Towards development of a malaria diagnostic: Generation, screening and validation of novel aptamers recognising *Plasmodium falciparum* lactate dehydrogenase

A thesis submitted in fulfilment of the requirements for the degree of

Doctor of Philosophy
(Biotechnology)

Rhodes University

Kelly-Anne Frith

(03f0103)

Supervisor: Prof. Janice L. Limson
Co-Supervisor: Dr Ronen Fogel

Biotechnology Innovation Centre (RUBIC)

October 2019

DECLARATIONS

I, KELLY-ANNE FRITH, do hereby declare that this thesis and work presented herein is that of my own. Where work of other researchers has been included in this thesis, the person responsible for producing that work has been duly acknowledged. This thesis is submitted in fulfillment of the degree of PhD at RHODES UNIVERSITY under the BIOTECHNOLOGY INNOVATION CENTRE. It has not been submitted for any other degree or examination at any other university.

KA Frith (signed eletronically)

……..

Signed

25 March 2019

……..

Date

Dedicated in loving memory to my late mother, father and brother…

… Remembered forever

ACKNOWLEDGEMENTS

Personal words of thanks:

To my loving husband, Prof. Roman Tandlich, words cannot express my gratitude for having you by my side through these years, for sharing the good times and celebrating my successes; but most of all, thank you for keeping me sane during the emotionally trying times, including the time writing up this thesis – It's been a bumpy road but we've finally made it!

To my son, Mr Dustian Frith-Tandlich – Mommy wrote her "book"!

To my friends and family near and far for your gentle words of encouragement – Thank you!

To my colleagues at NISC (Pty) Ltd for your support – Thank you!

Words of thanks in making this scholarly work possible:

First and foremost, my supervisor, Prof. Janice Limson, for her patience, guidance and support throughout the years – You've always been there for me and I would not be where I am without you.

My co-supervisor, Dr Ronen (Ron) Fogel, for his encouragement, enthusiasm, support, advice and endless hours of discussion on this work – I simply could not have done this without you.

The "aptamer team" in the Bio-SENS Research Group, Dr Shane Flanagan, Dr Lance Ho and Ms Mary Cromhout, for sharing and discussing ideas in the lab, as well as the remaining members of the Research Group through the years – it's been quite the journey.

Prof. Dean Goldring (UKZN), Mr Robert (Rob) Krause (UKZN), Dr Makobetsa Khati (CSIR), Dr Lia Rotherham (CSIR), Prof. Heinrich Hoppe, Dr Meesbah (Mez) Jiwaji, Dr Earl Prinsloo, Dr Pedro Estrela (UB), Mrs Margot Brookes, Mrs Michelle Isaacs, Mr Dustin Laming and Ms Taryn Swart for their provision of technical assistance, analytical methods and research input towards experimental work conducted herein – thank you.

The National Research Foundation (NRF)/German Academic Exchange Service (DAAD) In Country Scholarship for funding this research.

ABSTRACT

Malaria, caused by infection with the *Plasmodium* parasite, is one of the leading causes of death in under-developed countries. Early detection is crucial for the effective treatment of malaria, particularly in cases where infection is due to *Plasmodium falciparum.* There is, therefore, an enduring need for portable, sensitive, reliable, accurate, durable, self-validating and cost-effective techniques for the rapid detection of malaria. Moreover, there is a demand to distinguish between various infectious species causing malaria. Research in the area of malarial biomarkers has identified a unique, species-specific, epitope of *P. falciparum* lactate dehydrogenase (*Pf*LDH), enhancing prospects for the development of diagnostics capable of identifying the species causing malarial infection. In recent years, improvements have been made towards the development of rapid diagnostic tests for detecting malarial biomarkers. Owing to their low cost, ease of labeling, and high thermal stability (relative to antibodies), the development and synthesis of aptamers that target the malarial lactate dehydrogenase represents one of the key innovations in the field of rapid diagnostics for malaria. This study explored the generation of aptamers that specifically target *P. falciparum.*

Two sets of aptamers with diagnostically-supportive functions were generated independently, through parallel SELEX of recombinantly-expressed, full-length *Plasmodium falciparum* lactate dehydrogenase (r*Pf*LDH), and an oligopeptide comprising the *P. falciparum*-specific epitope on lactate dehydrogenase (LDHp). The latter offers a promising solution for generating aptamers capable of binding with high specificity to *P. falciparum.* In this work, an rLDH class of aptamers was generated when SELEX was performed using the full-length r*Pf*LDH protein as the target and the LDHp class of aptamers was generated when SELEX was performed using the oligopeptide LDHp as a target.

Aptamers were successfully generated through the process of SELEX (systematic evolution of ligands through exponential enrichment) following the study and application of several optimisation steps, particularly during the amplification stage of SELEX. Optimisation steps included the study of improvements in PCR conditions; role of surfactants (Triton-X), modifying the PCR clean-up protocol; and agarose gel excision. Structurally-relevant moieties with particular consensus sequences (GGTAG and GGCG) were found in aptamers both reported here and previously published, confirming their importance in recognition of the target. Novel moieties particular to this work (ATTAT and poly-A

stretches) were identified. Clades of consensus sequences were identified in both the rLDH and LDHp groups of aptamers, where sequences in the rLDH clade did not show preferential binding to r*Pf*LDH while those in the LDHp clade (particularly LDHp 3 and 18) were able to recognise and bind only LDHp.

Of the 19 sequences returned from the parallel SELEX procedures for r*Pf*LDH (11 sequences) and LDHp (8 sequences), six r*Pf*LDH and all eight LDHp sequences underwent preliminary screening and those with low responses eliminated. Of the eight LDHp-targeting aptamer sequences, five were preliminarily shown to bind to LDHp, whereas only two r*Pf*LDH-targeting sequences were shown to bind to the target (rLDH 4 and 7). To this small selection of r*Pf*LDH oligonucleotide sequences, two more (rLDH 1 and 15) were chosen for further study based on their sequences, secondary and predicted tertiary conformations. Sequences chosen for further study were therefore: rLDH 1, 4, 7 and 15 in the rLDH class, and LDHp 1, 3, 11, 14 and 18 in the LDHp class.

Binding properties of the aptamers towards their targets were investigated using enzyme-linked oligonucleotide assays (ELONA), fluorophore-linked oligonucleotide assays (FLONA), electromobility shift assays (EMSA), surface plasmon resonance (SPR), and GelRed dissociation assays, while applications towards aptasensors were explored using electrochemical impedance spectroscopy (EIS) and fluorescent microscopy. Some inconsistencies were seen for specific aptamer to target binding interactions using specific techniques; however, generally, binding to the targets was observed across the techniques assessed. These varied responses demonstrate the need to screen and validate aptamers using a variety of techniques and platforms not necessarily specific for the proposed application.

From the aptamer binding screening studies using ELONA, the most promising aptamers generated were identified as LDHp 11, rLDH 4, rLDH 7 and rLDH 15. Aptamer rLDH 4, which was generated against r*Pf*LDH, exhibited preferential and specific binding to the lactate dehydrogenase from *P. falciparum*, over the recombinantly-expressed lactate dehydrogenase from *Plasmodium vivax* (r*Pv*LDH), albeit with lowered responses compared to LDHp 11 in ELONA and EMSA studies. However, in kinetic ELONA studies rLDH 4 showed binding to both r*Pf*LDH and r*Pv*LDH. Aptamer rLDH 7 showed high affinity for r*Pf*LDH and r*Pv*LDH in kinetic studies using ELONA. However, screening studies with ELONA indicates that aptamer rLDH 7 may not be suitable for diagnostic tests in serum samples given its non-specific binding to human serum albumin (HSA). Aptamer rLDH 15

exhibited species specificity for r*Pf*LDH in screening studies using ELONA but showed affinity towards r*Pv*LDH (albeit lower relative to its affinity for r*Pf*LDH) in kinetic studies using ELONA. LDHp 11, generated against the *Pf*LDH peptide, showed a clear preference for r*Pf*LDH when compared to r*Pv*LDH and other control proteins, in both sets of ELONA studies conducted, as well as EMSA, thus possessing a strong ability to identify the presence of *Plasmodium falciparum* owing to its generation against the species-specific epitope. While LDHp 1 demonstrated binding to plasmodial LDH in a flow-through system (SPR), so reiterating ELONA responses, it did not perform well in the remaining methodologies. Aptamers rLDH 1 and 15 and LDHp 3, 14 and 18 exhibited a mixed set of results throughout the target protein screening analyses and were, thus, not considered for selective binding in *P. falciparum* parasite bodies.

In studies aimed at exploring biosensor assemblies utilising the developed aptamers, both rLDH 4 and LDHp 11, along with rLDH 7, LDHp 1 and pL1, demonstrated *in situ* binding to the native *Pf*LDH in fluorescent microscopy. LDHp 11 exhibited FITC-based fluorescence equivalent to the anti-r*Pf*LDHp IgY antibody in confocal fluorescent microscopy indicating superior binding to the native *Pf*LDH compared to the remaining aptamers. An examination of electrochemical impedance as a platform for a biosensor assembly did not, in these studies, exhibit the required sensitivity using physiologically relevant concentrations of analyte expected for pLDH following infection with *Plasmodium* spp.

Malstat/LDH activity was explored for application in a colorimetric aptasensor. A decrease in both r*Pf*LDH and r*Pv*LDH activity was observed following incubation with the tested aptamers, but rLDH 1, rLDH 7 and LDHp 14 did not exhibit similar decreases in r*Pv*LDH activity. Aptamers rLDH 1, 4 and 7 and LDHp 11 and 14 were, therefore, not selected as candidates for LDH capture in LDH activity-based diagnostic devices for *P. falciparum*. The decreases in pLDH activity in the presence of aptamers could hold promise as direct or antagonistic malaria therapeutic agents. Preliminary studies on the application of aptamers as malaria therapeutic agents, while of interest, should be viewed with due caution given the challenges of aptamers reaching the intracellular native plasmodial LDH hosted within the red blood cells.

In conclusion, this work has shown the ability of the LDHp 11 aptamer, generated in these studies, to selectively bind r*Pf*LDH over r*Pv*LDH, and to bind to the native *Pf*LDH in fluorescent microscopy, indicating that this aptamer holds promise as a biorecognition element in malaria biosensors and

other diagnostic devices for the detection, and differentiation, of *P. falciparum* and *P. vivax*. The use of a species-specific epitope of *P. falciparum* as a target in aptamer generation paves the way for similar such studies aimed at generating aptamers with species selectivity for other *Plasmodium* species.

TABLE OF CONTENTS

LIST OF FIGURES

CHAPTER 1

CHAPTER 2

LIST OF TABLES

CHAPTER 2

CHAPTER 3

CHAPTER 4

CHAPTER 5

CHAPTER 6

LIST OF EQUATIONS

Equation 2.1 $Recovery\ (\%) = \frac{ssDNA\ out\ (ng)}{ssDNA\ in\ (ng)} \times 100$

Equation 3.1 $\varphi = \Sigma\ [q_i / (\varepsilon d_i)]$

Equation 4.1 $Assay\ response\ (\Delta OD_{450nm}) = \left(\frac{\Gamma_{max} \times [aptamer]}{K_D + [aptamer]}\right)$

Equation 4.2 $Change\ in\ GelRed\ fluorescence\ (\Delta, Em_{600nm}) = Em_{600nm}\ of\ ssDNA_{\ LDHp^+} - Em_{600nm}\ of\ ssDNA_{LDHp^-}$

Equation 5.1 $Change\ in\ response\ (\Delta) = Response_{\ ([LDHp] = x\ nM)} - Response_{([LDHp] = 0\ nM)}$

Equation 5.2 $FITC{+}Pf\ bodies\ (\%) = \frac{Parasite\ bodies\ with\ FITC\ fluorescence\ (n)}{Parasite\ bodies\ with\ DAPI\ fluorescence\ (n)} \times 100$

LIST OF ABBREVIATIONS

AC	Alternating current
ANOVA	Analysis of variance
APAD/H	3-acetylpyridine nicotinimide adenine dinucleotide
APTEC	Aptamer-tethered enzyme capture
ATP	Adenosine triphosphate
bp	Basepair
BSA	Bovine serum albumin
C	Capacitance (EIS)
DAPI	4',6-diamidino-2-phenylindole
DMSO	Dimethyl sulfoxide
DNA	Deoxyribonucleic acid
dsDNA	Double-stranded deoxyribonucleic acid
EDC	1-ethyl-3-(3-dimethylaminopropyl) carbodiimide
EDTA	Ethylenediaminetetra acetic acid
EIS	Electrochemical impedance spectroscopy
ELISA	Enzyme-linked immunosorbent assay
ELONA	Enzyme-linked oligonucleotide assay
EMSA	Electrophoretic mobility shift assays
FITC	Fluorescein isothiocyanate
FLONA	Fluorophore-linked oligonucleotide assay
FP	Forward primer
GAPDH	Glyceraldehyde-3-phosphate dehydrogenase
HDT	Hexanedithiol
hLDH	Human lactate dehydrogenase
HMCKN	Hepes, MgCl (magnesium chloride), CaCl (calcium chloride), KCl (potassium chloride) and NaCl (sodium chloride)
HRP-II	Histidine rich protein 2
HSA	Human serum albumin
HSD	Honest significant difference
IntDen	Integrated fluorescent intensity
K_D	Dissociation constant
LDH	Lactate dehydrogenase
LDHp	*P. falciparum*-specific lactate dehydrogenase peptide (LISDAELEAIFDC)
MCH	Mercaptohexanol
mLDH	Mammalian (bovine) lactate dehydrogenase
MSA	Multiple sequence alignment
NAD/H	Nicotinamide adenine dinucleotide
NBT	Nitro blue tetrazolium
NHS	*N*-hydroxysuccinimide

OD	Optical density
PAGE	Polyacrylamide gel electrophoresis
PBS	Phosphate buffered saline
PCR	Polymerase chain reaction
PDB	Protein database
PES	Phenazine ethosulphate
*Pf*LDH	*Plasmodium falciparum* lactate dehydrogenase
pLDH	*Plasmodium* lactate dehydrogenase
*Pv*LDH	*Plasmodium vivax* lactate dehydrogenase
R_{CT}	Charge transfer resistance
RDT	Rapid diagnostic test
R_{max}	Theoretical binding capacities
RNA	Ribonucleic acid
RP	Reverse primer
r*Pf*LDH	Recombinant *Plasmodium falciparum* lactate dehydrogenase
rpm	Repetitions per minute
r*Pv*LDH	Recombinant *Plasmodium vivax* lactate dehydrogenase
RRU	Relative response units
RS	Solution phase resistance
RU	Response units
SA-HRP	Streptavidin-linked horseradish peroxidase
SAM	Self-assembled monolayer
SDS	Sodium dodeyl sulphate
SELEX	Systemic evolution of ligands by exponential enrichment
SPR	Surface plasmon resonance
ssDNA	Single-stranded deoxyribonucleic acid
TBE	Tris, borate, EDTA
TBS+	Tris buffered saline (with Nonidet P-40)
TMB	3,3’,5,5’-tetramethylbenzidine
UV	Ultraviolet
W/Z_W	Warburg modulus

LIST OF OUTPUTS

Patents

Frith KA, Cromhout M, Fogel R, Goldring D and Limson JL (2014) ARIPO Patent (AP) *P2014007847*. "Diagnosis of malaria" (ZA 2013/05850). Available at: http://regionalip.aripo.org/wopublish-search/public/patents

M Cromhout, Fogel R, Frith KA and Limson JL (2015) ARIPO Patent (AP) *P2015008263*. "Analysis of human immune status" (ZA 2014/01017). Available at: http://regionalip.aripo.org/wopublish-search/public/patents

Original article

Parts of this thesis were published with Open Access (CC-BY 4.0) in:

Frith KA, Fogel R, Goldring J, Krause R, Khati M, Hoppe H, Cromhout ME, Jiwaji M, Limson JL (2018) Towards development of aptamers that specifically bind to lactate dehydrogenase of *Plasmodium falciparum* through epitopic targeting. *Malaria Journal.* **17**(1): 191. doi:10.1186/s12936-018-2336-z

CHAPTER 1

Literature review and general introduction

1.1. Malaria and the *Plasmodium* parasite genus

Malaria remains one of the widest spread global causes of mortality today. From 2011 to 2018, malaria remained endemic in 104 countries worldwide (WHO, 2012a; 2018). The World Malaria Report has identified that approximately 90% (WHO, 2012a; 2016) of the 220 million worldwide cases, and 99.7% of cases reported in Africa (WHO, 2018), were caused by the malarial infectious agent: *Plasmodium falciparum*.

Global preventative measures taken against malaria infections, which include WHO-approved chemicals, intermittent preventative treatments and more commonly mosquito nets, are actively working in decreasing rates of malaria infection and mortality. The incidence of malaria-related deaths reported worldwide decreased from 863 000 in 2008, 607 000 in 2010, 429 000 in 2015 to 435 000 in 2017 (WHO, 2009; 2012a; 2016; 2018). However, Africa accounted for 93 % of all malaria-related deaths in 2017 (WHO, 2018). The majority of malaria deaths worldwide (61 %) occur in vulnerable segments of the population (specifically the elderly, pregnant women and children under the age of 5) with Africa having the highest statistic for child mortality (WHO, 2018).

1.1.1. Life-cycle of Plasmodium parasites

Malaria is caused by the protozoan parasite belonging to the *Plasmodium* genus. The parasites are transmitted through the bite of the female *Anopheles* mosquito (Walker *et al*., 2009) when the mosquito takes a blood meal. There are many species of the *Plasmodium* genus, with many infecting animals and humans alike. For example, the zoonotic *Plasmodium* species, *Plasmodium knowlesi*, has been known to infect humans when its natural host are South-East Asian macaques (Centre for Disease Control (CDC), 2018).

Anthropinistic, or human-affecting, *Plasmodium* species colonise 2 hosts: mosquitoes and humans. Three distinct infection phases of the *Plasmodium* life-cycle occur in these hosts, each phase with

their own distinctive cellular and metabolic profiles (CDC, 2018). These are shown in **Figure 1.1**.

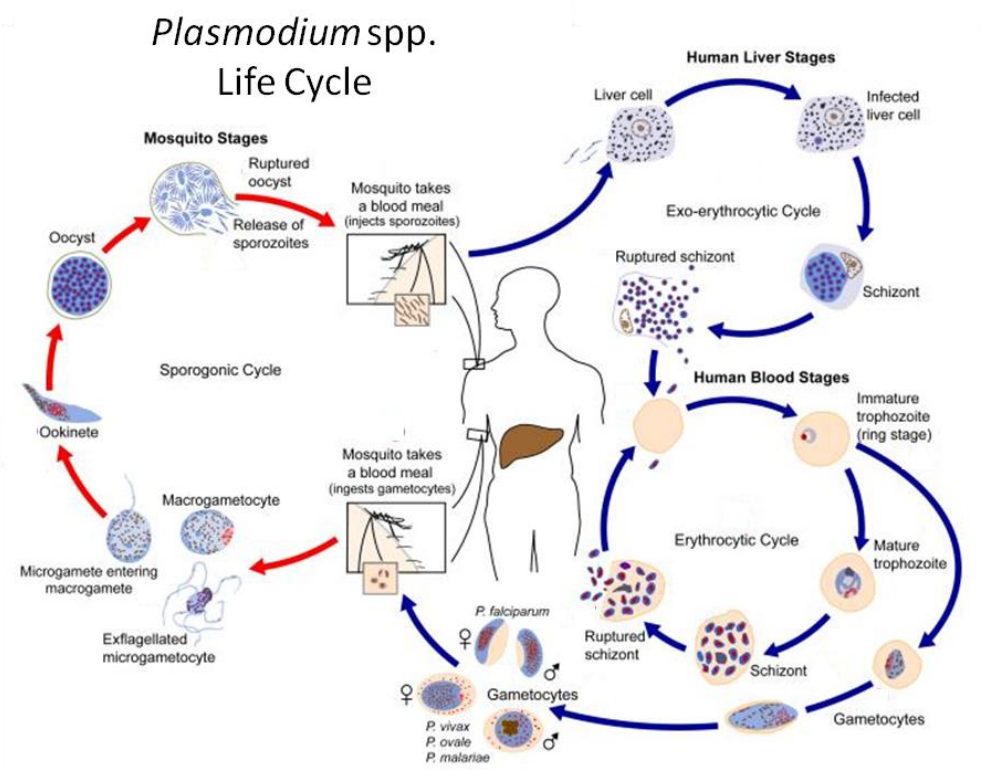

Figure 1.1: The life-cycle of *Plasmodium* spp.
Copyright obtained from the US Centre for Disease Control and Prevention – CDC found at: https://www.cdc.gov/dpdx/malaria/index.html, accessed 5 February 2019, reproduced under the Open Access CC-BY License

The life-cycle is initiated by a *Plasmodium*-infected mosquito taking a blood meal from a susceptible human. During feeding, the mosquito injects sporozoites in its saliva into the human blood stream (CDC, 2018). Sporozoites then travel to the liver where they infect the liver cells, or hepatocytes (the exo-erythrocytic cycle in the "Human Liver Stage" in **Figure 1.1**). In the liver, the sporozoites mature and multiply to form a multinucleate, aggregate organism termed a "schizont". The schizont then ruptures and releases merozoites into the blood, initiating the "Human Blood Stage" (**Figure 1.1**) of the life-cycle (CDC, 2018).

During the human blood stage, the merozoites infect red blood cells and develop to form immature ring-like trophozoites. This is the symptomatic stage of the human infection (CDC, 2018). The erythrocytic life-cycle can then follow two paths: asexual and sexual reproduction (**Figure 1.1**). In asexual reproduction indicated in **Figure 1.1** as the "Erythrocytic Cycle", the immature ring-like

trophozoites in the red blood cells develop into mature trophozoites and multiply mitotically until the schizont, and concomitantly infected red blood cell, ruptures releasing a new wave of merozoites into the blood stream (CDC, 2018).

Sexual reproduction of the *Plasmodium* life-cycle is initiated by the ring-stage trophozoite differentiating into male and female gametocytes (CDC, 2018; **Figure 1.1**). These gametocytes are ingested by another female mosquito upon taking a blood meal from the human host, thereby starting the sporogenic life-cycle in its mosquito host (**Figure 1.1**). The gametocytes mature forming macrogametocytes (female) and microgametocytes (male) which fuse in the stomach of the mosquito forming a flagellated ookinete (zygote). The mobile ookinetes move to the midgut wall of the mosquito where they mature to form oocysts (CDC, 2018). These rupture releasing sporozoites which will initiate a new cycle in another human host.

1.1.2. Clinical features of malaria inferred by Plasmodium in the human host

Malaria, the disease caused by infection with *Plasmodium* parasites, exhibits a wide range of symptoms in the human body (CDC, 2018). Mild to severe symptoms (possibly culminating in death) generally appear after a few days (for *Plasmodium falciparum*), a few weeks (one to four weeks, *Plasmodium ovale* and *Plasmodium vivax*) or up to a few months (*Plasmodium malariae*) following the initial infection (Coppel *et al*., 1998; CDC, 2018). This long period of dormancy is due to a longer exo-erythrocytic or liver stage in the human host and addition of a hypnozoite stage in the life-cycle (Coppel *et al.,* 1998).

The severity of malaria and the associated symptoms can be categorised into uncomplicated and complicated forms of malaria. Symptoms of uncomplicated malaria include fever, chills, headache, nausea and vomiting, body aches and fatigue (CDC, 2018). The onset of these symptoms is cyclic in nature with each cycle presenting two days (for *P. falciparum*, *P. vivax* and *P. ovale*) to three days (for *P. malariae*) apart, and lasting up to 10 hours before symptoms ease. Complicated malaria is caused by abnormalities in the patient's blood or organs, resulting in serious complications and/or organ failure (CDC, 2018). This category of malaria manifests to include: cerebral malaria (presenting with psychological distress, fainting, seizures and coma); anaemia and haemoglobinuria (presenting with destruction of red blood cells); acute respiratory distress syndrome (ARDS); low blood pressure; kidney failure; and, hypoglycaemia and associated metabolic acidosis (CDC, 2018).

Clinical symptoms are generally associated with the asexual erythrocytic cycle (**Figure 1.1**) in the human host stage of the lifecycle of the *Plasmodium* parasite (CDC, 2018). As the trophozoites mature to form schizonts in the red blood cell, a number of waste products, such as glucose phosphate isomerise and haemozoin, are formed and accumulate in the red blood cell as the parasites grow and metabolise nutrients (Srivastava *et al*., 1992; Olivier et al., 2014). When the schizont and red blood cell rupture, these waste products are released along with the merozoites into the human blood stream. The presence of these toxic products, glucose phosphate isomerise and haemozoin, stimulate the body's natural defence system to produce macrophages and cytokines (Olivier *et al*., 2014). It is this defensive response by the body that results in the symptoms commonly observed with uncomplicated malaria, specifically, those of fever and chills (Martiney *et al*., 2000).

1.1.3. Parasitic strategies of Plasmodium in the human host

The ability of the *Plasmodium* parasite to avoid attack and clearance by the human host's immune system accounts for the pathogenicity of the parasite (Coppel *et al.,* 1998). There are two ways by which the *Plasmodium* parasite is able to do this:

(1) The first method is through cyto-adherence of the *Plasmodium*-infected red blood cells to: endothelial cells lining capillary walls; non-infected red blood cells (a phenomenon called "rosetting") and other infected red blood cells (autoagglutination; Coppel *et al.,* 1998). This adherence is attributed to the parasite's expression of molecular adhesins, named erythrocyte membrane protein 1 (EMP1), on infected red blood cells' surfaces (Coppel *et al.,* 1998). The *Plasmodium falciparum* EMP1 (*Pf*EMP1) protein has been characterised extensively and may pose as a target in therapeutics (Leech *et al*., 1984; Chaiyaroj *et al*., 1994; Bull *et al*., 1998).

(2) Secondly, the parasite is able to avoid clearance from the human body by remaining in the liver and red blood cells for extended periods of time (Coppel *et al.,* 1998). This period of time is dependent on the species, as previously discussed in **Chapter 1.1.2**.

Detection of malaria in the human body will be discussed in the subsequent section of this chapter (**Chapter 1.2**).

1.2. Detection and diagnostics of malaria

Similarly to intracellular pathogenesis in the human body (**Chapter 1.1.3**), cyto-adherence and the intracellularity of the *Plasmodium* parasite may limit the direct detection of *Plasmodium* spp. in human blood. Although positive strides in the field of malaria diagnostics have been made in recent years, there still remain areas in which improvements can be made. Current methods of malaria diagnosis include: colourimetry (Whiley *et al.*, 2004); spectrophotometry (Alifrangis *et al.*, 2005); fluorescence (Carret *et al*., 2005); polymerase chain reaction (PCR; Whiley *et al.*, 2004); mass spectroscopy (Demirev *et al*., 2002); microfluidic cell enrichment (Kong *et al*., 2015); magnetic resonance relaxometry (Kong *et al*., 2015); loop-mediated isothermal amplification (Hsiang *et al*., 2014); and, the gold standard: microscopy (Carret *et al*., 2005). However, although these techniques may be sensitive with reported sensitivities as low as 10 parasites per microlitre of blood, they remain laboratory based techniques which require skilled personnel and expensive equipment.

Indirect detection of malaria via a *Plasmodium* biomarker can therefore be utilised as a means of malaria detection in a diagnostic device.

1.3. Biomarkers for malaria detection

Biological markers – or biomarkers – are cellular, biochemical, or molecular indicators that are used to measure an epidemiological response, pathogenic disease, or therapeutic effect (Hulka, 1991). There are three main classes of biomarker that exist (Frank & Hargreaves, 2003):

1. Biomarkers produced by the pathogen. These can be used to monitor the progress of the pathogenic infection following initial infection and therapy, e.g. enzymes, RNAs.
2. Biomarkers produced by the host in response to an infection. The presence of antigens results in the production of antibodies by the human body that specifically bind to pathogenic proteins, which can be measured to monitor disease progression and clearance, e.g. antibodies, cytokines.
3. Biomarkers in the form of a by-product produced or utilised by the pathogen or upon pathogenic infection, e.g. co-factors such as nicotinamide adenine dinucleotide (NAD/H).

Biomarkers can be used as an indicator of infection before the resulting disease becomes symptomatic, and thus prevent the onset of disease (Dal-Bianco *et al.*, 2007; Jain *et al*., 2014). In other words, biomarkers facilitate the early detection of the disease.

To facilitate such early diagnosis, the biomarker would also need to be produced by the pathogen in sufficiently high concentrations to be detectable. For blood parasites, such as *Plasmodium* spp., a suitable biomarker would quantitatively indicate the burden of infection in whole blood or serum, regardless of the infection locale and diluting influences of human sera (Jain *et al*., 2014). Furthermore, the ideal biomarker would need to assist in the classification of the type of infection, including the inter-individual differences (Hulka, 1991). This will aid in the identification of pathogen susceptibilities, and assist in the specific treatment of the infection. Therefore, the ideal biomarker for species recognition needs to be produced in high quantities and be specific for a particular pathogen. For example, early detection of *Plasmodium* sp. infection through the sensitive and selective biorecognition of any given biomarker (further discussed below) can facilitate treatment of a given *Plasmodium* sp. This is of particular importance given the rapid presentation of symptoms of malaria.

Biomarkers do offer an advantage in the indirect detection of malaria by way of the *Plasmodium* parasite over direct detection, e.g. via microscopy, due to the numerous methodologies and approaches that can be utilised in the production of the diagnostic device. Similarly to the locale of the parasite bodies, the location of the biomarker (whether it is intracellular or extracellular) needs to be considered in the development of such malaria detection devices. The biomarker's native location is important in the development of such malaria detection devices as it could influence the device's efficacy.

Biomarkers specifically produced by the *Plasmodium* parasite and are known indicators of infection, and which have been considered targets in diagnostic devices in the detection of *Plasmodium* species include: histidine-rich protein 2 (HRP2); aldolase; glycolytic lactate dehydrogenase (LDH) (Moody, 2002); and, glyceraldehyde-3-phosphate dehydrogenase (GAPDH) (Krause *et al*., 2017).

Plasmodium falciparum histidine rich protein 2 (*Pf*HRP II), aldolase and lactate dehydrogenase (LDH) are currently used as biomarkers in several commercial diagnostic rapid diagnostic tests (RDTs) (Kifude *et al*., 2008). As aldolase lacks the specificity required for identifying and discriminating *Plasmodium* species, immunosensors incorporating aldolase as a biomarker are used in conjunction with *Pf*HRP II (Bell *et al.*, 2006). *Pf*HRP II offers sensitivity as an antigen marker of *P. falciparum* (Grobusch *et al.*, 2003). While *Pf*HRP II lacks antigenic variance between species and is specific for *P. falciparum*, it cannot be used for species discrimination (Bell *et al.*, 2006). To achieve said species

discrimination, specificity and selectivity are instilled in a single sensor by combining *Pf*HRP II and aldolase. Should antigenic variance of *Pf*HRP II exist across strains within a species, it may lead to false positives as this antigen may bind to antibodies non-specifically (Grobusch *et al.*, 1999; Iqbal *et al.*, 2004). Furthermore, the antigen may not bind to the antibodies resulting in false negatives. False results lead to the misdiagnosis and mistreatment of malaria increasing the number of drug resistant species (White & Olliero, 1996).

*Pf*HRP II is present in the cytoplasm and on the membrane of the infected red blood cell and is, consequently, susceptible to attack by the immune system of the human host (Bell *et al*., 2006). Circulating *Pf*HRP II also remains in the blood for up to 2 weeks after clearance of the parasite making it a poor candidate for monitoring the efficacy of drug treatment and real-time monitoring of infection by resulting in false positives and prolonging treatment (Tjitra *et al.*, 2001). However, rapid diagnostic tests targeting *Pf*HRP II have reportedly failed to detect some *P. falciparum* parasitaemias and this is due to deletions in the gene from isolates from Peru, India and Africa and due to different amino-acid sequences arising from single nucleotide polymorphisms (Baker *et al*., 2005; Gamboa *et al*., 2010; Bharti *et al*., 2016).

Plasmodium LDH (pLDH), on the other hand, does not remain in the bloodstream once the malaria infection has cleared, minimising the frequency of false positives (Gerstl *et al*., 2010). Thus, pLDH presents as a more viable target than *Pf*HRP II when monitoring treatment responses and clearance of the parasite from the human host/patient. pLDH further presents as a viable target as it does not display antigenic variance within a species and is, therefore, species specific (Piper *et al*, 1999). The LDH gene, which encodes the peptide sequence of the LDH subunit, does not display any genetic diversity across *P. falciparum* strains found in Asia, Africa and South America (Simpalipan *et al*., 2018). This genetic conservation renders *Pf*LDH ideal as a target biomolecule in the development of malaria RDTs (Simpalipan *et al*., 2018). Detection of pLDH offers a means by which to discriminate between species based on unique epitopes on the protein (Piper *et al*, 1999). Such species include *P. falciparum*, *P. vivax* and *P. yoelii*. pLDH further presents as a viable target as it is produced throughout all stages of its life-cycle (Florens *et al.*, 2002).

1.3.1. Plasmodium lactate dehydrogenase (pLDH)

Lactate dehydrogenase (LDH) is a tetrameric enzyme essential in the production of energy during

anaerobic glucose metabolism. Plasmodial LDH (pLDH) possesses a vital function in the glycolytic pathway under anaerobic conditions for the generation of energy in the form of ATP (Piper *et al*., 1999). Using the nicotinamide adenine dinucleotide (NAD^+) cofactor, LDH reversibly catalyses the oxidation of lactate into pyruvate during the final phase of glycolysis under anaerobic, or microaerophillic, conditions. Given the importance of pLDH in glycolysis for the survival and longentivity of the parasite, it stands to reason that it would be expressed at significant levels throughout all stages of the parasite lifecycle, particularly in the erythrocytic cycle in the human body (Piper *et al*., 1999). *Plasmodium* sp. upregulate the expression of LDH in the erthrocytic stages of infection, thus pLDH will remain at a concentration 30 to 100 times greater than that of the host, or even the uninfected, erythrocyte (Vivas *et al*., 2005). The upregulated expression of LDH occurs in the merozoite (83.9 %) and gametocyte (78.8 %) life-cycle stages of the *Plasmodium* life-cycle (Florens *et al.*, 2002). Lower levels of LDH expressed in the intracellular immature trophozoite stage of the *Plasmodium* life-cycle may lower the sensitivity of the RDT (Miller *et al*., 2001).

Excess pLDH is advantageous in the development of a sensing device utilising pLDH as a biomarker in the detection of malaria as such a device would inherently be rendered sensitive to pLDH, as well as resistant to the diluting effects of large volumes of human sera. Interference by human LDH (hLDH) could be anticipated when analysing and detecting pLDH, concentrations of which are dependent on the level of parasitaemia and, hence, enzyme concentrations.

Plasmodium LDH (pLDH) was selected as a diagnostic tool for malaria pathogenicity as it is water-soluble, residing primarily in the cytoplasm of the parasite in nature (Bell *et al.*, 2006). Typically, during the diagnostic assay for this enzyme, lysis of the cells and merozoites is required to release pLDH (Moody *et al*., 2000).

1.3.2. Species-specific epitopes of pLDH

Plasmodial LDH is of particular interest with respect to selective detection of malaria given that amino acid sequence and resulting structure of pLDH is conserved within the *Plasmodium* genus. Furthermore, speciation within the *Plasmodium* genus can be observed through unique epitopes on the surface of the *Plasmodium*-derived protein (Piper *et al*, 1999), but not the human protein. Analysis of the amino acid sequences of pLDH molecules reveals that these have common, genus-specific epitopic regions on the surface of the enzyme that can be used for antibody binding for

broad biorecognition of *Plasmodium spp*. (Hurdayal *et al.*, 2010). Such sequence conservation is observed when the *Plasmodium spp* lactate dehydrogenase amino acid sequences are aligned with that from human (*Homo sapiens*) lactate dehydrogenase using ClustalW (**Figure 1.2**). The amino acid sequences of *Plasmodium* LDH have 26 % sequence similarity with that of human LDH; however, there is no conserved sequence stretches. There is, however, greater than 90 % amino acid sequence homology between the catalytic residues throughout the *Plasmodium* genus (Brown *et al*., 2004; Turgut-Balik *et al*., 2004).

Plasmodium LDH sequences, which traverse to the species-specific epitopes known to exist, are conserved across wild types of *P. falciparum* found in Africa, Asia and South America (Talman *et al*., 2007; Simpalipan *et al*., 2018). The sequences for *P. vivax*, *P. malariae* and *P ovale* LDH contain conserved regions with mutations, thereby varying the amino acid sequence across wild types (Talman *et al*., 2007). Despite the high degree of consensus amongst the LDH of *Plasmodium* species, unique species-specific epitopic regions, in addition to the pan-specific epitopic regions, do exist. The synthesis of these unique epitopes for pLDH paves the way for the development of diagnostic techniques for *in vitro* and *in vivo* testing (Tomar *et al.*, 2006). The location of this species-specific epitope sequence is highlighted in bold under the solid line in the sequence alignment in **Figure 1.2**. Hurdayal and co-workers describe the isolation and identification of an epitope specific to *P. falciparum*, *P. vivax* and *P. yoelli.* These were then expressed as short chain peptides between 12 and 16 amino acid residues long and antibodies raised against these peptides thereafter. This provided a preliminary demonstration of the promise for the specificity needed to achieve a sensor that has the ability to detect and discriminate between the various *Plasmodium* species.

Biological recognition elements raised against these regions can thus be utilised for inter-species discrimination (Piper *et al.*, 1999). As there have been reports that the synthesis of these unique epitopes for pLDH provides diagnostic techniques with viable biomarkers for *in vitro* testing (Tomar *et al*., 2006). Hurdayal and co-workers (2010) demonstrated that by raising antibodies against the synthesised species-specific antigenic epitope region (of 12 amino acid residues in length), selective, epitope-specific bio-affinity was achieved between species of *Plasmodium*, specifically *P. falciparum* and *P. vivax*, amongst others. Therefore, by raising antibodies against the species-specific peptide sequence, the required increased level of bioaffinity specificity may be achieved (Hurdayal *et al*., 2010; Mouatcho & Goldring, 2013).

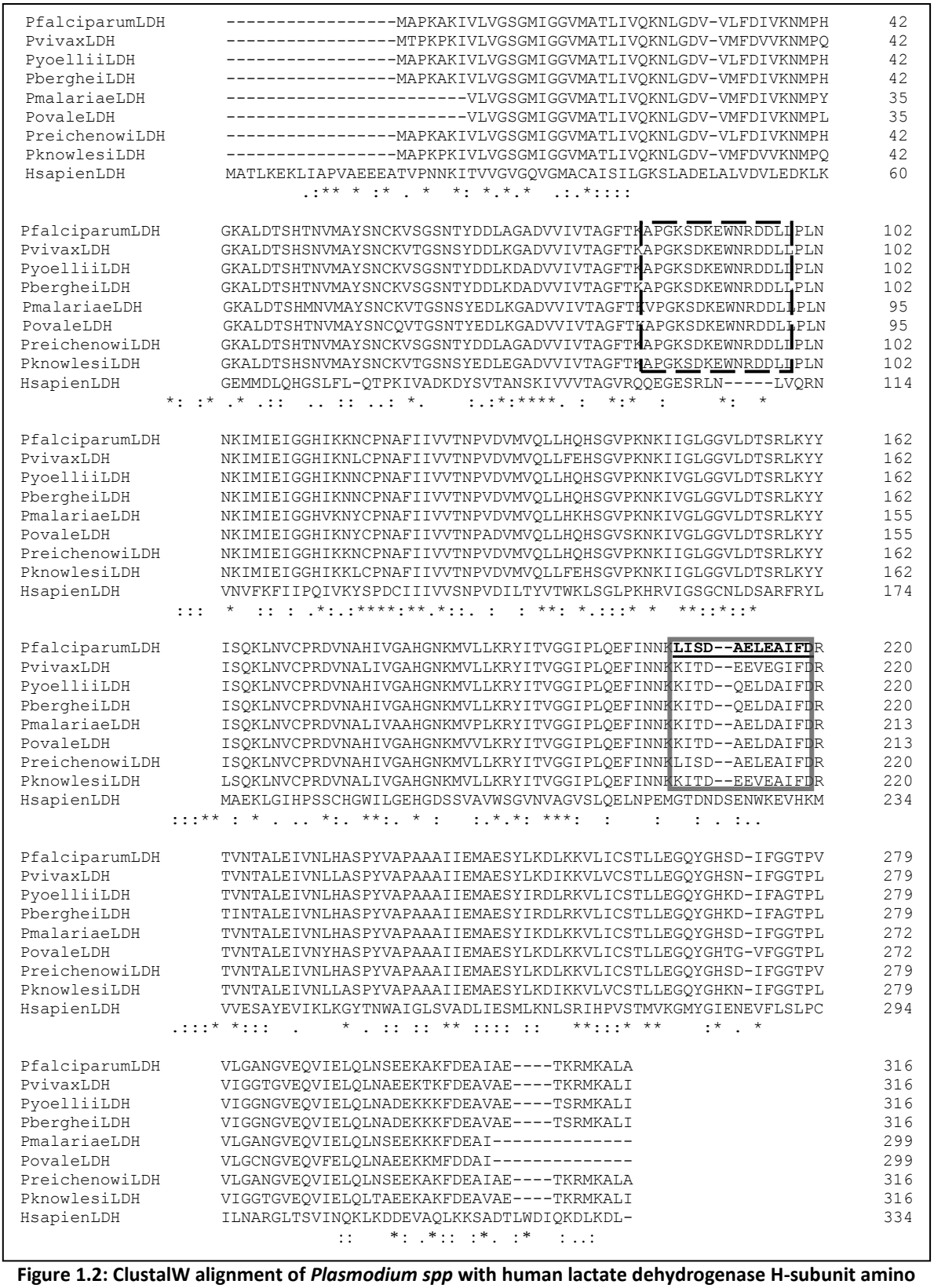

Figure 1.2: ClustalW alignment of *Plasmodium spp* with human lactate dehydrogenase H-subunit amino acid sequences (expanded from Hurdayal *et al.*, 2010).

The unique epitope specific for *P. falciparum* is underlined; similar epitopes in malarial LDH are boxed in grey; the common *Plasmodium* pan-specific epitope is boxed in dashed black.

Uniprot IDs are: *P. falciparum* LDH: Q71T02; *P. vivax* LDH: Q4PRK9; *P. yoellii* LDH: Q7RHU8; *P. berghei* LDH: P84793; *P. malariae* LDH: Q6JH31; *P. ovale* LDH: Q6JH32; *P. reichenowi* LDH: Q5R2J8; *P. knowlesi* LDH: B3L8Y6; and, *H. sapiens* LDH: P07195.

Figure 1.3 shows the three-dimensional location of the species-specific epitopic peptide (LISDAELEAIFD; with a green ribbon backbone and CPK ball and stick sidechains) found on the pLDH subunit (pale pink spacefill). The location of this peptide is well suited for biorecognition as it is a distance from the pan-specific epitope (APGKSDKEWNRDDLL; blue ribbon backbone and CPK stick sidechains in **Figure 1.3**) (Hurdayal *et al*., 2010). This epitopic region is also at a distance from the lactate/pyruvate binding site thereby nullifying interference from substrate binding at the enzyme's active site. The peptide location is ideally suited as a target for capture molecules, such as antibodies and aptamers, as this epitopic region is not hidden following polymerisation of the subunits and remains exposed on the surface of the whole naturally-occurring tetrameric protein form.

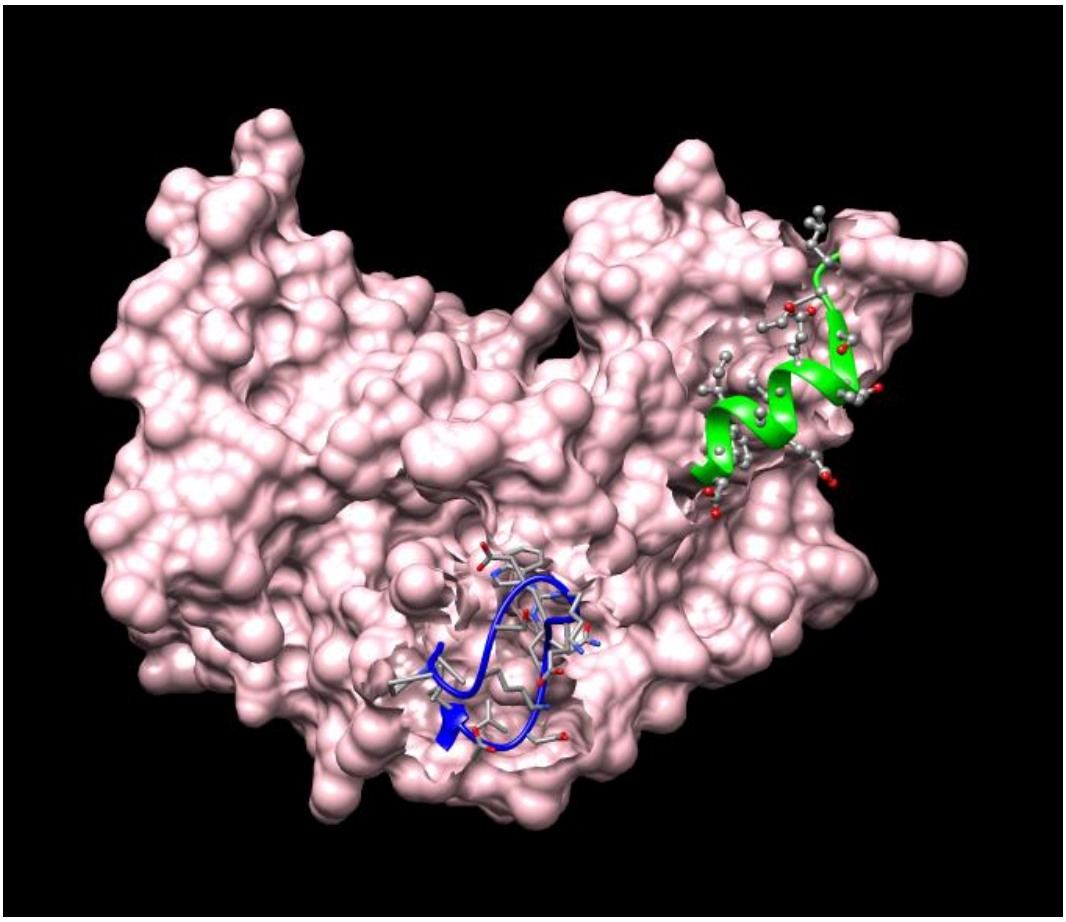

Figure 1.3: Crystallographic structure of a single *Pf*LDH subunit (PDB Accessions No.: 2A94) highlighting location of the *Pf*LDH species-specific peptide.
Image rendered in UCSF Chimera V1.10.2 (Pettersen *et al*., 2004; http://www.cgl.ucsf.edu/chimera)
r*Pf*LDH: pale pink space-fill;
*Pf*LDH species-specific epitope (LISDAELEAIFD): backbone: green ribbon; sidechains: CPK ball and sticks;
Plasmodium pan-specific epitope (APGKSDKEWNRDDLL): backbone: blue ribbon; sidechains: CPK sticks

Therefore, by using this unique epitope which exist a distance away from the shared, common epitopic regions (as those shown in **Figure 1.3**), selective detection of the *P. falciparum* can be achieved by means of specific *Pf*LDH antibody binding. Binding of *Pf*LDH or *Pv*LDH to such antibodies, employing the use of immunochromatography, can therefore offer the RDT operator a means of differentiating between *Plasmodium* species.

1.4. Conventional methods of detecting the biomarker, pLDH, for the diagnosis of malaria

Currently, pLDH is a focus of active detection through various platforms and methodologies. Use of the sensitive chromogenic Malstat assay for pLDH has been utilised to measure the viability of cultured *Plasmodium* parasites in the laboratory and clinical settings, initially for the purposes of drug sreening (Makler *et al*., 1993; Miller *et al*., 2001; Zofou *et al*., 2011). The Malstat assay was further developed by Dirkzwager and co-workers (2015) in the aptamer-tethered enzyme capture (APTEC) assay. This assay sensitively detects and measures pLDH activity as an indicator of the presence of *Plasmodium* as an indicator of malaria infection, while human LDH activity is measured less sensitively (Dirkzwager *et al*., 2015). The APTEC assay and most other malaria biomarker detection methods rely on immunochromatography as the main principle behind the development of malaria diagnostic devices. The APTEC and Malstat assays are further explored in **Chapter 5**.

1.4.1. Immunosensors: Immunochromatographic rapid diagnostic tests (RDTs)

Immunosensors are affinity-based sensors in which the immunochemical response is coupled to a transducer (Luppa *et al*., 2001). One of the ligands, often the biorecognition molecule (such as an antibody, aptamer, antacalin or molecularly imprinted polymer), is immobilised onto the surface of the transducer. Upon binding of the antigen to the immobilised biorecognition molecule, a response is elicited by the transducer which is then detected by the transducer and translated into a readable signal (Luppa *et al*., 2001). Examples of transducers include electrodes which detect electrochemically active molecules; thermistors which detect heat; photon counters which detect light; and, piezoelectric devices which detect changes in mass.

One such example of an immunosensor is that of the rapid diagnostic test or RDTs. RDTs primarily make use of immunochromatographic techniques. As an alternative to the current techniques previously mentioned (**Section 1.3**), immunochromatography-based RDTs, which use biological capture molecules, offers advantages such as speed, accuracy, simplicity, sensitivity, cost-

effectiveness, ease of use and interpretation, and portability which allows for bed-side testing and field application (Luppa *et al*., 2001). Immunosensing RDTs do not require extensive training of personnel or expensive equipment. The methodology is easy to follow and results are easily interpreted. Immunosensors can include antibodies and/or aptamers as the capture biomolecule and hold a great deal of promise for commercialisation and patenting.

RDTs, a major research focus for malaria detection devices, immunochromatographically detect malarial biomarkers, the antigen, to their respective antibodies, or immunorecognition molecule. These devices can detect one species having one immobilised antibody for a particular antigen and a control antibody. Alternatively, RDTs can contain the species-specific antibody and a pan-specific antibody that is capable of binding to the genus of that species. RDTs can also distinguish between species by having more than one species-specific antibody, the pan-specific antibody and/or the control antibody. They are ideal for point-of-care or bedside testing and field applications.

Traditionally, immunosensors are manufactured using antibodies specific for the target molecules (Laczka, 2014). Antibodies are either polyclonal or monoclonal. Polyclonal antibodies recognise many epitopes on one antigen, are less specific and can distinguish genera (Byrne *et al*., 2009). They are inexpensive and quick to produce (Leenaars & Hendriksen, 2005; Seida, 2017). Monoclonal antibodies, on the other hand, bind to one epitope on one antigen eliciting a highly specific response discriminating between species within the genus (Byrne *et al*., 2009). Production of these antibodies is costly and can take a long time (Leenaars & Hendriksen, 2005; Seida, 2017).

Antibodies found in immunosensing are typically mammal serum immunoglobulin G (IgG). However, antibodies from chickens (specifically chicken egg yolks, thus called IgY due to their presence in egg yolks) have become more attractive in infectious disease detection, prevention and treatment as large quantities of these antibodies can be efficiently and cost-effectively isolated (Gassmann *et al.*, 1990). IgY antibodies are ideally suited for use in a mammalian system as there is no activation of the mammalian complement system, or cross-reactivity, owing to the phylogenetic distance between chickens and mammals (Larsson *et al.*, 1988). Therefore, by generating IgY antibodies against a malarial target in a chicken for use in a human system, a large phylogenetic distance remains between all species involved, greatly reducing the possibility of cross-reactivity. This is beneficial for use in a diagnostic device in which false positives need to be eradicated.

Although IgY antibodies offer many advantages over IgG antibodies, there remain drawbacks in the use of antibodies. Generally, there remains a batch-to-batch variation as antibodies produced from one chicken will differ from another as they are produced *in vivo*. Being proteinaceous macromolecules, IgY antibodies are inherently temperature sensitive (impacting on their shelf-life) and can denature irreversibly when exposed to high temperatures of >65 °C (Pilz *et al*., 1977). IgY antibodies have a low structural stability as the conformation of the β-structure of the IgY molecule is disordered (Shimizu *et al*., 1992). Also, there is no hinge region in the IgY heavy chain lowering flexibility which may result in inactivation of the antibody, especially when exposed to low/acidic pH far below physiological conditions, temperatures >65 °C and proteolytic enzymes (Pilz *et al*., 1977).

In order to remain clinically significant for malaria diagnostics, the sensitivities of the rapid diagnostic tests need to have a lower limit of detection of 100 parasites per µl of blood or serum for sensitive detection of *Plasmodium* infection in the human host (WHO, 2003). *Pf*HRP II-, aldolase- and lactate dehydrogenase (LDH)-based RDTs are commercially available diagnostic tests used in the detection of malaria (Kifude *et al*., 2008). Furthermore, devices with *Pf*HRP II are used in most commercial RDTs, such as Malaquick®, Parasight F® and Paracheck®-*Pf* (Kifude *et al*., 2008). However, many of the present commercial *Pf*LDH RDTs have variable results owing to their sensitivity towards extreme heat and humidity – which often decreases the efficacy of antibody-based techniques (Chiodini *et al*., 2007; WHO, 2012b; Hsiang *et al*., 2014). Moreover, the sensitivity of RDTs may be lowered due to rapid antibody or cellular attack and subsequent clearance of the parasites circulating in the human body (Moody *et al*., 2000). Also, a large proportion of the circulating antigen may remain in the human body during testing and the resulting amount of detected antigen may not correlate with the concentration of antigen as well as parasite present in the human body, as schematically shown in **Figure 1.4** (Bell *et al*., 2006). Therefore, any discrepancies and variations in the concentrations of the antigen and the parasite must be compensated for, regardless of the type of antigen.

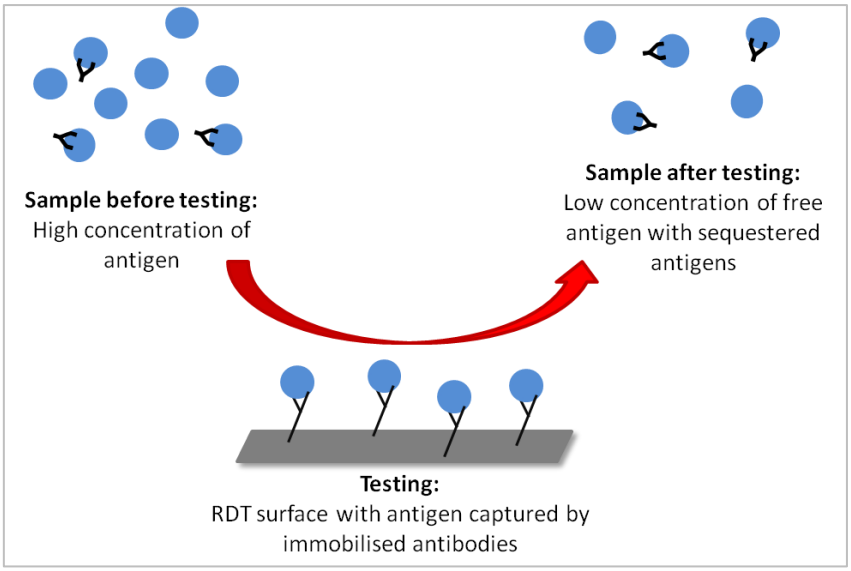

Figure 1.4: Schematic diagram depicting the concentration of free antigen in a blood sample before and after rapid diagnostic testing with an antibody-based RDT.

RDTs that use pLDH make use of *P. falciparum*-specific and pan-specific antibodies as active components of the immunochromatographic tests. Together, these allow the clinical practitioner to positively identify whether the patient has malaria resulting from infection with *P. falciparum* or another species of *Plasmodium* (Bell *et al.*, 2006). However, the results obtained from the present commercial pLDH RDTs, similar to other such RDTs, are also widely variable owing to vulnerabilities towards extreme heat and humidity (WHO, 2012c). It has been reported that the pLDH tests perform poorly when parasitemia levels are low (Ashley *et al*., 2009). The pLDH RDT OptiMAL®, manufactured by Bio-RAD (France), has been reported to have a sensitivity as low as >50 parasites/µl (Moody & Chiodini, 2002). Furthermore, there are reports that this RDT is not suitably sensitive when analysing low concentrations of parasite with sensitivities ranging from 76 % to 95 % with parasitaemia levels less than 100 parasites/µl (Coleman et al., 2002; Iqbal *et al*., 2001, Palmer *et al.*, 1998). Simpalipan and co-workers (2018) recently demonstrated that the OptiMAL-IT RDT exhibited lower sensitivity (10.5%) than previously reported at levels of parasitaemia >100 parasites/µl. There have been reports that the pan-specific antibodies have a lowered affinity towards *P. ovale* and *P. malariae* parasites, thus lowering detection sensitivity for the LDH sensor and demonstrating the existence of slight variations in the common epitopic regions of these species (Bigaillon *et al*., 2005). Therefore, a more sensitive, and reliable, technique for pLDH detection is required as an indicator for malaria.

*Pf*HRPII-based RDTs tend to out-perform pLDH-based RDTs at low levels of parasitaemia. The most sensitive RDT that is capable of differentiating between *P. falciparum* and *P. vivax* is FMV ag

(Republic of Korea) with a sensitivities of 150 parasites/µl for *P. falciparum* and 250 parasites/µl for *P. vivax* (Lee *et al*., 2011). Paracheck™-Pf (Orchid Biomedical Systems, India), SD Bioline malaria Ag-Pf (Standard Diagnostics Inc., Republic of Korea) and SD Bioline malaria Ag-Pf/pan (Standard Diagnostics Inc., Republic of Korea) had 100 % sensitivity in blood samples with 501 – 1000 parasites/µl (Djallé *et al*., 2014). Antibodies to *P. ovale*, *P. malariae* and *P. yoelli* have been raised (Bell *et al*., 2006; Hurdayal *et al.*, 2010). These *Plasmodium* RDTs noted herein are the more researched and studied of the many immunosensor-based RDTs available commercially worldwide (Jain *et al*., 2014).

As a technology, RDTs are not without drawbacks. Limitations of RDTs include the stage-specific expression of the antigen; intra-species variation of the antigenic region; and, *in vivo* stability of the antigen (Bell *et al*., 2006). The use of RDTs are further limited by technical problems that include personnel training, quality and assurance of RDT performance, accuracy of results and the packaging of the kits (Mouatcho & Goldring, 2013). The lack of precision during the development and implementation of RDTs leads to misdiagnosis (which impacts negatively on the RDT assessment) and incorrect drug prescription, both of which influence the emergence of drug-resistant strains of malaria (Mouatcho & Goldring, 2013). A key feature of an RDT is the ease of use and clear interpretation of diagnostic results. Should health practitioners not fully understand the instructions and are unable to interpret the results, the quality and accuracy of the RDT is diminished (Harvey *et al*., 2008). Furthermore, the various commercially available RDTs have different protocols and instructions that ensure the correct and effective use of that RDT; and, if health practitioners are not adequately trained on the use of a specific RDT, the effectiveness of the RDT is undermined (Mouatcho & Goldring, 2013).

The vulnerability of commercial malaria immunochromatographic RDTs towards extreme heat and humidity owing to the use or antibody-based platforms (WHO, 2012a) has paved the way for the exploration of aptamers. Aptamers offer an alternative to antibodies as a capture and sensing ligand to detect proteins, small molecules and whole microorganisms and represents a more heat stable and robust alternative biological capture molecule for use in immunosensing.

1.5. Aptamers – A novel sensing technology

Aptamers (from the Latin “aptus”: to fit) are short biopolymers, often as single-stranded

oligonucleotides, which offer high affinity (K_D constants of pM to nM) and specificity to specific target molecules against which they are selected (Tuerk and Gold, 1990). Aptamers can either be composed of RNA or DNA, or modified oligo-based, e.g. glycol nucleic acid (GNA), locked nucleic acid (LNA), peptide nucleic acid (PNA), therose nucleic acid (TNA) and SOMAmers, which are composed of structural elements, such as benzene, not normally observed in single-stranded nucleic acids (Gold *et al.*, 2012; Jolly *et al*., 2016). At the advent of affinity-based short chain oligonucleotides, RNA was the preferred choice as they were viewed as being more structurally diverse (Zhu *et al*., 2015). Today, single-stranded DNA aptamers have gained in popularity as they are inherently more stable and cheaper and quicker to produce (Lakhin *et al*., 2013). However, the choice of RNA versus DNA depends on the overall application of the aptamer.

Aptamers are synthesised and isolated *in vitro* using a technique called SELEX (Systemic Evolution of Ligands by EXponential enrichment) from a library of up to 10^{18} random oligonucleotide sequences (Tuerk and Gold, 1990; Lakhin *et al*., 2013; SELEX will be discussed further in **Chapter 2**). Aptamers are analogous to antibodies and represent an alternative biorecognition agent to the antibodies (Tuerk and Gold, 1990; Ellington and Szostak, 1990). They can be generated against a wide range of targets from small molecules to larger proteins (Pendergrast *et al*., 2005). As biological capture molecules, aptamers offer many advantages over antibodies such as stability and robustness; ease of production; lowered sensitivity to heat and humidity; reversible denaturation; ease of modification; low immunogenicity and toxicity; extended half-life; altered protein/target activity; disrupting and blocking docking sites on enzymes and other such functional proteins; and, disrupting protein-protein interactions (for protein targets) (Jayasena, 1999; Han *et al*., 2010; Pendergrast *et al*., 2005).

1.5.1. Structure-function relationship for aptamer-target binding

Each aptamer is unique in structure owing to their varied length and residue sequence: aptamers have a variable region of 30 to 50 bases in length flanked by constant sequence fragments, or primer regions, to facilitate manipulation or modification of the oligonucleotide (Lakhin *et al*., 2013). The unique sequence offers the aptamer a specific three-dimensional structure that results from their unique ribonucleic (RNA) or deoxyribonucleic (DNA) residue sequence through Watson-Crick base-pairing and/or non-canonical intramolecular interactions (Tuerk and Gold, 1990; Macaya *et al*., 1993). Stable conformations such as G-quadruplexes, hairpins and loops, like those seen in RNA structures, facilitate the binding of the oligonucleotide to the target upon heat destabilisation of the oligonucleotide prior to target binding and capture (Han *et al*., 2010). Alternatively, conformational

changes can occur upon oligonucleotide binding to the target at which point the oligonucleotide adapts a more stable and structured tertiary structure suited for binding to that specific target (Han *et al*., 2010).

Aptamers are able to elicit these oligonucleotide-target interactions via a combination of van der Waals forces, hydrogen bonding and electrostatic interactions (Pendergrast *et al*., 2005). Structure-specific oligonucleotide-target interactions occur between the oligonucleotide backbone sugars/phosphates and the protein chain (Nery *et al*., 2009). Furthermore, a given aptamer is able to take on different conformations in solution (Xu & Ellington, 1996), facilitating complementarity through shaping to the most ideal tertiary structure (Harmann & Patel, 2000), and offering the aptamer a degree of flexibility for target binding. The method of target binding to their oligonucleotide can be categorised into two groups, namely the target can be an embedded group or an outside-binding group (Han *et al*., 2010).

Embedded targets are nestled within a binding pocket formed by the unique conformation elicited by the oligonucleotide sequence. This is generally found to occur with the smaller targets, such as short-chained peptides and small molecules (Nery *et al*., 2009).

The larger targets, including proteins and microorganisms, are generally found to be outside-binders as their large structures typically have surface motifs ideal for aptamer docking (Han *et al*., 2010). As a result, these larger targets may have more than one optimally binding aptamer; and, conversely, one aptamer may bind numerous protein targets in that the aptamer is able to cross-react with not only their intended target but a target similar in structure (Lakhin *et al*., 2013). This can include isoforms of the same protein, as in the case of RNA aptamers that were selected against DNA polymerase β but were also able to bind to DNA polymerases κ (Gening *et al*., 2006). The inherent flexibility of the aptamer may facilitate integration of the aptamer into the binding site on the larger macromolecule, allowing the aptamer to reach amino acid sequences and peptide structures that can not ordinarily be reached by other ligands, such as antibodies, substrates and co-factors (Nery *et al*., 2009). Such characteristics afford aptamers the ability to distinguish between isomeric forms of targets (small molecules), closely related targets (proteins) and altered conformations of the target (protein enzymes) (Seiwert *et al*., 2000).

1.5.2. Applications of aptamers

1.5.2.a. Aptamers in therapeutics

Aptamers can fulfil specific functional roles through their binding interactions with protein targets: either competitively and non-competitively inhibit or induce a reaction in the bound target molecule when binding occurs (Lupold *et al*., 2002). Aptamers themselves exhibit antagonistic (i.e. inhibitory) behaviour in protein-protein interactions by altering and/or blocking docking sites present on enzymes and other such functional proteins (Jayasena, 1999; Han *et al*., 2010). Use of antagonistic aptamers to limit, alter or inhibit the natural functioning of a biologically important functional protein in a pathogen forms the premise of aptamers in therapeutics (Keefe *et al.*, 2010). An example of an antagonistic aptamer used in therapeutics is that of the vascular endothelial growth factor (VEGF165) RNA aptamer that prevents angiogenesis in the treatment of age-related macular degeneration (Ruckman *et al*., 1998; Lee *et al*., 2005). On the other hand, aptamers as agonists can activate or enhance a target's activity, thus soliciting a functional response, e.g. 4-IBB RNA aptamers that induce and co-stimulate T-cell receptors (Sullenger *et al*., 2008); and, the vascular endothelial growth factor receptor-2 aptamer on human endothelial cells (Ramaswamy *et al*., 2015).

Altered protein interactions (especially, enzyme activity) by a proteinaceous target upon aptamer binding that result in an effective therapeutic outcome has led to the application of aptamers in the field of therapeutics (Pendergrast *et al*., 2005).

The versatility of aptamers can be utilised through conjugation with therapeutically active agents in the field of therapeutics. Through conjugation with an active agent, aptamers in therapeutics have been used to deliver chemotherapeutic agents, gold/silver nanorods, dendrimers, siRNA, and photoagents directly to the cell (Davydova *et al*., 2011). These therapeutic aptamers modified with these biologically active molecules have been shown to transport and deliver therapeutic agents directly to the site of action be it on the cell surface for cell targeting aptamers or within the cell for smaller biomolecule targeting aptamers (Chen *et al*., 2008a).

1.5.2.b. Aptamer detection agents in diagnostics

The ease of production and ease of modification of the oligonucleotide sequences comprising aptamers has allowed the application of aptamers in the field of diagnostics. Aptamers are

"artificial" biological molecules that are synthesised and can, thus, be functionalized. This facilitates incorporation into biosensor designs as they extend their inherent effects of high stability and sensitivity to the diagnostic device (Prasad *et al*., 2016). Aptamer-based biosensors require a small volume of sample (<5 µl) without a loss in sensitivity (Ocaña *et al*., 2012). Aptamers have also shown specificity to their selected targets when used to detect their high-affinity target in complex media and biological fluids, such as blood and urine, eliminating non-specific binding (Zhou *et al*., 2014).

Aptamers that target intracellular proteins do pose a challenge in the field of molecular detection and diagnostics in biosensor development as access of aptamer is limited by the cellular components, specifically cellular membranes. Fortunately, the ease of aptamer modification in their chemical synthesis facilitates conjugation of intracellular enzyme substrates and/or cofactors required by the host cell machinery, facilitating the active uptake of the aptamer into the cell (Homann & Göringer, 2001). Furthermore, smaller aptamers less than 10 kDa have the capability of accessing targets on cell surfaces and within cells that were previously inaccessible to the larger antibodies (Lorger *et al*., 2003).

The versatility of aptamers can be utilised in the various strategies used in aptamer-based diagnostic devices. In target detection for the purposes of diagnostics, aptamers have been conjugated to radionuclides, gold nano particles, quantum dots, carbon nanotubes and fluorophores for specific detection of cellular and biomolecular targets (Davydova *et al*., 2011). Aptamers have also been conjugated to cofactors and enzymes for reaction-based detection of targets. Similarly to conventional antibody-based detection, activation of these conjugated molecules results in a measurable response that can be recorded signifying aptamer binding and hence presence of the target. This reporter-based method of target binding and detection is particularly useful in clinical and laboratory settings when a visual response is ideally required. An example of the use of such reporter assays include colorimetric assays, such as the enzyme-linked oligonucleotide assay (ELONA) (discussed further in **Chapter 1.7.2.a** and **Chapter 2**), involving aptamers conjugated to horseradish peroxidise that is then used in a measurable colour generation (Drolet *et al*., 1998). Coupling the aptamer to a fluorophore reporter molecule is particularly useful for target detection using fluorescent and epifluorescent microscopy (Ulrich *et al*., 2004). Through visualisation of the fluorescing reporter molecule, localisation of the target within the cell can be ascertained. This is advantageous as not only is the presence of the target shown, but also where in the cell the targets accumulate.

In sensor design, four basic strategies have previously been employed in the fabrication of aptamer-based diagnostic devices: target-induced structure switching, target-induced displacement, sandwich-type binding, and competitive modes (Han *et al*., 2010).

By utilising the mode of aptamer binding to the target, various unique and novel methods of eliciting a response indicating positive target recognition have been employed. One such method is that of a "molecular switch"; which utilises proximity of a covalently-linked electrochemical beacon (ferrocene) on a self-assembled aptamer to the gold electrode surface (Radi *et al.*, 2006). The ferrocene on the free end of a target-free aptamer lies at a distance from the transducer surface; however, upon target binding, the conformational changes undergone by the aptamer move the ferrocene beacon a distance away from the transducer surface signalling a positive binding event. Aptamer switches can be further classed into split and fused aptamers. Split aptamer switches employ two fragments of an aptamer that self-assemble upon target interaction, changing the fluorescent signal (Yamamoto *et al*., 2000). Fused aptamer switches use two different aptamers that have been conjugated to one another where one aptamer binds to the target and the other is used for signal transduction (Stojanovic and Kolpashchikov*,* 2004). Here, the aptamer used for signal transduction is activated upon conformation changes incurred when the targeting aptamer binds to its target. Target-induced dissociation/association aptamer switch utilised the immobilised complementary sequence of the aptamer, and works in an "on" mode and "off" mode (Han *et al*., 2010). In "off" mode, the target-aptamer complex dissociates from the tethered complementary strand, and a positive interaction is seen on the transducer as a decrease in signal. The signal "on" mode uses the same principle as the "off" mode with the exception that once the target-aptamer complex dissociates from the aptamer's immobilised complementary strand, another labelled aptamer binds to the immobilised complementary strand, thus creating or enhancing a signal response on the transducer.

Sandwich-type binding can be utilised when specific targets have more than one binding site, particularly on opposite sides of the target. For example, two different aptamers recognising their respective fibrinogen and heparin binding sites on thrombin can be used in a sandwich assay that selectively detects thrombin when one aptamer is immobilised and the other modified with a reported molecule specific for the assay (Ikebukuro *et al*., 2005). The ELISA-type method of aptamer binding can be utilised, for example, during ELISA or similar sandwich-type binding assay in which an enzyme, fluorescent probe (Xu *et al*., 2012), gold nanoparticle (Wang *et al*., 2009), quantum dot

(Bagalkot *et al.,* 2007) or electrochemical probe (Kang *et al.*, 2008) is covalently-linked to the second aptamer facilitating measurement of binding between the target and aptamer. When covalently linked to a fluorophore, e.g. fluorescein isothiocyanate (FITC), aptamers can facilitate the specific detection of their target cell or molecule within the cell through flow cytometry and microscopy (Blank *et al*., 2001).

Wandtke and co-workers (2015) and González and co-workers (2016) described the available aptamer-based technologies used to detect viruses and viral infections, such as human immunodeficiency virus, hepatitis B and C viruses, severe acute respiratory syndrome (SARS), H5N1 avian influenza and Ebola virus.

1.5.2.c. Aptamers with affinity to multiple targets: Cross-reactivity

Similarly to antibodies, there exist aptamers selected against one specific target that have exhibited binding to multiple targets, in addition to the one target for which they were selected. Such aptamers do not necessarily result from particular evolutionary pressures placed on enrichment in the SELEX process, but may simply arise from the ability of the aptamer to bind to the target and other structurally similar molecules. These pan- or multi-aptamers bind both their target and others similar in structure with high affinity. Nguyen and co-workers (2014) developed multi-target aptamers that exhibited an inherent flexibility which aided in the aptamer's recognition of three different pesticides. However, the mechanism by which this occurred was not elucidated. Similarly, Gening and co-workers (2006) showed that aptamers can bind to similar targets that are from another family. They generated four aptamers against DNA polymerase β that were able to bind and inhibit DNA polymerase κ, a polymerase of another family. On the other hand, Xu and Ellington (1996) showed that RNA aptamers selected against a peptide epitope of human immunodeficiency virus type I Rev have the ability to bind to the Rev protein by inducing a conformational change in the epitopic region on the protein. They note that these particular aptamers have the potential to disrupt protein structure, and concomitant enzyme activity, leading to therapeutic benefits of such aptamer-target interactions.

Cross-reactivity can thus be explored and applied to targeted specificity of an aptamer: much like antibodies raised against a peptide fragment (this same residue sequence occurs as an epitope on a whole protein) that are capable of binding to that peptide epitope on a whole native protein,

aptamers selected against a peptide fragment can be similarly used to selectively bind to the whole protein through interaction with the epitope (Xu & Ellington, 1996).

1.6. Considerations for diagnostic devices

In the design of an aptamer-based biosensor – aptasensors – through a process known as SELEX (Systemic Evolution of Ligands by EXponential enrichment), the major factors that should be considered include (Prasad *et al*., 2016):

1. The aptasensor needs to be resistant to stress and function at an appropriate pH and under various conditions (e.g. temperature) that appropriately mimic the target-containing matrix. For example, an aptamer expected to bind to an *in vivo* target in serum should function under physiological conditions.
2. The secondary and tertiary structures of the aptamer should be known to ensure that the best design strategy that facilitates optimal target recognition is employed in the development of the aptasensor. For example, an aptamer that forms a relatively large tertiary structure at the site of electrode attachment will require a greater surface area in which to fold.
3. Aptamer immobilisation and fabrication of the aptasensor should be quick and easy to, at the research and development level, enhance throughput of analyses and improving the efficiency of data generation; and, that the commercial level, facilitate production for distribution and sale.
4. The aptasensors should have a high specificity and sensitivity to detect low concentrations, even trace concentrations, of the analyte in complex matrices.

Design of the aptasensors should be such that the aptamer retains its biological activity and ability to detect the target molecules; therefore, diffusion of analyte/target to the ligand/aptamer and transport of unbound analyte/target away from the ligand/aptamer is important (Schultz, 1996). In the case of an indirect diagnostic devise employing an enzymatic reaction, substrate to the enzyme and product away from transducer surface should not be limiting as accumulation of the product as the transducer surface may cause interference (Schultz, 1996). Consequently, the strength, and rate of binding and the enzymatic reaction is of importance in any kinetic analysis (Schultz, 1996).

In aptamer-based diagnostic devices and sensors, as aptamers undergo conformational changes when exposed to the target, the immobilised aptamer needs to be adequately spaced and

orientated on the sensing platform of the diagnostic device to limit steric hindrance (Schultz, 1996). To promote binding between the target and aptamer, the target also needs to be orientated such that the binding site on the target is exposed to the aptamer (Schultz, 1996). Unfortunately, not much can be done with respect to orientation in the case of a free analyte/target. Pertaining to biosensors in particular that utilise transducers, the conformational change effected upon aptamer-target binding may alter the local environment affecting transducer response (Lubin & Plaxco, 2010) To achieve a suitable response in the design of the aptamer-based diagnostic device, the biomolecular design and strategy used in the diagnostic or sensing device is therefore of importance in facilitating interaction between target and aptamer through correct conformation. Furthermore, nucleic acids have been coupled to various nanomaterials that have lead to an improved design of biosensors (Chiu *et al*., 2009).

1.7. Methods and techniques used to develop aptamers and measure binding interactions between aptamers and target analyte

1.7.1. Systemic Evolution of Ligands by EXponential enrichment (SELEX) and aptamer development

Aptamers are synthesised and isolated *in vitro* using a technique called SELEX (Systemic Evolution of Ligands by EXponential enrichment) from a library of up to 10^{18} random oligonucleotide sequences flanked by a constant primer region on both 5' and 3' ends (Tuerk & Gold, 1990). As shown in **Figure 1.5**, SELEX requires repetitive cycles of oligonucleotide selection, amplification and complementary strand digestion.

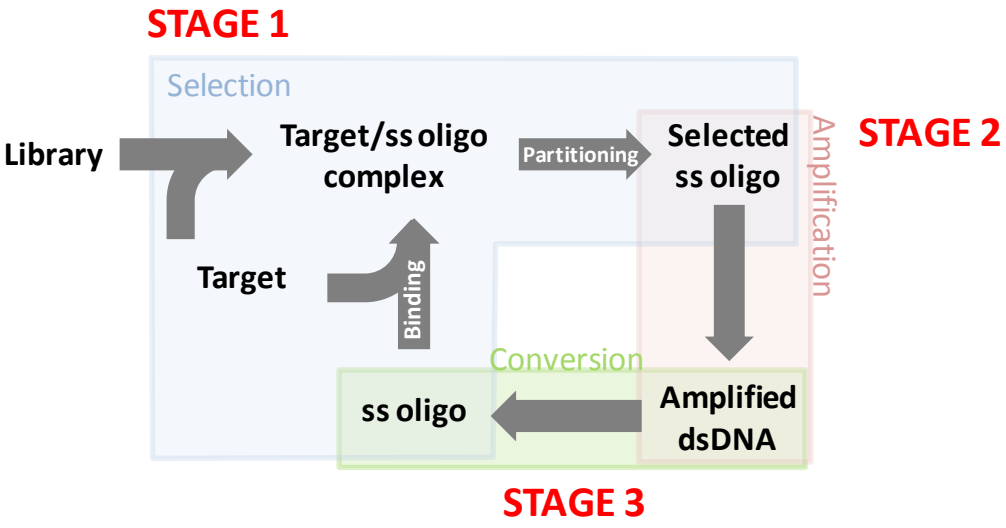

Figure 1.5: Schematic of a generalised single round of the SELEX procedure.

An initial binding event involves interaction between the target and the single-stranded oligonucleotide/DNA library forming a target/oligonucleotide complex (shown by the term "Binding" in the "Selection" phase of SELEX illustrated in **Figure 1.5**). For the research conducted herein, a single-stranded DNA (ssDNA) library was used at the selection step; however, selection can be performed with RNA as was initially conducted by Tuerk and Gold (1990).

Following Selection (**Figure 1.5**), unbound oligonucleotides are removed from the target/oligonucleotide mix through partitioning such as with nitrocellulose membranes (Smolarsky & Tal, 1970; Wong & Lohman, 1993), magnetic beads (Stoltenburg *et al.*, 2005) and capillary electrophoresis (Mendonsa & Bowser, 2004). The oligonucleotides are separated from their bound targets using heat denaturation and/or change in salts and salt concentration, releasing the unbound ssDNA from the target (the "Partitioning" step in **Figure 1.5**).

Regeneration of the retained pool to act as a library in subsequent cycles of SELEX then occurs. In the case of DNA-based aptamer generation, the retained, selected single-stranded oligonucleotides are amplified via polymerase chain reaction (PCR) resulting in amplification of the complementary strand rendering double-stranded DNA (dsDNA). This is the "Amplification" step in Stage 2 shown in **Figure 1.5**. The DNA is amplified until sufficient dsDNA has been produced for digestion.

Complementary DNA strand digestion of the amplified pool, regenerating ssDNA sequences, is

achieved through addition of lambda exonuclease (indicated by the term “Exonuclease” in the “Conversion” phase of SELEX illustrated in **Figure 1.5**) to the dsDNA suspension (Avci-Adali *et al*., 2010). Due to its preferential digestion of dsDNA over ssDNA and non-phosphorylated counterparts, lambda exonuclease is preferred in SELEX. However, it is in the Conversion step at Stage 3 that RNA aptamers can be generated through reverse transcription (Ellington & Szostak, 1990).

These single-stranded oligonucleotides will then be used in selection of target binders for the following round of SELEX thus repeating the aforementioned cycle and enriching the pool of binding oligonucleotides. This cycle, shown in **Figure 1.5**, may be repeated five to twenty times until sufficient saturation of binding oligonucleotides has been reached.

Following SELEX, the selected oligonucleotides undergo a screening process in which they are separated or individualised according to sequence and wherein binding interactions with the intended target are measured. Individual sequences are screened for their ability to bind to the target and the conditions under which binding occurs. Binding between the amplified oligonucleotide inserts and their target is measured using an enzyme-linked oligonucleotide assay (ELONA). Oligonucleotide candidates that successfully bind to the target/s are then sequenced. An ideal SELEX procedure would result in a large percentage of inserts with the same (or at least sequentially similar) insert sequence. Finally, structural analysis of the three-dimensional structure given by the sequence is conducted.

1.7.2. Screening of aptamers: methods of assessing aptamer-target affinity

There exist many methods and technologies by which to quantitatively and qualitatively measure the affinity interactions between the aptamer and the target. Such methods and technologies include, to mention a few: colorimetric, spectrophotometric and fluorescent binding assays using chemical reactions, reporter molecules and nanoparticles; microscopy using reporter molecules; flow cytometry using fluorescent reporters; magnetic resonance imaging using superparamagnetic iron oxide nanoparticles and/or gadolinium; electrochemistry and electrochemical impedance spectroscopy; colorimetric lateral flow technology; and, surface plasmon resonance (Zhou *et al*., 2014). Some of these methods pertinent for the research presented in this work are discussed below, and include enzyme linked oligonucleotide assays (ELONA), surface plasmon resonance (SPR),

electrophoretic mobility shift assays (EMSA), *in situ* and *ex situ* fluorimetry, and electrochemical impedance spectroscopy (EIS).

1.7.2.a. Enzyme Linked OligoNucleotide Assay (ELONA)

Aptamer binding to the target proteins or molecules is commonly determined using an ELONA (Enzyme Linked OligoNucleotide Assay), a technique adapted from the sandwich-type ELISA (Enzyme-Linked ImmunoSorbent Assay) configuration. **Figure 1.6** shows a schematic of the sandwich-type molecular building scheme used in ELONA for the measurement of aptamer affinity for the target. Here, this ELONA has been drawn to show the detection of LDH. It can be noted that ELONA is not limited to the reagents depicted in **Figure 1.6** and reagents can be suitably substituted.

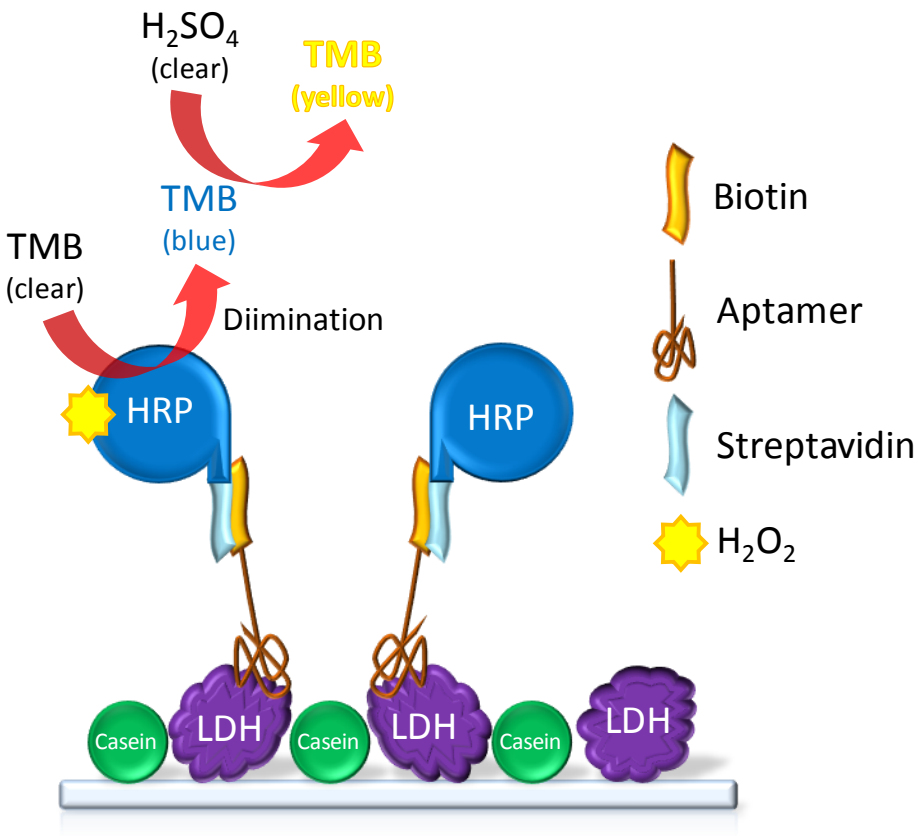

Figure 1.6: Schematic of ELONA sandwich-type assay.
Note: LDH = lactate dehydrogenase, HRP = horseradish peroxidise, TMB = 3,3',5,5'-tetramethylbenzidine, H_2SO_4 = sulphuric acid, H_2O_2 = hydrogen peroxide

ELONA is based on the increased affinity of the biotinylated oligonucleotide to the immobilised target peptide in which the oligonucleotide is the capture and/or detector molecule (Drolet *et al.*,

1998). **Figure 1.6** represents this set up using LDH as a target example as it pertains to the work presented herein. ELONA is both quantitative and qualitative as the amount of bound high-affinity oligonucleotide is indicative of the quantity of the target bound. Similar to ELISA, ELONA utilises a detector entity that attaches to the capture molecule (Drolet *et al*., 1998). In this case, the detector enzyme is horse radish peroxidise conjugated to streptavidin (SA-HRP) which in turn non-covalently binds to the biotin of the biotin-linked oligonucleotide. SA-HRP allows for the colorimetric determination of the presence of the target peptide by oxidising the chromogenic substrate, 3,3',5,5'-tetramethylbenzidine (TMB), in presence of hydrogen peroxide producing a blue colour (Josephy *et al*, 1982). The enzymatic reaction is stopped with the addition of sulphuric acid which then produces a yellow colour.

1.7.2.b. Surface Plasmon Resonance (SPR)

Surface Plasmon Resonance (SPR) is a technology used to qualitatively and quantitatively measure the binding interactions between an immobilised ligand and a free analyte in real-time, without the use of labels. Upon binding of analyte to the immobilised ligand (or molecules to the functionalised chip surface), the resulting mass of these bound molecules change the oscillation wave conditions on the chip surface. The altered surface conditions refract and change the resonance angle of the incident light reflected off the chip's metal base, which acts as the sensor signal. The change in the resonance angle is linearly proportional to the number of bound molecules on the sensor surface of the chip (Stenberg *et al*., 1991). SPR effectively measures the arbitrary response (measured in Response Units, RU) of homogenous or heterogenous biological interactions involving proteins or peptides, lipids, oligonucleotides, small molecules or drugs, monolayer and polymer surfaces, as well as hybridisation interactions (Green *et al*., 2000). SPR provides relevant information on the rate of adsorption; association and dissociation kinetics; equilibrium dissociation constants (K_D); and, theoretical binding capacities (R_{max}) of the ligand-analyte interaction (Nahshol *et al.*, 2008).

SPR has been used as a diagnostic device with many advances recently being made in the technology (Singh, 2016). However, SPR-based diagnostic sensing devices, although sensitive with picogram limits of detection and offer high throughput screening, are cumbersome in that they are large instruments and do require expertly trained personnel and are costly in their maintenance and operation; and, therefore, do not fulfil the basic requirements of a biosensor and RDT (Nguyen *et al*., 2015; Firdous *et al*., 2018).

1.7.2.c. Electrophoretic Mobility Shift Assay (EMSA)

The electrophoretic mobility shift assay (EMSA) can be performed as a qualitative measure of binary binding interaction and strength between the aptamer and the protein (Fried & Crothers, 1981). This technique is based on the principle that movement of the aptamer and protein complex through the polyacrylamide or agarose gel is less than that of the free aptamer and free protein due to the increased molecular weight of the complex (Gaillard & Strauss, 2000). **Figure 1.7** schematically demonstrates the EMSA principle and the anticipated outcome.

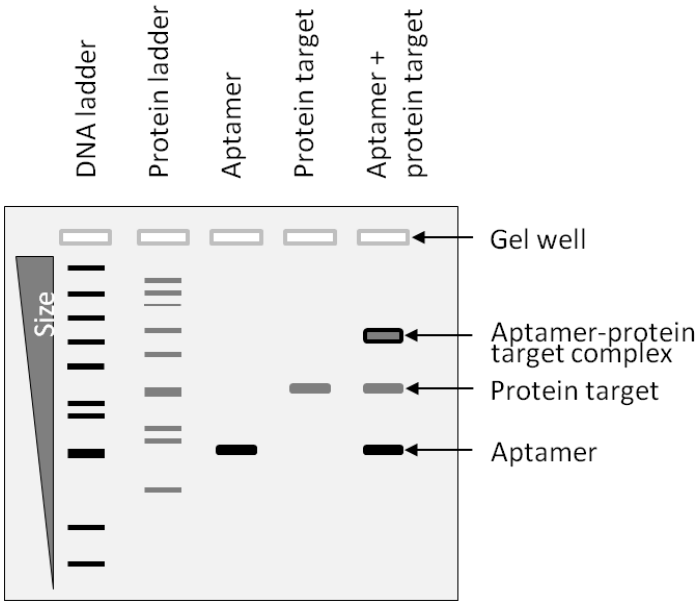

Figure 1.7: A schematic of aptamer, target protein and aptamer-target protein complex migration on polyacrylamide or agarose gel electrophoresis during EMSA.

EMSA is used as a confirmatory and qualitative technique, rather than quantitative, simply proving binding of the aptamer to the target protein (McKeague & Derosa, 2012). This is seen as slower migration of the aptamer-protein complex in gel electrophoresis as shown in **Figure 1.7**. Furthermore, major conformational changes can also be noted when banding resolution is of high quality. There are, however, a number of factors that may interfere with the EMSA, including: stock and reaction buffer differences; aptamer activation and sample preparation, which are crucial for any aptamer/target interaction; and, terminal end modifications on both the aptamer and protein (such as biotinylation of aptamer and His-tags on protein) that may interfere with movement through the gel (Holden & Tacon, 2011). EMSA is limited by the fact that it is ineffective with small molecule targets (Gaillard & Strauss, 2000). EMSA is, also, limiting in that incubation reactions have

to occur prior to electrophoresis to ensure sufficient binding between biomolecules and, thus, binding kinetics can not necessarily be followed. This technique is relatively inexpensive and, once optimised, quick to perform. There are variants of the EMSA based on the type of interaction and biomolecules involved, and when used in conjunction to other techniques (such as western blotting), information on the identity of binding interaction and three-dimensional structure of the biocomplex can be gleamed (Holden & Tacon, 2011). Therefore, is a useful technique to confirm binding interactions of developed or unstudied aptamers, and is particularly useful when requiring this information on a number of samples due to the speed and cost of the technique.

1.7.2.d. Fluorimetry

Fluorimetry quantitatively measures the emission of photons from fluorescent molecules – fluorophores – that have been excited at a lower wavelength. Fluorimetry is used in the analytical and visual fluorescent detection of an analyte of interest in optic sensors and techniques.

Fluorimetry offers a more sensitive detection method than colourimetry and UV-vis spectroscopy in the detection of trace amounts of an analyte, which originates from the intrinsic intensity of excited light/photons over and above a low background (Froehlich, 1989). The incident fluorescence of biological molecules can also be used for their detection; however, this natural fluorescence is less sensitive necessitating the need for additional fluorescent markers and dyes, or fluorophores, for visualisation of these biomolecules. Conventional methods of assaying use covalently linked fluorescent reporter molecules to biomolecules of interest, with their fluorescence as a positive indication of binding (Tyagi & Kramer, 1996; Hamaguchi *et al.*, 2001; Deng *et al*., 2014).

Fluorophores, the fluorescent molecules that are used as markers, are covalently linked to the biological molecule, such as fluorescein isothiocyanate (FITC), when exploring interactions between biomolecules that are known to occur (The & Feltkamp, 1970). For example, through the up-conversion of the nanoparticle from a longer to shorter wavelength in a nanoparticle-conjugated aptamer, (anti-Stokes) fluorescence can be used in target detection in bioassays conducted in complex matrices (Zhou *et al*., 2014).

Fluorescent molecules can also be used in the form of a dye capable of sensitively binding to the biomolecule of interest, such as those fluorescent dyes used to detect RNA and/or DNA, namely

ethidium bromide (Waring, 1965), 4',6-diamidino-2-phenylindole (DAPI; Kapuscinski, 1995), and 5,5'-(6,22-dioxo-11,14,17-trioxa-7,21-diazaheptacosane-1,27-diyl)bis(3,8-diamino-6-phenylphenanthridin-5-ium) iodide, or GelRed (Mao & Leung, 2010). The binding to RNA and/or DNA can occur through either intercalation or minor groove binding, at which time will undergo a conformational change facilitating emission of photons at a given excitation wavelength resulting in observable fluorescence. The sensitive visual response of emitted photons given by the fluorophores under a particular wavelength of light, thus fluorescence, is ideally suited for applications in microscopy, DNA detection and biosensors, in which low concentrations of analyte can be detected.

Fluorimetric spectroscopy

Fluorescent assays are an application of fluorimetry that utilise fluorescent markers and dyes in detection of biological molecules (Labarca & Paigen, 1979). Fluorescent assays are of particular use when analyzing the binding between small biomolecules or epitopic excerpts to larger capture molecules, particularly where the sensitivity of other techniques hinder an observable response. Fluorescent assays are particularly useful tools in that background fluorescence, in addition to that brought on from the intrinsic fluorescence of biological molecules, such as proteins, is non-existent, and interference is minimal as only emitted light at a given wavelength is detected. Assays in which DNA is involved in binding events require dyes that are able to elicit their fluorescent response only when bound to DNA, and so produce a strong signal indicative of positive binding against the negligible background signal. Bolger and co-workers (1997) used Hoechst stain 33258 in an assay to detect the presence of DNA in a recombinant protein solution as part of a DNA quantitation kit. In their case, however, the fluorescent Hoechst stain was used a reporter molecule to simply establish DNA presence/absence as it preferentially binds to adenine (A) and thymine (T) rich regions (Portugal & Waring, 1988). Joseph and co-workers (1996) showed that a decrease in fluorescence of YOYO DNA stain was indicative of thrombin binding and postulated that this was because the nano-environment surrounding the dye changed. Similarly, McKeague and co-workers (2014) utilised the principle of fluorescent quenching using SYBR Green I as an aptamer intercalator dye in their Ochratoxin A biosensor. Also, Wood and Bishop (2004) demonstrated a decrease in ethidium bromide fluorescence was as a result of L-argininimide binding to their aptamers. As an alternative, GelRed is an unstudied example of such a marker and dye as an indicator of binding in a fluorescent assay.

GelRed, used in this work, is a homodimer of ethidium bromide with a polyether and amide bridges

(Mao & Leung, 2010); and, has an excitation and emission wavelength of 295 nm and 600 nm, respectively. GelRed intercalates between nucleotide residues, as well as binds to the phosphate backbone of DNA based on electrostatic interactions with the positively charged GelRed molecules (Crisafuli *et al*., 2014). GelRed has a tendency to bind to guanine-rich (G-rich) moieties (Guo *et al*., 1992); therefore, those aptamer sequences with a higher G content will tend to fluoresce with greater intensity. Furthermore, as GelRed is an intercalator and also binds to dsDNA with greater sensitivity than ssDNA (Biotium FAQs, 2013), it stands to reason that GelRed molecules will intercalate more readily, and with greater sensitivity, in a more organised and stable tertiary structure akin to that of dsDNA. GelRed is also able to bind more readily to oligonucleotides with shorter length rendering it more sensitive than its monomeric counterpart, ethidium bromide. Furthermore, it is non-toxic, non-mutagenic and environmentally safe (Ohta *et al*., 2001; Biotium, 2013). As GelRed is environmentally safe, thus easy to dispose, and stable at room temperature, it is ideal for use in fluorescent assays.

As previously described, fluorescent assays are based on the ability of this fluorescent dye to bind to DNA, emitting a readable fluorescence. However, GelRed assays are based on quenching of fluorescence as GelRed molecules disengage from the DNA molecule as conformational changes in the oligonucleotide aptamer tertiary structure occur upon binding interactions with the target protein, polypeptide or molecule (**Figure 1.8**).

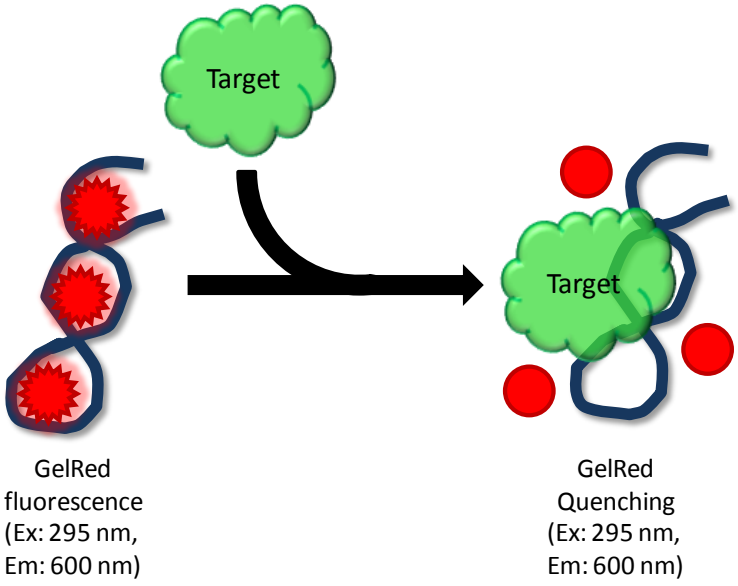

Figure 1.8: Schematic of GelRed assay principle

Detectable fluorescent quenching is, hence, indicative of positive binding between aptamer and target as demonstrated in **Figure 1.8** by the release of GelRed molecules upon target-aptamer binding. Furthermore, as GelRed is more sensitive than other commercial fluorescent markers and dyes that are used in laboratories and capable of binding to low molecular weight or short-chain oligonucleotides (Biotium, 2013), fluorescent assays incorporating GelRed are ideally suited for quantitatively measuring the capture of small targets by oligonucleotide aptamers.

Fluorescent microscopy

Fluorimetry can also be applied in microscopy, as fluorescent microscopy. Fluorescent microscopy uses fluorophores as tags, dyes, and/or stains to visualise biological interactions at the cellular and sub-cellular level (Cremer & Cremer, 1978).

Immunofluorescent microscopy uses fluorophores that are covalently linked to functional biological molecules, such as antibodies and aptamers, to visually confirm inherent specific properties, functions and analyte binding interactions (The & Feltkamp, 1970). The fluorophore-tagged antibodies/aptamers and, indirectly, the analyte (a polypeptide or co-factor) can then be observed to congregate in a particular locale. Under the light of a particular wavelength (the excitation wavelength), the fluorophore will illuminate at a given emission wavelength, revealing cellular regions where the analyte predominates and elicits its particular function. Given the sensitivity of fluorescence and intensity of photon-emitting fluorophore tags, a qualitative representation of analyte concentration can be detected in the cellular body (Froehlich, 1989). Fluorophore tags commonly used in fluorescent microscopy, and have further application in fluorescent or optical sensors, include: fluoroscein and its derivatives (fluoroscein isothiocyanate (FITC) and fluoroscein amidate (FAM)); rhodamine and analogues thereof (such as tetramethylrhodamine (Cy3)); Texas Red; and, the Alexa Fluor® range (Panchuk-Voloshina *et al*., 1999).

Fluorescent Biosensors

Fluorescent-based optical diagnostic devices employ fluorescently-labelled biological recognition molecules capable of eliciting a sensitive response with negligible background signal (Nagl & Wolfbeis, 2008; Lemke & Schultz, 2011; Luppa *et al*., 2016). Many strategies have been employed in the detection of analytes using fluorescent aptamers. Potyrailo and co-workers (1998) directly detected thrombin using a FITC-tagged ssDNA aptamers. The more complex aptamer beacons, also

known as aptamer switches, employ the distance dependant phenomenon known as fluorescent resonance energy transfer (FRET); and incorporate covalently linked fluorophores that emit fluorescence as their respective quenching molecules are moved a distance (10 nm) from one another as the aptamer conforms upon analyte binding (Trevino & Levy, 2014). Nutiu and Li (2003) demonstrated quenching in fluorescence upon analyte binding as the fluorophore and quencher are brought in close proximity to one another upon. Aptamer beacon biosensors have successfully been used in the detection of cocaine (Stojanovic *et al*., 2001; Li *et al*., 2007); thrombin (Mir *et al*., 2008); adenosine triphosphate (Zuo *et al*., 2007); and, theophylline (Ferapontova *et al*., 2008).

1.7.2.e. Electrochemical Impedance Spectroscopy (EIS)

Voltammetry is an inherently sensitive technique based on current measurements at conductive electrode surfaces following oxidation or reduction of a target analyte. Electrical detection of biomolecular interactions by way of a potentiostat is highly desirable due to its suitability to low-cost portable sensors that can be used in the field by non-specialised personnel. The use of label-free techniques has the added advantage of reducing costs and avoiding the need for sample pre-treatment. Recent research shows the use of nanostructured materials to enhance sensitivity through enhanced surface area, electroconducting properties, stability and reproducibility in biological sensors (Jianrong *et al.*, 2004) and indeed for application in voltammetric immunosensors (Cho *et al.*, 2008). Electrochemical impedance spectroscopy (EIS), on the other hand, measures variations in charge transfer resistance and layer capacitance brought about by a biomolecular interaction at the electrode surface. In the presence of charged redox markers in solution, EIS becomes a particularly sensitive technique since the capture of target proteins at the surface will induce measurable variations in the electrostatic barrier to the redox marker (Estrela *et al*, 2008; Keighley *et al*, 2008). Factors that would, hence, affect resistance include the thickness and porosity of the layer; distance of binding event from the electrode surface; and, the presence and concentration of conducting material in the layer, such as carbon nanotubes and nanoparticles. Many strategies have been employed in the development of EIS-based affinity analyses of target and aptamers binding (Xu *et al*., 2009).

1.8. Knowledge Gap

The development of a small, rapid, cost-effective, simple to use, easy to interpret, reliable, accurate, long-lasting and portable self-validating sensing technique for malaria detection, which is able to discriminate between several malarial species, remains an elusive target. However several strides

have been made locally and internationally in recent years in the development of new diagnostic methods. Outside of microscopy based tests, diagnostic methods, largely based on detection of malarial biomarkers via antigen tests have moved from research into commercial production over several years.

While tremendous scope exists for the identification of further biomarkers, currently research has targeted the *Plasmodium falciparum* histidine rich protein II (*Pf*HRP II) as well as on *Plasmodium* lactate dehydrogenase (pLDH) and aldolase. For reasons previously discussed, *Pf*HRP II and aldolase are not suitable for the specificity and species discrimination of *Plasmodium* that is required.

Plasmodial LDH presents a viable biomarker for RDT-based diagnosis, as it is not only produced throughout all stages of the *Plasmodium spp.* life-cycle but is conserved within a species (Florens *et al.*, 2002). This is observed when the *Plasmodium spp.* lactate dehydrogenase amino acid sequences are aligned with that from human (*Homo sapiens*) lactate dehydrogenase using ClustalW (**Figure 1.2**). Bigaillon and co-workers (2005) report that pan-specific antibodies used in some RDTs lower the affinity for *P. ovale* and *P. malariae* thus exhibiting a lowered detection sensitivity compared to the conventional methods of diagnosis. There is, thus, a need for biological recognition elements capable of distinguishing between *Plasmodium spp*. This can be achieved through manipulation of species-specific epitopic regions on certain biomarkers. There exist common epitopic regions on the surface of pLDH that can be used for broad biorecognition of *Plasmodium spp*. (Hurdayal *et al.*, 2010). In addition, unique species-specific epitopic regions also exist at a distance from the common epitopic regions on the surface of pLDH (Hurdayal *et al.*, 2010).

Studies have reported on the synthesis of unique peptide sequences of pLDH serving as viable biomarkers for *in vitro* testing (Tomar *et al.*, 2006) as well as the soluble expression of *Pf*LDH (Berwal *et al.*, 2008). Furthermore, by raising antibodies against these unique and species-specific peptides sequences, the level of specificity required can be obtained (Hurdayal *et al*., 2010). However, for the feasibility of this approach to be increased, significant enhancement in sensitivity for pLDH detection is warranted.

Reports of aptamers raised against an epitopic region of a macromolecular peptide capable of detecting the larger peptide have been reported for the Rev-1 protein (Xu and Ellington, 1996;

Robertson *et al*., 2004), gliadin (Amaya-González *et al*., 2015), Ras-binding domain of Raf-1 (Kimoto *et al*., 2002) and the mitogen-activated protein kinase ERK2 (Bianchini *et al*., 2001). However, there have been no reports in which an aptamer raised against a species-specific epitopic peptide (LDHp here) was used to discriminately bind to the larger peptide (r*Pf*LDH here) at the site of the epitope through LDHp tertiary structure mimicry in the larger protein.

1.9. Aim and objectives

The aim of this research was to develop a novel technology in the form of aptamers that are capable of specifically binding to lactate dehydrogenase of *Plasmodium falciparum*, for use in a sensing device.

The detailed objectives of this research were:

1. To generate single-stranded DNA oligonucleotides, or aptamers, capable of binding to recombinant *Plasmodium falciparum* lactate dehydrogenase and the *Plasmodium falciparum*-specific lactate dehydrogenase peptide in two separate, but parallel, SELEX procedures (**Chapter 2**).
2. To overcome the study-specific challenges and limitations inherent in SELEX, specifically those introduced by the polymerase chain reaction-based amplification used within the SELEX process (**Chapter 2**).
3. To analyse and evaluate SELEX-produced ssDNA sequences capable of binding to recombinant *Plasmodium falciparum* lactate dehydrogenase and the *Plasmodium falciparum*-specific lactate dehydrogenase peptide, covering PCR-amplified artefacts carried through SELEX (**Chapter 3**).
4. To identify and compare sequence families and conserved motifs on ssDNA aptamers within a SELEX pool for a given target (r*Pf*LDH versus LDHp aptamers) and within a given library across targets (r*Pf*LDH and LDHp aptamers versus elsewhere) (**Chapter 3**).
5. Using predicted secondary and tertiary structures, to ascertain structure-motif locales used for recombinant *Plasmodium falciparum* lactate dehydrogenase and the *Plasmodium falciparum*-specific lactate dehydrogenase peptide binding (**Chapter 3**).
6. To determine affinity of generated aptamers to recombinant *Plasmodium falciparum* lactate dehydrogenase and the *Plasmodium falciparum*-specific lactate dehydrogenase peptide using ELONA, FLONA, competitive dissociation assays (GelRed assays), EMSA and SPR, and compare

affinities of generated aptamers with control proteins, specifically human serum albumin, mammalian LDH and recombinant *Plasmodium vivax* LDH (**Chapter 4**).

7. To evaluate the application of chosen aptamers in an aptamer-based biosensor using platforms and technologies in favour of aptasensing, specifically EIS, as well as the *in situ* detection of *Plasmodium falciparum* lactate dehydrogenase through fluorescent and epifluorescent microscopy (**Chapter 5**).

CHAPTER 2

SELEX and identification of oligonucleotide aptamers binding to recombinant *Plasmodium falciparum* LDH and *Plasmodium falciparum*-specific LDH peptide

2.1. Preface

In this chapter, the SELEX (Systemic Evolution of Ligands by EXponential enrichment) process was applied to generate oligonucleotide sequences (aptamers) capable of binding to a species-specific epitope of *Plasmodium falciparum* lactate dehydrogenase (*Pf*LDH). Separately, a further suite of aptamers were generated to bind to the entire *Pf*LDH molecule, using the recombinant *Pf*LDH protein.

2.2. Introduction

2.2.1. Overview of the SELEX procedure

Aptamers are synthesised and isolated by an *in vitro* technique called SELEX (Systemic Evolution of Ligands by EXponential enrichment). This centres on the isolation of candidate sequences from a library of up to 10^{18} distinct molecules – each comprising random oligonucleotide sequences, flanked by constant primer regions at both 5' and 3' ends (Tuerk & Gold, 1990; Lakhin *et al*., 2013). As depicted in **Figure 2.1**, SELEX using single-stranded DNA molecules as aptamer candidates is an iterative cycle that can be categorised into three distinct stages: oligonucleotide selection (Stage 1), PCR amplification (Stage 2) and complementary strand digestion (Stage 3).

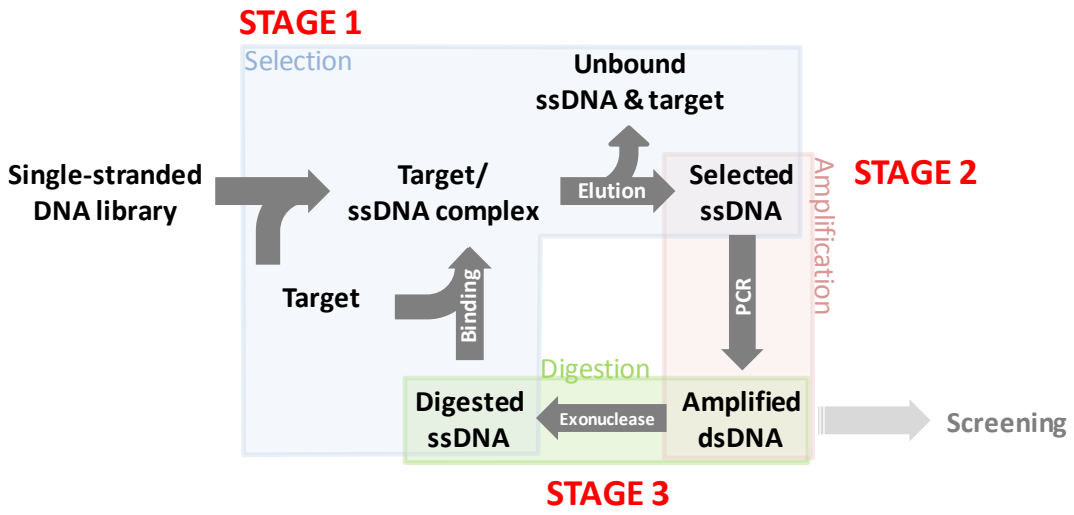

Figure 2.1: Detailed schematic of the various phases of a typical SELEX procedure for single-stranded DNA aptamers, highlighting the three main stages of SELEX occurring within a cycle of SELEX.
Stage 1: Selection; Stage 2: PCR amplification & Stage 3: Exonuclease digestion

2.2.2. Stage 1 of SELEX: Selection

The first stage – Stage 1 – of the SELEX process (**Figure 2.1**), also known as the selection step, starts with an initial binding event involving interaction between the target and the single-stranded DNA (ssDNA) oligonucleotides of the library, forming target/ssDNA complexes. Aptamers are able to elicit these oligonucleotide-target interactions via a combination of van der Waals forces, hydrogen bonding and electrostatic interactions (Pendergrast *et al*., 2005). Structure-specific oligonucleotide-target interactions occur between the oligonucleotide backbone sugars/phosphates and the protein chain (Nery *et al*., 2009). Following this interaction, those oligonucleotides capable of binding to the protein target with high affinity (i.e. those which form part of the target/ssDNA complexes) are selected through partitioning by facilitating the separation of unbound oligonucleotides from the target/ssDNA mixture.

There have been many advances in the methods used to partition unbound from target-bound oligonucleotides, including nitrocellulose membranes (Smolarsky & Tal, 1970; Wong & Lohman, 1993). Gopinath (2007) provides an comprehensive overview of the relevant methods used to partition bound from unbound oligonucleotides. Other than nitrocellulose membrane filtration, partitioning methods include the use of affinity surfaces, affinity tags, column matrices/chromatography, cross-linking, gel electrophoresis, antibody-based partitioning, centrifugation, surface plasmon resonance (SPR), flow cytometry, capillary electrophoresis, and

automated selection. Stoltenburg and co-workers (2005) report the use of magnetic beads for rapid and efficient high-affinity oligonucleotide capture, and have coined the term FluMag-SELEX for this type of SELEX. Microfluidic SELEX partitions binding oligonucleotides from non-binding oligonucleotides in a silica microline-based continuous-flow system in which target immobilisation can be either streptavidin-based (Hybarger *et al*., 2006) or magnetic bead-based (Lou *et al*., 2009). Berezovski and co-workers (2005) developed a non-SELEX-based method of aptamer generation using non-equilibrium capillary electrophoresis of equilibrium mixtures (NECEEM) as a partitioning method.

As the techniques listed above suggest, partitioning, or selection, methods typically employ an initial immobilization of the target onto a solid support, followed by binding of high-affinity oligonucleotides from a pool of free oligonucleotides. Conversely, Nutiu and Li (2003) developed a structure switching, or capture SELEX, in which labeled oligonucleotides from the oligonucleotide pool are tethered to the inert matrix by means of a known complementary region, forming a duplex structure. Upon exposure to the free target, the oligonucleotides preferentially bind to the target, resulting in a conformation change in the oligonucleotide resulting in the release of the oligonucleotide from the matrix. Thus, high-affinity binders are co-eluted with the target. However, methods such as nitrocellulose membrane filtration, chromatography, capillary electrophoresis and magnetic bead-based partitioning are techniques most frequently used in SELEX procedures. Their advantage exists in that they offer a speedy and high throughput method with the use of minimal sample (<100 µl) (Gopinath, 2007) – ideal in terms of the high number of cycles, and thus selections/partitioning events, performed during SELEX.

Following partitioning, separation of ssDNA from the ssDNA/target complexes can be achieved through use of heat denaturation, or by changing the salt composition and/or pH of the solvent the ssDNA/target complexes are in (Gould & Matthews, 1976; Wang *et al*., 2012).

Ideally, an attempt to recover the majority of the ssDNA molecules capable of binding to the target – while simultaneously minimising recovery of non-binding molecules – should be made, to ensure maximum recovery of positively-binding ssDNA while limiting loss of ssDNA ensuring greater product yields in later steps of SELEX.

Factors directly influencing oligonucleotide recovery in the selection phase of SELEX include:

1. Target concentration, as the higher the target molecule concentration, the great the number of binding sites within the pool and the greater the recovery (Wang *et al*., 2012);
2. Non-specific selection of those oligonucleotides with low affinity, which are retained with the target during the partitioning, but may be lost upon enrichment (Wang *et al*., 2012; Spill *et al*., 2016); and,
3. Retention of unbound oligonucleotides trapped on the partitioning matrix, which are non-specific and false-positive binders (Wang *et al.*, 2003).

The proportion of separated binding ssDNA molecules extracted from this phase of SELEX needs to be monitored to ensure increasing enrichment of the pool with sequences capable of binding the target.

The ssDNA enrichment can be calculated as a percentage of the mass of oligonucleotides recovered over the mass of oligonucleotides initially used. Oligonucleotide recovery following the initial cycle of SELEX can be expected to be between 10^{13} of the 10^{15} oligonucleotides within the intitial library, equating to a recovery yield of 0.1 to 4.0 %; however, the number of binding oligonucleotides recovered will increase with the successful enrichment of target-binding oligonucleotides as SELEX progresses (Ellington & Szostak, 1990).

2.2.3. Stage 2 of SELEX: Polymerase chain reaction (PCR)-amplification

The second stage of SELEX – Stage 2 (**Figure 2.1**) – involves the amplification of the target-binding ssDNA sequences isolated in Stage 1, using the polymerase chain reaction (PCR). PCR amplification results in the synthesis of the complementary strand of the ssDNA recovered following selection, producing double-stranded DNA (dsDNA).

During this phase of SELEX, DNA is amplified (by varying the cycles of PCR) until sufficient dsDNA has been produced for further use, a quantity that varies between studies. Compared to conventional PCR, in which a homogenous template is amplified, there exists a number of inherent challenges in the PCR stage of SELEX. Some of these are: lowered product yield, the possibility of introducing mutations, and inaccurate replication of the original template (i.e. amplification fidelity) and the introduction of primer-based oligomers within the pool of DNA undergoing amplification (primer

dimerization). These are limitations that need to be overcome in the generation of target-binding oligonucleotides during the complex SELEX process.

Many of the limitations identified above arise from the inherent challenges of using PCR amplification to amplify a template that is heterogeneous in sequence (Kalle *et al*., 2013). Given that the library template contains up to 10^{18} unique sequences and random sequences (Lakhin *et al*., 2013; Tolle *et al.*, 2014). Therefore, the difficulties and limitations across different SELEX processes can differ quite substantially from each other, as each template library sample differs from the next (Dieffenbach & Dveksler, 2003). Furthermore, the PCR amplification for a given template pool, as in the case of the DNA template library, for any given target can differ substantially from each other because amplification of a heterogeneous mixture of DNA template can introduce a number of very different errors and artefacts (Kalle *et al*., 2013). In short, what may work in one experimental set-up, may not work in another, as each reaction cycle and setting is unique (Kalle *et al*., 2013).

In addition, the host of materials sourced from the various suppliers elicit various degrees of response with varying degrees of success. For example, primers, and indeed library template sequences, that contain GC-rich (guanosine and cytosine rich) regions may result in shortened by-products as the looped structures formed at the GC-rich regions can cause the polymerase to jump (Musheev & Krylov, 2006). Therefore, the PCR amplification in each SELEX needs to be troubleshot and optimised to ensure optimal oligonucleotide production.

To overcome these challenges faced in the amplification of target-binding oligonucleotides during SELEX, there are various considerations that may be explored on a case-by-case basis, in order to improve the product outcome and yield of PCR amplification, such as:

1. Employing suggestions given by the trouble-shooting guide supplied by the manufacturer's of PCR reagents, specifically:
    a. Optimising the annealing time and temperature during PCR;
    b. Increasing the denaturation time;
    c. Adjusting the volume/comcentration of template DNA;
    d. Optimising the primer concentration;
    e. Adjusting the volume/concentration of *Taq* polymerase added to the reaction mix; and,

   f. Increasing the purity of template DNA by adding an additional wash step in the preceding DNA purification and concentration step (https://worldwide.promega.com/.../gotaq-flexi-dna-polymerase-m829.pdf?la=en),
2. Lengthening the oligonucleotide template to limit the production of erroneous by-products (Drabovich & Krylov, 2004),
3. The use of emulsion PCR to increase the fidelity of the polymerase activity towards the amplification of DNA (Williams *et al*., 2006; Shao *et al.*, 2011) and prevent loss of rare high-affinity aptamers that are difficult to amplify (Levay *et al*., 2015),
4. Inclusion of additives in the PCR amplification, such as formamide, glycerol, Tween-20, Nonidet P-40, DMSO and betaine to limit non-specific annealing of ssDNA (Varadaraj & Skinner, 1994; Kang *et al*., 2005),
5. Use of single-stranded DNA binding proteins to prevent non-specific binding of DNA polymerase to ssDNA (Rapley, 1994),
6. Use of asymmetric PCR which promotes amplification of the template strand over the complementary strand, resulting in an unequal molar ratio of ssDNA and dsDNA post PCR amplification (Wu & Curran, 1999), and
7. Use of gel-based capillary electrophoresis PCR to separate the fragments of longer length from the desired amplification product (Skeidsvoll & Ueland, 1995; Zhang *et al*., 2001).

Similar to conventional PCR, of particular concern is the generation of superfluous amplification artefacts/by-products, specifically primer dimers and concatemers and extended oligonucleotide fragments, leading to hybridised dsDNA, as shown in **Figure 2.2** (Musheev & Krylov, 2006; Tolle *et al.*, 2014). Primer dimers and concatemers form through self-annealing of the primer fragments; due to their rapid assembly, they are rapidly amplified during subsequent PCR amplifications (Drabovich & Krylov, 2004; Musheev & Krylov, 2006; Tolle *et al.*, 2014; **Figure 2.2.a**). However, the extended lengths of PCR by-product are formed as a result of the amplification of short single-stranded primers that have annealed to the random region in the template oligonucleotide (**Figure 2.2.b**), and will herein be referred to as “over-amplified PCR product” or as “over-amplification” of the target-binding oligonucleotides.

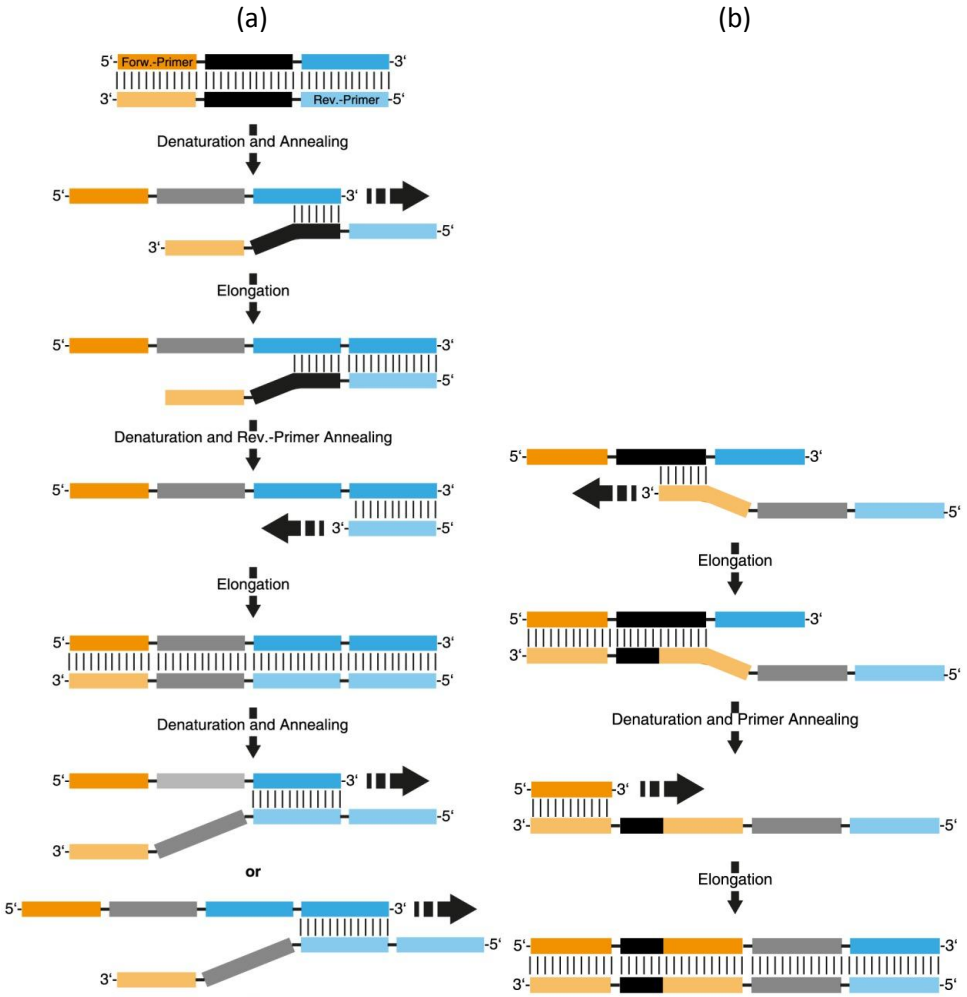

Figure 2.2: The proposed mechanism of (a) primer concatemer by-product formation ("ladder type") and (b) extended length by-product formation ("non-ladder type") by PCR amplification.
(Tolle *et al.*, 2014; reproduced under the Open Access CC-BY License)

Unlike conventional PCR with known template, when amplifying a random oligonucleotide library, the oligonucleotide template is finite whilst a fraction of unincorporated PCR primer remain in excess (Musheev & Krylov, 2006). This excess of PCR primer, which is not incorporated into PCR amplified oligonucleotide, may hybridise to one another in the absence of target DNA to which they would ordinarily anneal (Musheev & Krylov, 2006). As the template library can undergo up to 20 rounds of SELEX, with each round containing between two and six PCR PCR amplification reactions, production of PCR amplification by-products can be aggravated by the numerous PCR rounds that the library undergoes. As the amplification artefacts become the predominant molecules within the reaction, the desired PCR products – the target-binding oligonucleotides – diminish in proportion following numerous rounds of PCR to eventually disappear after an additional *n* cycles of PCR (Musheev & Krylov, 2006). Therefore, the yield of amplified target-binding oligonucleotide decreases

as the lengths of amplified by-product increase. Thus, the production of these by-products progressively inhibits the enrichment of the target-binding oligonucleotide pool (Tolle *et al.*, 2014).

Identification of these amplification artefacts is by the characteristic presence of a distinct laddered band profile of the amplicon when the various fragments are separated by agarose or polyacrylamide gel electrophoresis (Drabovich & Krylov, 2004; Musheev & Krylov, 2006; Tolle *et al.*, 2014). Until recently, agarose offered the advantage of ease of excision and removal of resolved target-binding dsDNA from the gel, removing the undesired primer dimers, concatemers, and over-amplified by-products. However, recently, strides have been made in the development of new buffers and cleaning reagents that make the extraction of DNA possible from polyacrylamide gels, which was not previously possible (http://www.mn-net.com/Portals/8/attachments/Redakteure_Bio/Protocols/DNA%20clean-up/UM_PCRcleanup_Gelex_NSGelPCR.pdf). Polyacrylamide gel electrophoresis (PAGE) is, herein, preferred in that it offers high resolution of resolved DNA with quick results – high band resolution is achieved in less than 20 minutes.

2.2.4. Stage 3 of SELEX: Exonuclease-based digestion

Finally, in Stage 3 of SELEX (**Figure 2.1**), complementary DNA strand digestion regenerating ssDNA from the pool amplified in Stage 2 is achieved through the use of lambda exonuclease to the dsDNA suspension (Avci-Adali *et al*., 2010). Lambda exonuclease favourably degrades 5'-phosphorylated dsDNA in a 5' to 3' direction over ssDNA and non-phosphorylated counterparts (Little, 1967). Therefore, 5'-phosphorylation of the reverse primer must be ensured should dsDNA lambda exonuclease digestion be the preferred route during SELEX (**Figure 2.1**).

2.2.5. Repeating cycles in SELEX: Stages 1 to 3

The ssDNA generated from the exonuclease digestion (Stage 3 of SELEX) is then used in selection of target binders in the following round of SELEX thus repeating the aforementioned cycle and enriching the pool of binding oligonucleotides. This cycle, shown in **Figure 2.1**, may be repeated five to twenty times or until sufficient saturation of binding oligonucleotides has been reached (Tuerk & Gold, 1990; Wang *et al*., 2012).

The degree to which the ssDNA pool has been enriched with high affinity oligonucleotides needs to be monitored with each round of SELEX ensuring increasing enrichment and preventing loss of

binding oligonucleotides. The number of binding oligonucleotides can, hence, be calculated as a percentage of the mass of oligonucleotides recovered over the mass of oligonucleotides initially used. Selection in the initial cycle of SELEX will have approximately 10^{13} of the 10^{15} oligonucleotides recovered equating to a recovery yield of 1.0 to 4.0 % (Ellington & Szostak, 1990). However, as these binding oligonucleotides are enriched during the amplification phase and non-binders removed during the selection phase, the number of binding oligonucleotides recovered will increase. Sufficient cycles of SELEX are performed until a yield of 55 to 85 % has been achieved where a higher recovery and yield is preferred (Ellington & Szostak, 1990).

2.2.6. Isolation of DNA and binding analyses following SELEX

Following SELEX, the selected oligonucleotides undergo a screening process in which they are separated or individualised according to sequence, and binding interactions with their target are measured (Berezhnoy *et al*., 2012; Rotherham *et al*., 2012).

Screening entails sequencing of the ssDNA within the final SELEX pool: this is initiated by regaining their double-stranded structure through PCR amplification following the final round of selection. A small portion of this dsDNA is ligated into a suitable vector in order to separate the pool of oligonucleotides into individual sequences. The ligated vector is then used to transform competent cells which are then cultured as isolated colonies as a means of exponentially copying the sequence ensuring sufficient template DNA. Growth of bacterial colonies, concomitantly, simplifies selection of particular inserts by amplifying the inserted orphaned sequence using the host cell machinery, simultanously permitting easy identification of the oligonucleotide sequence along with fabrication of candidate ssDNA sequences using the separated colonies via PCR. Preliminary binding between the amplified ssDNA oligonucleotide inserts and their target is measured using an enzyme-linked oligonucleotide assay (ELONA) (Drolet *et al*., 1996). Oligonucleotide candidates that successfully bind to the target/s are sequenced; and, finally, structural analysis of the three-dimensional structure given by the sequence is conducted.

2.3. Aims

1. To identify and minimise the study-specific difficulties and limitations encountered during SELEX during the generation of ssDNA oligonucleotide sequences, or aptamers, capable of

discriminately binding to the *Plasmodium falciparum*-specific peptide, as well as the whole recombinant *P. falciparum* lactate dehydrogenase in SELEX.

2. To identify ssDNA oligonucleotide sequences, or aptamers, capable of discriminatory binding to the *Plasmodium falciparum*-specific peptide, as well as to the full recombinant *P. falciparum* lactate dehydrogenase enzyme.

2.4. Methodology

2.4.1. Reagents

General chemicals and reagents were purchased at Sigma Aldrich (Germany) unless otherwise specified as follows. Recombinant His-tagged *Plasmodium falciparum* LDH (rLDH or r*Pf*LDH) and *P. falciparum*-specific IgY were obtained from Professor Dean Goldring (UKZN, Pietermaritzburg, South Africa) following cloning, expression and purification (Hurdayal *et al*., 2010). The unmodified *Plasmodium falciparum*-specific LDH epitope peptide (LDHp; LISDAELEAIFDC) was sourced from GL Biochem (China). Oligonucleotides (library and primers) were generated by Integrated DNA Technologies (IDT; USA).

PCR reaction reagents used in SELEX (GoTaq® Flexi DNA Polymerase kit) was purchased from Promega, USA. The PCR reaction reagents used during aptamer screening (KAPA Taq PCR kit) was purchased from KAPA Biosystems (South Africa). The dNTPs were purchased from Fermentas, Thermo Scientific, USA. Molecular-grade bovine serum albumin (BSA) was purchased from New England Biolabs (UK). Nucleospin® Gel and PCR clean-up kits were purchased from Macherey-Nagel GmbH & Co. KG (Germany). GelRed® (10 000 X) was purchased from Biotium (USA). Lambda exonuclease (5000 U/ml) was purchased from New England Biolabs (UK). PGEM-T Easy vector and all associated reaction components were purchased from Promega (USA). The low range O'GeneRuler DNA ladder (25-700 bp) was purchased from Fermentas/Thermo Fisher Scientific (South Africa). The PierceTM prestained protein molecular weight (MW) marker or protein ladder was purchased from ThermoFisher Scientific, USA.

Nonidet P-40 (10 % v/v) was purchased from Roche (Germany). PnP fat-free milk powder was purchased from Pick 'n Pay (Grahamstown, South Africa). Streptavidin-linked horse radish peroxidase (SA-HRP, 2.0 μg/ml) was purchased from Kirkegaard and Perry Laboratories (USA).

3,3',5,5'-tetramethylbenzidine (TMB) and peroxidase solution was purchased from Pierce (USA). The binding buffer used for aptamer-target interactions was 1X HMCKN buffer, pH 7.4, comprised 2 mM HEPES, 0.2 mM $MgCl_2$, 0.2 mM $CaCl_2$, 0.2 mM KCl and 15 mM NaCl. The Tris-buffered saline buffer, pH 7.6, for ELONA contained 144 mM NaCl and 25 mM Tris pH 7.6. The water used in all experiments was ultrapure

Milli-Q® water (TOC ≤ 5 ppb; resistivity (25 °C) = 18.2 MΩ.cm) from Merck KGaA (Germany).

2.4.2. Apparatus

All PCR thermocycling was performed on a MJ Mini Personal Thermo Cycler (Bio-RAD, USA). Polyacrylamide Gel Electrophoresis (PAGE) and agarose gel electrophoresis were performed using the PowerPac Basic Gel Electrophoresis equipment (BioRAD, USA). Electrophoresed gels were visualised under UV transillumination using a GelDoc™ EZ Imager (BioRAD, USA) controlled by Image Lab 4.0.1 software (BioRAD Laboratories, USA) and ChemiDoc XRS+ Molecular Imaging System (BioRAD, USA), respectively. DNA was quantified using a NanoDrop2000 Spectrophotometer (ThermoScientific, USA). Other UV-Vis spectrophotometric measurements were performed using the $Powerwave_x$ multiplate reader (Bio-Tek Instruments, USA).

2.4.3. Separation and visualisation of proteins by polyacrylamide gel electrophoresis (PAGE)

Recombinant *Plasmodium falciparum* lactate dehydrogenase (r*Pf*LDH, 0.95 (stock A), 0.95 (stock B) and 0.50 mg/ml), recombinant *Plasmodium vivax* lactate dehydrogenase (r*Pv*LDH, 0.18 and 0.50 mg/ml), human serum albumin (HSA, 1.0 mg/ml), bovine serum albumin (BSA, 1.0 mg/ml) and mammalian LDH (mLDH, 0.30 mg/ml) were initially heat-denatured in PBS, pH 7.4, at 100 °C for 5 min. Denatured proteins were resolved on a 10 % polyacrylamide gel (N,N,N',N'-tetramethylethylene-diamine (TEMED), ammonium persulphate (APS) and acrylamide/ bisacrylamide (30% 37.5:1) prepared in Miili-Q water) containing 1 % sodium dodecyl sulphate (SDS) at <60 V for 1 hour in TBE buffer (45 mM Tris base, 45 mM boric acid, 1.3 mM EDTA, pH 8.0, containing 1 % SDS). The All-Blue prestained protein molecular marker was used as a protein ladder. The PAGE gels were post-stained with Coomassie Brilliant Blue staining solution for 1 hour at 37 °C and destained twice at 37 °C with methanol-acetic acid (80:20 %) destain solution and once with Milli-Q H_2O, until proteins were suitably visible. Stained gels were viewed under visible light using a GelDoc™ EZ Imager linked up to Image Lab 4.0.1 software.

2.4.4. Synthesis of aptamers against recombinant PfLDH and LDH peptide

Aptamer synthesis was performed according to Rotherham and co-workers (2012), based on the originally-published work of Tuerk & Gold (1990). A library of 10^{14} – 10^{18} single-stranded DNA (ssDNA) sequences 90 bases in length consisting of a 49-nucleotide stretch of randomised sequence flanked by constant regions for primer annealing) was sourced from Integrated DNA Technologies (IDT, USA). The generalised sequence of the library was thus:

5'-GCCTGTTGTGAGCCTCCTAAC(N49)CATGCTTATTCTTGTCTCCC-3'.

Identification of oligonucleotides against recombinant *Pf*LDH (designated rLDH) and a species-specific *Pf*LDH epitopic peptide (designated LDHp) was performed in parallel through the method of SELEX (Tuerk & Gold, 1990; Rotherham *et al*., 2012). In total, eight rounds of selection were performed during SELEX.

2.4.5. Selection of target-binding oligonucleotides

2.4.5.a. Preparation and activation of nitrocellulose filter membranes

Selection of oligonucleotides capable of binding to rLDH and LDHp, shown in the schematic in **Figure 2.1**, using nitrocellulose membrane filtration as a partitioning method, was adapted from Smolarsky and Tal (1970) and Wong and Lohman (1993). Briefly, nitrocellulose filter membranes (pore size of 0.45 μm, Merck Millipore, USA) were activated through alkaline hydrolysis through incubation in 0.5 M KOH solution for 20 min at room temperature, rinsing with Milli-Q H_2O, further incubating in 0.1 M Tris, pH 7.4 for 45 min and finally rinsing with HMCKN buffer prior to use.

2.4.5.b. Incubation of target-binding oligonucleotides

The ssDNA library (20 μl; final concentration = 1590 nM) was heat denatured at 95 ^{o}C for 10 min in HMCKN buffer, cooled at -20 ^{o}C for 5 min and further rested at room temperature for 5 min before passing through prepared filter membranes to remove non-specifically-binding species (negative selection). Target protein/peptide (with a final concentration of 1590 nM) was added to the effluent and binding allowed to proceed at room temperature for 1 hour under mild agitation (<50 rpm). The unbound ssDNA and target-ssDNA mixtures were then separated by being passed through freshly prepared activated nitrocellulose membranes (positive selection). The membrane was subsequently rinsed with HMCKN buffer to remove unbound ssDNA. Based on nitrocellulose binding principles, it was

assumed that all protein/target-aptamer complexes are retained on the nitrocellulose filter (Wong & Lohmann, 1993).

2.4.5.c. Extraction of rPfLDH-binding and LDHp-binding oligonucleotides

The ssDNA-target complexes retained at the nitrocellulose membrane (**Chapter 2.4.5.b**) were eluted by immersion in 200 µl nitrocellulose elution buffer (7 M urea, 100 mM citrate buffer and 3 mM EDTA, pH 8.0) and heating to 100 ^{o}C for 5 min. The ssDNA was extracted from the elution buffer via a phenol-chloroform extraction in which 600 µl of phenol:chloroform:isoamyl alcohol (25:24:1; saturated with 10 mM Tris, pH 8.0, 1 mM EDTA) was added to the nitrocellulose elution buffer. This was mixed and incubated with agitation at room temperature for 30 min. Tubes were centrifuged for 5 min at 7 100 x *g* at room temperature (RT). The top layer or aqueous phase was removed and retained. To maximise recovery of ssDNA, an additional volume of 100 µl of sterile Milli-Q water was added to the phenol:chloroform:isoamyl alcohol with nitrocellulose filters; the suspension thoroughly mixed; and, centrifuged for 5 min at 7 100 x *g* (RT). Again, the aqueous phase or top layer was carefully removed and combined with the previously removed aqueous phase. To the 300 µl of aqueous phase, 600 µl of chloroform:isoamyl alcohol (24:1) was added. This was thoroughly mixed and centrifuged at 7 100 x *g* for 5 min at RT. The top layer or aqueous phase was removed and set aside. A further 100 µl of sterile Milli-Q water was added to the chloroform:isoamyl alcohol; thoroughly mixed; centrifuged at 7 100 x *g* for 5 min (RT); and, the top or aqueous layer carefully removed and combined with the previously removed aqueous phase. The extracted ssDNA in the combined aqueous phases was precipitated similarly to Avci-Adali and co-workers (2010) by adding 30 µl of 3M sodium acetate buffer, pH 5.2, 3.3 µl of glycogen (20 g/l) and 1 ml of absolute ethanol to the aqueous phase and incubating overnight for approximately 16 h at -80 ^{o}C. Following centrifugation at 4 ^{o}C for 30 min at 9 100 x *g*, a white precipitate was seen. The ethanol mixture was carefully removed (effluent) and 80 % ($^{v}/_{v}$) ethanol added to the precipitate. The ssDNA was centrifuged for a further 5 min at 4 ^{o}C at 9 100 x *g*. The ethanol was carefully removed (retained as "wash effluent" for further analysis) and the pellet allowed to air dry at room temperature for 2 to 4 h. The ssDNA pellet was resuspended in 30 µl sterile Milli-Q H_2O. The concentration and purity of ssDNA was quantified and assessed, respectively, using the NanoDrop2000 Spectrophotometer with sterile Milli-Q H_20 as the blank. A portion (5 µl) of ssDNA was set aside and stored at -20 °C.

2.4.5.d. Calculation of recovered oligonucleotides capable of binding to rPfLDH and LDHp

The concentration and purity of the extracted and eluted ssDNA obtained at the end of the selection step, was quantified using a NanoDrop 2000 Spectrophotometer (ThermoScientific, USA). This quantified ssDNA was used to calculate the mass (ng) of ssDNA that binds to the target during the selection (described as "ssDNA out"). By using the mass (ng) of ssDNA that was initially used in the selection (described as "ssDNA in"), the yield of positively binding ssDNA can be calculated as a percent recovery as follows:

$$Recovery\ (\%) = \frac{ssDNA\ out\ (ng)}{ssDNA\ in\ (ng)} \times 100 \qquad \textbf{Equation 2.1}$$

2.4.5.e. Fractionation of single-stranded DNA of Selection in SELEX (Stage 1)

To qualititatively evaluate the presence and purity of partitioned ssDNA from r*Pf*LDH- and LDHp-bound ssDNA following nitrocellulose filtering during the Selection –or Stage 1 – of SELEX, the ssDNA effluent and wash fractions were extracted, as described in **Chapter 2.4.5.c**. The ssDNA fractions were resolved on 8 % ($^{w}/_{v}$) polyacrylamide gel at $\leq$120 V for 20-30 min in TBE buffer (45 mM Tris base, 45 mM boric acid, 1.3 mM EDTA, pH 8.0). PAGE gels were post-stained with 1 X GelRED and viewed under UV with a ChemiDoc XRS+ Molecular Imaging System. DNA PAGE images were inverted for improved annotating.

2.4.6. Polymerase chain reaction (PCR)-based amplification of selected oligonucleotides

Amplification of ssDNA was performed by PCR, producing amplified double-stranded DNA (dsDNA).

2.4.6.a. PCR temperature profile

The optimised temperature profile used for PCR was performed as follows: 95 ^{o}C for 3 min (initiation step); 4 – 20 cycles at 95 ^{o}C for 1 min (denaturation), 59 ^{o}C for 1 min (annealing) and 72 ^{o}C for 1.5 min (elongation); and, 72 ^{o}C for 8 min (final elongation step) on a MJ Mini Personal Thermo Cycler.

2.4.6.b. PCR reaction mix recipe

PCR master reaction mix (GoTaq® Flexi DNA Polymerase kit) was prepared as per manufacturer's instruction: 0.2 mM dNTPs, 3.5 mM $MgCl_2$, 0.5 μM forward primer (5'-GCCTGTTGTGAGCCTCCTAAC-3'), 0.5 μM reverse primer (5'-GGGAGACAAGAATAAGCATG-3') and 10 μg/ml BSA. The reverse primer was modified with a phosphate group at the 5'-end for lambda exonuclease attachment and activity.

2.4.6.c. Optimisation of PCR amplification by altering PCR cycle numbers

The number of PCR cycles required optimisation during the amplification stage of SELEX to prevent over-amplification of the dsDNA and the inclusion of unwanted PCR products. From the 1 ml reaction master mix, 200 μl was removed. To this 200 μl of PCR reaction mixture, 2 U of *Taq* polymerase was added, plus 1 μl, or ~10 ng, of template DNA. This was sub-divided into 10 reaction tubes each containing 20 μl of the PCR reaction mixture. A template-free negative control was also included during PCR optimisation. The 20 μl reaction tubes were removed from the thermocycler after every second cycle following four rounds of PCR, e.g. 0, 4, 6, 8, 10, 12, 14, 16, 18, 20 cycles, with the blank control undergoing the maximum number of PCR cycles.

2.4.6.d. Polyacrylamide gel electrophoresis (PAGE) for PCR optimisation

PCR optimisation reactions were assessed for over-amplification by means of PAGE using 8 % ($^{w}/_{v}$) polyacrylamide gels (N,N,N',N'-tetramethylethylene-diamine (TEMED), ammonium persulphate (APS) and acrylamide/ bisacrylamide (30% 37.5:1) prepared in Miili-Q water) electrophoresed at $\leq$120 V for 20-30 min in TBE buffer (45 mM Tris base, 45 mM boric acid, 1.3 mM EDTA, pH 8.0) until the dye front was within 0.5 cm of the bottom edge of the gel. PAGE gels were post-stained with 2.5 μM ethidium bromide solution, and later 1 X GelRED, and viewed under UV with a ChemiDoc XRS+ Molecular Imaging System. DNA PAGE images were inverted for improved annotating. The chosen number of optimised cycles was based on that number of cycles which lacked over-amplification, seen as banding or smearing above the target band.

2.4.6.e. PCR amplification of the remaining ssDNA template

The remaining template DNA and 5 U of *Taq* polymerase was added to the remaining PCR master mix, which was aliquoted into smaller PCR tubes for PCR using a protocol with the optimised number

of cycles, as well as the final extension time. The $MgCl_2$ concentration was decreased to 1.5 mM after the third round of SELEX to reduce the mutation rate.

2.4.6.f. Purification and concentration of PCR amplification product

Using the Nucleospin® gel and PCR clean-up kit

Generally, PCR products were pooled for each round of PCR and purified and concentrated using the Nucleospin® Gel and PCR clean-up kit. Briefly, a 2:1 volume ratio of NT buffer (dsDNA binding buffer) to the pooled PCR products was added. The solution was incrementally added to a Nucleospin® clean-up column and centrifuged at 7 100 x *g* for 1 min at RT. The initial centrifugation was done twice to moisten the filter and promote DNA retention. Bound dsDNA was washed twice with an ethanol-based NT3 buffer (wash buffer) with each wash undergoing centrifugation at RT at 7 100 x *g* for 1 min. Excess ethanol-based Wash buffer was removed by centrifuging for 3 – 5 min at 7 100 x *g* at RT. The dsDNA was eluted in 50 µl sterile Milli-Q water. DNA was quantified using a NanoDrop2000 Spectrophotometer.

Using an agarose gel excision

Amplified DNA was purified by gel excision (Fuke & Thomas, 1970) by initially running the dsDNA on a 2.5 % ($^{w}/_{v}$) agarose gel with 1 X GelRED at 80 V for 1.5 to 2 h in TBE buffer, pH 8.0. Target 90 bp dsDNA was visualised on a UV transilluminator and carefully sliced out of the gel using a scalpel blade. A volume of 300 µl NTI binding buffer was added per 100 mg of gel. The gel slices in NTI buffer were heated at 50 ^{o}C until the agarose gel slice had dissolved. Target dsDNA was, again, concentrated using Nucleospin® clean-up columns, as per the manufacturer's guidelines and as previously described in **Chapter 2.4.6.f**.

2.4.6.g. Quality assessment of PCR product through PAGE

Quality of amplified dsDNA from the remaining ssDNA obtained through the selection step was determined by PAGE using 8 % ($^{w}/_{v}$) polyacrylamide gels at $\leq$120 V for 20-30 min in TBE buffer (45 mM Tris base, 45 mM boric acid, 1.3 mM EDTA, pH 8.0). PAGE gels were post-stained with 2.5 µM ethidium bromide solution, and later 1 X GelRED, and viewed under UV with a ChemiDoc XRS+

Molecular Imaging System. Lane profiles on PAGE gels were analysed using FIJI (Fiji is just ImageJ) v1.5e (available at http://imageJ.nih.gov/ij).

2.4.6.h. Optimisation of PCR amplification parameters for the removal of unwanted PCR amplification products

Exploration of amplification artefact formation during PCR amplification

In order to determine whether the undesired fragments in the PCR product profile observed on PAGE resulted from primer dimerisation and concatemerisation, the possibility of primer dimerisation and concatemerisation was probed. This was achieved by annealing only forward and reverse primers (5.0 µM) at 59 ^{o}C for 10 min using the MJ Mini Personal Thermo Cycler. No PCR amplification nor thermocycling was performed. The products were directly visualising on PAGE (performed as described in **Chapter 2.4.6.g**) with the exception that bands were resolved at <60 V for 30 min, and visualised as described in **Chapter 2.4.6.d**.

Non-specific primer and DNA library elongation during PCR amplification

To further probe the formation of concatemers, which are suspected in the PCR product profile resolved by PAGE, primers and ssDNA library were PCR amplified as carried out in **Chapter 2.4.6.g**, with the exception that 25 PCR cycles were carried out. Products thereof were resolved using PAGE at 50 V for 1.5 h (until the dye front had migrated sufficiently) and visualised as described in **Chapter 2.4.6.d**.

Modifications to the PCR reagent mixture and temperature profile

To enhance the replication fidelity of PCR, varying reaction parameters were tested, as suggested by the manufacturer's troubleshooting guide (available at https://worldwide.promega.com/). Amplification products were analysed during the optimisation of PCR amplification to minimise the generation of superfluous amplification by-products whilst ensuring ample target dsDNA amplification. The tested modifications included analysis of the effect that addition of PCR additives, specifically 0.01 % ($^{v}/_{v}$) Triton, to the PCR reaction mix had on dsDNA purity and yield. The effects of an adjusted annealing temperature on the amplification product profile was also investigated. Specific annealing temperatures investigated were: 50, 54 and 59 ^{o}C.

Removal of PCR fragments >150 bp through DNA binding buffer dilution

In order to obtain dsDNA products with a greater yield of the expected amplicon size (90 bp), the removal of the larger unwanted PCR products during DNA concentration (using the Nucleospin® Gel and PCR clean-up kit, as detailed in **Chapter 2.4.6.f**) was tested. Following an unfavourable and unsuccessful PCR amplification containing mainly amplification artefacts (visualised using the PCR product profile on PAGE), the ratio of NT buffer : sterile Miili-Q H_2O dilution ratio was adjusted from 1 : 1 to 1 : 5, as per the manufacturer's recommendation. Diluting the NT buffer allowed the elution of larger fragments >150bp and the retention of smaller fragments (<150 bp) during DNA concentration. The effluent containing the dsDNA fragments <150 bp was reserved, and underwent purification and concentration as per the general protocol above.

2.4.7. Exonuclease digestion of complementary oligonucleotide strand

Following sufficient amplification of dsDNA (≥4.5 μg dsDNA per round of SELEX), dsDNA was converted to ssDNA by lambda exonuclease digestion carried out for 4 h at 37 ^{o}C a rate of ~1 U exonuclease per microgram dsDNA to produce ssDNA, similar to previous research (Avci-Adali *et al.,* 2010). The produced ssDNA was purified similarly to that of the PCR products using the Nucleospin® Gel and PCR clean-up kit as per manufacturer's instruction (**Chapter 2.4.6.f**). A PAGE was performed as previously described (**Chapter 2.4.6.g**) to confirm the single-stranded nature of the samples by the visible absence of dsDNA. The resulting ssDNA was used for selection during the following round of SELEX. Eight rounds of selection were performed during SELEX.

SELEX note: The dsDNA from the final 3 rounds of SELEX was pooled, digested with lambda exonuclease to produce ssDNA and a final selection cycle was performed.

2.4.8. Screening and identification of binding sequences

2.4.8.a. Production of competent Escherichia coli JM109 cells

Aseptic technique were employed in the production of competent *Escherichia coli* JM109 cells. A 50 μl culture of *E. coli* JM109 cells (kindly gifted by Margot Brookes, Rhodes University, Grahamstown, South Africa) in nutrient broth was diluted in 5 ml of sterile nutrient broth, and incubated overnight (~16 h) at 37 ^{o}C under agitation. The overnight culture was diluted 20-fold in sterile Luria broth to achieve an OD_{600nm} of between 0.3 and 0.6 OD units. This diluted culture was

centrifuged at 5000 x *g* for 15 min at 4 °C. The pelleted cells were kept on ice from this point forward. The pelleted cells were resuspended in 50 ml of sterile cold (~4 °C) 0.1 M $MgCl_2$, incubated on ice for 20 min, and centrifuged at 5000 x *g* for 15 min at 4 °C. The supernatant was discarded. The remaining pellet was resuspended in 12.5 mls of sterile cold (~4 °C) 0.1 M $CaCl_2$, incubated on ice for 2 h, thereafter centrifuged at 5000 x *g* for 15 min at 4 °C. The supernatant was again discarded and supernatant gently resuspended in 1.25 mls of sterile cold (~4 °C) 0.1 M $CaCl_2$. Aliquots of these pelleted cells in 0.1 M $CaCl_2$ were added to aliquots of equal volume of 30 % ($^{v}/_{v}$) sterile glycerol in Luria broth (70 %). Unused glycerol stocks of competent *E. coli* JM109 cells were then stored at -80 °C.

2.4.8.b. Ligation of dsDNA fragments into pGEM® -T Easy vector

The amplified dsDNA consortia were ligated into the pGEM®-T Easy vector as per the manufacturer's instructions (https://www.promega.com/-/media/files/resources/protocols/technical-manuals/0/pgem-t-and-pgem-t-easy-vector-systems-protocol.pdf). Ten microlitre (10 µl) ligation reactions were prepared as shown in **Table 2.1**.

Table 2.1: Components of ligation reactions used in the screening of oligonucleotide products of SELEX selected for LDHp and r*Pf*LDH

Reaction component	SELEX pool targetting r*Pf*LDH	SELEX pool targetting LDHp	Positive control	Negative control
2X Rapid ligation buffer	5.0 µl	5.0 µl	5.0 µl	5.0 µl
pGEM®-T Easy vector	5.0 ng/µl	5.0 ng/µl	5.0 ng/µl	5.0 ng/µl
dsDNA	4.5 ng/µl	6.4 ng/µl	-	-
Control dsDNA	-	-	0.8 ng/µl	-
T4 DNA Ligase	3.0 U	3.0 U	3.0 U	3.0 U

These ligation reactions were gently mixed, and incubated overnight (~16 h) at 4 °C. Ligated products were then used to transform competent cells.

2.4.8.c. Transformation of competent cells with the ligated vector

Following ligation, the dsDNA-vector consortia were transformed into competent *E. coli* JM109 cells (**Chapter 2.4.8.a**), according to the manufacturer's protocol and using aseptic technique. Briefly, on ice, 20 µl of ligation reaction (**Table 2.1**) was added to 50 µl of thawed competent cells (**Chapter 2.4.8.a**) and gently mixed (the negative control contained no ligation reaction). The competent cell

and ligated vector suspensions were heat-shocked for 45 s at 42 ^{o}C, thereafter immediately placed on ice for 2 min. A volume of 950 µl of Super Optimal broth with Catabolite repression (SOC) media was added to each reaction tube, and incubated for 2 h at 37 ^{o}C with stirring at 200 rpm.

2.4.8.d. Blue/white screening of recombinants

Luria agar plates, containing 100 µg/ml ampicillin, 20 mg/ml 5-bromo-4-chloro-3-indolyl-β-D-galactopyranoside (X-Gal) and 0.1 µM isopropyl β-D-1-thiogalactopyranoside (IPTG), were prepared for the blue/white screening of recombinants. One hundred microlitres (100 µl) of each of the transformed cell reactions (**Chapter 2.4.8.c**) was plated onto prepared Luria agar plates using aseptic technique, and incubated for 48 h at 37 ^{o}C. **Table A.1** in **Appendix A** provides the transformation efficiencies for oligonucleotide fragment lengths selected against LDHp and r*Pf*LDH.

Sixteen (16) white colonies (containing oligonucleotide fragments selected against r*Pf*LDH) and 18 white colonies (containing oligonucleotide fragments selected against LDHp) were re-streaked onto a second set of Luria agar plates and selected for fragment length screening via PCR amplification.

2.4.8.e. Fragment-length screening of ligated dsDNA through PCR amplification

The region with the insert was PCR amplified using pUC/M13 universal primers specific for the insert region of the PGEM-T Easy vector. White colonies selected for fragment length screening were resuspended in 25 µl sterile Milli-Q H_2O, vigorously stirred, and heated to 95 ^{o}C for 10 min. The resuspended colonies were directly used for PCR amplification of ligated dsDNA fragments.

Confirmation of ligation of aptamer candidates via PCR-based amplification of ligated dsDNA

This PCR reaction mix was prepared according to the manufacturer's instruction, and contained 0.15 mM dNTPs, 5 µM pUC/M13 forward primer (5'-CCCAGTCACGACGTTGTAAAACG-3'), 5 µM pUC/M13 reverse primer (5'-AGCGGATAACAATTTCACACAGG-3'), and 16 U *Taq* polymerase. Aliquots (50 µl) of this PCR reaction master mix were prepared, to which 1 µl of resuspended colony/cell debris was added.

PCR temperature profile for amplification of ligated dsDNA

The temperature profile used for PCR amplification of ligated dsDNA was performed as follows: 95 ^{o}C for 3 min (initiation step); 30 cycles at 95 ^{o}C for 30 s (denaturation), 54 ^{o}C for 30 s (annealing) and 72 ^{o}C for 60 s (elongation); and, 72 ^{o}C for 8 min (final elongation step) on a MJ Mini Personal Thermo Cycler.

Size determination of amplified dsDNA fragments through PAGE

PCR-amplified vector inserts were measured using PAGE, similar to previous descriptions (**Chapter 2.4.6.g**), with the exception that PAGE was resolved at 60 V for 60 – 80 min prior to visualisation. Given the expected size of the inserted dsDNA (~90 bp – 100 bp), the length of vector dsDNA expected on either side of the insert (45 bp forward binding site at the 5' side and 175 bp reverse binding site at the 3' side) and the combined primer lengths (23 bp pUC/M13 forward primer and the 23 bp pUC/M13 reverse primer), colonies containing a dsDNA PCR product of 355 – 365 basepairs were identified as having the correctly-sized dsDNA insert, and were retained for further screening.

2.4.8.f. PCR amplification of target-binding oligonucleotide directly from E. coli colony

Amplicons from colonies containing correctly-sized inserts were further amplified and modified with 5'-biotin, as per the recipe and temperature profile used in the PCR amplification step used during SELEX, as described in **Chapter 2.4.6**. Briefly, the KAPATaq PCR reaction mix was prepared according to the manufacturer's instruction , and contained 0.1 mM dNTPs, 1.0 mM $MgCl_2$, 0.2 μM 5'-biotinylated forward primer (5'-GCCTGTTGTGAGCCTCCTAAC-3'), 0.2 μM 5'-phosphorylated reverse primer (5'-GGGAGACAAGAATAAGCATG-3') and 1 μl of resuspended cell debris. The PCR temperature profile was performed as described in **Chapter 2.4.6.a.** These PCR-amplified fragments lengths were resolved on PAGE as described in **Chapter 2.4.6.g**.

Following amplification of sufficient dsDNA (≥ 4.5 μg), the amplified dsDNA was exonuclease-digested to ssDNA as previously described.

Biotinylated ssDNA sequences obtained in the above manner were used in a preliminary binding assay using ELONA.

2.4.9. Preliminary enzyme-linked oligonucleotide assay (ELONA) of binding of PCR amplified oligonucleotides to immobilised rPfLDH and LDHp

Preliminary ELONA binding analyses involved oligonucleotides that were isolated and amplified directly from the transformed cells. Binding of the selected synthesised sequences to their respective targets, r*Pf*LDH and LDHp, and control protein (bovine serum albumin (BSA) was evaluated using ELONA (Drolet *et al*., 1996). A single measurement was conducted for BSA and the aptamer control due to the limited quantities of PCR-amplified oligonucleotide available. A schematic of ELONA is presented in **Figure 2.3**, in which the various steps has also been included, in the context of aptamer to LDH peptide binding.

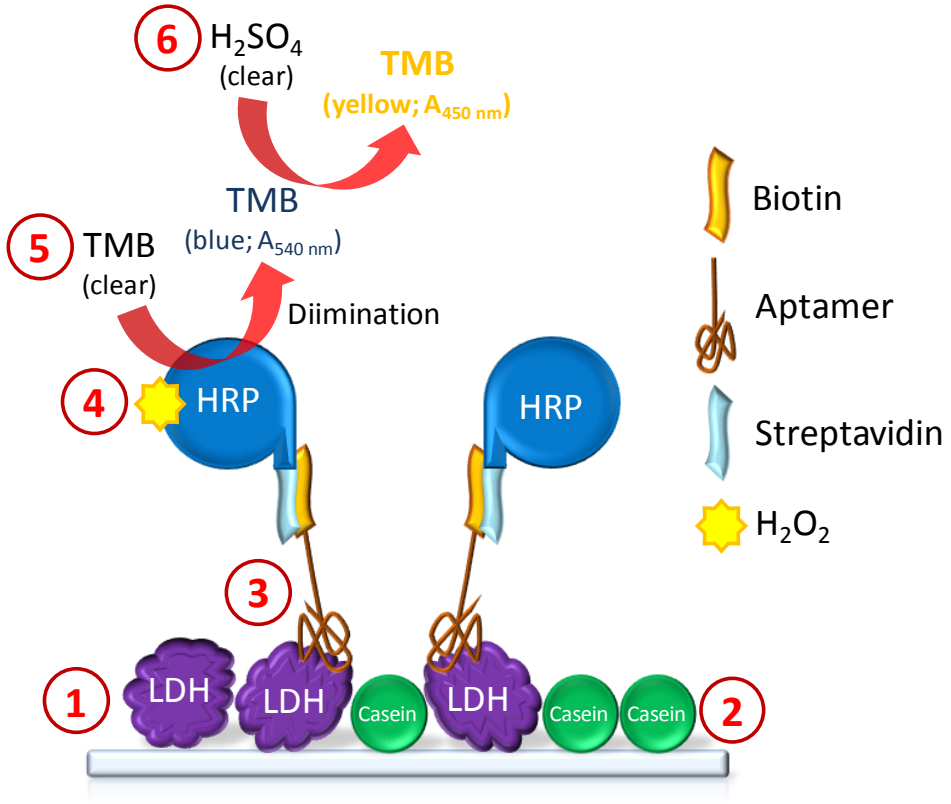

Figure 2.3: Detailed schematic of ELONA sandwich-type assay.
1: Target immobilisation. 2: Casein blocking. 3: Biotin-aptamer binding. 4: Streptavidin-horse radish peroxidise coupling. 5: TMB colour reaction through diimination (colour development read at 540 nm). 6: Reaction cessation through addition of sulphuric acid (end-point absorbance read at 450 nm).

Briefly, 500 ng of target or control protein was dissolved in 10 mM $NaHCO_3$ buffer, pH 8.5, and was added to each well of a 96-well ELISA plate and incubated overnight at 4 ^{o}C in a covered plate (Step 1 in **Figure 2.3**). The plate was then washed three times with 300 µl of 25 mM Tris-buffered saline

(TBS) buffer, pH 7.6 containing 0.1 % (v/v) Nonidet P-40 (NP-40), designated TBS+ hence forth. Wells were then blocked with 100 µl of 2 % (w/v) fat-free milk solution in TBS+, incubating for 1 hour at 4 ^{o}C (Step 2 in **Figure 2.3**). The plate was washed three times with 300 µl TBS+. Biotinylated oligonucleotides (generally 200 nM), suspended in HMCKN buffer was added to each sample well and incubated at room temperature for 2 h (Step 3 in **Figure 2.3**). The plate was then washed twice with 300 µl HMCKN buffer followed by a further three washes with 300 µl TBS+. Streptavidin-linked horse radish peroxidase (SA-HRP; 1 SA: 2.5 HRP; 0.1 mg/ml) was diluted 1:1000 in TBS+, of which 100 µl was added to each well (Step 4 in **Figure 2.3**). The plate was covered and incubated at 37 ^{o}C for 2 h and unbound SA-HRP removed from the system by rinsing the plate 4 times with 300 µl TBS+. Thereafter, 50 µl of the TMB solution consisting of the chromogenic substrate, 3,3',5,5'-tetramethylbenzidine (TMB), and hydrogen peroxide was added to each well (Step 5 in **Figure 2.3**); and, after 8 min, following visible colour formation, the reaction was stopped with 50 µl of 2 M sulphuric acid (stop solution) (Step 6 in **Figure 2.3**). UV-vis absorbance values at 450 nm were measured for each well using the Powerwave$_x$ multiplate reader. All measurements were performed in quadruplicate (n = 4).

2.4.10. Data measurement and analysis

All measurements were performed in, at minimum, triplicate with the exception of the SELEX yield calculations and oligonucleotide concentration data outputs on the NanoDrop2000 Spectrophotometer, which were performed using singular readings. Presented results are the means of measurements, while reported error bars and uncertainties represent one standard deviation from the mean. Statistically-significant differences in the means of measurements for all suitable analyses were performed, with the exception of the preliminary ELONA, using Kruskal-Wallis ANOVA, with Dunn's Multiple Comparison Test applied afterwards as a *post-hoc* test. For all statistical tests, statistical significance, α, was assigned to be 0.05.

2.5. Results and discussion

2.5.1. Size confirmation of recombinant PfLDH, recombinant PvLDH, mammalian LDH, HSA and BSA

To confirm the purity, subunit association and integrity of the proteins to be used for SELEX, the electrophoretic profile of the proteins was confirmed using semi-denaturative polyacrylamide gel

electrophoresis (PAGE). Semi-denaturative PAGE, in which protein samples are only partially denatured, was selected in order to preserve the quarternary structure of the proteins used for SELEX. In this technique, the protein solutions were only heat-denatured (100°C for 5 min) prior to SDS-PAGE. For complete denaturation of protein solutions to occur for proper size determination and positive identification of the protein monomeric subunits, protein solutions would need to be heated in the presence of a suitable surfactant or reducing agent, such as 1% SDS, dithiothreitol or 2-mercaptoethanol (Caprette, 2012). The addition of SDS only during the boiling stage ensures that SDS attaches to the protein molecules to impart the correct charge to the proteins for electrophoretic separation, but maintains the subunit association.

Electrophoresis of target, recombinant *Plasmodium falciparum* lactate dehydrogenase (r*Pf*LDH), and control, recombinant *Plasmodium vivax* lactate dehydrogenase (r*Pv*LDH), mammalian lactate dehydrogenase (mLDH), human serum albumin (HSA) and bovine serum albumin (BSA), proteins stained with Coomasie Brilliant Blue was performed to confirm size and subunit composition of these proteins (**Table 2.2**) as indicated by banding rendered in polyacrylamide (**Figure 2.4**).

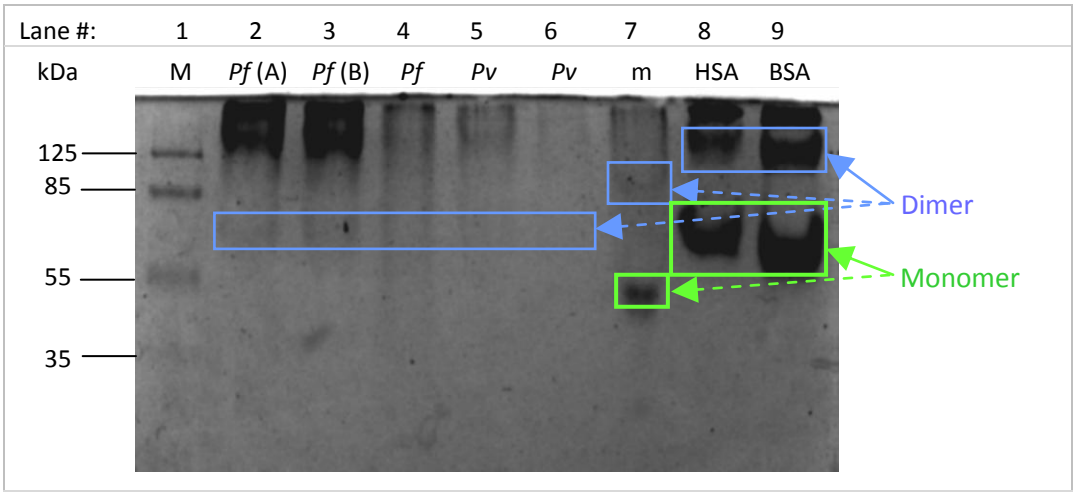

Figure 2.4: SDS-PAGE (10 %) of heat-denatured target, r*Pf*LDH, and control proteins, r*Pv*LDH, mLDH, HSA and BSA.

Blue box: dimer; green box: monomer

Lane 1: protein molecular weight marker (M); Lane 2: 0.95 mg/ml r*Pf*LDH (sample A) in PBS, pH 7.4; Lane 3: 0.95 mg/ml r*Pf*LDH (sample B) in PBS, pH 7.4; Lane 4: 0.50 mg/ml r*Pf*LDH in HMCKN, pH 7.4; Lane 5: 0.18 mg/ml r*Pv*LDH in PBS, pH 7.4; Lane 6: 0.50 mg/ml r*Pv*LDH in HMCKN, pH 7.4; Lane 7: 0.30 mg/ml mLDH (supplier stock); Lane 8: 1.0 mg/ml HSA in PBS, pH 7.4; Lane 9: 1.0 mg/ml BSA in PBS, pH 7.4.

Banding relative to subunit sizes was observed for r*Pf*LDH, r*Pv*LDH, mLDH, HSA and BSA in **Figure 2.4**. **Table 2.2** shows the calculated molecular weights of subunit forms of protein standards, r*Pf*LDH, r*Pv*LDH, mLDH, HSA and BSA, based on the relative fronts calculated using the Bio-RAD Image Lab 4.0.1 software.

Table 2.2: Relative fronts and molecular weight sizes of subunits observed by bands in PAGE of protein standards, r*Pf*LDH, r*Pv*LDH, mLDH, HSA and BSA, shown in Figure 2.4.

	Lane (in Figure 2.4)	Monomer		Homodimer	
		Relative front*	Molecular Weight (kDa)	Relative front*	Molecular Weight (kDa)
r*Pf*LDH (A)	2	-	NO**	0.265	68.7
r*Pf*LDH (B)	3	-	NO**	0.252	71.4
r*Pf*LDH	4	-	NO**	-	NO**
r*Pv*LDH	5	-	NO**	0.292	63.3
r*Pv*LDH	6	-	NO**	-	NO**
mLDH	7	0.382	48.0	0.161	94.6
HSA	8	0.274	66.9	0.081	121.3
BSA	9	0.303	63.0	0.100	114.1

The protein, r*Pf*LDH, shown in lanes 2, 3 and 4 in **Figure 2.4**, had a band at 68.7 kDa (or 71.4 kDa as in Lane 3) indicative of the presence of homodimer subunit organisation (**Table 2.2**). These molecular weights shown in **Table 2.2** are less than those predicted and stated by Hurdayal and co-workers (2010) for the relative subunit, but these differences can be related to automatic corrections the software may have included when determining the size relative to the analytical front as well as gel-loading capacity. The presence of protein smearing in Lanes 2, 3 and 4 in **Figure 2.4**, which ends relative to the 35 kDa molecular weight marker band indicates presence of the 39 kDa monomeric subunit of r*Pf*LDH shown by Hurdayal and co-workers (2010) or 37 kDa monomeric subunit of r*Pf*LDH shown by Krause (2016) to occur; however, this band was not observed as the concentration of this particular subunit was below the detectable quantity. Similar to r*Pf*LDH, r*Pv*LDH exhibited a band at approximately 63.3 kDa (lanes 5 and 6, respectively, **Figure 2.4**). However, Krause (2016) reported that r*Pv*LDH has a monomeric subunit of approximately 37 kDa, indicating that the bands in Lane 5 and 6 represent the dimeric form of the protein. As with r*Pf*LDH, the monomeric subunit, given as a molecular weight of 39.0 kDa (Hurdayal *et al.*, 2010), was not observed as the concentration of that particular subunit was below the detectable limit. The bands above 125 kDa (Lanes 2 – 6, **Figure 2.4**) suggest the presence a high molecular mass protein conformation and suggest the presence of tetrameric forms of r*Pf*LDH (Lanes 2 – 4) and r*Pv*LDH

(Lanes 5 and 6). However, further confirmatory analysis on the subunit composition of the protein suspension is required through fast protein liquid chromatography (FPLC) or dynamic light scattering (Petsev *et al.*, 2000). Therefore, these data suggest that the homodimeric form of r*Pf*LDH and r*Pv*LDH predominantly exist in the protein solutions that will be used for SELEX.

When performing a buffer exchange for r*Pf*LDH and r*Pv*LDH from phosphate buffer (lanes 2 and 3 and lane 5, respectively, **Figure 2.4**) to HMCKN, pH 7.4, (lanes 4 and 6, respectively, **Figure 2.4**) much of the protein sample was lost resulting in a lower protein concentration and, hence, diminished intensity of the bands for the various subunit forms through the polyacrylamide gel.

According to the BioRAD bulletin 6040 on troubleshooting PAGE (page 73, available at http://www.bio-rad.com/webroot/web/pdf/lsr/literature/Bulletin_6040.pdf), mobility and banding for mLDH (lane 7) was irregular due to the addition of salt, namely high concentrations of ammonium sulphate (NH_3SO_4) salt, during the purification process of the commercial mammalian LDH stock. This persisted despite attempts to remove NH_3SO_4 from mLDH stock aliquots. Two quartenary structures of mLDH were observed in Lane 7 in **Figure 2.4** and sized in **Table 2.2**: the monomer and dimer with molecular weights of 48.0 kDa and 94.6 kDa, respectively. However, due to the irregular mobility and banding for mLDH in Lane 7 in **Figure 2.4**, the increased electrophoretic mobility lead to the observed increased and apparent molecular weight of this mLDH. A molecular weight of 35.0 kDa has previously been reported for this particular mammalian, or bovine, LDH (Apella & Markert, 1961).

HSA and BSA both had two predominating bands at 66 kDa (lane 8, **Figure 2.4**) and 63 kDa (lane 9, **Figure 2.4**), respectively, and 121.3 kDa (lane 8, **Figure 2.4**) and 114.1 kDa (lane 9, **Figure 2.4**), indicative of the size of an albumin monomer and homodimer, respectively. These sizes are in accordance with those reported by the manufacturer of HSA (http://www.sigmaaldrich.com/life-science/metabolomics/enzyme-explorer/enzyme-reagents/human-albumin.html) and BSA (http://www.sigmaaldrich.com/lifescience/biochemicals/biochemicalproducts.html?TablePage=103994915).

The molecular weights and subunit composition of r*Pf*LDH, r*Pv*LDH, HSA and BSA were, therefore, confirmed in accordance with literature. The characterisation data of r*Pv*LDH, HSA and BSA can be

used as positive controls for the eventual binding analyses of oligonucleotides selected against the *P. falciparum* specific LDH peptide (LDHp) and r*Pf*LDH generated through Systemic Evolution of Ligands by Exponential enrichment (SELEX).

As Coomasie brilliant blue has a propensity to interact with basic amino acid residues (arginine and lysine) and polyaromatic amino acid residues (tryptophan, tyrosine and phenylalanine) (Compton & Jones, 1985; Congdon *et al.*, 1993), the species-specific 1 kDa LDHp polypeptide (LISDAELEAIFDC) would have been inadequately stained and subsequently not visualised due to insufficient and weak Coomasie brilliant blue binding sites, such as the one phenylalanine (F), even if a greater cross-linking was used in the preparation of the PAGE. Furthermore, given the small molecular size of 1 kDa, there exists the strong likelihood that the species-specific LDHp polypeptide would not have been appropriately resolved on the 10% PAGE along with the whole proteins assessed and would, hence, have migrated off PAGE gel. Therefore, the 1 kDa species-specific LDHp polypeptide was not resolved on SDS or native PAGE.

2.5.2. Fractionation of single-stranded DNA of Selection in SELEX (Stage 1)

The selection stage of SELEX for oligonucleotide aptamers against r*Pf*LDH (**Chapter 2.4.5**) requires a step involving quantification of the target-binding single-stranded DNA (ssDNA) obtained during a round of SELEX. Such a quantification was not performed on PAGE due to the utilisation of more rapid, inherently sensitive instrumentation, namely the NanoDrop™ Microvolume Spectrophotometer, which utilises UV/Vis spectrometry to quantitatively measure DNA (A_{260nm}) and other biomolecules (A_{280nm}) (https://tools.thermofisher.com/content/sfs/brochures/Thermo-Scientific-NanoDrop-Products-Nucleic-Acid-Technical-Guide-EN.pdf). Hence, while PAGE analysis was performed following exonuclease digestion of dsDNA to ssDNA and again throughout the amplification stage of SELEX, it was performed to provide a qualititative measurement of the purity and oligonucleotide length of the library at these aforementioned stages of SELEX (Chai *et al*., 2011; Kalle *et al.,* 2013).

Due to the limited quantity of available ssDNA that was known to bind to the respective target in SELEX, as shown by the UV-Vis quantification data, all available target-binding ssDNA was used in the amplification thereof for the subsequent round of SELEX. To evaluate the presence of unbound ssDNA that remains following target-oligonucleotide interaction and nitrocellulose filtering in the

selection stage of SELEX, eluted effluents (denoted in **Figure 2.5** by "E" in lanes 3, 4, 7, and 8) and wash effluents (denoted in **Figure 2.5** by "W" in lanes 5, 6, 9 and 10) were retained and purified. A portion of each of the effluents for both LDHp and r*Pf*LDH in the final round of SELEX were resolved on PAGE (**Figure 2.5)**.

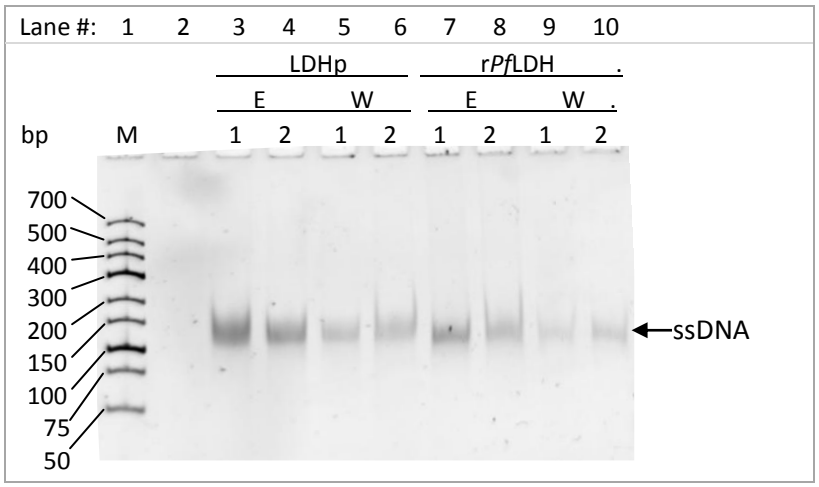

Figure 2.5: Unbound ssDNA from the eluted effluent (E) and wash effluent (W) following selection from a round of SELEX on 10% PAGE.

Lane 1: O'GeneRuler low range DNA molecular mass marker (M; Fermentas, ThermoScientific, USA); Lane 3 & 4: LDHp effluents; Lane 5 & 6: LDHp washes; Lane 7 & 8: r*Pf*LDH effluents; Lane 9 & 10: r*Pf*LDH washes.

The presence of a single well-resolved band in lanes 3 through to 10 in **Figure 2.5** indicates that a substantial number of single-stranded oligonucleotides did not bind to their respective target. These non-binding oligonucleotides did not adapt the correct tertiary conformation or exhibited weak interactions with the target; and, hence, flushed through during the selection process as unwanted single-stranded oligonucleotides (Yarus and Berg, 1967). The unbound oligonucleotides were thus present in the effluent and wash effluent following nitrocellulose filter-based separation of binding oligonucleotides and non-binding oligonucleotides as waste. Desired oligonucleotides were those that bound to their respective target/s that, in turn, bound to the nitrocellulose membrane.

The resolution of desired ssDNA with a known length of approximately 90 bp which appears between the 100 bp and 150 bp markers is compared to the resolution of dsDNA and is further discussed in **Chapter 2.5.6**.

2.5.3. Investigation of challenges inherent in the isolation of aptamers against recombinant PfLDH and PfLDH-specific peptide during SELEX

2.5.3.a. Optimisation of PCR parameters during Stage 2 of SELEX cycles

Amplification occurred through a polymerase chain reaction (PCR) in the second stage of a single SELEX round, the end-product of which is dsDNA created from ssDNA obtained from the Selection – or Stage 1 – of SELEX (**Figure 2.1**). One phase of the PCR amplification step required optimisation of the number of cycles to limit the production of non-specific PCR artefacts. Careful attention was, therefore, needed when conducting PCR in the second stage of SELEX, during each cycle of SELEX. Fractions of alternating PCR amplification cycles of a small quantity of amplified template DNA were analysed at each round of SELEX to assess the number of PCR cycles required to prevent the introduction of non-specific PCR by-products.

Specifically, the creation of non-specific PCR by-products to be avoided were: primer-dimer, primer concatemer and template dsDNA and primer concatemer formation. PAGE analysis of the quality of dsDNA generated during various PCR amplification cycles by the production of non-specific PCR by-products indicated a cycle-dependent formation of amplification artefacts, as shown in **Figure 2.6**. The concatemerisation of template dsDNA and/or primer forming fragments with longer base-pair length is, herein, referred to as over-amplification.

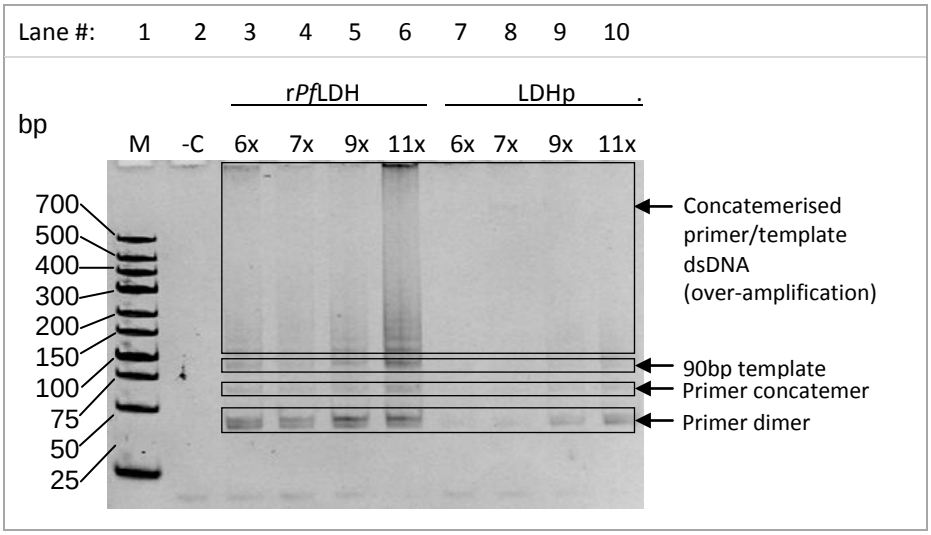

Figure 2.6: PAGE (10 %) analysis of amplification artefacts generated during PCR amplification of SELEX ssDNA pools.

Lane 1: DNA molecular mass marker (M); Lane 2: DNA control; Lane 3 - 6: r*Pf*LDH-targeted dsDNA during PCR cycle optimisation; Lane 7 - 10: LDHp-targeted dsDNA during PCR cycle optimisation

From **Figure 2.6**, the optimum number of PCR cycles chose with which to proceed with the next PCR stage would be 6x for LDHp oligonucleotides and 4x for r*Pf*LDH oligonucleotides. Six cycles would be optimal for LDHp given the complete absence of concatemerised primer/template dsDNA (over-amplification). The number of optimal PCR cycles for r*Pf*LDH-binding oligonucleotides would be problematic, given the evidence in **Figure 2.6**, as the lowest number of PCR cycles sampled (six cycles) also contains concatemerised primer/template dsDNA. Therefore, fewer PCR cycles than those tested here would need to be performed to raise sufficient dsDNA, with the strong possibility that a second PCR optimisation (and PCR amplification of the entire DNA fraction) would need to be performed. In the round of SELEX presented in **Figure 2.6**, inclusion of a sample following four PCR cycles (4x) would have provided affirmation on the presence of concatemerised primer/template dsDNA for r*Pf*LDH.

Specifically, this shows concatemerised dsDNA oligonucleotides (over-amplification) against the LDHp and r*Pf*LDH targets, as well as primer-dimers and primer concatemers formed, during PCR cycle optimisation of an unused round of SELEX. These non-specific PCR products may be capable of some binding to the target molecules, LDHp and r*Pf*LDH, resulting in false-positive binding and interference with selection and SELEX in its entirety as these fragments will be carried through SELEX (Crameri & Stemmer, 1993; Tuerk *et al*., 1992). These unwanted dsDNA fragments are essentially a combination of primers and/or template DNA annealing to one another, forming DNA concatemers (Quan & Tian, 2009).

Drabovich & Krylov (2004), Musheev and Krylov (2006) and Tolle and co-workers (2014) describe the production of PCR amplification by-products produced as a result of non-specific annealing of primer fragments to the template DNA. Herein, two self-annealing primers are referred to as primer-dimers, and three or more primers are referred to as primer-concatemers; both of which are visible in lane 3 to lane 10 in **Figure 2.6**. Primer-dimers are expected to have a length of approximately 40 bp, whilst primer-concatemers have a length of ≥60 bp and increase incrementally by 20 bp with the addition of primer lengths.

DNA concatemerisation is facilitated by the fact that short oligonucleotides (either primer or template DNA) are flexible and stable with respect to hybridisation; they have the ability to easily fold and self-anneal resulting in mis-annealments and unwanted secondary structures (Brownie *et al*., 1997; Tolle *et al.*, 2014). During PCR amplification, mis-annealed oligonucleotides are amplified

and erroneously elongated as the polymerase continues the elongation from the forward primer binding site until it reaches the reverse primer binding site (Jensen & Straus, 1993; Thompson *et al*., 2002; Tolle *et al.*, 2014). A schematic of such laddered and non-laddered oligonucleotide formation was previously presented in **Figure 2.2** (Tolle *et al.*, 2014).

Some of the longer concatemerised primer/template dsDNA (over-amplification) seen particularly in lane 6 for 11 PCR cycles of r*Pf*LDH-binding dsDNA in **Figure 2.6** was presued to include target-binding dsDNA that may have hybridised and subsequently been amplified during PCR (Musheev & Krylov, 2006). The presence of these longer-lengthed oligonucleotides promotes non-specific binding of shorter oligonucleotide sequences, namely primers, due to the absence of available primer annealing sites on the duplexed template DNA (Musheev & Krylov, 2006). The presence of these longer lengths of dsDNA also prohibits the formation of the desired target-binding oligonucleotides (Tolle *et al.*, 2014). Therefore, concatemers comprising template DNA and primer concatemers dominate the pool of PCR products, and are typically longer in length than the original 90bp template fragment and monomeric primer fragment, respectively (Crameri & Stemmer, 1993; Ouellet *et al*., 2015); and, migrate accordingly in PAGE based on the fragment base-pair length (Sun & Akerman, 2014), as shown most noticeably in Lane 6 in **Figure 2.6**.

Significant, i.e. visible primer-dimer formation and primer and dsDNA concatemerisation (shown in **Figure 2.6**), were only observed in later SELEX rounds, namely after round 4, of SELEX. Tolle and co-workers (2014) noted that their non-specific PCR amplification by-products were produced after the third round of SELEX. Pan and co-workers (2008) report that, after a number of SELEX rounds, the flanking primers mis-anneal through base-pairing, thus incorporating into the random sequence, forming tertiary structures themselves or flanking those structures necessary for target binding. Furthermore, the cross-hybridisation between the template DNA and primer is known to promote the observed over-amplification, more recently referred to in literature as high molecular weight by-products (Ouellet *et al*., 2015), due to the inherent presence of the primer sequence. Thus, as SELEX continues, these amplification products are consistently present with little to no discrimination between the correct sequence and mis-annealed sequence (Crameri & Stemmer, 1993). These products do not competitively bind to the target during selection, but frequently occur and are "competitive" in the amplification phase of SELEX (Crameri & Stemmer, 1993; Tuerk *et al*., 1992). As SELEX continues – round after round – production of PCR amplification primer dimers and concatemers are enhanced owing to the numerous PCR reactions and cycles that the template DNA

undergoes. Hence, they occur more frequently as SELEX continues.

Due the aforementioned production of amplification artefacts, a great deal of optimisation is thusly required during the amplification step of SELEX. This was reiterated by Dieffenbach and Dveksler (2003), who explained that each SELEX process is unique and presents its own challenges given that each template library is different from the next owing to the different properties of the unique DNA template sequences. This is due to the heterogeneous nature of the DNA template library, which can introduce a number of very different errors and artefacts (Kalle *et al*., 2013). Furthermore, and as was experienced in this work, the different materials sourced from the various suppliers elicit varying results. Whilst performing PCR amplification, optimisation was therefore required, limiting over-amplification and concatemerisation, which are directly influenced by the number of PCR cycles: too few cycles insufficiently amplified the desired 90bp ssDNA or dsDNA (e.g. six PCR cycles as shown in lanes 7-9 in **Figure 2.6** for amplified DNA targeted for LDHp and lane 3 and 7 in **Figure 2.6** when an annealing temperature of 50 ^{o}C was used); while too many cycles introduced unwanted lengths of dsDNA (over-amplification) (e.g. 11 PCR cycles as seen in lane 6 of **Figure 2.6** for amplified DNA targeted to LDHp).

It stands to reason that continuously amplifying the same oligonucleotide sequences repeatedly within a round of SELEX, as well as over a number of rounds of SELEX, will heavily affect the integrity and functionality of the binding dsDNA (Pan *et al*., 2008). In essence, this equates to SELEX having a life-span with respect to the number of rounds of PCR that can be undertaken across the entire SELEX procedure before the amplification artefacts begin to dominate the available pool of sequences. Shtatland and co-workers (2000) devised a SELEX method in which the initial primer sequence was replaced with an alternate binding sequence after the third round of SELEX, thus eliminating the occurrence of these unwanted primer artefacts. Wu and Curran (1999) and Citartan and co-workers (2012) also implemented the use of asymmetric PCR for the production of a diverse pool of oligonucleotides in which the formation of non-specific PCR products was limited. Asymmetric PCR using a reverse primer to forward primer ratio of 15:1 was found to be optimal for dsDNA of longer basepair length (Tabarzad *et al*., 2014). Therefore, as observed in **Figure 2.6** by the disappearance of the target 90bp band and the emergence of non-specific product on these PAGE gels, there was evidence that the SELEX process was exhausted after a number of rounds of SELEX involving symmetric PCR. This can be attributed to the fact that the same sequences of oligonucleotides repeatedly undergo amplification (as discussed), complementary strand digestion

(exposing DNA to nuclease activity) and UV exposure during the agarose gel excision of the desired 90bp oligonucleotide band (known to have mutagenic effects on DNA, particularly on cytosine), as outlined in **Chapter 2.5.4.b.** Hence, steps must be taken to reduce repeated exposure to such treatments to ensure the longevity and integrity of the DNA.

2.5.3.b. Catalysing a hybridisation reaction for primer dimerisation and concatemerisation of primer sets and/or library template

Primer dimers, concatemers and oligonucleotide artefacts have been problematic as, despite best efforts, they re-emerge in subsequent rounds of PCR and SELEX (Tolle *et al*., 2014). A primer hybridisation study (**Figure 2.7**) can be used as an indication of emerging primer concatemers and oligonucleotide artefacts containing a sequence complementary to that of the primers formed through the non-specific hybridisation of primers and the library. These primer concatemers and primer complement-containing artefacts can be of approximately the same length of nucleotides as that of the target oligonucleotide length and thus are unavoidably co-excised during the gel excisions. Here, reverse and forward primers and dsDNA were amplified using a 25-cycle PCR reaction. This primer hybridisation study, shown in **Figure 2.7,** makes use of a portion of artefact-free dsDNA from a round of SELEX, as described in **Chapter 2.4.6.h**.

Migration of forward primer (Lane 3, **Figure 2.7**) was observably further than that of the reverse primer (Lane 2, **Figure 2.7**). One would expect that this differing migration pattern would be attributed to the difference in size between the two primers. However, as the forward primer has 21 nucleotides and the reverse primer has 20 nucleotides, this evidently cannot be true. Therefore, the observed migration patterns for the forward and reverse primers can be attributed to a sequence-specific migration of ssDNA, which is known to be more pronounced in boric acid-containing polyacrylamide gels (Biyani & Nishigaki, 2003) as used herein (see **Chapter 2.4.6.d**).

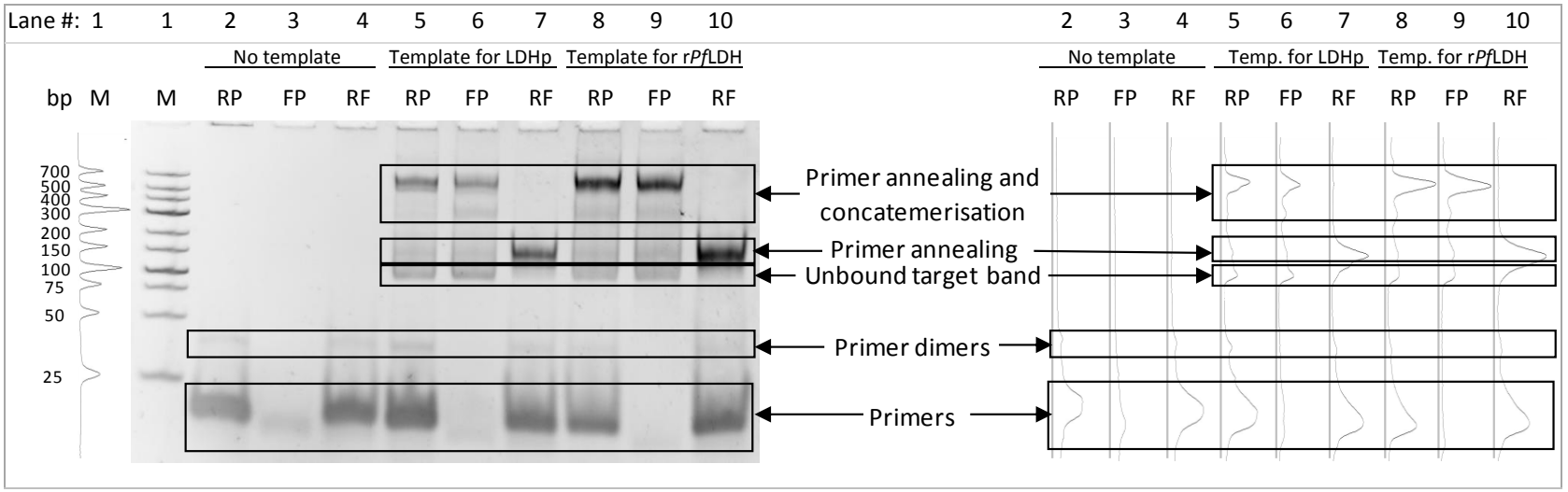

Figure 2.7: PAGE (10 %) of primer-hybridisation study using annealed primers (performed at 59 °C; no template; no amplification) and SELEX template dsDNA for LDHp and r*Pf*LDH following 25 PCR cycles (no anealing at 59 °C), with lane profiles.

RP: reverse primer; FP: forward primer; RF: reverse and forward primers.

Lane 1: DNA molecular mass marker (M); Lane 2: reverse primer only; Lane 3: forward primer only; Lane 4: reverse and forward primers; Lane 5: reverse primer with LDHp-specific oligonucleotides; Lane 6: forward primer with LDHp-specific oligonucleotides; Lane 7: forward and reverse primers with LDHp-specific oligonucleotides; Lane 8: reverse primer with rLDH-specific oligonucleotides; Lane 9: forward primer with rLDH-specific oligonucleotides; Lane 10: forward and reverse primers with rLDH-specific oligonucleotides.

A banding pattern emerged in Lanes 5, 6, 8 and 9 in **Figure 2.7** for the self-annealing forward and reverse primer concatemers indicating that they are steadily polymerizing, at the potential annealing sites shown in **Table 2.3**. Musheev and Krylov (2006) report that such artefacts arise from the use of poorly designed primers and library that have a tendency to self-anneal due to the presence of complementary regions on the forward and reverse primers. Since this primer study was conducted on an oligonucleotide "pool" consisting of a variety of sequences (10^{14} to 10^{18} different sequences) (Lakhin *et al*., 2013; Tolle *et al.*, 2014), primer-sequence complementation could not be done on those oligonucleotides selected for their respective targets (LDHp and r*Pf*LDH) during the SELEX process. The fact that the heterodimerisation and, to an extent, homodimerisation can occur between the forward and/or reverse primers, as seen by the solid lines between sequences in **Table 2.3**, is the basis for the observed banding seen in PAGE (**Figures 2.6** and **2.7**).

When the selected oligonucleotides were annealed with forward or reverse primers, laddering was created as demonstrated in Lanes 5, 6, 8 and 9 in **Figure 2.7**. This evidences that varying lengths of long chained reverse (Lanes 5 and 8) and forward (Lanes 6 and 9) primer concatemers annealed to the selected template oligonucleotides when included in the reaction mix. The afore-mentioned homodimers and heterodimers, thus, indiscriminately annealed to the flanking primers of the approximate 90 bp length of selected oligonucleotide for LDHp and r*Pf*LDH, creating an oligonucleotide length of approximately 130 – 135 bp, seen as the prominent band in Lanes 7 and 10 in **Figure 2.7**. Tolle and co-workers (2014) also reported the formation of such laddering as a result of the PCR amplification of multiple reverse primer clones in the absence and presence of a short-length ssDNA library. Lu (2014) demonstrated that similar laddering was observed when short ssDNA oligonucleotides were hybridised at 37 °C for 10 minutes; however, they measured the propensity of the short ssDNA to anneal in the presence and absence of zinc (Zn^{2+}). Therefore, with further evidence shown in the literature, the formation of primer dimers and oligonucleotide concatemers was determined as hybridisation will occur during and throughout the PCR amplification cycling. Given that the PCR technique is well-established, it can be expected that the hybridisation seen in **Figure 2.7** would in effect be nullified through the denaturation step of PCR. However, in the case of the SELEX for LDHp and r*Pf*LDH, these PCR by-products re-emerged and were a recurring problem in the enrichment of target-binding oligonucleotides.

2.5.3.c. Establishing the primer hybridisation reaction

To establish where possible complementation would occur between primers, a primer dimer analysis of forward and reverse complementation was performed using the online tool, Oligoanalyser 3.1 (https://eu.idtdna.com/analyzer/Applications/OligoAnalyzer). This tool provides probability of where complementation could occur by providing the user with sequence alignments, as well as the strength of these interactions by providing the Gibb's Free Energy (ΔG in kcal/mole). Only those dimers with the maximum ΔG (kcal/mole) measured at 59 ^{o}C were included in **Table 2.3** as these structures and values refer to the free energy for the ideal complementation of the primer sequence.

Table 2.3: Expected sites of complementation between hetero-and homodimers of primers (from Chapter 2.4.6.b.), and the corresponding Gibb's Free Energy at 59 ^{o}C for primer dimerisation using OligoAnalyzer 3.1.
(https://eu.idtdna.com/analyzer/Applications/OligoAnalyzer)
| indicates a strong bind interaction and : indicates a weak binding interation

	Primer	Complementation	ΔG (kcal/mole)
a	Forward primer homodimer	5' GCCTGTTGTGAGCCTCCTAAC ||| ::: ::: ::: ::: 3' CAATCCTCCGAGTGTTGTCCG	-3.29
b	Reverse primer homodimer	5' GGGAGACAAGAATAAGCATG |||| 3' GTACGAATAAGAACAGAGGG	-5.38
c	Forward and reverse heterodimers	5' GCCTGTTGTGAGCCTCCTAAC :: : : |||| 3' GTACGAATAAGAACAGAGGG	-6.24
d		5' GCCTGTTGTGAGCCTCCTAA || 3' GTACGAATAAGAACAGAGGG	-3.07
e	Forward and reverse complement heterodimer	5' GCCTGTTGTGAGCCTCCTAAC : : : ||| : 3' CCCTCTGTTCTTATTCGTAC	-4.74
f	Forward complement and reverse heterodimer	5' GGGAGACAAGAATAAGCATG ||| 3' GTTAGAGGCTCACAACAGGC	-3.90

Upon annealing at 59 ^{o}C, reverse primers annealed to one another forming a homodimer producing a band 38 – 44 basepairs in length on PAGE (**Figure 2.7**). The most probable complementation that arises from this pairing is shown in **Table 2.3b** as the reverse primer homodimer with a ΔG of -5.38 kcal/mole, indicating a strong complementation. Complementation of the forward and reverse primer mixture (Lanes 4, 7 and 10 in **Figure 2.7**) lead to primer dimerisation of reverse primer homodimer complementation. Concomitantly, heterodimerisation with a ΔG of -6.24 kcal/mole (**Table 2.3c**) also resulted; however, the length of this complemented oligonucleotide was similar to

that of un-annealed primers (20 – 21 nucleotides) thereby masking development of another band on PAGE (**Figure 2.7**) indicating a length of 23 basepairs. Homodimersation also occurred with the forward primer (**Table 2.3a**); however, this interaction is weaker than the reverse primer homodimer and heterodimer with a ΔG of -3.29 kcal/mole. As for the heterodimers (Lane 4, **Figure 2.7**), banding was similar to that seen for the reverse primer dimer indicating that dimerisation primarily resulted from reverse primer complementation, as well as forward and reverse heterodimerisation, given that the reverse primer homodimer and the forward and reverse heterodimers exhibited ΔG of -5.38 kcal/mole and -6.24 kcal/mole, respectively, indicative of strong interactions. This has been shown to occur when primers are in excess or insufficient template DNA is present (Musheev & Krylov, 2006).

Secondary structures of primer homodimers and heterodimers generated using MFold (http://mfold.rna.albany.edu/?q=mfold/dna-folding-form; Zuker, 2003) are shown in **Figure 2.8**, specifically the forward homodimers (a), reverse homodimers (b), forward primer to the reverse primer (c) and forward primer to the complement of the reverse primer (d).

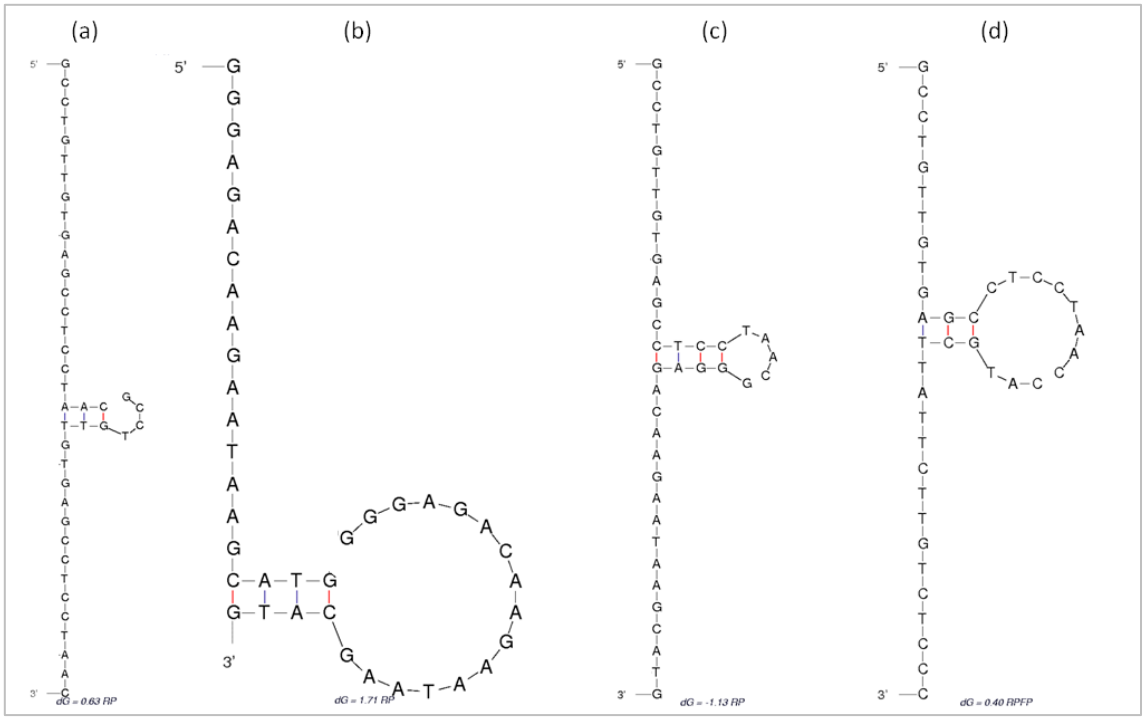

Figure 2.8: Secondary structure prediction of forward homodimers (a), reverse homodimers (b), forward to reverse heterodimer (c) and forward to reverse complement heterodimer (d) of primers in Chapter 2.4.6.b.
Images generated using MFold (http://mfold.rna.albany.edu/?q=mfold/dna-folding-form; Zuker, 2003)

Heterodimerisation (**Figure 2.8c, d**) between the forward primer and the reverse complement region (as would appear in the library and all generated oligonucleotide sequences) also annealed with an overlap of 1 to 2 nucleotides on either side of the binding moiety, seen in **Table 2.3**. This heterodimerisation, and the observed lengths that increase incrementally by approximately 20 bp, rendering the laddering observed in **Figures 2.6** and **2.7,** demonstrate that these primers are likely to build up on a unit-by-unit basis, increasing by one primer length as the forward strand is exponentially amplified, with a length of heterogeneity in between each primer run. The given concatemer sequence (5'-GCCTGTTGTGAGCCTCCTAACACTTTGCACATGCTTATTCTTGTCTCCCATGCCTG TTGTGAGCCTCCTAACCTCATGCTTATTCTTGTCTCCC-3') which is used in later analyses, and further discussed in this Chapter, empirically demonstrates that this is physically feasible. Moreover, observed laddering of the bands on PAGE (**Figures 2.6** and **2.7**) indicate that this is indeed the case. Furthermore, Tolle and co-workers (2014) also demonstrate this laddering effect with this same set of primers. **Figure 2.8** shows that secondary structures are possible within the annealed heterodimer primer sequences and, as *Taq* polymerase has no proof-reading activity, amplification anomalies, such as repeated motifs and sequence jumps, may result (Lawyer *et al*., 1993). These anomalies will limit the diversity of the pool of oligonucleotide sequences as a known error will be repeated, but more likely hinder amplification of desired PCR products (Tolle *et al*., 2014), as was the case, as unwanted additional primer lengths will indiscriminately anneal to the flanking regions of the 90 bp oligonucleotides resulting in over-amplification.

Identifying the primer hybridisation reaction using ssDNA library template

The different modes of primer dimerisation shown in **Table 2.3** and **Figures 2.6, 2.7** and **2.8** infer the likelihood that variable regions will differ in length between the flanking primer regions; and, further, that concatemerised sequences of target length will differ in their forward and/or reverse primer composition and configuration. Known primer dimers as well as ssDNA library were amplified for an extended number of cycles to comparatively ascertain the effect of primer and library template hybridisation on banding, particularly on the 90 bp target band (**Figure 2.9**).

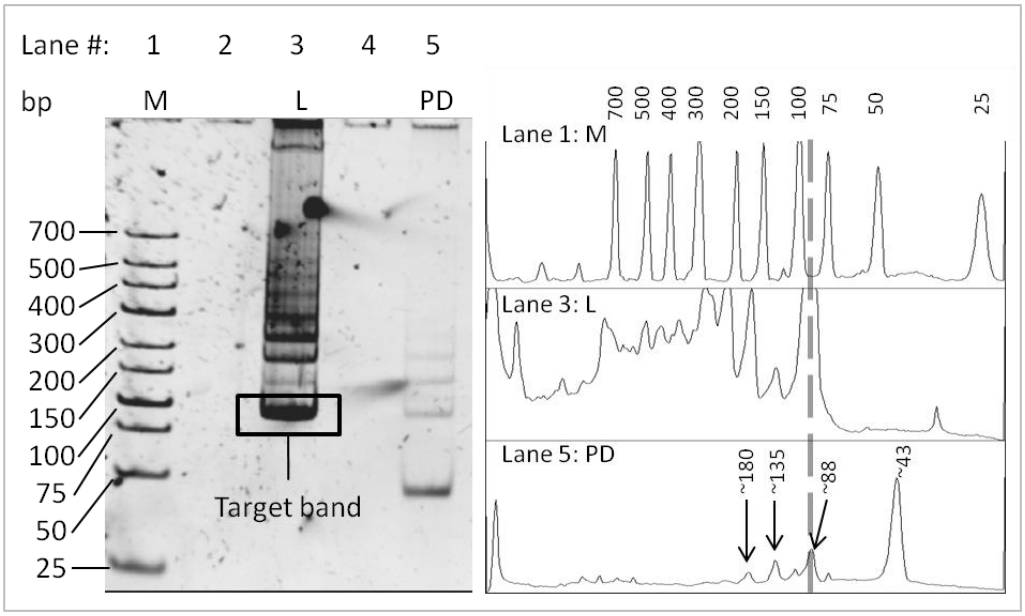

Figure 2.9: PAGE (10 %) of non-specifically amplified library (L) and primer-dimer(PD) dsDNA following 25 PCR cycles (left panel), with lane profiles (right panel).
Lane 1: DNA molecular mass marker (M); Lane 3: amplified library DNA (L); Lane 5: amplified primer dimer (PD); dashed line in the right panel indicates locale of 90 bp target band.

Figure 2.9 demonstrates that the amplified library and primer dimer banding exhibited similar band laddering of equal proportion indicating that the same primer dimerisation and concatemerisation occurred here and as previously seen in **Figures 2.6, 2.7,** and **2.8**. Furthermore, absence of dsDNA bands of approximately 60 and 100 bp in Lane 5 of non-specifically amplified primer-dimer dsDNA are indicative of the monomeric building of primers onto each of the flanking primer regions found on the library sequence. The banding showing 20 bp incremental increases in dsDNA length seen in the lane profiles (**Figure 2.9**) is indicative of primers increasing in proportionate length forming larger concatemers. Therefore, the non-specific annealing of primers to the template appear to be directly involved in the observed laddering. The peak indicative of dsDNA at 88 bp in Lane 5 (bottom lane profile, right panel, **Figure 2.9**) was of concern due to its likely co-localization with the 90 bp band (indicated by dashed line in right panel in **Figure 2.9**) following PCR. This 88 bp length of dsDNA would consistently appear as a PCR artefact during the amplification step in SELEX, co-concentrated during column purification, and most likely co-excised during an agarose gel excision, thereby reducing fidelity in the pool of oligonucleotides. Theoretically, it remains unlikely that these primer concatemers would bind to the target proteins with their removal occurring during the selection step of SELEX. However, evidence of library concatemers and primer dimers present in the oligonucleotide pool generated during SELEX was shown and is discussed in **Chapter 2.5.3.d** and **Chapter 3**.

2.5.3.d. Primer dimer and concatemer products of primer sets and/or library template

Library concatemers and primer dimers present in the oligonucleotide pool generated did occur in the SELEX process (**Table A.2** in **Appendix A**). **Table 2.4** shows the different representative concatemers that were obtained using this same primer set and library obtained from an overamplified ssDNA pool. **Figure 2.2** by Tolle and co-workers (2014) illustrates the formation of such anomalous PCR by-products.

Table 2.4: Clones with different classes of primer concatemers obtained from previous SELEX targeting LDHp and r*Pf*LDH.

Blue text: forward primer, green text: reverse primer, red text overlapping nucleotides, black text: variable region

Forward primer: GCCTGTTGTGAGCCTCCTAAC
Forward primer complement: CGGACAACACTCGGAGATTG
Reverse primer: CATGCTTATTCTTGTCTCCC
Reverse primer complement: GGGAGACAAGAATAAGCATG
Sequence with primer dimer: Example: LDHp 23 (Table A.2) GCCTGTTGTGAGCCTTCCTAACCCCATGCTTATTCTTGTCTCCC
Sequence with forward and reverse primer: Example: LDHp 2 (Table A.2) GCCTGTTGTGAGCCTCCTAACATGCTTATTCTTGTCTCCCTTGCCTGTTGTGAGCCTCCTAACCCC ATGCTTATTCTTGTCTCCC
Sequence with forward and reverse primer, and short variable region: Example: rLDH 5 (Table A.2) GCCTGTTGTGAGCCTCCTAACATGCTTATTCTTGTCTCCCGCGCCTGTTGTGAGCCTCCTAACAC TTTGCACATGCTTATTCTTGTCTCCC
Sequence with forward and multiple reverse primers: Example: LDHp 16 (Table A.2) GCCTGTTGTGAGCCTCCTAACCCCATGCTTATTCTTGTCTCCCATGCTTATTCTTGTCTCCCATGC TTATTCTTGTCTCCCATGCTTATTCTTGTCTCCCATGCTTATTCTTGTCTCCC
Sequence with multiple forward and reverse primers (ordered): Example: LDHp 41 (Table A.2) GCCTGTTGTGAGCCTCCTAACCCCATGCTTATTCTTGTCTCCCATGCCTGTTGTGAGCCTCCTAAC CCCATGCTTATTCTTGTCTCCCGTGCCTGTTGTGAGCCTCCTAACATGCTTATTCTTGTCTCCC
Sequence with multiple forward and reverse primers (unordered): Example: LDHp 25 (Table A.2) GCCTGTTGTGAGCCTCCTAACCCCATGCTTATTCTTGTCTCCCATGCTTATTCTTGTCTCCCGTGC CTGTTGTGAGCCTCCTAACCCCATGCTTATTCTTGTCTCCC Example: rLDH 28 (Table A.2) GCCTGTTGTGAGCCTCCTAACATGCTTATTCTTGTCTCCCATGCTTATTCTTGTCTCCCATGCTTA TTCTTGTCTCCCATGCCTGTTGTGAGCCTCCTAACATGCTTATTCTTGTCTCCC

DNA sequences generated during SELEX, capable of binding to r*Pf*LDH and LDHp, asserted that primer dimerisation and primer/template concatemerisation did indeed occur (**Table 2.4**), and that fusion of these lengths of DNA were primarily primer-based. The formation of concatemers with primers sets that have fused together, or with a variable region of merely two nucleotides, accounts for the laddering pattern seen in **Figures 2.6** and **2.9**, and to some extent **Figure 2.7** too, as primers are seen to fuse together and monomerically build to yield the sequences shown in **Table 2.4**. This creates concatemers that are in multiples of approximately 20 bp or 40 bp– the mean length of the forward and reverse primer, and is in agreement with bioinformatic analyses presented in **Table 2.3** and **Figure 2.8**. Tolle and co-workers (2014) demonstrate this exact same occurrence of primer concatemerisation in which full-length primers fuse to each other creating longer lengths of oligonucleotides. Their presence could be explained as the target dsDNA of 90 bp underwent a number of agarose gel excision procedures experienced by the over-amplified pools of ssDNA, the excised gel slices inherently contained the amplified concatemers shown in **Table 2.4**, owing to their similarity in length to the target 90 bp DNA. From **Table 2.4** and **Table A.2**, there is evidence that the favoured conformation of primers in the concatemers appears to be one in which the forward and reverse primers, both in the forward direction, alternate creating a forward-reverse-forward-reverse primer hybrid. Furthermore, the emergence of these concatemers could have occurred in the final PCR of SELEX, prior to ligation into the PGEM-T vector.

Therefore, this evidence shows that primer dimer and concatemer artefacts can easily be produced during the PCR amplification process. Long primer sequences and poor primer design of the primers used from literature (Drabovich & Krylov, 2004; Musheev & Krylov, 2006; Avci-Adali *et al*., 2010; Rotherham *et al*., 2012; Tolle *et al.*, 2014) can be attributed to this. Despite the challenges faced with primer design and formation of primer dimer and concatemer artefacts during PCR amplification, there are indeed further optimisations in the PCR amplification protocol that are require to ensure generation of sufficient and suitable target-binding oligonucleotides in the PCR amplification – Stage 2 – of the SELEX process.

2.5.4. Optimisation of PCR amplification parameters in the isolation of aptamers against recombinant PfLDH and PfLDH-specific peptide

2.5.4.a. Exploring the use of Triton X and annealing temperature to lower amplification artifact formation

To address the concern over insufficiently-amplified 90 basepair PCR product during the PCR optimisation step, PCR products when amplified in the presence and absence of a non-ionic detergent (Triton-X) were compared (**Figure 2.10**). Simultaneously, a range of annealing temperatures was studied based initially on the primers' melting temperature (T_m) (**Figure 2.10**).

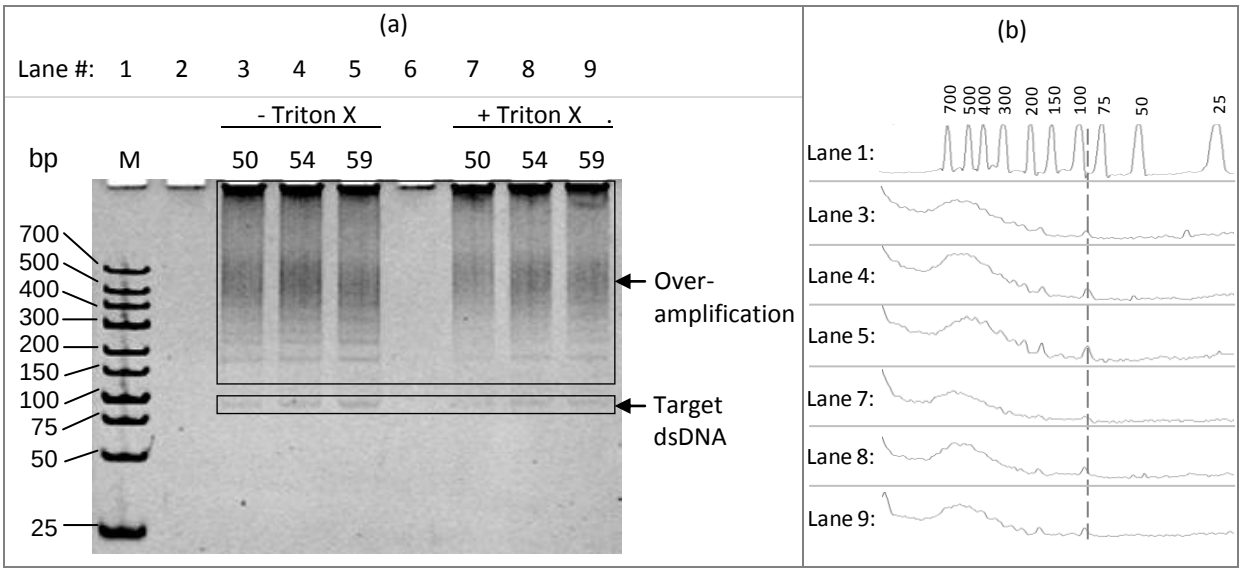

Figure 2.10: PAGE (10 %) of (a) over-amplified dsDNA oligonucleotides, with lane profiles; and (b) during PCR optimization of annealing temperature and presence and absence of 0.01 % Triton-X.
Lane 1: DNA molecular mass marker (M); Lane 3-5: Absence of Triton-X; Lane 7-9: Presence of Triton-X; Lane 3 & 7: Annealing temperature = 50 ^{o}C; Lane 4 & 8: Annealing temperature = 54 ^{o}C, Lane 5 & 9: Annealing temperature = 59 ^{o}C. Dashed line in (b) indicates locale of 90bp target-binding oligonucleotide band.

The relative intensities of the bands of the target-binding dsDNA and the high molecular weight smear, or over-amplification, were calculated using FIJI v1.5e and are shown in **Table 2.5**, in which a relative response unit (RRU) of 0 (zero) is indicative of the absence of DNA and an RRU of 1 (one) is indicative of DNA saturation on the polyacrylamide gel.

Table 2.5: The relative intensities in relative response units (RRU) of the target-binding dsDNA and over-amplification on PAGE shown in Figure 2.10, determined using FIJI v1.5e.

	Annealing Temp (^{o}C)	Absence of Triton X (RRU)	Presence of Triton X (RRU)
Target dsDNA	50	0.056 ± 0.014	0.040 ± 0.020
	54	0.071 ± 0.012	0.086 ± 0.017
	59	0.100 ± 0.018	0.093 ± 0.014
Over-amplification	50	0.268 ± 0.165	0.205 ± 0.172
	54	0.295 ± 0.167	0.233 ± 0.169
	59	0.264 ± 0.151	0.234 ± 0.158

Note: RRU given as mean number of light pixels in designated area ± the intrinsic error calculated by FIJI, and is not a statistically calculated error.

As shown in lanes 7, 8 and 9 in **Figure 2.10**, the addition of Triton X did not result in a definitive increase in the amplification yield of the desired dsDNA of 90bp. Furthermore, **Table 2.5** shows that the mean RRU for target dsDNA bands in the absence and presence of Triton X for the respective annealing temperatures are similar. The use of Triton X was proposed, given that addition of non-ionic detergents to a PCR reaction mixture enhances *Taq* polymerase activity (Innis *et al*., 1988; Varadaraj & Skinner, 1994; Kang *et al*., 2005). Additionally, Triton X is believed to prevent: 1) formation of secondary structures during amplification that may interfere with amplification; and, 2) DNA polymerase from self-conjugating, thus stabilising the enzyme (Bachmann *et al*., 1990). Given this, it was interesting to note in **Table 2.5** that the presence of Triton X resulted in an overall decreased RRU across all annealing temperatures analysed; and, therefore, indicates that the presence of Triton X in the PCR reaction mix results in a lowered dsDNA yield.

Simultaneously, to prevent over-amplification seen as a high-molecular-weight smear also seen in lanes 3, 4, 5, 7, 8 and 9 in **Figure 2.10**, a range of annealing temperatures was studied based initially on the primers melting temperature (T_m). This was investigated since less primer dimerisation and non-specific template binding would be expected to occur by changing the annealing temperature (Ishii & Fukui, 2001; Roux, 2009). Annealing temperatures included the prescribed temperature of 54 ^{o}C (lanes 4 and 8), a lower temperature of 50 ^{o}C (lanes 3 and 7) and a higher temperature of 59 ^{o}C (lanes 5 and 9). **Figure 2.10** and, more so, **Table 2.5** show that an increase in band intensity of the target dsDNA was seen with an increase in annealing temperature both in the presence and absence of Triton X indicating a greater presence of dsDNA, with the greatest relative response of 0.100 ± 0.018 RRU observed for the annealing temperature of 59 ^{o}C in the absence of Triton X.

Therefore, the absence of Triton X with an annealing temperature of 59 ^{o}C was considered optimal for PCR amplification in this study.

2.5.4.b. Removal of undesired amplification artefacts following PCR amplification

Two physical methods of removing unwanted lengths of dsDNA following PCR amplification were utilised during this SELEX process to ensure a more purified dsDNA template. These included 1) diluting the PCR clean-up kit binding buffer (**Figure 2.11**); and, 2) the inclusion of a gel excision from agarose (**Figure 2.12**) to remove any primer artefacts, namely primer dimers and concatemers.

Dilution of the binding buffer of the PCR Clean-up kit as a means of removing undesired PCR amplification artefacts

The removal of unwanted DNA fragments through diluting the NT binding buffer of the Nucleospin® Gel and PCR clean-up kit (Macherey-Nagel GmbH & Co. KG, Germany) was carried out according to the manufacturer's product manual (available at http://www.mnnet.com/Portals/8/attachments/Redakteure_Bio/Protocols/DNA%20clean-up/UM_PCRcleanup_Gelex_NSGelPCR.pdf). As per the manufacturer's guidelines, the over-amplified DNA was retained in the binding column and the desired shorter oligonucleotides were eluted into the capture vessel. The aim was such that the fraction containing the shorter oligonucleotides would then be re-amplified thereby limiting the degree of over-amplification. Based on the Nucleospin® Gel and PCR clean-up kit (Macherey-Nagel GmbH & Co. KG) guidelines, a binding buffer dilution of 1:5.5 NT binding buffer to distilled sterile water was used facilitating a cut-off of approximately 150 basepairs. This dilution would ideally ensure that all oligonucleotides of 100 bp and lower would be eluted from the binding column but saved in the capture vessel, thereby limiting the amount of over-amplified products that are co-eluted with the dsDNA in the PCR clean-up and concentration (as per the Macherey-Nagel GmbH & Co. KG product manual).

Figure 2.11 shows the PAGE-resolved banding pattern of the concentrated rLDH- and LDHp-binding PCR-amplified SELEX dsDNA and, as a test sample, the LDHp-binding dsDNA fractions to be retained in the binding column (>150) and the fraction that was eluted but saved in the capture vessel (<150), following the 1:5.5 NT buffer:water rinse step.

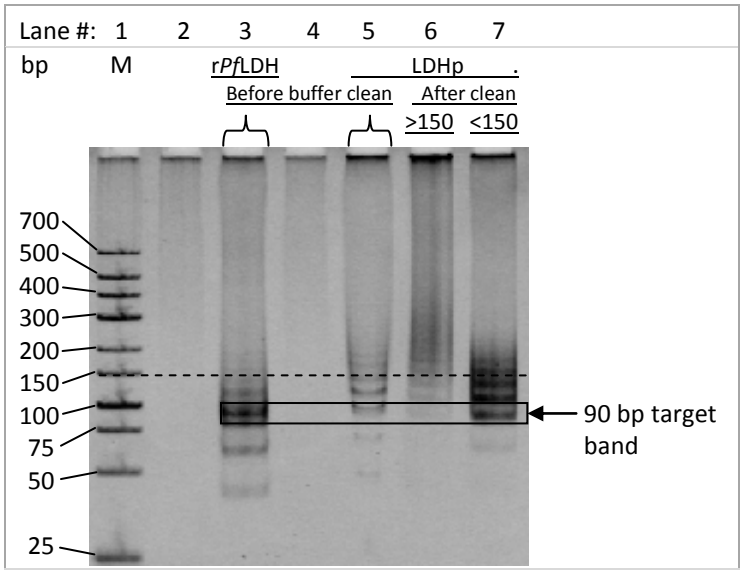

Figure 2.11: PAGE (10 %) of over-amplified and concatemerised LDHp- and r*Pf*LDH-binding dsDNA oligonucleotide fractions before and after separation, and subsequent concentration, with the 1:5.5 binding buffer:water PCR clean-up kit.

Lane 1: DNA molecular mass marker (M); Lane 3: concentrated rLDH-binding dsDNA after PCR; Lane 5: concentrated LDHp-binding dsDNA after PCR; Lane 6: captured LDHp-binding dsDNA above 150 basepairs in length; Lane 7: effluent of LDHp-binding dsDNA less than 150 basepairs in length

Comparing lanes 6 and 7 (**Figure 2.11**), the 1:5.5 NT buffer to water rinse separated the dsDNA lengths that were longer than 150 basepairs from those less than 164 bp with some degree of overlap. This is evidenced by the high molecular weight smearing seen more prominently in lane 6 (>150 bp) compared to in lane 7 (<150 bp). However, both lanes contained dsDNA artefacts of approximately 90 to 200 bp in length – and around the cut-off length of 150 bp – indicating that separation of lengths of dsDNA is not clearly defined. Furthermore, as shown in lanes 6 and 7 (**Figure 2.11**), target 90 bp LDHp-binding dsDNA can be seen in both the >150 (lane 6) and <150 bp (lane 7) fractions following the 1:5.5 NT buffer to water rinse. These two fractions contained differing proportions of the 90 bp length of dsDNA given the differing intensities of the 90 bp bands, and not complete removal of this particular length of dsDNA. Even though there was separation of some of the extended lengths of dsDNA, lengths of dsDNA from approximately 90 to 200 bp were present in both fractions that were retained in the column and those present in the effluent, resulting in an incomplete separation of the lower lengths of dsDNA from the dsDNA pool. Furthermore, a lower dilution could not be used as this would introduce additional dsDNA artefacts, such as primer dimers.

Therefore, diluting the NT binding buffer alone during the PCR clean-up step was insufficient in removing unwanted artefacts from the PCR product mix; hence, the need for gel excision of the

target 90 bp oligonucleotides. Also, diluting the NT binding buffer in the process of concentrating the target-binding PCR product as a means of removing undesired PCR artefacts may be better suited to separation of PCR artefacts that vastly differ in size and thus distribution within a given lane in a resolving gel.

Agarose gel excision of the target-binding dsDNA

Purification and amplification products by gel excision remains the most generally accepted method of removing superfluous by-products in PCR amplification of the 90 bp target-binding dsDNA (Sun *et al*., 2012). **Figure 2.12** is a PAGE analysis of the expected over-amplification and primer artefacts that would have similarly been seen on a 2.5 % agarose gel (although some difference in the resolution of banding can be expected between PAGE and agarose gels given the different principles in how DNA is resolved). Also shown in this figure is the location of the gel excision slice taken in the purification of the 90 bp target-binding dsDNA, indicated by a dotted red box.

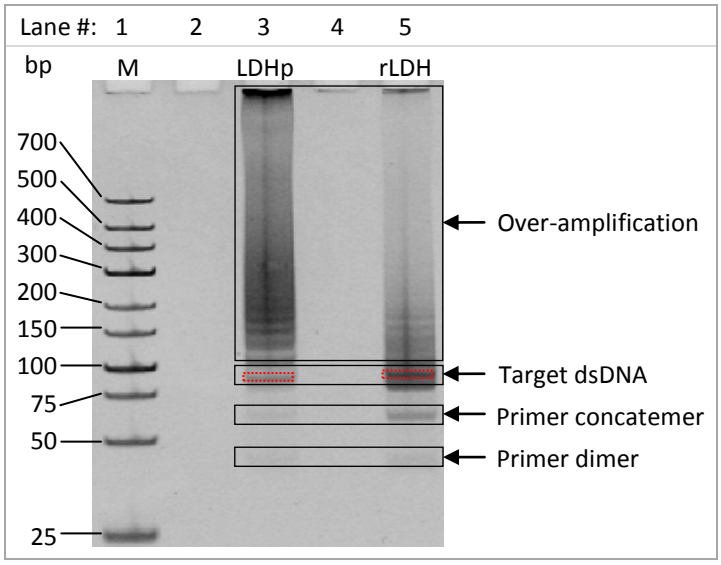

Figure 2.12: PAGE (10 %) of target-binding dsDNA, over-amplified and concatemerised dsDNA oligonucleotides against the LDHp and rLDH targets following PCR.
Dotted boxes indicate where the gel slice was excised.
Lane 1: DNA molecular mass marker (M); Lane 3: LDHp-targeted dsDNA; Lane 5: rLDH-targeted dsDNA.

The target-binding dsDNA band of approximately 90 basepairs in length, labelled in **Figure 2.12**, was carefully excised (**Chapter 2.4.6.f.ii**) and amplified (**Chapter 2.4.6.a-e**). Agarose gel excision proved to be the only certain method by which to remove any and all undesired artefacts that were in the PCR sample as only the excised dsDNA was taken further in subsequent purification, concentration

and further amplifications. The major disadvantage of agarose gel excision was the loss of a large mass of the desired dsDNA length in the cleaning process, as well as in the DNA mass of the entire sample. Initial mass quantities of dsDNA following PCR and prior to agarose gel excision were upwards of 10 µg; however, following the agarose gel excision, the final yields of artefact-free 90-bp target-binding dsDNA averaged around 200 ± 73 ng. This 98 % loss indicated a significant removal of the amplified DNA, presumed to contain significant amounts of DNA, specifically superfluous amplification by-products and artefacts. To obtain the required yields of DNA for further SELEX rounds, further PCR optimisation and amplification was therefore required to obtain the required amounts of artefact-free 90-bp dsDNA to proceed with SELEX. However, and as Kalle and co-workers (2013) report, the primer dimers and concatemers (PCR by-products) were re-created in each round of PCR given the heterogonous, multi-sequence nature of the template dsDNA. This is despite the target-binding oligonucleotide pool sequence enrichment that one expects in later rounds of SELEX. Tominimise this effect, gel excision was performed in each round of SELEX, but only on alternating rounds of PCR. Following this, in all PCR amplification steps, the use of agarose gel excision combined with the binding buffer dilution method proved adequate in creating the required quantity of clean and artefact-free dsDNA.

With the PCR amplification parameters optimised for, whilst eliminating the occurrence of primer concatemers, oligonucleotides of approximately 90kb in size capable of binding to the protein targets, LDHp and rPfLDH, can be generated.

2.5.5. Generation of target dsDNA through PCR amplification at the end of Stage 2 of SELEX

After cyclic rounds of optimised PCR (**Chapter 2.5.3.a**), PCR clean-up incorporating an NT buffer dilution and precision gel excision of the excised dsDNA (**Chapter 2.5.4.b**) of approximately 90 bp in length, a mass of at least 4.5 µg of artefact-free dsDNA was sufficiently produced for exonuclease digestion and/or cloning. A PAGE of the amplified and excised dsDNA was sampled on PAGE (**Figure 2.13**).

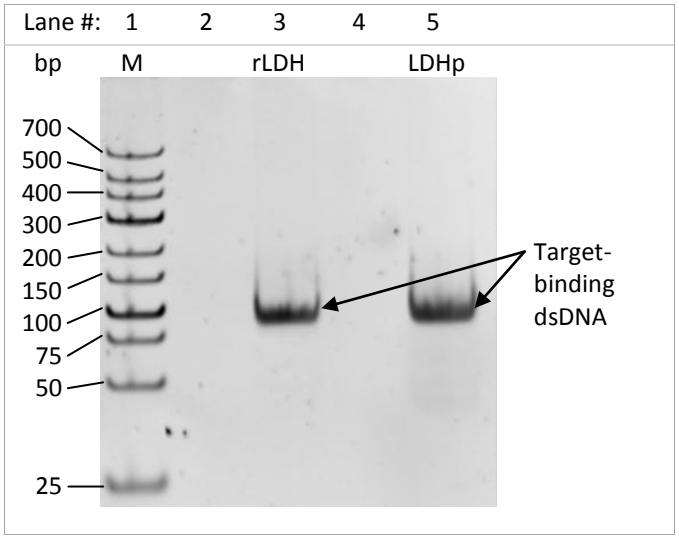

Figure 2.13: PAGE (10 %) of dsDNA after the final round of SELEX for r*Pf*LDH and LDHp.
Lane 1: DNA molecular mass marker (M); Lane 2: rLDH dsDNA; Lane 3: LDHp dsDNA

Amplified and excised dsDNA was sampled on PAGE to ascertain the quality of dsDNA prior to exonuclease digestion and/or cloning to ensure that undesired PCR artefacts were not carried over through to the exonuclease digestion and/or cloning stage as these by-products could result in false-positive binding and be mistaken as target-binding oligonucleotides.

Once at least 4.5 µg artefact-free dsDNA, quantified using UV-Vis and assessed on PAGE (**Figure 2.13),** had resulted from PCR amplification, , the round of SELEX could proceed to the next step: lambda exonuclease digestion.

2.5.6. Stage 3 of SELEX: Exonuclease digestion of target-binding dsDNA to ssDNA

Lambda exonuclease digestion was required for digestion of the 5'-phosphorylated complementary DNA strand in a 5' to 3' direction, thus regenerating ssDNA from dsDNA (Avci-Adali *et al*., 2010). Ninety-basepair target-binding dsDNA free of primer dimers, primer oligomers and product-product oligomers was required for exonuclease digestion to prevent introduction of anomalous oligonucleotides capable of binding the target proteins during selection (Pan *et al*., 2008). **Figure 2.14** demonstrates the observed difference in migration between the concentrated PCR-amplified dsDNA and ssDNA following exonuclease digestion.

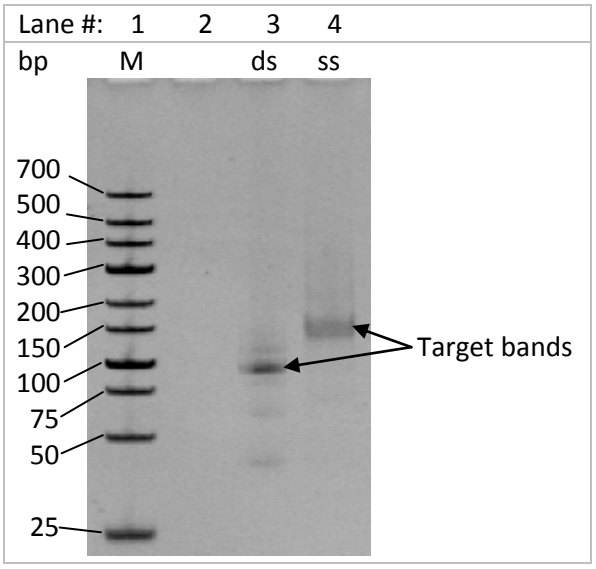

Figure 2.14: PAGE (10 %) of dsDNA and ssDNA during a round of SELEX.
Lane 1: DNA molecular mass marker (M); Lane 3: dsDNA; Lane 4: ssDNA

As shown in **Figure 2.14**, ssDNA (Lane 4) migration on PAGE was slower than that of dsDNA (Lane 3) evidenced by the differing migration patterns of dsDNA and ssDNA. As per general PAGE principles, this can be accounted for by the nucleotide composition and absence of negatively charged antisense strand of ssDNA lessening the net negative charge of the ssDNA slowing migration during PAGE (**Figure 2.14**) (Stellwagen & Stellwagen, 2009). Furthermore, ssDNA is less constrained than dsDNA and therefore inherently more flexible and can more readily take on secondary structures that hinder migration through PAGE (Maniaits *et al*., 1975; Stellwagen & Stellwagen, 2009). Additional banding of approximately 40 and 60 bp observed in Lane 3 of **Figure 2.14** for dsDNA were non-specifically digested by the exonuclease enzyme, as has been previously reported by Avci-Adali and co-workers (2010), resulting in ssDNA free of contaminating oligonucleotide artefacts. However, a limiting effect of this non-specific digesting of dsDNA was a substantial loss in ssDNA – valuable ssDNA necessary for a competent Selection.

Successful achievement of this ssDNA free from undesirable contaminating oligonucleotide artefacts for selection against LDHp and r*Pf*LDH is presented in **Figure 2.15**.

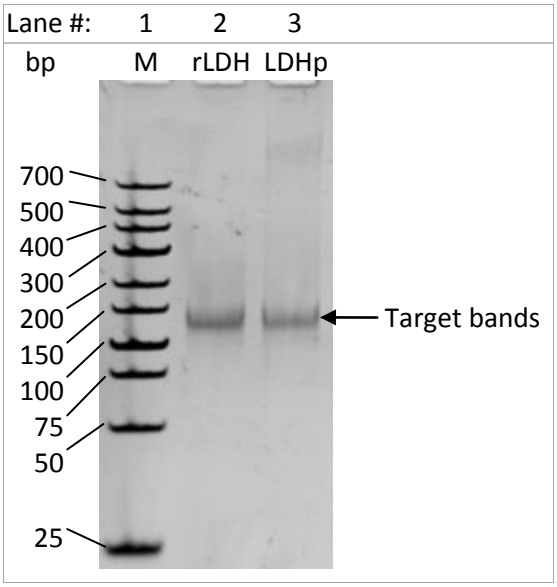

Figure 2.15: PAGE (10 %) of ssDNA during the final round of SELEX for r*Pf*LDH and LDHp.
Lane 1: DNA molecular mass marker (M); Lane 2: rLDH ssDNA; Lane 3: LDHp ssDNA

This artefact-free ssDNA (**Figure 2.15**) was achieved following exonuclease digestion; is representative of the ideal ssDNA which was sought in all of the eight rounds of SELEX; and, was subsequently used in Stage 1 of SELEX, Selection, in the subsequent round of SELEX (as per the SELEX cycle depicted in **Figure 2.1**).

2.5.7. SELEX of recombinant PfLDH and PfLDH-specific peptide

2.5.7.a. Overview of SELEX performed for rPfLDH and LDHp

An exonuclease-based SELEX (**Figure 2.1**) targeting recombinant *Pf*LDH (r*Pf*LDH) and *Pf*LDH peptide (LDHp) incorporating PCR amplification optimisations outlined in **Chapter 2.5.3** and **Chapter 2.5.4** were performed in parallel. **Figure 2.16** is a schematic of the SELEX process performed for the generation of r*Pf*LDH- and LDHp-binding oligonucleotides discussed herein, showing the deviations from the standard linear SELEX procedure discussed below.

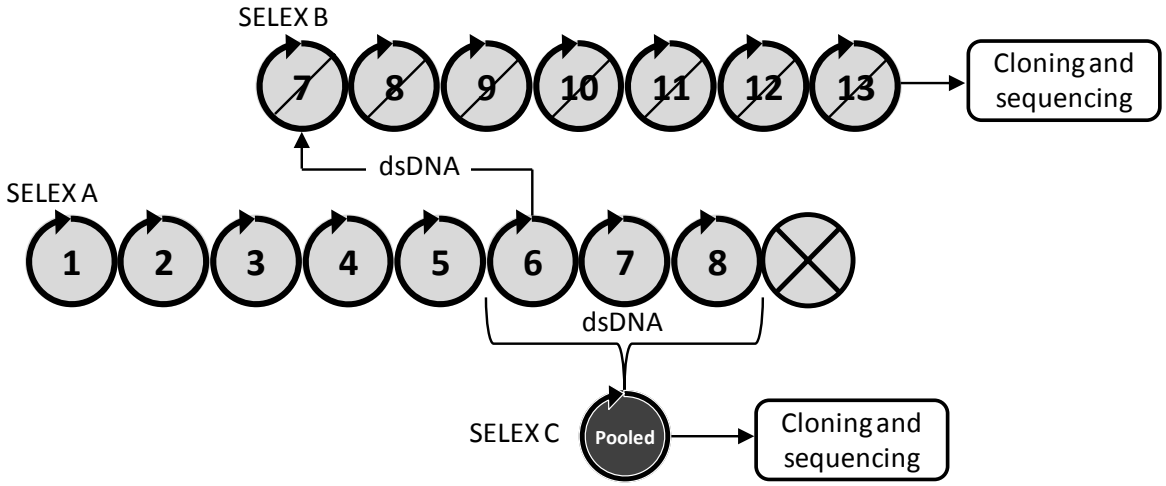

Figure 2.16: Schematic representation of SELEX pathway performed in the generation of r*Pf*LDH and LDHp-binding oligonucleotides.

Eight traditional rounds of SELEX were performed (SELEX A, **Figure 2.16**). As dsDNA stored from Rounds six through to eight were combined, the final ninth selection was dubbed "pooled". Pooling of the last three rounds of SELEX was performed in order to enrich the sequence diversity. Whilst performing SELEX for r*Pf*LDH and LDHp in SELEX A, a complete loss of dsDNA occurred during the PCR amplification in Round 8, indicated by the circle and cross on **Figure 2.16**. This loss of target-binding dsDNA likely resulted from the over-production of undesired PCR by-products and extended lengths of dsDNA resulting from product-product hybridisation, nullifying amplification of the shorter 90 bp target oligonucleotides (Tolle *et al.*, 2014). This loss of DNA resulted in the need to return to Round 6, and repeat the selection step for Round 7 using the preserved aliquot of dsDNA from Round 6 and diverged to SELEX B (**Figure 2.16**). Of those 35 clones that were sequenced in SELEX B, only one contained a variable region, and was taken further and dubbed rLDH 7. (Preliminary binding analysis of rLDH 7 is shown in **Chapter 2.5.8**) From this point, SELEX diverged from the original path of cyclic SELEX rounds as DNA from Rounds 6, 7 and 8 were preserved for possible use at a later stage.

Following cloning and sequencing of oligonucleotides after the 13th round of SELEX B, sequences were returned predominantly consisting of primer concatemers, as shown in **Table 2.5**, created during SELEX B. Thus, SELEX B is represented in **Figure 2.16** with the round cycle symbols with the strike-through indicating that oligonucleotide products of no practical use came from this SELEX. The emergence of these primer concatemers was discussed in **Chapter 2.5.3**. Upon analysis of the sequences returned following SELEX B, SELEX A was revisited (**Figure 2.16)**. This entailed the pooling

of Rounds 6, 7 and 8 from SELEX A, and another round of selection (the resurgence of SELEX C, **Figure 2.16**) to retrieve r*Pf*LDH- and LDHp-binding oligonucleotides. Lakhin and co-workers (2013) and Spill and co-workers (2016) provide some discussion pertaining to problems and uncertainties faced in aptamer synthesis in general; however, there is scant literature on retracing and repeating rounds of SELEX and the effect on the final target-binding oligonucleotides. Mosing and co-workers (2005) and Levay and co-workers (2015) demonstrate that no homology exists within both of the sequence pools of target-binding oligonucleotides in both literature and those sequences that they generated, despite using the same target and library. Therefore, one can deduce that a different set of oligonucleotide sequences could be obtained from a diverging SELEX for the same target, in this case r*Pf*LDH and LDHp, using the same template DNA/library. The homology between cloned r*Pf*LDH- and LDHp-binding oligonucleotide sequences obtained following SELEC C (**Figure 2.16**) are discussed in **Chapter 3**.

2.5.7.b. Percent recoveries of rPfLDH- and LDHp- binding oligonucleotides in SELEX

The mass of ssDNA binding to r*Pf*LDH and LDHp from the oligonucleotide pool was recorded in Stage 1, selection, throughout SELEX. From the recorded masses, the percent (%) recoveries were calculated as per **Equation 2.1**. The percent recoveries, which were monitored throughout SELEX, were used as a measure of the proportion of ssDNA capable of binding to the respective targets. The percent recoveries for the parallel SELEX targeting both r*Pf*LDH and LDHp are illustrated in **Figure 2.17**.

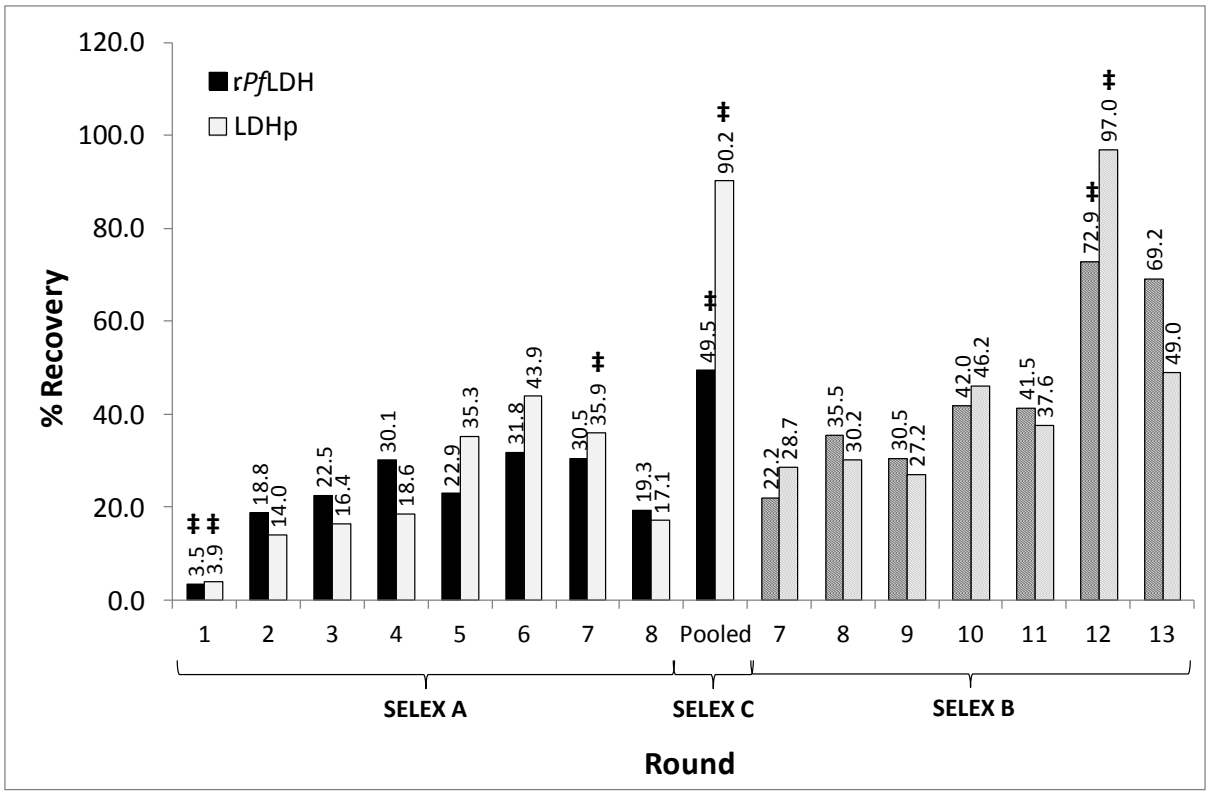

Figure 2.17: Percent (%) recovery of ssDNA during the SELEX process for the recombinant LDH (rLDH) and LDH peptide (LDHp) targets.
‡ denotes a counter or negative selection

Oligonucleotides with high affinity to the targets, r*Pf*LDH and LDHp, were generated following nine rounds of SELEX: 8 traditional rounds and 1 round incorporating pooled DNA from Rounds 6-8 (**Figure 2.17**). This is within the range of the number of cycles expected for the enrichment of oligonucleotides for a given target as literature reports that enrichment of high-affinity aptamers ranges from 5 to 15 rounds or cycles (Liu *et al*., 2011; Mascini *et al*., 2012), but the emergence of common motif families vital for target recognition have been reported from Round 8 (Spiga *et al*., 2015). Sequence motifs that have emerged in the generation of r*Pf*LDH and LDHp-binding oligonucleotides are discussed further in **Chapter 3**. Consequently, a SELEX with too many cycles can result in the emergence and recycling of non-specific by-products capable of binding to the target (Crameri & Stemmer, 1993; Tuerk *et al*., 1992), which accounts for the fact that the sequences returned for SELEX B for both r*Pf*LDH and LDHp (**Figure 2.16** and **2.17**) were predominantly concatemers, as shown in **Table 2.4**.

A final enrichment of 49.5 % and 90.2 % was observed for the r*Pf*LDH and LDHp, respectively. A ssDNA enrichment of 49.5 % for r*Pf*LDH is similar to that reported by Lee and co-workers (2012),

who reported a final ssDNA enrichment for r*Pv*LDH of 50.0 % after the 10th round of SELEX. An enrichment of approximately 50 % implies that approximately half of the oligonucleotides were partitioned in the selection stage of SELEX whilst the remaining 50 % bound to the target. Similarly to the 90.2 % recovery of the smaller peptide, LDHp, Yang and co-workers (1998) report a nitrocellulose-based ssDNA recovery greater than 90 % after 14 rounds for cellulose and cellobiose. Therefore, the enrichments reported herein are consistent with similar findings in literature.

The percent recovery for LDHp seen in **Figure 2.17** followed the expected increasing trend for Rounds 1 through to 6. Lee and co-workers (2012) also observe such an increasing trend in the percent of r*Pv*LDH-binding ssDNA from Rounds 1 through to 5 in their SELEX. Counter selections, shown in **Figure 2.17**, were performed in Round 1 and 7 of SELEX for LDHp. Counter selections were performed in the initial round of SELEX to remove non-specific binding of oligonucleotides to the nitrocellulose (Wong & Lohman, 1993). Another counter selection was performed when a substantial rise in percent recovery was observed in the preceding two rounds of SELEX, such as in the case of Round 4, 5 and 6 for LDHp (**Figure 2.17**). Such increases in percent recovery could indicate conjugation of ssDNA target binders or non-specific ssDNA binding to the nitrocellulose membrane resulting in false-positive binding (Wang *et al.*, 2003). These non-specific binders, therefore, need to be removed from the oligonucleotide pool to ensure enrichment of the ssDNA oligonucleotides that are able to bind to r*Pf*LDH and LDHp. Thus, a counter selection was performed for LDHp in Round 7 (**Figure 2.17**). The observed decrease in percent recovery from Rounds 6 to 7 indicates that non-specific binders were retained on the nitrocellulose membrane, thus eliminated from the oligonucleotide pool used in the positive selection for LDHp, resulting in the elution of only those oligonucleotides with the highest affinity for LDHp. Such a decrease in percent recoveries following the counter selection was also observed in the r*Pv*LDH SELEX by Lee and co-workers (2012).

On the other hand, the enrichment trend for r*Pf*LDH in SELEX A (**Figure 2.17**) appeared less consistent. For example, a 7.2 % decrease in recovery was observed from Round 4 to Round 5, indicating the loss of r*Pf*LDH-binding oligonucleotides in the pool. Thereafter, an 8.9 % increase in recovery was observed in Round 6. Like LDHp, a steady decrease in recovery was observed from Round 6 through to Round 8, until the complete loss of DNA for r*Pf*LDH in Round 8. SELEX B was initiated using dsDNA from Round 6, as shown in **Figure 2.16.** Rounds 7 through to 13 in SELEX B for both r*Pf*LDH and LDHp followed a similar trend to one another with a general increase in enrichment

for Round 7 to 12, likely due to the unbeknownst enrichment of targeting-binding concatemers which eventually out-competed the desired oligonucleotide sequences (Tolle *et al.*, 2014). The decrease in enrichment observed in SELEX B in **Figure 2.17** prompted the cessation of SELEX and progression on to cloning and sequencing; thereafter, followed by the pooling of Rounds 6 to 8 from SELEX A and initiation of SELEX C, as discussed previously in **Chapter 2.5.3.a**.

The ssDNA pooled sample for r*Pf*LDH and LDHp (**Figure 2.16** and **2.17**) were then further PCR amplified and ligated into a vector as outlined in the **Chapter 2.4.8**.

2.5.8. Identification of oligonucleotide sequences capable of binding the targets, recombinant PfLDH and LDH peptide

Following insertion of dsDNA amplified from r*Pf*LDH- and LDHp-binding ssDNA of SELEX C into the PGEM-T Easy vector and competent JM109 *E. coli* cells, blue-white screening utilising disruption of the β-galactosidase gene positively identified clones containing the correctly-sized insert corresponding to introduction of aptamers were then picked. Clones were further selected at random to undergo preliminary screening. Selected colonies were directly PCR amplified using the pUC/M13 universal primers. These primers were chosen based on the fact that they flank the inserted selected oligonucleotide sequence a distance away from the insertion site. Identification of clones with an insert of the correct length of 350 to 360 basepairs was based upon analysis of the colony PAGE for r*Pf*LDH and LDHp (**Figure 2.18**). A basepair length of 350 to 360 bp would be consistent with the length of DNA between the pUC/M13 universal primers specific for the insert region of the PGEM-T Easy vector containing inserted dsDNA; and can, therefore, be used as a means of positively identifying the presence of the desired oligonucleotide of 90 bp in length. Basepair length measurements were taken from the PAGE well for each sample to the band in question.

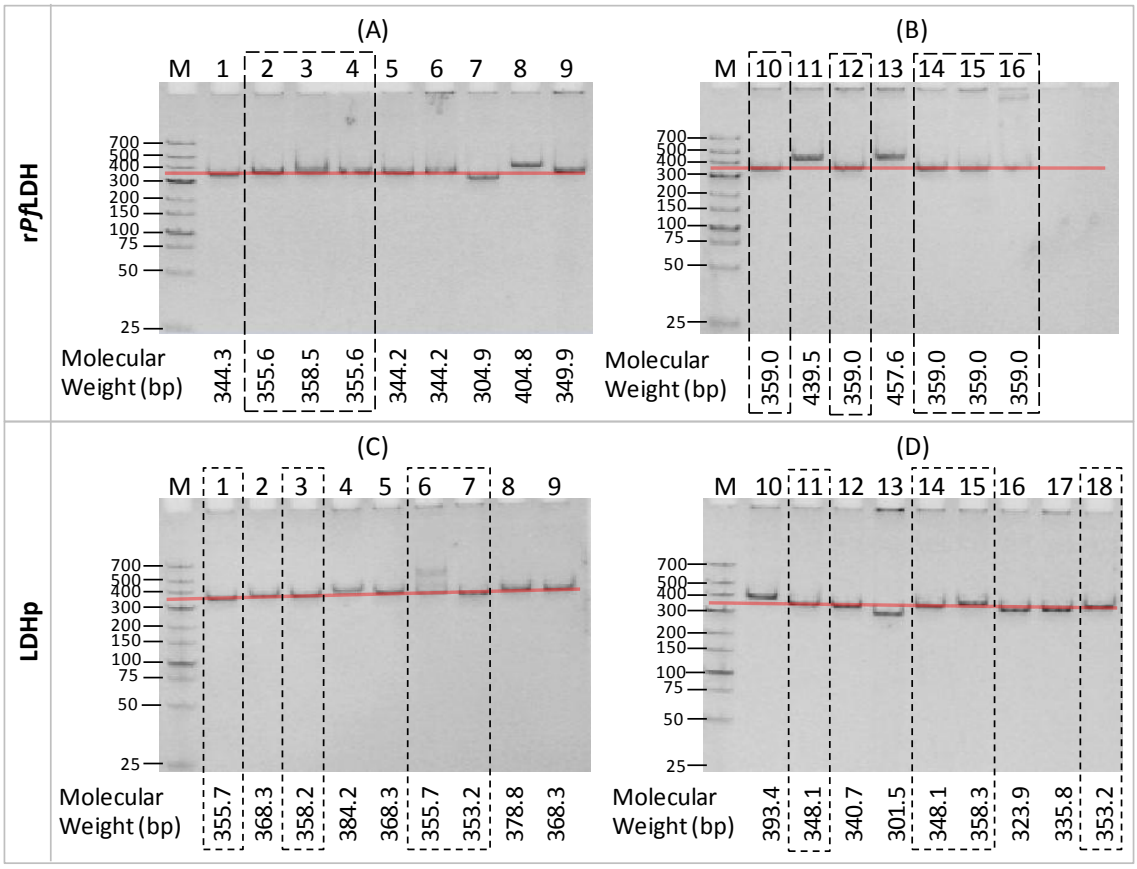

Figure 2.18: PAGE (10 %) and molecular weights of the PCR amplified regions using the pUC/M13 universal primers for chosen clones containing the inserted dsDNA used in selection against r*Pf*LDH (A and B) and LDHp (C and D) (assigned according to number).

M: DNA molecular mass marker. Clones are designated by number LDHp 1 – 18 and rLDH 1 – 16. Red line across gels indicates the desired band size according to the ladder. Dashed box indicates clones chosen based on their calculated molecular weight falling between 350 and 360 basepairs.

Based on molecular weight, clones with the r*Pf*LDH-specific inserts chosen for further study are highlighted in **Figure 2.18** and include clone 2, 3, 4, 10, 12, 14, 15 and 16. Clones with the LDHp-specific insert chosen for further study included 1, 3, 6, 7, 11, 14, 15 and 18. Clone 1 for the target r*Pf*LDH was chosen as a control as the length of amplified DNA did not fall within the desired range and, thus, was believed to contain primer artefacts. Therefore, a total of 8 out of 18 clones were shown to have an insert of the correct length for the target LDHp; and, 9 out 16 clones had an insert of the correct length for rLDH. Oligonucleotides showing binding to their specified target were numbered and hence named according to their originating colony and clone number. For example, the 90 bp oligonucleotide amplified from clone 1 targeting r*Pf*LDH was named rLDH 1. These selected clones identified as positively containing the insert were then picked at random to undergo preliminary screening.

2.5.9. Screening of aptamer candidates via preliminary ELONA binding assay

As previously discussed (**Chapter 2.5.3**), careful consideration was required to prevent over-amplification and inclusion of primer concatemers during PCR amplification of the 90 bp oligonucleotides; and, as the binding events required DNA to be in its single-stranded form, a large quantity of dsDNA was required to get sufficient quantities of ssDNA following exonuclease digestion for use in the preliminary enzyme-linked oligonucleotide assay, or ELONA. As the preliminary ELONA was performed with PCR amplified inserts directly from the transformed colonies, only a limited number of binding events could be studied. The preliminary ELONA is limited by the high quantities required for each triplicate sample, yet only a limited supply of ssDNA required for the preliminary ELONA could be generated owing to the limitations in amplifying and purifying 90 bp ssDNA caused by erroneous PCR by-products. ELONA (as detailed in **Chapter 1)** is an adapted sandwich-type immunosorbent assay used to measure binding between the amplified, or synthesised, oligonucleotide and their target (Drolet *et al*., 1998). The preliminary ELONA binding assay involved amplification of the insert from selected clones highlighted in **Figure 2.18**, exonuclease digestion of these oligonucleotides and, finally, the preliminary ELONA binding assay performed (**Figure 2.19** for the r*Pf*LDH aptamers and **Figure 2.20** for LDHp aptamers).

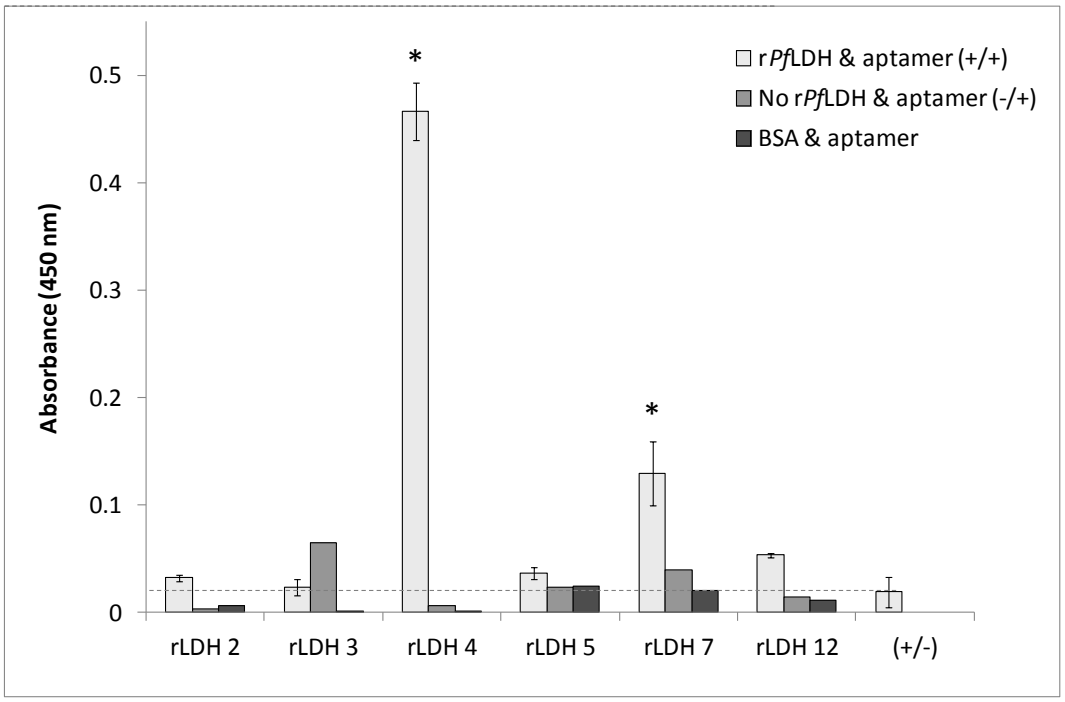

Figure 2.19: Preliminary binding affinity ELONA (absorbance at 450 nm) on colony PCR amplified inserts against r*Pf*LDH (*n* = 3).
Dotted line indicates mean of the r*Pf*LDH in absence of aptamer (+/- control) and used as a baseline response.
Statistics: r*Pf*LDH & aptamer: $F(6,18) = 61.73$; $p < 0.0001$)
* Tukey's multiple comparison's test: $p \leq 0.05$

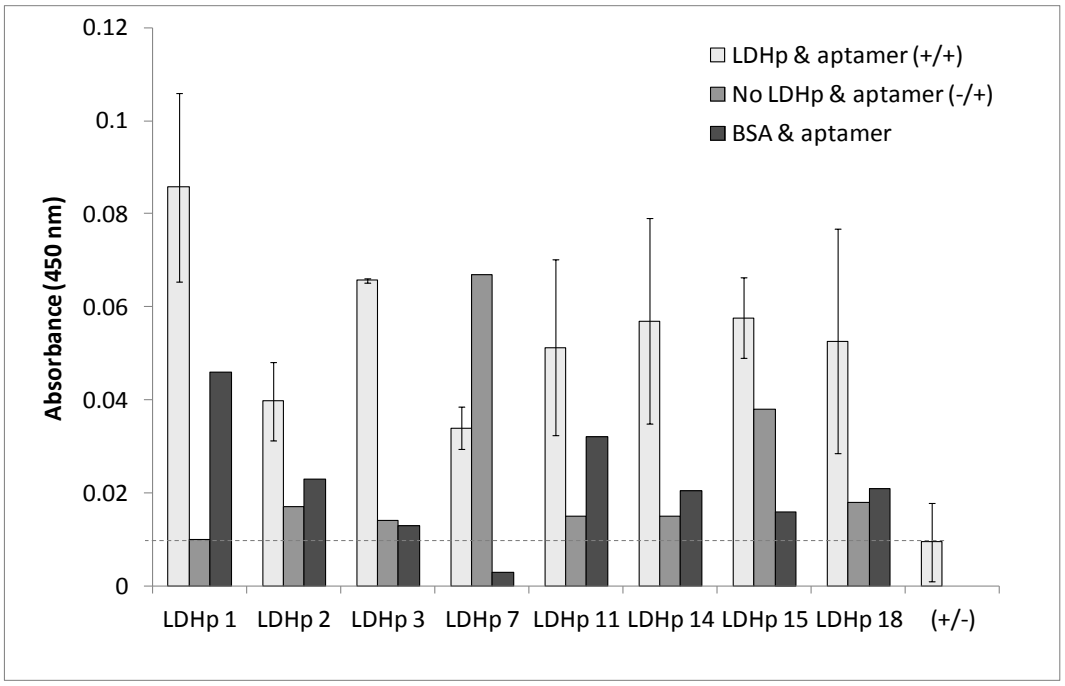

Figure 2.20: Preliminary binding affinity ELONA (absorbance at 450 nm) on colony PCR amplified inserted against LDHp (*n* = 3).
Dotted line indicates mean of LDHp in absence of aptamer (+/- control) and was used as a baseline response.
Statistics: LDHp & aptamer: $F(8,24) = 1.025$; $p = 0.45$)

Figure 2.19 demonstrates the binding affinities of PCR-amplified oligonucleotides, rLDH 2, 3, 4, 5, 7 and 12 to r*Pf*LDH and bovine serum albumin (BSA) indicated by the absorbance at 450 nm. The amplified oligonucleotide with the highest recorded affinity was rLDH 4, followed by rLDH 7, rLDH 12, rLDH 5, and rLDH 2. A negligible response for rLDH 3 was observed as the recorded response did not exceed that of the r*Pf*LDH control (+/-). Also, the response rLDH 5 did not far exceed that of all the controls, as shown in **Figure 2.19**. Therefore, rLDH 2, 3, 5 and 12 were removed from contention as high-affinity r*Pf*LDH-binding oligonucleotides.

Given the low number of rLDH oligonucleotides that showed strong positive binding over the controls, further colonies containing r*Pf*LDH-targeting oligonucleotides were randomly selected for sequencing and structure analysis eventhough they had not undergone any preliminary ELONA screening. These randomly selected colonies included rLDH 1 despite the colony PCR-amplified oligonucleotide having a length of 344.3 bp, below the targeted 350 – 360 bp length (colony rLDH 5 and 6 similarly presented as alternatives). Colony rLDH 15 was also randomly selected for further sequencing and structure analysis as colony PCR-amplified oligonucleotides from this colony were within the required 350 – 360 bp length.

Figure 2.20 demonstrates the binding affinities of PCR-amplified oligonucleotides, LDHp 1, 2, 3, 7, 11, 14, 15 and 18 to LDHp and bovine serum albumin (BSA) indicated by the absorbance at 450 nm. The amplified oligonucleotide with the highest recorded affinity was LDHp 1 and the lowest was LDHp 7. However, LDHp 7 and 15 exhibited high non-specific binding seen in the absence of protein (no LDHp and aptamer (-/+) control). Therefore, LDHp 7 and 15 were eliminated for contention in future binding analyses. PCR-amplified oligonucleotides from colony LDHp 2 was substantially out-performed in binding response to LDHp compared to its counterparts to the same protein target. LDHp 1 and 3 exhibited responses for LDHp above those in the absence of protein and, therefore, were considered for future binding analyses. PCR-amplified oligonucleotides from colonies LDHp 11, 14 and 18 exhibited similar affinities to LDHp given by the responses at 450 nm. The observed responses of LDHp 11, 14 and 18 to LDHp were above those observed for those in the absence of protein (-/+) and in the presence of BSA (BSA & aptamer). Oligonucleotide sequences targeting LDHp were limited to those that were studied in the preliminary ELONA and no more colonies were randomly selected for further study.

Thus, colonies containing sequences that showed positive binding at the preliminary phase – 4 out of 8 for r*Pf*LDH and 5 out of 8 for LDHp – were sequenced (Inqaba Biotec, South Africa) using pUC/M13 universal forward and reverse primers. Therefore, the sequences that were selected for commercial synthesis (IDT, USA) were: rLDH 1, 4, 7 and 15; LDHp 1, 3, 11, 14 and 18. These oligonucleotides (aptamers, given their binding to respective targets were hence sequenced and commercially synthesised with 5'-modifications, which included 5'-biotin (for ELONA), 5'-SH (thiolation for electrochemical impedance spectroscopy, EIS), 5'-NH (for EIS and surface plasmon resonance, SPR) and 5'-FITC (for confocal microscopy). Further analysis on these chosen sequences was thus carried out.

2.6. Conclusion

Aptamers specific for recombinant *Pf*LDH (rLDH) and species-specific *Pf*LDH peptide (LDHp) were developed using the exonuclease-SELEX method. However, SELEX does come with its challenges which present a concern for all researchers in the field of aptamer design and synthesis in that each SELEX requires its own optimisation procedures. The production of unwanted primer artefacts in the pursuit of clean desired DNA was highlighted as the main concern in the synthesis of oligonucleotides selected against r*Pf*LDH and LDHp. The final PCR amplification optimisations taken further included: the optimisation of the PCR cycles (outlined in **Chapter 2.4.6.c** and **Chapter 2.5.3.**),

absence of Triton X, and an annealing temperature of 59 ^{o}C (**Chapter 2.5.4**). The primer hybridization study (**Chapter 2.5.3.b** and **c**) showed that the banding seen following PCR amplifications was indeed as a result of the formation of primer dimers and concatemers, primer-product concatemers and over-amplification leading to the formation of longer lengths of dsDNA eluted along with the target 90-bp oligonucleotides. This concurs with the literature (Dieffenbach & Dveksler, 2003; Drabovich & Krylov, 2004; Musheev & Krylov, 2006; Kalle *et al*., 2013; Tolle *et al.*, 2014). On return of the sequences obtained following the second SELEX, SELEX B (**Figure 2.16**), retention of these undesired artefacts in SELEX was proven as the obtained sequences (**Table 2.4**) consisting predominantly of primers dimers and the same five classes of concatemers, which were understandably found in oligonucleotide pools for both targets: r*Pf*LDH and LDHp. A final percent recovery of 90.2 % was observed for those aptamers targeted for LDHp and 49.5 % for those aptamers targeted for r*Pf*LDH (**Figure 2.17**). Therefore, the oligonucleotide pool for r*Pf*LDH and LDHp consisted of 49.5 and 90.2 % targeting-binding oligonucleotides. The cloning procedure resulted in the identification of inserts relative to the correct 90-bp size of the desired r*Pf*LDH- and LDHp-binding oligonucleotides. Preliminary analysis via ELONA showed that the aptamer rLDH 4 bound to a greater extent than other rLDH aptamers, but rLDH 1, 4, 7 and 15 were selected for sequencing (analysis of which is in **Chapter 3**) and commercial synthesis for further binding analyses (**Chapters 4 and 5**). LDHp 1, 3, 11, 14 and 18 showed the highest binding indicated by higher absorbance and were, therefore, sequenced (analysis of which is in **Chapter 3**) and selected for commercial synthesis for further binding analyses (**Chapters 4 and 5**).

CHAPTER 3

Analyses of recombinant *Pf*LDH- and *Pf*LDH peptide-binding oligonucleotide aptamer sequence and structure

3.1. Preface

In this chapter, oligonucleotide (now aptamer) sequence and predicted secondary and tertiary structure analyses of successfully selected aptamer sequences, LDHp 1, 3, 11, 14 and 18 and rLDH 1, 4, 7 and 15, capable of binding to recombinant *Plasmodium falciparum* LDH (r*Pf*LDH) and *Plasmodium falciparum*-specific LDH peptide (LDHp) are presented.

3.2. Introduction

3.2.1. Aptamer structure-function relationship

The high affinity and specificity that aptamers offer during target molecule binding is due to their specific three-dimensional structure that results from their unique ribonucleic (RNA) or deoxyribonucleic (DNA) residue sequence (Tuerk & Gold, 1990). The aptamer's residue-dependant tertiary structure is brought about by Watson-Crick base-pairing and/or non-canonical intramolecular interactions (Macaya *et al*., 1993). Conformational changes of the aptamer tertiary structure can occur prior to target binding for which stable three-dimensional tertiary structures (G-quadruplex and hairpins) are formed; or, upon binding to the target whereby the aptamer forms a more systematic and ordered structure ideal for specific target binding (Han *et al*., 2010). Aptamers are able to elicit these oligonucleotide-target interactions via van der Waals forces, hydrogen bonding and electrostatic interactions (Pendergrast *et al*., 2005).

As discussed in **Chapter 1.4.1**, there are various classifications of aptamer-target binding. Aptamers have diverse application in both therapeutic and diagnostic fields (**Chapter 1.4.3**). As biological capture molecules, aptamers offer many advantages over antibodies as discussed in **Chapter 1.4**.

A selected pool with high affinity for a pure protein or low molecular weight target usually consists of relatively few sequences that can be grouped into a small number of families based on primary and secondary sequence similarities. These sequence-similar families can often span aptamers generated for a particular target across different libraries (Tasset *et al*., 1997). Furthermore, these families can be found in the reverse sequence and/or with a one-residue difference that may or may not affect target recognition. These different families are often able to compete with each other for binding to the target, demonstrating that they bind to single or overlapping epitopes (Morris *et al*., 1998). Should grouping of these families in a common area occur, a truncated aptamer can be used to bind to the target, nullifying the existence of unimportant DNA sequence stretches (Jayasena, 1999).

Levay and co-workers (2015) showed that monitoring the formation, and subsequent retention, of common sequence motifs with the progression of SELEX via high-throughput sequencing assisted in identifying common families, and resulting conformations, necessary for target capture. A tool with which to monitor sequence motif enrichment through the progression of SELEX is Next Generation Sequencing, which facilitates sequencing of numerous DNA samples within a single pool (Schütze *et al*., 2011). Levay and co-workers (2015) further confirmed that a particular motif and secondary/tertiary conformation was necessary in target capture. This was demonstrated by introducing mutations into these motifs and secondary/tertiary structures. Furthermore, it has been shown that retention of these moieties across aptamers from different libraries is largely given by the target against which the aptamer families are selected (Takahashi *et al*., 2016). Therefore, identification of common motifs and/or residue families through careful analysis of an aptamers given sequence is important.

3.2.2. Analysing aptamer sequences

Oligonucleotide sequence analysis software and oligonucleotide secondary structure prediction software are useful tools when identifying frequently occurring oligonucleotide moieties and aptamer secondary structures. The mechanism by which these commonly occurring moieties facilitate the binding of the aptamer to the target can then be determined. Aptamers containing those relevant moieties can then be grouped into families (Morris *et al*., 1998). Identification of these families in the analysis of present and future aptamer sequences and secondary structures will assist in understanding the biomolecular interactions responsible for the binding of the aptamer to a specific target (Morris *et al*., 1998). This will lead to identifying which nucleotides, moieties and

secondary structures are responsible for binding specifically to a given epitope, secondary structure or functional group on its specific target. As this binding occurs at a molecular level where structure facilitates function, it is important that both the forward and reverse aptamer sequences are analysed. Elucidated: a secondary structure given by a specific sequence will retain its form when viewed from a different aspect, although the sequence will be mirrored. Thus, when analysing the aptamer/target complexation, more attention towards secondary structure formation is required; and, this aptamer/target interaction is not necessarily based on the aptamer sequence alone (Morris *et al*., 1998).

To fully understand and characterise the aptamer-target binding interaction, the nucleotide sequence of the aptamer needs to be explored (Katilius *et al*., 2007). With the sequence of the aptamer known, the secondary and tertiary structures that the aptamer is likely to adopt under specific conditions can be ascertained using structure prediction software, such as MFold, RNAComposer. However, since the popularisation of aptamers, more modelling software programs have since been developed, such as FASTAptamer (Alam *et al*., 2015) and APTANI (Caroli *et al*., 2016). By identifying structures and the related sequence motifs, short sequences that are involved in binding of the aptamer to the target can be identified to: (1) identify aptamer families shown to have high affinity to the target; and, (2) understand the biochemistry of DNA-protein binding (Davies *et al*., 2012). As aptamers capable of binding to their target are selected from a pool of oligonucleotides that may have affinity for the target, more than one aptamer is likely to bind to the target with high affinity (Carothers *et al*., 2004; Caroli *et al*., 2016). Short consensus sequences possibly involved in target binding that may be located on a structurally important segment of the aptamer need to be identified. The role of such short consensus motif sequences across aptamers needs to be ascertained in target binding to gain a better understanding into the chemistry. Sequence-structure data can, hence, be utilised in the development and application of aptamers in real-world settings.

Chapter 2 showed the rise of PCR amplification artefacts carried through the SELEX B resulted in the rise of primer-dimers and concatemerised sequences following SELEX B. An example of such a concatemer, C7, was used as a negative control and as a comparison for subsequent analyses. A further number of ssDNA oligonucleotide sequences capable of binding to their respective targets were identified through preliminary screening following SELEX C. From SELEX C, a select group of aptamers each capable of binding to r*Pf*LDH and LDHp, respectively, was assessed in terms of

sequence, secondary and tertiary structure (**Chapter 3**) and binding affinity (**Chapter 4**). Of that select group of aptamers, short consensus sequence motifs were identified for predicting the manner by which the target binds.

3.3. Aims

1. Using sequence analysis tools, ClustalW and/or DNAMAN Sequence Analysis software, to analyse and compare sequences for r*Pf*LDH- and LDHp-binding aptamers, rLDH 1, 4, 7 and 15 and LDHp 1, 3, 11, 14 and 18, respectively.
2. To identify and compare sequence families and motifs common for aptamers, rLDH 1, 4, 7 and 15 and LDHp 1, 3, 11, 14 and 18, with comparison to previously published aptamers for *Plasmodium* LDH.
3. To predict secondary and tertiary structure aptamer structures for rLDH 1, 4, 7 and 15 and LDHp 1, 3, 11, 14 and 18, using available tools.

3.4. Methodology

3.4.1. Sequence analysis tools

To identify closely-related sequences, all aptamer sequences (including those reported in the **Table B.1, Appendix B**) were aligned and compared using:

- ClustalW (http://www.ebi.ac.uk/Tools/msa/clustalw2/; Larkin *et al*., 2007),
- MUSCLE MSA (https://www.ebi.ac.uk/Tools/msa/muscle/; Edgar, 2004), and/or
- DNAMAN Sequence Analysis software (http://www.lynnon.com/index.html; Lynnon Corporation, Canada).

Single-stranded sequences were analysed in the 5’ → 3’ directions.

Following identification of closely-related sequence clusters, consensus subsequences (subsequences analysed in 5’ → 3’ and 3’ → 5’) within these clusters were identified using ClustalW-aligned sequences and subsequent analysis of the alignment using mView (https://www.ebi.ac.uk/Tools/msa/mview/; Brown *et al*., 1998).

3.4.2. Secondary structure prediction of generated aptamers

Preliminary identification and comparison of secondary structures of the primers and aptamer candidate sequences identified for both recombinant r*Pf*LDH and the species-specific peptide (LDHp) were modelled using Mfold software (http://mfold.rna.albany.edu/?q=mfold/dna-folding-form; Zuker, 2003). To maintain parity with the SELEX conditions, structure prediction was conducted using the following environmental constraints: temperature was constrained to 23 ^{o}C; the sodium concentration was constrained to 15.0 mM; and, the magnesium concentration was constrained to 0.2 mM to maintain parity with SELEX conditions.

Following preliminary identification, more detailed prediction using pseudoknot prediction of RNA analogues of the DNA sequences were performed (i.e. converting all thymidine ('T') residues into uracil ('U') residues). Dot-bracket notations of predicted secondary structures were generated using VSFold V5.23 (http://www.rna.it-chiba.ac.jp/~vsfold/cgi-bin/run_vsfold5_23.cgi; Dawson *et al*., 2006). The model selected were the default parameters of the Effective Flory model, selecting the following additional parameters: a folding temperature of 20 °C, permitting pseudoknot determination, including the presence of $[Mg(H_2O)_6]^{2+}$. Possibly conserved secondary structures between the various sequences determined using this method are highlighted and compared qualititatively to one-another in the relevant results section.

3.4.3. Tertiary structure prediction of generated aptamers

Three-dimensional (3D) tertiary single-stranded primer and DNA aptamer structures proceeded using RNA-transposed sequence analogues of the DNA sequences. These were generated using RNAComposer (http://rnacomposer.cs.put.poznan.pl/; Popenda *et al*., 2012).

Generated molecular graphic files (Protein Data Bank (".pdb")) files were rendered in UCSF Chimera (http://www.cgl.ucsf.edu/chimera; Pettersen *et al*., 2004). Molecular surfaces were coloured according to coulombic potential using the Coulombic colouring surface analysis tool. Coulombic surface potential was calculated according to Coulomb's law:

$$\varphi = \Sigma [q_i / (\varepsilon d_i)] \qquad \textbf{Equation 3.1}$$

Where, φ is the potential, q are the atomic partial charges, d are the distances from the atoms, and ε is the distance-dependent dielectric (UCSF, 2013). The force field model for the atomic partial charges of standard residues was the default AMBER ff14SB. Coulombic surface colouring was adjusted for the highly negative nature of native DNA: red indicates negative coulombic potential (-25 kcal/(mol*e)); white indicates neutral coulombic potential (-10 kcal/(mol*e)); and, blue indicates positive coulombic potential (2 kcal/(mol*e)).

Tertiary structures of the LDHp peptide were rendered in DeepView V3.9 (latest version available at https://spdbv.vital-it.ch/; Guex & Peitsch, 1997), as well as in UCSF Chimera and molecular surfaces coloured as described for ssDNA.

3.4.4. Data measurement and analysis

Presented quantitative results in this Chapter are the means of independent measurements ($n \geq 3$), while all reported error bars and uncertainties represent one standard deviation from the mean. Statistical analyses were performed using Graphpad Prism, version 6.1. The statistical significance level for statistical analyses, α, was set at 0.05. Statistical data are presented for H for Kruskal-Wallis H-test, with the determined statistic value, as well as the degrees of freedom in parentheses. The Dunn's multiple comparisons test was used as a post-hoc test. Data p-values are also presented for the given data set.

3.5. Results and discussion

3.5.1. Recombinant PfLDH and PfLDH peptide aptamer sequence content

All sequences of the appropriate and correct length resulting from SELEX C in the enrichment of oligonucleotides for the adaptation of binding to r*Pf*LDH and LDHp are shown in **Table B.1** in **Appendix B**. From **Chapter 2**, aptamers rLDH 4 and 7 were selected for further analysis as they exhibited the highest affinity to their target protein during the preliminary ELONA. Similarly, LDHp 1, 3, 11, 14 and 18 were selected for further analysis as they exhibited the highest affinity to their target peptide during the preliminary ELONA. Aptamers rLDH 1 and 15 were randomly selected for further sequencing and structure analysis. The sequences of aptamers identified in **Chapter 2** with affinity for r*Pf*LDH and LDHp were, therefore, rLDH 1, 4, 7 and 15 and LDHp 1, 3, 11, 14 and 18,

respectively. The sequences of these selected aptamers, along with the sequences of the published LDH aptamers, are listed in **Table 3.1**. A concatemer control, C7, was also included.

Selected aptamers, rLDH 1, 4, 7 and 15 and LDHp 1, 3, 11, 14 and 18, consisted of 90 to 100 basepairs in length. Interestingly, sequences containing more than 5 consecutive adenine (poly-A) stretches within the variable region were not uncommon amongst the sequences generated by SELEX in **Chapter 2**. These poly-A stretches are found in aptamers targeting both r*Pf*LDH (all sequences, with the exception of rLDH 7 from SELEX B) and LDHp (Specifically LDHp 14, **Table 3.1**). For aptamers generated against r*Pf*LDH (**Table B.1, Appendix B**), the presence of these poly-A regions demonstrates an inherent stability of sequence and structure considering that this region is conserved amongst r*Pf*LDH-targeting aptamers. Interestingly, of the 11 sequences for r*Pf*LDH-targeting oligonucleotides, 10 occur a distance of 8 nucleotide bases from the 5'-end into the variable region, while only rLDH 15 contains the poly-A region 20 nucleotide bases into the variable region. Aptamer LDHp 18, however, does contain a purine-rich region consisting of predominantly guanines and adenines at this same locale within the variable region of the sequence. Abe and co-workers (1996) showed that poly-A stretches in RNA bind to mouse HuC. The evolutionary inclusion of this poly-A sequence in the aptamer's sequence may be due to the progressive degradation of other affinity binders or a preferential bias for that base in the selection and amplification method used for aptamer generation (Takahashi *et al*., 2016). Beelman and Parker (1995) note that a poly-A tail protects mRNA from exoribonuclease degradation and so stabilising mRNA. Similarly, this form of inherent protection may be similar for ssDNA in that the poly-A stretch within the aptamer sequence may offer the aptamer an inherent protection from nuclease digestion, particularly when ssDNA molecules are not chemically modified for protection in the commercial synthesis. The structural purpose and possible influence of the poly-A tail is discussed further in this Chapter.

Table 3.1: DNA sequences of selected aptamers with affinity to r*Pf*LDH and LDHp, selected from Chapter 2.
Included: concatenated-primer control sequence, C7, and previously published aptamers for *Plasmodium* spp.
Forward primer regions are shown shaded and reverse primer regions are underlined.

Name	Sequence (5' to 3')		
	Forward primer region	Variable region	Reverse primer region
	Aptamers selected using recombinant full-length protein, r*Pf*LDH		
rLDH 1	GCCTGTTGTGAGCCTCCTAAC	TCACGGGCAAAAAAAAAACCGTTGTGCACTTGCTGGTTGGCGGCGGTAGGT	CATGCTTATTCTTGTCTCCC
rLDH 4	GCCTGTTGTGAGCCTCCTAAC	CAGCTCGTAGAAAAAAAAAGATATTGCTTCAATTATCTCCTCGCGTTCAATTAACCCAG	CATGCTTATTCTTGTCTCCC
rLDH 7	GCCTGTTGTGAGCCTCCTAAC	CCAGAATAGGGACTGCTCGGGATTGCGGATGAGTCTGGGTGGGACATGG	CATGCTTATTCTTGTCTCCC
rLDH 15	GCCTGTTGTGAGCCTCCTAAC	TTTAAAGTTGCTATTTAACCAAAAAAAAAAAAAtAAAAAAGTCGAGCCGGCCC	CATGCTTATTCTTGTCTCCC
	Aptamers selected using peptide epitode, LDHp		
LDHp 1	GCCTGTTGTGAGCCTCCTAAC	CAGGAAGCGACCTACTAAAGTGATATTATAGATTCACGGGAGCGTGGTG	CATGCTTATTCTTGTCTCCC
LDHp 3	GCCTGTTGTGAGCCTCCTAAC	TGTTACGCGGGAGAACAATTATGACCAAACCACCGATGTTAAACTCATT	CATGCTTATTCTTGTCTCCC
LDHp 11	GCCTGTTGTGAGCCTCCTAAC	CTACTGTTGATATGAGTGATAGGGCGGCGCGCTTATCTAGTGTATTGTG	CATGCTTATTCTTGTCTCCC
LDHp 14	GCCTGTTGTGAGCCTCCTAAC	AGCGTTCACAGCGCAAAAAAGGTAACACGTTTTACTGGACGGGCCGAGC	CATGCTTATTCTTGTCTCCC
LDHp 18	GCCTGTTGTGAGCCTCCTAAC	AGTCCTCACGTGTCAGGAAATATGTTGAATCATGAGGATAAAACTGTGT	CATGCTTATTCTTGTCTCCC
	Control sequence containing concatemerised primers		
C7	GCCTGTTGTGAGCCTCCTAAC	ACTTTGCA	CATGCTTATTCTTGTCTCCCAT GCCTGTTGTGAGCCTCCTAAC CTCATGCTTATTCTTGTCTCCC
	*Pf*LDH-specific aptamers from literature		
pL1*	CACCTAATACGACTCACTATAGCGGATCCG	AGTTCGATTGGATTGTGCCGGAAGTGCTGGCTCGAAC	CTGGCTCGAACAAGCTTGC
pL2*	CACCTAATACGACTCACTATAGCGGATCCG	GAACTCATTGGCTGGAGGCGGCAGTACCGCTTGAGTTC	CTGGCTCGAACAAGCTTGC
2004s°	CGTACGGTCGACGCTAGC	ACGCGAGCAGGTGGTAGAATCATAATGGCCTGATC	CACGTGGAGCTCGGATCC
2008s°	CGTACGGTCGACGCTAGC	CTGGGCGGAGACCATAGTGACCCAGCCGTCTAC	CACGTGGAGCTCGGATCC
2009s°	CGTACGGTCGACGCTAGC	TAGGTGGCCAGAAGGTAGAACCATAGTGGTCTGGTA	CACGTGGAGCTCGGATCC
2021°	CGTACGGTCGACGCTAGC	AGAATGGCGGGAGAGCCTTAGCGACCATTCGTAC	CACGTGGAGCTCGGATCC

* *Pf*/*Pv*LDH aptamers from Lee *et al.* (2012)
° *Pf*LDH aptamers from Tanner *et al.* (2013)

Exploration of the nucleotide composition needs to be performed to (1) ascertain sequence diversity within a group of aptamers from a single library; and, (2) elucidate the stability of the aptamer inherently given by the sequence (Blind & Blank, 2015; Takahashi *et al*., 2016). The total number of nucleotides, as well as the nucleotide composition (in percentage), of each of the generated aptamers and aptamer controls are shown in **Table 3.2**. **Table 3.2** shows nucleotide composition for the entire sequence in which forward and reverse primer sequences have been included.

Table 3.2: Proportion (%) of adenine (A), thymine (T), guanine (G) and cytosine (C) for each entire oligonucleotide aptamer sequence.

Aptamer	Total N	A (%)	T (%)	G (%)	C (%)	GC (%)
rLDH 1	92	19.6	28.3	26.1	26.1	52.2
rLDH 4	100	26.0	31.0	15.0	28.0	43.0
rLDH 7	90	16.7	27.8	31.1	24.4	55.5
rLDH 15	94	33.0	27.7	14.9	24.5	39.4
LDHp 1	90	22.2	28.9	24.4	24.4	48.9
LDHp 3	90	24.4	30.0	17.8	27.8	45.6
LDHp 11	90	15.6	35.6	25.6	23.3	48.9
LDHp 14	90	22.2	25.6	23.3	28.9	52.2
LDHp 18	90	23.3	32.2	21.1	23.3	44.4
C7	94	13.8	37.2	16.0	33.0	48.9
pL1*	86	23.3	23.3	26.7	26.7	53.5
pL2*	87	23.0	21.8	26.4	28.7	55.2
2004s°	71	22.5	18.3	32.4	26.8	59.2
2008s°	69	18.8	15.9	31.9	33.3	65.2
2009s°	72	22.2	19.4	34.7	23.6	58.3
2021°	70	21.4	17.1	32.	28.6	61.4

* *Pf*/*Pv*LDH aptamers from Lee *et al.* (2012)

° *Pf*LDH aptamers from Tanner *et al.* (2013)

As enrichment of specific nucleotides focuses primarily on the variable regions, averages of nucleotide base composition across the oligonucleotide pools for targets, r*Pf*LDH and LDHp, were determined using the variable regions of all sequences for each r*Pf*LDH- and LDHp-targeting pool (**Table B.1**). These are compared to previously published aptamers (Lee *et al*., 2012; Tanner *et al*., 2013) (**Figure 3.1**).

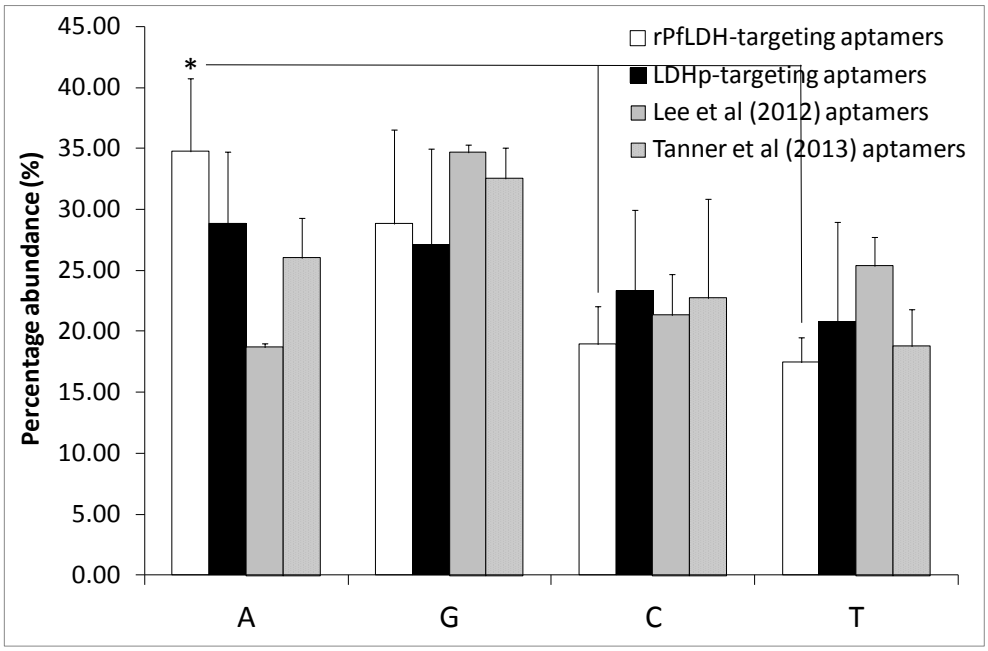

Figure 3.1: The distribution of adenine (A), thymine (T), guanine (G) and cytosine (C) of the variable regions for oligonucleotide aptamer sequence groups based on target, r*Pf*LDH and LDHp.
These are compared to previously published aptamers (Lee *et al*., 2012; Tanner *et al*., 2013).
Statistics: Kruskal-Wallis statistical significance test: $H(15,100) = 26.28$, $p < 0.0001$;
* Dunn's multiple comparison test: $p \leq 0.05$.

Percent abundance of residues in the final SELEX pools for r*Pf*LDH and LDHp are reported in **Figure 3.1**. In line with the stretches of poly-A regions in r*Pf*LDH-targeting oligonucleotide sequences observed in **Table 3.1**, **Figure 3.1** shows that the percentage abundance of adenine (A) was comparatively higher in r*Pf*LDH-targeting oligonucleotide sequences than the remaining aptamer groups across their SELEX pools (34.74 ± 6.02 % for A, versus 28.83 ± 7.68 %, 19.98 ± 3.10 % and 17.47 ± 2.02 % for G, C and T, respectively). The abundance of A for r*Pf*LDH-targeting oligonucleotides indicates enrichment of the nucleotide. In particular, aptamer rLDH 15, with an adenine content of 33.0 %, exhibited the highest A content than the remaining bases compared to the remaining aptamers (**Table 3.2**). This is attributed to the stretch of 15 adenine bases in the poly-A stretch for rLDH 15 – the longest poly-A stretch when compared with the remaining aptamer sequences. Similar to the enrichment of A observed across generated rLDH aptamers, A enrichment was also observed in only one of the eleven LDHp-targeting aptamers: LDHp 14 (**Table 3.1**). Adenine enrichment for LDHp-targeting aptamers, hence, resulted in an abundance of A (28.84 ± 5.91 %), seen in **Figure 3.1,** over G, C and T (27.09 ± 7.88 %, 23.30 ± 6.63 % and 20.77 ± 8.17 %, respectively). Therefore, it appears the adenine was concentrated in the poly-A region for LDHp 14 and the r*Pf*LDH-targeting aptamers.

Furthermore, **Table 3.2** and **Figure 3.1** show evidence of enrichment of adenine (A; r*Pf*LDH = 34.74 ± 6.02 %; LDHp = 28.84 ± 5.91 %) and guanine (G; r*Pf*LDH = 28.83 ± 7.68 %; LDHp = 27.09 ± 7.88 %) for generated aptamers targeting r*Pf*LDH and LDHp across their SELEX pools over cytosine (C; r*Pf*LDH = 18.95 ± 3.10 %; LDHp = 23.30 ± 6.63 %) and thymine (T; r*Pf*LDH = 17.47 ± 2.02 %; LDHp = 20.77 ± 8.17 %). This is similar to nucleotide enrichment for aptamers from Lee and co-workers (2012) and Tanner and co-workers (2012), both of whom demonstrate enrichment of G in their aptamer sequences.

Enrichment of adenine residues during SELEX may not necessarily extend from the SELEX process: the nucleotide bias for A seen in **Figure 3.1** may result from a similar bias present in the original library pool. Takahashi and co-workers (2016) demonstrated the existence of nucleotide bias inherent in a library extending into later SELEX rounds, where a nucleotide is preferentially selected over the other nucleotides.

Table 3.3 compares the percent (%) homology for ssDNA aptamers generated in this study and in other published work in their 5’ to 3’ direction as given in **Table 3.1** using DNAMAN sequence analysis software.

Table 3.3: Percent (%) homology (generated by DNAMAN; Lynnon Corporation) of the variable regions of the ssDNA aptamers against rLDH and LDHp.

	C7	LDHp 1	LDHp 3	LDHp 11	LDHp 14	LDHp 18	rLDH 1	rLDH 4	rLDH 7	rLDH 15	pL1	pL2	2004s	2008s	2009s	2021s
C7	-	50.00	11.36	22.22	25.00	18.18	29.17	24.53	28.95	25.00	32.43	33.33	33.33	23.53	29.73	25.71
LDHp 1		-	25.81	44.74	26.83	36.59	40.00	28.57	31.91	36.73	39.39	34.21	38.89	21.43	40.54	28.12
LDHp 3			-	39.47	35.90	51.43	21.28	33.33	37.93	37.14	22.86	37.04	54.84	50.00	45.16	52.94
LDHp 11				-	24.44	34.78	28.57	35.56	30.56	14.29	29.73	35.29	30.56	32.35	40.54	40.00
LDHp 14					-	37.78	46.51	32.65	23.08	46.67	29.73	24.32	27.78	32.35	29.73	22.86
LDHp 18						-	35.90	33.33	28.21	35.56	27.03	32.43	44.44	40.62	45.95	34.29
rLDH 1							-	29.41	36.36	43.59	29.73	25.81	37.14	26.47	37.14	28.57
rLDH 4								-	22.50	39.13	37.84	34.21	36.11	29.41	40.54	31.43
rLDH 7									-	25.53	29.03	36.84	38.24	30.77	25.71	26.67
rLDH 15										-	27.03	21.05	30.56	28.12	29.73	31.43
pL1*											-	44.83	36.36	28.12	33.33	22.86
pL2*												-	37.50	25.00	39.39	32.14
2004s°													-	46.43	66.67	43.75
2008s°														-	46.43	45.16
2009s°															-	43.75
2021s°																-

* *Pf*/*Pv*LDH aptamers from Lee *et al.* (2012)

° *Pf*LDH aptamers from Tanner *et al.* (2013)

A range of between 11.36 to 66.67 % sequence homology was obtained between synthesised oligonucleotides when conducting a two sequence alignment of the variable regions. Homology of the LDHp group of aptamers ranged from 24.44 % (LDHp 11 compared with LDHp 14) to 51.43 % (LDHp 3 compared to LDHp 18). Similarly, the percent homology for the class of r*Pf*LDH-targeting oligonucleotides ranged from 22.50 % (rLDH 4 compared to rLDH 7) to 43.59 % (rLDH 1 compared to rLDH 15). Assuming that comparing two randomly-generated sequences would result in a ~25 % alignment through chance co-presence of the same nucleotide at the same compared position, this average of 35.60 % may indicate some specific enrichment of certain nucleotides at certain locations was occurring in these two pools, or a continuation of the effects of nucleotide bias in the library, discussed previously.

Homology of synthesised oligonucleotides was then compared with that in literature. Percent homologies ranged from 21.05 % for pL2 (Lee *et al.*, 2012) and rLDH 15 to 39.39 % for pL1 and LDHp 1 (**Table 3.3**). When the synthesised aptamers were compared with those generated by Tanner and co-workers (2013), percent homologies ranged from 21.43 % (2008s aligned with LDHp 1) to 54.84 % (2004s aligned with LDHp 3).

All shared sequence homologies for synthesised sequences and pL1 and pL2 are well below 70.0%, the percentage of homology which is the cut-off value stipulated in their patent application for claiming a unique aptamer (Ban *et al*., 2012). All shared sequence homologies for synthesised sequences and those by Tanner and co-workers (2013) are below the 85.0% as stipulated in their patent application (Tanner *et al*., 2013).

3.5.2. Sequence similarity between rPfLDH and LDHp sequences

A neighbour-joining tree (**Figure 3.2**), generated using MUSCLE MSA (https://www.ebi.ac.uk/Tools/msa/muscle/), is a representation of the relatedness (or "maximum likelihood of relation" (Gascuel & Steel, 2006)) of the sequences to one another, with respect to their sequences, by clustering them based on sequence similarity (Saitou & Nei, 1987). **Figure 3.2** is a representation of the relatedness between the variable sequence regions (shown in **Table 3.1**) of sequences generate against r*Pf*LDH and LDHp presented in this thesis, as well as concatemer C7, including previously published sequences by Lee and co-workers (2012) and Cheung and co-workers (2013).

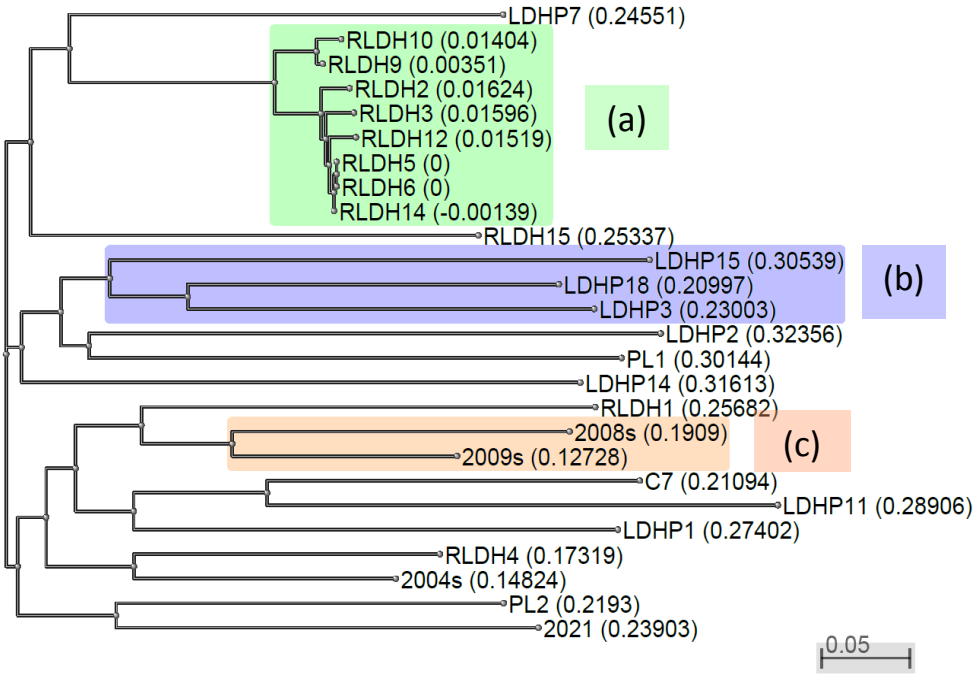

Figure 3.2: Neighbour-joining tree (dendogram with real distances) of generated sequences, compared with the concatemerised control, C7, and previously published sequences pL1 and pL2 by Lee and co-workers (2012) and 2004s, 2008s, 2009s and 2021s by Cheung and co-workers (2013), generated using MUSCLE MSA.
(https://www.ebi.ac.uk/Tools/msa/muscle/)
Distance indicator: 0.05 ≈ 2.5 nucleotides
(a) Green box: rLDH 10, 9, 2, 3, 12, 5, 6 and 14; (b) Blue box: LDHp 15, 18 and 3; and, (c) Red box: 2008s and 2009s

The real-distance dendogram, or neighbour-joining tree, presented in **Figure 3.2** shows similarity between the various oligonucleotide sequences, as well as groups of aptamers that are evolutionarily related. The distance indicator of 0.05 indicates a nucleotide difference of around 2.5 nucleotides between compared sequences. Moreover, **Figure 3.2** shows groups of aptamers that did not diverge greatly from each other through the evolutionary process of SELEX (Levay *et al*., 2016), and are thus evolutionarily similar. Such sequence clusters identified were: (a) rLDH 10, 9, 2, 3, 12, 5, 6 and 14 (green box); (b) LDHp 15, 18 and 3 (blue box); and, (c) 2008s and 2009s (red box). These groups highlighted in **Figure 3.2** contain aptamer sequences grouped as per the targets against which they were selected, specifically **Figure 3.2a** are r*Pf*LDH-targeting aptamers (in green) and **Figure 3.2c** are aptamers selected against r*Pf*LDH transcribed from a *P. falciparum* 3D7 cDNA library (in red), while **Figure 3.2b** are LDHp-targeting aptamers (in blue).

Eight of the eleven r*Pf*LDH-targeting oligonucleotide sequences identified in **Table B.1** are clustered together (**Figure3.2a**, green box), the short distance between them indicating that they are very closely related to one-another. This conserved family of aptamers, however, did not exhibit

significant r*Pf*LDH binding in the preliminary ELONAs (**Figure 2.19**). Given that this conserved family of aptamers were carried through SELEX, indicating some binding to the r*Pf*LDH target, it is possible that the biotinylation of these aptamers in the prelimanary ELONA (via use and incorporation of biotinylated forward primer into the sequences) affected the tertiary conformation of the folding necessary for target detection (Baldrich *et al*., 2004). Nevertheless, the absence of observable binding of aptamers in this particular group of aptamers to r*Pf*LDH in preliminary ELONA resulted in none of these aptamers being selected for further analysis.

Despite the presence of the poly-A stretch seen in the three rLDH aptamers, rLDH 1, 4 and 15, and the 6-A stretch in LDHp 14 (**Table 3.1**), clustering of these aptamers was not immediately evident in in **Figure 3.3.** This lack of clustering demonstrates that these aptamers are not related to one another through evolution, but rather enrichment of the poly-A stretch. Similarly, the clustering of aptamers selected for r*Pf*LDH generated by Cheung and co-workers (2013), specifically pL1 and pL2, do not exhibit clustering within the pool of compared sequences in **Figure 3.3**. This can be expected given the 44.83 % sequence homology between the two aptamers (**Table 3.3**).

Regarding the LDHp-targeting aptamers, a lesser cluster (smaller with regard to both number of represented sequences and degree of similarity) compared to that found for rLDH-targeting aptamers was also identified following multiple sequence alignment (MSA; blue box, **Figure 3.3**). This cluster contained aptamers LDHp 3, LDHp 15 and LDHp 18. While similar in sequence evolution to each other (evident by the clustering), they are less similar than groups presented in the green (**Figure3.2a**) and blue boxes (**Figure3.2c**) evidenced by the distances indicated in parentheses behind the sequence name. Further to this, LDHp 3 and LDHp 18 have a 51.43 % sequence homology (**Table 3.3**).

Of particular interest, rLDH 1, 4 and 15, were found distributed across the remaining aptamers, but not limited to a family or group of aptamers (**Figure 3.2**). This demonstrates that they were evolutionarily unique. Similarly to the rLDH range of aptamers, the LDHp range of aptamers exhibited divergence in nucleotide sequence. This diversity in sequence across aptamers selected for this small molecule illustrates the innate pool diversity from which the aptamers were selected. Furthermore, the divergence in studied sequences is indicative of the existence of various aptamer structure conformations, binding moieties and chemistries involved in the small peptide target binding (McKeague& DeRosa, 2012).

Conversely, while C7 and LDHp 11 were clustered in the same node, the distance (~20 nt) indicates divergence from each other through the evolutionary process of SELEX (Levay *et al.*, 2016), indicating that LDHp 11 does not significantly resemble the concatemer, C7, such that LDHp 11 would be considered a concatemerised PCR by-product. Therefore, the clustering of C7 and LDHp 11 in **Figure 3.2** demonstrates that while these two sequences are unique, they do share evolutionarily similar subsequences and/or nucleotides, so much so that they were considered of the same clade.

Previously published sequences from Tanner and co-workers (2013), specifically 2008s and 2009s, were clustered; this clustering is represented in the red box (**Figure 3.2c**). Similarly to C7 and LDHp 11, this demonstrates that these two sequences are evolutionarily similar (46.43 % sequence homology), so much so that they were considered of the same clade.

In order to evaluate whether sequence enrichment may have occurred, further analysis of the aptamer sequences found within the same clades was performed. This was conducted in order to identify consensus regions or common motifs found within the aptamer sequences. **Figure 3.3** shows the multi-sequence alignment of selected aptamers for r*Pf*LDH and LDHp using MUSCLE MSA (https://www.ebi.ac.uk/Tools/msa/muscle/), as per the shaded regions in **Figure 3.2**. Variable sequence regions (shown in **Table 3.1**) used included: (a) rLDH 10, 9, 2, 3, 12, 5, 6 and 14 (green box); (b) LDHp 15, 18 and 3 (blue box); and, (c) 2008s and 2009s (red box), and were aligned in a 5' to 3' direction.

(a) r*Pf*LDH-targeting cluster: Green box from Figure 3.2:

(b) *Pf*LDH-specific peptide, LDHp, targeting cluster: Blue box from Figure 3.2:

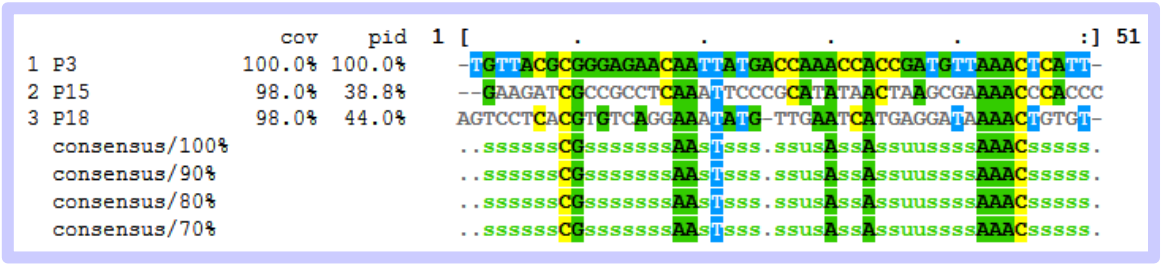

(c) Previously published *Pf*LDH-targeting cluster: Red box from Figure 3.2:

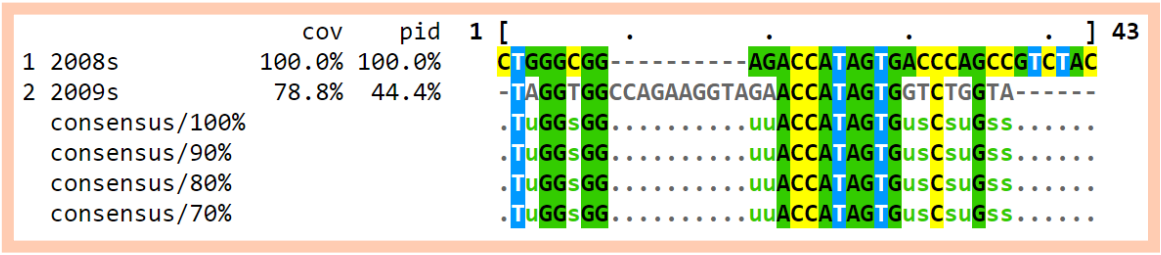

Figure 3.3: MView (Brown *et al*., 1998) alignment of aptamers, according to groups shown in Figure 3.2, generated using MUSCLE MSA.

(a) Green box: rLDH 10, 9, 2, 3, 12, 5, 6 and 14; (b) Blue box: LDHp 15, 18 and 3; and, (c) Red box: 2008s and 2009s

The alignment of rLDH aptamers in **Figure 3.3a** shows subsequence consensus of approximately 100% for all the identified sequences in the cluster in **Figure 3.2**. The multiple sequence alignments in **Figure 3.3** demonstrate the lower sequence diversity for the rLDH group caused by the presence of the poly-A region: alignment of the variable region show strong subsequence consensus across the clustered rLDH aptamers.

The distances between the sequences in the group shown in the blue box (**Figure 3.2a**), according to the distance indicator, are less than 0.1 indicating that these sequences evolutionarily differ from one another by an average of one nucleotide. This is evident in **Figure 3.3a** by the differing of two to four nucleotides outside of the poly-A sequence within the variable region. For example, rLDH 3 and

rLDH 12 vary by approximately 1.56 nucleotides (**Figure 3.2a**). This can be seen in **Figure 3.3a** in which there are two A/T substitutions in the variable region of rLDH 3 when compared to rLDH 12, apart from the poly-A region with an added three adenines in rLDH 3. When making these distance predictions based on sequences, the additional AAA sequence in rLDH 3, compared to rLDH 12, are scored differently than the A/T substitutions, so their evolutionary distances remain relatively close, as per the gap and bestfit principles (Haeberli, 2002).

Conversely, the LDHp-targeting group of sequences shown in **Figure 3.3b** exhibits a more limited consensus. A 70%+ consensus for only 11 conserved nucleotides along the length of the variable region of the single-stranded oligonucleotide sequence is evident. For example, LDHp 3 and LDHp 15 show a 44.4% sequence similarity (**Figure 3.3b**) and are scored with a difference of 26.77 nucleotides (**Figure 3.2**).

Similarly to **Figure 3.3b** for the LDHp group of sequences, the group presented in red (**Figure 3.3c**) comparing 2008s and 2009s (Cheung *et al*., 2013) show similar evolutionary traits and conserved sequences with 44% sequence similarity (**Figure 3.3c**). The 2008s and 2009s sequence evolutionary difference was scored at 15.91-nucleotide difference, which can be seen by the shift of the consensus region about eight nucleotides into the variable region of aptamer 2008s compared to 2009s (**Figure3.3c**).

Figure 3.4 shows the multi-sequence alignment of selected aptamers for r*Pf*LDH and LDHp using MUSCLE MSA (https://www.ebi.ac.uk/Tools/msa/muscle/). Variable sequence regions (shown in **Table 3.1**) of aptamers LDHp 1, 3, 11, 14 and 18, rLDH 1, 4, 7 and 15, and concatemer C7, including previously published aptamers by Lee and co-workers (2012) and Cheung and co-workers (2013) were aligned in a 5’ to 3’ direction.

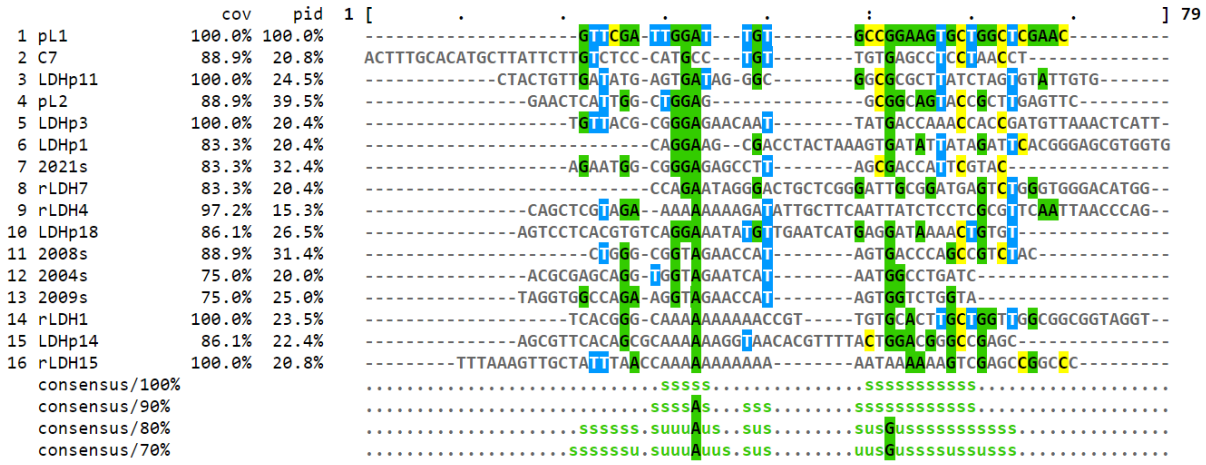

Figure 3.4: MView (Brown *et al*., 1998) alignment of selected aptamers, rLDH 1, 4, 7 and 15 and LDHp 1, 3, 11, 14 and 18, and compared with concatemer control, C7, and previously published aptamers by Lee and co-workers (2012) and Cheung and co-workers (2013), generated using MUSCLE MSA.

Note: Common nucleotides across aptamer sequences, i.e. nucleotides with consensus regions of 70-100 %, are so noted in the consensus lines and further highlighted in green

From **Figure 3.4**, only two nucleotides (A and G) in two different regions of the variable region of the aptamers were identified as having 80 % consensus across all the tested sequences. Given that the variable regions consist of a random (intrinsically semi-random) arrangement of four nucleotides, there will be some consensus across the aptamer sequences analysed. **Figure 3.4** showed that there is no alignment with 100 % consensus between the majority of the generated aptamers. The lack of overall consensus across the selected aptamers in **Figure 3.4** is therefore expected given the divergence in targets within the pools that SELEX proceeded in and the sequence divergences between the selected sequences, noted in **Figure 3.2** above.

Despite the limited consensus across all the tested sequences, a number of conserved subsequences do exist within the aptamer pools. These facilitate the binding reaction between the aptamer and the target, and can be found across a number of aptamers for a given target across different libraries (Tasset *et al*., 1997). These different families are thus responsible for the specificity inferred by the aptamer to the target, as well as offer sites for high affinity binding (Battig & Wang, 2014). Common moieties found in aptamer sequences were highlighted and compared within the aptamers' variable regions (**Table 3.4**) and locations compared with the secondary structures in **Figure 3.6**.

Table 3.4: Sequence of the variable region for the ssDNA LDH aptamers generated with common moieties noted.

Key: Solid underlining: GGTAG-type moiety; bold: ATTAT-type moiety; italics: GGCG-type moiety; zigzagged underlining: GC-rich region

Aptamer	Variable Region Sequence (5' to 3')
C7	ACTTTGCACATGCTTATTCTTGTCTCCCATGCCTGTTGTGAGCCTCCTAAC
rLDH 1	TCACGGGCAAAAAAAAAACCGTTGTGCACTTGCTGGTTGGCG*GCGG*TAGGT
rLDH 4	CAGCTCGTAGAAAAAAAAAGATATTGCTTC**AATTAT**CTCCTCGCG**TTCA**ATTAACCCAG
rLDH 7	CCAGAATAGGGACTGCTCGGGATT*GCGG*ATGAGTCTGGGTGGGACATGG
rLDH 15	TTTAAAGTTGCTATTTAACCAAAAAAAAAAAAATAAAAAAGTCGA*GCCGG*CCC
LDHp 1	CAGGAAGCGACCTACTAAAGTGAT**A**TTAT**AGA**TTCACGGGA*GCG*TGGTG
LDHp 3	**TGTTAC***GCGG*GAGAACA**ATTAT**GACCAAACCACCGA**TG**TTA**AACTCATT
LDHp 11	CTACTGTTGATATGAGTGATAG*GGCG*GCGCGC**TTATC**TGTATTGTG
LDHp 14	AGCGTTCACAGCGCAAAAAAGGTAACACGT**TTTACT**GGACG*GGCCG*AGC
LDHp 18	AGTCCTCACGTGTCAGGAAATATGTTGAATCATGAGGATAAAACTGTGT
pL1*	GTTCGATTGGATTGT*GCCGG*AAGTGCTGGCTCGAAC
pL2*	GAACTCATTGGCTGGA*GGCG*GCAGTACCGCTTGAGTTC
2004s°	ACGCGA*GCAGG*TGGTAGAATCATAATGGCCTGATC
2008s°	CTGG*GCGGT*AGAACCATAGTGACCCAGCCGTCTAC
2009s°	TAGG*TGGC*CAGAAGGTAGAACCATAGTGGTCTGGTA
2021s°	AGAATG*GCGGG*AGAGCCTTAGCGACCATTCGTAC

* r*Pf*/r*Pv*LDH aptamers from Lee *et al.* (2012)
° r*Pf*LDH aptamers from Tanner *et al.* (2013)

As shown in **Table 3.4**, this is plausible given that the presence and location of the GC-rich regions in both LDHp 14 and rLDH 15 are located at the same locale in the variable region of the aptamer's sequence, i.e. towards the 3'-end of the variable region of the aptamer's sequence. Apart from the GC-rich region, both LDHp 14 and rLDH 15 contain one other common moiety: the GTTG-type moiety, shown by dotted underlining in **Table 3.4**. The existence of these two common moieties in LDHp 14 and rLDH 15 reiterates the clustering of these two aptamers seen in **Figure 3.2**.

It is of importance to explore the structure-motif relationship to determine whether or not the location of these motifs on structures hold any bearing on target binding. The sub-sequence motifs and their respective locale on secondary structures formed will be further discussed in the next section.

3.5.3. Secondary structure prediction and analysis of aptamers generated in SELEX for rPfLDH and LDHp

The selection of similar sequence motifs from pools of different lengths can potentially be attributed to what has been called “the tyranny of short motifs” (Bartel & Szostak, 1993). In other words, a shorter motif has a greater initial chance of survival because it is present in a random sequence pool at a higher frequency than is a longer motif. A longer motif will be preferentially selected only if its affinity for a target is much higher than that of the shorter motif. As enrichment of short motifs occurs preferentially over the longer sequences during the selection and enrichment procedure of SELEX, these short motifs would occur more frequently throughout a given pool of aptamers produced against a single target (Bell *et al*., 1998).

The binding properties given by the sequence and tertiary structure of protein-binding nucleic acid aptamers determine the location and affinity of the binding interaction. Sequence motifs and structural moieties assist in the understanding and determination of the protein target and aptamer interaction; thus, the similarities of these moieties needs to be compared across aptamers generated for certain targets through SELEX. A structure and sequence comparison is, thus, required. Oligonucleotide structure prediction algorithms assist in determining possible secondary structures. The most probable secondary structures (generated from MFold) that arise from these variable regions flanked by the constant primer regions are shown in **Figure 3.5**. These secondary structures were calculated to occur spontaneously in solution, as evidenced by the negative ΔG value.

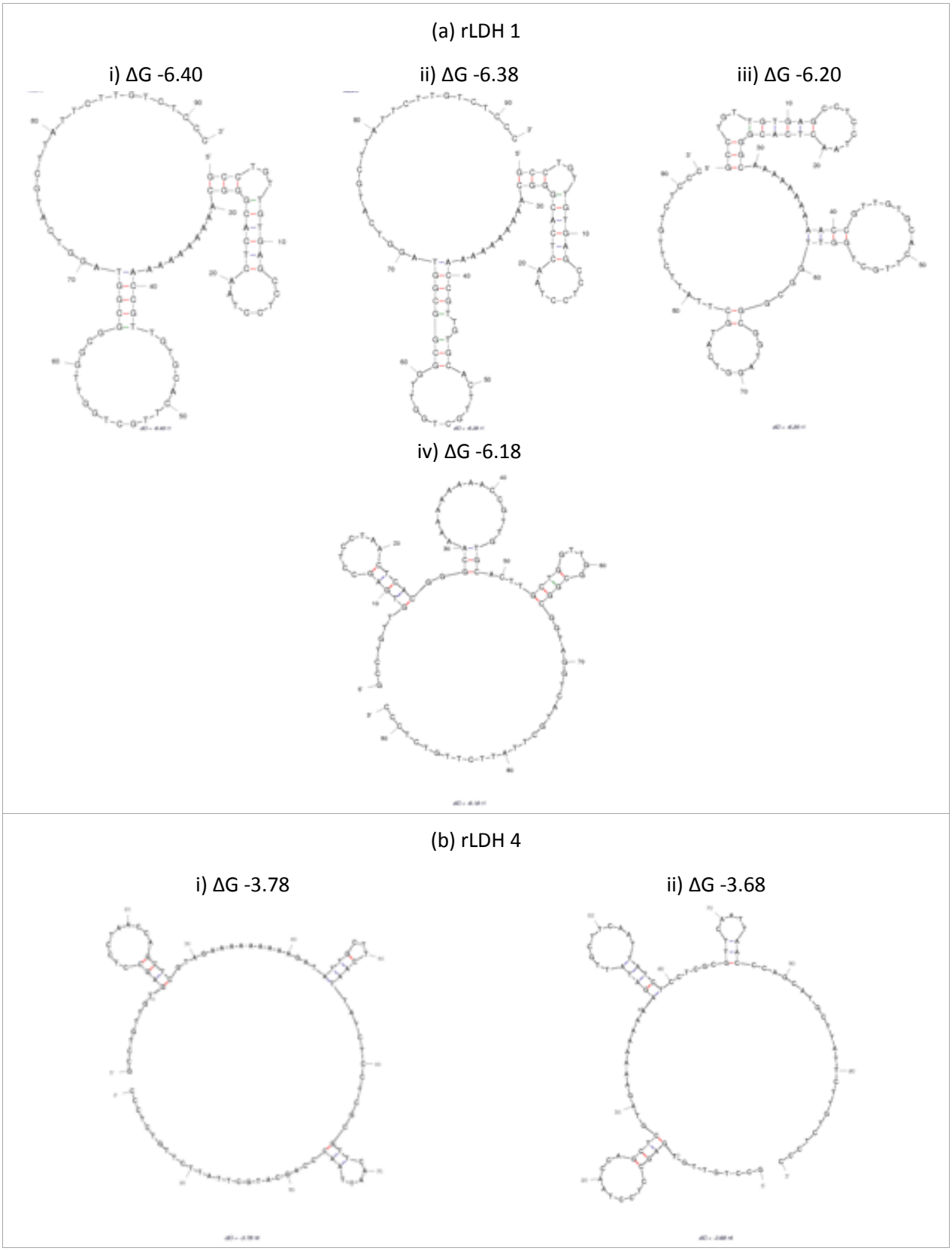

Figure 3.5: Continues on following page

Figure 3.5 continued…

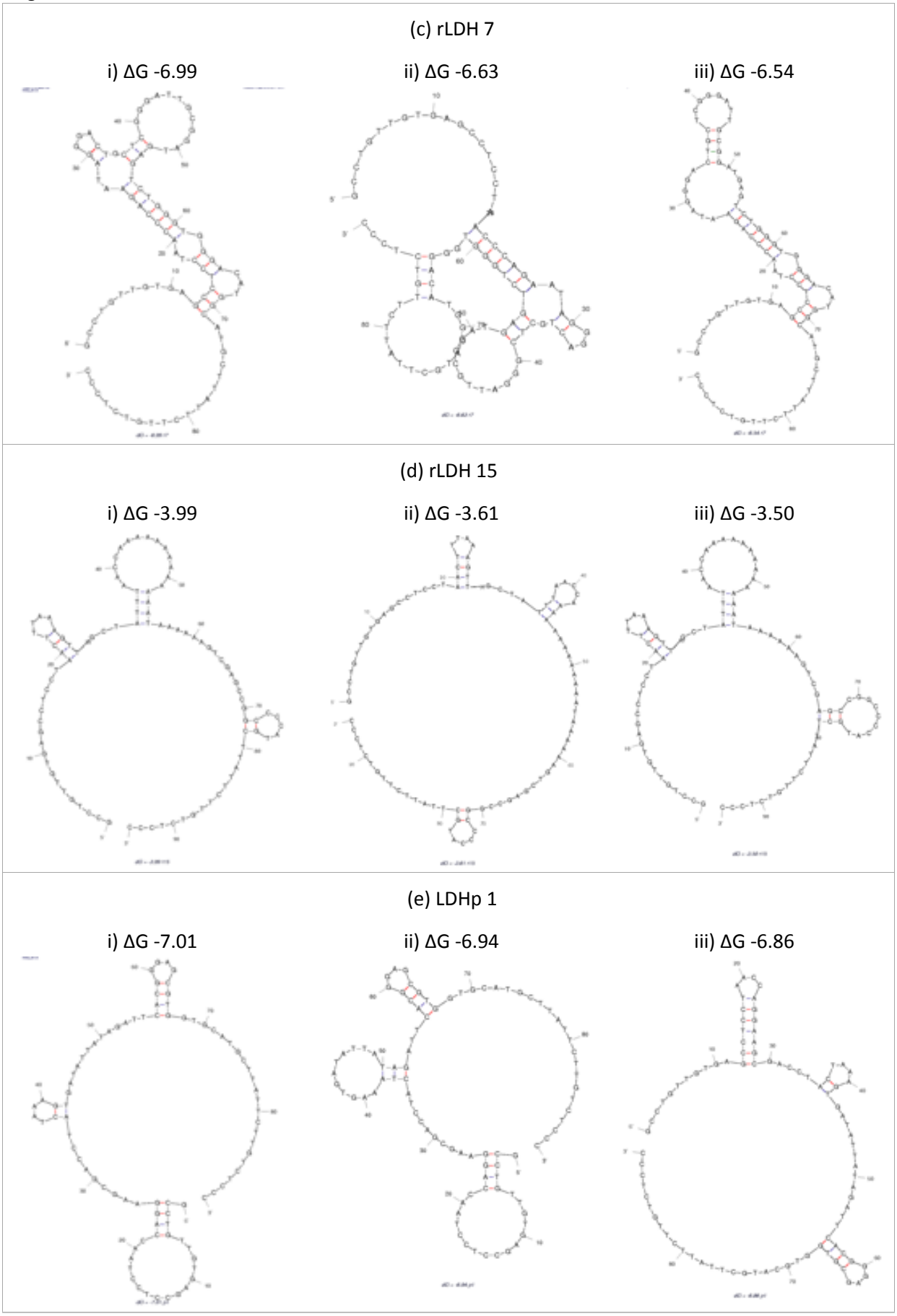

Figure 3.5: Continues on following page

Figure 3.5 continued…

(f) LDHp 3

i) ΔG -3.26

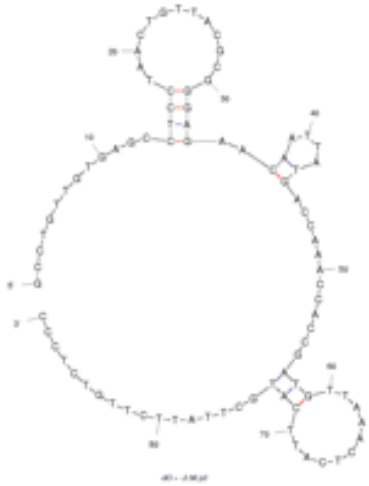

ii) ΔG -3.29

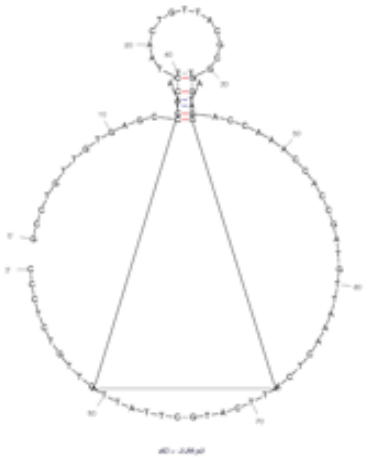

(g) LDHp 11

i) ΔG -3.67

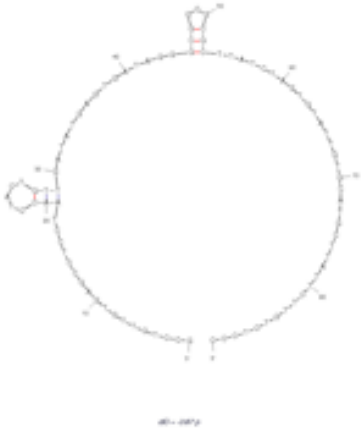

ii) ΔG -3.34

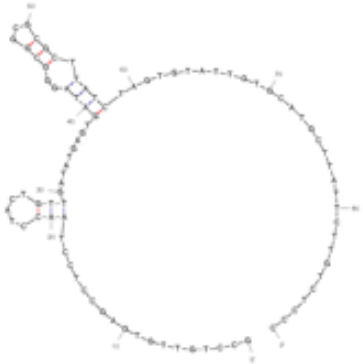

iii) ΔG -2.85

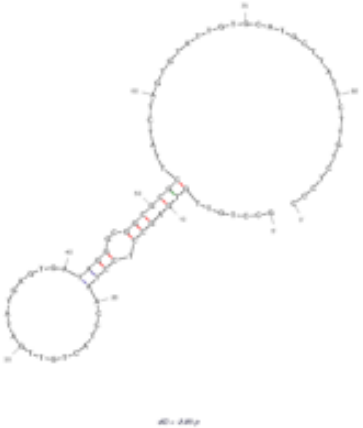

iv) ΔG -2.76

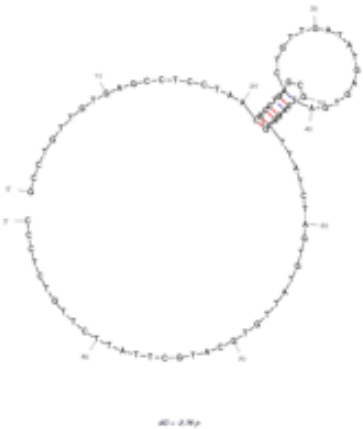

Figure 3.5: Continues on following page

Figure 3.5 continued…

(h) LDHp 14

i) ΔG -8.02

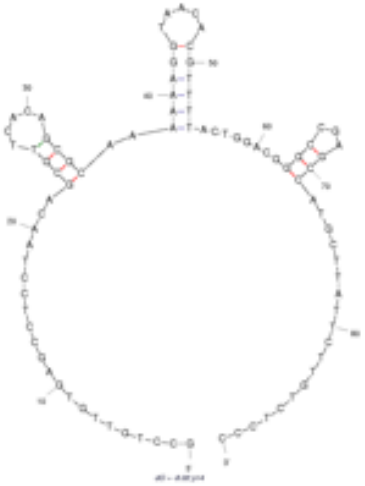

ii) ΔG -7.92

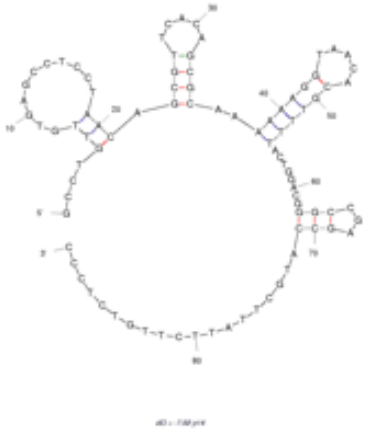

iii) ΔG -7.22

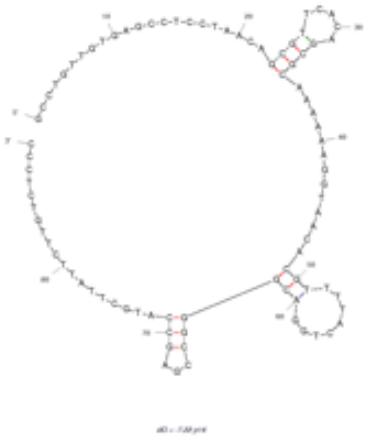

iv) ΔG -7.11

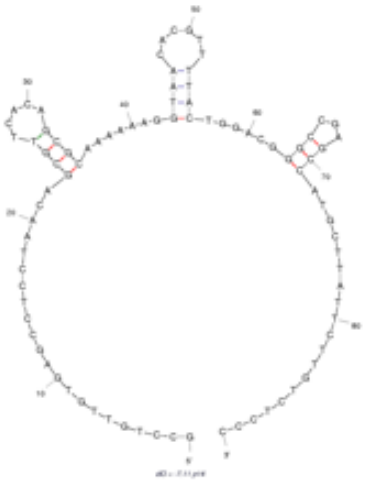

(i) LDHp 18

i) ΔG -6.63

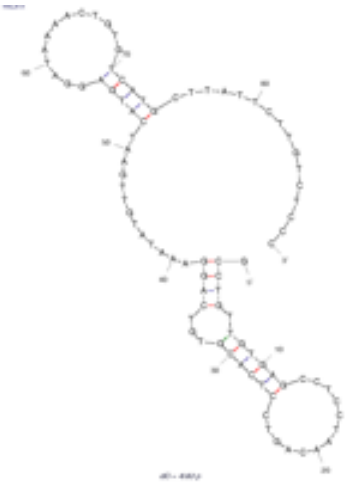

ii) ΔG -6.61

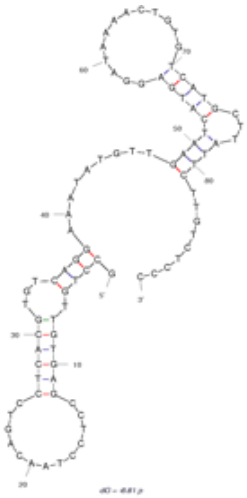

iii) ΔG -6.03

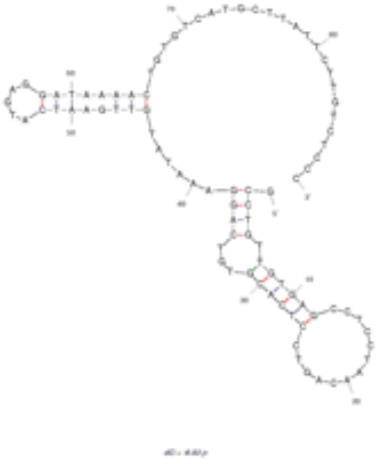

Figure 3.5: Predicted secondary structures (generated from Mfold) of ssDNA aptamers and corresponding ΔG (kcal/mol) for each ssDNA aptamer secondary structure.

Observed in **Figure 3.5**, secondary structures consist mostly of stem and loop substructures that branch off a bulbous main loop in various configurations and orientations. Interestingly, structures for rLDH 1, rLDH 7 and LDHp 18 contain stem-loop-stem-loop substructures creating “elbows” giving rise to more complex secondary structures. The formation of stem-loop structures appears typical of aptamer secondary structure formation (Huizenga & Stozak, 1995; Jian *et al*., 1996). Furthermore, secondary structures for LDHp 3 and 11 illustrate a folded loop structure in which stem-loop substructures fold in leading to what may be considered as a highly convoluted structure. Aptamers with a convoluted secondary structure are likely to bind smaller targets, as observed in a preliminary ELONA in **Chapter 2**, embedding the target within the oligonucleotide structure.

Predominating moiety sequences and their locations on structures are shown in **Figure 3.6**.

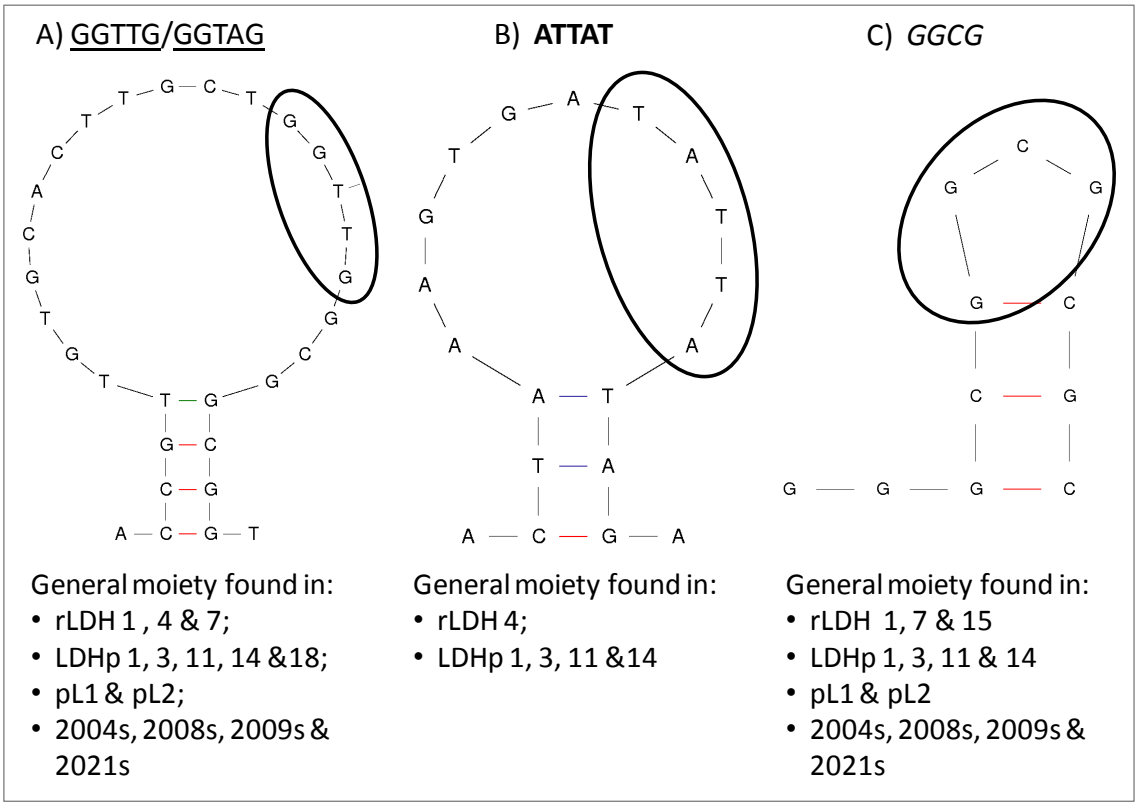

Figure 3.6: Moieties found on secondary structures of aptamers generated with examples of moiety location encircled [A) *GGTTG/GGTAG; B) ATTAT; C) GGCG].
*Moieties with the general sequence, GGTAG or GGTTG (differing by one nucleotide) are present on the loop structure of selected aptamers. The example shown here indicates GGTTG.

Cheung and co-workers (2013) showed that the binding moiety, $C_6G_7G_8[TA]G_{11}$, of the aptamer 2008s plays a pivotal role in target recognition and binding to *Plasmodium* LDH. With the exception of rLDH 15, the general GGTAG moiety (single underlining; **Table 3.4**, **Figure 3.6A**), also found in aptamer sequences with single nucleotide derivations in this moiety and/or the reverse sequence thereof, was found predominantly on the loop structure of all aptamers analysed, demonstrating that this moiety sequence, location and tertiary structure plays a role in target recognition. The moiety, ATTAT (**Figure 3.6B** and in bold in **Table 3.4**), can also be found on the stem-loop structure of the synthesised aptamers. However, this particular moiety appears to occur frequently in the aptamers selected against the *P. falciparum*-specific peptide indicating its relevance in the tertiary structure of aptamers against the smaller LDHp target. A possibility is that this sequence can be attributed to the flexibility of adenine and thymine bonding facilitating complexation with LDHp.

The sequence, GCGG and reverse of (GGCG) (in italics), is present in 10 of the 15 analysed sequences in **Table 3.4**. This sequence forms part of a binding moiety in the stem and stem-loop secondary structures of pL1, 2008s and LDHp 11 (**Figure 3.6C**) and, thus too, forms an integral three-dimensional structure necessary for recognition and binding of the aptamer to the *Pf*LDH target. LDHp 11, LDHp 14 and rLDH 15 contain a GC-rich stem-loop structure (underlined with zig-zagging in **Table 3.4**) incorporating the GCGG moiety (shown in **Figure 3.6C**). Due to the inherent stability of the GC rich stem-loop, the resulting tertiary structure may play an important role in the specific and high affinity complexation of the aptamers to the *P. falciparum*-specific peptide and recombinant *Pf*LDH. However, further investigation into this particular binding site is required. Interestingly, rLDH 7 contains four runs of three guanines, sufficient to form an intramolecular G-quadruplex tertiary structure. The presence of these G-rich runs demonstrates a true evolution of the rLDH 7 sequence structure in the enrichment during the SELEX procedure. Furthermore, the presence of this G-quadruplex structure facilitates and enhances the stability of the rLDH 7-*Pf*LDH interaction.

Moieties with the same or similar sequences within the aptamers have the general sequences: GTTGC (dotted underlining in **Table 3.4**). This moiety may or may not be incorporated into a secondary or tertiary structure relevant for binding to the target. However, due to the presence of this sequence within the variable region of analysed aptamer sequences, it is evident that this moiety and any resulting structure are relevant for correct folding of the single-stranded DNA sequences and their recognition of *Plasmodium* LDH.

Furthermore, the recurrences of the moieties shown in **Figure 3.6** demonstrate an increased conservation of residues in the LDHp pool of aptamers, shown in **Table 3.4**. This may be further explained by the simpler structure that the target, LDHp, has in comparison with the whole recombinant r*Pf*LDH (McKeague & DeRosa, 2012). Therefore, these moieties shown in **Figure 3.6** may be pivotal in recognition and binding of the ssDNA aptamer to the helical LDH peptide.

Single-stranded oligonucleotides have an inherent flexibility when folding throughout the SELEX process, particularly in the selection but also during the amplification steps. Therefore, secondary and tertiary structures and moieties that are not immediately visible in the 5' to 3' forward direction are possible. This can lead to the formation of particular moieties such as the prominent adenine (A) nucleotide runs seen in the synthesised aptamers, rLDH 1, 4, 15 and LDHp 14 created by imperfect alignment of nucleotides. These moieties and structures would result from the single-stranded oligonucleotides twisting and folding or looping back resulting in unidirectional base-pairing of the single strand (e.g. 3' complementing with 3' ends) creating a more complex and convoluted tertiary structure (Brahms *et al*., 1966; Leng & Felsenfeld, 1966; Isaksson *et al*., 2004). However, as the location of this twisting and folding can only be hypothesised based on the reversed complementary base-pairing of the sequence, the number of known tertiary structures given by an aptamer sequence can be innumerable and/or incalculable with presently available oligonucleotide structure prediction software.

Therefore, the location of short sub-sequence motifs appear to be important in secondary structure formation, and may lend themselves to target recognition (**Table 3.4**).

Table 3.5 shows the dot-bracket notations of the predicted tertiary structures, determined using VSFold, which is used in the rendering of pseudoknots in RNA. Therefore, the pairing observed in **Table 3.5** is loosely based on RNA folding. Secondary basepairing occurs when the step loop structures tend to fold in onto each other creating a tertiary structure.

Table 3.5: Dot-bracket notations of the predicted secondary structure folding of aptamers, generated using VSFold.
Parameters: dots indicate no basepairing; round brackets indicate basepairing or stem formations; square brackets indicate secondary basepairing; temperature of 20 °C with pseudoknot calculations included in presence of $[Mg(H_2O)_6]^{2+}$; Flory polymer solvent model selected.
Aptamers: LDHp 1; LDHp 3; LDHp 14; LDHp 18; rLDH 1; rLDH 7 rLDH 15; pL1; 2008s and concatemer, C7.

Aptamer	Sequence (5' to 3') ·	ΔG (kcal/mol)
Negative control sequences		
C7	GCCTGTTGTGAGCCTCCTAACACTTTGCACATGCTTATTCTTGTCTCCCATGCCTGTTGTGAGCCTCCTAACCTCATGCTTATTCTTGTCTCCC ...(((((.[[[[....)))))).....(((((.....)))))).....(((((.....)))))]]]].....	-14.34
Sequences generated through SELEX using *rPf*LDH as the target		
rLDH 1	GCCTGTTGTGAGCCTCCTAACTCACGGGCAAAAAAAAAACCGTTGTGCACTTGCTGGTTGGCGGCGGTAGGTCATGCTTATTCTTGTCTCCC .....(((((.....))))).(((((.....(((((((.((((....)).))))))).(((.....))).....)))))....	-35.88
rLDH 4	GCCTGTTGTGAGCCTCCTAACCAGCTCGTAGAAAAAAAAAGATATTGCTTCAATTATCTCCTCGCGTTCAATTAACCCAGCATGCTTATTCTTGTCTCCC ....[[[[.((((....]]]]..)))))..((((.....(((((((.....)).)))))....((((.....))))...)))).....	-29.12
rLDH 7	GCCTGTTGTGAGCCTCCTAACCCAGAATAGGGACTGCTCGGGATTGCGGATGAGTCTGGGTGGGACATGGCATGCTTATTCTTGTCTCCC .(((((..((....[[[[....))..)))))..((((..]]]]..))))....((((..[[[))))..((((....]]]...))))....	-38.58
rLDH 15	GCCTGTTGTGAGCCTCCTAACTTTAAAGTTGCTATTTAACCAAAAAAAAAAAAAATAAAAAAGTCGAGCCGGCCCATGCTTATTCTTGTCTCCC ....((((((.....)))).]]]..((((.[[[[))))).....]]]].....(((.[[[[.))).....]]]].....	-18.39
Sequences generated through SELEX using LDHp as the target		
LDHp 1	GCCTGTTGTGAGCCTCCTAACCAGGAAGCGACCTACTAAAGTGATATTATAGATTCACGGGAGCGTGGTGCATGCTTATTCTTGTCTCCC .((((((.....)))).))))..((((...[[[...((((.....))))..((((((]]].)))))))....))))....	-29.86
LDHp 3	GCCTGTTGTGAGCCTCCTAACTGTTACGCGGGAGAACAATTATGACCAAACCACCGATGTTAAACTCATTCATGCTTATTCTTGTCTCCC .....((((((.....(((.....)))[[[[.[[[...[[[.....((((]]]....))))...)))))))..]]]]]]].	-18.59
LDHp 11	GCCTGTTGTGAGCCTCCTAACCTACTGTTGATATGAGTGATAGGCGGCGCGCTTATCTAGTGTATTGTGCATGCTTATTCTTGTCTCCC .....((((((....((((..[[[)))).....]]](((((.((.....)))))))..((((.....))))))))).....	-20.76
LDHp 14	GCCTGTTGTGAGCCTCCTAACAGCGTTCACAGCGCAAAAAAGGTAACACGTTTTACTGGACGGGCCGAGCCATGCTTATTCTTGTCTCCC ((((((((((((((.....)).)))))))[[[[.....(((((..]]]])))))).)))))))).(((.....))).....	-34.95
LDHp 18	GCCTGTTGTGAGCCTCCTAACAGTCCTCACGTGTCAGGAAATATGTTGAATCATGAGGATAAAACTGTGTCATGCTTATTCTTGTCTCCC .((((.((((((.((.....)).))))))...)))))...((((..[[[[))))..((((.....)))))......]]]].....	-24.65
***rPf*LDH-binding aptamers drawn from the literature**		
pL1*	CACCTAATACGACTCACTATAGCGGATCCGAGTTCGATTGGATTGTGCCGGAAGTGCTGGCTCGAACCTGGCTCGAACAAGCTTGC ...((.((((((.....)))))).((((((((..]]].)))))))..(((((.....)))))[[[.....((((]]]...)))))...	-39.69
2008s°	CGTACGGTCGACGCTAGCCTGGGCGGAGACCATAGTGACCCAGCCGTCTACCACGTGGAGCTCGGATCC (((..(((((..((((.....))))..)))))...(((((.....))).)).)))).(((.....)))	-30.22

Dot-bracket notations, determined using VSFold (http://www.rna.it-chiba.ac.jp/~vsfold/cgi-bin/run_vsfold5_23.cgi; Dawson *et al*., 2006), were generated to linearly represent the predicted secondary folding are shown in **Table 3.5**. VSFold is used in the rendering of pseudoknots in single-stranded ribonucleic acid (RNA), and data presented are a representation of predicted folding for ssDNA.

Similar to secondary structure analysis using the MFold-based predicted secondary structures, the dot-bracket representation of secondary structure predictions that included pseudoknot formation indicate similar moieties and motifs exist across the various aptamer classes. The different families of moieties are highlighted in different colours in **Table 3.5**. These moieties are located between parentheses in the dot-bracket notation of secondary structures and are indicated by dots between bracketed parentheses. The round brackets indicate basepairing and the resultant formation of folded ssDNA stem structures, while the square brackets indicate further folding of these stem-loop structures creating pseudoknots (Antczak *et al*., 2018).

In the selected sequences for the r*Pf*LDH- and LDHp-targeting oligonucleotides, there exist conserved areas, indicated by shading in different colours in **Table 3.5**. While there was some overlap in these motif sequences across the different classes of aptamers, certain secondary structures containing certain families of motifs were conserved amongst the r*Pf*LDH- and LDHp-targeting oligonucleotides. Areas of basepairing give rise to the formation of loops containing sequence motifs believed to play a role in target binding, as discussed in the previous section. In **Table 3.5**, three different moiety families common across the rLDH sequences are shown, specifically the GCGG moiety indicated in purple, the ATTAT moiety in red and GGTTG moiety in pink. The rLDH 15 sequence, for example, contains the TATT (grouped with ATTAT) moiety not only on a stem-loop structure (shown in **Figure 3.6**), but also on a pseudoknot structure (indicated by the square brackets in **Table 3.5**) is believed to be of importance in target recognition and binding.

The LDHp-targeting sequences similarly highlight three different binding motifs found on stem-loop structures. Specifically, such motifs were: the GCGG moiety indicated in blue and the ATTAT (or similar) moiety in green. However, a sub-moiety emerged amongst the LDHp class of sequences: CGG, highlighted in yellow. This sub-moiety, also found predominantly on secondary structures indicated by the dot-bracket notation in **Table 3.5**, was too small to be considered pertinent in the

overall structure-recognition element proposed by secondary target-binding oligonucleotide structures.

As previously shown in **Figure 3.6**, the previously published aptamers also contain these identified moieties (GCGG, ATTAT and GGTTG), which also appear to have a sequence-structure relationship.

Table 3.5 demonstrates that the appearance of these moieties was not only beneficial with respect to the uncomplicated secondary structures such as MFold-based stem-loops (**Figure 3.6**), but that their location transcends to more complex secondary structures such as pseudoknots. Pseudoknots, while limited to secondary structure predictions and outputs, do offer the prediction of more complicated structures based on oligonucleotide chemistries – likened to a pseudo tertiary structure (Antczak *et al*., 2018). Given the localisation of common motifs on pseudoknots and uncomplicated secondary structures (**Table 3.5**), the appearance of pseudoknots may play a role in target binding. Identification of these motifs with respect to the three-dimensional rendering of the ssDNA oligonucleotide tertiary structures were hence explored and discussed in the following section.

3.5.4. Tertiary structure prediction

The tertiary structures of previously identified families of motifs were visualised by rendering three-dimentional (3D) images of the oligonucleotide aptamer sequences, from which important information on the location of potential binding sites could be obtained. Of the three-dimensional oligonucleotide prediction software currently available, RNAComposer (http://rnacomposer.cs.put.poznan.pl/; Popenda *et al*., 2012) was chosen as this tool is able to model the DNA with more freedom guided by the flexibility of single-stranded RNA folding, and conforming less to the conventions in most DNA folding programs. These predicted 3D tertiary structures are calculated based on binding predictions of RNA folding governed by known conventions and, therefore, have a tendency to adopt a base-paired double helix formation. However, the analysis of tertiary structure and target binding prediction is intended to be a guide as it is limited as actual interactions between aptamers and protein targets cannot be performed due to limiting software available, which is capable of suitably predicting these interactions on a molecule to molecule basis.

Examples of the most probable aptamer tertiary structures generated that require further discussion are rLDH 4 (**Figure 3.7**) and LDHp 11 (**Figure 3.8**), while the 3D rendered tertiary structures of the remaining aptamers are shown in **Figure 3.9**.

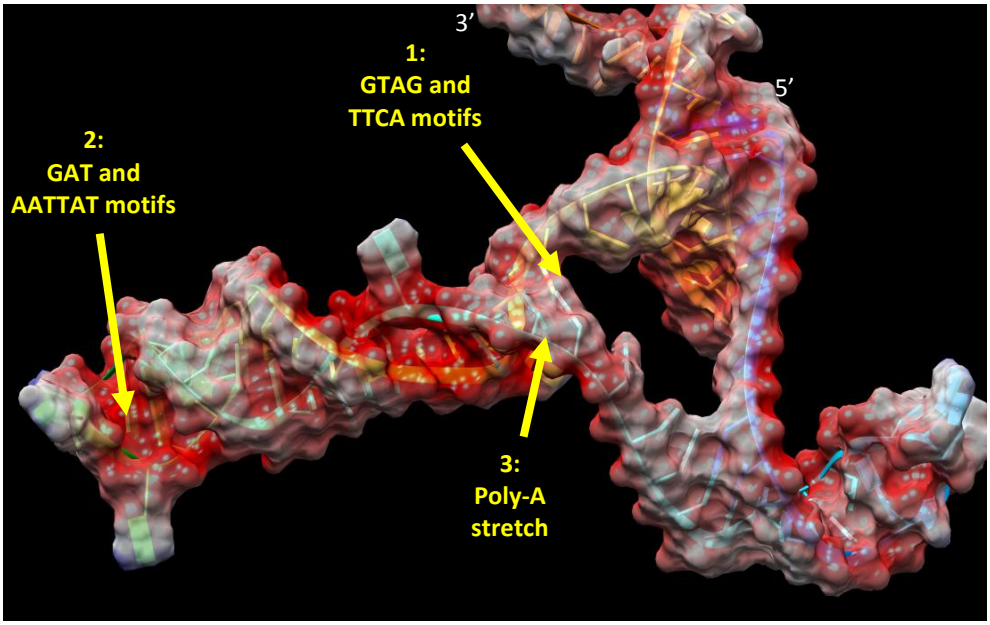

Figure 3.7: Predicted 3-dimentional tertiary structure of rLDH 4 generated using RNA composer with image rendering in Chimera.
Red: negative coulombic potential; white: neutral coulombic potential; blue: positive coulombic potential

With reference to **Figure 3.7**, the second guanine (G) in the motif GTAG (from **Table 3.4** and **Figure 3.6A**) base-paired with cytosine (C) of TTCA (from **Table 3.4** and **Figure 3.6B**), both located in the largest binding pocket of the rLDH 4 3D tertiary structure, as indicated by arrow 1. Given the size of this possible binding pocket, it is likely that this pocket is well suited to binding and interacting with larger targets. The sequence GAT, found as part of the GGTAG motif (**Figure 3.6A**) and AATTAT, resembling motif B in **Figure 3.6**, are found in close proximity to one another and may, in fact, form a helical groove binding pocket with negative coulombic potential (indicated by arrow 2), well suited as binding moiety for smaller targets or proteinaceous secondary structures. The structure of aptamer rLDH 4 depicted in **Figure 3.8** appears ideal for binding to larger molecules, such as r*Pf*LDH. Binding of rLDH 4 to r*Pf*LDH, as well as other species of LDH, will be explored in the following Chapter.

The 3D rendered tertiary structure of LDHp 11 is shown in **Figure 3.8** and includes a side view (**Figure 3.8A**) and a view into the helical structure of LDHp 11 (**Figure 3.8B**).

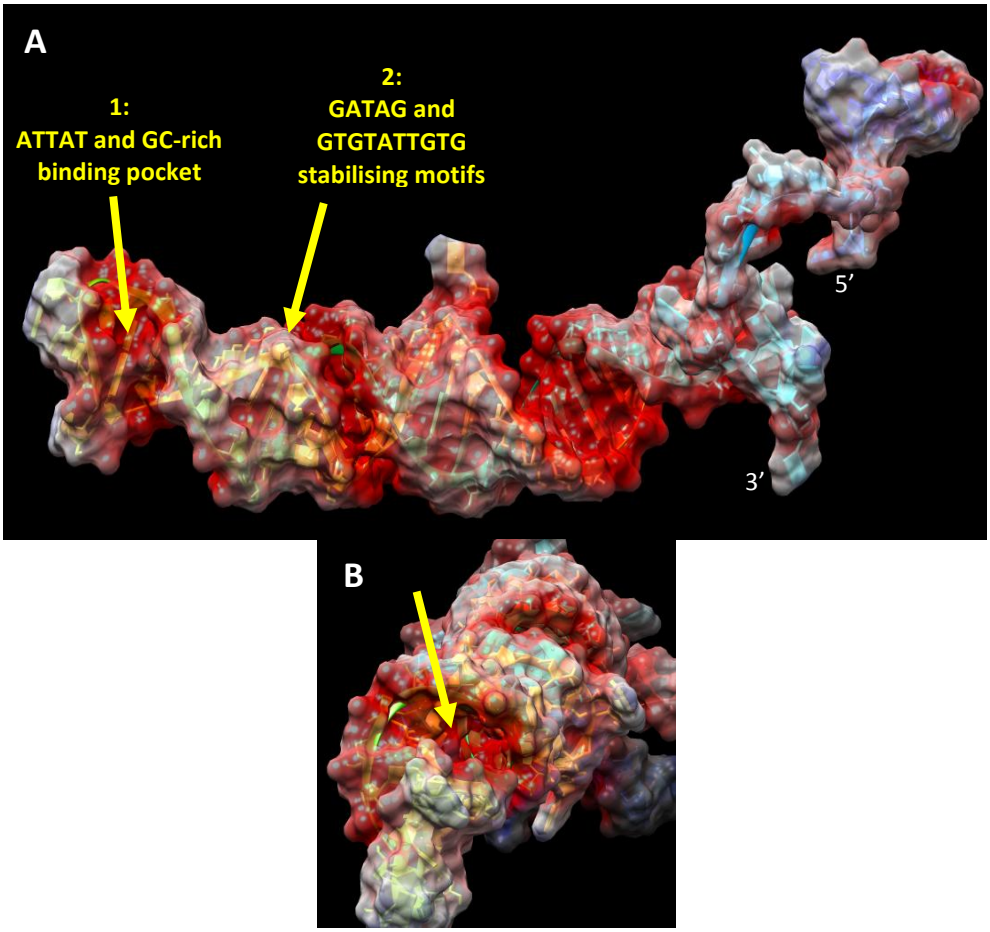

Figure 3.8: Predicted 3-dimentional tertiary structure of LDHp 11 generated using RNA composer with image rendering in Chimera.
A: Side view; B: View into the helical structure. Red: negative coulombic potential; white: neutral coulombic potential; blue: positive coulombic potential.

Binding motif B (highlighted in **Figure 3.6B**) with sequence ATTAT was also present in the LDHp 11 sequence (**Table 3.4**) and was located on a helical groove binding pocket (arrow 1 in **Figure 3.8**). The GC-rich region alongside this pocket offers an inherent stability which may play a pivotal role for the target binding mechanism (Nelson *et al*., 1987). Other motifs identified in the LDHp 11 sequence, namely GATAG and GTGTATTGTG (arrow 2 in **Figure 3.8**), are seen to base-pair in proximity to the afore-mentioned binding pocket and therefore, although not directly involved in possible target binding, may play a role in stabilising the tertiary structure. Both of these probable binding sites are found at a distance away from the 5'-end, and may reduce possible interference caused by any 5'-modifications required for aptamer immobilisation for sensor design. A clear view down the binding site's predicted tertiary structure is shown in **Figure 3.6B**, clearly showing the grooved binding site (arrow).

Identified pockets of interest in **Figure 3.7** and **Figure 3.8**, and where sequence motifs are prominent have polarisation and charge suitable for target binding. Generated aptamer tertiary structures are shown in **Figure 3.9**, in comparison to the tertiary structures derived from r*Pf*LDH sequences previously published, pL1 (Lee et al., 2012) and 2008s (Cheung *et al*., 2013), as well as the concatemer, C7.

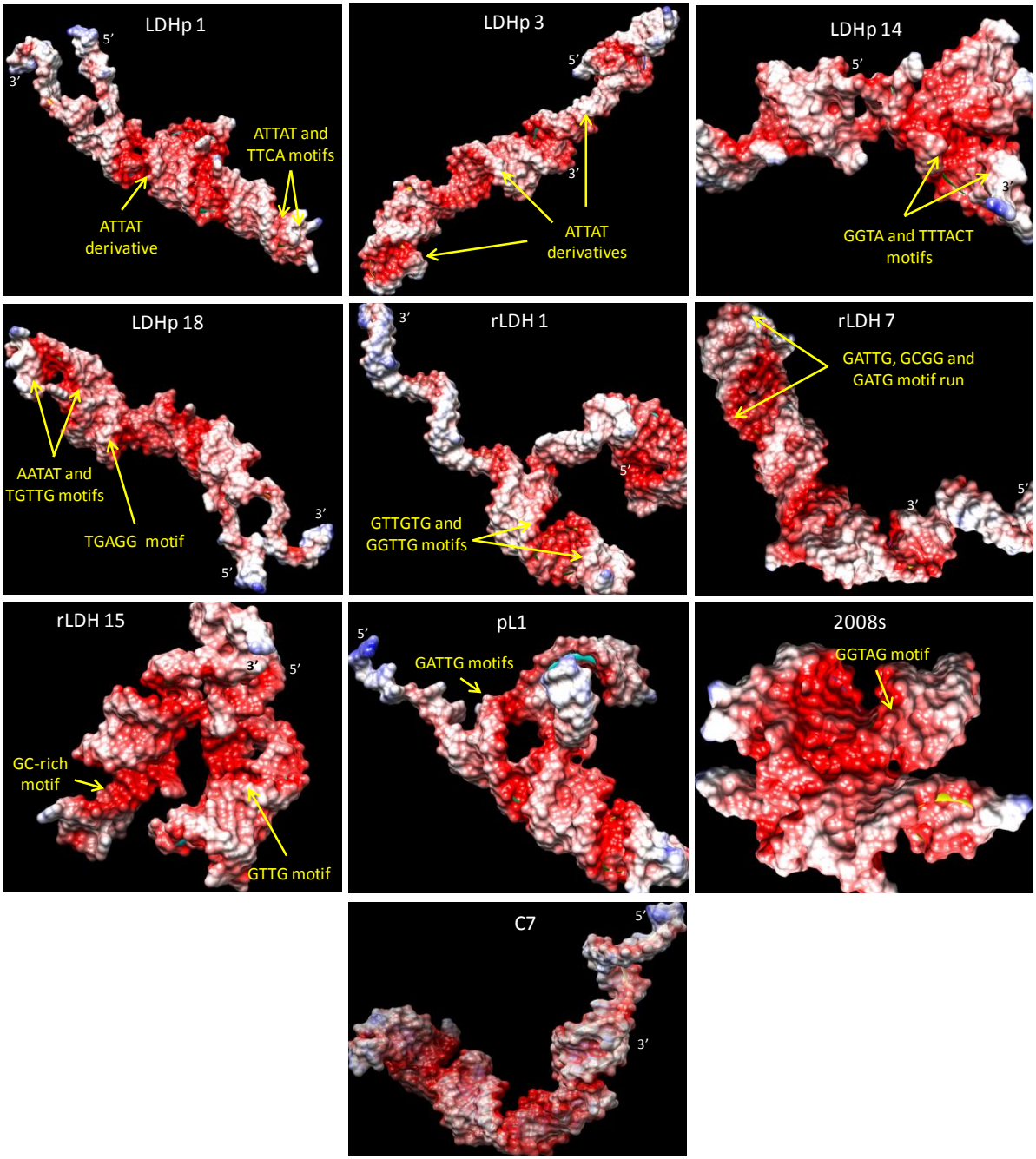

Figure 3.9: Predicted 3-dimentional tertiary structure of generated aptamers using RNA composer with image rendering in Chimera.
Aptamers: LDHp 1; LDHp 3; LDHp 14; LDHp 18; rLDH 1; rLDH 7 rLDH 15; pL1; 2008s and concatermer, C7. Red: negative coulombic potential; white: neutral coulombic potential; blue: positive coulombic potential.

Interestingly, the generated LDHp aptamer tertiary structures display an apparent commonality across aptamers: the binding motif ATTAT, shown in **Figure 3.6B** and **Figure 3.9**, exists on similar tertiary structures, which can be described as a binding pocket "hand", indicating that it may indeed play a role in binding to the smaller LDHp target and the LDHp moiety on r*Pf*LDH, in particular. Interestingly, the GTAG moiety on the LDHp aptamers is generally located in close proximity to ATTAT moiety either sequentially or structurally. Therefore, it is likely that both moieties are equally important in creating a small molecule binding pocket, and may in fact work synergistically when capturing and binding the smaller target, LDHp. These pockets are slightly polar in nature and therefore are suited for binding to polar amino acids, such as leucine-isoleucine (L-I) "arm" on the LDHp helix, as shown in the rendered Deepview (Guex & Peitsch, 1997) and Chimera (Pettersen *et al*., 2004) images in **Figure 3.10**.

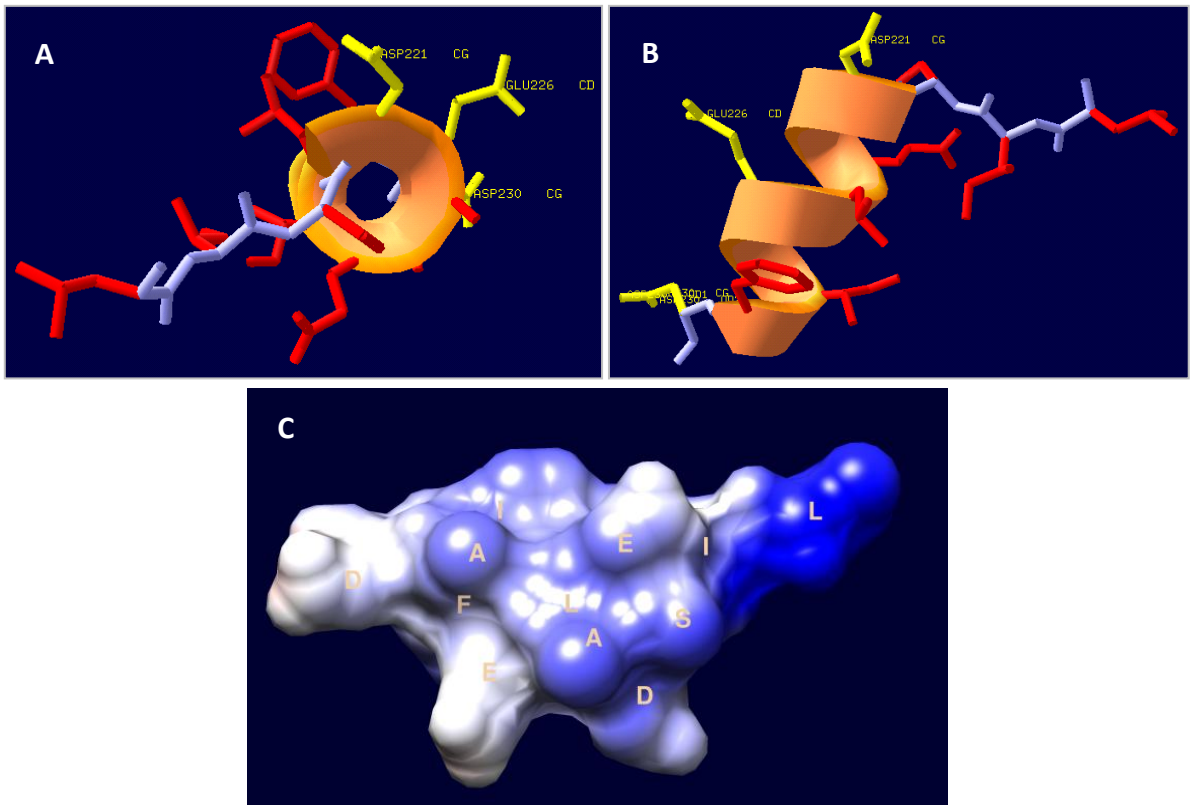

Figure 3.10: Crystallographic structures of the species-specific peptide found on *Pf*LDH subunit with a view down the helix (A) and from the side (B) rendered in DeepView (A and B) and Chimera (C).
A and B: Helix: orange ribbon; loop: grey sticks; polar residues: yellow sticks; non-polar residues: red sticks.
C: Red: negative coulombic potential; white: neutral coulombic potential; blue: positive coulombic potential.

The peptide sequence, LISDAELEAIFD, tends to spontaneously fold into the same helical structure (shown in **Figure 3.10**) that exists in the whole protein when in a buffered saline solution, offering

stability during the antibody and aptamer synthesis and selection process. This can be (and was) confirmed using protein folding software, such as Abalone. However, the loop structure (grey sticks) does not have the molecular forces that offer stability rendering the loop structure relatively flexible in the peptide tertiary structure and, transcendently, the whole *Pf*LDH. Understandably, inclusion of this peptide sequence into the whole protein leads to the stabilisation of the loop structure, which may play a role in speciation during synthesis of the capture molecules.

Figure 3.10 shows the polar (yellow sticks) and non-polar (red sticks) residues of the species-specific peptide (LDHp). When looking through the barrel of the helix, the polar more hydrophilic residues are all on the same side of the helix with the non-polar hydrophobic residues on the opposite side of the helix highlighting the difference between the exposed and protected residues. The polar residues, aspartic acid and glutamic acid, offer possible binding sites for antibody and aptamer interactions due not only to their exposure to the aqueous environment but to the length and charge of these residues. These residues could facilitate binding between the peptide target and the antibody or aptamer through binding interactions including van der Waals forces, hydrogen bonding and electrostatic interactions between molecular groups. They can be likened to projecting "fingers" on a helical "hand".

The poly-A stretches seen in rLDH 1, 4 and 15 (**Figures 3.7** and **3.9**) are located at flexible bridging sites between loop structures, granting the aptamers an intrinsic flexibility facilitating binding to the larger r*Pf*LDH target. The GTAG and GCGG general moieties are common throughout all generated aptamers for LDHp and r*Pf*LDH (**Table 3.4**; **Figure 3.6**), and, with the exception of rLDH 4 as previously discussed, behave autonomously, creating their own unique tertiary structures. As seen in **Figure 3.9**, these motifs are generally located on a major helical groove well suited as a binding site (Varani *et al.*, 2000; Reiter *et al.*, 2008). The GC-richness of these motifs and regions offer an inherent stability to these tertiary structures (Nelson *et al*., 1987); and, therefore, are ideally suited to binding a particular epitope on the target, r*Pf*LDH.

In LDHp 3 and 14 and rLDH 7 and 15 in **Figure 3.9**, the primer sequences were also seen to fold in on the aptamer sequence directly facilitating the formation of potentially important binding sites and motifs, rendering the presence of these primer sequences important in the formation of the overall 3D tertiary structure. Furthermore, the primers were located a distance away from binding motifs

for rLDH 7 and 15, whereas primer-containing tertiary structures encompassed binding motifs for LDHp 3 and 14 – further highlighting characteristics prominent in the two groups of size-dependant aptamers. Unlike secondary structures illustrated in **Figure 3.5** in which primers appear not to be involved in secondary structure formation, immobilisation of these four aptamers could disrupt their given tertiary structures, and will affect target binding, particularly for LDHp 3 and 14, in which the primers aid to evolve the tertiary structures. It further stands to reason that end modifications for the purposes of immobilisation may also disrupt binding due to the relative size of these modifying molecules in comparison to nucleotides, such as addition of biotin as a modifier (Wang *et al*., 2014; Hernandez *et al*., 2013). In particular, a 5' modification on rLDH 15, LDHp 14 and, to an extent, LDHp 3, will disrupt target binding as this end is embedded in the tertiary structure and steric space will be required to accommodate the 5' modification molecule. These are factors relating to aptamer immobilisation that will need careful consideration in later binding analyses and sensor design.

On the other hand: either one or both flanking primers were also seen not to be directly involved in folding of the tertiary structure (rLDH 4 in **Figure 3.7**, LDHp 11 in **Figure 3.8** and LDHp 1, and 18 and rLDH 1 and 7 in **Figure 3.9**); and, therefore, are not directly involved in tertiary structure formation. These protruding primer and primer binding regions are freely available to anneal to flanking primer regions of another aptamer molecule through primer homodimer and/or heterodimer formation, as previously discussed in **Chapter 2.5.3.c** and **Chapter 2.5.3.d**. More importantly, they are ideally suited for 5'- and 3'-modification as it is unlikely that these end modifications will disrupt the tertiary structures; hence, target binding will remain unaffected. However, these free 5' and 3' ends can be exploited as docking sites for aptamer immobilisation in sensor design with limited effect on target binding, offering a crucial advantage over bound 5' and 3' ends.

Similarly to those binding motifs and their tertiary structures identified in the generated LDHp and r*Pf*LDH aptamers, the previously published aptamers also contained their own unique set of sequence motifs (**Table 3.4**). As seen in **Figure 3.9**, the families of motifs found in the previously published aptamers were found in structural locales, and given their size, are well-suited as binding sites for larger proteins, such as recombinant *P. falciparum* and *P. vivax* LDHs. GATTG, found in pL1 (Lee et al., 2012), was located on a leg of a larger triangular binding moiety ideally structured to dock the larger r*Pf*LDH and r*Pv*LDH. GGTAG, found in 2008s (Cheung *et al*., 2013), was located on the lip of a binding groove, as previously seen for generated aptamers. Cheung and co-workers (2013) have since filed the three-dimensional structure of aptamer, 2008s, binding to *P. falciparum* LDH under

the PDB accession number 3ZH2.

With sequence families and motifs across aptamers now known, possible secondary and tertiary structures elucidated and potential target-binding sites identified, the qualitative and quantitative analysis of r*Pf*LDH and LDHp binding to synthesised aptamers, LDHp 1, 3, 11, 14 and 18 and rLDH 1, 4, 7 and 15, can be determined (**Chapters 4** and **5**).

To visibly assess and compare commercially synthesised biotinylated aptamer purity, sizes and migration pattern on polyacrylamide gel for later purposes of the electrophoretic mobility shift assay, GelRed-stained polyacrylamide gel electrophoresis was performed on all biotinylated aptamers (**Figure 3.11**).

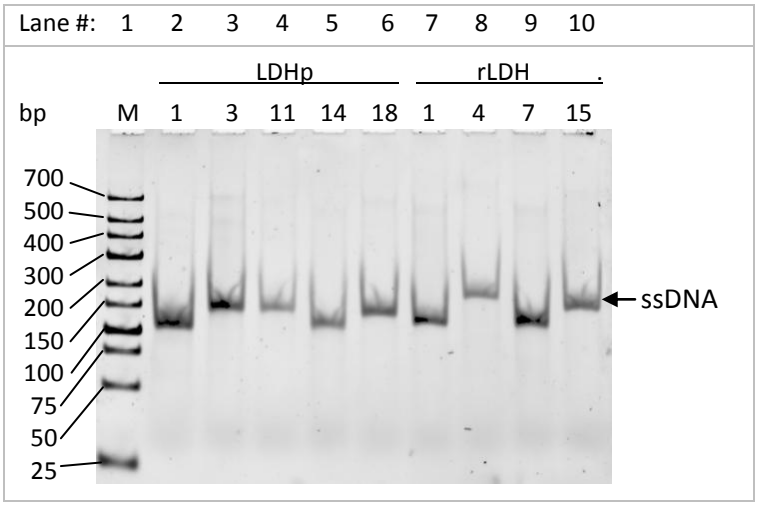

Figure 3.11: PAGE (10 %) of selected synthesised biotinylated aptamers.
Lane 1: Low molecular weight DNA mass marker; Lane 2: LDHp 1; Lane 3: LDHp 3; Lane 4: LDHp 11; Lane 5: LDHp 14; Lane 6: LDHp 18; Lane 7: rLDH 1; Lane 8: rLDH 4; Lane 9: rLDH 7; and, Lane 10: rLDH 15.

Differing migration patterns can be observed in **Figure 3.11** for synthesised biotinylated aptamers. For reasons discussed in **Chapter 2.5.6**, equivalent lengths of synthesised ssDNA were observed to migrate slower than dsDNA aptamers in PAGE (**Figure 3.11**). Resolved lengths of aptamers on PAGE in Lanes 2 to 10 are, therefore, not indicative of their true length as would been seen if the dsDNA equivalent were resolved on PAGE and compared to the double-stranded DNA molecular marker in Lane 1 (**Figure 3.11**). The resolved lengths of aptamers in **Figure 3.11** are, however, indicative of their folded conformations, and associated migration profile caused by their charge : length ratios in

the PAGE matrix (Stellwagen & Stellwagen, 2009). Thus, with respect to PAGE in **Figure 3.11**, only comparative analyses can be done.

Migration of ssDNA of rLDH 4 (Lane 8, **Figure 3.11**) was hindered due to the longer length of this aptamer (100 bp), and the concomitant tertiary structural differences between this aptamer and the other aptamers. This too occurred for rLDH 15, which is 94 bp in length. It is further plausible that migration was hindered for aptamers rLDH 4 owing to the occurrence of open gaps in their tertiary structures (**Figure 3.7**); a "circular" tertiary structure that can be likened to circular DNA (Stellwagen & Stellwagen, 2009). Such gaps are indicative of unpaired nucleotides (54 nucleotides in the case of rLDH 4, **Table 3.5**), or circular DNA structure formations, and are located between the TTCCA and GTAG motif (1) and poly-A region (3) of aptamer rLDH 4 (in **Figure 3.7**), where there was an absence of base-pairing, cross-linking and tertiary helices. Migration of rLDH 15 in PAGE (Lane 10, **Figure 3.11**) was hindered due to the observed bending or curvature of the aptamer's tertiary structure seen in **Figure 3.9** (Stellwagen & Stellwagen, 2009).

Even though LDHp 1 (Lane 2, **Figure 3.11**) and LDHp 11 (Lane 4, **Figure 3.11**) are of the same base pair length (90 bp), these two aptamers exhibited differing migration patterns where LDHp 11 migration was less than that for LDHp 1. This can be attributed to the differing tertiary structure, and resulting exposed surface charge, that aptamer LDHp 1 forms at room temperature facilitating movement through PAGE (Gagnon and Maxwell, 2011). The more rapid migration of aptamer LDHp 1 and LDHp 14 can be attributed to a greater surface-exposed negative coulombic potential (the visible red in **Figure 3.9**). This exposure of negative coulombic potential causes the aptamers to migrate further in PAGE owing to electrostatic interactions (Stellwagen & Stellwagen, 2009). The more rapid migration of LDHp 1, LDHp 14, rLDH 1 and rLDH 7 aptamers compared to the remaining aptamers in **Figure 3.11** can be attributed to the nucleotide composition with these aptamers having a higher GC content compared to the remaining aptamers (**Table 3.2**). This further migration is due to the fact that these ssDNA aptamers, which have a greater GC-content, migrate further during PAGE (Stellwagen *et al.*, 2007). This difference in migration on PAGE can be attributed to the likelihood that the higher GC content will create a more convoluted tertiary structure owing to the hairpin structures that are likely to result from the GC content (Stellwagen *et al.*, 2007). Therefore, ssDNA migration through gel electrophoresis is not solely dependent on sequence length, but also needs to factor in residue content.

3.6. Conclusions

While this conserved family of aptamers presented in **Figure 3.3a** was strongly represented in the work, aptamers rLDH 2, 3, 5, 6, 9, 10, 12 and 14 failed the preliminary ELONAs with the absence of r*Pf*LDH binding. These sequences were not selected for further studies. While LDHp 3 and LDHp 18 shared consensus regions, demonstrating a 44 % sequence similarity and alignment, they did demonstrate binding in the preliminary ELONA, and were thus selected for further analysis in **Chapter 4**.

Secondary structures of the aptamers involved binding leading to stem-loop structures (LDHp 1, LDHp 14, rLDH 4 and rLDH 15) and elbow structures protruding from a larger loop (rLDH 1, rLDH 7 and LDHp 18). Those aptamers which were predominated by a convoluted secondary structure were seen to embed the target, LDHp, within the secondary structure. More complex folding in which the main loop (or sections thereof) folded in on itself was also observed (LDHp 3 and LDHp 11). Of the selected aptamers, it was observed that those with a high degree of folding were more suited to binding to the smaller target (LDHp); whereas, those with a simpler secondary structure tend to bind more strongly to the larger target (r*Pf*LDH). The identified motifs common in the generated aptamer sequences and those found in previously published aptamer sequences are located in 3D structures that are of interest in binding due to inherent stability, as with the GC-rich region of LDHp 11 (also evolutionarily unique)or base-pairing seen with the GTAG motif in rLDH 4. The common motif, ATTAT, locale on pertinent binding pockets may play a significant role in target binding, particularly for LDHp. Finally, the presence of these sequence families and motifs increases the relatedness of those aptamers generated against r*Pf*LDH and LDHp presented in this work. Binding of generated aptamers to r*Pf*LDH and LDHp is further elucidated in **Chapter 4**.

CHAPTER 4

Screening of selected generated oligonucleotide aptamers by binding affinity to *Plasmodium falciparum* LDH and *Plasmodium falciparum*-specific LDH peptide

4.1. Preface

In this chapter, screening of the binding affinity between sequences described in **Chapter 3**, LDHp 1, 3, 11, 14 and 18 and rLDH 1, 4, 7 and 15, to the Plasmodial biomarker, lactate dehydrogenase (LDH), from *Plasmodium falciparum (Pf*LDH) and *Pf*LDH-specific peptide, LDHp, was explored.

This was achieved using screening techniques common to the literature: enzyme-linked oligonucleotide assays (ELONA), fluorophore-linked oligonucleotide assays (FLONA), electrophoretic mobility shift assays (EMSA), fluorescent dye displacement assays and Surface Plasmon Resonance affinity analyses (SPR). The binding capacity of screened aptamers to their targets was compared to binding to other proteins, such as human serum albumin (HSA), as well as LDH enzymes from other species, such as *Plasmodium vivax* (r*Pv*LDH), mammalian (bovine) LDH (mLDH), and human LDH (hLDH). With binding capacity proven, these target-binding oligonucleotides are, hence, referred to as “aptamers”. Generated aptamers were screened in order to elucidate their affinity for the target analyte using these techniques for their intended application in biosensors, which is discussed in further detail in **Chapter 5**.

4.2. Introduction

From the work presented in **Chapters 2 and 3**, a number of single-stranded DNA oligonucleotides/aptamers were generated following SELEX (**Chapter 2**). A pool of single-stranded oligonucleotides exists capable of binding to given targets, r*Pf*LDH and LDHp, were identified and preliminarily tested for binding to r*Pf*LDH and LDHp, over structurally similar proteins (**Chapter 2**). Of the dozens of individual oligonucleotides within this pool, common motifs and moieties were identified on target-binding oligonucleotides (**Chapter 3**). These oligonucleotides require screening to determine their target binding efficacies. To assess the effectiveness of the oligonucleotides/ aptamers to binding to and capturing r*Pf*LDH, aptamers LDHp 1, 3, 11, 14 and 18 and rLDH 1, 4, 7

and 15 need to be screened to evaluate their separate abilities to bind their targets. Especially, specificity and affinity of their binding will identify potential sequences as suitable bioagents for use in diagnostics.

4.2.1. Brief background

Prior reports of the *Plasmodium falciparum*-specific lactate dehydrogenase (LDH) oligopeptides, LDHp, demonstrated its validity as an epitope, whereby IgY antibodies generated against the peptide discriminated between a *P. falciparum* and *Plasmodium vivax* LDH via Western blots, immunofluorescence and enzyme-linked immunosorbtion assays, ELISA (Hurdayal *et al*., 2010). These antibodies are capable of being integrated into sensing technologies capable of discriminating between the presence of these two species of malaria (Hurdayal *et al*., 2010), similar to other peptide-specific malarial diagnostic tests (Tomar *et al*., 2006; Verma *et al*., 2013). Similar to the above works, protein targets used in screening procedures in this Chapter include both the *P. falciparum*-specific oligopeptide, LDHp, and the whole recombinant *P. falciparum* LDH (*Pf*LDH) as principal target proteins. Control proteins consisted of potential diagnostic interferents: *P. vivax* LDH (*Pv*LDH) as an intra-*Plasmodium* genus control, mammalian (bovine) LDH (mLDH) and human LDH as mammalian "host" control proteins, and human serum albumin (HSA) as a common protein within the diagnostic matrix i.e. human blood.

Aptamers have several advantages over antibody based techniques which can be explored to establish rapid diagnostic tests that are less sensitive to storage temperatures and conditions and are cheap to synthesize (as discussed in **Chapter 1**). Soukup *et al.* (1996) demonstrated improved affinity for RNA aptamers selected for a 21-nucleotide homopurine/homopyrimidine duplex DNA target at pH 6 versus pH 7.4. The manipulation of pH and temperature in the sensing environment, therefore, has implications in the overall production and effectiveness of the biosensor (Cho *et al.*, 2009). These factors are however carefully controlled to ensure that the aptamer's conformation, pivotal in the binding mechanism to the target protein (Mairal *et al*., 2008), is not greatly affected.

While the specific conformation that aptamers adopt is ultimately dictated by their nucleotide base sequence (Tuerk and Gold, 1990; Macaya *et al*., 1993), reports indicate that to aid the folding of the aptamer to an appropriate conformation a pretreatment step consisting of heating the aptamer to high temperatures, such as 90 °C is often required By heating the aptamer suspension to denaturing

temperatures and cooling the aptamer suspension to room temperature thereafter, the aptamer adopts a particular subset of possible three-dimensional conformations, which facilitates subsequent target recognition (Tuerk and Gold, 1990; Ellington & Szostak, 1990). There have been reports that aptamers are able to spontaneously conform to their tertiary structure in the absence of any heat-activation, but retain the binding affinity that they would otherwise exhibit following heat-activation (Ying *et al*., 2011; Jeong & Paeng, 2012). This ability of aptamers to conform to their tertiary structures in the presence of their target opens up a host of possibilities for the application of aptamers in signal transduction schemes in the field of optical-, electrochemical-, or mass-based sensing and diagnostics (Cho *et al.*, 2009). In particular, the ability of an aptamer to conform in the presence of target plays a pivotal role in aptamer applications such as aptabeacons, which have a specific conformation prior to and after target binding (Mairal *et al*., 2008).

4.2.2. Aptamer screening techniques as a measure of target binding

Aptamer screening techniques used to assess target binding include: enzyme-linked oligonucleotide assays (ELONA; used for screening aptamers in this Chapter), nanoparticle-linked oligonucleotide assays, fluorophore-linked oligonucleotide assays (FLONA; this Chapter), electrophoretic mobility shifts assays (EMSA; this Chapter), fluorescent dye displacement assays (this Chapter), filter-binding assays, electrochemical impedance spectroscopy (EIS; tested in **Chapter 5**), SPR (this Chapter), QCM/D, isothermal titration calorimetry (ITC) and capillary electrophoresis (Kim & Gu, 2014; McKeague *et al*., 2015a; Ruscito & DeRosa, 2016).

The screening techniques discussed in this Chapter, particularly ELONA, FLONA, EMSA, SPR, and fluorescent dye displacement or GelRed® assay, were performed to evaluate the generated aptamers' capabilities for specific binding to the target proteins, LDHp and r*Pf*LDH.

4.2.2.a. Fluorophore-linked oligonucleotide assays (FLONA) to measure aptamer-target binding

Similar to the enzyme-linked oligonucleotide assay (ELONA) in design (ELONA principles described elsewhere in **Chapter 1.7.2.a** and **Chapter 2.4.9**), this aptamer screening assay is also used in the detection of target proteins (Tyagi & Kramer, 1996; Hamaguchi *et al.*, 2001; Cho *et al*., 2010; Deng *et al*., 2014). FLONA differs from ELONA in that the reporting agents, fluorophores (**Chapter 1.7.2.d**) are conjugated directly to the aptamers as opposed to separate molecules which are then incubated with the aptamer-target complex (Anderson *et al*., 2008). A variety of fluorophores can be

commercially conjugated to the aptamers for use in FLONA; including: fluorescein (also known as FIT-C or 6-FAM); the polymethine compounds, cyanine-3 (Cy3) and cyanine-5 Cy5; and tetramethylrhodamine (Anderson *et al*., 2008). As with ELONA, FLONA is both quantitative and qualitative, as the amount of target-bonded oligonucleotide is indicative of the quantity of the target bound.

4.2.2.b. Displacement-based fluorescent aptamer-target assays

In DNA-based aptamer-target binding analyses, fluorescent molecules capable of sensitively intercalating with the secondary structures of DNA can be used to detect aptamers and measure their conformational changes via displacement of the fluorescing intercalator. The change in fluorescent intensity in GelRed®-based fluorescent displacement assays, reported in this Chapter, are based on alterations of fluorescence caused by the change in number and state of GelRed® molecules bound to the aptamer molecule while it undergoes conformational changes upon interacting with the target molecule (**Figure 1.8**). A detectable decrease in fluorescent signal (quenching) is indicative of positive binding between aptamer and target and subsequent release of GelRed® molecules upon target-aptamer binding. Fluorescent displacement assays have been previously used to measure binding between DNA and small molecules, oligonucleotides and proteins, using ethidium bromide as the fluorescent reporter molecule (Tse & Boger, 2004).

GelRed® is a homodimer of ethidium bromide linked via a polyether bridge (Mao & Cheung, 2010). These molecules have an excitation and emission wavelength of 295 nm and 600 nm, respectively. GelRed® binds to DNA in two manners: it intercalates between nucleotide residues, and binds to the negatively-charged phosphate backbone of DNA via electrostatic attraction with the positively-charged GelRed® molecules (Crisafuli *et al*., 2014). These molecules are routinely applied for the fluorescent detection of DNA and RNA, following gel electrophoretic separation of samples containing these nucleic acids. Furthermore, as GelRed® is more sensitive than other commercial fluorescent markers and dyes that are used in laboratories and capable of binding to low molecular weight or short-chain oligonucleotides (Biotium, 2013), fluorescent assays incorporating GelRed® are ideally suited for quantitatively measuring the capture of small targets by oligonucleotide aptamers.

The intercalative activity of GelRed® to double-stranded DNA elicits a more sensitive response that it would to ssDNA (Biotium FAQs, 2013). Such an apparent response results from the hydrophobic

internal environment of the dsDNA to which GelRed® binds minimising fluorescent quenching otherwise caused by the presence of water. Hence, when considering binding to the single-stranded aptamers it is reasonable to assume that GelRed® molecules will intercalate more readily, and exhibit greater fluorescence, in aptamers with a more complex and stable tertiary structure compared to those with more linear structures. GelRed® is also able to bind more readily to oligonucleotides with shorter length rendering it more suitable for this purpose than its monomeric counterpart, ethidium bromide. Furthermore, it is non-toxic, non-mutagenic and environmentally safe (Ohta *et al*., 2001; Biotium, 2013). For these reasons, it is suitable for use in fluorescent displacement assays.

4.2.2.c. Electrophoretic mobility shift assay (EMSA) in aptamer-target affinity

Electrophoretic mobility shift assays (EMSA) can be performed as a qualitative measure of binary binding interaction, kinetics and strength of the DNA and protein interaction (Hellman & Fried, 2007). The use of polyacrylamide gel electrophoresis (PAGE) to measure binding interactions between DNA and proteins was first proposed by Fried and Crothers (1981) when studying the *lac* repressor-operator interaction. Subsequently, this was applied to aptamer and protein interactions by Latham and co-workers (1994). This technique is based on the principle that migration of an aptamer-protein complex through the gel matrix differs from either the free aptamer or free protein. This may be due to the: increased molecular weight of the complex (Gaillard & Strauss, 2000); changes in the shape of the aptamer-protein complex; and/or the corresponding decrease in charge-to-weight ratio (Gagnon and Maxwell, 2011).

This technique has been widely applied to aptamer research. The principle of this technique in aptamer-target binding interactions is illustrated schematically in **Figure 1.7**. Sosic and co-workers (2011) used EMSA to assess binding of modified DNA aptamers to human thrombin. EMSA has been used to measure the binding of DNA aptamers to whole bacterial cells, specifically *Salmonella enterica* serovars (Joshi *et al*., 2009). Cheung and co-workers (2013) used EMSA to characterise binding of their aptamers, 2008s, to r*Pf*LDH with a measured K_D of 56 ± 18 nM, thereafter Godonoga and co-workers (2016) used EMSA to measure binding of a rectangular DNA origami scaffold of the same aptamer to r*Pf*LDH.

EMSA is predominately used as a confirmatory and qualitative technique, rather than a quantitative measure of affinity (McKeague & Derosa, 2012), particularly when a number of developed or unstudied aptamers require assessment. This technique is relatively inexpensive and quick to perform, albeit the required optimisation. Assessment of the use of EMSA for aptamer-target binding will be assessed in this Chapter.

4.2.2.d. Surface plasmon resonance to measure aptamer binding to LDH

In addition to ELONA, quantitative information can be garnered on aptamer-target interaction through surface plasmon resonance (SPR). Binding interactions between an immobilised ligand and a free analyte result in the real-time change in the oscillation wave conditions on the chip surface. The altered surface conditions refract and change the resonance angle of the incident light reflected off the chip's metal base, which acts as the sensor signal. The change in the resonance angle upon biomolecular interactions produces an arbitrary response (measured in Response Units, RU) used as a measure of the binding interactions (Stenberg *et al*., 1991). This technique provides information on the rate of adsorption; association and dissociation kinetics; equilibrium dissociation constants (K_D); and, theoretical binding capacities (R_{max}) of ligand-analyte interactions (Nahshol *et al.*, 2008).

Furthermore, SPR is an attractive tool in the label-free analysis of aptamer-target interactions as it facilitates the high throughput screening of the individual oligonucleotide aptamers generated from the SELEX process (Smith & Corn, 2003). An added advantage of high throughput screening by means of SPR translates to screening a wider range of structurally similar targets and control proteins for specificity (Strehlitz *et al*., 2008). These factors make SPR the tool of choice in assessing the binding interactions between aptamers and their target and control proteins. SPR was therefore, explored within the context of the work to observe and determine binding of generated and previously published aptamers to their respective target proteins, as well as control proteins.

The SPR chip surface design and modification stipulates the oscillation wave conditions and refractive index; and, are ideally suited to specific experimental applications. Generally, SPR chips have an inert metal base, such as silver and gold, with a self-assembled monolayer of carboxy-modified polysaccharides to facilitate capture of the immobilised interactant, the ligand. Various methods of biomolecule immobilisation can be used in the creation of the SPR solid support capture surface for the analyte of interest

Typically, biomolecular ligand immobilisation involves protein-linking conjugation techniques to the SPR chip surface using covalent linking via functional groups such as amine (-NH_2), thiol (-SH) and aldehyde (-COOH) groups (Nguyen *et al*., 2015). Amine coupling, used to immobilise ligands in this study, utilises reactive intermediates such as 1-ethyl-3-(3-dimethylaminopropyl) carbodiimide (EDC) and *N*-hydroxysuccinimide (NHS) (Mädler *et al*., 2009). Amine-modified aptamers have been immobilised on SPR chips, for the development of a biosensor for blood proteins (Zheng *et al*., 2011). Thrombin-binding aptamers have previously been immobilised and investigated using SPR (Baldrich *et al*., 2004). Baldrich and co-workers (2004) investigated immobilisation of thiolated aptamers to gold SPR chip surface and biotinylated aptamers to streptavidin coated SPR chips surfaces in the detection of thrombin. They found that immobilised thiolated aptamer exhibited dissociation constants in the nanomolar range; however, immobilised biotinylated aptamer did not demonstrate similar thrombin binding. Baldrich and co-workers (2004) attempted to demonstrate binding of biotinylated aptamers to thrombin by inverting the ligand-analyte arrangement through thrombin immobilisation via biotin-streptavidin coupling and carbodiimide chemistry, but to no avail, concluding that modification with biotin inhibited aptamer-thrombin binding.

An alternative approach to measuring affinity between the aptamer and target is to immobilise the protein target directly to the SPR chip surface, thereby using the target protein as ligand and the aptamer as analyte. Misono and Kumar (2005) demonstrate this configuration in their analysis of an RNA aptamer binding to immobilised human influenza A haemagglutinin, using a Biacore CM4 SPR system. Using a Biacore CM5 SPR chip with a standard carboxylated surface, Win and co-workers (2006) demonstrated RNA aptamer binding to immobilised codeine through a succinimidyl group linker. Both configurations, namely immobilised aptamer as ligand and free target as analyte versus immobilised target as ligand and free aptamer as analyte, offer similar sensitivities and binding kinetics.

Looking specifically at chips available for the purposes of this research, the GLC chip (used with the ProteOn™ XPR36 protein interaction array system from Bio-RAD (http://www.bio-rad.com/en-us/sku/176-5011-proteon-glc-sensor-chip)) is designed for compact amine coupling with minimal mass transport effects. These chips have a carboxy-modified alginate self-assembled monolayer on a gold base. This layer's net negative charge is well-suited for covalent attachment of proteins as the ligand, followed by binding interactions with oligonucleotides as the analyte as non-specific charge-based interactions are minimised. The GLC chip surface can be further modified as in the case of the

NLC chips: these have been modified with NeutrAvidin and are designed for immobilisation of a single monolayer of biotinylated molecules through affinity interactions (http://www.bio-rad.com/en-ch/sku/1765021-proteon-nlc-sensor-chip).

Drawbacks of covalent coupling of ligands to SPR sensors exist (Nguyen *et al*., 2015): firstly, the chemical activation for covalent attachment of biomolecules may involve non-specific chemical modification of residues at the active sites of enzymes or recognition moieties on proteins affecting substrate recognition and analyte binding, respectively. Secondly, chemical activation may also result in the non-specific coupling of proteins to one another through activation of surface functional groups. Finally, use of inappropriate blocking agents can inactivate the biomolecules by blocking binding sites of the protein disabling analyte recognition. SPR measuring the aptamer-target interaction will be discussed in this Chapter in the context of r*Pf*LDH and r*Pv*LDH as ligands and aptamers, LDHp 1, LDHp 11 and rLDH 4 as analytes.

4.3. Aim

Using a combination of ELONA, FLONA, GelRed® assays, EMSA and SPR, to:

1. Screen generated aptamers, LDHp 1, 3, 11, 14 and 18 and rLDH 1, 4, 7 and 15 for their ability to bind to the biomarker, lactate dehydrogenase (LDH), from *Plasmodium falciparum (Pf*LDH), with high affinity. This will be explored through a comparison of the findings from the variety of screening techniques employed in this Chapter.
2. Identify aptamers capable of binding r*Pf*LDH and LDHp with specificity, compared to control proteins HSA, as well as LDH from other species, namely *Plasmodium vivax* (r*Pv*LDH) and mammalian LDH (mLDH).
3. Determine affinities for each of the afore-mentioned aptamers to r*Pf*LDH and/or LDHp.

4.4. Methodology

4.4.1. Reagents

Reagents for ELONA are as described in **Chapter 2.4.1**. Biotinylated and fluorescein(FITC)-labelled aptamers, LDHp 1, 3, 11, 14, 18 rLDH 1, 4, 7, 15, pL1, 2008s and concatemer, C7, were generated by Integrated DNA Technologies (IDT; USA). Recombinant proteins, r*Pf*LDH and r*Pv*LDH, were kindly

gifted by Prof Dean Goldring. Mammalian (bovine) LDH, mLDH was purchased from Sigma Aldrich (Germany). Human LDH (hLDH) isoenzyme V was purchased from Abcam (United Kingdom) through BiocomBiotech (Pretoria).

Reagents for DNA and protein staining in PAGE for electrophoretic mobility shift assay (EMSA) are described in **Chapter 2.4.1.** With the exception of the 1× HMCKN, pH 7.4, running buffer, aptamers and protein target, all reagents used for Surface Plasmon Resonance (SPR) were purchased from Bio-Rad Laboratories, USA. All other reagents were purchased from Sigma Aldrich (Germany).

4.4.2. Apparatus

Apparatus for ELONA are as described in **Chapter 2.4.2**. Fluorescent intensities for the GelRed® assay fluorescence (excitation = 295 nm; emission = 600 nm) and fluorophore-linked oligonucleotide assay (excitation = 595 nm; emission = 510 nm) were measured using the SynergyMx fluorimeter / spectrophotometer linked to Gen5 v1.10 software (Biotek, USA).

Apparatus for DNA and protein staining in PAGE for electrophoretic mobility shift assay (EMSA) are described in **Chapter 2.4.2.**

Surface Plasmon Resonance (SPR) was performed on ProteOn XPR36 Protein Interaction Array System, controlled via ProteOn Manager™ 3.1.0 software (Bio-Rad Laboratories, USA). Degassing of solvents used in SPR was performed using an Instruvac® Rocker 400 oil-less vacuum pump (M.R.C. Ltd, Israel). Binding analyses were performed using carboxylic-acid modified GLC chips and NeutrAvidin-modified NLC chips (Bio-RAD Laboratories, USA).

4.4.3. Enzyme-linked oligonucleotide assay (ELONA) of biotinylated aptamers and protein binding

ELONA using biotinylated aptamers to measure aptamer affinity to r*Pf*LDH and LDHp was performed as described in **Chapters 1.6.2.a** and **Chapter 2.4.9**. A schematic of ELONA is presented in **Figure 4.1**, in which the various steps has also been included, in the context of aptamer to LDH peptide binding.

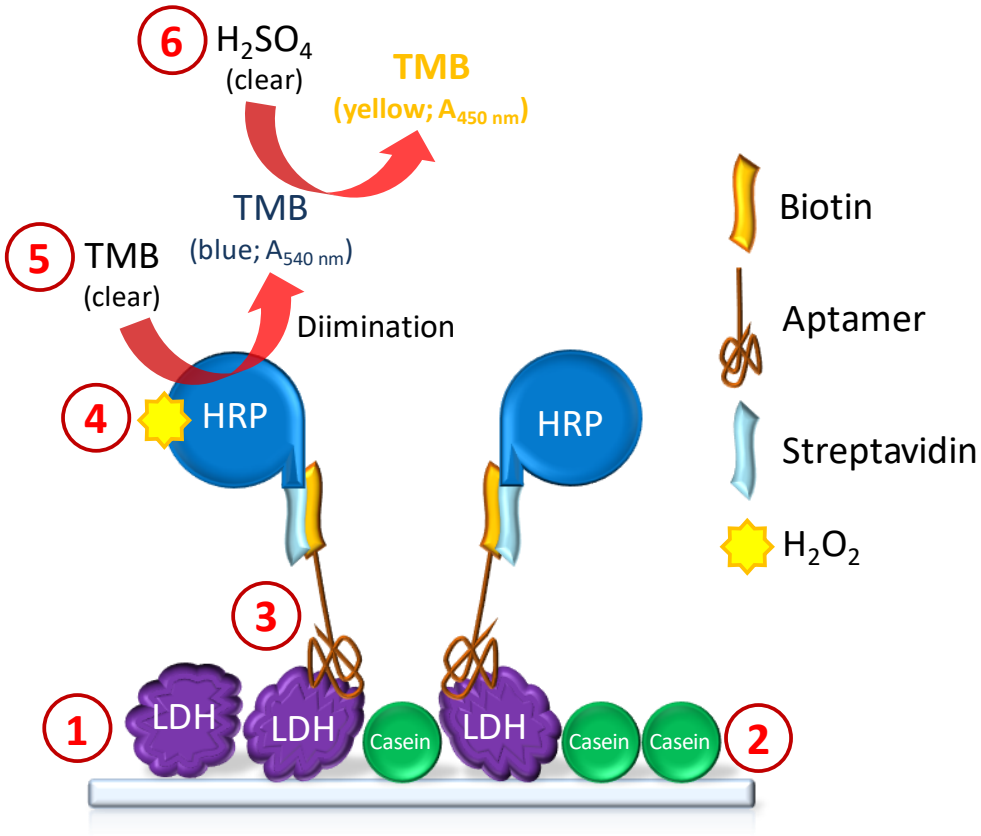

Figure 4.1: Detailed schematic of ELONA sandwich-type assay, using LDH as a target protein.
1: Target immobilisation. 2: Casein blocking. 3: Biotin-aptamer binding. 4: Streptavidin-horse radish peroxidise coupling. 5: TMB colour reaction through diimination (colour development read at 540 nm). 6: Reaction cessation through addition of sulphuric acid (end-point absorbance read at 450 nm).

Similarly to ELONA described in **Chapter 2.4.9**, ELONA performed in this section did not include bovine serum albumin (BSA) as an immobilised proteinaceous positive control. Instead, human serum albumin (HSA), mammalian (bovine) lactate dehydrogenase (mLDH) and recombinant *Plasmodium vivax* LDH (r*Pv*LDH), in addition to target proteins r*Pf*LDH and LDHp, were used to evaluate affinity of synthesised aptamers.

For all ELONA tests, five hundred nanograms (100 µl of 0.005 mg/ml) of each of these afore-mentioned proteins was immobilised (Step 1 in **Figure 4.1**), and rinsing performed as previously described in **Chapter 2.4.9**. Milk powder/casein blocking and rinsing (Step 2 in **Figure 4.1**) was performed as described in **Chapter 2.4.9**.

To investigate and assess aptamer binding, changes in Step 3 (**Figure 4.1**) of ELONA were as follows:

- To evaluate the influence of aptamer concentration on binding to immobilised polypeptide (r*Pf*LDH, LDHp and r*Pv*LDH), the following concentrations of aptamer were prepared in 1× HMCKN: 0, 50, 100, 200/250, 500 and 1000 nM.
- The influence of pH was explored by performing aptamer-target binding similarly described in **Chapter 2.4.5.b** with the exception that the HMCKN binding buffer was set to pH 5.2.
- The effect of heat denaturation on aptamer binding to target proteins and control proteins was assessed using an aptamer concentration maintained at 200 nM. For assessment of heat denaturation effects, aptamer-target interactions were prepared similarly described in **Chapter 2.4.5.b** with the exception that aptamers did not undergo heat denaturation and remained at room temperature.

Steps 4 through 6 (**Figure 4.1**) of ELONA proceeded as described in **Chapter 2.4.9**.

4.4.4. Fluorescently-linked oligonucleotide assay (FLONA) of generated aptamers to rPfLDH

Affinity of synthesised fluorescein-labelled aptamers (excitation = 490 nm; emission = 520 nm) to proteins were investigated. A schematic of FLONA is presented in **Figure 4.2**, in which the various steps has also been included, in the context of aptamer to LDH binding.

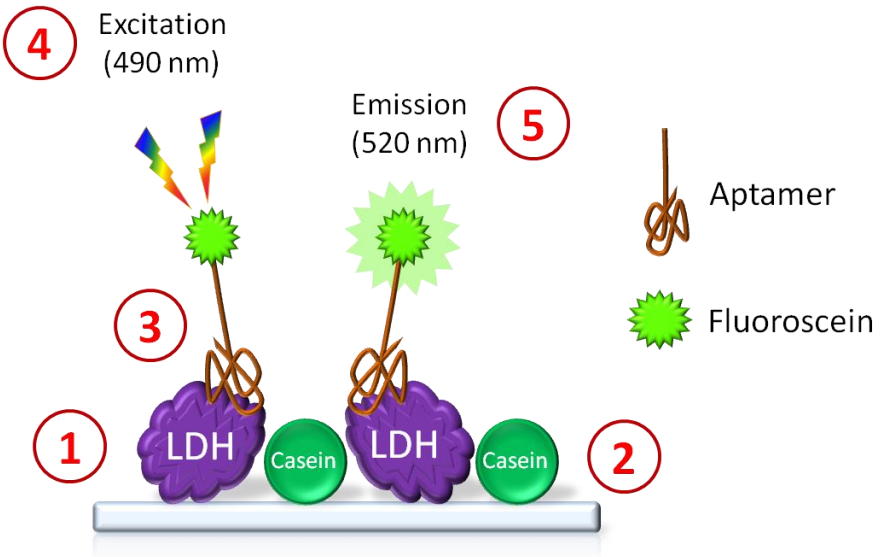

Figure 4.2: Detailed schematic of FLONA affinity assay, using LDH as a target protein.
1: Target immobilisation. 2: Casein blocking. 3: Fluorophore-tagged aptamer binding. 4: Excitation of fluoroscein (490 nm). 5: Record measurable readings at 520 nm.

FLONA proceeded very similarly to the methodology used for ELONA (**Chapter 2.4.9**). For each of the target or control proteins, five hundred nanograms of the protein was immobilised into a well of a 96-well ELISA plate using 10 mM $NaHCO_3$ buffer, pH 8.5. This was covered and incubated overnight at 4 ^oC (Step 1 in **Figure 4.2**). The plate was then washed three times with 300 µl of 25 mM Tris-buffered saline (TBS) buffer, pH 7.6 containing 0.1 % (v/v) Nonidet P-40 (NP-40), designated TBS+ hence forth. Wells were subsequently blocked using 100 µl of 2 % (w/v) fat-free milk solution in TBS+, incubating for 1 hour at 4 ^oC (Step 2 in **Figure 4.2**). The plate was washed three times with 300 µl TBS+.

Fluorescein-tagged oligonucleotides (200 nM), heat-activated at 65 °C and suspended in 5X HMCKN buffer (similarly described in **Chapter 2.4.5.b**), were added to each sample well and incubated in the dark at room temperature for 2 hours (Step 3 in **Figure 4.2**). The plate was then washed twice with 300 µl aliquots of HMCKN buffer followed by a further three washes with 300 µl aliquots of TBS+. An additional volume (100 µl) of HMCKN was added to each well prior to reading. Fluorescence (excitation = 490 nm; emission = 520 nm) was measured (Step 4 [excitation] and 5 [emission] in **Figure 4.2**) in a spectral scan from 500 to 600 nm using the SynergyMx fluorimeter/ spectrophotometer linked to Gen5 v1.10 software. All measurements were performed in quadruplicate (*n* = 4).

4.4.5. GelRed® assays assessing binding interactions between generated aptamers and LDH target peptides

GelRed® intercalation with r*Pf*LDH and LDHp (0, 0.1, 0.5, 1.0, 1.25 and 1.5 µM) was assessed with 1× dilution of GelRed® fluorescent stain. Fluorescent intensity (excitation and emission at 295 nm and 600 nm, respectively) was measured using the SynergyMx fluorimeter/spectrophotometer linked to Gen5 v 1.10 software.

GelRed® assays (schematic presented in **Figure 1.8**) were carried out by preparing 1, 10, 50, 75 and 100 nM of pL1 and LDHp 1, 3, 11, 14 and 18 as per **Chapter 2.4.5.b**. The aptamers were then decanted into microtitre plate wells containing 1× GelRed, which subsequently had 0.5 µM of the LDHp peptide added. Fluorescent emission spectra of GelRed-aptamer complexes (1× GelRed® and 1 to 100 nM aptamer) in presence and absence of LDHp (0.5 µM) were measured from 350 nm to

750 nm, relative fluorescent unit (RFU) output were standardised for 100 RFU. Quenching or enhancement responses was normalised against the fluorescent response of the LDHp polypeptide.

4.4.6. Electrophoretic Mobility Shift Assay (EMSA) of ssDNA aptamers and rPfLDH, rPvLDH and mammalian LDH (mLDH)

Electrophoretic mobility shift assay (EMSA) was performed by initially preparing a 50 nM solution of an aptamer for binding through heat denaturation and incubation with a specified concentration of protein for 1 hour, as described in **Chapter 2.4.5.b**. The aptamers screened using ELONA were: 2008s (Cheung *et al*., 2013), pL1 (Lee *et al*., 2012), rLDH 1, rLDH 4, rLDH 7, rLDH 15, LDHp 1, LDHp 3, LDHp 11, LDHp 14 and LDHp 18. The proteins used for aptamer capture were: r*Pf*LDH, r*Pv*LDH and mammalian LDH (mLDH).

The incubated aptamer/protein mixture underwent PAGE on a 6 % ($^{w}/_{v}$) polyacrylamide gel at <60 V for approximately 1 hour in TBE buffer (45 mM Tris base, 45 mM boric acid, 1.3 mM EDTA, pH 8.0) using PowerPac Basic Gel Electrophoresis equipment. Polyacrylamide gels were post-stained in two phases: initially, with 2.5 µM GelRed® (**Chapter 2.4.6.d**) to view ssDNA under UV, and, secondly, Coomasie brilliant blue (**Chapter 2.4.3**) staining solution (and acetic acid-methanol-based destain solution) to view protein under white light, both using a GelDoc™ EZ Imager linked up to Image Lab 4.0.1 software.

Optimisation of r*Pf*LDH concentration took place in the presence of 100 nM rLDH 4 aptamer, varying the r*Pf*LDH concentration as follows: 0.0, 0.07, 0.14, 0.28, 0.56, 1.125, 2.25, 4.5 and 9.0 µM r*Pf*LDH. A further control consisting only of 9.0 µM r*Pf*LDH and no aptamer was included. Similarly, the influence of varying concentrations of rLDH 4 aptamer was similarly assessed using 1.75 µM of r*Pf*LDH, varying the aptamer concentration: 0, 10, 25, 50, 100, 200, 500, 750 and 1000 nM. Again, the aptamer control contained only 1000 nM rLDH 4 with 0 µM r*Pf*LDH. Aptamer rLDH 4 was used as a case study.

4.4.7. Surface plasmon resonance (SPR) of selected generated aptamer binding to immobilised proteins

The SPR running buffer (HMCKN, pH 7.4) was vacuum-degassed for a minimum duration of 1 h per litre. The sensor chip surface was initially primed using a running buffer rinse (HMCKN, pH 7.4),

followed by preconditioning of the horizontal and vertical channels on the chip surface sequentially with 0.5 % ($^{w}/_{v}$) SDS and 100 mM HCl. Activation of the chip surface was achieved through 1 M 1-ethyl-3-(3-dimethylaminopropyl)carbodiimide / 1 M N-hydroxysuccinimide (EDC/NHS) for 300 s at 30 µl/min. Protein ligand solutions of r*Pf*LDH (128.2 nM), r*Pv*LDH (128.2 nM) and human serum albumin (256.4 nM) were prepared in 10 mM sodium acetate buffer, pH 4.0, as determined by pre-concentration pH probing, interacted with the activated surface at a flow rate of 30 µl/min for 300 s. For qualitative aptamer analyses, immobilised protein ligand amounted to 1671.3 ± 189.6 RU for r*Pf*LDH, 2151.5 ± 87.6 RU for r*Pv*LDH and 1013.5 ± 124.1 RU for HSA. For quantitative analyses, immobilised protein ligand amounted to approximately 1200 RU for r*Pf*LDH, r*Pv*LDH and HSA. Excess activated carboxyl groups on the surface were deactivated using 1 M ethanolamine-HCl, flowed over the surface for 300 s at 30 µl/min. At a concentration of 200 nM for the qualitative analyses and concentrations of 1.0 to 20.0 µM for the quantitative analyses, the chosen aptamers (LDHp 1, LDHp 11, rLDH 4 and pL1), dissolved in HMCKN, heat-activated and allowed to interact with immobilised protein ligand for 90 s at 25 µl/min. Exposure to the aptamers was followed by a dissociation step of 600 s duration. Blanking injections were prepared and performed similarly to chosen aptamer solutions using 10 mM Tris-EDTA buffer, pH 8.0, as stock buffer. Aptamer docking/binding sites on – and adsorbed Tris-EDTA from the buffer injections to – the immobilised protein ligands were regenerated by a single injection of 1 M guanidine in 10 mM Tris-HCl, pH 6.8, at 100 µl/min for 18 s. Therefore, regeneration steps were performed following each analyte and blank injection. Aptamer analyte interaction with the protein ligands was double-referenced against the interspot (channel surface outside of the intersecting channel areas) and buffer injections. Referencing against the buffer injections was performed to limit the effects of mass transfer caused by differing salt concentrations in the binding buffer. Unless noted otherwise, all experiments were performed at 24 °C. Separate GLC chips were used for aptamer binding analyses.

4.4.8. Data measurement and analysis

All measurements were performed in, at minimum, triplicate. Presented results are the means of independent measurements ($n \geq 3$), while all reported error bars and uncertainties represent one standard deviation from the mean. Statistical analyses were performed using Statistica Version 13 and/or Graphpad Prism, version 6.1. The statistical significance level for statistical analyses, α, was set at 0.05. Statistical data are presented for *H* for Kruskal-Wallis H-test and F for One-Way ANOVA, with the determined statistic value, as well as the degrees of freedom in parentheses. The *p*-values for data are presented for the given data set.

4.4.8.a. Statistics performed for ELONA and FLONA

Gaussian distribution was used to determine if data was normally distributed (α = 0.05). For datasets consisting of equal numbers of measurements per sample, the distributions of which were normal (i.e. parametric datasets) significant difference was determined using one-way analysis of variance (One-Way ANOVA), followed by the Tukey's Honest Significant Difference *post hoc* test to identify significantly different samples. Non-parametric datasets were tested for significant difference using the Kruskal-Wallis H-test, followed by Dunn's Multiple Comparison Test to identify significantly-different samples within those datasets.

4.4.8.b. Calculation of dissociation constants of biotinylated aptamers for rPfLDH, LDHp and rPvLDH using ELONA

Kinetic data determined from ELONA analyses were used to calculate the apparent dissociation constants (K_D) of aptamer-r*Pf*LDH/r*Pv*LDH/LDHp interactions. ELONA assay responses were fitted via non-linear regression (Least-Squares minimisation) to a variant of a previously-described Langmuir equivalent binding isotherm equilibrium formula (Brahms *et al*., 1966), using Statistica® (**Equation 4.1**), and further presented in Frith *et al.* (2018):

$$Assay\ response\ (\Delta OD_{450nm}) = \left(\frac{\Gamma_{max} \times [aptamer]}{K_D + [aptamer]}\right) \qquad \textbf{Equation 4.1}$$

Where [*aptamer*] is the specified concentration of the aptamer used during ELONA (in M); ΔOD_{450nm} is the change in the ELONA absorbance for [*aptamer*], relative to the assay response when [*aptamer*] = 0 M); K_D is the modelled apparent dissociation constant of the aptamer-r*Pf*LDH/r*Pv*LDH complex (in M); and, Γ_{max} is the modelled maximal assay response for the aptamer-r*Pf*LDH/r*Pv*LDH complex, essentially calculated the assay response as [*aptamer*] → ∞.

The [*aptamer*] and ΔOD_{450nm} were used to calculate the values of the parameters, K_D and Γ_{max}. A Wald test of the parameters was performed to calculate the significance of the K_D and Γ_{max} non-linear regression coefficients, in which values showing that ΔOD_{450nm} is dependent on [*aptamer*] for a given aptamer-r*Pf*LDH/r*Pv*LDH complex is indicated by $p < 0.05$.

4.4.8.c. GelRed® assays

Changes in GelRed fluorescence in the presence of LDHp at various concentrations of the peptide were calculated as per **Equation 4.2**:

$$Change\ in\ GelRed\ fluorescence\ (\Delta, Em_{600nm}) = Em_{600nm}\ of\ ssDNA_{\ LDHp^{+}} - Em_{600nm}\ of\ ssDNA_{LDHp^{-}}$$

Equation 4.2

Grouped multiple *t*-tests were performed on the change in GelRed fluorescence (Δ, Em_{600nm}) for 100 nM fluorescent responses of concatemer C7, pL1, rLDH 4, LDHp 1, 3, 11, 14 and 18, as well as on pairwise comparisons of the various concentrations of aptamer in absence and presence of the *Pf*LDH-specific peptide, LDHp. Statistical significance was determined with α set at 0.05.

4.4.8.d. Surface Plasmon Resonance (SPR)

SPR data analyses were performed on both ProteOn Manager™ 3.1.0 software and BIAevaluation Version 4.1.1 (GE Healthcare Bio-Sciences AB, Sweden), assuming 1:1 Langmuir binding kinetics. Unpaired *t*-tests were performed comparing r*Pv*LDH and r*Pf*LDH kinetic responses for LDHp 1 binding.

4.5. Results and Discussion

4.5.1. Enzyme-linked oligonucleotide assay (ELONA) binding analyses of aptamers to target and control proteins

The extent and specificity of binding of each of the synthesised 5'-biotinylated aptamers to r*Pf*LDH and LDHp were performed using ELONA. Using ELONA, a variety of experimental conditions to improve binding extent was also performed in conjunction with the evaluation of the generated aptamers' target-binding potential. These are detailed in the various sections, hereafter.

4.5.1.a. Heat-activation-dependency of aptamer binding to HSA, mLDH, LDHp, rPfLDH and rPvLDH

Herein, ELONA was used to investigate the spontaneous conformation of aptamers to their tertiary structures in presence of the target under standard assay conditions (i.e. at room temperature or 22 °C) in aptamer-protein binding to determine the influence of heat-denaturation (95 °C for 10 min; -20 °C for 5 min; 22 °C for 5 min) in subsequent aptamer-protein interactions.

This investigation into spontaneous structure conformation in the absence of a heat-denaturation step aids in the better understanding of the interaction and binding between aptamers and their targets, as well as control proteins. By knowing the conditions under which aptamer-target interactions can effectively and sensitively take place, the eventual application of such aptamers in a diagnostic device can be better formulated and optimised for maximum biosensor performance. As there have been reports that aptamers are able to spontaneously conform to their tertiary structure without prior heat-activation but in the presence of the target (Jeong & Paeng, 2012), therein motivates for the investigation into the possibility that the aptamers presented in this work may spontaneously conform in the presence of the target without initial heat-activation, and hence bind to the specific target eliciting a response.

ELONA was, hence, used to measure the response when non-heat activated aptamers (rLDH 1, 4, 7 and 15 and LDHp 1, 3, 11, 14 and 18, as well as 2008s and pL1, as positive aptamers controls) are brought into proximity with the targets, LDHp and r*Pf*LDH (**Figure 4.3**). Additional proteins used as controls included human serum albumin (HSA) and mammalian LDH (mLDH), both expected to be found in high concentrations in the analyte matrix, as well as recombinant *P. vivax* LDH (r*Pv*LDH) to assess inter-species binding specificity. For this study, tested proteins were maintained at a fixed concentration, similar to work reported by Stoltenburg *et al*. (2016) and Sypabekova *et al*. (2017).

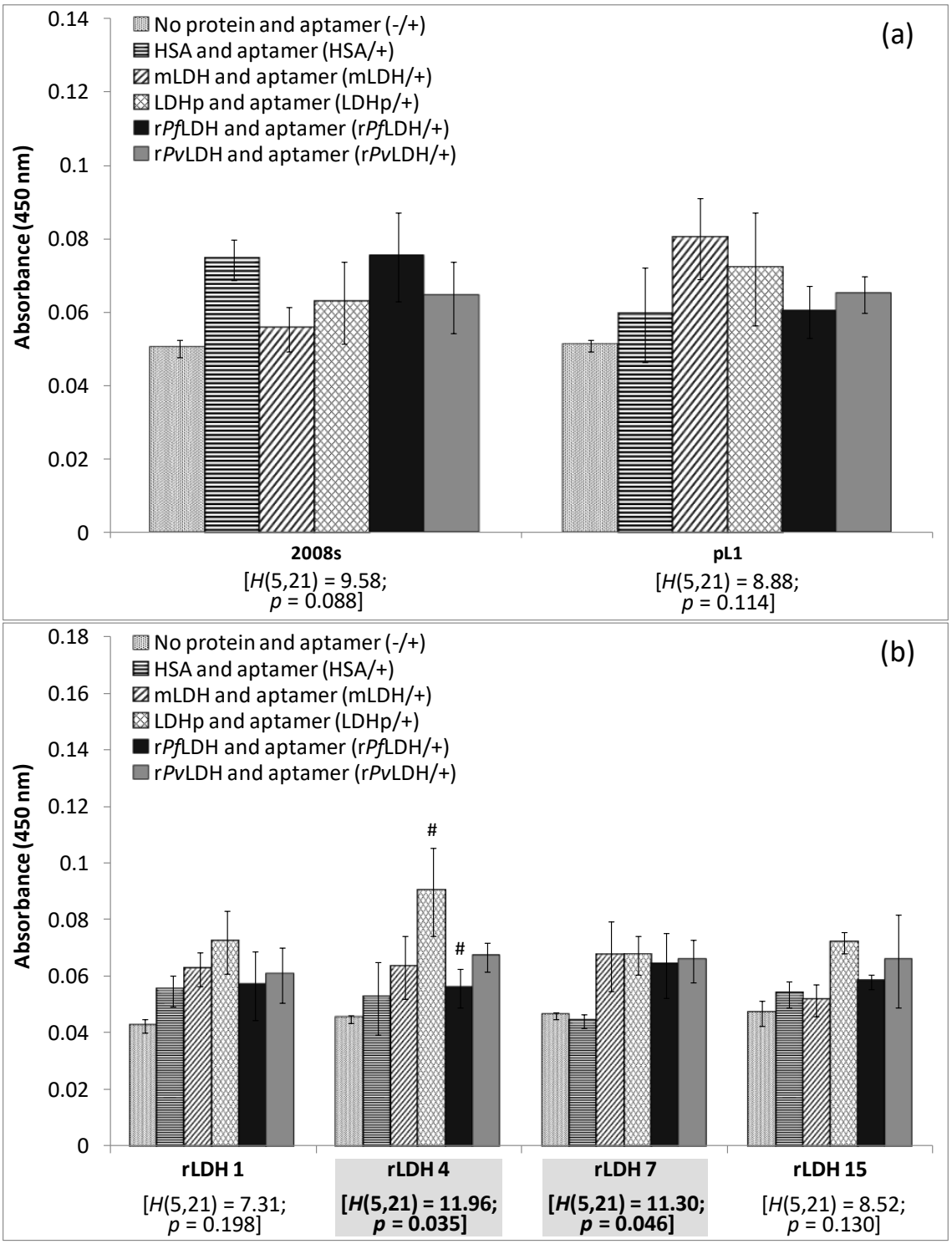

Figure 4.3: Continued on following page

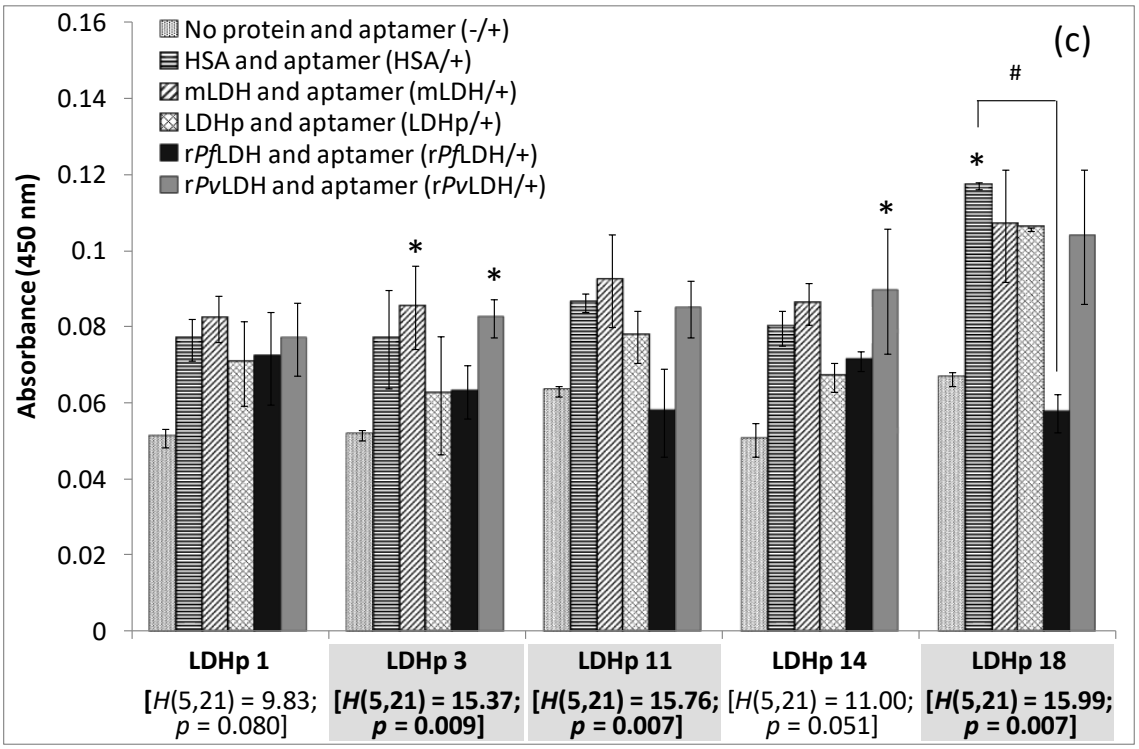

Figure 4.3: Binding affinity of non-heat-activated biotinylated ssDNA aptamers, controls 2008s and pL1 (a), and r*Pf*LDH- (b) and LDHp-targeting (c), to HSA, mLDH, LDHp, r*Pf*LDH and r*Pv*LDH determined using ELONA.
Number of replicates, *n*, vary between 3 and 5.
Statistics: Kruskal-Wallis *H*-test for statistical significance followed by Dunn's Multiple Comparisons test
Shaded bold - indicates statistical significance using the Kruskal-Wallis *H*-test ($p \leq 0.05$),
* - indicates statistically-significantly larger ELONA responses compared to the absence of aptamers (Dunn's Multiple Comparison Test: $\alpha = 0.05$),
# - indicates statistically-significantly larger ELONA responses of the aptamers to the protein indicated, compared to the other protein/s investigated (Dunn's Multiple Comparison Test: $\alpha = 0.05$)

When comparing the performance across proteins for studied non-heat-activated aptamers, Kruskal-Wallis *H*-test significance ($p \leq 0.05$; indicated in shaded bold type) was observed for binding of non-heat activated rLDH 4 ($H(5,21) = 11.96$; $p = 0.035$), rLDH 7 ($H(5,21) = 11.30$; $p = 0.046$) (**Figure 4.3b**), LDHp 3 ($H(5,21) = 15.37$; $p = 0.009$), LDHp 11 ($H(5,21) = 15.76$; $p = 0.007$) and LDHp 18 ($H(5,21) = 15.99$; $p = 0.007$) (**Figure 4.3c**), across studied proteins.

LDHp 18, however, did show high-affinity binding to LDHp when it was not heat-activated indicated by the assay response (colourimetric absorbance at 450 nm) of 0.106 ± 0.003 OD (**Figure 4.3c**); however, LDHp 18 also demonstrated statistically significant and non-specifically higher binding to HSA with 0.117 ± 0.003 OD ($p \leq 0.05$). In a Dunn's multiple comparisons test, ELONA responses for LDHp 18 to HSA and LDHp showed significance to each other (indicated buy the # symbol in **Figure 4.3c**). These data indicate that non-heat-activated – LDHp 18 has a propensity to bind spontaneously

and non-specifically, albeit sensitively, to HSA, mLDH, LDHp and r*Pv*LDH.

Interestingly, when rLDH 4 was not heat-activated (**Figure 4.3b**), this aptamer exhibited low $OD_{450\ nm}$ responses for HSA, mLDH, r*Pf*LDH and r*Pv*LDH, but exhibited statistically significantly ($\alpha < 0.05$) higher binding to LDHp (0.090 ± 0.004 OD) over, specifically, r*Pf*LDH (0.056 ± 0.003 OD), indicated by # in **Figure 4.3b**. This is in direct contradiction to observed ELONA responses with heat-activated aptamers (see following section and **Figure 4.4**).

ELONA $OD_{450\ nm}$ responses for non-heat-activated aptamers, 2008s, pL1, rLDH 1, 4, 7, 15 and LDHp 1, 3, 11, and 14, to HSA, mLDH, LDHp, r*Pf*LDH and r*Pv*LDH were not statistically significantly greater than $OD_{450\ nm}$ responses for aptamers in the absence of protein (-/+ control). Moreover, non-heated aptamers, rLDH 1, 7, 15 and LDHp 1, 3, 11 and 14, against r*Pf*LDH and LDHp, respectively, exhibited similar non-specific binding to control proteins, HSA, mLDH and r*Pv*LDH evidenced by the lack of statistically significant (Dunn's multiple alignment statistics: $\alpha > 0.05$) increases in $OD_{450\ nm}$ responses for generated aptamers to r*Pf*LDH and LDHp, respectively, over HSA, mLDH and r*Pv*LDH control proteins (**Figure 4.3**). This non-specific binding demonstrates that the aptamers that did not undergo heat treatment are incapable of distinguishing between peptide and/or protein macromolecules. This lack of discriminatory recognition is as a result of the inability of the aptamers to conform to the correct secondary and tertiary structure, i.e. conformation (Ellington & Stostak, 1990). Although the ELONA OD response observed for LDHp 18 was significant for HSA, LDHp and r*Pf*LDH, as previously discussed, the spontaneous and non-specific nature in which this non-heated aptamer binds to these proteins renders the use of non-heat-activated LDHp 18 in a diagnostic device as unsuitable. Therefore, heat-denaturation of aptamers is required to facilitate aptamer conformation to the appropriate tertiary structure capable of target recognition and discrimination between LDHp and/or r*Pf*LDH, and HSA, mLDH and r*Pv*LDH. The effect of heat-denaturation of generated aptamers on target and control proteins will be related to their secondary and tertiary structures, and will be explored further in the following section.

4.5.1.b. Heat-activated aptamer binding to HSA, mLDH, LDHp, rPfLDH and rPvLDH

ELONA was used to investigate the performance of heat-denatured (95 °C for 10 min; -20 °C for 5 min; 22 °C for 5 min) pretreated aptamers binding to proteinaceous targets under room temperature (22 °C). The performance of heat-activated rLDH aptamers to LDHp and, vice versa,

LDHp aptamers to r*Pf*LDH was investigated (**Figure 4.4**). Control proteins included human serum albumin (HSA) and mammalian LDH (mLDH), both expected to be found in high concentrations in the analyte matrix, as well as recombinant *P. vivax* LDH (r*Pv*LDH) to assess inter-species binding specificity.

Figure 4.4 illustrates the ELONA responses of previously published aptamers found to bind to *rPf*LDH: aptamer 2008s (Cheung *et al*., 2013; Tanner *et al*., 2013) and aptamer pL1 (Ban *et al*., 2012; Lee *et al*., 2012). Despite the differences in operating buffer composition between these reported aptamers and the ones generated in this study, 2008s (0.1 M NaCl and 10 mM phosphate buffer) and pL1 (20 mM Tris, 50 mM NaCl, 5 mM KCl, 5 mM $MgCl_2$, pH 8.0) were heat-activated in 1× HMCKN, and binding allowed to proceed in 1× HMCKN as binding buffer in order to accurately compare responses across all aptamers.

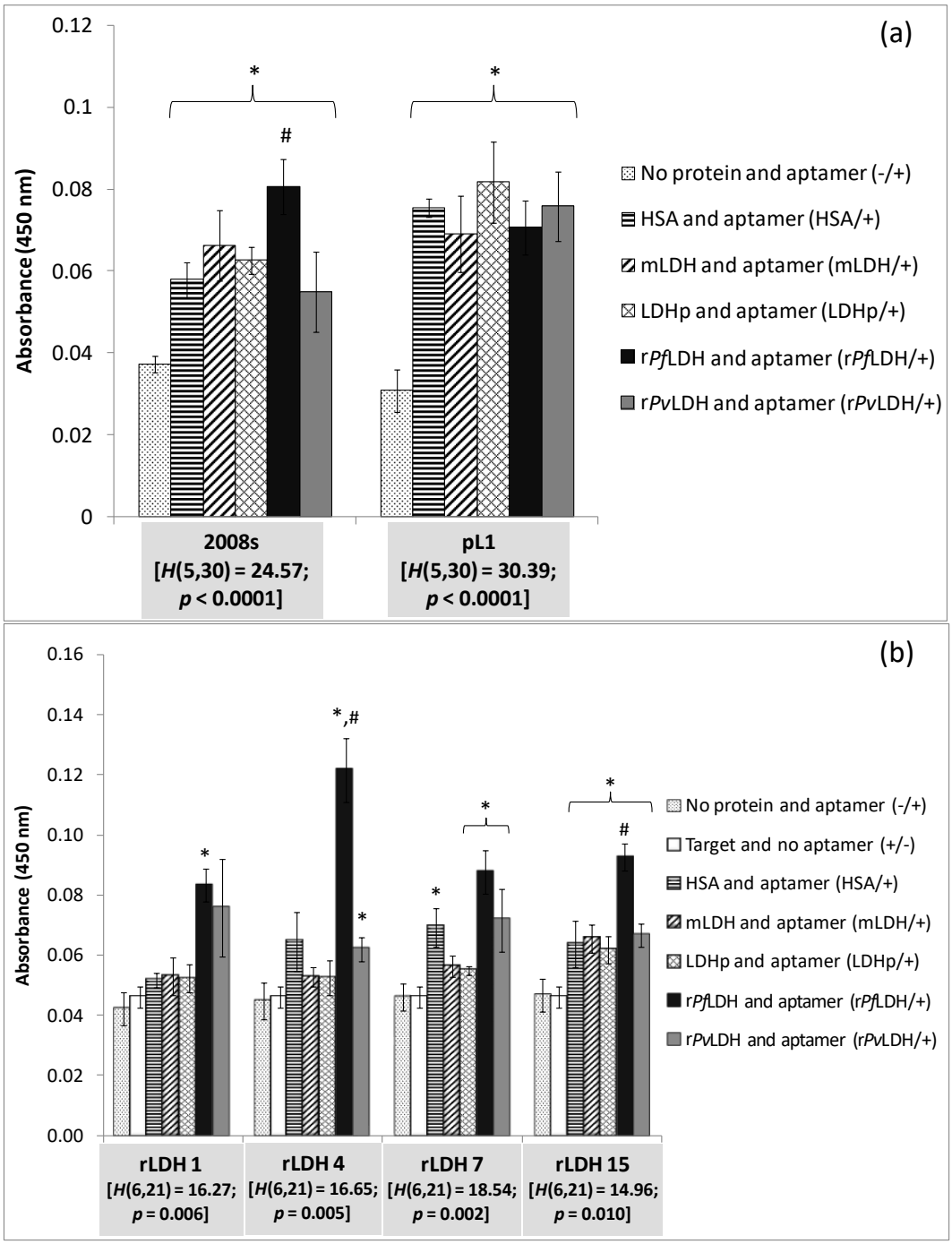

Figure 4.4: Continued on following page

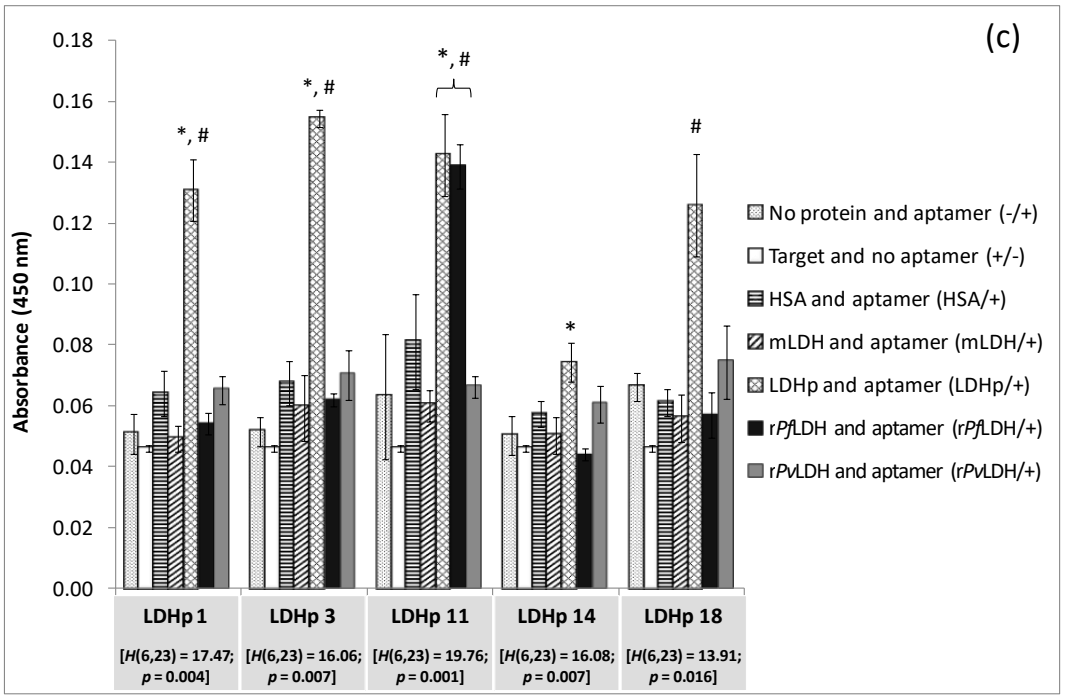

Figure 4.4: Binding specificity of previously published biotinylated ssDNA aptamers, 2008s and pL1 (a), and r*Pf*LDH- (b) and LDHp-targeting (c) to HSA, mLDH, LDHp, r*Pf*LDH and r*Pv*LDH, as determined by ELONA using 1× HMCKN, pH 7.4, as binding buffer (*n* = 5).

Statistics: Kruskal-Wallis H-test for statistical significance with Dunn's multiple comparisons *post hoc* test;
Shaded bold - indicates statistical significance using the Kruskal-Wallis H-test ($p \leq 0.05$),
* - indicates statistically-significantly larger ELONA responses compared to the absence of aptamers (Dunn's multiple comparisons *post hoc* test: $\alpha < 0.05$),
# - indicates statistically-significantly larger ELONA responses of an aptamer to the protein indicated, compared to the other protein/s investigated (Dunn's multiple comparisons *post hoc* test: $\alpha < 0.05$)

The ELONA results (**Figure 4.4**) show protein-dependent variation in assay responses. The $OD_{450\ nm}$ responses of 2008s and pL1 binding to protein and control targets (HSA, mLDH, LDHp, r*Pf*LDH and r*Pv*LDH) were statistically significantly higher (Dunn's multiple comparison *post hoc* test: $\alpha \leq 0.05$) compared to the aptamer binding in the absence of protein target (no protein and aptamer control), as indicated by the * symbol in **Figure 4.4a**. Binding of heat-denatured 2008s exhibited increased binding signal to r*Pf*LDH (0.081 ± 0.007 OD) compared to the other proteins indicated by the increased optical density responses thereof (Dunn's multiple comparisons *post hoc* test: $\alpha \leq 0.05$; indicated by the # symbol in **Figure 4.4a**). Aptamer 2008s also exhibited statistically significantly higher OD response and, thus binding, to r*Pf*LDH compared to r*Pv*LDH (0.0806 ± 0.0068 OD for r*Pf*LDH vs. 0.0548 ± 0.0098 OD for r*Pv*LDH; $p \leq 0.05$) indicating preferential binding to r*Pf*LDH in 1× HMCKN binding buffer, pH 7.4. Using a fluorescent assay, Lee and co-workers (2012) demonstrated that pL1 bound to both r*Pv*LDH and r*Pf*LDH with high affinity, which will be further discussed in **Chapter 4.5.1.d**. These observed colourimetric (OD_{450nm}) data shown in **Figure 4.4a** are corroborated by the recent report by Cheung and co-workers (2018) in which they report the preferential binding

of 2008s to r*Pf*LDH over r*Pv*LDH in phosphate buffered saline-Tween 20 (PBST) buffer. They also report the absence of speciation between r*Pf*LDH and r*Pv*LDH for aptamer pL1 in a Tris-Tween 20 buffer (50 mM NaCl, 5 mM KCl, 5 mM $MgCl_2$, 0.01% Tween 20 and 20 mM Tris, pH 8) according to the original report by Lee and co-workers (2012). However, OD responses for 2008s and pL1 recorded in **Figure 4.4a** were lower than those reported for ELONA in Cheung *et al*. (2018), indicating that 1× HMCKN, pH 7.4, lowered the affinity of these two aptamers for r*Pf*LDH and r*Pv*LDH, without significantly impacting the specificity. At this juncture, one can note the lack of statistical data presented for ELONA in the report by Cheung and co-workers (2018) as only one set of data was provided in their report. This lack of reported statistical data limits the significance of the data presented in Cheung *et al*. (2018); therefore, the OD responses observed in the ELONA shown in Cheung *et al*. (2018) could be idiosyncratic.

When comparing the performance of a given heat-activated r*Pf*LDH-binding aptamer across the studied proteins (**Figure 4.4b**), Kruskal-Wallis *H*-test significance ($p \leq 0.05$; indicated in bold type) was observed for binding of all heat-activated aptamers, specifically rLDH 1 ($H(6,21) = 16.27$; $p = 0.006$), rLDH 4 ($H(6,21) = 16.65$; $p = 0.005$), rLDH 7 ($H(6,21) = 18.54$; $p = 0.002$) and rLDH 15 ($H(6,21) = 14.96$; $p = 0.010$), indicating that ELONA responses for aptamer binding to r*Pf*LDH, r*Pv*LDH, LDHp, mLDH, HSA and the negative control were significantly different.

Of the sampled aptamers raised against the recombinant protein, r*Pf*LDH, illustrated in **Figure 4.4b**, binding of rLDH 4 aptamer to r*Pf*LDH (0.120 ± 0.011 OD) produced a significantly higher colourimetric response than the same sequence binding to the control proteins mLDH (0.053 ± 0.003 OD), HSA (0.065 ± 0.010 OD) and r*Pv*LDH (0.062 ± 0.004 OD, significant vs. negative control), indicated by the Dunn's statistical comparison ($\alpha \leq 0.05$; indicated the # symbol). Shown in **Figure 4.4b**, rLDH 4 exhibits a preference for r*Pf*LDH and discriminates between r*Pf*LDH and r*Pv*LDH, given that the signal against r*Pv*LDH does not differ statistically from the HSA control. Both r*Pv*LDH and HSA $OD_{450\ nm}$ responses are statistically higher than the no protein and aptamer and target and no aptamer controls ($\alpha > 0.05$; indicated by the * symbol).

Colourimetric assessment of rLDH 15 aptamer binding to the target r*Pf*LDH (0.093 ± 0.012 OD) showed statistically-significantly higher ($\alpha \leq 0.05$; indicated by the # symbol) binding than to the control mLDH, HSA and r*Pv*LDH (with ODs of 0.065 ± 0.005 OD, 0.064 ± 0.008 OD and 0.067 ± 0.004 OD, respectively [**Figure 4.4b**]) indicating that it too exhibits species specificity. Interestingly, the

secondary structures shown in **Figure 3.5** (**Chapter 3.5.3**) for rLDH 4 and rLDH 15 do not show extensive canonical base-pairing indicating a more complex tertiary structure (refer to **Figure 3.6** and **3.9** for tertiary structures) may be governing binding interactions between this sequence and the target protein. Although rLDH 1 and rLDH 7 aptamers do show positive binding to r*Pf*LDH, the high signal obtained for rLDH 1 binding to r*Pv*LDH suggests binding to a common motif shared between the proteins; while, the high levels of rLDH 7 binding to HSA compared to r*Pf*LDH suggests that the aptamer, rLDH 7, may lack specificity for r*Pf*LDH in human serum samples.

None of the rLDH aptamers tested demonstrated statistically significant binding to LDHp (Dunn's multiple comparison: $\alpha \leq 0.05$; **Figure 4.4b**), either compared to control proteins or baseline assay responses. Moreover, the statistically significant results for rLDH 4 in which binding to r*Pf*LDH is significantly higher than LDHp in **Figure 4.4b** are in opposition to data presented in **Figure 4.3b** in which higher responses were observed for LDHp over r*Pf*LDH. This indicates that heat-activation is required for target recognition and speciation, particularly for rLDH 4 aptamer. The low degree of consensus between the LDHp group of aptamers and the rLDH aptamers (**Chapter 3.5.2**) may indicate that the rLDH aptamers generated in this study bind to other sites than that modelled by LDHp. Furthermore, the absence of binding may also be as a result of incorrect orientation of r*Pf*LDH at the time of binding during ELONA. Therefore, r*Pf*LDH-binding aptamers, rLDH 1, 4, 7 and 15, may bind to sites on r*Pf*LDH that are not analogous, or that do not mimic, the secondary and tertiary structure of LDHp. This is reminiscent of the behaviour of polyclonal antibodies that have been raised against a whole protein and affinity purified because within the pool of antibodies there would be multiple antibodies against the range of available epitopes acting as binding sites (Lipman *et al*., 2005). Higher titres of antibodies against one epitope over another are, therefore, likely to occur. Conversely, aptamers recognise and interact with a limited region of the target protein (Aptekar *et al*., 2015) – demonstrated here by three rLDH aptamers detecting r*Pf*LDH (rLDH 4, 7 and 15), one rLDH aptamer detecting r*Pv*LDH (rLDH 1) and none of these rLDH aptamers detecting the r*Pf*LDH peptide, LDHp.

Assessing binding of rLDH to the aptamers selected against the *Pf*LDH-specific peptide, LDHp, further assist in *Plasmodium spp*. discrimination in a practical application, as shown by Hurdayal and co-workers. The recombinant LDH (r*Pf*LDH) provides the correctly assembled conformation of the peptide and native secondary structure in this study. Of the eight colonies that contained the

inserted oligonucleotides for LDHp binding, four (LDHp 1, 3, 11 and 18) bound to the target LDHp (**Figure 4.4c**).

When comparing the performance of a given heat-activated LDHp-binding aptamer across the studied proteins (**Figure 4.4c**), Kruskal-Wallis *H*-test significance ($p \leq 0.05$; indicated in bold type) was observed for binding of all heat-activated aptamers, specifically LDHp 1 ($H(6,23) = 17.47$; $p = 0.004$), LDHp 3 ($H(6,23) = 16.06$; $p = 0.007$), LDHp 11 ($H(6,23) = 19.76$; $p = 0.001$), LDHp14 ($H(6,23) = 16.08$; $p = 0.007$) and LDHp 18 ($H(6,23) = 13.91$; $p = 0.016$).

Binding analysis of the pool of aptamers generated against the LDH epitopic oligopeptide indicated that four aptamers (LDHp 1, 3, 11 and 18) bind strongly to the target LDHp indicated by ELONA absorbance at 450 nm (**Figure 4.4c**). This binding to LDHp was statistically significantly greater than the remaining proteins, as indicated by Dunn's multiple comparisons statistical significance tests ($\alpha \leq 0.05$; indicated by the # symbol; **Figure 4.4c**). These four LDHp aptamers had similar signal intensities with LDHp in the assay (with an average OD of 0.138 ± 0.013 OD for these four aptamers). The four aptamers demonstrated significant (Kruskal-Wallis *H*-test: $p \leq 0.05$) binding to the target LDHp compared to mLDH, HSA, r*Pv*LDH and the other controls. Binding of these aptamers to the LDHp with similar OD values and the lack of binding to r*Pv*LDH, is strongly indicative of discrimination of the aptamers between the selected *Plasmodium spp*. Species specificity towards r*Pf*LDH is thus intimated as the sequence of the r*Pf*LDH peptide used is unique to *P. falciparum* and is, hence, not present in *P. vivax* LDH (Hurdayal *et al.*, 2010).

Only one of the four peptide-specific aptamers, LDHp 11, bound to a significant extent to both the recombinant protein, r*Pf*LDH, and the peptide. The LDHp 11 aptamer exhibits selective recognition of the epitope when in the appropriate conformation in the recombinant protein (**Figure 4.4c**). LDHp 11 can, therefore, bind to the recombinant LDH similarly to the findings of Hurdayal *et al*. (2010), who validated the immunogenicity of this peptide construct using antibodies. Furthermore, from **Figure 3.5**, **Chapter 3.5.3**, the vastly different secondary structures for LDHp 11 demonstrate a form of structural flexibility which may facilitate binding to both the smaller peptide (LDHp) and larger polypeptide (r*Pf*LDH). Therefore, this discovery of species-specificity shown by LDHp 11 facilitates the further development of a sensing technique by which to specifically detect *P. falciparum* in a biosensor and is an important finding in this study.

Generated aptamers, rLDH 1, 4, 7, and 15 and LDHp 1, 3, 11, 14, and 18, that were non-heat-activated, having not undergone heat-denaturation, did not exhibit the same behaviour in general as they did when heat-activated at 95 °C and snap-cooled at -20 °C (**Figure 4.4b** and **Figure 4.4c**, respectively). Given the non-specific binding of non-heat-activated aptamers (**Figure 4.3**) and differential binding of heat-activated aptamers (**Figure 4.4b** and **Figure 4.4c**), rLDH 1, 4, 7 and 15 and LDHp 1, 3, 11, 14 and 18, to a variety of proteins tested presented herein, these aptamers do indeed require heat-activation in order to conform to the necessary tertiary structures required for target recognition. This may serve as a limitation in the application of these generated aptamers in particular molecular constructions used in diagnostic devices, such as aptabeacons. Aptabeacons require an aptamer to conform from its native state in solution to the correct tertiary conformation when in contact with the target, exposing the conjugated reporter molecule upon target binding (Baldrich, 2010). The generated aptamers are, therefore, not suitable candidates for application as aptabeacons on a sensing platform as they require heat activation and the resulting tertiary conformation to be able to suitably and selectively recognise and bind r*Pf*LDH and LDHp.

4.5.1.c. pH-dependency of aptamer binding to rPfLDH

ELONA was used to probe the effect that the pH of the aptamer-target binding solution, in this case 1× HMCKN, has on the binding of aptamers, rLDH 1, 4, 7 and 15 and LDHp 1, 3, 11, 14 and 18 (200 nM), to r*Pf*LDH. The control used was absent of r*Pf*LDH; but, similar to the test condition, did contain 200 nM of the afore-mentioned aptamers. Binding solutions with constant salt contents of pH 5.2 and 7.4 were used as examples (**Figure 4.5**) as a lower and more acidic pH has been previously shown to positively influence aptamer-target binding (Ahmad *et al*., 2011). A concentration of 200 nM of 5'-biotinylated aptamer was used for this analysis. Binding buffers with constant salt contents but different pH demonstrate that influence of pH along without interference by mitigating factors such as the change in ions and salt compositions (Ellis and Morrison, 1982).

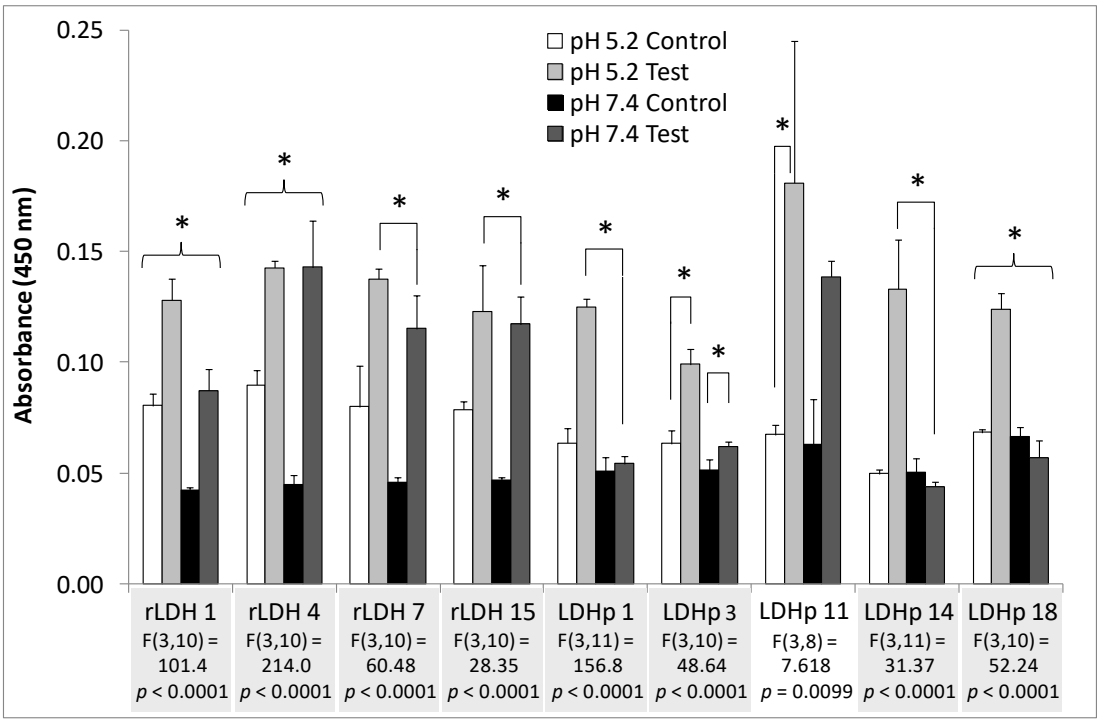

Figure 4.5: pH dependency of ELONA responses, using binding of 200 nM heat-denatured ssDNA aptamers, rLDH 1, 4, 7 and 15 and LDHp 1, 3, 11, 14 and 18, to 500 ng r*Pf*LDH at pH 5.2 and pH 7.4, compared to control ([r*Pf*LDH] = 0 nM, [aptamer] = 200 nM).

Buffer used: 1× HMCKN. Number of replicates, $n = 3$.

Statistics: Statistical significance using One-Way ANOVA was given where $p \leq 0.05$

Shaded bold - indicates statistical significance using the One-Way ANOVA with $p < 0.0001$.

* Tukey's HSD *post hoc* test where $\alpha = 0.05$.

Comparing the influence of pH on ELONA responses presented in **Figure 4.5**, proportionately increased assay responses (absorbance at 450 nm) across measured aptamers in the control samples (no r*Pf*LDH) was observed at pH 5.2 compared to pH 7.4, with the exception of LDHp 11, 14 and 18. This may indeed be caused by the more favourable electrostatic environment caused by the drop in pH and associated decrease in negative charge of the molecules, but this indicates an increase in non-specific binding of the aptamer to the control sample under these conditions.

Comparing the influence of pH on ELONA responses presented in **Figure 4.5**, proportionately increased assay responses (absorbance at 450 nm) across measured aptamers in the test samples (binding to r*Pf*LDH) were observed at pH 5.2 compared to pH 7.4, with the exception of rLDH 4 ($F(3,10) = 214.0$; $p < 0.0001$). One-Way ANOVA indicated that a significant difference in the binding extent across tested aptamers existed ($p \leq 0.05$). One-Way ANOVA statistical significance ($p < 0.0001$) was shown across aptamers binding to r*Pf*LDH at pH 5.2 over pH 7.4, with the exception of LDHp 11 ($F(3,8) = 7.618$; $p = 0.0099$). This statistically significant increase in $OD_{450\ nm}$ response for the

rLDH aptamers (except rLDH 4) at pH 5.2 over pH 7.2 does not necessarily indicate that the aptamers are binding to r*Pf*LDH with a higher affinity as the controls showed similar increases in affinity the lower pH in the absence of target protein. Aptamer rLDH 1, on the other hand, did exhibit significant increases in the presence of the target protein at pH 5.2 over pH 7.4. The test samples (with r*Pf*LDH) for the LDHp group of aptamers did exhibit increases in $OD_{450\ nm}$ response at pH 5.2 over pH 7.4, with the exception of LDHp 11, while the respective controls (no r*Pf*LDH) for the remaining LDHp aptamers did not exhibit such increases in response. $OD_{450\ nm}$ responses for the controls at pH 7.4 showed little deviation for the various of aptamers unlike the $OD_{450\ nm}$ responses for the controls at pH 5.2. This increase in ELONA response above the background (ie that of the controls) at pH 5.2 versus pH 7.4 indicates that such responses can be attributed to increased binding interactions between r*Pf*LDH and aptamers, rLDH 1, LDHp 1, 3, 14 and 18.

The increase in assay response results from the electrostatic effect that the lower pH, pH 5.2, has on the overall charge of whole recombinant protein, *Pf*LDH (pI = 7.3; Artimo *et al*., 2012), as well as the electrostatic attraction that the charged protein has towards the negatively charged aptamers (Ahmad *et al*., 2011). (The r*Pf*LDH-specific peptide (pI = 3.4), not used in the pH dependency analysis, would be negatively charged at both pH values used). Ahmad and co-workers (2011) reported similar findings in their fluorescent bead assay based analysis on the effect of binding solution pH on aptamer-target binding for platelet derived growth factor B (PDGF-BB; pI = 9.3). They report that a decrease in pH and increase in the overall net positive charge of the target protein resulted in an improved aptamer affinity for the target PDGE-BB indicated by a decrease in the K_d. Therefore, the observed increases in OD response at pH 5.2 over the OD responses at pH 7.4 for rLDH 1 and LDHp 1, 3, 14 and 18 shown in **Figure 4.5** can be expected and attributed to the electrostatic effect that lowering the binding buffer pH has on the affinity of the aptamer to the target (Ahmad *et al*., 2011).

The statistically significant difference in OD_{450nm} response between rLDH 4 to r*Pf*LDH at pH 5.2 and 7.4 (0.143 ± 0.003 OD versus 0.143 ± 0.21 OD, respectively) indicates that rLDH 4 is not wholly affected by the pH of the binding solution. Furthermore, the sensitive $OD_{450\ nm}$ responses, albeit statistically insignificantly different responses, of LDHp 11 at pH 5.2 and pH 7.4 (0.181 ± 0.064 OD and 0.139 ± 0.007, respectively) indicates that LDHp 11 can sensitively bind to r*Pf*LDH. The observed sensitivity of the $OD_{450\ nm}$ responses for both rLDH 4 and LDHp 11 at pH 5.2 and pH 7.4 implies that these two aptamers can be utilised at both physiological pH and more acidic pH with little adverse effect on the selectivity exhibited by the aptamers. Aptamers rLDH 4 and LDHp 11 are able to

sensitively detect r*Pf*LDH, at both pH 5.2 and 7.4.

Unlike previous reports of aptamer sensitivity to changes in pH (Ilgu & Nilsen-Hamilton, 2016), a certain level of stability is inferred on rLDH 4 and LDHp 11 aptamers due to their ability to withstand a change in pH. Therefore, the evidence demonstrated in **Figure 4.5** indicates that generated aptamers, rLDH 4 and LDHp 11, are not limited by the pH of the local environment in which they will be used to elicit binding, and consequential detections response, in the analytical device in which they will eventually be used. The indiscriminative, yet sensitive, response at the two pH values for rLDH 4 and LDHp 11 implies that a buffering and detection micro-environment with a more acidic pH can be utilised in future experimentation. A more acidic buffering and detection system can, hence, be used in future malaria sensing applications and sensor configurations: the rLDH 4 and LDHp 11 aptamers' sensitivity will not be limited by the acidity of the binding matrix in which the aptamer may be applied.

However, as the eventual matrix in which these aptamers will be applied in human blood (pH = 7.4), it is the OD responses for aptamer-target binding at pH 7.4 that would be a true indication of aptamer binding in human blood. Thus, rLDH 4 and LDHp 11 hold promise in the *in vitro* and *in vivo* detection of *Plasmodium falciparum* LDH. Therefore, 1× HMCKN binding buffer at pH 7.4 was used in all consecutive studies.

4.5.1.d. Binding affinity kinetics of tested aptamers for rPfLDH and rPvLDH using ELONA

The kinetics of aptamer concentration-dependent ELONA assay responses was examined for generated aptamers, rLDH 4, 7 and 15, LDHp 1, 3, 11, 14 and 18, and concatemer, C7, as well as pL1 and 2008s (Ban *et al*., 2012; Lee *et al*., 2012; Cheung *et al*., 2013; Tanner *et al*., 2013; Cheung *et al*., 2017). Binding to r*Pf*LDH and r*Pv*LDH was examined. The kinetics of aptamer concentration-dependent ELONA assay responses was also separately examined for the LDHp class of aptamers, LDHp 1, 3, 11, 14 and 18 to the *Pf*LDH-specific peptide, LDHp. Examples of the corresponding ELONA-based colour changes for binding kinetics of r*Pf*LDH-binding aptamers, LDHp 1 and 11, rLDH 4 and 7, 2008s (Cheung *et al*., 2013; Tanner *et al*., 2013) and concatemer control, C7, are shown in **Figure C.1 Appendix C**.

The concentration-dependant increase in binding, shown in **Figure 4.6**, leads to calculable binding

kinetics through non-linear regression models (Langmuir regression model) and fitting using a least-squares model. The concatemer control, C7, used as a classical negative and primer control, did not show such an aptamer concentration-dependant increase. Due to their performances in ELONA presented in **Figures 4.5**, binding kinetics and regression model fits for aptamers LDHp 11 and rLDH 4 are presented in **Figure 4.6** as case studies in the discussion on the apparent affinity constants, K_D, and Γ_{max}.

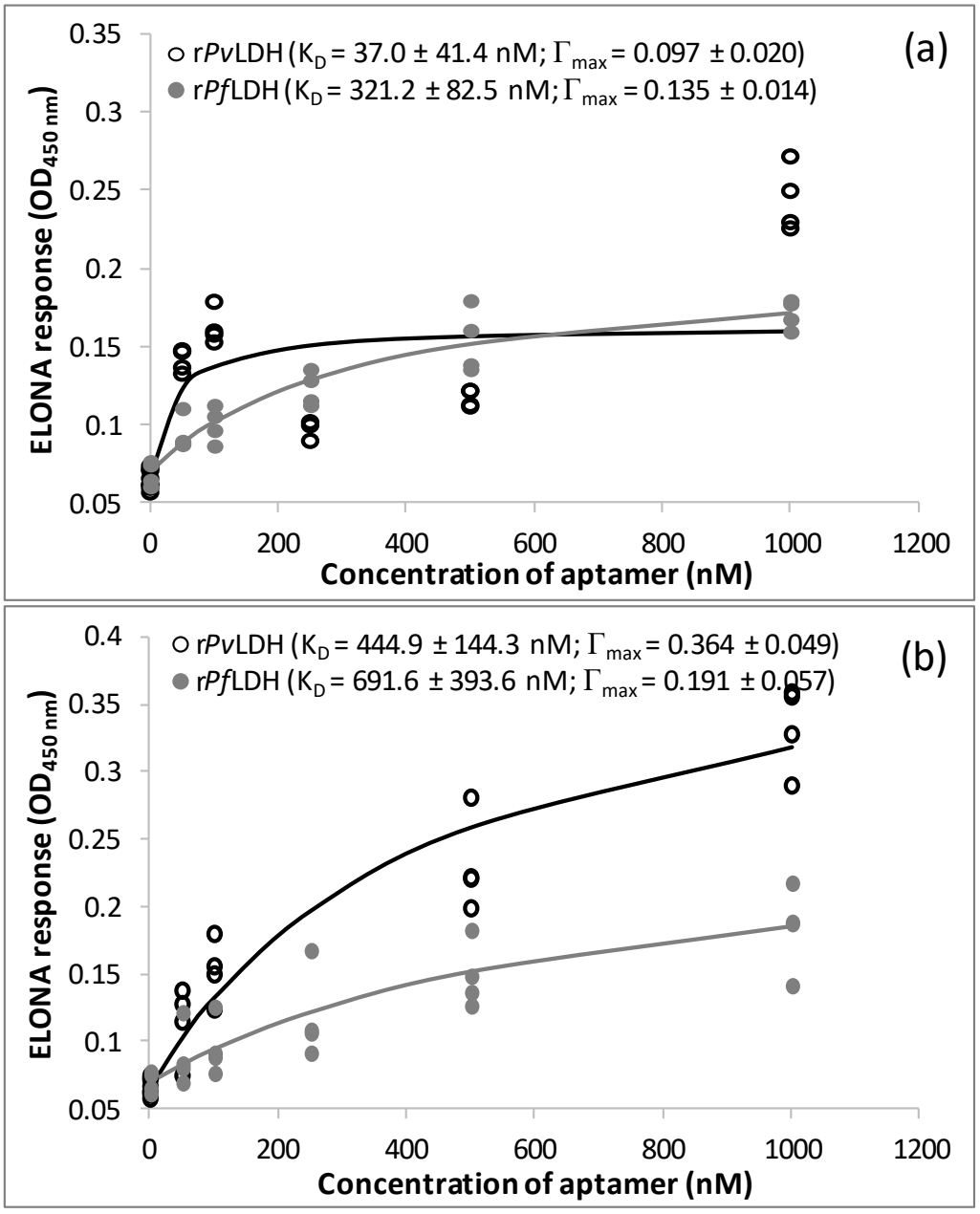

Figure 4.6: ELONA-assessed (A_{450nm}) binding kinetics of 0, 50, 100, 250, 500 and 1000 nM biotinylated LDHp 11 (a) and rLDH 4 (b) to r*Pf*LDH and r*Pv*LDH (*n* = 4).

Note: K_D = apparent binding constant using a Least Squares fitting model; Γ_{max} = Kendell's correlation coefficient

In addition to the binding kinetics and regression model fits exampled in **Figure 4.6**, those for rLDH 7, rLDH 15 and LDHp 1, concatemer C7, as well as pL1, to r*Pf*LDH and r*Pv*LDH were determined and are shown in **Figure C.2 Appendix C**. Binding kinetics and regression model fits for LDHp 1, 3, 11, 14 and 18 to LDHp are shown in **Figure C.3 Appendix C**. Averages and standard errors of the apparent affinity constants, K_D, and Γ_{max} for generated aptamers, LDHp 1, 3, 11, 14 and 18, rLDH 4, 7 and 15, and the concatemer, C7, as well as the previously published aptamers, pL1 (Ban *et al*., 2012; Lee *et al*., 2012) and 2008s (Cheung *et al*., 2013; Tanner *et al*., 2013; Cheung et al., 2017), to r*Pf*LDH and r*Pv*LDH, as determined through ELONA, are presented in **Table 4.1**. Included in **Table 4.1** are the averages and standard errors of the apparent affinity constants, K_D, and Γ_{max} for generated aptamers, LDHp 1, 3, 11, 14 and 18 to LDHp.

Table 4.1: K_D values for aptamers LDHp 1, LDHp 11, rLDH 4, rLDH 7, rLDH 15, C7 and pL1 binding to immobilised proteins, r*Pf*LDH, r*Pv*LDH and LDHp, as determined using ELONA.

K_D: estimated apparent dissociation constant (M) of the aptamer-target complex; Γ_{max}: estimated maximal assay response for the aptamer-target complex.

Aptamer	Apparent affinity constant, K_D (nM) ±SE						Reference
	r*Pf*LDH		r*Pv*LDH		LDHp		
	K_D	Γ_{max}	K_D	Γ_{max}	K_D	Γ_{max}	
C7	NR	NR	NR	NR	-	-	This work
LDHp 1	927.3 ± 915.0	0.068 ± 0.039	CNM > 1000	0.230 ± 0.106	96.0 ± 63.2	0.060 ± 0.011*	This work
LDHp 3	-	-	-	-	CNM > 1000	CNM > 1000	This work
LDHp 11	321.2 ± 82.5*	0.135 ± 0.014*	37.0 ± 41.4 CNM	0.097 ± 0.020*	CNM > 1000	CNM > 1000	This work
LDHp 14	-	-	-	-	CNM > 1000	CNM > 1000	This work
LDHp 18	-	-	-	-	81.1 ± 63.8	0.053 ± 0.011*	This work
rLDH 4	691.6 ± 393.6	0.191 ± 0.057*	444.9 ± 144.3*	0.364 ± 0.049*	-	-	This work
rLDH 7	39.9 ± 15.7*	0.180 ± 0.014*	26.3 ± 3.2*	0.283 ± 0.050*	-	-	This work
rLDH 15	80.7 ± 17.1*	0.129 ± 0.007*	268.7 ± 67.2*	0.501 ± 0.429*	-	-	This work
pL1	159.5 ± 167.8 CNM	0.022 ± 0.005*	79.2 ± 12.7*	0.209 ± 0.010*	-	-	This work
	38.7 ± 1.3	-	16.8 ± 0.6	-	-	-	Lee *et al*., 2012
	6.2	-	2.9	-	-	-	Cheung *et al*., 2017
2008s	42.0 – 59.0	-	-	-	-	-	Cheung *et al*., 2013
	43.0	-	NR	-	-	-	Cheung *et al*., 2017

* Wald test produced a probability, *p* of < 0.05 for this parameter.

CNM: Could not model – positive binding occurred, but no valid modelled K_D was obtained

CNM > 1000: Could not model – linear dependence indicates that apparent K_D of a target did not fall within the tested concentration range i.e. K_D > 1000 nM

NR: No response – no evidence of binding, relative to the baseline assay response.

No detectable response (NR) was recorded for aptamers that did not exhibit binding to r*Pf*LDH or r*Pv*LDH. Could not model (CNM) was recorded for aptamers that exhibited maximal OD_{450nm} responses that were greater than baseline assay responses, i.e. $\Gamma_{max} > 0$, but for which K_D values could not be determined. These K_D values that cannot be calculated had a standard error greater than its average resulting in failure of the model. Aptamer for which a linear dependence indicated that the apparent K_D of a target did not fall within the tested concentration range were designated CNM > 1000, i.e. K_D > 1000 nM. The Wald test was performed to measure the validity of the measured parameter to the aptamer concentration-dependent OD_{540nm} response: The Wald test assesses whether the parameter distribution within the confidence interval is necessary for the described mathematical dependence i.e. the certainty that K_D and Γ_{max} are > 0 for the dataset investigated. A parameter (K_D or Γ_{max}) that passed the Wald test for a given aptamer was indicated in **Table 4.1** by an asterisk (*). Failure of the Wald test for a given parameter tested for an aptamer using the model shown in **Equation 4.1** was indicated by $p < 0.05$.

Γ_{max}, similar to the R_{max} for conventional binding affinity analysis, is an estimated parameter extrapolated from the measured assay response recorded for aptamer-protein kinetic ELONAs i.e. the $\Delta OD_{450\ nm}$. It is impossible to compare the Γ_{max} between different aptamer-LDH target pairs to evaluate differences in binding affinity for this study as responses inherently varied between kinetic studies. These slight variations in assay responses were due to slight differences in execution of the assay, e.g. TMB substrate exposure time, day-to-day variations in ambient temperatures. Kinetic comparisons between aptamers and targets are limited to the apparent dissociation constant, K_D, Γ_{max}, and the associated Wald test on that parameter, and not overall responses. The K_D, Γ_{max}, and the associated Wald test were, therefore, used to determine if statistically-significant binding between an aptamer and the LDH target in a given study took place.

For binding of the negative concatemerised aptamer control, C7, to r*Pv*LDH and r*Pf*LDH, no detectable response (NR) was recorded (**Table 4.1**). This lack of response indicates that the primer-binding sequences flanking the randomised region enriched during SELEX in this study did not bind to r*Pv*LDH and r*Pf*LDH themselves, as could be expected of this negative control.

K_D values could not be determined for the binding of r*Pv*LDH to aptamers LDHp 1 and LDHp 11. The kinetics for aptamer LDHp 1 and LDHp 11 binding to r*Pv*LDH followed a linear, rather than hyperbolic trend within the concentration range used in this study. The linear dependence indicated that the

apparent K_D of a target did not fall within the tested concentration range, i.e. K_D > 1000 nM, and resulted in a Could Not Model (CNM > 1000) annotation for these aptamer-target pairs (**Table 4.1**). A measurable K_D could be obtained if the concentration range of aptamers LDHp 1 and LDHp 11 increased, but the concentration range would need to surpass all practicalities of the purposes of this research, particularly that which is based on ELONA.

Of the two peptide aptamers, LDHp 1 and LDHp 11, examined here, the modelled K_D between aptamer LDHp 11 and r*Pf*LDH of 321.2 ± 82.5 nM (**Table 4.1**) indicated preferential binding of this aptamer to r*Pf*LDH over r*Pv*LDH, evident in **Figure 4.3c** and **4.4**. The lack of Wald test significance (p > 0.05) and high variability in modelled K_D (927.3 ± 915.0 nM) and Γ_{max} (0.068 ± 0.039) for the binding of LDHp 1 to r*Pf*LDH indicates that this aptamer exhibited binding responses that were independent of aptamer concentration. This is further seen in the lack of visible colour change with increasing LDHp 1 concentration (**Figure C.1 Appendix C**). Liu and co-workers (2019) similarly describe the generation of *Plasmodium* LDH epitope-derived peptide aptamers against the synthesised, mutant sequence, KITTTDEEVEGIFD, using *in silico* modelling. Using a fluorescence-linked immunosorbent assay, or FLISA, they showed that their aptamers bound with an affinity of 35.7 nmol.

Aptamer rLDH 4 (generated against the whole recombinant *Pf*LDH) binding to r*Pf*LDH demonstrated higher modelled K_D values (691.6 ± 393.6 nM) compared to LDHp 11 to the same protein, indicating a lower affinity between this aptamer and the protein (**Figure 4.4**). The lower K_D of 444.9 ± 144.3 nM obtained for binding of rLDH 4 to *rPvLDH* indicated a lack of species-specificity by this aptamer, albeit with a statistically insignificant difference (determined using a pairwise *t*-test: p > 0.05) between the K_D values for r*Pf*LDH and r*Pv*LDH for this aptamer. LDHp 11, thus, exhibits greater sensitivity and species-specificity, compared to rLDH 4, as not only is the K_D value of LDHp 11 for r*Pf*LDH lower, but LDHp 11 did not display modelled and measurable binding to r*Pv*LDH. Furthermore, and as shown in **Figure C.1 Appendix C**, aptamer LDHp 11 displayed greater binding to r*Pf*LDH over r*Pv*LDH given by the $OD_{450\,nm}$ responses for LDHp 11 binding to r*Pf*LDH being higher than that of r*Pv*LDH using static ELONA (**Figure 4.4c**).

A K_D of 80.7 ± 17.1 nM (**Table 4.1**) was determined for binding interactions between rLDH 15 and r*Pf*LDH. This indicates that rLDH 15 exhibited a stronger affinity for r*Pf*LDH than LDHp 11. This is further reiterated by an ELONA-based colour response with increasing concentrations of rLDH 15

(**Figure C.1 Appendix C**). However, a K_D of 268.7 ± 67.2 nM between rLDH 15 and r*Pv*LDH shows preferential, but not specific binding to r*Pf*LDH by this aptamer. Of the aptamers generated in this study, rLDH 7 exhibited the lowest K_D for both tested targets (39.9 ± 15.7 nM for r*Pf*LDH and 26.3 ± 3.2 nM for r*Pv*LDH, respectively), indicating similar high affinities to both targets (**Table 4.1**, **Figures 4.4**). (Aptamer rLDH 7 however also showed non-specific binding to HSA during ELONA studies).

The values obtained here are nevertheless similar to those previously reported with a K_D of 42.0 nM (isothermal titration colorimetry [Cheung *et al*., 2013]), 43.0 nM (ELONA [Cheung *et al*., 2017]), 56 ± 18 nM (electromobility shift assay [Cheung *et al*., 2013]) and 59 nM (surface plasmon resonance [Cheung *et al*., 2013]) for aptamer 2008s generated against r*Pf*LDH (**Table 4.1**). Aptamer rLDH 15 will be further investigated for species-specific binding between r*Pf*LDH and r*Pv*LDH.

Previously published aptamer, pL1 (Lee *et al.,* 2012), exhibited an apparent K_D value of 79.2 ± 12.7 nM for r*Pv*LDH. This measured K_D value was one of the highest affinities recorded in this study for that protein. However, despite producing ELONA responses above the baseline, pL1 did not produce a modelled K_D for r*Pf*LDH using the methods detailed in this study, resulting in a CNM determination (**Table 4.1, Figure C.2, Appendix C**).

To validate ELONA responses, fluoroscein-linked aptamer binding to rPfLDH was explored in fluorophore-linked oligonucleotide assays (FLONA).

4.5.2. FLONA of aptamer-target affinity interactions for rPfLDH and rPvLDH

As an alternative to ELONA, the fluorophore-linked oligonucleotide assay (FLONA) was explored to measure the affinity between r*Pf*LDH and generated aptamers. Fluorescein was chosen as the reporter molecule in this fluorescence-based assay due to its innate sensitivity in the blue-green wavelength spectrum (Al-Hakiem *et al*., 1981). Through FLONA, affinity interactions were ascertained between immobilised r*Pf*LDH and generated fluorscein-tagged aptamers, LDHp 1, LDHp 11, rLDH 4, rLDH 7, concatemer control, C7, and previously published aptamer by Lee and co-workers (2012), pL1 (**Figure 4.7**).

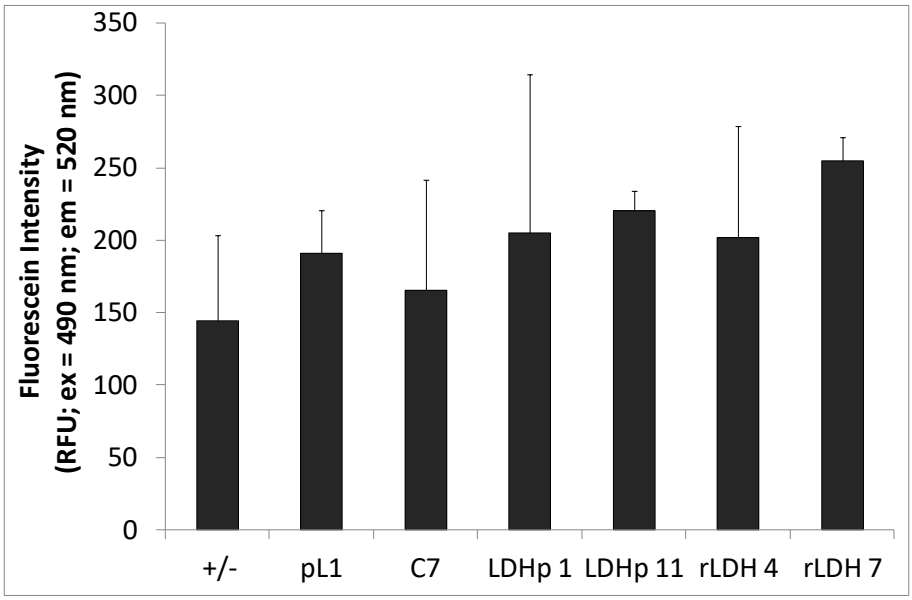

Figure 4.7: Binding affinity of fluorescein-tagged ssDNA aptamers (LDHp 1, LDHp 11, rLDH 4, rLDH 7) and the control aptamers, pL1 (Lee et al., 2012) and concatemer, C7, to the target, r*Pf*LDH, as determined by FLONA (*n* = 4).

Statistics: One-Way ANOVA *F*-test ($p \leq 0.05$): $F(6,20) = 1.124$; $p = 0.3838$
*Tukey's HSD *post hoc* test ($\alpha \leq 0.05$)

A general increase in the average fluorescent response was observed for aptamers, pL1, LDHp 1, LDHp 11, rLDH 4 and rLDH 7, over that of the concatemer, C7 (**Figure 4.7**). These fluorescein-tagged aptamers also exhibited increases in fluorescent response over the control blank. However, these increases in responses over the control blank and also concatemer, C7, were not statistically significant ($F(6,20) = 1.124$; $p = 0.3838$). Furthermore, these increases in response were not sensitive as was hypothesised given the innate sensitivity of fluorescein (Froehlich, 1989). Lee and co-workers (2012) showed that their aptamer pL1 exhibited fluorescent sensitivity in the presence of both r*Pf*LDH and r*Pv*LDH in which an aptamer concentration of 200 nM resulted in a fluorescent response of approximately 2.7×10^5 (≈270 000) RFU. This is substantially greater than the resultant fluorescence of 200 RFU exhibited in **Figure 4.7**. As ELONA suggested that pL1 bound to r*Pf*LDH with low affinity, a response lacking in sensitivity could be expected in FLONA. This indifference could be due to the fact that the 5'-modified fluorophore tag on the aptamers prevented the aptamer from adopting the correct tertiary conformation necessary to bind to the immobilised r*Pf*LDH (Ruscito & DeRosa, 2016). Lack of statistically significant fluorescent decreases in response upon addition of LDHp to the studied aptamer-GelRed® solutions could be due to the inability of the fluorophore-tagged aptamers to bind to the immobilised r*Pf*LDH due to the unfavourable orientation of the protein on the 96-well plate (Schultz, 1996; Kwon *et al*., 2004; LaBaer & Ramachandran, 2005).

LDHp 11 was chosen as a representative of aptamers generated within this work. However, given the evident lack of statistically sensitive responses of aptamers, C7, pL1, LDHp 1, LDHp 11, rLDH 4 and rLDH 7) to r*Pf*LDH using fluorimetry in 96-well plates, any further studies exploring interactions between fluorescein-tagged aptamers and immobilised recombinant LDH peptides using FLONA were abandoned. It was further evident that fluorimetry using 96-well plates similar to ELONA was not suitably sensitive to measure the smaller expected responses produced from the r*Pf*LDH-aptamer interactions. However, in a later study, fluorescein-tagged aptamers will be used to detect native *Pf*LDH *in situ* using the more sensitive confocal fluorescent and epifluorescent microscopy (**Chapter 5**).

Certain methods proving aptamer binding to LDHp and r*Pf*LDH in which both probe and target are free and in solution phase facilitate complexation by performing better than others providing conclusive responses. Such is the case with GelRed displacement, or simply GelRed assays, where binding conditions are mimicked, simulating the conditions under which "Selection" during SELEX was performed, and enabling the heat-activated aptamers to freely take on a binding tertiary conformation in solution simultaneously binding to r*Pf*LDH. An alternative to FLONA with respect to the fluorescent detection of aptamer-target binding, a validation technique using displacement of GelRed® as the fluorescing reporter molecule were explored in the following section.

4.5.3. GelRed® displacement assays for determination of aptamer to rPfLDH binding

As LDHp was too small to be viewed on PAGE, limiting use of EMSA as a binding analysis tool for LDHp, an alternative method is required to visually confirm aptamer binding to LDHp. As a result, the use of fluorescent dyes and markers came as an immediate possibility. GelRed, used as a fluorescent marker for viewing DNA under UV during gel electrophoresis, was immediately available. GelRed® offers added advantages such as stability at room temperature and in light, as well as that of safety, as it is a non-toxic and environmentally friendly alternative to ethidium bromide. GelRed® readily intercalates with DNA and less readily to protein secondary structures. GelRed® has a tendency to bind to guanine-rich (G-rich) moieties (Guo *et al*., 1992); therefore, those aptamer sequences with higher guanine content will tend to fluoresce with greater intensity. Therefore, the premise behind this technique is: GelRed® fluorescence decreases as the intercalator is freed when the DNA conforms as the aptamer bind to its target.

The fluorescence emitted by the observed binding of GelRed® to r*Pf*LDH will interfere with solution-based binding analyses of aptamer to this larger macromolecule, seen in **Figure C.4 Appendix C**, as GelRed® molecules intercalate with cyclic amino acid residues, tryptophan and tyrosine, on the r*Pf*LDH surface, emitting a fluorescent response at 600 nm (Banerjee *et al*., 2014). Therefore, the use of GelRed® to qualitatively and quantitatively measure aptamer binding to r*Pf*LDH can be ruled out.

Solution-based fluorescence of GelRed® was shown to varying degrees upon GelRed® intercalation and binding to aptamers used in this study. No correlation was seen based on guanine content (percent content shown in **Table 3.2**, **Figure 3.1**, **Chapter 3.5.1**) as described by Guo and co-workers (1992) when using the monomeric form of GelRed, ethidium bromide. Neither was a correlation observed between emitted fluorescence and length of oligonucleotide, degree of base-pairing in its secondary structure or folding in its tertiary structures, as would perhaps be expected.

GelRed® has a propensity to bind to the phosphate backbone of DNA based on electrostatic interactions with the positively charged GelRed® molecules (Crisafuli *et al*., 2014). Furthermore, as GelRed® is an intercalator and also binds to dsDNA with greater sensitivity than ssDNA (Biotium FAQs, 2013), it stands to reason that GelRed® molecules will intercalate more readily, and with greater sensitivity, in a more organised and stable tertiary structure exhibiting complementary base-pairing akin to that of dsDNA. Therefore, fluorescent quenching will be based less on the intercalation of GelRed® with ssDNA aptamer when the target is bound: Weakly bound intercalating GelRed® molecules between nucleotides will be removed upon aptamer binding, whilst strongly bound GelRed® molecules within the aptamer 3D conformation and those not directly found at the binding motifs will elicit a response. Moreover, quenching of GelRed® fluorescence has recently been shown in the binding analysis of small molecules, i.e. Ni(II) complexes, to calf thymus DNA through displacement binding (Yu et al., 2017).

Using LDHp as the tested “small” molecule, affinity interactions were assessed between this target and aptamers generated against it in SELEX (LDHp 1, 3, 11, 14 and 18). Control aptamers included the concatemer C7 and pL1 (Lee *et al.*, 2012). Aptamer rLDH 4 binding to the whole recombinant *Pf*LDH was included to assess feasibility in using this approach on the larger protein. **Figure 4.8** shows that a general gain in fluorescence (Em = 600 nm) was observed at an aptamer concentration of 100 nM when 0.5 µM LDHp was added to the ssDNA-GelRed suspension, compared with responses of LDHp-C7 and r*Pf*LDH-rLDH 4.

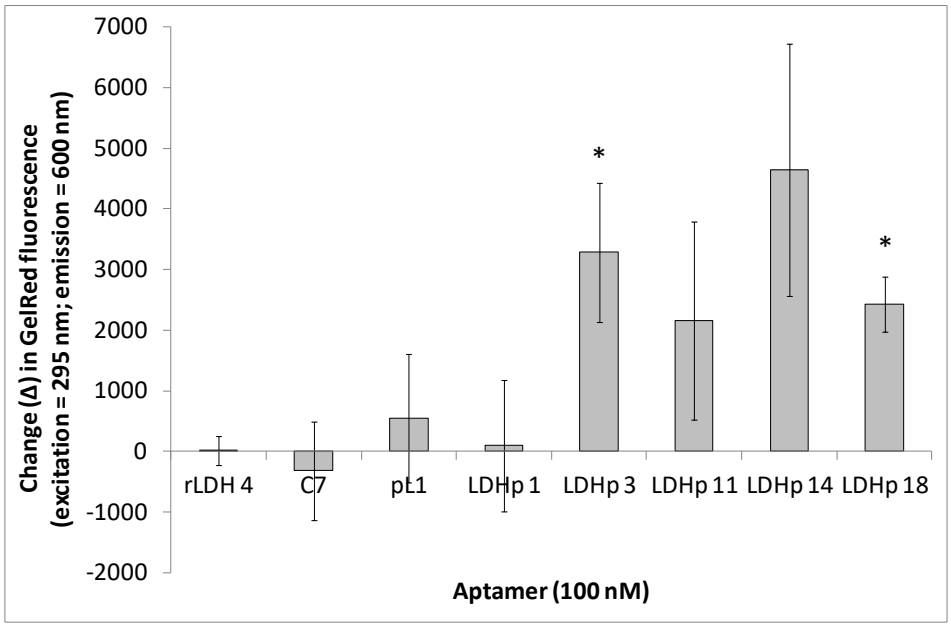

Figure 4.8: Change in fluorescence (em = 600 nm) of GelRed upon addition of 0.5 µM LDHp to 100 nM of aptamer.

r*Pf*LDH-rLDH 4 complexation was used as a control; aptamers: rLDH 4, c7, pL1, LDHp 1, LDHp 3, LDHp 11, LDHp 14 and LDHp 18; aptamer concentrations: 100 nM; LDHp: 0.5 µM; r*Pf*LDH: 1 µM; $n = 3$
Statistics: * denotes statistical significance of grouped, multiple *t*-tests ($p \leq 0.05$)

From **Figure 4.8**, neither the concatemer control C7 nor rLDH4 exhibited measureable shifts in the presence, or absence, of the peptide. An increase in fluorescence of 11.66 ± 238.9 RFU was observed for 100 nM rLDH 4 upon interactions with r*Pf*LDH. Only aptamers LDHp 3 and LDHp 18 exhibited statistically significant differences in fluorescence at 100 nM, with $p = 0.05$ and $p = 0.008$, respectively.

As aptamers LDHp 3, 11, 14 and 18 exhibited such increases in fluorescence (**Figure 4.8**), with LDHp 3 and 18 exhibiting statistically significant increases in fluorescent responses, it can be postulated that these two aptamers are indeed trapping GelRed molecules when interacting with LDHp. This is supported by the fact that, when interacting with the LDHp target, the tertiary structures of LDHp 3 and LDHp 18 conform to create helical structures (**Figure 3.9**), ideally suited to GelRed binding. This increase in GelRed fluorescence is postulated to further be attributed to the formation of hydrophobic or non-polar pockets ideally suited for GelRed trapping and intercalation created between the aptamer and LDHp molecules upon binding interactions. This increase in fluorescent response with the addition of LDHp across the tested aptamers strongly indicates that free GelRed® molecules (those not intercalated to the aptamers prior to target-binding) were physically entrapped when ssDNA aptamers bound to LDHp, and not released (and quenching occur) as reported in literature (Yu et al., 2017).

Further to the investigation reported in **Figure 4.8**, the concentration dependence of GelRed assay responses upon aptamer interactions (maintaining 0.5 µM LDHp) was explored. Concentration-dependence was tested on aptamers LDHp 1, 3, 11, 14 and 18, with pL1 as a control. Pairwise comparisons of fluorescent responses at each aptamer concentration in the presence (with LDHp) and absence (without LDHp) were performed using a grouped multiple *t*-test with statistical significance determined with α set at 0.05 (**Figure C.5 Appendix C**). Statistical pairwise comparisons were performed to ascertain the optimal aptamer concentration with which to record possible GelRed® fluorescent quenching upon addition of 0.5 µM LDHp. **Figure 4.9** shows the changes in fluorescence (Δ) at the concentrations of aptamers explored, specifically, 1, 10, 50 and 75 nM, following addition of LDHp to the ssDNA-GelRed suspension.

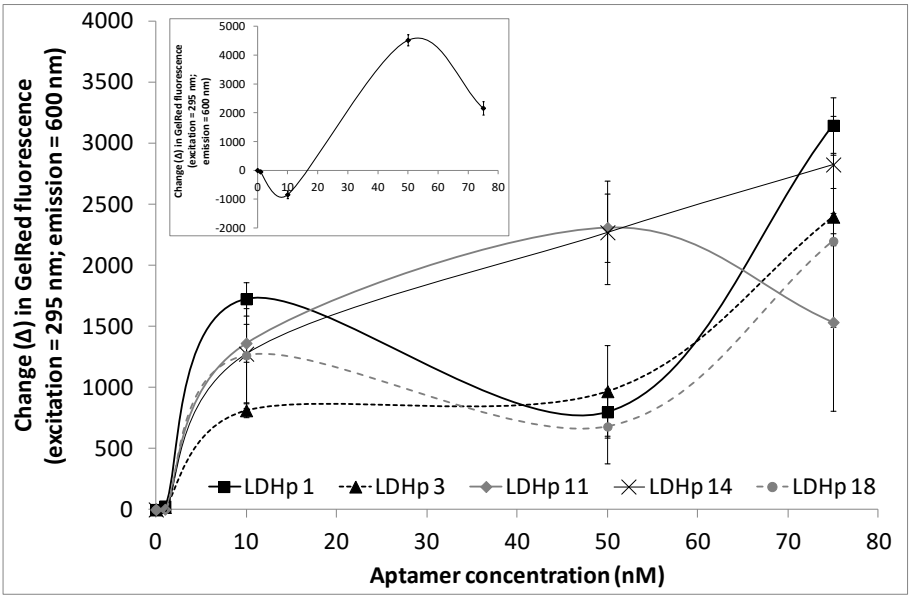

Aptamer	Significant nM ($p \leq 0.05$)
pL1	10, 50, 75
LDHp 1	10, 50, 75
LDHp 3	10, 75
LDHp 11	10, 50
LDHp 14	50, 75

Figure 4.9: Change in fluorescence (Δ) of GelRed dye at various concentrations of aptamer upon LDHp binding.
Insert: Δ GelRed fluorescence at various concentrations of pL1 upon LDHp binding.
Table insert: Aptamer concentrations (nM) found to be statistically significant (*t*-test: $p \leq 0.05$).
r*Pf*LDH-rLDH 4 complexation was used as a control; aptamers: rLDH 4, c7, LDHp 1, LDHp 3, LDHp 11, LDHp 14 and LDHp 18; LDHp aptamer concentrations: 1, 10, 50, 75 and 100 nM; rLDH 4 and c7: 100 nM; LDHp: 0.5 µM; r*Pf*LDH: 1 µM; $n = 3$; $p \leq 0.05$

Figure 4.9 shows that a general gain in fluorescence was observed upon increasing LDHp aptamer concentrations, with the exception of pL1 (insert, **Figure 4.9**) which showed quenching at 10 nM of pL1. This fluorescent gain at lower concentrations, again with the exception of 10 nM pL1, indicates that a higher proportion of free aptamer (with respective intercalated GelRed) was able to binding to LDHp, thus trapping more GelRed molecules within the LDHp-aptamer complex. The general gain in fluorescence and lack of quenching was extended to the higher concentrations of ssDNA aptamers,

despite the provision of more binding sites for target binding given the presence of an increased number of DNA molecules.

Increases in fluorescent responses were observed across aptamer concentrations; however, these displayed little concentration dependence (**Figure 4.9**). While quenching may be occurring upon binding of LDHp to the ssDNA-GelRed complexes, such effects are not occurring to a significant extent and certainly not sufficiently for an observable, clear and measurable fluorescent response. Two theories exist as to why this could occur: (1) tertiary conformation of the aptamer creating helices and pockets suited for GelRed intercalation upon interaction with LDHp; and, (2) trapping of the intercalator within the aptamer-target complex upon binding interaction. A lack of low concentration linearity in **Figure 4.9** prevented kinetic modelling. To fully ascertain the effects on GelRed fluorescence of LDHp binding to aptamers intercalated with GelRed, a scoping range of LDHp concentration needs to be further investigated.

Similar to GelRed binding conditions, electrophoretic mobility shift assays (EMSA) make provision for the mimicking of binding conditions under which "Selection" during SELEX was performed in which both probe and target are free enabling solution phase heat-activated aptamers to freely take on a binding tertiary conformation simultaneously binding and complexing to r*Pf*LDH. However, EMSA makes use of migration profiles of the complexed aptamer-target structure on PAGE.

4.5.4. Electrophoretic mobility shift assay (EMSA) of ssDNA aptamers and rPfLDH, rPvLDH and mammalian LDH (mLDH)

During the above binding analyses, a major influencing factor was the aptamer movement: whether or not aptamer, in its solution phase, was able to freely conform and take on its 3D tertiary structure following heat denaturation; as well as, whether or not sufficient space was available for the aptamer to orientate correctly for target binding. As a result, solution phase binding was preferred in which aptamer was free and target was either free or immobilised. Binding kinetics of aptamers to their targets, LDHp and r*Pf*LDH, are influenced by the phase in which they occur (McKeague & DeRosa, 2012). Daniel and co-workers (2013) demonstrate that affinity of aptamer-target conformations differ in solution and surface phases during kinetic binding.

EMSA relies on the formation of aptamer-target complexes when combinations of the aptamers and the target proteins were incubated together. Potential aptamer-target complexes were separated via PAGE and visualised using GelRed®, to view changes in the migration profile of the ssDNA. These electrophoretic mobility shift assays, or EMSAs were performed to assess to qualitative binding between selected aptamers and r*Pf*LDH. For the aptamer rLDH4, the influence of varying concentrations of either the target protein (**Figure 4.10**) or aptamer (**Figure 4.11**) on the resulting electrophoretic migration profiles are presented. Similar studies were used to determine optimal concentrations for screening of all the tested sequences against control proteins, r*Pv*LDH and mLDH (**Figure 4.12**). EMSA could not be performed using LDHp as this polypeptide was too small to be viewed on PAGE.

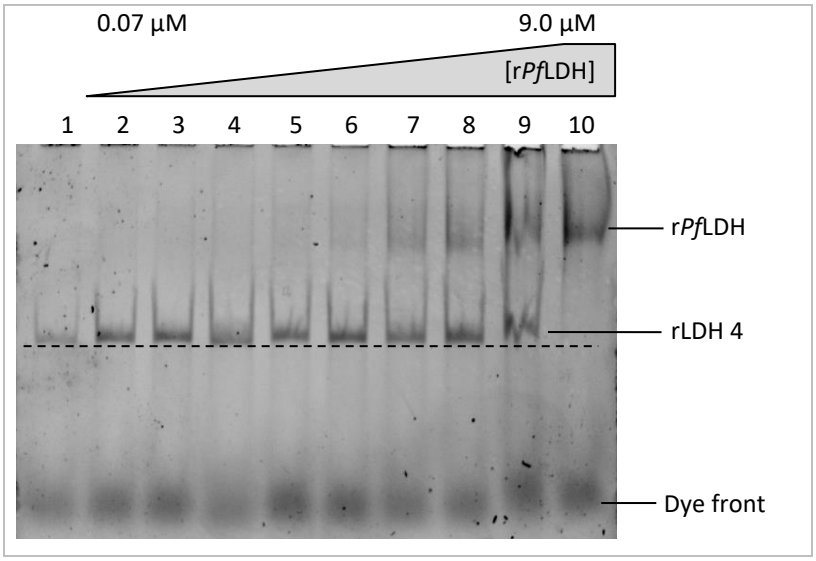

Figure 4.10: GelRed® visualisation of EMSA showing influence of varying *rPf*LDH concentrations when exposed to 100 nM of the aptamer rLDH 4.
Electrophoretic gel matrix: 6.0% Polyacrylamide in TBE buffer.
Shaded quadrilateral shows increasing concentration of r*Pf*LDH.
Lane 1: 0.0 µM r*Pf*LDH (with 50 nM rLDH 4); Lane 2: 0.07 µM r*Pf*LDH; Lane 3: 0.14 µM r*Pf*LDH; Lane 4: 0.28 µM r*Pf*LDH; Lane 5: 0.56 µM r*Pf*LDH; Lane 6: 1.125 µM r*Pf*LDH; Lane 7: 2.25 µM r*Pf*LDH; Lane 8: 4.5 µM r*Pf*LDH; Lane 9: 9.0 µM r*Pf*LDH; and, Lane 10: 9.0 µM r*Pf*LDH (with 0 nM rLDH 4).

Recombinant *Pf*LDH could be visualised at concentrations of 2.25 µM and above following GelRed® staining (Lane 10 of **Figure 4.10**, which contained only 9.0 µM of *rPf*LDH serves as an example of this). While GelRed® was intended to specifically detect DNA, reports of ethidium bromide staining of proteins have been long reported in literature (Vincent & Scherrer, 1979) and the structural similarities between GelRed® and ethidium bromide are known (Hao *et al*., 2018). For this reason, an upper limit for protein concentration for further EMSAs was set at 1.75 µM, to ensure that the maximum concentration of protein can be used to elicit the desired shift, whilst minimising any

interference from GelRed® fluorescence. This ensured that any additional band formation was not an artefact of GelRed-r*Pf*LDH fluorescence, but rather a true indication of ssDNA band formation and, hence, mobility shift.

Figure 4.11 illustrates that a very slight shift with further migration on the PAGE (towards a downward direction) can be observed within the main rLDH 4 aptamer band in the presence of *rPf*LDH (lanes 5 and 6). The formation of additional banding in the vicinity of r*Pf*LDH at higher concentrations is attributed to GelRed® fluorescence of the protein, as discussed above.

Due to the slight shift in the rLDH 4 band, EMSA optimisation by varying aptamer concentration was investigated using rLDH 4 as a case study, with a constant r*Pf*LDH concentration of 1.75 µM. **Figure 4.11** shows GelRed® stained polyacrylamide gel (a), sequentially co-stained Coomasie-stained polyacrylamide gel (b) and an overlay of both the GelRed® stained and Coomasie stained polyacrylamide gel images of the same PAGE gel (c).

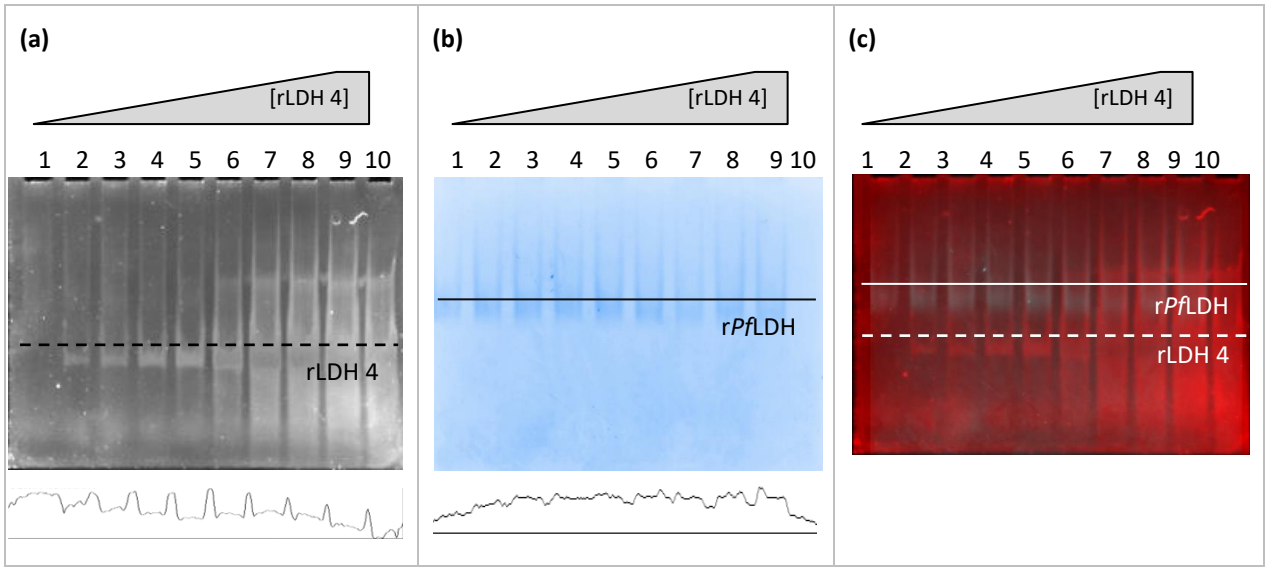

Figure 4.11: Parallel visualisation of nucleic acids (GelRed®) and proteins (Coomassie Brilliant Blue) of EMSAs showing influence of increasing rLDH 4 aptamer concentration in presence of 1.75 µM r*Pf*LDH.
Electrophoretic gel matrix: 6.0% Polyacrylamide in TBE buffer.
Shaded quadrilaterals show concentration of rLDH 4 aptamer.
(a) PAGE stained with GelRed® highlighting ssDNA; (b) PAGE stained with Coomasie highlighting recombinant protein; and, (c) overlay of GelRed® and Coomasie stained polyacrylamide gel images. Horizontal lines in (a) and (b) indicate positioning of band of interest as well as location of profiles (included below and aligned with PAGE images) for rLDH 4 (dashed lines) and r*Pf*LDH (solid lines).
Lane 1: 0 nM rLDH 4; Lane 2: 10 nM rLDH 4; Lane 3: 25 nM rLDH 4; Lane 4: 50 nM rLDH 4; Lane 5: 100 nM rLDH 4; Lane 6: 200 nM rLDH 4; Lane 7: 500 nM rLDH 4; Lane 8: 750 nM rLDH 4; Lane 9: 1000 nM rLDH 4; and, Lane 10: 1000 nM rLDH 4 (with 0 nM r*Pf*LDH)

Increasing concentrations of rLDH 4 above 200 nM created additional banding and smearing (**Figure 4.11a**) beyond the prominent band observable at lanes 2-4. The rLDH 4-r*Pf*LDH complex migrated further during PAGE as observed from lane 6 to 9 in **Figure 4.11b** at concentrations of and above 500 nM rLDH 4 when compared to the absence of r*Pf*LDH (lane 1). This observed shift in the migration of the rLDH 4-*Pf*LDH complex is shown in the zone profile in **Figure 4.11b** where the formation of a peak in lane 9 is observed – indicative of positive binding. Upon complexation of rLDH 4 to r*Pf*LDH, the molecular weight is effectively doubled, so in essence the complex should migrate a distance less than that observed for r*Pf*LDH. However, this complex migrates ahead of the protein alone, but also remains behind free aptamer. Therefore, an additional factor is at play during the migration of this complex: electrostatic charge. This observed mobility shift can also be attributed to the electrostatic influence that additional negatively charged ssDNA has on the migration of the complex (Cseke *et al*., 2011). As the rLDH 4-r*Pf*LDH complex forms, the positively charged moieties on the protein surface are nullified by the highly negative ssDNA backbone, giving the complex a higher overall negative charge, and a larger charge to surface net ratio, capable of migrating further through the polyacrylamide gel. Simultaneously, the added r*Pf*LDH will render the aptamer slightly more positive, resulting in an apparent retardation in migration. However, as seen in **Figure 4.11a**, this is not easily observed as the higher concentrations of aptamer resulted in smearing around the band of interest due to overloading. Therefore, both the charge of the rLDH 4-r*Pf*LDH complex, as well as its overall size influences migration. The overall charge-to-size ratio, therefore, directly influences any observed changes in migration as the lower the charge-to-size ratio, the slower and shorter the migration (Hellman & Fried, 2007). The complex migration patterns of both r*Pf*LDH and rLDH 4 observed in **Figure 4.11** attributed to the fact that salt concentrations and temperature continuously fluctuate within the course of an electrophoresis run, thereby affecting the local environmental conditions conducive for aptamer-target binding (Blind & Blank, 2015). However, given the influence of ssDNA conformation on its migration and the influence of aptamer concentration on conformation, there also exists the possibility that high concentrations of ssDNA migrate with a different profile to lower ones, and this could in effect be skewing the qualitative data assessment. This was minimised in the following experiments by selecting a fixed protein and aptamer concentration for further testing.

As rLDH 4 was used as an example of the expected behaviour that the r*Pf*LDH- and LDHp-specific aptamers would exhibit in the presence of r*Pf*LDH, their concentration-dependent behaviours are unconfirmed and would need to be optimised on an individual basis. However, for the purposes of standardisation across aptamers in EMSA, the same concentration profile was used for all aptamers.

GelRed-stained polyacrylamide gels were used to view the migrated ssDNA of an electrophoretic mobility shift assay, or EMSA, which was performed to assess to qualitative binding between selected aptamers and r*Pf*LDH, r*Pv*LDH and mammalian LDH, or mLDH (**Figure 4.12**). Selected aptamers included previously published aptamers, 2008s (Cheung *et al*., 2013; Tanner *et al*., 2013) and pL1 (Lee *et al*., 2012; Jeon *et al*., 2013), and the generated aptamers rLDH 1, 4, 7 and 15 and LDHp 1, 3, 11, 14 and 18. The control was aptamer alone in absence of any protein.

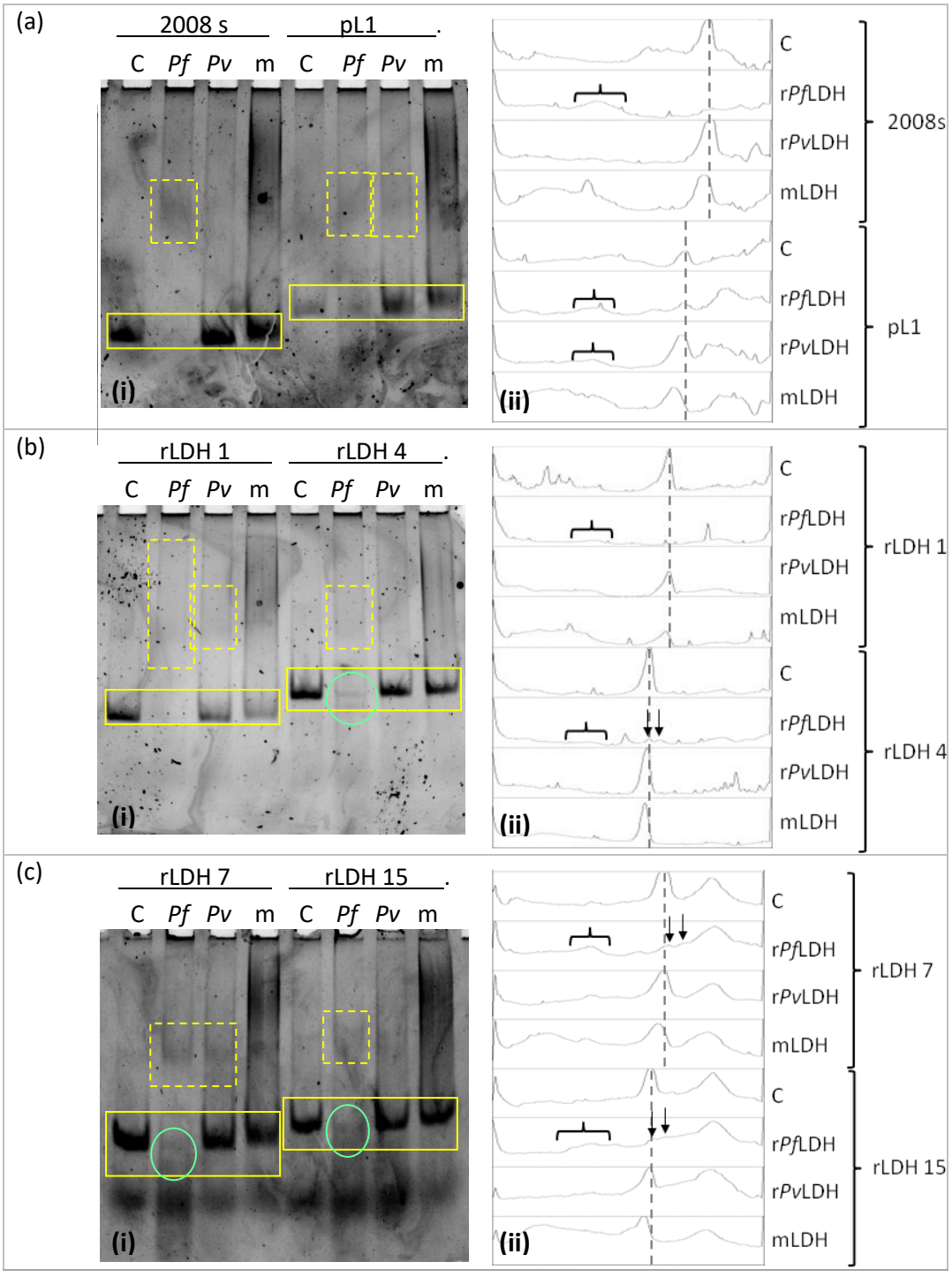

Figure 4.12 continued...

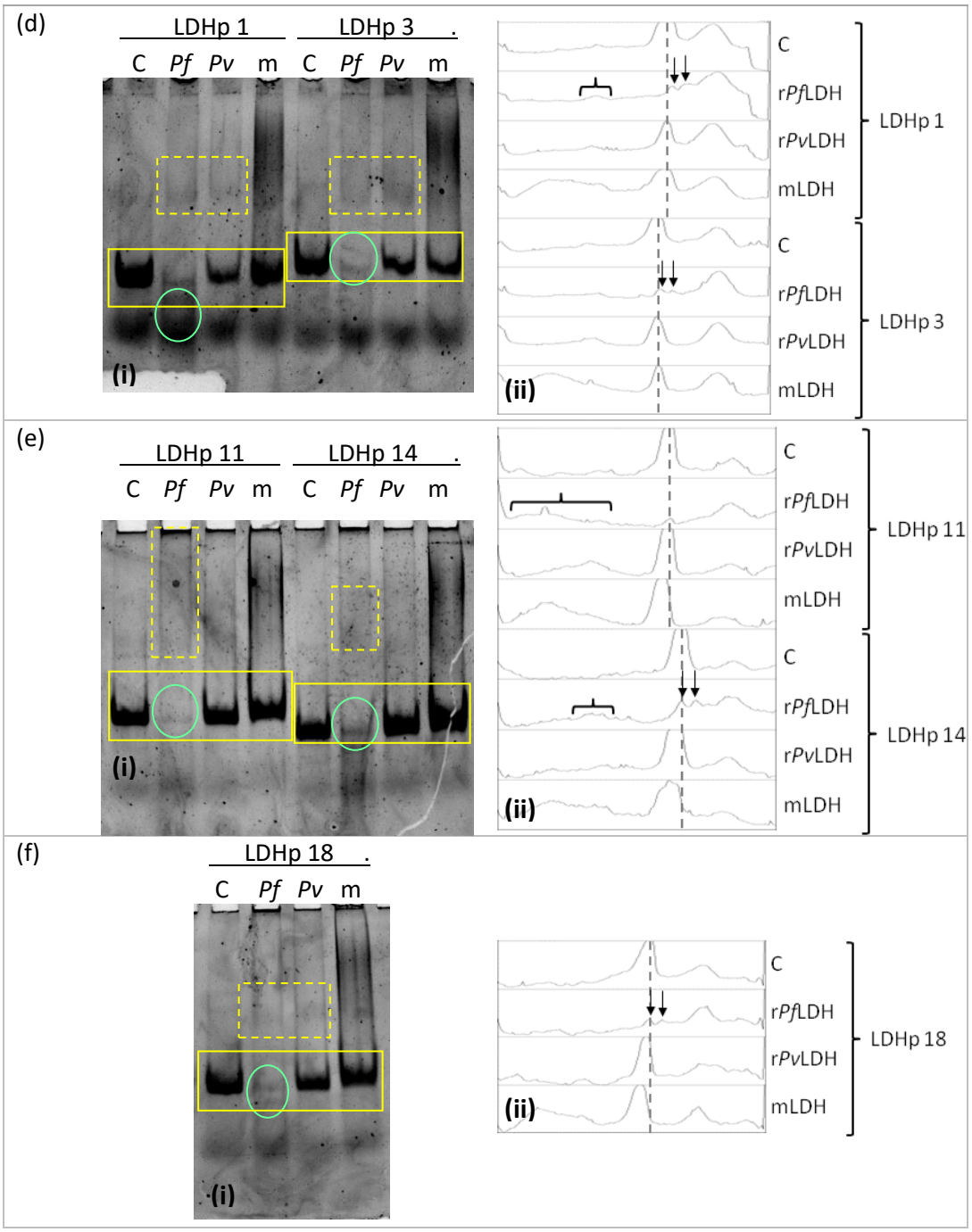

Figure 4.12: Screening of aptamers using PAGE-based EMSA using r*Pf*LDH, r*Pv*LDH and mammalian LDH, together with lanes profiles extracted from the gel images.

Aptamers: 2008 s (a), pL1 (a), rLDH 1 (b), rLDH 4 (b), rLDH 7 (c), rLDH 15 (c), LDHp 1 (d), LDHp 3 (d), LDHp 11 (e), LDHp 14 (e), and LDHp 18 (f).

i [PAGE]: Lanes 1 & 5: aptamer control (C); lanes 2 & 6: r*Pf*LDH (*Pf*); lanes: 3 & 7: r*Pv*LDH (*Pv*); and, lanes 4 & 8: mLDH (m); solid boxes highlight ssDNA aptamers; dashed boxes highlight co-localisation of protein and ssDNA aptamers; and, ovals/circles highlight double-banding of ssDNA aptamers.

ii [Lane profiles]: dashed line indicates 90 bp band ssDNA aptamer; arrows indicate double-banding of ssDNA; brackets indicate co-localisation of protein and ssDNA aptamers.

Observed in **Figure 4.12**, ssDNA aptamer sequences migrated at different rates which were consistent with their different sequence lengths and predominant tertiary structures. The various sequence lengths and predominant tertiary structures were initially reported in **Figure 3.9**. Hence, the main bands (indicated by C in **Figure 4.12**) in the absence of the proteins vary for the selected aptamers used in the EMSA analysis. The control band is hence indicated by C in **Figure 4.12**, and is indicative of the migration of the aptamer in the absence of proteins (and therefore non-interaction between an aptamer and a target).

Using the heat-activation and binding conditions described in **Chapter 2.4.5.b**, aptamer migration after incubation with r*Pf*LDH showed differing migration patterns compared to the other proteins, as seen in **Figure 4.12**. Relative to the control lanes and under these experimental conditions used, hindered band migration in the presence of r*Pf*LDH was observed for aptamer 2008s and with both r*Pf*LDH and r*Pv*LDH for pL1, evident by the absence and lowered intensity of aptamer banding for these aptamers in Lanes 2 and 6, respectively (**Figure 4.12(a)i**) (annotated as bracketed areas in **Figure 4.12(a)ii**). Given the location of the r*Pf*LDH dimer in previous studies (**Figure 2.4**), the emergence of the banding in **Figure 4.12** is indicative of co-localisation to the peptide and, hence, positive binding. This observed binding for 2008s and pL1 in the performed EMSA correlates with that of Cheung *et al.* (2013) and Lee *et al*. (2012). Nevertheless, complex band formations resulted for the remaining aptamers.

Co-localisation of all generated aptamers with r*Pf*LDH was observed, with the exception of LDHp 3 and 18 (**Figure 4.12d** and **f**). This indicated binding of aptamers LDHp 3 and 18 to r*Pf*LDH. Co-localisation, indicative of aptamer-protein binding, was observed for r*Pf*LDH and r*Pv*LDH for aptamers rLDH 1, rLDH 7, LDHp 1, LDHp 3 and LDHp 18, and indicates that there exist moieties on the surfaces of both r*Pf*- and r*Pv*LDH to which these aptamers (and pL1) have affinity. Complexation of r*Pv*LDH with LDHp 14, rLDH 4, rLDH 15 and 2008s can be disputed given the lack of defined banding.

Similarly to ethidium bromide, GelRed® has a tendency to intercalate with nucleotide-like cyclic tyrosine and tryptophan residues in proteins, emitting a response that would interfere with visible DNA under UV-Vis, rendering a false positive (Banerjee *et al*., 2014). This smearing for aptamers rLDH 1 and LDHp 11 to r*Pf*LDH can be attributed to aptamer-r*Pf*LDH complex movement through the gel based on electrostatic charge: the concomitant negative charge on the ssDNA as well as that on

the surface of r*Pf*LDH formed a more negatively charged aptamer-r*Pf*LDH complex, which was capable of migrating more rapidly, and further, through the polyacrylamide gel than r*Pf*LDH alone (Cseke *et al*., 2011).

As shown in the lane profiles in **Figure 4.12(a-f)ii**, aptamer migration in the presence of mLDH generally exhibited slower migration for most of the tested aptamers, with the exception of rLDH 1, LDHp 1 and LDHp 3, demonstrating weak and unstable binding to mLDH under the differing PAGE conditions. However, conclusive co-localisation could not be determined due to fluorescent interference from GelRed® to mLDH, previously discussed in **Chapter 4.5.2**. (The smear results from purification additives in the commercial preparation of mLDH which affected ssDNA and mLDH migration).

Interestingly, all LDHp and rLDH aptamers, with the exception of rLDH 1 (**Figure 4.12(b)**) and LDHp 11 (**Figure 4.12(e)**), developed double-banding of the ssDNA in the presence of r*Pf*LDH (encircled in **Figure 4.12(b)i** and **Figure 4.12(e)i** and indicated with arrows in **Figure 4.12(b)ii** and **Figure 4.12(e)ii**) where one band migrated further than that of aptamer alone. Also, the emergence of the double-banding of the ssDNA in the presence of r*Pf*LDH resulted in a decreased band intensity compared to r*Pv*LDH and mLDH, indicating a decreased ssDNA concentration in the localised area of band formation. The aptamers 3D conformation, which can take on many shapes and forms as previously shown in **Chapter 3.5.4**, formed following heat denaturation and incubation with its target r*Pf*LDH is convoluted and compact in structure. As this smaller structured form of aptamer molecule dissociated from r*Pf*LDH under PAGE conditions, it was propelled further through the gel based on size and charge (Blind & Blank, 2015), resulting in the in appearance of the second band. Alternatively, the observed banding patter for the aptamer could result from dissociated aptamers travelling through the gel, migrating down the electric field as PAGE continues (Pan *et al*., 2014). These reflections are typically indicative of weak binding aptamers, known to be true for LDHp 1, 3 and 14 given the more pronounce banding observed for these double bands and minimal to no co-localisation (**Figure 4.12(d)** and **(e)**). There also exists the possibility that this band doubling resulted from aptamer binding to degraded or cleaved sections of protein given that the protein stock solutions are not a homologous mixture (**Figure 2.4**). The observed double banding did not occur with aptamers in presence of r*Pv*LDH and mLDH. Two forms of positive binding were, therefore, demonstrated: retardation of ssDNA migration and co-localisation of aptamers with r*Pf*LDH

indicated stable binding; and, formation of double banding indicating dissociation of weak ssDNA aptamer binders to r*Pf*LDH.

4.5.5. Binding affinity determination of generated aptamer binding through surface plasmon resonance (SPR)

The affinity of aptamer-target interactions, directly influenced by tertiary conformation, differs in solution and surface phases during kinetic binding (Daniel *et al*., 2013). Daniel and co-workers (2013) demonstrate that the overall response and performance of the generated aptamers were affected, as evidenced by SPR-based binding analyses in which the binding capacity of free aptamer (solution phase) was compared with that of immobilised aptamer (surface phase). SPR-based binding analysis was performed on rLDH 4, LDHp 1, LDHp 11 and pL1 (Lee *et al*., 2012; Ban *et al*., 2012) to r*Pf*LDH, r*Pv*LDH and control proteins to ascertain binding affinities. A high concentration of aptamer (200 nM) was used in this instance to ensure that sufficient aptamer molecules were available to interact with visible sites present on the r*Pf*LDH target/ligand, limiting the effects of mass transport, providing a suitable environment for correct orientation, and improving solution-phase complexation. To counter the effects of mass transport experienced by aptamer analyte interaction and binding with the r*Pf*LDH target in kinetic binding analyses, such as SPR (Myszka *et al*., 1998), in which low association and dissociation flow rates were employed (discussed later in this Chapter). This concomitantly ensures that the aptamer was able to adopt the correct conformation and orientation for stable interaction and binding to the target, r*Pf*LDH.

4.5.5.a. Qualitative measures of aptamer binding to immobilised proteins

The aptamers that were selected for surface plasmon resonance (SPR) analysis were: rLDH 4, LDHp 1 and LDHp 11; and previously-published pL1 (Lee *et al*., 2012; Ban *et al*., 2012). C7 was included as a negative control.

Initially, proteins were deposited onto the sensor chip's alginate surface using established EDC/NHS covalent chemistry. SPR sensorgrams for all aptamers interacting with immobilised protein targets, r*Pf*LDH and r*Pv*LDH, demonstrated exponential association and dissociation curves, as seen between zero (0) to 90 s in **Figure 4.13**, with no apparent equilibrium reached after 90 s exposure to the aptamers. Qualitative dissociation rate constant (k_d) analyses of the dissociation curves show preliminary evidence (10^{-5} to 10^{-4} $.s^{-1}$) of high affinity interaction for aptamers tested.

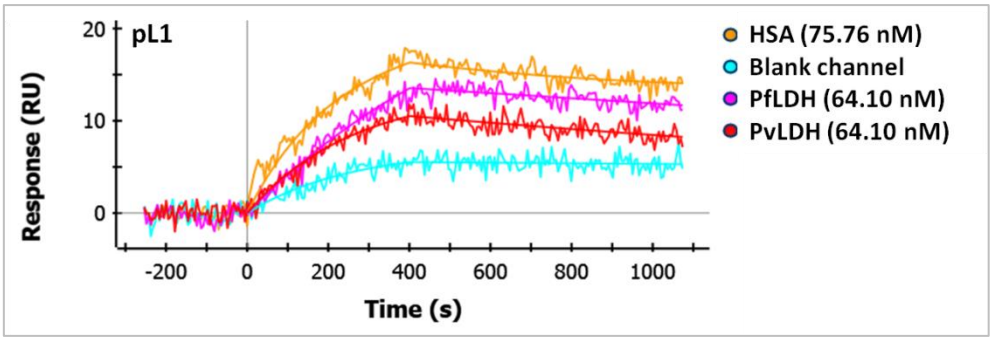

Figure 4.13: SPR sensorgrams of the control aptamer, pL1 (200 nM), binding to immobilised ligands HSA (1013.5 ± 124.1 RU), r*Pf*LDH (1671.3 ± 189.6 RU) and r*Pv*LDH (2151.5 ± 87.6 RU).

The control aptamer, pL1, was observed to bind to the alginate layer on the GLC chip surface with low affinity, exhibited by the low response seen in the SPR sensorgram (**Figure 4.13**) for the "blank channel". Interactions of all aptamers and the unactivated alginate layer were also observed on the SPR, exemplified in the sensorgrams in **Figure 4.13** and **Figure 4.14**.

The control aptamer, pL1, also exhibited binding to HSA, equivalent in this instance to any other protein-modified surface (**Figure 4.13**). This was anticipated – serum albumins have a tendency to adsorb and sequester random oligonucleotides (Malonga *et al*., 2006) – and binding of ssDNA to the HSA-modified surfaces was also exhibited with the other aptamers and the negative control sequence. This is suggested to be due to the concomitant binding effects of both the alginate layer and HSA.

SPR analysis using immobilised proteins indicated that the best performing aptamer generated for the purpose of *P. falciparum* versus *P. vivax* specificity was LDHp 11, similar to the findings outlined in the ELONA analyses (**Figure 4.4**), with SPR results shown in **Figure 4.14**.

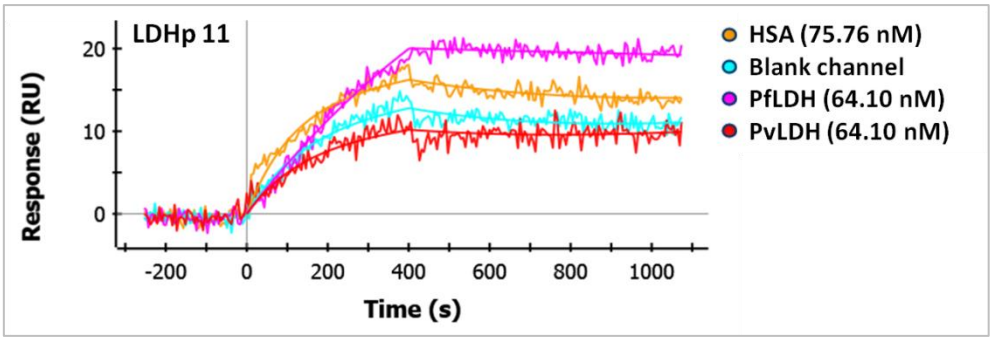

Figure 4.14: SPR sensorgrams of the control aptamer, LDHp 11 (200 nM), binding to immobilised ligands HSA (1013.5 ± 124.1 RU), r*Pf*LDH (1671.3 ± 189.6 RU) and r*Pv*LDH (2151.5 ± 87.6 RU).

LDHp 11 exhibited lowered binding to r*Pv*LDH compared to r*Pf*LDH, HSA and the alginate layer (blank channel), with a response of less than 10 RU, as shown in **Figure 4.14**. Furthermore, LDHp 11 binding to r*Pv*LDH is comparable to the alginate layer on the GLC chip surface. This indicates that binding of LDHp 11 to r*Pv*LDH is negligible and this interaction can be negated by the response exhibited by the alginate layer. However, mass transfer shifts in the baseline upon initial association (seen as an increase in RU within the initial 10 to 20 s of the association phase of aptamer to protein interaction and again in the initial 20 s of the dissociation phase, i.e. 400 s in **Figure 4.14**) were observed for the interaction of LDHp 11 to r*Pv*LDH. Furthermore, binding of LDHp 11 to HSA also exhibited a mass transfer shift in response with the characteristic shifts in baseline within the first 20 s of the association step and again around 400s in **Figure 4.14**.

The SPR sensorgrams in **Figure 4.15** show that the generated aptamers, rLDH 4 and rLDH 7, bound equivalently to both r*Pf*LDH and r*Pv*LDH. This observed binding interaction of rLDH 4 and rLDH 7 to both r*Pf*LDH and r*Pv*LDH occurred to a lesser extent during ELONA (**Figure 4.4**). The aptamer, rLDH 7, exhibited low binding to both r*Pf*LDH and r*Pv*LDH indicating a strong interaction of only a few rLDH 7 molecules present. The highest response was seen for LDHp 11 when interacting with r*Pf*LDH (**Figure 4.15**). This aptamer, LDHp 11, exhibited an observed lower binding to r*Pv*LDH than to the r*Pf*LDH.

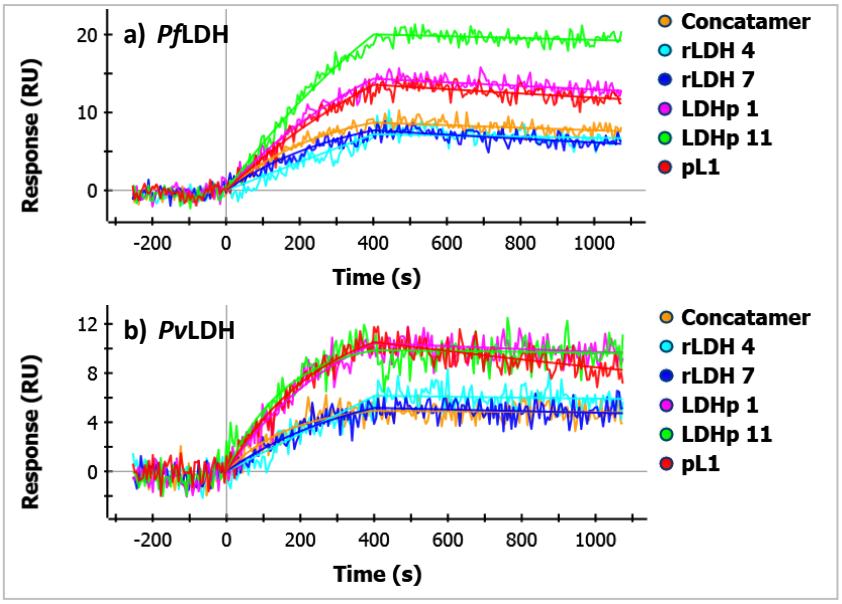

Figure 4.15: SPR sensorgrams comparing the interaction between tested aptamers (concatemer, rLDH 4, rLDH 7, LDHp 1, LDHp 11 and pL1) with either (a) 64.1 nM *Pf*LDH or (b) *Pv*LDH immobilised on the activated alginate surface of a GLC chip.

Therefore, LDHp 11, which was generated against the *P. falciparum*-specific epitopic peptide, successfully bound to r*Pf*LDH with greater binding capacity than to r*Pv*LDH (**Figure 4.15**). This reiterates that LDHp 11 is able to sensitively and specifically discriminate between the malarial species *P. falciparum* and *P. vivax* through varying affinities of binding interactions with their respective LDH enzymes. As binding was observed in these qualitative analyses, further optimisation was required with respect to the flow parameters, as well as the concentration of aptamer used for this assessment of binding.

4.5.5.b. Quantitative analysis of aptamer binding to immobilised proteins

A concentration dependent analysis was hence performed to yield quantitative data on the binding efficacies of the aptamers. Quantitative analyses of interactions between aptamers to r*Pf*LDH and r*Pv*LDH, with HSA as a control protein, were performed using a higher concentration range than that used in the qualitative analyses in the previous section. The concentrations of LDHp 1, LDHp 11, rLDH 4 and pL1 used in these analyses were: 0, 1.0, 2.5, 5.0, 10.0 and 20.0 µM. SPR sensorgrams (presented in **Figure 4.16**) illustrate the associations and dissociations of concentrations of LDHp 1 (a and b) and LDHp 11 (c and d).

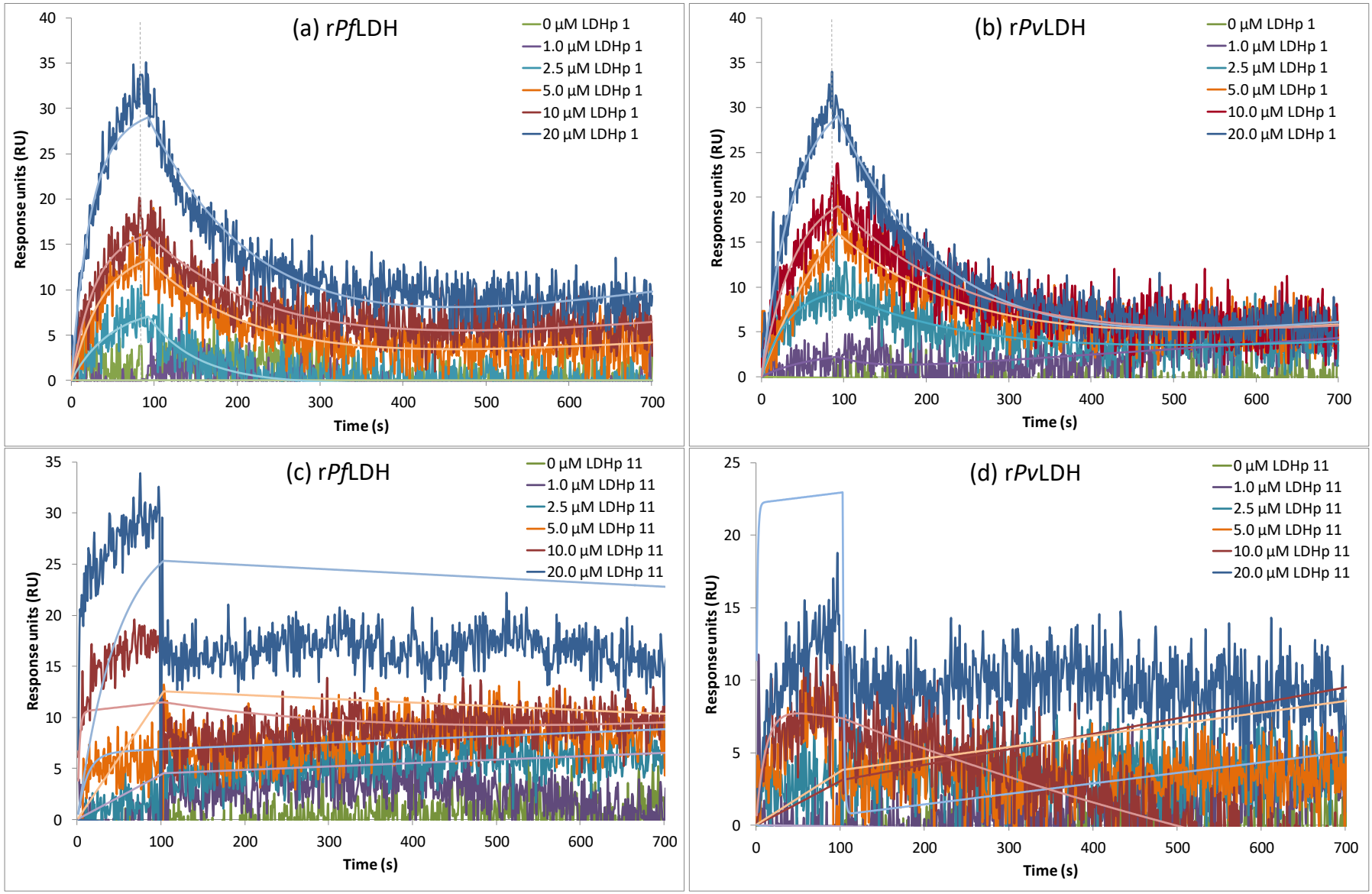

Figure 4.16: SPR sensorgrams of interaction between various concentrations of LDHp 1 and LDHp 11 with ~1200 RU r*Pf*LDH and r*Pv*LDH immobilised on the activated alginate surface of a GLC chip. Included: Local fitted analyses in smooth lines overlaid on curves. Aptamer concentrations: o, 1.0, 2.5, 5.0, 10.0 and 20.0 µM.

Of the four aptamers analysed, only LDHp 1 (**Figure 4.16** a and b) exhibited concentration-dependent binding interactions to r*Pf*LDH and r*Pv*LDH seen in the modellable SPR sensorgrams. LDHp 11, however, did not exhibit such characteristic SPR curves due to mass transfer baseline shifts. Therefore, k_a, k_d, K_D, R_{max}, and Chi^2 could only be calculated from SPR sensorgrams for LDHp 1, depicted in **Figure 4.16**, and are displayed in **Table 4.2**.

Table 4.2: Summary of SPR-based binding interactions between LDHp 1, LDHp 11, rLDH 4 and pL1 to the alginate matrix (blank), human serum albumin (HSA), r*Pv*LDH and r*Pf*LDH.
Statistics: Unpaired *t*-test: *p*-values of pairwise comparisons between r*Pf*LDH and r*Pv*LDH for LDHp 1 for each of the SPR kinetic parameters are also included; $p \leq 0.05$ signified by shaded cell

		Kinetic parameters				
		k_a (/M/s)	**k_d (/s)**	**K_D (M)**	**R_{max} (RU)**	**Chi^2 (RU)**
Blank	LDHp 1	NR				
	LDHp 11					
	rLDH 4					
	pL1					
HSA	LDHp 1	NR				
	LDHp 11	CNM				
	rLDH 4	NR				
	pL1					
r*Pv*LDH	LDHp 1	738.83 ± 377.86	$7.40 \pm 0.62 \times 10^{-3}$	$1.24 \pm 0.58 \times 10^{-5}$	78.84 ± 57.65	3.55 ± 0.98
	LDHp 11	CNM				
	rLDH 4	NR				
	pL1					
r*Pf*LDH	LDHp 1	904.33 ± 547.35	$8.73 \pm 1.06 \times 10^{-3}$	$1.30 \pm 0.73 \times 10^{-5}$	67.56 ± 38.33	5.11 ± 1.73
	LDHp 11	CNM				
	rLDH 4	NR				
	pL1					
	p-value	0.5558	0.0249	0.858	0.6983	0.836

The dissociation, or k_d, for LDHp 1 binding between r*Pf*LDH and r*Pv*LDH in **Table 4.2** showed statistical differences. However, none of the other parameters, specifically k_a, K_D, R_{max}, and Chi^2 showed any statistical differences between LDHp 1 binding to the two LDH species. This absence of statistical differentiation between the two proteins could be due to the observed mass-limiting capacity illustrated in the curves for LDHp 1 binding to r*Pf*LDH and r*Pv*LDH presented in **Figure 4.16** a and b (Svitel *et al*., 2007). Furthermore, the lack of statistical significance for LDHp 1 could be attributed to the fact that the concentration range used was relatively narrow, so affecting the

significance of the analysed output. A wider concentration would, therefore, be required to obtain statistically significant data.

While aptamer LDHp 11 (**Figure 4.16** c and d) exhibited associations to r*Pf*LDH and r*Pv*LDH, seen by increases in response units (RU) between 0 s and 90 s, the lack of a dissociation curve from 90 s similar to that observed for LDHp 11 (**Figure 4.16** a and b) demonstrated that this interaction of LDHp 11 and plasmodial LDH was mass-limiting (Schuck & Zhao, 2010). The inability of modelling of these SPR curves is further shown by the modelled curves (shown by smooth lines in **Figure 4.16** c) not fitting accurately over the generated SPR data. Therefore, SPR-based kinetics could not be modelled, and are thus indicated in **Table 4.2** with CNM (could not model). Furthermore, the fluctuation observed in the curve for 20 µM of LDHp 11 between 90 and 700 s in **Figure 4.16** c shows that there was weak or minimal binding interaction with the immobilised r*Pf*LDH. Furthermore, this fluctuation demonstrates that aptamer LDHp 11 was weakly, and repetitively, binding to immobilised r*Pf*LDH molecules elsewhere on the SPR chip spot surface as running buffer (HMCKN buffer, pH 7.4) was flowing over the immobilised protein in the dissociation phase of analyte interaction. This essentially resulted in LDHp 11 tumbling over the protein surface and weakly interacting with exposed proteinaceous binding sites. The occurrence of this tumbling effect could further indicate that the flow rate of 5 µl/min remained too high (Svitel *et al*., 2007). This inability of LDHp 11 to bind to immobilised r*Pf*LDH and r*Pv*LDH demonstrates that affinity interactions could not occur sufficiently to produce a measurable response from which affinity data could be modelled. This lack of a measurable high affinity interaction between LDHp 11 and r*Pf*LDH and r*Pv*LDH in the association phase could be attributed to:

(1) The flow-through system used in SPR directly prohibiting interaction of LDHp 11 to the protein in a time-dependent manner within the association phase by creating an additional physical momentum preventing binding interactions with the protein, despite utilisation of the slowest flow rate afforded by the Proteon XPR36 and associated software (Svitel *et al*., 2007; Schuck & Zhao, 2010).

(2) The length of the 90-bp LDHp 11 unwinding in the flow-through system as LDHp 11 sinuously flows over the active sites on the protein layer (McKeague *et al*., 2015b; Neves *et al*., 2015). While Nieuwlandt (2000) argue that longer the aptamers lead to a high-affinity target binders, this does not appear true of the SPR-based analysis of generated aptamers produced in this work.

The flow system may, however, support the prevention of non-specific binding of the aptamer to the target r*Pf*LDH and r*Pv*LDH, thereby promoting the specific, selective and sensitive binding (Whelan *et al*., 2002).

LDHp 1 remained the only aptamer of those aptamers analysed in the quantitative SPR analyses for which measurable kinetic data could be determined, while the remaining aptamers did not exhibit similar binding trends by means of SPR analysis. The flow-through system could be the predominating cause for the lack of observed binding in SPR for aptamers LDHp 11 and rLDH 4, previously shown to bind to r*Pf*LDH, in particular, through ELONA. These aptamers therefore did not exhibit similar trends to those previously reported in ELONA (**Table 4.1**). This disparity in reported and observed data is demonstrated in **Figure 4.16** when comparing the SPR sensorgram curves of LDHp 1, previously shown to be a poor binder with low affinity, versus LDHp 11, previously shown to be a strong binder with high affinity. This disparity, therefore, demonstrates that target-binding aptamers generated within these SELEX processes, described in **Chapter 2**, are more attuned to binding to r*Pf*LDH within a static system, such as ELONA, than to a flow-through system, such as SPR. Therefore, of the techniques, tools and approaches available to evaluate aptamer-target binding, not all techniques used to measure aptamer-target interactions can effectively be used to similarly measure affinity kinetics. From this SPR data, it appears that not all aptamers generated against a particular target in a single SELEX process demonstrate binding in the same manner: there exist few aptamers from the SELEX pool that may exhibit binding under certain conditions, whereas other aptamers from that same pool do not exhibit binding interactions under the same conditions. The following chapter will explore aptamer-r*Pf*LDH binding in a static system, conducive to aptamer-r*Pf*LDH binding, towards the fabrication of an aptasensor.

Furthermore, biomolecule orientation and steric hindrance during binding analyses is also of the utmost importance and goes hand-in-hand with binding kinetics. Freedom to adopt the correct orientation facilitating binding is given by the solution, which emphasises the advantage of having the aptamer free in solution for binding events, as in the case of EMSA and SPR in which the aptamer is the analyte. Steric hindrance is limited at low concentrations facilitating movement of the aptamer and interactions between the aptamer molecules and their targets. Binding of the aptamer molecules to the target is also affected by orientation of the target molecule as a visible binding site on the target is needed to sequester aptamers from solution, limiting observed responses and

affinities. Therefore, dissociation constants, a measure of binding affinity, can vary based on ligand orientation (Daniel *et al*., 2013).

4.6. Conclusion

In these screening analyses, binding properties of aptamers rLDH 1, 4, 7 and 15 and LDHp 1, 3, 11, 14 and 18 to r*Pf*LDH were investigated using ELONA, FLONA, GelRed displacements assays, EMSA and SPR. ('Screening' ELONA studies to examine binding of the aptamers to the targets and control molecules were performed as well as kinetic binding studies using ELONA). Screening ELONA studies (**Figure 4.4**) demonstrated that the four rLDH aptamers selected showed binding to r*Pf*LDH. ELONA-based colorimetric responses for rLDH 4 and 15 to recombinant *Pf*LDH were statistically significantly above that of rLDH 1 and 7 for the same protein (**Figure 4.4b**). The ELONA colorimetric responses for rLDH 4 and 15 exhibited signal above that of mammalian LDH, HSA and r*Pv*LDH. While four out of the five LDHp aptamers detected the peptide, only LDHp 11 was able to bind to r*Pf*LDH (**Figure 4.4c**) with significant K_D values (**Table 4.1**). None of the five LDHp aptamers demonstrated binding to r*Pv*LDH with modelled K_D values (**Table 4.1**). Furthermore, LDHp 11 showed detection responses to HSA, mLDH and r*Pv*LDH equivalent to that of the aptamer without protein control; no apparent affinity constant could be modelled for LDHp 11 to r*Pv*LDH binding in ELONA and SPR, supporting the specificity of the aptamer and the selectivity to LDHp and r*Pf*LDH. This data complements the reported findings of Hurdayal and co-workers (2010) on antibodies raised against the same peptide. This species-specificity and selectivity of LDHp 11, in particular, is promising for the development of a malaria biosensor detecting *P. falciparum*.

The calculated K_D value of pL1 to r*Pv*LDH using ELONA is higher than those stated by Lee and co-workers (2012) using fluorescence and those produced by Cheung and co-workers (2013). While recent studies by Cheung and co-workers (2017) determined K_D values for pL1 using ELONA (as presented herein), differences in experimental conditions such as buffer formulation and pH of the aptamer-protein binding buffer influence the binding kinetics. Both prior studies examining pL1 binding kinetics show a higher affinity of pL1 to r*Pv*LDH, similar to these findings presented herein (**Table 4.1**).

The ability of LDHp 11 to differentiate between r*Pf*LDH over LDH from other *Plasmodium* spp. is supported by K_D values of 321.24 ± 82.46 nM for LDHp 11 to r*Pf*LDH. Therefore, a key finding of this

work shows that an aptamer generated against a species-specific epitope of *Plasmodium falciparum* (LDHp 11) demonstrates greater specific binding to the recombinant *Plasmodium* LDH than aptamers generated against the whole recombinant protein; and, thus, LDHp 11 shows great promise in the ability to speciate between *Plasmodium* LDH, showing a clear preference for *Pf*LDH. The application of this particular aptamer as the biorecognition element in biosensors and other diagnostic devices is very promising. Our studies concur with Lee and co-workers (Ban *et al*., 2012; Lee *et al*., 2012) and Tanner and co-workers (Cheung *et al*., 2013; Tanner *et al*., 2013), but extend their findings with the addition of aptamers that differentiate between *P. falciparum* and *P. vivax* LDH and species of malaria employing a species-specific epitope. This is the first aptamer set where the aptamers were selected against a conserved peptide epitope on *P. falciparum* lactate dehydrogenase and the aptamers have specificity to the larger recombinant LDH protein. Of specific import to future studies is that aptamers generated against the species-specific epitope of r*Pf*LDH (peptide aptamers) detected only r*Pf*LDH and not r*Pv*LDH.

Fluorophore-linked oligonucleotide assays, or FLONA, demonstrated that fluorophore-tagged aptamers exhibited insignificant changes in response of the blank control and the control aptamer, C7, to r*Pf*LDH. Therefore, a definitive conclusion could not be drawn on fluorophore-tagged aptamer binding to r*Pf*LDH.

GelRed® was shown to fluoresce in the presence of larger proteins, namely r*Pf*LDH, due to intercalation of GelRed® molecules with the aromatic residues on the protein surface. GelRed® assays resulted in an increase in fluorescence upon addition of LDHp to the aptamer-GelRed® solution as the GelRed® molecules were trapped upon binding of LDHp aptamers to LDHp. Furthermore, statistically significant increases in fluorescent gain were observed with 100 nM LDHp 3 and 18 in the presence of LDHp demonstrating that binding interactions between aptamer and target were promising (**Figure 4.8**). With increasing aptamer concentrations, fluorescent gain was also observed at low aptamer concentrations as any change in fluorescence was more noticeable at these low concentrations. Although the GelRed® assays did not garner the expectant results, ie quenching effects, in relation to the confirmation of binding between LDHp and the LDHp aptamers, the data gathered on the fluorescence of GelRed® in presence of aptamer and target can lead to the utilisation of such GelRed® assays as a method to efficiently confirm binding between small molecule targets and their respective aptamers.

The EMSA analyses demonstrated that binding between larger proteins, specifically r*Pf*LDH, and aptamers can be shown using polyacrylamide gel electrophoresis. However, EMSA fails to differentiate the affinity of interaction between the various aptamers and r*Pf*LDH as it is limited to only qualitative output. Generally, and as literature has shown, positive binding is indicative of the slow migration of the oligonucleotide aptamer and larger protein target complex across PAGE. Aptamers pL1, 2008s, rLDH 1, 4, 7 and 15 and LDHp 1, 11 and 14 reflected this result with the predictive formation of smeared bands mid-way to the 90 bp band. Furthermore, positive binding was observed through the formation of a double band in the vicinity of the 90 bp band caused by formation of the more condensed 3D aptamer conformation following interaction with r*Pf*LDH as well as electrostatic interactions and charge differences of the aptamer and r*Pf*LDH complex. Although this double-banding phenomenon of aptamer-target binding in PAGE has not been reported on in literature, this observed variation from the negative control and r*Pv*LDH leads to the conclusion that confirmed binding between aptamers rLDH 4, 7 and 15 and LDHp 1, 3, 14 and 18 and r*Pf*LDH did in fact occur. Therefore, EMSA did demonstrate positive binding between aptamers and r*Pf*LDH.

SPR analysis showed that while quantitative analyses could be determined for selected aptamers, qualitative analysis was limiting for LDHp 11, rLDH 4 and the control aptamer pL1. Kinetic data could be determined for only one aptamer, the *Pf*LDH peptide- binding LDHp 1. Therefore, LDHp 1 binding to r*Pf*LDH was assessed in the flow-through system given by SPR. These data, therefore, show that aptamers selected for a certain targets using the same library do not necessarily exhibit the same propensity for binding under specific conditions rendered by the analysis technique utilised. Furthermore, given that LDHp 11 did not exhibit binding under these SPR-based conditions, it can be ascertained that LDHp 11 binding to rPfLDH requires further optimisation in a flow-through system and LDHp 11 exhibits preferential binding to r*Pf*LDH in a static system.

The summary table presenting the effectiveness of various techniques presented in this Chapter for the determination and assessment of generated aptamer binding to r*Pf*LDH and LDHp is shown in **Table 4.3**.

Table 4.3: Summary of effectiveness of various techniques used in this Chapter in the determination of target binding.

Technique	r*Pf*LDH-targeting aptamers		LDHp-targeting aptamers		Effective for aptamer binding analyses?	Concluding remark/s
	Aptamer/s tested	Response	Aptamer/s tested	Response		
ELONA	rLDH 1, 4, 7 and 15 pL1, 2008s and C7	Binding kinetics determined for r*Pf*LDH and r*Pv*LDH	LDHp 1, 3, 11, 14 and 18 C7	Binding kinetics determined for r*Pf*LDH, r*Pv*LDH and LDHp	Yes	Ideal for high-throughput aptamer binding analysis
FLONA	rLDH 4 and 7 pL1 and C7	Insensitive and statistically insignificant responses to r*Pf*LDH	LDHp 1 and 11 C7	Insensitive and statistically insignificant responses to r*Pf*LDH	No	Insensitive responses leave this method as undesirable in kinetic determination
GelRed displacement assays	rLDH 4, pL1 and C7	rLDH 4: No change observed; C7: decrease/quenching observed; pL1: increase observed	LDHp 1, 3, 11, 14 and 18 pL1	Increased responses in presence of LDHp	Yes	LDHp presence increased fluorescence; generally not concentration sensitive; further investigation required
EMSA	rLDH 1, 4, 7 and 15 pL1 and 2008s	Qualitative binding to r*Pf*LDH shown	LDHp 1, 3, 11, 14 and 18 C7	Qualitative binding to r*Pf*LDH shown for LDHp 1, 11 and 14	Yes	Qualitative, observable responses
SPR	rLDH 4 and 7 pL1	Quantitative responses observed for r*Pf*LDH, r*Pv*LDH and HSA	LDHp 1 and 11	Quantitative responses observed for r*Pf*LDH, r*Pv*LDH and HSA; qualitative responses observed for LDHp 1 to r*Pf*LDH and r*Pv*LDH	Yes	Qualitative responses limited to LDHp 1 (conditions conducive for binding); flow-through system not ideal for measuring binding for remaining aptamers

With the binding affinity of aptamers generated in this work to recombinant *Plasmodium falciparum* lactate dehydrogenase determined, the application of LDHp 11 as the biorecognition element in biosensors and other diagnostic devices could be explored. LDHp 11 as the biorecognition element in aptasensors is extremely promising, and further *in situ* detection native *Plasmodium falciparum* lactate dehydrogenase by generated aptamers, specifically LDHp 11 and rLDH 4, is required.

CHAPTER 5

Screening of generated aptamer sequences for potential use in aptasensors and therapeutics: detection of *Plasmodium falciparum* LDH and *Plasmodium falciparum*-specific LDH peptide using EIS, fluorescent microscopy and Malstat LDH activity assays

5.1. Preface

In this chapter, the ability of the generated aptamers to facilitate detection of the biomarker of malaria infection, lactate dehydrogenase (LDH), from *Plasmodium falciparum (Pf*LDH) was evaluated. This was achieved using both the full-length recombinant *rPf*LDH in addition to the *Pf*LDH-specific peptide, LDHp. Generated aptamers, LDHp 1, 3, 11, 14 and 18 and rLDH 1, 4, 7 and 15, from previous Chapters, were tested.

Evaluation was performed in the context of their function in several common biosensing platforms. As such, tested methodologies include electrochemical impedance spectroscopy (EIS) and fluorescence. *In situ* inspection of aptamer binding to native LDH in cultured *Plasmodium falciparum* parasite bodies was visualised using immunofluorescent microscopy. Utilising the Malstat LDH activity as an indicator of the presence of plasmodial LDH (pLDH), selected generated aptamers (LDHp 1 and 11 and rLDH 4 and 7) were explored as potential therapeutic bio-agents via LDH inhibition.

5.2. Introduction

5.2.1. Aptasensing using Electrochemical Impedance Spectroscopy (EIS) for analyte detection

Electrochemical impedance spectroscopy, or EIS, is a rapid label-free technique commonly used for analyte detection in bio-sensing. The electrochemical impedance signal is produced when a sinusoidal AC potential is applied to an electrochemical cell (Randviir & Banks, 2013). The electrochemical impedance signal is measured when a sinusoidal AC potential waveform is applied to the working electrode at varying frequencies to generate a spectrum of impedimetric responses (Randviir & Banks, 2013).

Applied as a sensing technique, EIS can be used to measure changes at an electrode's surface or in the electrolyte solution near the electrode surface, using a probing solution (Cataldo *et al*., 2018). A probing solution, such as the negatively-charged ferro-/ferricyanide redox couple, is used to measure changes in frequency-dependent electron transfer rates between the electrode and the redox couple: specifically dielectric properties, charge distribution and conductivity (Cataldo *et al*., 2018). The electron transfer limiting processes are illustrated by an impedance spectrum (e.g. Nyquist plot), which corresponds to measurable data including solution-phase resistance (R_S), charge transfer resistance (R_{CT}), double-layer capacitance (C) and, for systems exhibiting diffusion-limited mass transfer of the probes to the electrode surface, the Warburg impedance element (Z_W) (Cataldo *et al*., 2018; Chang & Park, 2010). Changes in spectra of electron transfer rates due to aptamer-target interaction can then be recorded as a measure of analyte binding to the aptamer (Cataldo *et al*., 2018).

To obtain quantitative data for the various elements of EIS, the impedance spectrum is modelled using various circuit component equivalents that would best describe the transistor effect observed in the impedance spectra (Cataldo *et al*., 2018). Changes in modelled resistance or capacitance, in particular, depend on the properties of the target analyte (de-los-Santos-Álvarez *et al*., 2008): a decrease in charge transfer resistance (R_{CT}) may be caused by a positively-charged analyte masking a negatively-charged aptamer, while an increase in R_{CT} may be caused by a negatively-charged protein analyte further repelling the negatively-charged ferro-/ferricyanide redox probe couple. The sensing electrodes can be modified for enhanced specificity and sensitivity for analyte detection through modification with complementary biorecognition molecules and nanoparticles (Chiu *et al*., 2009; Zhang *et al*., 2012; Meirinho *et al*., 2016).

Aptamers are often modified with functional groups to facilitate the method of immobilisation onto an electrode surface to create impedimetric aptasensors (de-los-Santos-Álvarez *et al*., 2008). For aptamer-based diagnostic sensing, aptamers are commonly immobilised onto the electrode surface through: physical adsorption, chemical adsorption, streptavidin-biotin interactions, or covalent attachment through amine-carboxyl pairing, gold-thiolated aptamer pairing (de-los-Santos-Álvarez *et al*., 2008; Chiu *et al*., 2009). Briefly, other methods of aptamer immobilisation to the electrode surface for EIS include, but are not limited to (Paniel *et al*., 2013): (1) Covalent attachment, frequently via coupling of amine-modified aptamers to carboxyl groups on the electrode surface; (2) Biomolecule conjugation, chiefly using biotin-modified aptamers immobilised via affinity reactions to

covalently-attached avidin/streptavidin at the surface of the electrode; and, (3) A nanomaterial-modified layer on the electrode surface that is used as a substrate of aptamer conjugation through covalent attachment, thiol-gold conjugation and/or self-assembly. However, the most effective method that produces the most reproducible EIS data arises from thiol-modified aptamers that have been directly, or even covalently, attached to the gold electrode surface by means of a self-assembled monolayer, particularly following a potassium hydroxide (KOH) pretreatment of the gold electrode (Fischer *et al*., 2009; Reich *et al.*, 2017).

There exist a number of design strategies for aptasensor configurations for EIS that are either "label-free" (lacking a reporter molecule) or do employ a reporter molecule (and are so "labelled") (Meirinho *et al*., 2016). Commonly employed design strategies include "apta-switches" (Trevino & Levy, 2014), "sandwich-type" aptasensors (Meirinho *et al*., 2016) and competitive binding (Han *et al*., 2010). However, strides are being made in the design and development of EIS based sensors incorporating various design strategies for improved or enhance disease detection.

EIS-based aptasensors for in the detection of *Plasmodium* spp., as an indicator of malaria infection, have been reported (Lee et al., 2012; Chakma *et al*., 2018; Singh *et al*., 2018).These predominately make use of self-assembled thiolated monolayers cast onto gold electrodes, to which the aptamers are subsequently attached. Using this method, Chakma and co-workers (2018) created a horseradish peroxidise II (HRP-II)-binding aptasensor, using their B4 aptamer. This aptasensor was reported to have a detection limit of ∼3.15 pM. Singh and co-workers (2018) developed a capacitive aptasensor for the detection of 100 fM − 100 nM of *P. falciparum* glutamate dehydrogenase, with a limit of detection of 0.77 pM in serum. More specifically to the detection of plasmodial LDH, Lee and co-workers (2012) used EIS in their fabrication of an aptasensor for detection of *Plasmodium vivax* LDH using their aptamer, pL1. Their aptasensor exhibited an *in vitro* detection limit of 108.5 fM and *in vivo* detection limit of 1 parasite/µl.

5.2.2. Applicability of aptamers in therapeutics against intra- and extracellular targets

Aptamers can fulfil specific functional roles through their binding interactions with protein targets: either competitively and non-competitively inhibit or induce a reaction in the bound target molecule when binding occurs (Lupold *et al*., 2002). Aptamers themselves exhibit antagonistic (i.e. inhibitory) behaviour in protein-protein interactions by altering and/or blocking docking sites present on

enzymes and other such functional proteins, thus altering or inhibiting the natural functioning of the enzyme (Jayasena, 1999; Han *et al*., 2010; Keefe *et al.*, 2010). Altering or inhibiting the enzymatic activity upon aptamer binding is an effective therapeutic outcome and has led to the application of aptamers in the field of therapeutics (Pendergrast *et al*., 2005).

Alternatively, through conjugation with therapeutically active agents (or even drugs), aptamers can induce therapeutic effects indirectly, so acting as drug delivery agents transporting the therapeutic directly to the site of action. The aptamer's site of action can be on the cell surface for cell targeting aptamers or within the cell for smaller biomolecule targeting aptamers (Chen *et al*., 2008a). Therapeutically active agents that have previously been coupled to aptamers for drug delivery include chemotherapeutic agents, gold/silver nanorods, dendrimers, siRNA, and photoagents directly to the cell (Davydova *et al*., 2011). Aptamers in drug delivery are generally subject to physiological conditions: (1) The hydrophilicity and solubility of aptamers in blood leads to improved bioavailability facilitating low doses and sensitive results in therapeutics; (2) aptamers are ideal as therapeutic agents as they exhibit lowered immunogenicity due to their size as they are generally three-fold smaller than antibodies; and, (3) the mammalian immune response is not programmed to recognise and react to oligonucleotides (Pendergrast *et al*., 2005).

Both DNA and RNA aptamers are, however, subject to degradation by nucleases within biological matrices, including blood, limiting applicability of aptamers in therapeutics (Lakhin *et al*., 2013). DNA aptamers are more effective at resisting nuclease degradation in biological fluids than RNA aptamers (Jayasena, 1999). To resist nuclease digestion, aptamers can be modified during aptamer synthesis; thus, increasing the longevity and stability of the aptamer (Rusconi *et al*., 2002; Narayanan *et al*., 2004; Peng & Damha, 2007; Hernandez *et al*., 2012). The ease of such modifications during oligonucleotide synthesis renders aptamers as ideal biological recognition molecules in the application of aptamers in the fields of therapeutics and diagnostics.

Most current reports on aptamers are for aptamers that specifically target extracellular or membrane-based proteins (Keefe *et al*., 2010). However, therapeutic aptamers specific for intracellular targets have been developed, known as intramers. Intramers employ unique expression systems, which can employ the host cell machinery, within the host cell ensuring accumulation at the site of action (Mi *et al.,* 2006; Ausländer *et al.,* 2011). Transport of the aptamer into the cell and delivery of the aptamer directly to the intracellular target can be through phagocytosis by utilising

the receptors on the cell surface through conjugation of the aptamer to the receptor's antigen (Davydova *et al.,* 2011). Chen and co-workers (2008) identified a cell-surface protein, called nucleolin, capable of binding and transporting DNA from the cell surface to the nucleus. Thus, nucleolin could chaperone phagocytised aptamers within the cell and to the targeted site of action. Uptake of phosphorothioate-modified aptamers into viable skin cells using electroporation has been shown (Regnier *et al*., 1998).

5.2.3. In situ aptamer-based, or oligofluorescent, detection of LDH in P. falciparum

Fluorescent microscopy uses fluorophores that are linked to functional biological molecules, such as antibodies and aptamers, to visually confirm inherent specific properties, functions and analyte binding interactions (The & Feltkamp, 1970). The cellular regions in which the analyte is concentrated in can be visualised under the light of a particular wavelength through the intensity of photon-emitting fluorophores tagged to the antibodies/aptamers (Froehlich, 1989). Fluorophore tags commonly used in fluorescent microscopy, having further application in fluorescent or optical sensors, include: fluoroscein and its derivatives (fluoroscein isothiocyanate (FITC) and fluoroscein amidate (FAM)); rhodamine and analogues thereof (such as tetramethylrhodamine (Cy3)); Texas Red; and, the Alexa Fluor® range (Panchuk-Voloshina *et al*., 1999).

To aid in identifying intracellular regions such as nuclei bodies and even mitochondria, tagged fluorophores are frequently co-stained with nucleic-acid stains in order to visualise cell nuclei (Dellinger & Gèze, 2001). DAPI and Hoechst stain are often interchangeable for this purpose, as both are dsDNA intercalators and minor groove binders with excitation and emission wavelengths around 360 nm and 460 nm, respectively (Biancardi *et al.*, 2013). They are both capable of permeating cell membranes of live and fixed, or dead, cells thereby providing cellular orientation and nuclear state (degradation and/or division of the nucleus) (Dellinger & Gèze, 2001). However, DAPI is used more widely for fluorescent probing of fixed cells (Zink *et al*., 2003). DAPI and Hoechst stains are sequence-specific probes, preferentially binding to AT-rich regions, thereby illuminating nuclear and mitochondrial DNA (Portugal & Waring, 1988; Dellinger & Gèze, 2001). This is particularly helpful when orientating and familiarising oneself with the sample, as well as identification of biomolecule location and action when probing with covalently-linked fluorophores.

An evaluation of the tandem use of two or more fluorescent dyes and tags can be performed using fluorescent microscopy to assess their co-distribution in relation to one another: co-localisation. An overlapping of these fluorescent signals within the same sub-cellular structure indicates a co-localisation; however, this does not necessarily mean that the two fluorescent molecules directly interact, but that they are simply retained in the same regions, since poor resolution may prevent this defining clarity (Dunn *et al.*, 2011). This concept of using FITC-tagged DNA aptamers co-localised with DAPI has been frequently shown in literature, with applications extending from detection in human glioblastoma multiforme cells (Tan *et al*., 2013) to virus detection (Li *et al*., 2015). Lindh and Persson (2009) demonstrated such detection of *P. falciparum* using a FITC-tagged RNA aptamer targeting erythrocyte membrane protein 1 (*Pf*EMP1). Fluorescent microscopic detection of *Pf*LDH using ssDNA aptamers remains elusive.

The *P. falciparum* LDH specific peptide was shown with peptide antibodies, to be a suitable antibody target whereby antibodies against the peptide differentiated between a *P. falciparum* and *P. vivax* LDH and by inference between the two species (Hurdayal *et al*., 2010). Immunofluorescent detection of *Plasmodium yoelli* LDH in *P. yoelli* parasite bodies using fluorescent microscopy has been shown by Hurdayal and co-workers (2010), while Krause and co-workers (2017) effectively demonstrated binding of the r*Pf*LDH-specific antibody to *P. falciparum* LDH in *P. falciparum* parasite bodies, and similarly showed detection of *P. falciparum* glyceraldehyde-3-phosphate dehydrogenase (GAPDH) using anti-r*Pf*GAPDH antibodies. Similarly, to results described by Hurdayal and co-workers (2010) and Krause and co-workers (2017), this work will also explore the application of these aptamers as *in situ* detectors of native *Pf*LDH in the *P. falciparum* parasite bodies using fluorescent labels in epifluorescent and confocal microscopy.

5.2.4. LDH activity for the detection of malaria

A standard method of detecting and measuring the viability of *Plasmodium* spp. in culture in the laboratory is by measuring LDH activity of the cultured parasites using the Malstat assay (Makler *et al*., 1993; Miller *et al*., 2001; Zofou *et al*., 2011). In the Malstat assay, APAD (3-acetylpyridine nicotinimide adenine dinucleotide) is used as a synthetic alternative to the LDH cofactor, NAD+ (nicotinimide adenine dinucleotide). APAD is selected as the LDH enzymes of *Plasmodium* spp. have a higher affinity for this synthetic cofactor compared to human LDH molecules (Gomez *et al*., 1997). A schematic of the LDH Malstat assay is shown in **Figure 5.1**.

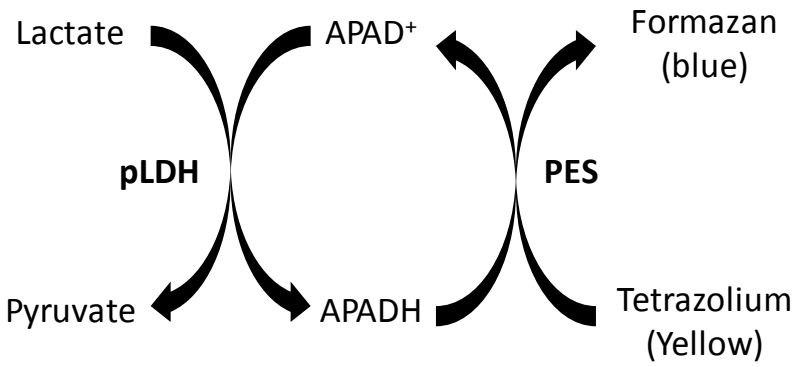

Figure 5.1: Scheme of the Malstat lactate dehydrogenase assay (adapted from Markwalter *et al*., 2015). pLDH: plasmodial lactate dehydrogenase; $APAD^+$: 3-acetylpyridine nicotinimide adenine dinucleotide; APADH: reduced 3-acetylpyridine nicotinimide adenine dinucleotide; PES: phenazine ethosulphate; tetrazolium refers to nitro blue tetrazolium, or NBT.

As plasmodial LDH (pLDH) converts lactate to pyruvate, APAD (3-acetylpyridine nicotinimide adenine dinucleotide) is reduced to APADH (**Figure 5.1**). In the presence of phenazine ethosulphate (PES), the reduction of the yellow nitro blue tetrazolium (NBT) salt by APADH results in the formation of a chromogenic blue-purple product, nitro blue formazan, which can be measured photometrically (600-650 nm) using UV-Vis (Zofou *et al*., 2011).

While the general use of the Malstat assay has been to test the viability of *Plasmodium* spp. cultures during antimalarial drug screening, many have recently utilised this quick and sensitive assay to measure pLDH as a biomarker for the diagnosis of malaria (Miller *et al*., 2001; Zofou *et al*., 2011). Markwalter and co-workers (2016) make use of the Malstat assay in the detection of *P. falciparum* by capturing *Pf*LDH using antibodies and magnetic beads. Cheung and co-workers (2015) utilise the fact that the plasmodial LDH activity remains unchanged when bound to the aptamer 2008s as a means of detecting malaria colourimetrically. Using immobilised aptamer 2008s, they captured *Pf*LDH and registered this binding interaction via colour development as nitro blue diformazan was produced in the Malstat-NBT/PES assay in a technique they refer to as aptamer-tethered enzyme capture (APTEC).

5.3. Aim

The studies presented in this Chapter aimed to evaluate the effectiveness of generated aptamers, LDHp 1 and 11 and rLDH 4 and 7, to detect the biomarker, lactate dehydrogenase, from *Plasmodium falciparum* (*Pf*LDH) for application in an aptamer-based biosensor. This was evaluated using biosensing techniques common to malarial detection: Electrochemical Impedance Spectroscopy (EIS), fluorescent microscopy and the Malstat lactate dehydrogenase (LDH) activity assays.

5.4. Methodology

5.4.1. Reagents

Aptamers bearing a 5'-biotin tag, specifically LDHp 1, 3, 11, 14 and 18, rLDH 1, 4, 7 and 15, pL1, 2008s and concatemer, C7, were sourced from Integrated DNA Technologies (IDT; USA). Thiolated LDHp 11 was purchased from IDT (USA). 5'-FITC-tagged aptamers, LDHp 1, LDHp 11, rLDH 4 and rLDH 7, pL1 and concatemer, C7, were also generated by IDT (USA). Thiol-tagged (5'-HS-C_6-) aptamers, LDHp 1, LDHp 11, rLDH 4 and rLDH 7, pL1 and concatemer, C7, were also sourced from Integrated DNA Technologies (IDT; USA).

The *Pf*LDH-specific antibody was supplied by Professor Dean Goldring (UKZN, Pietermaritzburg, South Africa). The FITC-tagged donkey anti-chicken IgG secondary antibody was supplied by Biotium, Inc., USA. Fluoroshield® was supplied by ImmunoBioScience Corp. (USA). All other reagents were purchased from Sigma Aldrich (Germany).

5.4.2. Apparatus

Electrochemical impedance spectroscopy (EIS) measurements were generated using a Metrohm AutoLab PGSTAT302N (EcoChemie, The Netherlands), controlled with NOVA 1.9 software (EcoChemie, Metrohm, The Netherlands). Gold stalk working electrodes (1.6 mm diameter active electrode surface area), Ag|AgCl (sat, KCl) reference electrodes, and platinum wire auxiliary electrodes were purchased from Bioanalytical Systems Inc (United States), as were Buëhler felt pads.

Epifluorescent and brightfield microscopy performed using a Zeiss AxioVert.A1 Inverted Fluorescence Microscope (Carl Zeiss Microscopy GmbH, Jena, Germany) using the ×50 objective.

Confocal microscopy was performed using a Zeiss LSM780 laser scanning confocal microscope (Carl Zeiss Microscopy GmbH, Jena, Germany) using the ×63 objective. Fluorescent and epifluorescent micrograph analysis and overlays, where relevant, were performed with Zen Blue Microscope Imaging Software 2011 (Carl Zeiss Microscopy GmbH, Jena, Germany).

Colour generation for the Malstat LDH activity assay was measured chromogenically, using a FLUOstar® Omega microplate reader (BMG Labtech, Germany) to act as a UV-Vis spectrophotometer.

5.4.3. Electrochemical impedance spectroscopy (EIS)

5.4.3.a. Cleaning the gold stalk electrodes for electrochemical impedance

Cleaning of the gold stalk electrodes was performed similarly to the procedure reported by Fischer and co-workers (2009). Briefly, gold stalk electrodes (n = 6) were polished with alumina powder slurry on a Buëhler felt pad. Gold electrodes were then rinsed with Milli-Q water, followed by a 3-min ultra-sonication in Milli-Q water. Gold electrodes were thereafter exposed to a solution of 1 : 4 mixture of 25% $^{v}/_{v}$ hydrogen peroxide (H_2O_2) : 50 mM potassium hydroxide (KOH) for 10 min. Subsequently, each electrode was pretreated using a single cathodic sweep from -0.2 V to -1.2 V at a rate of 0.05 V/s in 50 mM KOH. Cleaned electrodes were stored in nitrogen gas (N_2)-purged absolute ethanol until use. Directly prior to use, chemically-cleaned gold electrodes were rinsed with Milli-Q water and dried under streaming N_2 gas.

5.4.3.b. Functionalisation of gold stalk electrodes with ssDNA

A schematic on the construction and proposed functioning of the aptamer-functionalised gold electrode is presented in **Figure 5.2**.

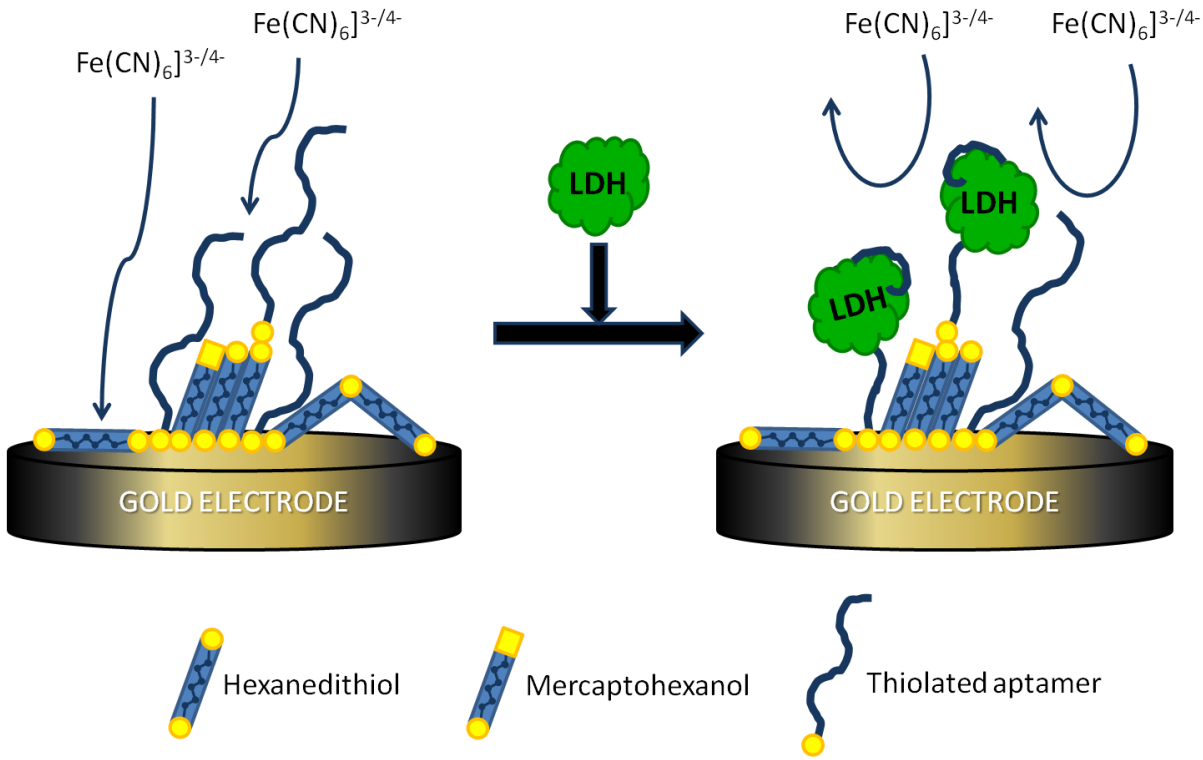

Figure 5.2: A schematic on the construction of the self-assembled aptamer-modified gold electrode for detection of *Plasmodium falciparum* lactate dehydrogenase by electrochemical impedance spectroscopy. Assembly of hexanedithiol and mercaptohexanol on the modified layer was based on Niklewski *et al.* (2004)

An aptamer immobilisation solution containing 0.3 mM hexanedithiol and 100 nM thiolated ssDNA aptamer, LDHp 11 (as a preliminary case study aptamer), in Milli-Q water was prepared in advance. Six microlitres (6 µl) of this DNA immobilisation solution was carefully placed on the N_2-dried gold of the vertically positioned gold stalk electrode (**Figure 5.2**), and placed in a humidifier chamber (capped with a microcentrifuge tube) at 4 °C for 16 hours. The ssDNA-modified gold electrodes were then rinsed with water and dried under a N_2 airstream.

Six microlitres (6 µl) of 1.0 mM mercaptohexanol (MCH) was carefully placed on the working electrode surface to ensure complete coverage of the electrode surface with thiol monolayer. The gold electrodes were then placed in a humidifier, and incubated at room temperature for 50 minutes. The functionalised ssDNA-MCH-modified gold electrodes were rinsed with water and dried under a N_2 airstream. Surface functionalisations of gold stalk electrodes for ssDNA immobilisation were freshly prepared for each new LDHp concentration measurement and its preceding blank ([LDHp] = 0 nM).

5.4.3.c. Preparing the ssDNA-modified gold electrode

Working electrodes were equilibrated for an hour at room temperature in a humidifying chamber with 30 µl of electrochemical impedance buffer: an equimolar solution of 5 mM potassium ferri/ferrocyanide ($[Fe(CN)_6]^{3-/4-}$) in 50 mM potassium phosphate buffer, pH 7.0, with 100 mM potassium sulphate. Electrochemical impedance measurements were performed directly thereafter as detailed in **Chapter 5.4.3e**.

5.4.3.d. Electrochemical impedance cell set-up

A conventional three-electrode working cell using a gold-stalk working electrode, platinum auxiliary electrode and silver/silver chloride (Ag/AgCl) reference electrode in a glass cell was employed.

5.4.3.e. Electrochemical impedance measurements

Impedimetric measurements were performed in 1.0 ml 50 mM potassium phosphate buffer enriched with 100 mM potassium sulphate, pH 7.0, containing an equimolar solution of 5 mM $[Fe(CN)_6]^{3-/4-}$ as probe solution (**Figure 5.2**). A sinusoidal potential with amplitude of 10 mV (rms), centred on the open-circuit potential (~0.29 V vs. Ag/AgCl for all datasets), was applied to the working electrode. Fifty measurements were taken, varying the oscillating frequency from 10 kHz to 0.01 Hz (in logarithmic decrements). A fresh probe solution was used with every new measurement. The concentrations of LDHp measured were: 0.1, 1.0, 10.0, 50.0 and 100.0 nM, and 3.5 µM.

5.4.4. Culturing Plasmodium falciparum parasites (3D7 strain)

Culturing of *P. falciparum* parasites was performed by the Centre for Chemico- and Biomedicinal Research (Rhodes University, Grahamstown, South Africa). The use of human red blood cells for culturing *P. falciparum* parasites was approved by the Rhodes University Ethics Committee (2011Q4-1). *Plasmodium falciparum* parasites (strain 3D7) were cultured in RPMI 1640 medium supplemented with 25 mM HEPES, 22 mM glucose, 2 mM L-glutamine, 0.65 mM hypoxanthine, 0.05 mg/ml gentamicin, 0.5% (w/v) Albumax II and 3% ($^{v}/_{v}$) haematocrit human red blood cells. Cultures were maintained at 37 ^{o}C in sealed culture flasks suffused with a 5% CO_2, 5% O_2, 90% N_2 gas mixture. When the culture contained predominantly mature stage parasites (trophozoites and schizonts) as judged by light microscopy of Giemsa-stained blood smears, further analyses shown in **Chapter 5.4.5** and **5.4.7** were performed.

5.4.5. In situ aptamer interaction with native PfLDH using epifluorescent and confocal microscopy

Predominantly mature stage parasites (trophozoites and schizonts) in red blood cells were pelleted by centrifugation (92 x *g*), washed and concentrated by resuspension in 750 µl PBS, pH 7.4. Round glass coverslips (12 mm diam.) were coated for 15 min with 1 mg/ml poly-L-lysine at room temperature. The glass coverslips were rinsed with 1 ml of 1X PBS, pH 7.4. *Plasmodium falciparum*-infected red blood cells, suspended in PBS (50 µl) were allowed to settle on the poly-L-lysine coated coverslips for 1 h. Unbound red blood cells were washed away using PBS. Bound red blood cells were lysed by exposure to 0.5 ml of 0.05 % $^{w}/_{v}$ saponin for 1 min and rinsed with PBS to remove haemoglobin and the remaining cell debris from the immobilised *P. falciparum* parasite bodies. Parasite bodies were fixed to the glass coverslips using 1 min incubation with ice-cold methanol. Unfixed parasite bodies were removed with a PBS wash. The coverslips were then blocked with 100 mg/ml HSA in PBS for 20 min.

Parasites fixed in this manner were incubated in the dark with 200 nM of heat-activated 5'-modified FITC-tagged aptamer prepared in 1x HMCKN buffer (similarly to **Chapter 4.4.4**, except heated to 65 °C) for 45 min. After incubation, coverslips were washed three times with PBS, pH 7.4. Fixed parasite bodies were incubated in 1 µg/ml DAPI in PBS for 1 min, before being briefly dipped in Milli-Q H_2O, dried, mounted with Fluoroshield® and allowed to dry in the dark overnight.

As a positive control, samples were also incubated for 45 min with IgY generated to the species-specific *P. falciparum* epitope (described by Hurdayal *et al*., 2010) followed by three washes with PBS, pH 7.4. To elicit a fluorescent response, the antibody control included 45 min incubation with the FITC-tagged (fluorscein-tagged) donkey anti-chicken IgG as secondary antibody. A negative control consisting of a prepared sample of fixed parasites, but lacking exposure to aptamers and antibodies, was prepared. For both controls, DAPI staining, mounting and drying proceeded as described above.

Microscopy samples were imaged using brightfield, epifluorescent and confocal fluorescent microscopy as described in **Chapter 5.4.2**. Micrograph images for were acquired using the same exposure and detector settings for each spectral channel, separately for epifluorescent and confocal fluorescent microscopy.

5.4.6. Aptamer inhibition on ex situ LDH activity

LDH activity was measured using the Malstat assay for *Plasmodium* LDH (Zofou *et al*., 2011). Activity of r*Pf*LDH (1 µg/ml), r*Pv*LDH (1 µg/ml) and human LDH (1 µg/ml) was measured using the Malstat assay. This was compared with the activity of these enzymes, also at a concentration of 1 µg/ml, in the presence of 1 µg/ml of *P. falciparum*-specific primary antibody (Ab) or 300 nM of aptamers. The following aptamers were tested: concatemer (C7), pL1 (Lee *et al*., 2012), 2008s (Cheung *et al*., 2013) and, from this work, LDHp 1, 3, 11, 14 and 18 and rLDH 1, 4, 7 and 15. Aptamers were heat-activated using the procedure outlined in **Chapter 2.4.5.b** and incubated with the LDH for for 1 hour under mild agitation (<50 rpm).

In quadruplicate, 25 µl of the aptamer-LDH mixture was added to 20 µl of a solution of 195.7 µM nitro blue tetrazolium (NBT) and 23.9 µM phenzine ethosulphate (PES) pipetted into the well of a 96-well microplate (Zofou *et al*., 2011). Thereafter, 100 µl of a mixture of Malstat (44.4 mM L-lactate, 33.2 µM 3-acetylpyridine nicotinimide adenine dinucleotide (APAD), 10.9 mM Tris buffer, pH 9.0, and 0.5 % $^{v}/_{v}$ Triton-X 100) was added to each of the wells.

LDH activity was measured through the formation of the purple diformazan product and measured spectrophotometrically at 600 nm. For each aptamer, data is presented as LDH activity in the presence of antibody/aptamer relative to LDH activity in absence of antibody/aptamer, and expressed as a percentage.

5.4.7. Aptamer inhibition on cultured P. falciparum parasites

The effects of the addition of aptamer on *in situ* LDH activity in cultured *P. falciparum* parasites was performed by the Centre for Chemico- and Biomedicinal Research (Rhodes University, Grahamstown, South Africa). For each screened aptamer, a single sample evaluating the therapeutic potential of the aptamer was conducted. For each aptamer, a 20 µM solution of aptamer added to parasite cultures in 96-well, clear plates and incubated for 48 hours in a 37 ^{o}C CO_2 incubator. After 48 hours, 20 µl of culture was removed from each well and combined with 125 µl of a mixture of Malstat and NBT/PES solutions in a fresh 96-well plate. Purple-blue product formation was quantified using a Spectramax M3 microplate reader (absorbance read at 620nm).

For each aptamer concentration, percent parasite viability (%) – the pLDH activity in compound-treated wells relative to untreated controls – was calculated.

5.4.8. Data measurement and analysis

Unless otherwise stated, all measurements were performed in, at minimum, triplicate. Presented results are the means of measurements, while reported error bars and uncertainties represent one standard deviation from the mean. Statistical analyses were performed using GraphPad Prism 6 (2012) and/or Statistica® 13 (2017).

5.4.8.a. Electrochemical impedance spectroscopy analyses

EIS data presented is the mean of four to six gold stalk electrodes, and reported error bars and uncertainties represent one standard deviation from the mean. Significant differences in the means of EIS responses for a single concentration of LDHp were performed using unpaired *t*-tests for data in the absence and presence of LDHp.

For multiple LDHp concentrations, the change in response of charge transfer resistance (R_{CT} in ohms, Ω) or capacitance (C in farads, F) of the specific concentration relative to the blank ([LDHp] = 0) was recorded as delta (Δ), and can be described using **Equation 5.1**:

$$Change\ in\ response\ (\Delta) = Response_{([LDHp] = x\ nM)} - Response_{([LDHp] = 0\ nM)} \qquad \textbf{Equation 5.1}$$

Statistical significance was determined using Kruskal-Wallis tests (level of significance: $p < 0.05$), followed by Dunn's HSD test was performed for multiple comparisons (level of significance: $\alpha < 0.05$). For all tests, the statistical significance level, *p*, was set at 0.05.

5.4.8.b. Fluorescent microscopy micrograph analyses

To assess mean fluorescent intensity, ImageJ 1.50i software was used for confocal fluorescent microscopy image analysis whereby areas of interest were highlighted using the same defined area for all cells to retain consistency; and, the integrated density value (IntDen) and area measured.

GraphPad Prism 5 was used to plot the mean fluorescent intensity (IntDen / Area) values for 12 parasites of interest across three micrograph frames.

For epifluorescent and confocal fluorescent microscopy, the relation (expressed as a percentage (%)) between *P. falciparum* bodies positively exhibiting FITC-based fluorescence using selected aptamers (concatemer C7, LDHp 1, LDHp 11, rLDH 4 and pL1), and the anti-r*Pf*LDHp IgY antibody, was calculated with respect to the total number of immobilised *P. falciparum* parasite bodies (indicated by DAPI fluorescence) across four micrograph frames, and can be described using **Equation 5.2**:

$$FITC{+}Pf\ bodies\ (\%) = \frac{Parasite\ bodies\ with\ FITC\ fluorescence\ (n)}{Parasite\ bodies\ with\ DAPI\ fluorescence\ (n)} \times 100 \qquad \textbf{Equation 5.2}$$

Statistical significance was determined using One-Way ANOVA (level of significance: $p < 0.05$), followed by Tukey's Honest Significant Difference (HSD) *post-hoc* test (level of significance: $\alpha < 0.05$). For all tests, the statistical significance level, *p*, was set at 0.05.

5.4.8.c. LDH activity/inhibition assay analyses

LDH activity/inhibition in the presence of the aptamer were calculated relative to LDH activity for the control absent of aptamer (or antibody), and expressed as relative fluorescent intensity (%). Statistical analyses for LDH activity/inhibition assays were performed on all data using One-Way ANOVA (level of significance: $p < 0.05$), followed by Tukey's HSD test (level of significance: $\alpha < 0.05$). For all tests, the statistical significance level, *p*, was set at 0.05.

5.5. Results and discussion

5.5.1. Electrochemical impedance spectroscopy (EIS)

Electrochemical impedance spectroscopy (EIS) was performed with the main goal of developing a point-of-care analytical method in which prompt, and reliable, testing for malaria (*P. falciparum*) can occur in the field.

This diagnostic device setup would theoretically incorporate generated aptamers that have been immobilised at the surface of a gold electrode in a self-assembled monolayer (SAM) format. To test the feasibility of EIS for the purposes of aptamer-based *Pf*LDH detection, 3.5 µM of LDHp was measured at the MCH-LDHp 11 modified gold electrode surface. LDHp was used in the direct detection as it is the primary target for LDHp 11, so ensuring that the aptamer adopts the correct tertiary conformation in the presence of its target. A positive response of LDHp-LDHp 11 interactions, which could have been seen as an increase – or even decrease – in the charge resistance (R_{CT}) and/or capacitance (C), would have signalled binding of the target polypeptides, r*Pf*LDH and the *Pf*LDH-specific peptide, LDHp, to the immobilised aptamers. Although related to the R_{CT}, use of the Warburg modulus (W) as an indication of analyte binding is rarely used for measuring analytical interactions as it is constrained as a measure of effective diffusion coefficients (Suni *et al*., 2008). Although C values can be used, the use of R_{CT} values is inherently more sensitive and lead to more affirmed results (Chang & Park, 2010). An increase in R_{CT}, given by an increase in the semi-circle on the Nyquist plot, is accepted as a positive indication that target to aptamer binding has occurred (Xu *et al*., 2006). However, and shown in **Figure 5.3**, the semi-circle observed in the Nyquist plot, from which the R_{CT} is calculated, was observed to decrease in the presence of a single concentration of target *Pf*LDH-specific peptide, LDHp (indicated as +LDHp), compared to the unassociated LDHp 11 aptamer (indicated as -LDHp).

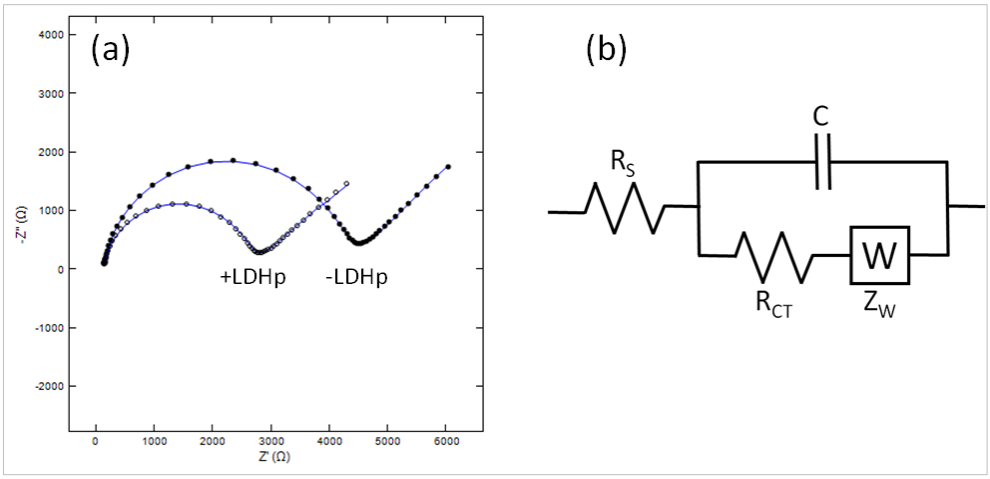

Figure 5.3: (a) Nyquist plot of LDHp 11-MCH gold stalk electrode in the presence (+LDHp) and absence of 3.5 µM LDHp (-LDHp).
(b) The electrical equivalent circuit (ie Randle's circuit) modelling the observed impedimetric response
Notes: Measured with 5 mM $[Fe(CN)_6]^{4-/3-}$ probe in 50 mM potassium phosphate buffer, pH 7.0.
Sinusoidal potential: 10 mV (rms); oscillating frequency: 10 kHz to 0.01 Hz.
C = capacitance; R_S = solution-phase resistance; R_{CT} = charge transfer resistance; Z_W = Warburg diffusion element, Z' = real part of impedance and Z'' = imaginary part of impedance response.

Figure 5.3a demonstrates a decrease in semi-circle width and associated *Z*' (Ω) upon target to aptamer binding, indicative of a decrease in the charge-transfer resistance, R_{CT}. The six replicates of Nyquist plots presented in **Figure 5.3a** for the immobilised LDHp 11 in the presence and absence of LDHp are presented in **Figure D.1**, **Appendix D**. Facilitated by self-assembly with MCH, these aptamers are immobilised in a vertical fashion at the electrode surface allowing greater flexibility and folding to its tertiary structure conformation in presence of the LDHp target (Reich *et al*., 2017). This positioning and conformational change of the aptamer in the presence of the peptide, LDHp, therefore exposes more of the electrode surface area to the negatively-charged probe, resulting in greater electron transfer at the electrode surface, resulting in the observed decrease in semi-circle width and modelled R_{CT}, similarly described by Keighley and co-workers (2008). Zayats and co-workers (2006) report a similar decrease in semi-circle width, and corresponding interfacial electrode transfer resistance, when measuring adenosine complexation with their immobilised aptamer. This observed decrease in semi-circle width could, therefore, be indicative of a change in the conformation of the 90-bp LDHp 11 aptamer.

For reference, the electrical equivalent, or Randle's circuit (**Figure 5.3b**), shows the circuit model that was used to calculate the solution and charge transfer resistances (R_S and R_{CT}, respectively, in ohms (Ω)), capacitance (C in Farads (F)) and Warburg diffusion modulus (Z_W in Mho) of LDHp 11-MCH layer in the presence and absence of LDHp.

Calculated from the Randle's circuit shown in **Figure 5.3b**, R_{CT} and C values of the MCH-LDHp 11 modified layer in presence and absence of the *Pf*LDH-specific peptide, LDHp, are reported in **Table 5.1**.

Table 5.1: Modelled equivalent circuit parameters of LDHp 11 aptasensor in absence and presence of 3.5 µM LDHp (*n* = 6).

Statistics: *t*-test: $p \leq 0.05$; significant difference indicated in bold

	- LDHp	**+ LDHp**	***p*-value of *t*-test**
R_S (Ω)	168.7 ± 20.0	161.0 ± 16.6	0.4874
R_{CT} (Ω)	3317 ± 570	2388 ± 410	**0.0088**
C (F)	$2.50 \pm 0.57 \times 10^{-7}$	$2.33 \pm 0.52 \times 10^{-7}$	0.6332
Z_W (Mho)	$4.34 \pm 0.16 \times 10^{-4}$	$5.19 \pm 0.11 \times 10^{-4}$	**< 0.0001**

A comparison of the average responses of LDHp 11 aptasensors (**Table 5.1**) demonstrates a statistically-significant decrease (p = 0.0088) in the mean modelled R_{CT} values upon interaction with 3.5 µM LDHp, from 3317 ± 570 Ω in the absence of the peptide to 2388 ± 410 Ω. As discussed previously, this decrease in the R_{CT} is attributed to the binding of LDHp 11 aptamer to LDHp peptide and associated change in aptamer conformation. The significant increase in the Warburg modulus from 4.34 ± 0.16 × 10^{-4} Mho to 5.19 ± 0.11 × 10^{-4} Mho upon interactions with LDHp can also be an indication of conformational changes occurring in the aptamer modified layer at the sensing surface.

Nguyen and co-workers (2018) show that capacitance can indeed be used to measure lung carcinoma cells (target) binding to aptamers in a microfluidic chip, and is therefore necessary to investigate. The capacitance (C) shown in **Table 5.1** demonstrates that a minor decrease in mean double-layer capacitance occurred: The change in C in the presence of LDHp peptide (2.33 ± 0.52 × 10^{-7} F) compared to responses recorded for LDHp11 alone (2.50 ± 0.57 × 10^{-7} F) was not statistically significant (p = 0.6332). Therefore, using capacitance (C) to measure target-aptamer binding for the peptide target to aptamer LDHp 11 is not recommended for aptasensor-based purposes presented in this thesis.

While statistically-significant responses in modelled impedimetric circuit element equivalents was recorded, the concentration of LDHp used in the above feasibility study was extremely high given the anticipated physiological concentrations of the *Pf*LDH. Considering that the mass of pLDH ranges from 0.013 to 0.269 pg/parasite in *P. falciparum* and 0.001 to 0.038 pg/parasite in *P. vivax*, which equates to 7.9 to 164.0 pM and 6.1 to 23.2 pM pLDH in *P. falciparum* and *P. vivax*, respectively, when parasitaemia is at 100 parasites/µl (Jang *et al*., 2019). To assess the feasibility of utilising the preliminary LDHp11 aptasensor for the detection of malaria, a separate study evaluating the sensor's response to lower LDHp concentrations in these ranges was explored.

A concentration-dependant response for R_{CT} and/or C was explored using increasing concentrations (0, 0.1, 1.0, 10.0, 50.0 and 100.0 nM) of LDHp measured at the MCH-LDHp 11 modified gold electrode (**Figure 5.4**). Data in **Figure 5.4** for a given LDHp concentration are presented as the change in responses (Δ) for a modified layer relative to the performed blank ([LDHp] = 0 nM) on the same surface. Values reported for these LDHp concentrations are that single or multiple measures using a set of four gold stalk electrodes.

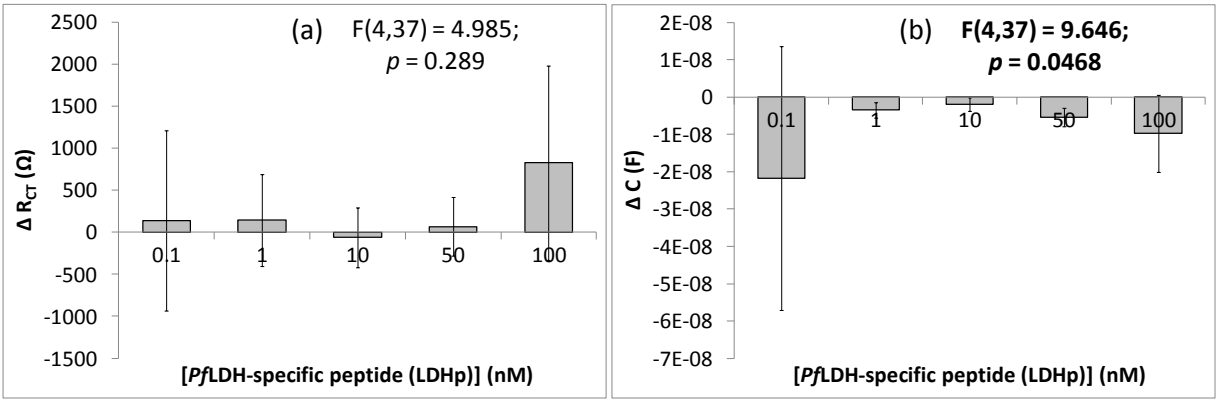

Figure 5.4: Change, presented as Δ, in (a) charge transfer resistance (R_{CT}) and (b) capacitance (C) of the MCH-LDHp 11 modified gold stalk electrodes using the *Pf*LDH-specific peptide, LDHp, as the analyte, determined from EIS.

LDHp concentrations: 0.1 nM (*n* = 6), 1.0 nM (*n* = 7), 10.0 nM (*n* = 10), 50.0 nM (*n* = 4) and 100.0 nM (*n* = 10)
Probe: 5 mM $[Fe(CN)_6]^{4-/3-}$ in 50 mM potassium phosphate buffer, pH 7.0
Statistics: Kruskal Wallis test: R_{CT}: F(4,37) = 4.985, *p* = 0.289; C: F(4,37) = 9.646, *p* = 0.0468
* Dunn's HSD test where $p \leq 0.05$

Multiple measures of four to six different electrodes were used to account for any variation in the surface topography that may be introduced through the cleaning and ssDNA-MCH layer construction (Guo *et al*., 1994; Hoogvliet *et al*., 2000). **Figure 5.4** demonstrates that there were no statistically significant increases or decreases in R_{CT} (R_{CT}: F(4,37) = 4.985, *p* = 0.289) at the various concentrations of LDHp relative to the absence of LDHp (ie the blank ([LDHp] = 0). The error presented in **Figure 5.4** showing the lack of any significant trend in response for R_{CT} across additions of 0.1 nM to 100 nM LDHp is as a result of the irreproducibility experienced across gold stalk electrodes despite efforts to maintain consistency throughout. Conversely, C did exhibit statistically significant decreases (C: F(4,37) = 9.646, *p* = 0.0468) at the various concentrations of LDHp relative to the absence of LDHp (ie the blank ([LDHp] = 0). Across the LDHp concentration range measured, C lacked concentration dependency owing to lack of a visible trend across the various concentrations tested. This inherent lack of sensitivity to LDHp concentrations displayed by both the R_{CT} and C rendered EIS as unsatisfactory in measuring the binding between LDHp and LDHp 11.

Utilising EIS, Lee and co-workers (2012) demonstrated that a positive linear correlation exists upon increasing *Pv*LDH concentration (0 pM – 1.0 nM) and R_{CT} (ohm) in their demonstration of *Plasmodium vivax* LDH detection using their aptamer, pL1.

The variability, or error, shown in **Figure 5.4** on a single concentration across six MCH-LDHp 11 modified gold stalk electrodes, is illustrated in **Figure D.1** in **Appendix D**. Additionally, **Figure 5.5** demonstrates the variability that was observed when various concentrations of LDHp were measured independently on, for example, three electrodes with the same modification.

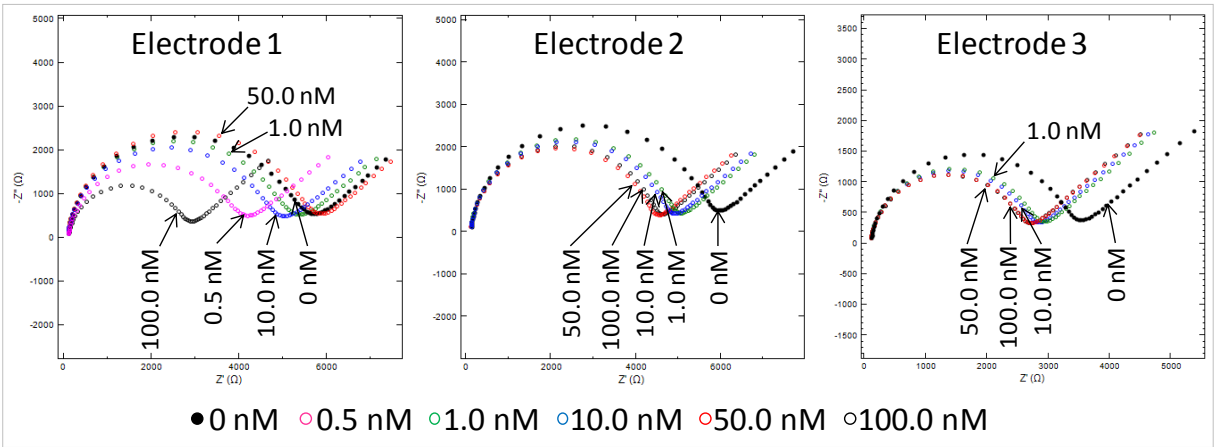

Figure 5.5: Nyquist plots of three different LDHp 11-MCH gold stalk electrodes (electrode 1, 2 and 3) with various concentrations of LDHp.
LDHp concentrations: 0, 0.5, 1.0, 10.0, 50.0 and 100.0 nM
Notes: Measured with 5 mM $[Fe(CN)_6]^{4-/3-}$ probe in 50 mM potassium phosphate buffer, pH 7.0.
Sinusoidal potential: 10 mV (rms); oscillating frequency: 10 kHz to 0.01 Hz.
Z' = real part of impedance and *Z''* = imaginary part of impedance

As illustrated in **Figure 5.4** and **5.5** and reiterated by the lack of statistically significant data ($p > 0.05$ in **Figure 5.4**), the variability in R_{CT}, given by the width of the semi-circle in the Nyquist plot and associated *Z'* (Ω) at such low concentrations of the target, LDHp, was significant (**Figure 5.5**). This lack of sensitivity at nanomolar concentrations using the hexanedithiol-aptamer-mercaptohexanol electrode surface assembly was further exemplified by the inter-electrode variability. While, there is a general tendency for impedimetric response to decrease (**Figures 5.3, 5.5** and **Table 5.1**), the current configuration of the aptasensor for LDHp 11 did not work at the relevant concentrations of LDHp peptide – akin to physiological concentrations expected for pLDH following infection with *Plasmodium* spp.

5.5.2. In situ binding of aptamers to native PfLDH through fluorescent microscopy

5.5.2.a. In situ binding of aptamers to native PfLDH through epifluorescent microscopy

Epifluorescent microscopy of FITC-tagged aptamer interactions in *P. falciparum* parasitic bodies was performed to evaluate aptamer binding to native *Pf*LDH. In addition to fluorophore-labelled aptamers, *P. falciparum* parasites were stained with nucleus-staining DAPI to demonstrate, or dispute, co-localisation of the FITC-tagged aptamers with the DAPI.

Figures 5.6 shows the accumulation of aptamers (observable green-channel fluorescence) in a number of immobilised *P. falciparum* parasitic bodies upon binding of FITC-tagged aptamers and FITC-anti-IgY-anti-*Pf*LDHp antibodies to native LDH using brightfield and epifluorescent microscopy ($\times$50 magnification).

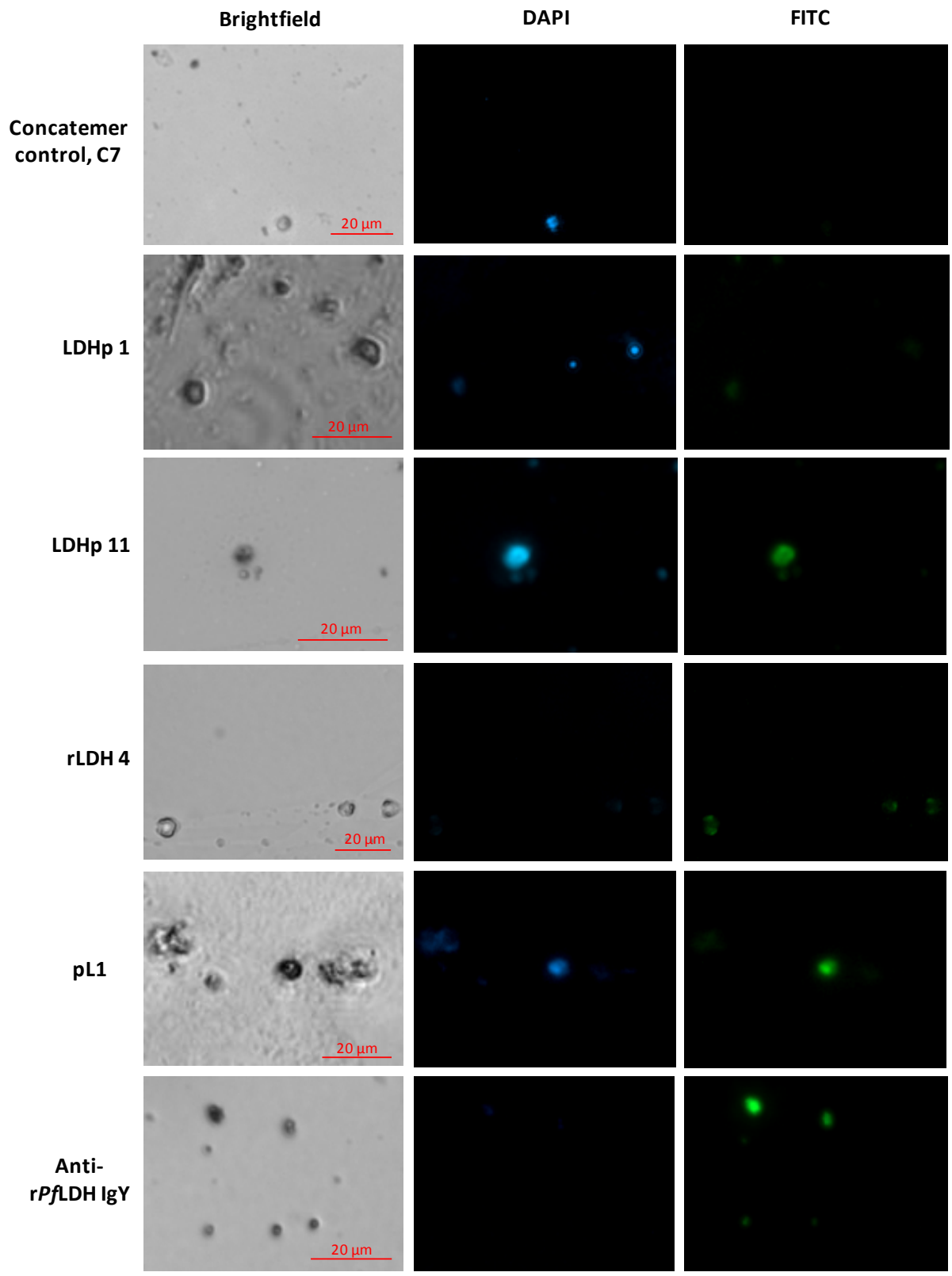

Figure 5.6: Binding of FITC-tagged aptamers and r*Pf*LDH-specific antibodies to native LDH in a number of immobilised *P. falciparum* parasite cell bodies washed with DAPI using brightfield and epifluorescent microscopy images and profiles (×50 magnification).

Left to right: Brightfield; blue channel (DAPI; excitation = 360 nm; emission = 460 nm), green channel (FITC; excitation = 490; emission = 525 nm) and merged blue- and green-channel fluorescent microscopy images. Aptamers: LDHp 1, LDHp 11, rLDH 4, pL1 and concatemer, C7.

Immobilised *P. falciparum* parasites shown in the brightfield images of **Figure 5.6** were predominantly of the trophozoite and schizont stage of the parasites' human host erythrocyte stage of their lifecycle, and were 3 to 5 µm in length.

The anti-r*Pf*LDH IgY antibody exhibited binding in the immobilised *P. falciparum* parasites, demonstrating the relevance of the antibody as a positive-binding indicator and as a positive control. The use of the anti-r*Pf*LDH antibody as a positive indicator of native LDH-binding has been shown before (Hurdayal *et al*., 2010; Krause *et al*., 2017).

Positive indications of binding over the background fluorescence were not seen for the concatemer, C7, seen by the indeterminable result for the control concatemer; therefore, it can be assumed that observed fluorescence in the *P. falciparum* bodies are not necessarily due to uptake of the aptamer into the parasite body, but indeed due to aptamer binding to native LDH. The presence of this background fluorescence has previously been observed through the non-specific uptake of fluorescing elements in the immobilised erythrocyte lipid bilayer membranes (Braun & Fromherz, 1997). The presence of the erythrocyte "ghosts" is not uncommon, particularly in fluorescent microscopy (Braun & Fromherz, 1997). Therefore, the presence of such a background "haze" is unavoidable in fluorescent microscopy, and is generally circumvented through adjusting the filters, contrast and spatial resolution to get the highest image quality (Sanderson *et al*., 2014).

LDHp 1 exhibited a low intensity of fluorescence in the immobilised parasite bodies (**Figure 5.6**), as well as a low colourimetric response in the ELONA (**Figure 4.4**), indicating a low affinity for *Pf*LDH. The aptamers, rLDH 4 and LDHp 11, were observed to bind in immobilised *P. falciparum* parasite bodies on the observed image frames, demonstrating positive target binding. These aptamer molecules were, therefore, readily taken up by a number of the *P. falciparum* bodies, and demonstrate binding to the native *Pf*LDH in the parasite bodies. The affinities for both rLDH 4 and LDHp 11 towards *Pf*LDH were also previously shown through colourimetric optical density responses shown in ELONA (**Figures 4.4** for rLDH 4 and LDHp 11). Qualitatively, it can be determined that aptamers rLDH 4 and LDHp 11 demonstrate preferable binding to native *Pf*LDH compared to the previously published aptamer, pL1 (Lee *et al*., 2012). Through this wide view in epifluorescent microscopy, aptamers rLDH 4 and LDHp 11, therefore, hold significant promise in the detection of *P. falciparum* LDH for application in aptasensors.

Figure 5.7 shows the observed cellular localisation of fluorescence in single immobilised *P. falciparum* parasitic bodies upon binding of FITC-tagged aptamers, LDHp 1, LDHp 11, rLDH 4, rLDH 7, pL1 and concatemer, C7, and FITC-anti-IgY-anti-*Pf*LDHp antibodies to native LDH of *P. falciparum*, using epifluorescent microscopy (with further digital magnification).

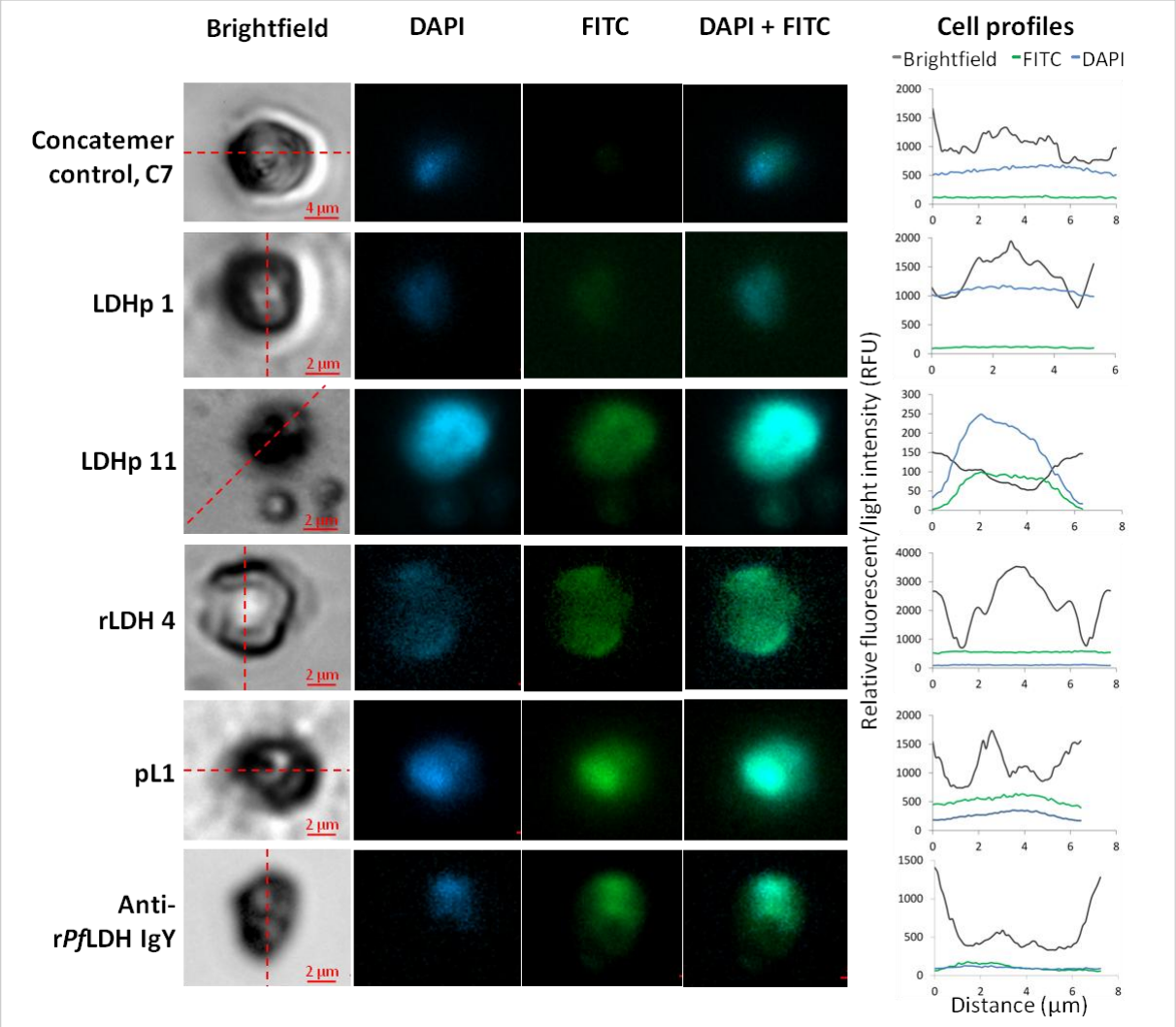

Figure 5.7: Localisation of FITC-tagged aptamers and r*Pf*LDH-specific antibodies in immobilised *P. falciparum* parasitic singular cell bodies washed with DAPI using brightfield and epifluorescent microscopy images and profiles.

Magnification: ×50 (with further digital magnification)
Left to right: Brightfield; blue channel (DAPI; excitation = 360 nm; emission = 460 nm), green channel (FITC; excitation = 490; emission = 525 nm) and merged blue- and green-channel fluorescent microscopy images.
Aptamers: LDHp 1, LDHp 11, rLDH 4, pL1 and concatemer, C7.
Red dashed lines indicate the cell profile.

Comparing the intensities of the brightfield and the blue channels in **Figure 5.7** indicates that DAPI was seen to bind strongly to the parasite's genetic material, shown by areas of greater intensity relative to the rest of the parasite body, and to a lesser extent to the outer membrane showing definition of the parasite body. Labelled oligonucleotides have been previously shown to localise within the nucleus, as demonstrated by Leonetti and co-workers (1991) with antisense oligomers. Therefore, fluorescence of tagged aptamers in the cytoplasm of the parasite body, i.e. not co-localised with DAPI fluorescence, would indicate positive binding (Hurdayal *et al*., 2010). In **Figure 5.7**, and similarly to the findings of Hurdayal and co-workers (2010), the FITC-tagged anti-r*Pf*LDH epitope IgY antibody out-competed DAPI in both fluorescent intensity and bound to native LDH with a greater observed intensity as well as in number of immobilised parasite bodies, thus displaying its suitability as a positive control.

While epifluorescent microscopy provided data with respect to overall binding, it did not however provide suitable resolution on co-localisation of the probed fluorophores within the parasite bodies (**Figure 5.7**). Thus, further investigation into localisation of aptamer binding was required to achieve affirmation of aptamer binding in native *P. falciparum* parasite bodies. Improved resolution of fluorescing parasite bodies was achieved through confocal fluorescent microscopy (**Figure 5.8** and **Figures 5.9**).

5.5.2.b. In situ binding of aptamers to native PfLDH through fluorescent confocal microscopy

Figures 5.8 shows the absence and presence of observable fluorescence in a number of immobilised *P. falciparum* parasitic bodies upon binding of FITC-tagged aptamers (LDHp 11, rLDH 4, L1 and concatemer, C7) and FITC-anti-IgY-anti-*Pf*LDHp antibodies to native LDH of *P. falciparum*, through the use of confocal microscopy.

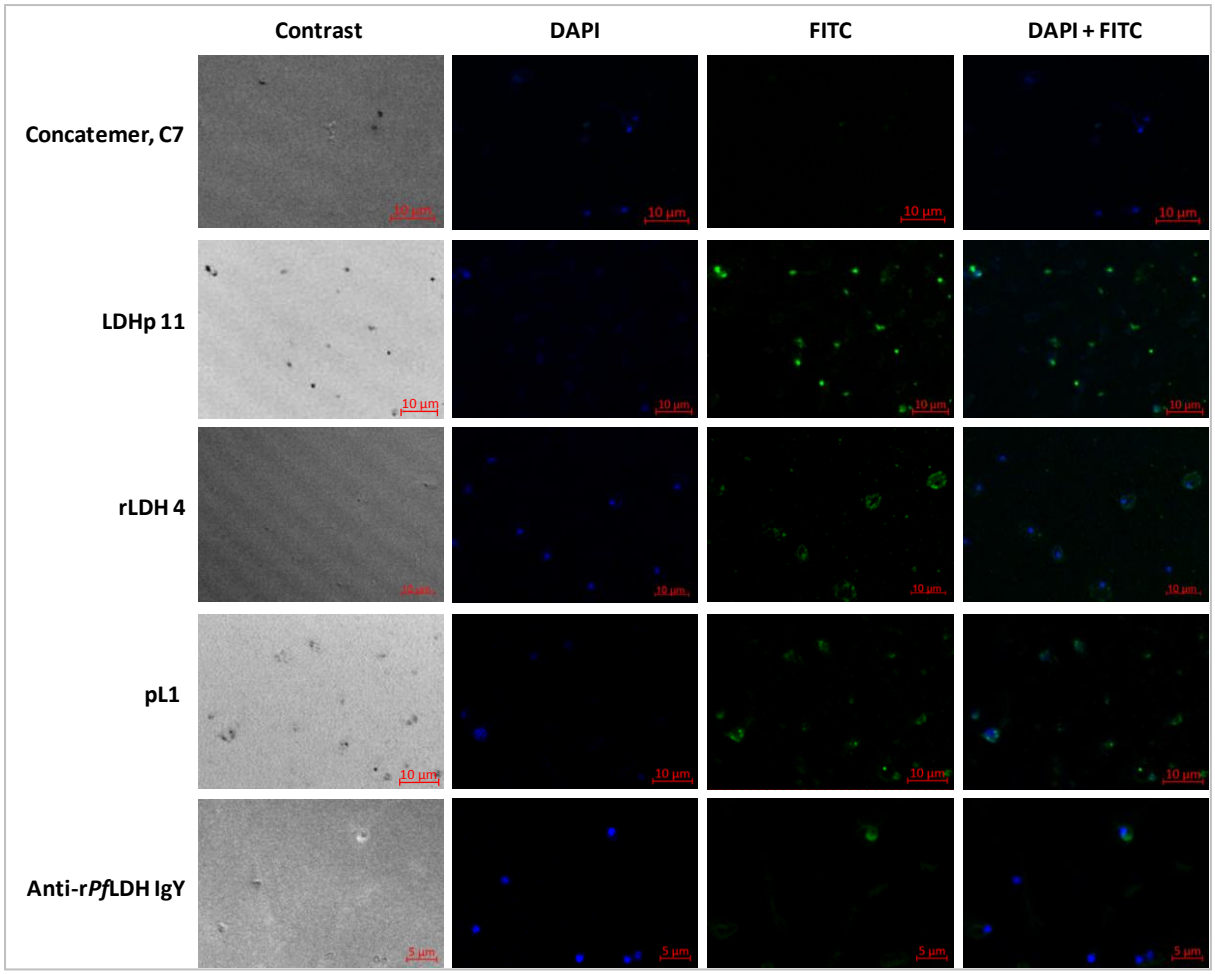

Figure 5.8: Confocal micrographs of a number of immobilised *P. falciparum* parasite cell bodies stained with DAPI and either FITC-tagged aptamers (LDHp 11, rLDH 4, pL1 and concatemer, C7), or r*Pf*LDH-specific antibodies to native LDH and FITC secondary antibodies (×63 magnification).
Left to right: Phase-contrast; blue channel (DAPI; excitation = 360 nm; emission = 460 nm), green channel (FITC; excitation = 490; emission = 525 nm) and merged blue- and green-channel fluorescent microscopy images.
[Confocal micrograph images captured by Dr Meesbah Jiwaji (Rhodes University)]

As previously shown in epifluorescent microscopy (**Figure 5.6**), immobilised *P. falciparum* parasites shown in **Figure 5.8** were predominantly of the trophozoite and schizont stage of the parasites' human host erythrocyte stage of their lifecycle, and were 3 to 5 µm in length.

Confocal fluorescent microscopy (**Figure 5.8**) exhibited, on average across the aptamers selected, a higher fluorescent intensity and improved optical resolution than epifluorescent microscopy. This optical technique has improved optical resolution and contrast, thus increased sensitivity, owing to the elimination, via a physical barrier or pin-hole, of superfluous, "out-of-focus" light during image capture (Hauch & Ratner, 2013).

Evaluation of the aptamers' binding profile using confocal microscopy indicated that the generated FITC-tagged aptamers, LDHp 1, LDHp 11, rLDH 4 and rLDH 7, appeared to bind to native LDH found in *P. falciparum* in blood cultures, similarly to the IgY antibody (**Figure 5.8**). Compared to the low fluorescence exhibited by the negative control concatemer, C7, generated FITC-tagged aptamers, LDHp 1, LDHp 11, rLDH 4 and rLDH 7 did exhibit a greater fluorescent intensity. Aptamer rLDH 4 showed positive binding to native *Pf*LDH. LDHp 1 exhibited a low fluorescent intensity compared to LDHp 11 and rLDH 4 when bound to the native *Pf*LDH, indicating lowered affinity, reiterating similar findings shown in **Figure 5.7**.

A closer inspection of the observed fluorescence in immobilised *P. falciparum* singular parasitic bodies upon binding of FITC-tagged aptamers, LDHp 1, LDHp 11, rLDH 4, rLDH 7, pL1, concatemer, C7, and FITC-anti-IgY-anti-*Pf*LDHp antibodies to native LDH of *P. falciparum* using confocal fluorescent microscopy (with further digital magnification), is shown in **Figure 5.9**.

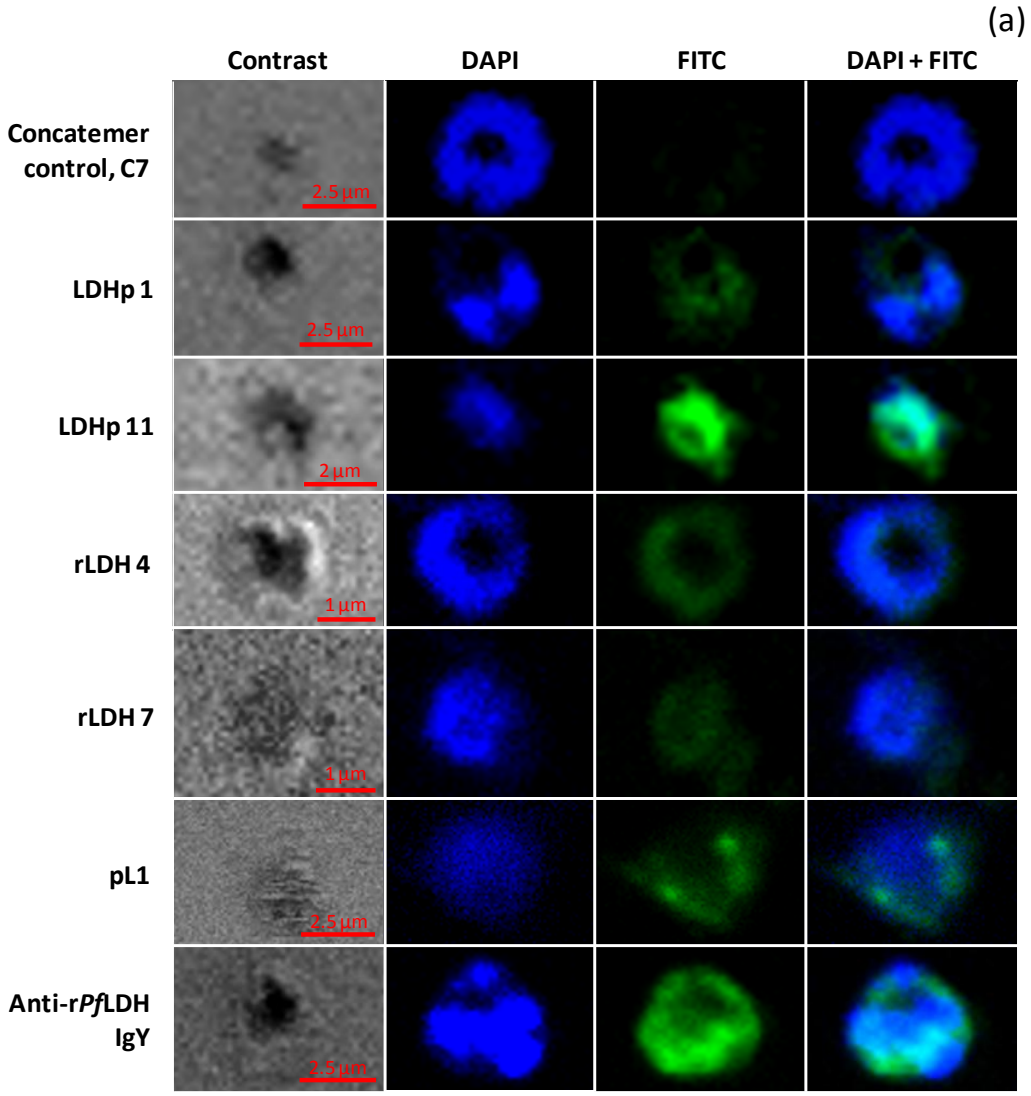

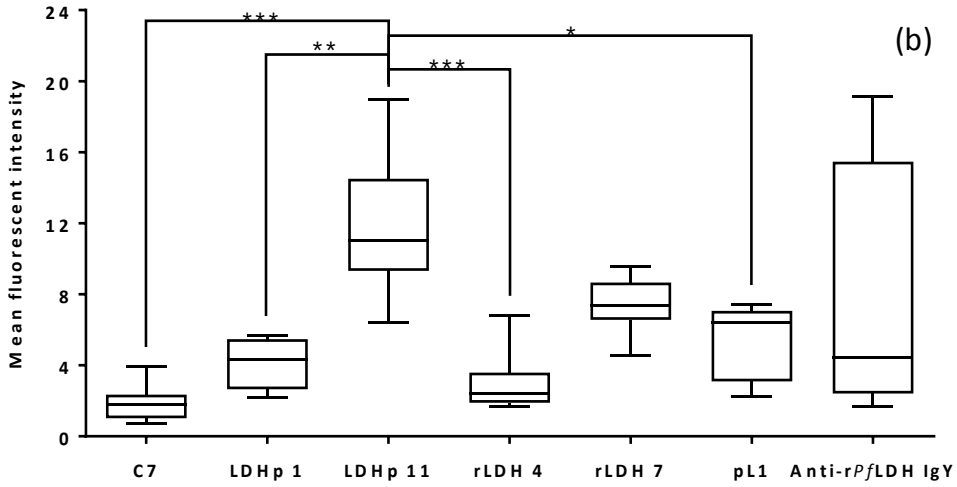

Figure 5.9: (a) Confocal micrographs of immobilised *P. falciparum* infected red blood cells stained with DAPI and either FITC-tagged aptamers or r*Pf*LDH-specific antibodies. (b) Quantification of FITC-tagged aptamers and r*Pf*LDH-specific antibody fluorescence associated with immobilized *P. falciparum* infected red blood cells ($n = 12$; $p < 0.05$).
Magnification: ×63 (with further digital magnification)
FITC tagged aptamers included LDHp 1, LDHp 11, rLDH 4, rLDH 7, pL1 and concatemer, C7. IgY antibodies against r*Pf*LDH were detected with FITC-labeled secondary antibody. Left to right: Phase-contrast; blue channel (DAPI; excitation = 360 nm; emission = 460 nm), green channel (FITC; excitation = 490; emission = 525 nm) and merged blue- and green-channel fluorescent microscopy images.
* Significant: p = 0.01-0.05 (Dunn's multiple comparison test)
** Very significant: p = 0.001-0.01 (Dunn's multiple comparison test)
*** Extremely significant: $p < 0.001$ (Dunn's multiple comparison test)

In all instances of the preliminary confocal microscopy imaging (**Figure 5.9a**), DAPI was seen to bind strongly to the parasite's nuclear material and, to a lesser extent, the outer membrane (previously seen in **Figure 5.7**). The cytosolic localisation of LDH is confirmed by the cellular fluorescence profile of anti-r*Pf*LDH IgY binding, in which the separation between the FITC-stained cytosol and nuclear material may be inferred. The distribution of LDH in the *P. falciparum* bodies visualised by the FITC-tagged aptamers in these micrographs was similar to that reported by Hurdayal and co-workers (2010) and Krause and co-workers (2017) using the anti-r*Pf*LDH IgY antibody in their study.

The control aptamer, pL1, also showed positive binding to native *Pf*LDH, including accumulation in sub-cellular parasite bodies (**Figure 5.9a**). The control oligonucleotide and concatemer, C7, showed negligible binding to the native LDH in the *P. falciparum* bodies indicating that the evidenced binding in the studied aptamers was not due to electrostatic interactions but specific binding as a result of the 3D conformation of the aptamer (depicted in **Figure 3.7**, **Chapter 3.5.4**). This can also be attributed to "ghosting" effects of non-specific FITC binding. The presence of the erythrocyte "ghosts" is not uncommon and has known to cause background interference, particularly in fluorescent microscopy (Braun & Fromherz, 1997).

Using confocal microscopy, the generated FITC-tagged aptamers, LDHp 1, LDHp 11, rLDH 4 and rLDH 7, appeared to bind to native LDH found in *P. falciparum* in blood cultures with a similar cytosolic profile to that obtained with the IgY antibody with comparable mean fluorescent intensities, compared to the low fluorescence exhibited by the negative control concatemer, C7 (**Figure 5.9b**). Aptamer LDHp 11, which demonstrated high binding affinity to the recombinant *Pf*LDH during ELONA studies (**Figures 4.4** and **4.6**, and **Table 4.1**), demonstrating partial co-localisation with DAPI in the nucleus of the parasitic bodies. Both rLDH 4 and 7 detected the native protein in fluorescent confocal microscopy (**Figure 5.9a**). However, the high absorbance value for HSA by rLDH 7 precludes this aptamer from further investigation.

5.5.2.c. Comparison of FITC-positive P. falciparum bodies in epifluorescent versus confocal fluorescent microscopy

The percent of *P. falciparum* bodies exhibiting FITC fluorescence with selected tagged aptamers (concatemer C7, LDHp 1, LDHp 11, rLDH 4 and pL1), and the anti-r*Pf*LDHp IgY antibody, was calculated with relation to the total number of immobilised *P. falciparum* parasite bodies (indicated

by DAPI fluorescence) across four micrograph frames represented in **Figure 5.6** and **5.8**. This percentage of fluorescing parasite bodies is indicative of positive binding to native *Pf*LDH found within the parasite bodies. **Table 5.2** presents the percent of positive binding for the FITC-tagged aptamers and anti-r*Pf*LDHp IgY antibody in *P. falciparum* parasite bodies, as a function of the total number of DAPI-fluorescing bodies, obtained through epifluorescent microscopy (**Figure 5.6**) and confocal microscopy (**Figure 5.8**).

Table 5.2: Percent FITC-positive *P. falciparum* bodies (%) using FITC-tagged aptamer and anti-r*Pf*LDH IgY antibodies, via confocal microscopy, compared with epifluorescent microscopy (*n* = 4).

	Percent FITC-positive *P. falciparum* bodies (%)	
FITC-tagged capture biomolecule	**Epifluorescent microscopy[a]**	**Confocal microscopy[b]**
Concatemer control, C7	12.77 ± 2.03	14.38 ± 12.66
LDHp 1	26.10 ± 9.34	76.89 ± 13.39*[$]
LDHp 11	62.79 ± 7.35*[$]	94.98 ± 3.01*[$]
rLDH 4	67.32 ± 13.28**[$]	43.87 ± 8.91*
pL1	37.82 ± 4.20	67.08 ± 6.14*[$]
Anti-r*Pf*LDHp IgY	71.26 ± 18.27**	78.21 ± 25.61*

Statistics: One-Way ANOVA ($p \leq 0.05$):
[a]Epifluorescent microscopy: $F(5,17): 19.85; p < 0.0001$
[b]Confocal microscopy: $F(5,17): 20.73; p < 0.0001$
* Denotes Tukey's HSD statistical significance of FITC-positive bodies over the C7 concatemer control
** Denotes Tukey's HSD statistical significance of FITC-positive bodies over the C7 concatemer control and pL1
[$] Denotes Tukey's HSD statistical significance of FITC-positive bodies equivalent to anti-r*Pf*LDHp IgY

The relative aptamer binding, indicated by the number of FITC-positive *P. falciparum* parasite schizonts and trophozoites, as a proportion of the total number of immobilised DAPI-fluorescing bodies for both epifluorescent and confocal fluorescent microscopy are given in **Table 5.2**.

The FITC-tagged negative control, concatemer, C7, did not exhibit fluorescence in the parasite schizonts and trophozoites that was more intense than that of the immobilised erythrocyte membranes (background), shown in **Figure 4.8** and **4.9**. C7 did, however, show presumed non-specific interactions with the one to three immobilised parasite bodies (of the ~30 parasite bodies immobilised per micrograph resulting in 12.77 ± 2.03 % for epifluorescence and 14.38 ± 12.66 % for confocal microscopy). Previous ELONA-based analyses in **Chapter 4.5.1.d**, show that C7 did exhibit a lack of response (NR = no response) towards r*Pf*LDH. Values presented in **Table 5.2** for aptamer binding was, therefore, representative of the one to three parasite bodies in which non-specific FITC

fluorescence and C7 binding occurred and, hence, can be negated. Non-specific binding of fluorescing elements in the immobilised erythrocyte lipid bilayer membranes has been shown (Braun & Fromherz, 1997). This result is greatly improved from those obtained through epifluorescent microscopy owing to the improved resolution, closer working distance and limited out-of-focus light inherent in confocal microscopy when capturing the fluorescing image (Sanderson *et al*., 2014).

Aptamer pL1 exhibited a statistically significant percentage binding of 67.08 ± 6.14 % in confocal microscopy over C7 (**Table 5.2**). This indicates that the previously published aptamer, pL1, was representative as a positive binding indicator for native *Pf*LDH binding, but was not as effective as the antibody that exhibited 78.21 ± 25.61 % binding. However, when analysing the proportion of immobilised parasite bodies exhibiting FITC fluorescence in confocal fluorescence microscopy, the FITC-tagged aptamer pL1 exhibited a statistically equivalent percentage of FITC-assessed binding to the anti-r*Pf*LDHp IgY antibody (p = 0.852) with 67.08 ± 6.14 % of parasites illuminating at the FITC wavelength. This corresponds with the report by Lee and co-workers (2012) in which they showed, through use of an assay, that fluorophore-tagged pL1 binds to r*Pf*LDH and r*Pv*LDH.

Using confocal fluorescent microscopy, FITC-tagged LDHp 1, LDHp 11, rLDH4 and pL1 were visualised in a greater proportion of immobilised *P. falciparum* parasite schizonts and trophozoites than the control, C7, indicated by the statistically significant increases in percent of FITC fluorescing bodies over C7 (**Table 5.2**). LDHp 11 exhibited statistically significant increases in the proportion of fluorescing parasite bodies over the concatemer control, C7, in both epifluorescent and confocal microscopy techniques (p < 0.0001). Unlike epifluorescent microscopy, the visualisation success rate of LDHp 11, per FITC-positive body, in fluorescent confocal microscopy (**Figure 5.8**) was higher than that of the anti-r*Pf*LDHp IgY antibody, binding of 94.98 ± 3.01 and 78.21 ± 25.61 % of the immobilised *P. falciparum* parasite bodies, respectively (**Table 5.2**). However, accumulation of FITC-tagged LDHp 11 was statistically equivalent to the anti-r*Pf*LDHp IgY antibody, indicating that LDHp 11 efficacy to accumulate and bind to immobilised parasite bodies was comparable with that expected of the anti-r*Pf*LDHp IgY antibody.

LDHp 1 exhibited a higher percentage of accumulated fluorescence in immobilised parasites in confocal microscopy compared to epifluorescent microscopy, with 76.89 ± 13.39 % of immobilised parasite schizonts and trophozoites exhibiting fluorescence in confocal microscopy compared to 26.10 ± 9.34 % in epifluorescent microscopy (**Table 5.2**). Furthermore, confocal microscopic analysis

showed that the number of immobilised parasite bodies in which accumulation of FITC-tagged LDHp 1 occurred was equivalent to the anti-r*Pf*LDHp IgY. Therefore, LDHp 1, LDHp 11 and pL1 can be used to successfully identify *P. falciparum* parasite bodies through visualisation by confocal microscopy. Moreover, LDHp 11 exhibited the highest mean fluorescent intensity (**Figure 5.9b**) of aptamers assessed using confocal fluorescent microscopy, intimating that LDHp 11 does indeed outperform LDHp 1 and pL1.

FITC-tagged rLDH 4 fluorescence using epifluorescent microscopy was observed in 67.32 ± 13.28 % of immobilised parasite bodies, which was statistically greater than C7 and pL1 ($p < 0.0001$ and $p = 0.0245$, respectively). This response exhibited by rLDH 4 is similar to that of the anti-r*Pf*LDHp IgY antibody ($p > 0.05$). In epifluorescent microscopy, the relative FITC-positive fluorescence of immobilised parasites using aptamers LDHp 11 (62.79 ± 7.35 %) and rLDH 4 (67.32 ± 13.28 %) was statistically equivalent to that of the anti-r*Pf*LDHp IgY antibody (71.26 ± 18.27).

The statistical equivalence ($p > 0.05$) demonstrates that LDHp 11 and rLDH 4 were observed to accumulate in similar proportions of immobilised *P. falciparum* parasite bodies, indicating comparable aptamer binding efficacies as the anti-r*Pf*LDHp IgY to native *Pf*LDH using epifluorescent microscopy. Furthermore, LDHp 11 and rLDH 4 exhibited FITC fluorescence with confocal fluorescent and epifluorescent microscopy, respectively, indicates higher sensitivity than the other tested aptamers. Therefore, LDHp 11 and rLDH 4 can be used to successfully identify *P. falciparum* parasite bodies, with equivalent efficacies to the anti-r*Pf*LDHp IgY antibody, through visualisation with epifluorescent microscopy.

5.5.3. Aptamer inhibition on LDH activity

5.5.3.a. Aptamer inhibition on ex situ LDH activity

Measuring the activity of plasmodial LDH (pLDH) as an indicator of the presence of *Plasmodium* spp. has been performed (Makler *et al*., 1993; Miler *et al*., 2001; Zofou *et al*., 2011). The use of antibodies (Markwalter *et al*., 2016) and aptamers (Cheung *et al*., 2015; Dirkzwager *et al*., 2015; Fraser *et al*., 2018) as capture elements in the immobilisation or tethering of *Plasmodium* LDH has also been explored for the purposes of *Pf*LDH detection as an indicator of malaria. Previous reports of aptamer tethered enzyme capture indicate that aptamer binding displayed little to no effect on pLDH activity

making the aptamer capture assays (based on the Malstat-NBT principle) ideal for the purposes of diagnostics. Few reports on the inhibitory effects of aptamer binding on pLDH or even other *Plasmodium* enzymes exist. Inhibition of enzyme activity following binding of aptamers has significant implications for the use of aptamers as antagonists in the field of therapeutics. Use of the Malstat assay to define an aptamer as a therapeutic element has, however, not been explored.

Here, LDH activity was measured at A_{620nm} using the Malstat assay, with NBT as colour indicator, to determine the effectiveness of using generated aptamers, rLDH 1, 4, 7 and 15 and LDHp 1, 3, 11, 14 and 18 along with control concatemer C7 and previously published aptamers, pL1 (Lee *et al*., 2012) and 2008s (Ban *et al*., 2013), as a potential therapeutic agent against malaria through inhibition of the pLDH activity. **Figure 5.10** shows the relative LDH activity of r*Pf*LDH and r*Pv*LDH in the in the absence of binding agent (control) and presence of *P. falciparum*-specific primary antibody (Ab), concatemer (C7), pL1 (Lee *et al*., 2012), 2008s (Cheung *et al*., 2013) and, from this work, LDHp 1, 3, 11, 14 and 18 and rLDH 1, 4, 7 and 15.

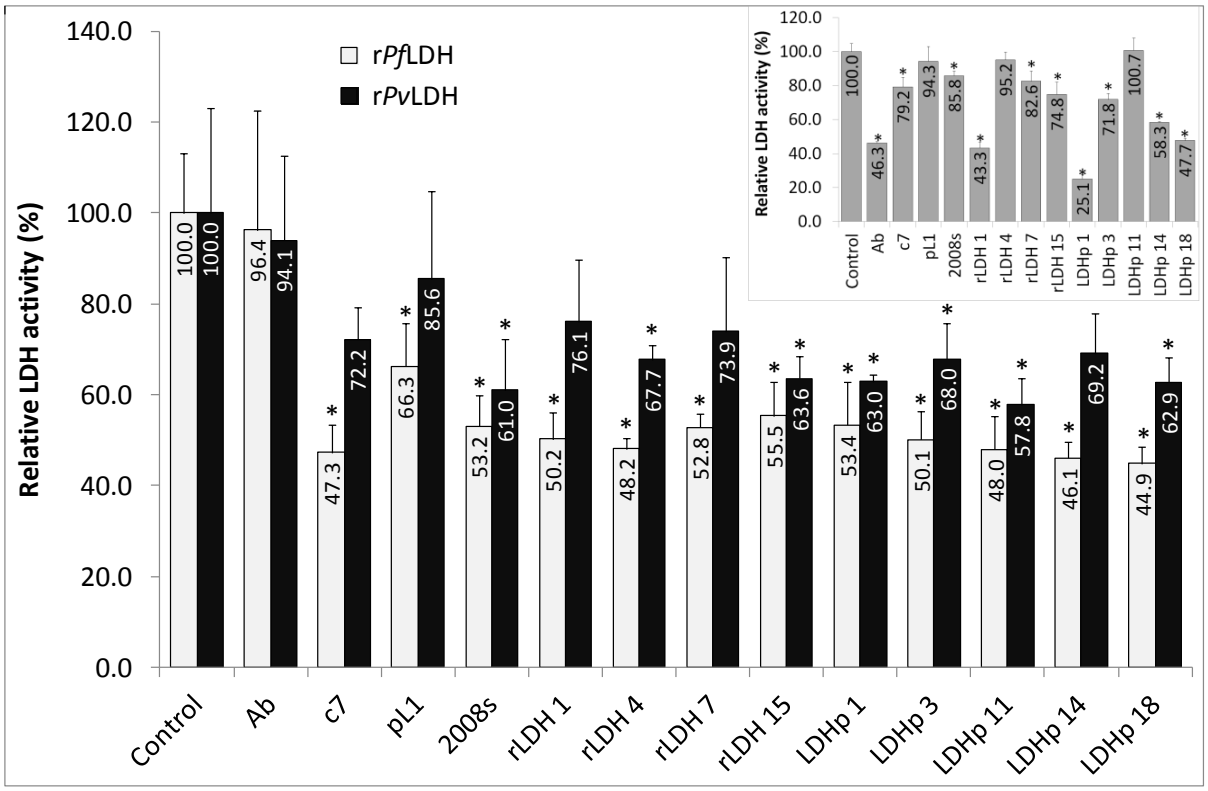

Figure 5.10: The relative activity of r*Pf*LDH, r*Pv*LDH and hLDH (insert) in the absence of binding agent (control) and presence of *P. falciparum*-specific primary antibody (Ab), concatemer (C7), pL1 (Lee *et al*., 2012), 2008s (Cheung *et al*., 2013) and LDHp 1, 3, 11, 14 and 18 and rLDH 1, 4, 7 and 15 (*n* = 4).
Statistics: One-Way ANOVA:
r*Pf*LDH: $F(13,42) = 12.39$, $p < 0.0001$;
r*Pv*LDH: $F(13,42) = 4.19$, $p = 0.0002$;
hLDH: $F(13,42) = 101.00$, $p < 0.0001$.
* Significant inhibition vs. control LDH activity, identified using Tukey's HSD test ($p \leq 0.05$).

Aptamers 2008s and C7 (control) were comparable with similar decreases in overall activity. Aptamer 2008s exhibited significantly decreased activity for r*Pf*LDH (56.2 ± 6.8 %, $p < 0.0001$) and r*Pv*LDH (61.0 ± 11.2 %, $p = 0.004$) in **Figure 5.10**, which is in contradiction to the report by Cheung and co-workers (2013). They report that plasmodial LDH exhibited no change in activity upon binding with aptamer 2008s despite its binding proximity to the LDH active site. Cheung and co-workers (2015) later utilise the fact that the plasmodial LDH activity remains indifferent whilst bound to the aptamer 2008s as a means of detecting malaria colorimetrically using aptamer-tethered enzyme capture (APTEC).

From **Figure 5.10**, *Plasmodium* parasite LDH activity showed no significant decrease following binding to the *P. falciparum*-specific primary IgY antibody relative to the control in which no binding agent was included. This indicates that the primary antibody had no inhibitory effect on activity of

both r*Pf*LDH and r*Pv*LDH. While no literature exists to directly compare the effect that coupling of the *P. falciparum*-specific IgY antibody used in this work on pLDH activity, others have looked at the effect that antibody binding has on human and plasmodial LDH activity. Kaushal and co-workers (1995) found that their monoclonal antibody (2A3B7) inhibited the LDH of both *P. falciparum* and *P. vivax*. This team have since used their plasmodial LDH antibody in an immunodot enzyme assay for the detection of LDH and diagnosis for malaria (Kaushal & Kaushal, 2002). Further to this study, Kaushal and Kaushal (2014) found that their monoclonal antibodies directed to the substrate-specific loop region of plasmodial LDH, 10C4D5 and 10D3G2, did indeed inhibit *Pf*LDH activity.

Even though sensitivity of *Plasmodium* LDH is enhanced with APAD given that *Plasmodium* LDH preferentially utilises APAD compared to the human LDH analogue (Gomez *et al*., 1997), human LDH (hLDH) activity was observed (**Figure 5.10**, insert). Observed decreases in relative activity of hLDH in the presence of aptamers can be attributed to the fact that human LDH has a low affinity for APAD; such an affinity interaction between hLDH and APAD was lessened in the presence of the aptamer. The insert to **Figure 5.10** shows the relative activity of human LDH in the presence of antibody and aptamers. The reduction in activity of hLDH, but not for r*Pf*LDH and r*Pv*LDH, shown in **Figure 5.10** (insert), in the presence of the antibody indicates that the antibody cannot be considered as a potential anti-plasmodial therapeutic agent; but its use in a diagnostic device utilising LDH activity would be feasible given that a reduction in activity was observed for hLDH but not r*Pv*LDH and r*Pf*LDH.

The relative activity of r*Pf*LDH was significantly reduced upon binding of aptamers relative to the control (**Figure 5.10**). This indicates that binding of aptamers inhibited r*Pf*LDH activity at the concentrations studied. The relative LDH activity for aptamers generated from this work, rLDH 1, 4, 7 and 15 and LDHp 1, 3, 11, 14 and 18, exhibited an LDH activities of between 44.9 % (LDHp 18) to 55.5 % (rLDH 15) relative to the control (100 %). On the other hand, the relative activity of r*Pv*LDH showed statistically significant ($F(13,42) = 4.19$, $p = 0.0002$) decreases following binding interactions with 2008s, rLDH 4, rLDH 15, LDHp 1, 3, 11, and 18, relative to the control in which a binding bioagent was absent (**Figure 5.10**). In the presence of these aptamers, r*Pv*LDH exhibited 57.8 to 68.0 % activity relative to the control. DNA aptamers have been known to inhibit enzyme activity as shown with 2-oxoglutarate (2OG)-dependent oxygenases (Krylova *et al*., 2012). The calculable decrease in r*Pf*LDH activity of between 44.5 (rLDH 15) and 55.1% (LDHp 18) shows that these aptamers, rLDH 1, 4, 7 and 15 and LDHp 1, 3, 11, 14 and 18, interacted with r*Pf*LDH at or near the

active site or cofactor binding site that significantly limited LDH activity. There exists the possibility that while the LDHp aptamers were selected for a secondary structure (α-helix and loop) away from the active site, it could be anticipated that aptamer localisation would occur at the active site stem and loop structure. These moderate interactions or even binding of the aptamer/s at the active site may limit LDH activity, but not directly inhibit LDH activity. It is also possible that there was a similar interaction of the aptamer with the co-factor binding site of the r*Pf*LDH enzyme. Those aptamers that significantly reduced r*Pf*LDH activity, specifically rLDH 1, 4 and 7, LDHp 1, 3, 11, 14 and 18, and 2008s, all share a common moiety: GGTTG/GGTAG (**Figure 3.5**). Given that all aptamers that significantly reduced r*Pf*LDH activity contain the GGTTG/GGTAG moiety within the variable region, it is understandable that this moiety may result in localisation at the LDH active site or cofactor-binding site interfering with enzyme activity. Aptamers with conserved short motifs found on the stem-loop structures of the aptamers have been shown to infer a loss of activity for an enzyme, for example the RNA aptamer N30yc2 inhibited activity of *Yersinia* protein tyrosine phosphatises, Yop51 (Bell *et al*., 1998). Therefore, even though some of the aptamers did not inhibit LDH activity, this does not necessarily imply that they did not bind to LDH; it does, however, imply that the aptamers bound and interacted with the LDH in such a way that they did influence LDH activity. However, the direct influence of aptamer binding on r*Pf*LDH activity can only be proven through rendering of crystal structure of the aptamer-r*Pf*LDH complex using nuclear magnetic resonance (NMR) or X-ray crystallography (Sakamoto, 2017).

Table 5.3 summarises whether statistically-significant inhibition of relative LDH activity occurs in the presence of the biorecognition elements analysed in **Figure 5.10**, in relation to the control. While this enzyme inhibition does have implications when considering their use in diagnostic devices based on pLDH activity in the detection of *P. falciparum* and *P. vivax*, there exists the possibility that such inhibitory effects may have potential for use in malaria therapeutics. Therefore, included in **Table 5.3** is the type of therapeutic the antibody and aptamer would be most effective: a combined therapeutic agent targeting both *P. falciparum* and *P. vivax* but not human LDH, or a species-specific therapeutic agent targeting only *P. falciparum* or *P. vivax* and not human LDH. If the aptamer or antibody was seen to bind to human LDH, this would render it ineffective as a therapeutic agent given that it would have a negative impact on LDH in human blood and the body, inhibiting human LDH activity, e.g. LDHp 1 (**Figure 5.10**, insert).

Conversely, while a decrease in pLDH activity would enhance the probability that the aptamer could be used therapeutically, the lack of a statistically meaningful change in pLDH activity would mean that the aptamer could be used as a capture molecule for a diagnostic device employing the sensitive Malstat assay.

Table 5.3: Aptamers exhibiting significant decreases in activity for r*Pf*LDH, r*Pv*LDH and hLDH relative to the control, drawn from Figure 5.10, and effectiveness using activity as a diagnostic method and/or as a therapeutic agent against malaria, categorised into aptamers binding both pLDH versus only one.

	r*Pf*LDH	r*Pv*LDH	hLDH	Utilising LDH activity for diagnostic purposes	Direct/antagonistic use as a therapeutic agent against malaria
Antibody	-	-	Inhibits	Both r*Pf*LDH and r*Pv*LDH	-
C7	Inhibits	-	Inhibits	Non-specific	Non-specific
pL1	Inhibits	-	-	-	*rPf*LDH-specific
2008s	Inhibits	Inhibits	Inhibits	-	-
rLDH 1	Inhibits	-	Inhibits	r*Pv*LDH-specific	-
rLDH 4	Inhibits	Inhibits	-	-	Both r*Pf*LDH and r*Pv*LDH
rLDH 7	Inhibits	-	Inhibits	r*Pv*LDH-specific	-
rLDH 15	Inhibits	Inhibits	Inhibits	-	-
LDHp 1	Inhibits	Inhibits	Inhibits	-	-
LDHp 3	Inhibits	Inhibits	Inhibits	-	-
LDHp 11	Inhibits	Inhibits	-	-	Both r*Pf*LDH and r*Pv*LDH
LDHp 14	Inhibits	-	Inhibits	r*Pv*LDH-specific	-
LDHp 18	Inhibits	Inhibits	Inhibits	-	-

While a general decrease in activity was observed in the presence of all aptamers for r*Pf*LDH, but only some aptamers for r*Pv*LDH and hLDH (**Figure 5.10** and **Table 5.3**), a broad decrease in activity was observed. This is important in that the sort of response observed for the different LDH enzymes in the presence of the aptamers does have implications were they to be used in the field of therapeutics. **Table 5.3** shows that aptamers rLDH 4 and LDHp 11 could be considered for further investigation as a therapeutic drug for *Plasmodium* spp. as they demonstrated significant reduction in LDH activity for both r*Pf*LDH and r*Pv*LDH, but not to hLDH. While the decrease in r*Pf*LDH activity with aptamer pL1 was statistically significant (and no decrease in activity was observed for r*Pv*LDH and hLDH), this decrease was the least sensitive of all aptamers analysed and would, therefore, not be recommended as a therapeutic agent. Aptamers pL1, rLDH 1 and 7 and LDHp 14 could be used in a diagnostic devise utilising r*Pv*LDH activity as an indicator of *P. vivax* infection given the lack of a statistically significant decrease in activity for r*Pv*LDH while r*Pf*LDH and hLDH activity were significantly decreased.

Aptamers 2008s, rLDH 15, LDHp 1, 3 and 18 exhibited statistically significant decreases in LDH activity for all species of LDH tested (r*Pf*LDH, r*Pv*LDH and hLDH). This would render these aptamers ineffective as either a therapeutic or in a diagnostic device due to these non-specific decreases in LDH activity.

5.5.3.b. Aptamer inhibition on cultured P. falciparum parasites – a scoping study

To assess the therapeutic potential of the generated aptamers, the aptamers were combined with cultured *P. falciparum* parasites over a 48-hour growth period (one blood stage cycle) to ascertain toxicity towards the live parasites. The Malstat assay measuring LDH activity can also be used to calculate the number of parasites present. (This work was conducted by the Centre for Chemico- and Biomedicinal Research.)

Figure 5.11 shows the percent parasite viability (%) obtained for the individual aptamers in the cultured *P. falciparum* parasite cells.

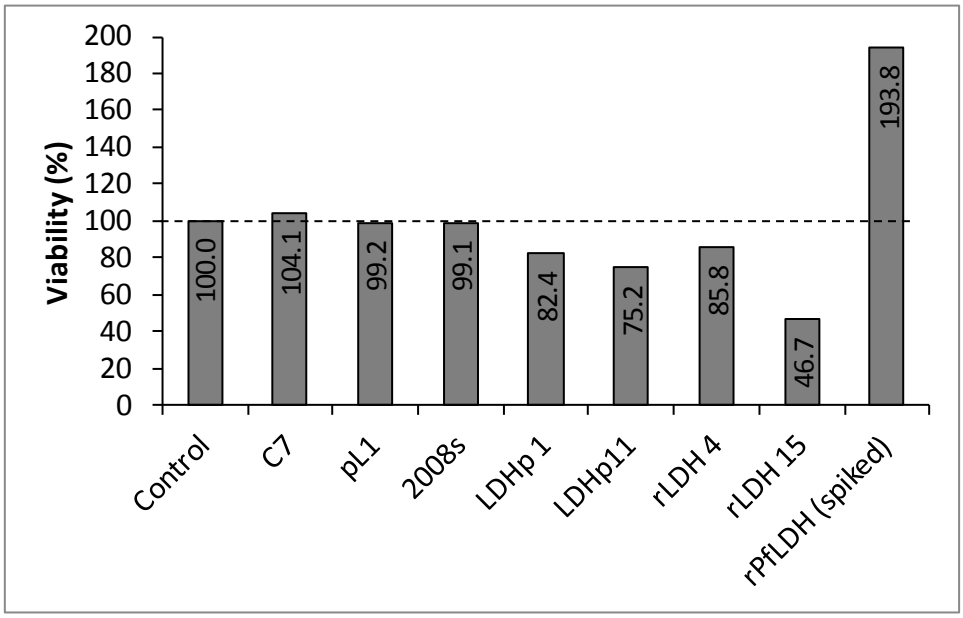

Figure 5.11: The percent viability of *P. falciparum* in the absence and presence of aptamers, C7, pL1, 2008s, LDHp 1, LDHp 11, rLDH 4 and rLDH 15 (*n* = 1).
Dashed line indicates 100% viability with live parasites

Figure 5.11 shows the results of the scoping study to determine the effect that a 48-hour incubation with the various aptamers had on viable *P. falciparum* parasites. A single-dose concentration was applied to a single blood culture, as concentrations and volumes of aptamers required for this assay was limiting. It must also be noted that these externally performed assays for the scoping analysis shown in **Figure 5.11** were not performed on whole parasites. As parasite bodies were lysed in the assay performed here, aptamers were able to gain access to the cellular *Pf*LDH in the assay matrix.

Both the negative control (no added aptamer) and the control aptamer C7 exhibited similar degrees of LDH activity (**Figure 5.11**), indicating that no significant inhibition of either propagation or LDH activity took place. The exogenous addition of r*Pf*LDH to the assay resulted in an increased LDH activity for that pool, as would be expected for standard additions (**Figure 5.11**). The standard addition can be used to validate the *Pf*LDH activity and can be used to quantify the amount of *Pf*LDH found in the parasite culture.

It is worth further analysis in future studies that some aptamer sequences exhibited inhibition of the *Pf*LDH activity assayed in the viability study. The aptamer rLDH 15, in particular, exhibited a 53.3% decrease in viability over the 48-hour period (**Figure 5.11**). Furthermore, LDHp 11 also exhibited a 24.8% decrease in viability over this same 48-hour period. The decrease in viability in the presence of rLDH 15 and LDHp 11 could indicate that (1) the aptamer actively inhibits parasite growth over 48 hours, or (2) the aptamer inhibited native *Pf*LDH activity.

However, given the evidence presented in **Figure 5.10**, LDHp 11 remained effective as only an inhibitory agent towards native *Pf*LDH, and did not necessarily exert toxic effects towards the live parasite cultures.

Little is known about how the aptamer could gain access to the parasite body, and the cellular *Pf*LDH, meaning that it cannot necessarily exert a toxic effect without gaining access to the cell and then the parasite. The cultured parasite assay used by the external laboratory was limited by the fact that the Malstat assay used routinely for screening drugs for antimalarial activity measures inhibition of pLDH activity. The inhibition is used by researchers to infer toxicity. In this study the red blood cells and the cultured *P. falciparum* bodies were perforated with Triton-X. The Malstat assay was then performed on the perforated parasite bodies; hence, aptamers permitting access of the

aptamer to the cellular *Pf*LDH present in the cellular debris. This assay was performed on parasite lysate after culturing without initially pelleting the cellular debris. Furthermore, unbound aptamer was not removed from the parasite debris mixture on which the assay was performed; hence, any inhibition observed could be related to direct inhibition of native *Pf*LDH.

Native *Pf*LDH in the presence of aptamer rLDH 15 exhibited activity of 46.7 % of the untreated *Pf*LDH control (**Figure 5.11**), whereas recombinant *Pf*LDH exhibited the least inhibition of those generated aptamers tested with activity of 55.5 % compared to the untreated r*Pf*LDH control (**Figure 5.10**). Therefore, rLDH 15 exhibited about a 50 % decline in activity for both recombinant and native *Pf*LDH enzymes. Conversely, LDHp 11 exhibited a greater inhibitory effect on the recombinant *Pf*LDH (48.0 %) compared to the cultured native *Pf*LDH (75.2%). Nevertheless, the observed decreases in cultured *P. falciparum* viability would also entail further follow-up in future studies.

Given the preliminary nature of the Malstat assay presented in **Figures 5.10** and **5.11**, as well as the assay limitations (especially, the lysis of parasties before assaying LDH activity), it remains that further research will need to be conducted to determine whether the aptamers enter the parasite cells and could serve as therapeutic agents through pLDH inhibition. Given the evidence presented above, use of these aptamers holds some promise for future studies directed at aptamers for *P. falciparum* therapeutics.

5.6. Conclusion

With respect to EIS-based aptamer-target interactions, the preliminary assessment of LDHp 11 (3.5 µM) binding interactions with the *P. falciparum*-specific peptide, LDHp, demonstrated feasibility of such an approach given the statistically significant decreases in charge transfer resistance (R_{CT}) and Warburg modulus (W). However, using lower concentrations akin to physiological concentrations expected for pLDH following infection with *Plasmodium* spp., no statically definitive trend was observed for the charge transfer resistance across the LDHp concentration range tested (RCT: $F(4,37) = 4.985$, $p = 0.289$). While capacitance expressed a statistically significant decrease with relation to the blank control (C: $F(4,37) = 9.646$, $p = 0.0468$), C lacked concentration dependency and hence sensitivity across the various LDHp concentrations tested. EIS, therefore, exhibited a lack of sensitivity to increasing nanomolar concentrations of the peptide. This lack of sensitivity at nanomolar concentrations using the hexanedithiol-aptamer-mercaptohexanol electrode surface

assembly for each nanomolar concentration was further exemplified by the inter-electrode variability. Therefore, the current configuration of the aptasensor for LDHp 11 did not work at the relevant, and necessary, concentrations of LDHp. This rendered EIS, in this instance as unsatisfactory in measuring the binding between LDHp and LDHp 11.

Of the aptamers, pL1, LDHp 1, LDHp 11 and rLDH 4 also were also confirmed to bind to native LDH in immobilised *Plasmodium falciparum* parasite bodies through epifluorescent and confocal fluorescent microscopy of FITC-tagged aptamers. Confocal fluorescence microscopy exhibited higher resolution than epifluorescence microscopy, providing greater sensitivity. The anti-r*Pf*LDH antibody demonstrated binding as previously shown by Hurdayal and co-workers (2010), whereas the concatemer, C7, demonstrated negligible binding indicating that minimal fluorescence observed for aptamers was due to passive uptake of oligonucleotide material into the nucleus of the parasite body. However, in most instances, aptamer fluorescence was co-localised with that of DAPI indicating either uptake into the nucleus but most likely the concentration of LDH in the sub-cellular region of the parasite body. Akin to the *Pf*LDH antibody, LDHp 11 exhibited the highest fluorescent intensity, with a relative FITC-assessed fluorescence in 62.49 % and 94.98 % of immobilised parasite bodies in epifluorescent microscopy and confocal fluorescent microscopy, respectively. Aptamer rLDH 4 also showed similar relative fluorescence to the *Pf*LDH antibody in epifluorescent microscopy but not so in confocal microscopy; while LDHp 1 exhibited an opposing trend with few fluorescing bodies in epifluorescent microscopy but with equivalent trends to that seen for the *Pf*LDH antibody. Mean fluorescent intensity analyses between rLDH 4 and LDHp 1 showed a lack of statistical significance between these two data sets. Therefore, epifluorescent microscopy visually demonstrated binding between LDHp 11 and rLDH 4 aptamers to native LDH in *P. falciparum*. Confocal fluorescent microscopy, on the other hand, showed that relative fluorescence of FITC-tagged LDHp 1, LDHp 11 and pL1 in immobilised parasite bodies were statistically equivalent to the *Pf*LDH antibody. Furthermore, LDHp 1 and LDHp 11 had a higher success rate of binding immobilised parasite bodies than C7, pL1 and rLDH 4, with ~95 % of parasite bodies with observed FITC fluorescence.

A decrease in LDH activity using the Malstat and NBT/PES assay was observed for r*Pf*LDH in the presence of aptamers C7, pL1, 2008s, rLDH 1, 4, 7 and 15 and LDHp 1, 3, 11, 14 and 18. Aptamers rLDH 4 and LDHp 11 hold promise as potential plasmodial LDH inhibitory agents given that observed decreases were seen in the presence of these two aptamers for r*Pf*LDH but not r*Pv*LDH nor hLDH.

Moreover, decreases in r*Pv*LDH activity were not observed for pL1, rLDH 1 and 7 and LDHp 14. Given their limited binding capacity to r*Pf*LDH in previous screening analyses, particularly ELONA, these aptamers could therefore be used in *P. vivax* diagnostic devices given that insignificant changes in r*Pv*LDH activity were observed for these four aptamers. Decreased viability was observed in live *P. falciparum* parasites in the presence of aptamers LDHp 11 and rLDH 15; however, given the limitations of the LDH assay on cultured *P. falciparum* parasites with respect to the aptamers accessing the intracellular target in the parasite within the red blood cell, thorough investigations into the feasibility of these aptamers in the field of therapeutics are required.

The summary table presenting the effectiveness of various techniques presented in this Chapter for the determination and assessment of generated aptamer binding to r*Pf*LDH and LDHp is shown in **Table 5.4**.

Table 5.4: Summary of effectiveness of various techniques used in this Chapter in the determination of target binding.

Technique	r*Pf*LDH-targeting aptamers		LDHp-targeting aptamers		Effective for aptamer binding analyses?	Concluding remark/s
	Aptamer/s tested	Response	Aptamer/s tested	Response		
EIS	Not tested	-	LDHp 11	R_{CT} : variable responses; no trends C: decreased; lack of concentration dependence	No	Irreproducible; low sensitivity and lack of concentration dependence
Fluorescent microscopy	rLDH 4 rLDH 7 pL1 C7	Binding and co-localisation of rLDH 4, rLDH 7 and pL1 shown, C7 did not bind	LDHp 1 LDHp 11 C7	Co-localisation observed; LDHp 11 demonstrated greater fluorescent intensity than other aptamers; C7 did not bind	Yes	Visual technique to show binding and localisation of aptamers in parasite bodies
LDH inhibition assay	rLDH 1, 4, 7 and 15 2008s and pL1 C7	rLDH 1 and 7 are r*Pv*LDH-specific; rLDH 4 shows binding to both r*Pf*LDH and r*Pv*LDH ; rLDH 15 inhibited native r*Pf*LDH; 2008s inhibited all LDH; pL1 only showed inhibition towards r*Pf*LDH C7 inhibited r*Pf*LDH and hLDH, not r*Pv*LDH	LDHp 1, 3, 11, 14 and 18 C7	LDHp 11 inhibited pLDH, showed r*Pf*LDH- and r*Pv*LDH-specificity, showed ~25 % decrease in native *Pf*LDH activity; C7 and LDHp 14 inhibited r*Pf*LDH and hLDH, not r*Pv*LDH	Yes	Inhibition rendered aptamers not suitable for *P. falciparum* diagnostics utilising LDH enzyme activity (LDHp 14, rLDH 1 and 7 could be used towards *P. vivax* diagnostic); not suitable for application in therapeutics

CHAPTER 6

Conclusions and future recommendations

6.1. General conclusions

This study (part of which is published in Frith *et al*., 2018) details the generation of two sets of aptamers with significantly different sequences and structures to those reported previously (Lee *et al*., 2012; Cheung *et al*., 2013). These aptamers were designed from first principles to have the potential to differentiate between malaria species based on selective binding to the lactate dehydrogenases expressed by *Plasmodium falciparum* versus *Plasmodium vivax*, referred to as *Pf*LDH and *Pv*LDH, respectively. Two sets of aptamers were generated independently through parallel SELEX using recombinant *Plasmodium falciparum* lactate dehydrogenase (r*Pf*LDH) as a target and the *P. falciparum*-specific lactate dehydrogenase peptide (LDHp) as the second target during SELEX.

Similar to previously-reported aptamers capable of binding r*Pf*LDH and r*Pv*LDH (Lee *et al*., 2012; Cheung *et al*., 2013), SELEX was performed on the whole pLDH proteins in the generation of aptamers presented herein: the rLDH class of aptamers. Furthermore, aptamers were generated for the first time against the *Pf*LDH peptide, representing an epitope unique to *P. falciparum*. This resulted in the LDHp class of aptamers – which were able to bind to the whole recombinant protein, as well as the initial LDHp target, owing to the similarity between the peptide and the peptide epitopic region on the surface of the larger recombinant *Pf*LDH. The ability of aptamers to bind to not only the specific target against which they were generated but also the larger protein motivates the need for such developments in SELEX, specifically dual target SELEX in which a single SELEX is performed on two structurally similar targets (similarly to those first proposed by Hicke *et al*., 2001).

In **Chapter 2**, aptamers specific to the recombinant LDH of *Plasmodium falciparum* (r*Pf*LDH) and species-specific *Plasmodium falciparum* LDH peptide (LDHp) were developed using the exonuclease-SELEX method. While a certain level of optimisation is required for SELEX, the main challenge experienced was the production of unwanted primer artefacts capable of non-specifically elongating to form extended lengths of DNA – termed over-amplification (Tolle *et al*., 2014). In **Chapter 2**,

numerous methods were evaluated to remove this over-amplification throughout SELEX: optimising PCR annealing temperatures; optimising the number of PCR cycles per amplification; adding Triton-X surfactant; modifying the PCR product purification protocol; and, agarose gel excision. To limit over-amplification and remove artefacts from the PCR amplified SELEX pool, a combination of the optimal PCR conditions was employed encompassing optimised PCR conditions, a modified PCR clean-up protocol and excised PCR amplified template DNA from agarose gel. These optimisation steps in the amplification stage of SELEX are required in every round of SELEX, regardless of target, owing to the fact that PCR inherently generates over-amplification products.

Successful SELEX resulted in a final percent recovery of 90.2 % for those oligonucleotides targeted for LDHp and 49.5 % for those oligonucleotides targeted for r*Pf*LDH. Preliminary ELONA binding analyses demonstrated PCR-amplified oligonucleotides from clones were capable of binding to their targets, and lead to the positive identification of aptamer candidates for further analyses.

Analysis of the primary sequences of aptamer candidates indicated that two main clades were identifiable in **Chapter 3**: one clade containing 8 of the 11 sequenced r*Pf*LDH-targeting aptamers (rLDH 2, 3, 5, 6, 9, 10, 12 and 14), and the second clade containing 3 of the 8 LDHp-targeting sequences (LDHp 3, 15 and 18). Separate multiple sequence alignments of these sequences show a high consensus between the rLDH aptamer cluster; however, the LDHp cluster showed less consensus across the three sequences. Aptamers comprising the rLDH cluster were from clones identified as incapable of binding to their targets and were, therefore, eliminated from additional binding analyses. Therefore, the generation of a number of similar sequences in SELEX demonstrates sequence enrichment, but this enrichment does not necessarily translate to high affinity interactions with the target (when assessed using ELONA), but these sequences could have been shown to bind to r*Pf*LDH using another screening technique. However, this was not explored within this thesis.

Mfold-based secondary structure predictions of the aptamers selected for further study identified two common secondary structures: stem-loop (LDHp 1, LDHp 14, rLDH 4 and rLDH 15) and elbow structures protruding from a larger loop (rLDH 1, rLDH 7 and LDHp 18). Moreover, pseudoknot predictions of these aptamers in **Chapter 3** show that these sequences adopt more complex structures than those immediately evident by Mfold. Therefore, while Mfold is the more utilised technique in secondary structure prediction for aptamers, it is relatively rigid in its computation of the chemistries used to generate the secondary structures. Even though pseudoknot prediction

software is specific for RNA folding, it can indicate the conformation expected of ssDNA based on similar chemistries. Based on the computational power for RNA folding, pseudoknot prediction software, therefore, has the ability to factor in the flexibility in its folding prediction of ssDNA conformations and is, hence, more representative of what the expected tertiary structure could resemble, compared to Mfold. Both pseudoknot predictions and tertiary structure analysis demonstrated that common moieties found in synthesised aptamers were located at distinct three-dimensional (3D) structures, such as ATTAT forming part of the possible negatively charged, non-polar aptamer binding pockets. Identification of these moieties aids in predicting how the aptamer binds to its target, and whether or not these binding interactions are extended to a family aptamers for a specific target generated with a specific library and further extended to aptamers generated from another independent SELEX library to the same target. Identification of these moieties in this work and other aptamers generated from a separate SELEX library to the given protein target aids in concluding that the moiety is indeed essential for r*Pf*LDH recognition and binding.

Structurally-complex aptamers with sequence diversity predominated in the aptamers selecting the smaller peptide target LDHp. Aptamers selecting the larger r*Pf*LDH, on the other hand, comprised of sequences with a greater consensus, owing to the poly-A region. The poly-A resulted in the formation of more complex and flexible helical tertiary structures not immediately evident in secondary structure-predicting software like that employed in other studies (Brahms *et al*., 1966; Isaksson *et al*., 2004), but visually represented using tertiary structure prediction with RNA analogues of the sequences. Few reports exist on the use of RNA analogue-based ssDNA aptamer pseudoknot and tertiary structure prediction (SantaLucia & Hicks, 2004; Cash *et al*., 2009). As the larger recombinant *Pf*LDH consists of a greater number of possible binding sites owing to varied peptide secondary structures on the surface of the protein, the poly-A consensus region in the rLDH class of aptamers and the resulting tertiary structures of these aptamers was unexpected. However, the presence of the poly-A region and inherent flexibility of the tertiary structures in the rLDH class of aptamer would facilitate aptamer binding interactions to the larger protein.

Of the 19 sequences generated through SELEX targeting r*Pf*LDH and LDHp, nine were chosen for further screening, based on both oligonucleotide sequence (rLDH 1 and 15) and their empirical ability to bind their target in the preliminary ELONA from **Chapter 2** (rLDH 4 and 7 and LDHp 1, 3, 11, 14 and 18).

Several screening techniques were used to conduct binding analyses of the generated aptamers to the targets, LDHp and r*Pf*LDH (**Chapter 4**). A comprehensive overview of the responses of each aptamer generated in this study in each of the screening techniques used is presented in **Table 6.1**.

From ELONA, binding kinetics of aptamer-target interactions were deduced, showing improved response sensitivity and concentration dependence over the fluorescent counterpart, FLONA (for which there was no provable binding between aptamers and r*Pf*LDH). Given the sensitive ELONA response, non-specific interactions were observed to serum albumins, particularly for the positive control aptamers. While ELONA should be the first method with which to screen aptamer-target binding affinity when embarking on SELEX for protein targets, additional validation techniques were required given this non-specificity to verify the observed interactions between aptamer and protein. Compared to ELONA, competitive fluorescent binding analyses using GelRed demonstrated a large extent of signal variability and general lack of sensitivity for the LDHp class of aptamers upon binding to LDHp. There exist few reports in literature on the use of fluorescent dye displacement that prove that this technique can be used to assess aptamer-target interactions for small molecules (Tse & Boger, 2004; Yu et al., 2017). However, these findings provide the groundwork for preliminary data for the utilisation of the GelRed assay for the binding analysis of aptamers to small peptides.

Assessment of binding interactions of aptamers to select proteins using EMSA (**Chapter 4**) showed that aptamer-r*Pf*LDH interactions generally had a differing migration profile to r*Pv*LDH and mLDH, indicative of specific binding of the aptamers to r*Pf*LDH. EMSA offered a quick method of qualitative analysis of whether an aptamer binds to its selected target, it displayed some limitations. Chiefly, the staining of the target *rPf*LDH protein by GelRed was identified as a limitation when conducting kinetic studies, in this case study instance.

While SPR (**Chapter 4**) is a standard method for measuring binding interactions between biological molecules, data presented herein indicated that use of SPR for such interactions in this study was also somewhat limited. Analysis of interactions between aptamers with extended lengths, such as these aptamers of 90 bp, and their targets (and controls) using SPR is limited given the flow requirements of such a system. Noted in this study was that use of a flow-through system prevented the aptamer from adopting the most preferred tertiary conformation adept for target recognition and binding, as well as sufficient contact time to facilitate such interactions.

Table 6.1: Overview of findings obtained from screening studies examining aptamers' binding interactions

"Target Binding" indicates the most relevant response obtained for the stipulated aptamer using the designated technique; "Binding Specificity" (*Pf* vs *Pv*) provided when aptamers were tested against r*Pf*LDH and r*Pv*LDH, where only one protein was tested, binding specificity was not determined. "Yes" indicates positive observed quantitative/qualitative binding to the protein; "No" indicates absence of observed binding; "Maybe" indicates unconfirmed, statistically insignificant or varying responses of aptamer to protein binding.

Screening technique and tested property of the aptamer		**Thesis Chapter**	**Negative Control, C7**	**r*Pf*LDH-targeting aptamers**				**Peptide-targeting aptamers**					**Positive controls**	
				rLDH 1	**rLDH 4**	**rLDH 7**	**rLDH 15**	**LDHp 1**	**LDHp 3**	**LDHp 11**	**LDHp 14**	**LDHp 18**	**pL1**	**2008s**
Target affinity assays														
ELONA	r*Pf*LDH-binding (K_D)	**4.5.1.**	No	Yes	Yes (691 ± 393 nM)	Yes (39 ± 15 nM)	Yes (80 ± 17 nM)	Yes (927 ± 914 nM)	No	Yes (321 ± 82 nM)	No	No	Yes (159 ± 167 nM, CNM)	Yes
	LDHp-binding (K_D)		-	No	No	No	No	Yes (96.0 ± 63.2 nM)	Yes (CNM > 1000)	Yes (CNM > 1000)	Yes (CNM > 1000)	Yes (81 ± 63 nM)	Yes	Yes
	r*Pv*LDH-binding (K_D)		No	Yes	Yes (444 ± 144 nM)	Yes (26 ± 3 nM)	Yes (268 ± 67 nM)	No (CNM > 1000)	No	No (CNM > 1000)	No	No	Yes (79 ± 12 nM)	Yes
	mLDH-binding		-	No	No	No	No	No	No	No	No	No	Yes	Yes
	HSA-binding		-	No	Maybe	Yes	No	No	No	No	No	No	Yes	Yes
	Binding specificity (r*Pf*LDH, r*Pv*LDH, LDHp, mLDH, HSA)		N/A	*Pf* > *Pv*	*Pf* > *Pv* ≈ HSA*	*Pf* > *Pv* ≈ HSA*	*Pf* > *Pv* ≈ HSA*	LDHp *Pf* #	LDHp	*Pf* LDHp	LDHp	LDHp	*Pf* *Pv* ≈ LDHp ≈ mLDH ≈ HSA	*Pf* ≈ *Pv* ≈ LDHp ≈ mLDH ≈ HSA
FLONA	r*Pf*LDH-binding	**4.5.2.**	No	-	No	No	-	No	-	No	-	-	No	-
GelRed	r*Pf*LDH-binding	**4.5.3.**	-	-	No	-	-	-	-	-	-	-	-	-
	LDHp-binding		No	-	-	-	-	No	Yes	Yes	Yes	Yes	Maybe	No
	Binding specificity (r*Pf*LDH, LDHp)		N/A	-	N/A	-	-	N/A	LDHp	LDHp	LDHp	LDHp	LDHp(?)	N/A
EMSA	r*Pf*LDH-binding	**4.5.4.**	-	Yes	Yes	Yes	Yes	Yes	Yes	Yes	Yes	Yes	Yes	Yes
	r*Pv*LDH-binding		-	Yes	No	Yes	No	Yes	Yes	No	No	No	Yes	No
	mLDH-binding		-	No	No	No	No	No	No	No	No	No	No	No
	Binding specificity (r*Pf*LDH, r*Pv*LDH, mLDH)		-	*Pf, Pv*	*Pf*	*Pf, Pv*	*Pf*	*Pf, Pv*	*Pf, Pv*	*Pf*	*Pf*	*Pf*	*Pf, Pv*	*Pf*

Screening technique and tested property of the aptamer		Thesis Chapter	Negative Control, C7	r*Pf*LDH-targeting aptamers				Peptide-targeting aptamers					Positive controls	
				rLDH 1	rLDH 4	rLDH 7	rLDH 15	LDHp 1	LDHp 3	LDHp 11	LDHp 14	LDHp 18	pL1	2008s
SPR	*rPf*LDH-binding (K_D)	**4.5.5.**	No	-	No	No	-	Yes (0.13 ± 0.07 µM)	-	Maybe (CNM)	-	-	Maybe	-
	*rPv*LDH-binding (K_D)		No	-	No	No	-	Yes (0.12 ± 0.06 µM)	-	Maybe (CNM)	-	-	Maybe	-
	HSA-binding		-	-	No	-	-		-	Maybe	-	-	Maybe	-
	Binding specificity (r*Pf*LDH, r*Pv*LDH, HSA)		N/A	-	N/A	N/A	-	*Pf, Pv*	-	*Pf*(?), *Pv*(?), HSA(?)	-	-	*Pf*(?), *Pv*(?), HSA(?)	-
Preliminary biosensing potential														
EIS	LDHp-binding	**5.5.1.**	-	-	-	-	-	-	-	Yes	-	-	-	-
Epifluore-scent Microscopy	Binding to parasite body	**5.5.2.a.**	No	-	Yes	Yes	-	Maybe	-	Maybe	-	-	Yes	-
Confocal Microscopy	Binding to parasite body	**5.5.2.b.**	No	-	Yes	Yes	-	Yes	-	Yes	-	-	Yes	-
Scoping therapeutic potential studies														
r*Pf*LDH Inhibition	*rPf*LDH inhibition	**5.5.3.a.**	Yes	Yes	Yes	Yes	Yes	Yes	Yes	Yes	Yes	Yes	Yes	Yes
	r*Pv*LDH inhibition		No	No	Yes	No	Yes	Yes	Yes	Yes	No	Yes	No	Yes
	hLDH inhibition		Yes	Yes	No	Yes	Yes	Yes	Yes	No	Yes	Yes	No	Yes
	Binding specificity (r*Pf*LDH, r*Pv*LDH, hLDH)		*Pf*(?), h(?)	*Pf,* h	*Pf, Pv*	*Pf,* h	*Pf, Pv,* h	*Pf, Pv,* h	*Pf, Pv,* h	*Pf, Pv*	*Pf,* h	*Pf, Pv,* h	*Pf*	*Pf, Pv,* h
Native *Pf*LDH Inhibition	Parasitised blood LDH inhibition	**5.5.3.b.**	No	-	Maybe	-	Yes	Maybe	-	Yes	-	-	No	No

Footnotes: -: Aptamer not included for testing for the specific screening study.

N/A: Not applicable.

* In ELONA screening studies, **Figure 4.4**, the binding extent of the indicated aptamer to r*Pv*LDH was equivalent to the low levels of binding observed for HSA.

\# Binding of the aptamer to the indicated pLDH was observed during kinetic ELONA studies (**Table 4.1**) but not in the ELONA screening (**Figure 4.4**).

Based on the binding analysis studies in **Chapter 4**, aptamers bind with high affinity and specificity to r*Pf*LDH possessing the potential to differentiate between malaria species based on selective binding to *Pf*LDH versus *Pv*LDH, while some show an ability to bind both LDH from *P. falciparum* and *P. vivax*.

From the ELONA screening analysis in **Chapter 4**, it was determined that the rLDH class of aptamers bound to r*Pf*LDH and r*Pv*LDH with higher colorimetric responses than the smaller epitopic peptide, LDHp, mammalian LDH (mLDH) and human serum albumin (HSA). In ELONA, rLDH 4 consistently bound to r*Pf*LDH to a greater extent than other rLDH aptamers. Aptamer binding to both r*Pf*LDH and r*Pv*LDH was observed in EMSA for aptamers rLDH 1 and 7; however, aptamers rLDH 4 and 15 exhibited specific r*Pf*LDH interactions demonstrating consistency with ELONA screening (**Figure 4.4**) under the tested conditions. However, in kinetic ELONA studies none of the rLDH class of aptamers showed species specificty (**Table 4.1**). This is attributed to differences in protein and aptamer concentrations for the EMSA, kinetic ELONA studies (**Table 4.1**) and the ELONA screening (**Figure 4.4**), as well as the variance in binding kinetics observed for the tested aptamer sequences. A specific sequence at a high concentration of r*Pv*LDH for example may show binding for a specific experiment. EMSA further showed that binding of the rLDH class of aptamers to mLDH did not occur. Statistically insignificant rLDH aptamer interactions to the r*Pf*LDH were shown for GelRed assays (unlike LDHp class of aptamers). SPR data provided conflicting results for rLDH 4 and 7 binding to the immobilised r*Pf*LDH and r*Pv*LDH (and HSA) and no kinetic data could readily be obtained using this method. However, binding between rLDH 4 aptamer to native LDH in *P. falciparum* was visually demonstrated using both epifluorescent and confocal microscopy (**Chapter 5**). Binding between rLDH 7 aptamer to native LDH in *P. falciparum* was validated using the more sensitive confocal fluorescent microscopy.

From **Chapter 4**, four of the five of the LDHp aptamers screened bound to the LDHp target, as determined using ELONA and/or GelRed assays; the exceptions being LDHp 14 using ELONA and LDHp 1 using the GelRed assay. Moreover, some LDHp aptamers were shown to bind to the larger recombinant *Pf*LDH with LDHp 11 exhibiting statistically significantly higher colorimetric responses for r*Pf*LDH over the remaining LDHp aptamers. Kinetic data for LDHp 1, 11 and 18 to r*Pf*LDH demonstrated the ability of these three aptamers to bind to the larger, protein – and not only the smaller peptide – indicating that they were able to complex to the tertiary conformation of the epitope found on the larger recombinant *Pf*LDH. This ability of LDH recognition was tested on r*Pv*LDH in ELONA whereupon the LDHp class of aptamers exhibited no binding interactions with r*Pv*LDH, as well as mammalian LDH (mLDH) and human serum albumin (HSA). At least one aptamer

candidate, LDHp 11, therefore shows a consistent ability to speciate between *Plasmodium* LDH: binding to not only the intended target, LDHp, but showing a clear preference for r*Pf*LDH over recombinant LDH from *P. vivax* (r*Pv*LDH), human serum albumin (HSA) and mammalian LDH (mLDH) using ELONA and EMSA. SPR showed that LDHp 11 as analyte was able to elicit a qualitative discrimination between the malarial species through binding interactions with their respective LDH enzymes; however, quantitative SPR showed non-discriminatory binding between the two *Plasmodium* LDHs. While similar in biomolecular arrangement, the fluorescence-based FLONA was unable to validate these ELONA results given the lack of sensitivity.

The ability of at least one of the LDHp aptamers to bind to the whole recombinant r*Pf*LDH, as well as the initial LDHp target, demonstrates a cross-over binding between targets. The LDHp class of aptamers showed no binding to LDH of another species, specifically *Pv*LDH, resulting in specific detection of r*Pf*LDH over r*Pv*LDH, eg. LDHp 1, 11 and 18. Compared to the eight total LDHp-targeting sequences produced from SELEX, this ability of these three LDHp-targeting aptamers to bind to both r*Pf*LDH and LDHp demonstrate that their tertiary structure conformations conferred such binding reactions. The sequences of aptamers rLDH 4 and rLDH 15 were comparable to those of the LDHp aptamers in that the sequences are distinct, so inferring unique tertiary structures. In ELONA screening studies (**Figure 4.4**), rLDH 4 and rLDH 15 indicated preferential binding to r*Pf*LDH relative to r*Pv*LDH as stated above (but not in kinetic ELONA studies). Indeed, rLDH 4 showed the highest OD response in the ELONA studies for r*Pf*LDH as per **Figure 4.4**. Therefore, the tertiary structures of the aptamers LDHp 11 and to a lesser extent rLDH 4 and rLDH 15 can infer preferential target recognition. Thus, aptamers generated against a smaller, structurally relevant moiety of a larger protein in a separate and parallel SELEX were able to bind to the larger protein and also distinguish between structurally similar species.

Following aptamer screening and simultaneous identification of aptamers capable of binding the recombinant *Pf*LDH, biosensor platforms (impedimetric, fluorescent, colorimetric) were explored based on the ultimate application of the aptamer as a biosensor for the detection of *Pf*LDH as a diagnostic agent. These were explored in **Chapter 5**, and included EIS and fluorescent microscopy as the sensing platforms, whereas Malstat/LDH activity assays explored colorimetric approaches.

Fluorescent microscopy showed clear detection of LDH in *P. falciparum* parasites using aptamers LDHp 1, LDHp 11, rLDH 4 and rLDH 7 (comparable to the mean fluorescent intensities of the anti-

r*Pf*LDHp IgY with LDHp 11 and above that of pL1). While LDHp 1 showed stable binding in a flow through system, SPR, it was also found to bind weakly to the native *Pf*LDH given the intensity of fluorescence in fluorescent microscopy, rendering this aptamer as not suitable for diagnostic purposes. LDHp 11 demonstrated strong binding, equivalent to the anti-r*Pf*LDH IgY antibody, given the FITC fluorescence intensity and the proportion of FITC-fluorescing bodies. Therefore, fluorescent microscopy visually demonstrated binding between LDHp 11 to native LDH in *P. falciparum*, substantiating the responses seen in ELONA, SPR and EMSA. This data compliments the results obtained with antibodies raised against the same peptide (Hurdayal *et al*., 2010). Species-specificity and selectivity of aptamer LDHp 11 is very promising for the development of a biosensor to detect *P. falciparum* and is an important finding in this study.

For EIS, while feasible given the statistically significant change in R_{CT} at the analyte concentration extreme of 3.5 µM LDHp, there was no appreciable R_{CT} change in EIS observed in **Chapter 5** using LDHp 11 as ligand across the LDHp concentration range prepared for physiologically-relevant levels of LDH. This lack of sensitivity demonstrated that EIS was not suitable for the detection of r*Pf*LDH. Further studies using any of these generated aptamers, will warrant the optimisation of the electrode surface assembly, sensor operation and operating target concentration range.

Malstat/LDH activity could be utilised in colorimetric aptasensing possibly for the application of a colorimetric diagnostic technique such as that of APTEC (Dirkzwager *et al*., 2015). In this work, the addition of aptamers to the reaction mix lead to a broad inhibition of r*Pf*LDH activity in the Malstat and NBT/PES assay, even for the C7 control. However, inhibition of r*Pv*LDH was not similarly observed for all aptamers, with only aptamers rLDH 4 and 15 and LDHp 1, 3, 11 and 18 exhibiting r*Pv*LDH inhibition. Those aptamers that did not significantly alter r*Pv*LDH activity, specifically rLDH 1 and 7 and LDHp 14, could be used in a diagnostic device utilising the APTEC method. Inhibition of native *Pf*LDH *in vitro* activity was similarly observed in cultured *P. falciparum* cells, particularly for aptamers LDHp 11 and rLDH 15, which hold promise as malaria therapeutic agents. However, considering the physiological and cell-based impediments and barriers of aptamer uptake into live parasites, use of aptamers as direct antagonists in *Plasmodium* parasites is currently limited.

Taken together, a general consistency in binding interactions of these generated aptamers to their targets was observed across the techniques used (for example, LDHp 11); however, inconsistencies were observed for specific aptamer-target interactions in particular techniques (rLDH 4, for

example). For example, when considering results for rLDH 4, ELONA presented as an accessible technique for the purposes of r*Pf*LDH detection. However, a poor fluorescent response was observed in FLONA, yet rLDH 4 binding was observed in fluorescent microscopy. Therefore, these inconsistencies in binding to r*Pf*LDH and LDHp, as well as the other control proteins, demonstrates the clear necessity to select a number of diverse aptamer-target binding assessment techniques that complement each other and provide a thorough inspection of binding such that a full assessment of the utilised technique/s is achieved. Furthermore, the validation technique used is dependent on the ultimate application of the aptamer: if the aptamer is designed for biosensing applications in an EIS platform in which the aptamer is immobilised, validation using EMSA may not be as relevant as ELONA, for example. The aptamer may be more conducive for target recognition and binding when immobilised since solution phase binding would perhaps offer more freedom to adopt different conformations. It is for this reason that aptamers generated in this study were able to show conclusive results which were further validated in fluorescent microscopy given the freedom of the aptamer to conform and adopt the necessary tertiary structure of *Pf*LDH recognition and binding. Therefore, having a complete understanding of the binding interactions between the specific aptamer and target across particular techniques aids in the development of a technique specific for the proposed biosensing platform in which the aptamer is to be used.

Also, another contributing factor to target recognition contributing to inconsistencies between techniques would also include the aptamers' 5'-modification, whether it is the larger biotin or fluorophore, or the smaller thiol group, as these would have an inherent effect on tertiary conformation. For example, thiolation of LDHp 11 for EIS lowered the affinity for LDHp, but biotinylated LDHp 11 was otherwise shown to bind to LDHp in ELONA and GelRed assays. Therefore, when screening aptamers for target binding, it is imperative that more than one platform is used to prove that the aptamer is indeed binding to the specific target. Moreover, the validation technique needs to be relevant for the ultimate application of the aptamer.

This study utilises aptamers generated in parallel against full-length r*Pf*LDH- and r*Pf*LDH peptide-targeting SELEX procedures able to differentiate between *P. falciparum* and *P. vivax* LDH employing a species-specific epitope, and could be extended to other species of malaria. The basis behind this discrimination is owing to the fact that aptamers, upon conformation into their particular tertiary structures, are able to specifically bind to their target. The ability of these aptamers presented in this thesis to detect native *Pf*LDH, therefore, paves the way to the application of these generated

aptamers as detection molecules in optical sensing techniques specifically employing fluorescent microscopy. Convenient and portable diagnostic tests that use technology that is main-stream in society and employ visualisation techniques, such as, microscopy, UV-vis colourimetry and fluorescence, are gaining much interest, as in the case of Brelauer and co-workers (2009), who developed a smart mobile phone device with an attached microscope capable of imaging *P. falciparum*, as well as tuberculosis, using both fluorescence and bright-field imaging. Such application of and advances in technology hold promise in the field of optical biosensors.

This work demonstrates key findings with respect to aptamer synthesis: target cross reactivity, species specificity and technique validation. A key finding from this work, specifically shown in ELONA and fluorescent microscopy, is that an aptamer generated against a species-specific epitope of *Plasmodium falciparum* (LDHp 11) demonstrated greater specific binding to r*Pf*LDH than the rLDH class of aptamers, themselves generated against the full-length r*Pf*LDH. This is the first aptamer set where the aptamers were selected against a conserved peptide epitope on *P. falciparum* lactate dehydrogenase and in which the aptamers have specificity to the larger recombinant LDH protein. While *Pf*LDH-specific (monoclonal) antibodies differentiated between a *P. falciparum* and *P. vivax* LDH (Hurdayal *et al*., 2010), the aptamers generated herein have similarly shown promise in that at least one aptamer (LDHp 11) has shown promise in speciation of *P. falciparum* and *P. vivax*. Therefore, application of a rapid diagnostic device incorporating LDHp 11 (inferring species specificity) in the development of an aptamer-based sensing technology is possible. This study paves the way to explore aptamer generation against targeted species-specific epitopes of other *Plasmodium* species.

6.2. Future recommendations

Future directions for SELEX

Since this SELEX process was conducted, advances in SELEX technologies and methodologies have been made. The current method of generating aptamer capable of binding to a specific epitope on a specific protein is not to perform two separate SELEX procedures (parallel SELEX) as was done in this work. Rather, a single, dual-target SELEX (hybrid SELEX) can be performed generating high-affinity target-binding-aptamers.

Furthermore, there have been numerous developments in commercially-available protocols and reagents since this work began. As an example, significant differences by Macherey-Nagel GmbH & Co. KG, the manufacturer of the Nucleospin Gel and PCR Clean-up kits (see their online protocol available at: http://www.mn-net.com/Portals/8/attachments/Redakteure_Bio/Protocols/DNA%20clean-up/UM_PCRcleanup_Gelex_NSGelPCR.pdf), to the advantage of those currently performing SELEX . Therefore, there is now no further need to run an agarose gel in the excision of DNA as they have developed a buffer system and protocol which allows for the extraction of DNA directly from polyacrylamide gels. Use of this technique would likely have reduced loss of precious target-binding dsDNA experienced during the SELEX of r*Pf*LDH- and LDHp-binding oligonucleotides, as:

1. Due to the high load capacity of polyacrylamide gels, extraction of dsDNA directly from PAGE expedites the purification and concentration of the desired 90-bp dsDNA as the additional step of running the agarose gel is not required.
2. Polyacrylamide gels are 1 mm in thickness compared to the varied thicknesses of agarose gels. The thinness that PAGE provides leads to less perpendicular diffusion, and possible loss of DNA, as a more concentrated DNA band is resolved on PAGE.

In conjunction with an agarose gel excision, dsDNA from all polyacrylamide gels in a given round of PCR amplification or SELEX could also have been extracted in instances where target-binding dsDNA recovery was low.

Applications of developed aptamers

While consensus sequences targeting r*Pf*LDH (rLDH 2, 3, 5, 6, 9, 10, 12 and 14) did not show binding to their target in ELONA, and given that ELONA has shown non-specific binding, potential binding of these sequences should be further explored using an alternative screening technique, such as EMSA or even FLONA. EMSA, simulating the selection conditions, would be more suited in the event that immobilisation of protein/oligonucleotide prior to binding hinders any interaction. Circular dichroism and X-ray crystallography could be used to explore secondary and tertiary LDHp 11 stability, respectively, upon interactions with r*Pf*LDHp, as well as the recombinant *Pf*LDH. This will also ascertain, and confirm, binding sites between LDHp 11 and r*Pf*LDH.

Future research should explore the use of these generated aptamers in a biosensor assembly using clinical samples. Aptamers, rLDH 4 and LDHp 11, can be incorporated into a biosensor assembly

using colourimetry, fluorescence and/or chemiluminescence to detect *Plasmodium falciparum* in clinical samples, such as whole blood. Such an application can be further extended to the use of gold nanoparticles to colorimetrically measure binding of aptamers rLDH 4 and LDHp 11 to r*Pf*LDH as little interference is inferred by the gold nanoparticles. Studies on the distribution of LDH within the parasite probed with IgY and aptamers using immunoelectron microscopy at different stages of parasite intra-erythrocytic development are also proposed.

Other Plasmodium targets

Currently, there is no antibody- or aptamer-based RDT available for the detection of *Plasmodium knowlesi*. Therefore, scope exists to develop aptamers for this strain of malaria for application in sensing and detection technologies.

Aptasensing

The microscopy study can be further extended to explore the distribution of LDH within the parasite probed with IgY and aptamers using immunoelectron microscopy at different stages of parasite intra-erythrocytic development. Therefore, further exploration into fine-tuning fluorescent assays to sensitively detect *Pf*LDH over other protein targets is also recommended for future researchers.

REFERENCES

1. Abe R, Sakashita E, Yamamoto K, Sakamoto H (1996) Two different RNA binding activities for the AU-rich element and the poly(A) sequence of the mouse neuronal protein mHuC. *Nucleic Acids Research*. **24**(24) 4895-4901.

2. Ahmad KM, Oh SS, Kim S, McClellen FM, Xiao Y, Tom Soh H (2011) Probing the limits of aptamer affinity with a microfluidic SELEX platform. *PLoS ONE*. **6**(11): e27051. doi:10.1371/journal.pone.0027051.

3. Alam KK, Chang JL, Burke DH (2015) FASTAptamer: A bioinformatic toolkit for high throughput sequence analysis of combinatorial selections. *Molecular Therapy – Nucleic Acids*. **4**(3): e230. doi:10.1038/mtna.2015.4

4. Al-Hakiem MHH, Landon J, Smith DS, Nargesi RD (1981) Fluorimetric assays for avidin and biotin based on biotin-induced fluorescence enhancement of fluoroscein-labeled avidin. *Analytical Chemistry*. **166**(2):264-267.

5. Alifrangis M, Enosse S, Pearce R, Drakeley C, Roper C, Khalil IF, Nkya W, Ronn AM, Theander TG, Bygjerg IBC (2005) A simple, high-throughput method to detect *Plasmodium falciparum* single nucleotide polymorphisms in the dihydrofolate reductase, dihydropteroate synthase, and *P. falciparum* chloroquine resistance transporter genes using polymerase chain reaction- and enzyme-linked immunosorbent assay-based technology. *Aerican Journal of Tropical Medicine and Hygeine.***72**: 155-162.

6. Amaya-González S, López-López L, Miranda-Castro R, de-los-Santos-Álvarez N, Miranda-Ordieres AJ, Lobo-Castañón MJ (2015) Affinity of aptamers binding 33-mer gliadin peptide and gluten proteins: Influence of immobilization and labeling tags. *Analytica Chimica Acta*. **873**: 63-70.

7. Anderson BJ, Larkin C, Guja K, Schildbach JF (2008) Using fluorophore-labeled oligonucleotides to measure affinities of protein-DNA interactions. *Methods in Enzymology*. **450**: 253-272.

8. Antczak M, Popenda M, Zok T, Zurkowski M, Adamiak WR, Szachniuk M (2018) New algorithms to represent complex pseudoknotted RNA structures in dot-bracket notation. *Bioinformatics*. **34**(8): 1304-1312.

9. Apella E, Markert CL (1961) Dissociation of lactate dehydrogenase into subunits with guanidine hydrochloride. *Biochemical and Biophysical Research Communications*. **6**: 171-176.

10. Aptekar S, Arora M, Lawrence CL, Lea RW, Ashton K, Dawson T, Alder JE, Shaw L (2015) Selective Targeting to glioma with nucleic acid aptamers. *PLoS ONE* 10(8): e0134957. https://doi.org/10.1371/journal.pone.0134957

11. Artimo P, Jonnalagedda M, Arnold K, Baratin D, Csardi G, de Castro E, Duvaud S, Flegel V, Fortier A, Gasteiger E, Grosdidier A, Hernandez C, Ioannidis V, Kuznetsov D, Liechti R, Moretti S, Mostaguir K, Redaschi N, Rossier G, Xenarios I, Stockinger H (2012) ExPASy: SIB bioinformatics resource portal. *Nucleic Acids Research.* **40**(W1): W597-W603.

12. Ashley EA, Touabi M, Ahrer M, Hutagalung R, Htun K, Luchavez J, Dureza C, Proux S, Leimanis M, Lwin MM, Koscalova A, Comte E, Hamade P, Page A-L, Nosten F, Guerin PJ (209) Evaluation of three parasite lactate dehydrogenase-based rapid diagnostic tests for the diagnosis of falciparum and vivax malaria. *Malaria J.* **8**: 241.

13. Ausländer D, Wieland M, Ausländer S, Tigges M, Fussenegger M (2011) Rational design of a small molecule-responsive intramer controlling transgene expression in mammalian cells. *Nucleic Acids Research*. **39**(22):e155.

14. Avci-Adali M, Paul A, Wilhelm N, Ziemer G, Wendel HP (2010) Upgrading SELEX technology by using Lambda exonuclease digestion for single-stranded DNA generation. *Molecules*. **15**: 1-11.

15. Bachmann B, Lüke W, Hunsmann G (1990) Improvement of PCR amplified DNA sequencing with the aid of detergents. *Nucleic Acids Research*. **18**(5): 1309.

16. Bagalkot V, Zhang L, Levy-Nissenbaum E, Jon S, Kantoff PW, Langer R, Farokhzad OC (2007) Quantum dot-aptamer conjugates for synchronous cancer imaging, therapy, and sensing of drug delivery based on bi-fluorescence resonance energy transfer. *Nano Letters*. **7**: 3065-3070.

17. Baker J, McCarthy J, Gatton M, Kyle DE, Belizario V, Luchavez J, Bell D, Cheng Q (2005) Genetic diversity of *Plasmodium falciparum* histidine-rich protein 2 (PfHRP2) and its effect on the performance of PfHRP2-based rapid diagnostic tests. *Journal of Infectious Diseases*. **192**: e870-e877.

18. Baldrich E, Restrepo A, O'Sullivan CK (2004) Aptasensor development: Elicidation of critical parameters for optimal aptamer performance. *Analytical Chemistry*. **76**: 7053-7063.

19. Baldrich E (2010) Aptamer: Versatile tools for reagentless aptasensing. *In Recognition Receptors in Biosensors*. Zourob M (Ed) Springer, New York, USA. Pp 675-722.

20. Ban C, Jeon W, Lee S (2012) DNA aptamer specifically binding to pLDH (*Plasmodium* lactate dehydrogenase). US patent 0316325 A1. United States Patent Application Publication. Available at http://www.google.com/patents/US20120316325. Accessed 21/9/2014.

21. Banerjee A, Majumder P, Sanyal S, Singh J, Jana K, Das C, Dasgupta D (2014) The DNA intercalators ethidium bromide and propidium iodide also bind to core histones. *FEBS Open Bio*. **4**: 251-259.

22. Bartel DP, Szostak JW (1993) Isolation of new ribozymes from a large pool of random sequences. *Science* **261:** 1411-1418.

23. Battig, MR, Wang Y (2014) Chapter 17 – Nucleic acid aptamers for biomaterials development. In *Natural and Synthetic Biomedical Polymers*. Kumbar SG, Laurencin CT, Deng M (Eds.) Elsevier, UK. Pp 287-299.

24. Beelman CA, Parker R (1995) Degredation of mRNA in eukaryotes. *Cell*. **81**(2): 179-183.

25. Bell SD, Denu JM, Dixon JE, Ellington AD (1998) RNA molecules that bind to and inhibit the active site of a tyrosinase phosphatase. *Journal of Biological Chemistry*. **273**: 14309-14314.

26. Bell D, Wongsrichanalai C, Barnwell JW (2006) Ensuring quality and access for malaria diagnosis: how can it be achieved? *Nature Reviews*. **4**: 7-20.

27. Berezhnoy A, Stewart CA, McNamara JO, Thiel W, Giangrande P, Trinchieri G, Gilboa E. (2012) Isolation and optimisation of murine IL-10 receptor blocking oligonucleotide aptamers using high-throughput sequencing. *Molecular Therapy*. **20**(6): 1242-1250.

28. Berezovski M, Musheev M, Drabovich A, Krylov SN (2005) Non-SELEX selection of aptamers. *Journal of the American Chemical Society*. **128**: 1410-1411.

29. Berwal G, Gopalan N, Chandel K, Prasad GBKS, Prakash S. (2008) *Plasmodium falciparum*: Enhanced soluble expression, purification and biochemical characterization of lactate dehydrogenase. *Experimental Parasitology*. **120:** 135–141.

30. Bharti PK, Chandel HS, Ahmad A, Krishna S, Udhayakumar V, Singh N (2016) Prevalence of pfhrp2 and/or pfhrp3 gene deletion in *Plasmodium falciparum* population in eight highly endemic states in India. *PLoS ONE*. **11**(8):e0157949. doi: 10.1371/journal.pone.0157949.

31. Biancardi A, Biver T, Secco F, Mennucci B (2013) An investigation of the photophysical properties of minor groove bound and intercalated DAPI through quantum-mechanical and spectroscopic tools. *Physical Chemistry Chemical Physics.* **15:** 4596-4603.

32. Bianchini M, Radrizzani M, Brocardo MG, Reyes GB, Solveyra CG, Santa-Coloma TA (2001) Specific oligobodies against ERK-2 that recognize both the native and the denatured state of the protein. *Journal of immunological Methods*. **252**: 191-197.

33. Bigaillon C, Fontan E, Cavallo JD, Hernandez E, Spiegel A (2005) Ineffectiveness of the Binax NOW malaria test for diagnosis for *Plasmodium ovale* malaria. *Journal of Clinical Microbiology*. **43**: 1011.

34. Bio-RAD Laboratories, Inc. (2016) Bulletin 6040 A guide to polyacrylamide gel electrophoresis and detection. http://www.bio-rad.com/webroot/web/pdf/lsr/literature/Bulletin_6040.pdf (Accessed 24/10/2016)

35. Biotium (2013) FAQs for GelRed™ and GelGreen™ Dyes. http://216.19.65.49/product/ product_info/ other/GelRed%20and%20GelGreen%20FAQ.pdf (Accessed 22/1/2016)

36. Biyani M, Nishigaki K (2003) Sequence-specific and nonspecific mobilities of single-stranded oligonucleotides observed by changing the borate buffer concentration. *Electrophoresis*. **24**(4) 628-33.

37. Blank M, Weinschenk T, Priemer M, Schluesener H (2001) Systematic evolution of a DNA aptamer binding to rat brain tumor microvessels. Selective targeting of endothelial regulatory protein pigpen. *Journal of Biological Chemistry.* **276**: 16464–16468.

38. Blind M, Blank M (2015) Aptamer selection technology and recent advances. *Molecular Therapy – Nucleic Acids*. **4**(1): e223. doi:10.1038/mtna.2014.74

39. Bolger R, Lenoch F, Allen E, Meiklejohn B, Burke T (1997) Fluorescent dye assay for detection of DNA in recombinant protein products. *BioTechniques*. **23**: 532-537.

40. Brahms J, Michelson AM, van Holde KE (1966) Adenylate oligomers in single- and double-strand conformation. *Journal of Molecular Biology*. **15**: 467-488.

41. Braun D, Fromherz P (1997) Fluorescence interference-contrast microscopy of cell adhesion on oxidized silicon. *Applied Physics A*. **65**: 341-348.

42. Brelauer DN, Maamari RN, Switz NA, Lam WA, Fletcher DA (2009) Mobile Phone Based ClinicalMicroscopy for Global Health Applications. *PLoS ONE*. **4**: e6320. doi:10.1371/journal.pone.0006320

43. Brown NP, Leroy C, Sander C (1998) MView: A Web compatible database search or multiple alignment viewer. *Bioinformatics*. **14**(4): 380-381.

44. Brown WM, Yowell CA, Hoard A, Vander Jagt TA, Hunsaker LA, Deck LM, Royer RE, Piper RC, Dame JB, Makler MT, Vander Jagt DL (2004) Comparitive structural analysis and kinetic properties of lactate dehydrogenases from the four species of human malarial parasites. *Biochemistry*. **43**: 6219-6229.

45. Brownie J, Shawcross S, Theaker J, Whitcombe D, Ferrie R, Newton C, Little S (1997) The elimination of primer-dimer accumulation in PCR. *Nucleic Acids Research*. **25**: 3235-3241.

46. Bull P, Lowe B, Kortor M, Molyneux C, Newbold C, Marsh K (1998) Parasite antigens on the infected red cell surface are targets for naturally acquired immunity to malaria. *Nature Medicine*. **4**: 358-360.

47. Byrne B, Stack E, Gilmartin N, O'Kennedy R (2009) Antibody-based sensors: Principles, problems and potential for detection of pathogens and associated toxins. *Sensors*. **9**: 4407-4445.

48. Caprette DR (2012) Preparing protein samples for electrophoresis. Experimental Biosciences. (Online resource). Rice University, Houston, Texas, United States. Accessed 14 Jan 2019. Available at: https://www.ruf.rice.edu/~bioslabs/studies/sds-page/denature.html.

49. Caroli J, Taccioli C, De La Fuente A, Serafini P, Bicciato S (2016) APTANI: a computational tool to select aptamers through sequence-structure motif analysis of HT-SELEX data. *Bioinformatics*. **32**(2) 161–164.

50. Carothers JM, Oestreich SC, Davis JH, Szostak JW (2004) Informational complexity and functional activity of RNA structures. *Journal of the American Chemical Society*. **126**(16): 5130-5137.

51. Carret CK, Horrocks P, Konfortov B, Winzeler E, Qureshi M, Newbold C, Ivens A (2005) Microarray-based comparative genomic analyses of the human malaria parasite *Plasmodium falciparum* using Affymetrix arrays. *Molecular and Biochemical Parasitology*. **144**: 177-186.

52. Cash KJ, Heeger AJ, Plaxo KW, Xiao Y (2009) Optimisation of a reusable, DNA pseudoknot-based electrochemical sensor for sequence-specific DNA detection in blood serum. *Analytical Chemistry*. **81**(2): 656-661.

53. Cataldo R, Leuzzi M, Alfinito E (2018) Modelling and development of electrical aptasensors: a short review. *Chemosensors*. 6:20. doi:10.3390/chemosensors6020020

54. Centre for Disease Control (CDC) (2018) Malaria: About Malaria. https://www.cdc.gov/malaria/about/. Accessed 2 February 2019.

55. Chai C, Xie Z, Grotewold E (2011) SELEX (Systematic Evolution of Ligands by EXponential Enrichment), as a powerful tool for deciphering the protein–DNA interaction space. In: *Plant Transcription Factors*. Yuan L andand Perry S (Eds) Methods in Molecular Biology (Methods and Protocols), Vol 754. Humana Press

56. Chaiyaroj SC, Coppel RL, Novakovic S, Brown GV (1994) Multiple ligands for cytoadherence can be present simultaneously on the surface of Plasmodium falciparum-infected erythrocytes. *Proceedings of the National Academy of Sciences of the United States of America*. **91**: 10805-10808.

57. Chakma B, Jain P, Singh NV, Goswami P (2018) Development of electrochemical impedance spectroscopy based malaria aptasensor using HRP-II as target biomarker. *Electroanalysis*. **30**(8): 1847-1854.

58. Chang B-Y, Park S-M (2010) Electrochemical impedance spectroscopy. *Annual Review of Analytical Chemistry*. **3**: 207-229.

59. Chen CH, Dellamaggiore KR, Ouellette CP, Sedano CD, Lizadjohry M, Chernis GA, Gonzales M, Baltasar FE, Fan AL, Myerowitz R, Neufeld EF (2008a) Aptamer-based endocytosis of a lysosomal enzyme. *Proceedings of the National Academy of Sciences of the United States of America.* **105**(41): 15908-15913.

60. Chen X, Kube DM, Cooper MJ, Davis PB (2008b) Cell surface nucleolin serves as receptor for DNA nanoparticles composed of pegylated polylysine and DNA. *Mol*ecular *Therapy.* **16**(2): 333-342.

61. Cheung YW, Kwok J, Law AWL, Watt RM, Kotaka M, Tanner JA (2013) Structural basis for discriminatory recognition of Plasmodium lactate dehydrogenase by a DNA aptamer.

Proceedings of the National Academy of Sciences of the United States of America. **110**: 15967-15972.

62. Cheung YW, Dirkzwager RM, Wong WC, Cardoso J, Costa JDN, Tanner JA (2018) Aptamer-mediated *Plasmodium*-specific diagnosis of malaria. *Biochimie*. **145**: 131-136. DOI: 10.1016/j.biochi.2017.10.017.

63. Chiodini PL, Bowers K, Jorgensen P, Barnwell JW, Grady KK, Luchavez J, Moody AH, Cenizal A, Bell D (2007) The heat stability of *Plasmodium* lactate dehydrogenase-based and histidine-rich protein 2-based malaria rapid diagnostic tests. *Transactions of the Royal Society of Tropical Medicine and Hygiene*. **101**: 331-337.

64. Chiu T-C, Huang C-C (2009) Aptamer-functionalized nano-biosensors. *Sensors*. **9**: 10356-10388.

65. Cho EC, Choi J-W, Lee M, Koo KK (2008) Fabrication of an electrochemical immunosensor with self-assembled peptide nanotubes. *Colloids and Surfaces A*. **313-314:** 95-99.

66. Cho EJ, Lee JW, Ellington AD (2009) Applications of aptamers as sensors. *Annual Reviews in Analytical Chemistry*. **2**: 241-264.

67. Cho M, Xiao Y, Nie J, Stewart R, Csordas AT, Oh SS, Thomson JA, Soh HT (2010) Quantitative selection of DNA aptamers through microfluidic selection and high-throughput sequencing. *Proceedings of the National Academy of Sciences of the United States of America*. **107**(35): 15373-15378.

68. Citartan M, Tang TH, Tan SC, Hoe CH, Saini R, Tominaga J, Gopinath SCB (2012) Asymmetric PCR for good quality ssDNA generation towards DNA aptamer production. *Songklanakarin Journal of Science and Technology*. **34**: 125–131.

69. Coleman RE, Maneechai N, Ponlowat A, Kumpitak C, Rachapaew N, Miller RS, Sattabongkot J (2002) Failure of the OptiMAL® rapid malaria test as a tool for the detection of asymptomatic malaria in an area of Thailand endemic for *Plasmodium falciparum* and *P. vivax*. *American Society of Tropical Medicine and Hygiene.***67**: 563-565.

70. Compton SJ, Jones CG (1985) Mechanism of dye response and interference in the Bradford protein assay. *Analytical Biochemistry*. **151**: 369-374.

71. Congdon RW, Muth GW, Splittgerber AG (1993) The binding interaction of coomasie blue with proteins. *Analytical Biochemistry*. **213**: 407-413.

72. Coppel RL, Brown GV, Nussenzweig V (1998) Adhesive proteins of the malaria parasite. *Current opinion in Microbiology*. **1**: 472-481.

73. Crameri A, Stemmer WPC (1993) 10^{20}-Fold aptamer library amplification without gel purification. *Nucleic Acids Research*. **21**: 4410.

74. Cremer C, Cremer T (1978) Considerations on a laser-scanning-microscope with high resolution and depth of field. *Microscopica Acta*. **81**: 31-44.

75. Crisafuli FAP, Ramos EB, Rocha MS (2014) Characterising the interaction between DNA and GelRed fluorescent stain. *European Biophysics Journal*. **44**: 1-7.

76. Cseke LJ, Kirakosyan A, Kaufman PB (2011) DNA footprinting and gel retardation assay. *In* Handbook of molecular and cellular methods in biology and medicine (3rd Ed.) Cseke LJ, Kirakosyan A, Kaufman PB, Westfall MV (Eds) CRC Press, Florida, USA. pp 338-350.

77. Dal-Bianco MP, Köster KB, Kombila UD, Kun JFJ, Grobusch MP, Ngoma GM, Matsiegui PB, Supan C, Salazar CLO, Missinou MA, Issifou S, Lell B, Kremsner P (2007) High prevalence of asymptomatic *Plasmodium falciparum* infection in Gabonese adults. *American Journal of Tropical Medicine and Hygiene*. **77**(5): 939–942.

78. Daniel C, Roupioz Y, Gasparutto D, Livache T, Buhot A (2013) Solution-phase vs surface-phase aptamer-probe affinity from a label-free kinetic biosensor. *PloS ONE*. **8**:e75419. DOI: 10.1371/journal.pone. 0075419.

79. Davies DR, Gelinas AD, Zhang C, Rohloff JC, Carter JD, O'Connell D, Waugh SM, Wolk SK, Mayfield WS, Burgin AB, Edwards TE, Stewart LJ, Gold L, Janjic N, Jarvis TC (2012) Unique motifs and hydrophobic interactions shape the binding of modified DNA ligands to protein targets. *Proceedings of the National Academy of Sciences of the United States of America.* **109**(49): 19971-19976

80. Davydova AS, Vorobjeva MA, Venyaminova AG (2011) Escort aptamers: new tools for the targeted delivery of therapeutics into cells. *Acta Naturae*. **3**(4): 12-29.

81. Dawson W, Fujiwara K, Futamura Y, Yamamoto K, Kawai G (2006) A method for finding optimal RNA secondary structures using a new entropy model (vsfold). *Nucleosides, Nucleotides, and Nucleic Acids.* **25**: 171-189.

82. Dellinger M, Gèze M (2001) Detection of mitochondrial DNA in living animal cells with fluorescence microscopy. *Journal of Microscopy*. **204**: 196-202.

83. de-los-Santos-Álvarez N, Lobo-Castañón MJ, Miranda-Ordieres AJ, Tuñón-Blanco P (2008) Aptamers as recognition elements for label-free analytical devices. *Trends in Analytical Chemistry*. **27**(5): 437-446.

84. Demirev PA, Feldman AB, Kongkasuriyachi D, Scholl P, Sullivan D, Kumar N (2002) Detection of malaria parasites in blood by laser desorption mass spectroscopy. *Analytical Chemistry*. **74**: 3262-3266.

85. Deng B, Lin Y, Wang C, Li F, Wang Z, Zhang H, Li X-F, Le XC (2014) Aptamer binding assays for proteins: The thrombin example – A review. *Analytica Chimica Acta*. **837**: 1-15.

86. Dieffenbach CW, Dveksler GS (2003) PCR primer: a laboratory manual. 2nd Ed. Cold Spring Harbour Laboratory Press, USA. Pp. 520.

87. Dirkzwager RM, Kinghorn AB, Richards JS, Tanner JA (2015) APTEC: aptamer-tethered enzyme capture as a novel rapid diagnostic test of malaria. *Chemical Communications*. **51**: 4697-4700.

88. Djallé D, Gody JC, Moyen JM, Tekpa G, Ipero J, Madji N, Breurec S, Manirakzia A (2014) Performance of Paracheck™-Pf, SD Bioline malaria Ag-Pf and SD Bioline malaria Ag-Pf/pan for diagnosis of falciparum malaria in the Central African Republic. *BMC Infectious Diseases*. **14**: 109.

89. Drabovich A, Krylov SN (2004) Single-stranded DNA-binding protein facilities gel-free analysis of polymerase of polymerase chain reaction products in capillary electrophoresis. *Journal of Chromatography A*. **1051**: 171-175.

90. Drolet DW, Moon-McDermott L, Romig TS (1998) An enzyme-linked oligonucleotide assay. *Nature Biotechnology*. **14**: 1021-1025.

91. Dunn KW, Kamocka MM, McDonald JH (2011) A practical guide to evaluating colocalisation in biological microscopy. *American Journal of Physiology-Cell Physiology*. **300**: C723-C742.

92. Edgar RC (2004) MUSCLE: multiple sequence alignment with high accuracy and high throughput. *Nucleic Acids Research.* **32**(5): 1792-1797.

93. Ellington AD, Szostak JW (1990) *In vitro* selection of RNA molecules that bind specific ligands. *Nature*. **346**: 818-822.

94. Ellis KJ, Morrison JF (1982) Buffers of constant ionic strength for studying pH-dependent processes. *Methods in Enzymology*. **87**: 405-426.

95. Estrela P, Paul D, Li P, Keighley SD, Migliorato P, Laurenson S, Ko-Ferrigno P. (2008) Label-free detection of protein interactions with peptide aptamers by open circuit potential measurement. *Electrochemica Acta*. **53:** 6489 – 6496.

96. Ferapontova EE, Olsen EM, Gothelf KV (2008) An RNA aptamer-based electrochemical biosensor for detection of theophylline in serum. *Journal of the American Chemistry Society*. **130**: 4256-4258.

97. Firdous S, Anwar S, Rafya R (2018) Development of surface plasmon resonance (SPR) biosensors for use in the diagnostics of malignant and infectious diseases. *Laser Physics Letters*. **15**(6): 065602. DOI: 10.1088/1612-202X/aab43f

98. Fischer LM, Tenje M, Heiskanen AR, Masuda N, Castillo J, Bentien A, Emneus J, Jakobsen MH, Boisen A (2009) Gold cleaning methods for electrochemical detection applications. *Microelectronic Engineering*. **86**: 1282-1285.

99. Florens L, Washburn MP, Raine JD, Anthony RM, Grainger M, Haynes JD, Moch, JK, Muster N, Sacci JB, Tabb DL, Witney AA, Wolters D, Wu Y, Gardner MJ, Holder AA, Sinden RE, Yates JR, Carucci DJ (2002) A proteomic view of the *Plasmodium falciparum* life cycle. *Nature*. **419**: 520-526.

100. Frank R, Hargreaves R (2003) Clinical biomarkers in drug discovery and development. *Nature Reviews Drug Discovery*. **2**(7): 566-580.

101. Fraser LA, Kinghorn AB, Dirkzwager RM, Liang S, Cheung YW, Lim B, Shiu SC, Tang MSL, Andrew D, Manitta J, Richards JS, Tanner JA (2018) A portable microfluidic aptamer-tethered enzyme capture (APTEC) biosensor for malaria diagnosis. *Biosensors andand Bioelectronics*. **100**: 591-596.

102. Fried M, Crothers DM (1981) Equilibria and kinetics of lac repressor–operator interactions by polyacrylamide gel electrophoresis. *Nucleic Acids Research*. **9**: 6505−6525.

103. Frith KA, Fogel R, Goldring J, Krause R, Khati M, Hoppe H, Cromhout ME, Jiwaji M, Limson JL (2018) Towards development of aptamers that specifically bind to lactate dehydrogenase of *Plasmodium falciparum* through epitopic targeting. *Malaria Journal.* **17**(1): 191. doi:10.1186/s12936-018-2336-z

104. Froehlich P. (1989) Understanding the sensitivity specification of spectrofluorometers. *International Laboratory*. **19**: 42-45.

105. Fu XH (2008) Electrochemical measurement of DNA hybridization using nanosilver as label and horseradish peroxidase as enhancer. *Bioprocess and Biosystems Engineering*. **31**: 69-73.

106. Fuke M, Thomas CA, Jr. (1970) Isolation of open-circular DNA molecules by retention in agar gels. *Journal of Molecular Biology*. **52**(2): 395-397.

107. Gagnon KT, Maxwell ES (2011) Electrophoretic mobility shift assay for characterizing RNA–protein interaction. In: Nielsen H. (eds) *RNA*. *Methods in Molecular Biology (Methods and Protocols)*, vol 703. Humana Press.

108. Gaillard C, Strauss F (2000) DNA loops and semicatenated DNA junctions. *BMC Biochemistry*. **1**: 1-7.

109. Gamboa D, Ho MF, Bendezu J, Torres K, Chiodini PL, Barnwell JW, Incardona S, Perkins M, Bell D, McCarthy J, Cheng Q.(2010) A large proportion of P. falciparum isolates in the Amazon region of Peru lack pfhrp2 and pfhrp3: implications for malaria rapid diagnostic tests. *PLoS ONE*. **5**(1):e8091. doi: 10.1371/journal.pone.0008091.

110. Gascuel O, Steel M (2006) Neighbor-joining revealed. *Molecular Biology and Evolution*. **23**(11): 1997-2000.

111. Gassmann M, Thommes P, Weiser T, Hubscher U (1990) Efficient production of egg yolk antibodies against a conserved mammalian protein. *FASEB*. **4**: 2528-2532.

112. Gening LV, Klincheva SA, Reshetnjak A, Grollman AP, Miller H (2006) RNA aptamers selected against DNA polymerase β inhibit the polymerase activities of DNA polymerases β and κ. *Nucleic Acids Research*. **34**(9): 2579-2586.

113. Gerstl S, Dunkley S, Mukhtar A, De Smet M, Baker S, Maikere J (2010) Assessment of two malaria rapid diagnostic tests in children under five years of age, with follow-up of false-positive pLDH test results, in a hyperendemic *falciparum* malaria area, Sierra Leone. *Malaria J.* **9**: 28.

114. Godonoga M, Lin TY, Oshima A, Sumitomo K, Tang MSL, Cheung YW, Kinghorn AB, Dirkzwager RM, Zhou C, Kuzuya A, Tanner JA, Heddle JG (2016) A DNA aptamer recognizing a malaria protein biomarker can function as part of a DNA origami assembly. *Nature Scientific Reports*. **6**: 21266. doi:10.1038/srep21266.

115. Gold L, Janjic N, Jarvis T, Schneider D, Walker JJ, Wilcox SK, Zichi D (2012) Aptamers and the RNA world, past and present. *Cold Spring Harbor Perspectives in Biology*. **4**(3): a003582. doi:10.1101/cshperspect.a003582

116. Gomez MS, Piper RC, Hunsaker LA, Royer RE, Deck LM, Makler MT, Vander Jagt DL (1997) Substrate and cofactor specificity and selective inhibition of lactate dehydrogenase from the malarial parasite *P. falciparum*. *Molecular and Biochemical Parasitology*. **90**(1): 235-246.

117. González VM, Martin ME, Fernáandez G, Gargia-Sacristán A (2016) Use of aptamers as diagnostics tools and antiviral agents for human viruses. *Pharmaceuticals (Basel)*. **9**(4):78.

118. Gopinath SCB. (2007) Methods developed for SELEX. *Analytical and Bioanalytical Chemistry.* **387**(1):171-182. https://doi.org/10.1007/s00216-006-0826-2

119. Gould H, Matthews HR (1976) Separation methods for nucleic acids and oligonucleotides. *In Laboratory Techniques in Biochemistry and Molecular Biology*. Vol 4. Work TS, Work E. (Eds). North-Holland-American Elsevier Publishing, Amsterdam-New York.-Pp 241-252.

120. Green RJ, Frazier RA, Shakesheff KM, Davies MC, Roberts CJ, Tendler SJ. (2000) Surface plasmon resonance analysis of dynamic biological interactions with biomaterials. *Biomaterials*. **21**: 1823-1835.

121. Grobusch MP, Alpermann U, Schwenke S, Jelinek T, Warhurst DC (1999) False-positive rapid tests for malaria in patients with rheumatoid factor. *Lancet.* **353**: 297.

122. Grobusch MP, Hanscheid T, Gobels K, Slevogt H, Zoller T, Rogler G, Teichmann D (2003) Comparison of three antigen detection tests for diagnosis and follow-up of falciparum malaria in travellers returning to Berlin, Germany. *Parasitological Research.* **89**: 354–357.

123. Guex N, Peitsch MC (1997) SWISS-MODEL and the Swiss-PdbViewer: An environment for comparative protein modeling. *Electrophoresis.* **18**: 2714-2723.

124. Guo L-H, Facci JS, McLendon G, Mosher R (1994) Effect of gold topography and surface pretreatment on the self-assembly of alkanethiol monolayers. *Langmuir*. **10**: 4588-4593.

125. Guo Q, Lu M, Marky LA, Kallenbach NR (1992) Interaction of the dye ethidium bromide with DNA containing guanine repeats. *Biochemistry*. **10**: 2451-2455.

126. Haeberli P (2002) BestFit. (c)1982-2002. Accelrys Inc. A subsidiary of Pharmacopeia, Inc. Available at: http://www.biology.wustl.edu/gcg/bestfit.html. Accessed: 5 March 2019.

127. Hamaguchi N, Ellington A, Stanton M (2001) Aptamer beacons for the direct detections of proteins. *Analytical Biochemistry*. **294**: 126-131.

128. Han K, Liang Z, Zhou N (2010) Design strategies for aptamer-based biosensors. *Sensors*. **10**: 4541-4557.

129. Hao YY, Liu L, Zhang LH, Huang QL, Wang F, Li J, Xu JQ, Wang LH (2018) Real-time label-free analysis of the thermostability of DNA structures using GelRed. *Nuclear Science and Techniques*. **29**: 138. https://doi.org/10.1007/s41365-018-0486-x

130. Harmann T, Patel DJ (2000) Adaptive recognition by nucleic acid aptamers. *Science*. **287**(5454): 820-825.

131. Harvey SA, Jennings L, Chinyama M, Masaninga F, Mulholland K, Bell DR (2008) Improving community health worker use of malaria rapid diagnostic tests in Zambia: package instructions, job aid and job aid-plus-training. *Malaria J.* **7**: 160.

132. Hauch KD, Ratner BD (2013) Microscopy for biomaterials science. In *Biomaterials Science* (3rd Ed.) Ratner BD, Hoffman AS, Schoen FJ, Lemons JE (Eds.) Academic Press, Elsevier, Oxford, United Kingdom. Pp 677-692.

133. Hernandez FJ, Stockdale KR, Huang L, Horswill AR, Behlke MA, McNamara JO (2012) Degradation of nuclease-stabilized RNA oligonucleotides in mycoplasma-contaminated cell culture media. *Nucleic Acids Therapy*. **22**(1): 58-68.

134. Hernandez LI, Flenker KS, Hernandez FJ, Klingelhutz AJ, McNamara JO, Giangrande PH (2013) Methods for evaluating cell-specific, cell-internalising RNA aptamers. *Pharmaceuticals*. **6**: 295-319.

135. Hellman LM, Fried MG (2007) Electrophoretic mobility shift assay (EMSA) for detecting protein-nucleic acid interactions. *Nature Protocols*. **2**: 1849-1861.

136. Hicke BJ, Marion C, Chang YF, Gould T, Lynott CK, Parma D, Schmidt PG, Warren S (2001) Tenascin-C aptamers are generated using tumor cells and purified protein. *Journal of Biological Chemistry*. **276**(52): 48644-48654.

137. Holden N, Tacon C (2011) Principles and problems of the electrophoretic mobility shift assay. *Journal of Pharmacological Toxicology Methods*. **63**: 7-14.

138. Homann M, Göringer HU (2001) Uptake and intracellular transport of RNA aptamers in African trypanosomes suggest therapeutic "piggy-back" approach. *Bioorganic and Medicinal Chemistry*. **9**(10): 251-2580.

139. Hoogvliet JC, Dijksma M, Kamp B, van Bennekom WP (2000) Electrochemical pretreatment of polycrystalline gold electrodes to produce a reproducible surface roughness for self-assembly: A study in phosphate buffer pH 7.4. *Analytical Chemistry*. **72**(9): 2016-2021.

140. Hsiang MS, Greenhouse B, Rosenthal PJ (2014) Point of care testing for malaria using LAMP, loop mediated isothermal amplification. *Journal Infectious Diseases*. **210**: 1167-1169.

141. Huizenga DE, Stozak JW (1995) A DNA aptamer that binds adenosine and ATP. *Biochemistry*. **34**: 656-665.

142. Hulka BS (1991) Epidemiological studies using biomarkers: Issues for epidemiologists. *Cancer Epidemiology, Biomarkers and Prevention*. **1**(1): 13-19.

143. Hurdayal R, Achilonu I, Choveaux D, Coetzer THT, Goldring JPD (2010) Anti-peptide antibodies differentiate between plasmodial lactate dehydrogenases. *Peptides*. **31**: 525-532.

144. Hybarger G, Bynum J, Williams RF, Valdes JJ, Chambers JP (2006) A microfluidic SELEX prototype. *Analytical and Bioanalytical Chemistry*. **384**(1): 191-198.

145. Ikebukuro K, Kiyohara C, Sode K (2005) Novel electrochemical sensor system for protein using the aptamers in sandwich manner. *Biosensors and Bioelectronics*. **20**: 2168–2172.

146. Ilgu M, Nilsen-Hamilton M (2016) Aptamers in analytics. *Analyst*. **141**: 1551-1568.

147. Innis MA, Myambo KB, Gelfand DH, Brow MAD (1988) DNA sequencing with Thermus aquaticus DNA polymerase and direct sequencing of polymerase chain reaction-amplified DNA. *Proceedings of the National Academy of Sciences of the United States of America*. **85**: 9436-9440.

148. Iqbal J, Hira PR, Cher A, Al-Enezi AA (2001) Diagnosis of imported malaria by *Plasmodium* lactate dehydrogenase (pLDH) and histidine-rish protein 2 (*Pf*HRP-2)-based immunocapture assays. *American Journal of Tropical and Medical Hygiene.* **64**: 20-23.

149. Iqbal J, Siddique A, Jameel M, Hira PR (2004) Persistent histidine-rich protein 2, parasite lactate dehydrogenase, and panmalarial antigen reactivity after clearance of *Plasmodium falciparum* monoinfection. *Journal of Clinical Microbiology*. **42**: 4237-4241.

150. Isaksson J, Acharya S, Barman J, Cheruku P, Chattopadhyaya J (2004) Single-stranded adenine-rich DNA and RNA retain structural characteristics of their respective double-stranded conformations and show directional differences in stacking pattern. *Biochemistry*. **43**: 1596-1601.

151. Ishii, K Fukui M (2001) Optimisation of annealing temperature to reduce bias caused by a primer mismatch in multitemplate PCR. *Applied and Environmental Microbiology*. **67**(8(:3753-3755.

152. Jain P, Chakma B, Patra S, Goswami P (2014) Potential biomarkers and their applications for rapid and reliable detection of malaria. *BioMed Research International*. **2014**: 852645. http://dx.doi.org/10.1155/
2014/852645

153. Jang IK, Tyler A, Lyman C, Kahn M, Kalnoky M, Rek JC, Arinaitwe E, Adrama H, Murphy M, Imwong M, Ling CL, Proux S, Haohankhunnatham W, Rist M, Seilie AM, Hanron A, Daza G, Chang M, Das S, Barney R, Rashid A, Landier J, Boyle DS, Murphy SC, McCarthy JS, Nosten F, Greenhouse B, Domingo GJ (2019) Simultaneous quantification of *Plasmodium* antigens and host factor C-reactive protein in asymptomatic individuals with confirmed malaria by use of a novel multiplex immunoassay. *Journal of Clinical Microbiology*. **57**(1): pii: e00946-18. doi: 10.1128/JCM.00948-18.

154. Jayasena SD (1999) Aptamers: An emerging class of molecules that rival antibodies in diagnostics. *Clinical Chemistry.***45**(9): 1928-1650.

155. Jensen MA, Straus N (1993) Effect of PCR conditions on the formation of heteroduplex and single-stranded DNA products in the amplification of bacterial ribosomal DNA spacer regions. *Genome Research*. **3**(3): 186–194.

156. Jeon W, Lee S, Manjunatha DH, Ban C (2013) A colorimetric aptasensor for the diagnosis of malaria based on cationic polymers and gold nanoparticles. *Analytical Biochemistry*. **439**: 11-16.

157. Jeong S, Paeng IR (2012) Sensitivity and selectivity on aptamer-based assay: The determination of tetracycline residue in bovine milk. *The Scientific World Journal*. Article ID 159456: 1-10. doi:10.1100/2012/159456.

158. Jian F, Kumar RA, Jones RA, Patel DJ (1996) Structural bases if RNA folding and aptamer recognition in an AMP-RNA aptamer complex. *Nature*. **382**: 183-186.

159. Jiang Y, Fang X, Bai C (2004) Signaling aptamer/protein binding by a molecular light switch complex. *Analytical Chemistry*. **76**(17): 5230-5235.

160. Jianrong C, Yuqing M, Nongyue H, Xiaohua W, Sijiao L. (2004) Nanotechnology and biosensors. *Biotechnology Advances.* **22**: 505-518.

161. Jolly P, Estrela P, Ladomery M (2016) Oligonucleotide-based systems: DNA, microRNAs, DNA/RNA aptamers. *Essays in Biochemistry*. **60**(1): 27-35.

162. Joseph MJ, Taylor JC, McGown LB, Pitner B, Linn CP (1996) Spectroscopic studies of YO and YOYO fluorescent dyes in a thrombin-binding DNA ligand. *Biospectroscopy*. **2**: 173-183.

163. Josephy PD, Eling T, Mason RP (1982) The horseradish peroxidase-catalyzed oxidation of 3,5,3',5'-tetramethylbenzidine. Free radical and charge-transfer complex intermediates. *Journal of Biological Chemistry*. **257**: 3669-3675.

164. Joshi R, Janagama H, Dwivedi HP, Senthil Kumar TMA, Jaykus LA, Schefers J, Sreevatsan S (2009) Selection, characterisation, and application of DNA aptamers for the capture and detection of *Salmonella enteric* serovars. *Molecular and Cellular Probes*. **23**(1): 20-28.

165. Kalle E, Gulevich A, Rensing C (2013) External and semi-internal controls for PCR amplification of homologous sequences in mixed templates. *Journal of Microbiological Methods*. **95**:285-294.

166. Kang J, Lee MS, Gorenstein DG (2005) The enhancement of PCR amplification of a random sequence DNA library by DMSO and betaine: Application to *in vitro* combinatorial selection of aptamers. *Journal of Biochemical and Biophysical Methods*. **64**: 147-151.

167. Kang Y, Feng K-J, Chen J-W, Jiang J-H, Shen G-L, Yu R-Q (2008) Electrochemical detection of thrombin by sandwich approach using antibody and aptamer. *Bioeectrochemistry*. **73**: 76-81.

168. Kapuscinski J (1995). DAPI: a DNA-specific fluorescent probe. *Biotechnic and Histochemistry.* **70**: 220–33.

169. Katalius E, Flores C, Woodbury NW (2007) Exploring the sequence space of a DNA aptamer using microarrays. *Nucleic Acids Research.* **35**(22): 7626-7635.

170. Kaushal DC, Kaushal NA, Chandra D (1995) Monoclonal antibodies against lactate dehydrogenase of *Plasmodium knowlesi*. *Indian Journal of Experimental Biology*. **33**(1): 6-11.

171. Kaushal DC, Kaushal NA (2002) Diagnosis of malaria by detection of plasmodial lactate dehydrogenase with an immunodot enzyme assay. *Immunological Investigations*. **31**(2): 93-106.

172. Kaushal NA, Kaushal DC (2014) Production and characterization of monoclonal antibodies against substrate specific loop region of *Plasmodium falciparum* lactate dehydrogenase. *Immunological Investigations*. **43**(6): 556-571.

173. Keefe AD, Pai S, Ellington A (2010) Aptamers as therapeutics. *Nature Reviews Drug Discovery.* **9**: 537–550.

174. Keighley SD, Li P, Estrela P, Migliorato P (2008) Optimization of DNA immobilization on gold electrodes for label-free detection by electrochemical impedance spectroscopy. *Biosensors and Bioelectronics***. 23**: 1291 – 1297.

175. Kifude CM, Rajasekariah HG, Sullivan DJ Jr, Stewart VA, Angov E, Martin SK, Diggs CL, Waitumbi JN. (2008) Enzyme-linked immunosorbent assay for detection of *Plasmodium falciparum* histidine-rich protein 2 in blood, plasma, and serum. *Clinical and Vaccine Immunology*. **15**: 1012–1018.

176. Kim YS, Gu, MB (2014) Advances in aptamer screening and small molecule aptasensors. *Advances in Biochemical Engineering and Biotechnology*. **140**: 29-67.

177. Kimoto M, Shirouzu M, Mizutani S, Koide H, Kaziro Y, Hirao I, Yokoyama S (2002) Anti-(Raf-1) RNA aptamers that inhibit Ras-induced Raf-1 activation. *European Journal of Biochemistry*. **269**: 697–704.

178. Kong TF, Ye W, Peng, WK, Hou HW, Preiser PR, Hguyen N-T, Han J (2015) Enhancing malaria diagnosis through microfluidic cell enrichment and magnetic resonance relaxometry detection. *Scientific Reports*. **5**: 11425. DOI:10.1038/srep11425

179. Krause RGE (2016) Developing antibodies against *Plasmodium* lactate dehydrogenase, glyceraldehyde-3-phosphate dehydrogenase and phosphoethanolamine-N-methyltransferase. MSc Thesis (UKZN). Pp.106.

180. Krause RGE, Hurdayal R, Choveaux D, Przyborski JM, Coetzer THT, Goldring JPD (2017) Plasmodium glyceraldehyde-3-phosphate dehydrogenase: A potential malaria diagnostic target. *Experimental Parasitology*. **179**: 7-19.

181. Krylova SM, Koshkin V, Bagg E, Schofield CJ, Krylov SN (2012) Mechanistic studies on the application of DNA aptamers as inhibitors of 2-oxoglutarate-dependent oxygenases*. Journal of Medicinal Chemistry*. **55**(7): 3546-3552.

182. Kwon Y, Han Z, Karatan E, Mrksich M, Kay BK (2004) Antibody arrays prepared by cutinase-mediated immobilization on self-assembled monolayers. *Analytical Chemistry*. **76**(19): 5713-5720.

183. LaBaer J, Ramachandran N (2005) Protein microarrays as tools for functional proteomics. *Current Opinion in Chemical Biology*. **9**(1): 14-19.

184. Labarca C, Paigen K (1979) A simple, rapid and sensitive DNA assay procedure. *Analytical Biochemistry.* **102**: 344-352.

185. Laczka O (2014) Immunosensors: Using antibodies to develop biosensors for detecting pathogens and their toxins. In: Gopalakrishnakone P. (eds) Toxinology. Springer, Dordrecht. Pp 19. doi.org/10.1007/978-94-007-6645-7_16-1

186. Lakhin AV, Tarantul VZ, Gening LV (2013) Aptamers: Problems, solutions and prospects. *Acta Naturae*. **5**(4): 34-43.

187. Larkin MA, Blackshields G, Brown NP, Chenna R, McGettigan PA, McWilliam H, Valentin F, Wallace IM, Wilm A, Lopez R, Thompson JD, Gibson TJ, Higgins DG (2007) Clustal W and Clustal X version 2.0. *Bioinformatics*. **23**(21): 2947-8.

188. Larsson A, Carlander D, Wilhelmsson M (1988) Antibody response in laying hens with small amounts of antigen. *Food and Agricultural Immunology*. **10**: 29-36.

189. Latham JA, Johnson R, Toole JJ (1994) The application of a modified nucleotide in aptamer selection: novel thrombin aptamers containing –(1-pentynyl)-2'-deoxyuridine. *Nucleic Acids Research*. **22**(14): 2817-2822.

190. Lawyer FC, Stoffel S, Saiki RK, Chang SY, Landre PA, Abramson RD, Gelfand DH (1993) High-level expression, purification, and enzymatic characterization of full-length *Thermus aquaticus* DNA polymerase and a truncated form deficient in 5' to 3' exonuclease activity. *Genome Research*. **2**(4): 275-287.

191. Lee GC, Jeon ES, Le DT, Kim TS, Yoo JH, Kim HY, Chong CK (2011) Development and evaluation of a rapid diagnostic test for *Plasmodium falciparum*, *P. vivax*, and mixed species malaria antigens. *American Journal of Tropical and Medical Hygiene*. **85:** 989–993.

192. Lee JH, Canny MD, De Erkenez A, Krilleke D, Ng YS, Shima DT, PArdi A, Jucker F (2005) A therapeutic aptamer inhibits angiogenesis by specifically targeting the heparin binding domain. *Proceedings of the National Academy of Sciences of the United States of America*. **102**(52): 18902-18907.

193. Lee S, Song K-M, Jeon W, Jo H, Shim Y-B, Ban C (2012) A sensitive aptasensor towards Plasmodium lactate dehydrogenase for the diagnosis of malaria. *Biosensor and Bioelectronics*. **35**: 291-296.

194. Leech JH, Barnwell JW, Miller LH, Howard RJ (1984) Identification of a strain-specific malarial antigen exposed on the surface of Plasmodium falciparum-infected erythrocytes. *Journal of Experimental Medicine*. **159**: 1567-1575.

195. Leenaars M, Hendriksen CF (2005) Critical steps in the production of polyclonal and monoclonal antibodies: Evaluation and recommendations. *ILAR J*. **46**(3): 269-279.

196. Lemke EA, Schultz C (2011) Principles for designing fluorescent sensors and reporters. *Nature Chemical Biology*. **7**: 480-483.

197. Leng M, Felsenfeld G (1966) A study of polyadenylic acid at neutral pH. *Journal of Molecular Biology*. **15**: 455-466.

198. Leonetti JP Mechti N, Degols G, Gagnor C, Lebleu B (1991) Intracellular distribution of microinjected antisense oligonucleotides. *Proceedings of the National Academy of Sciences of the United States of America*. **88**: 2702-2706.

199. Levay A, Brenneman R, Hoinka J, Sant D, Cardone M, Trinchieri G, Przytycka TM, Bereshnoy A (2015) Indeifying high-affinity aptamer ligands with defined cross-reactivity using high-throughput guided systematic evolution of ligands by exponential enrichment. *Nucleic Acids Research*. **43**(12):e8. doi: 10.1093/nar/gkv534

200. Li P, Zhou L, Yu Y, Yang M, Ni S, Wei S (2015) Characterisation of DNA aptamers generated against the soft-shelled turtle iridovirus with antiviral effects. *BMC Veterinary Research*. **11**: 245.

201. Li Y, Qi H, Peng Y, Yang J, Zhang C (2007) Electrogenerated chemiluminescence aptamer-based biosensor for the determination of cocaine. *Electrochemistry Commununications*. **9**: 2571-2575.

202. Lindh J, Persson T (2009) Selection of RNA-aptamers as anti-malaria agents. Patent: CA 2714121 A1. Available at: http://www.google.com/patents/CA2714121A1?cl=en. (Accessed: 30/01/2016)

203. Lipmann NS, Jackson LR, Trudel LJ, Weis-Garcia F (2005) Monoclonal versus polyclonal antibodies: Distinguishing characteristics, applications, and information resources. *ILAR Journal*. **46**(3): 258-268.

204. Little JW (1967) An Exonuclease induced by Bacteriophage Lambda. 2. Nature of enzymatic reaction. *Journal of Biological Chemistry*. **242**: 679.

205. Liu J, You M, Pu Y, Liu H, Ye M, Tan W (2011) Recent developments in protein and cell-targeted aptamer selection and applications. *Current Medicinal Chemistry*. **18**(27): 4117-25.

206. Lorger M, Engstler M, Homann M, Göringer HU (2003) Targeting the variable surface of African trypanosomes with variant surface glycoproteins-specific serum stable RNA aptamers. *Eukaryot Cell.* **2**: 84–94.

207. Lou X, Qian J, Xiao Y, Viel L, Gerdon AE, Lagally ET, Atzberger P, Tarasow TM, Heeger AJ, Soh HT (2009) Micromagnetic selection of aptamers in microfluidic channels. *Proceedings of the National Academy of Sciences of the United States of America*. **106**(9): 2989-2994.

208. Lu S (2014) Zn2+ Blocks annealing of complementary single-stranded DNA in a sequence-selective manner. *Scientific Reports*. **4**: 5464. doi:10.1038/srep05464.

209. Lubin AA, Plaxco KW (2010) Folding-based electrochemical biosensors: the case for responsive nucleic acid architectures. *Accounts of Chemical Research*. **43**(4): 496-505.

210. Lupold SE, Hicke BJ, Lin Y, Coffey DS (2002) Identification and characterization of nuclease-stabilized RNA molecules that bind human prostate cancer cells via the prostate-specific membrane antigen. *Cancer Research*. **62**(14): 4029-4033.

211. Luppa PB, Sokoll LJ, Chan DW (2001) Immunosensors – principles and applications to clinical chemistry. *Clinica Chimica Acta.***314**: 1-26.

212. Luppa PB, Bietenbeck A, Beaudoin C, Gianetti A (2016) Clinically relevant analytical techniques, organizational concepts for application and future perspectives of point-of-care testing. *Biotechnology Advances*. doi:10.1016/j.biotechadv.2016.01.003

213. Macaya RF, Schultze P, Smith FW, Roe JA, Feigon J (1993) Thrombin-binding DNA aptamer forms a unimolecularquadruplex structure in solution. *Proceedings of the National Academy of Sciences of the United States of America*. **90**: 3745-3749.

214. Mädler S, Bich C, Touboul D, Zenobi R (2009) Chemical cross-linking with NHS esters: A systematic study on amino acid reactivities. *Journal of Mass Spectrometry*. **44**: 694-706.

215. Mairal T, Cengiz Özalp V, Lozano Sánchez P, Mir M, Katakis I, O'Sullivan CK (2008) Aptamers: molecular tools for analytical applications. *Analytical and Bioanalytical Chemistry*. **390**(4): 989-1007.

216. Makler MT, Ries JM, Williams JA, Bancroft JE, Piper RC, Gibbins BL, Hinrichs DJ (1993) Parasite lactate dehydrogenase as an assay for *Plasmodium falciparum* drug sensitivity. *American Journal of Tropical Medicine and Hygiene*. **48**(6): 739-741.

217. Malonga H, Neault JF, Arakawa H, Tajmir-Riahi HA (2006) DNA interaction with human serum albumin studied by affinity capillary electrophoresis and FTIR spectroscopy. *DNA and Cell Biology*. **25**: 63-68.

218. Maniatis T, Jeffrey A, van deSande H (1975) Chain length determination of small double- and single-stranded DNA molecules by polyacrylamide gel electrophoresis. *Biochemistry*. **14**(17): 3787-3794.

219. Mao F, Leung WY (2010) Methods of using dyes in association with nucleic acid staining or detection and associated technology. US patent: US2010323453(A1). Accessed 24 Jan 2016.

220. Markwalter CF, Ricks KM, Wright DW (2015) Immunomagnetic capture and colorimetric detections of malarial biomarker *Plasmodium falciparum* lactate dehydrogenase. *Analytical Biochemistry*. **493**: DOI: 10.1016/j.ab.2015.10.003

221. Martiney JA, Sherry B, Metz CN, Espinoza M, Ferrer AS, Calandra T, Broxmeyer HE, Bucala R (2000) Macrophage migration inhibitory factor release by macrophages after ingestion of *Plasmodium chabaudi*-infected erythrocytes: Possible role in the pathogenesis of malarial anemia. *Infection and Immunity*. **68**(4): 2259-2267.

222. Mascini M, Palchetti I, Tombelli S (2012) Nucleic acid and peptide aptamers: fundamentals and bioanalytical aspects. *Angewandte Chemie International Edition.* **51**(6): 1316-32.

223. McKeague M, DeRosa MC (2012) Challenges and opportunities for small molecule aptamer development. *Journal of Nucleic Acids*. Article ID 748913, 20 pages.

224. McKeague M, Velu R, Hill K, Bardoczy V, Meszaros T, DeRosa MC (2014) Selection and characterization of anovel DNA aptamer for label-free fluorescence biosensing of Ochratoxin A. *Toxins*. **6**: 2435-2452.

225. McKeague M, De Girolamo A, Valensano S, Pascale M, Ruscito A, Velu R, Frost NR, Hill K, Smith M, McConnell EM, DeRosa MC (2015a) Comprehensive analytical comparison of strategies used for small molecule aptamer evaluation. *Analytical Chemistry*. **87**(17): 8608-8612.

226. McKeague M, McConnell EM, Cruz-Toledo J, Bernard ED, Pach A, Mastronardi E, Zhang X, Beking M, Francis T, Giamberardino A, Cabecinha A, Ruscito A, Aranda-Rodriguez R, Dumontier M, DeRosa MC (2015b) Analysis of in vitro aptamer selection parameters. *Journal of Molecular Evolution*. **81**(5-6): 150-61.

227. Meirinho SG, Dias LG, Peres AM, Rodrigues LR (2016) Voltammetric aptamers for protein disease biomarkers detection: A review. *Biotechnology Advances*. **34**(5): 941-953.

228. Mendonsa SD, Bowser MT (2004) *In vitro* evolution of functional DNA using capillary electrophoresis. *Journal of the American Chemical Society*. **126**(1): 20-21.

229. Mi J, Zhang X, Rabbani ZN, Liu Y, Su Z, Vujaskovic Z, Kontos CD, Sullenger BA, Clary BM (2006) H1 RNA polymerase III promoter-driven expression of an RNA aptamer leads to high-level inhibition of intracellular protein activity. *Nucleic Acids Research*. **34**(12): 3577-3584.

230. Milla P, Dosio F, Cattel L (2012) PEGylation of proteins and liposomes: a powerful and flexible strategy to improve the drug delivery. *Current Drug Metabolism*. **13**(1): 105-119.

231. Miller RS, McDaniel P, Wongsrichanalai C (2001) Following the course of malaria treatment by detecting parasite lactate dehydrogenase. *British Journal of Haematology.* **113**: 558-559.

232. Mir M, Jenkins ATA, Katakis I (2008) Ultrasensitive detection based on an aptamer beacon electron transfer chain. *Electrochemistry Communications*. **10**: 1533-1536.

233. Misono TS, Kumar PKR (2005) Selection of RNA aptamers against human influenza virus hemagglutinin using surface plasmon resonance. *Analytical Biochemistry*. **342**(2): 312-317.

234. Moody A, Hunt-Cooke A, Gabbett E, Chiodini P (2000) Performance of the OptiMAL malaria antigen capture dipstick for malaria diagnosis and treatment monitoring at the Hospital for Tropical Diseases, London. *British Journal of Haematology*. **109**: 891-894.

235. Moody A (2002) Rapid diagnostic tests for malaria parasites. *Clinical Microbiology Reviews*. **15**: 66-78.

236. Moody A, Chiodini P (2002) Non-microscopic method for malaria diagnosis using OptiMAL IT, a second-generation dipstick for malaria pLDH antigen detection. *British Journal of Biomedical Science*. **59**: 228-231.

237. Morris GE, Sedgwick SG, Ellis JM, Pereboev A, Chamberlain JS, Man NT (1998) An epitope structure for the C-terminal domain of dystrophin and utrophin. *Biochemistry*. **4**: 11117-11127.

238. Mosing RK, Mendonsa SD, Bowser MT (2005) Capillary electrophoresis-SELEX selection of aptamers with affinity for HIV-11 reverse transcriptase. *Analytical Chemistry*. **77**: 6107-6112.

239. Mouatcho J, Goldring J (2013) Malaria rapid diagnostic tests: Challenges and prospects. *Journal of Medical Microbiology.* **62**: 1491-1505.

240. Musheev MU, Krylov SN (2006) Selection of aptamers by systematic evolution of ligands by exponential enrichment: addressing the polymerase chain reaction issue. *Analytica Chimica Acta.* **564**(1): 91–96.

241. Myszka DG, He X, Dembo M, Morton TA, Goldstein B (1998) Extending the range of rate constants available from BIACORE: Interpreting mass transport-influenced binding data. *Biophysical Journal.* **75***:* 583−594.

242. Nagl S, Wolfbeis OS (2008) Classification of chemical sensors and biosensors based on fluorescence and phosphorescence. In *Standardisation and Quality Assurance in Fluorescence Measurements I*. Volume 5. Resch-Genger U (Ed) Springer, Berlin, Germany. Pp 325-346.

243. Nahshol O, Bronner V, Notcovich A, Rubrecht L, Laune D, Bravman T (2008) Parallel kinetic analysis and affinity determination of hundreds of monoclonal antibodies using the ProteOn XPR36. *Analytical Chemistry.* **383**: 52-60.

244. Narayanan S, Gall J, Richert C (2004) Clamping down on weak terminal base pairs: oligonucleotides with molecular caps as fidelity-enhancing elements at the 5'- and 3'terminal residues. *Nucleic Acids Research*. **32**(9): 2901-2911.

245. Neidle S (2016) Quadruplex nucleic acids as novel therapeutic targets. *Journal of Medicinal Chemistry*. **59**(13): 5987-6011.

246. Nery AA, Wrenger C, Ulrich H (2009) Recognition of biomarkers and cell-specific molecular signatures: Aptamers as capture agents. *Journal of Separation Science*. **32**: 1523-1530.

247. Neves MA, Blaszykowski C, Bokhari S, Thompson M (2015) Ultra-high frequency piezoelectric aptasensor for the label-free detection of cocaine. *Biosensors and Bioelectronics*. **72**: 383-392.

248. Nguyen HH, Park J, Kang S, Kim M (2015) Surface Plasmon Resonance: A versatile technique for biosensor applications. *Sensors*. **15**(5): 10481-10510.

249. Nguyen N-V, Yang C-H, Liu C-J, Kuo C-H, Wu D-C, Jen C-P (2018) An aptamer-based capacitive sensing platform for specific detection of lung carcinoma cells in the microfluidic chip. *Biosensors*. **8**: 98-110.

250. Nguyen V-T, Kwon YS, Kim JH, Gu MB (2014) Multiple GO-SELEX for efficient screening of flexible aptamers. *Chemistry Communications*. **50**: 10513-10516.

251. Nieuwlandt D (2000) *In vitro* selection of functional nucleic acids. *Current Issues in Molecular Biology*. **2**(1): 9-16.

252. Niklewski A, Azzam W, Strunskus T, Fischer RA, Wöll Ch (2004) Fabrication of self-assembled monolayers exhibiting a thiol-terminated surface. *Langmuir*. **20**(20): 8620-8624.

253. Nutiu R, Li Y (2003) Structure-switching signaling aptamers. *Journal of the American Chemistry Society*. **125**: 4771-4778.

254. Ocaña C, Pacios M, del Valle M (2012) A reusable impedimetric aptasensor for detection of thrombin employing a graphite-epoxy composite electrode. *Sensors* (Basel). **12**(3): 3037-3048.

255. Ohta T, Tokishita S, Yamagata H (2001) Ethidium bromide and SYBR Green I enhance the genotoxicity of UV-irradiation and chemical mutagens in *E. coli*. *Mutation Research*. **492**: 91-97.

256. Olivier M, VanDen Ham K, Shio MT, Kassa FA, Fougeray S (2014) Malarial pigment hemozoin and the innate inflammatory response. *Frontiers in Immunology*. 5: 25. doi: 10.3389/fimmu.2014.00025

257. Ouellet E, Foley JH, Conway EM, Haynes C (2015) Hi-Fi SELEX: A high-fidelity digital-PCR based therapeutic aptamer discovery platform. *Biotechnology and Bioengineering*. **112**: 1506-1522.

258. Palmer CJ, Lindo JF, Klaskala WI, Quesada JA, Kaminsky R, Baum MK, Ager AL (1998) Evaluation of the OptiMAL test for rapid diagnosis of *Plasmodium vivax* and *Plasmodium falciparum* malaria. *Journal of Clinical Microbiology*. **36**: 203-206.

259. Pan W, Xin P, Clawson GA (2008) Minimal primer and primer-free SELEX protocols for selection of aptamers from random DNA libraries. *Biotechniques*. **4**(3):351-360.

260. Pan Y, Karns K, Herr AE (2014) Microfluidic electrophoretic mobility shift assays for quantitative biochemical analysis. *Electrophoresis*. **35**(15): 2078-2090.

261. Panchuk-Voloshina N, Haugland RP, Bishop-Stewart J, Bhalgat MK, Millar PJ, Mao F, Leung WY, Haugland RP (1999) Alexa dyes, a series of new fluorescent dyes that yield exceptionally bright, photostable conjugates. *Journal of Histochemistry and Cytochemistry*. **47**: 1179-88.

262. Paniel N, Baudart J, Hayat A, Barthelmebs L (2013) Aptasensor and genosensor methods for detection of microbes in real world samples. *Methods*. **64**: 229-240.

263. Pendergrast PS, Marsh HN, Grate D, Healy JM, Stanton M (2005) Nucleic acid aptamers for target validation and therapeutic applications. *Journal of Biomolecular Techniques*. **16**: 224-234.

264. Peng CG, Damha MJ (2007) G-quadruplex induced stabilization by 2'-deoxy-2'-fluoro-d-arabinonucleic acids (2'F-ANA). *Nucleic Acids Research.* **35**: 4977–4988.

265. Petsev DN, Thomas BR, Yau S-T, Vekilov PG. (2000) Interactions and aggregation of apoferritin molecules in solution: Effects of added electrolytes. *Biophysical Journal*. **78**(4): 2060-2069.

266. Pettersen EF, Goddard TD, Huang CC, Couch GS, Greenblatt DM, Meng EC, Ferrin TE (2004) UCSF Chimera – a visualization system for exploratory research and analysis. *Journal of Computational Chemistry*. **25**: 1605-1612.

267. Pilz I, Schwarz E, Palm W (1977) Small-angle X-ray studies of the human immunoglobulin molecule. *European Journal of Biochemistry*. **75**: 195-199.

268. Piper R, Lebras J, Wentworth L, Hunt-Cooke A, Houzé S, Chiodini P, Makler M. (1999) Immunocapture diagnostic assays for malaria using *Plasmodium* lactate dehydrogenase (*P*LDH*). American Journal of Tropical and Medical Hygiene*. **60**:109–118.

269. Popenda M, Szachiuk M, Antczak M, Purzycka KJ, Lukasiak P, Bartol N, Blazewicz J, Adamiak RW (2012) Automated 3D structure composition for large RNAs. *Nucleic Acids Research*. **40**: e112. doi:10.1093/nar/gks339

270. Portugal J, Waring MJ (1988) Assignment of DNA binding sites for 4',6-diamidine-2-phenylindole and bis-benzimide (Hoechst 33258). A comprehensive footprinting study. *Biochimica et Biophysica Acta*. **28**: 158-168.

271. Potyrailo RA, Conrad RC, Ellington AD, Hieftje GM (1998) Adapting selected nucleic acid ligands (aptamers) to biosensors. *Anaytical Chemistry*. **70**: 3419-3425.

272. Prasad A, Mahato K, Maurya PK, Chandra P (2016) Biomaterials for biosensing applications. *Journal of Analytical and Bioanalytical Techniques*. **7**: e124. doi:10.4172/2155-9872.1000e124.

273. Quan J, Tian J (2009) Circular polymerase extension cloning of complex gene libraries and pathways. *PLoS ONE*. 4(7): e6441. doi:10.1371/journal.pone.0006441.

274. Radi A-E, Sánchez JLA, Baldrich E, O'Sullivan CK (2006) Reagentless, Reusable, Ultrasensitive Electrochemical Molecular Beacon Aptasensor. *Journal of the American Chemical Society*. **128**(1): 117-124.

275. Ramaswamy V, Monsalve A, Sautina L, Segal MS, Dobson J, Allen JB. (2015) DNA Aptamer Assembly as a Vascular Endothelial Growth Factor Receptor Agonist. *Nucleic Acid Therapeutics*. **25**(5): 227-234. doi:10.1089/nat.2014.0519.

276. Randviir EP, Banks CE (2013) Electrochemical impedance spectroscopy: An overview of bioanalytical applications. *Analytical Methods*. **5**(5): 1098-1115.

277. Rapley R (1994) Enhancing PCR amplification and sequencing using DNA-binding proteins. *Molecular Biotechnology*. **2**(3): 295-298.

278. Regnier V, Le Doan T, Préat V (1998) Parameters controlling topical delivery of oligonucleotides by electroporation. *Journal of Drug Targeting.* **5**(4): 275–289.

279. Reich P, Stoltenburg R, Strehliz B, Frense D, Beckmann D (2017) Development of an impedimetric aptasensor for the detection of *Staphylococcus aureus*. *International Journal of Molecular Sciences*. **18**: 2484. doi:10.3390/ijms18112484

280. Reiter NJ, Maher LJ, Butcher SE (2008) DNA mimicry by a high-affinity anti-NF=κB RNA aptamer. *Nucleic Acids Research*. **36**: 1227-1236.

281. Robertson MP, Knudsen SM, Ellington AD (2004) *In vitro* selection of riboaymes dependent on peptides for activity. *RNA*. **10**(1): 114-127.

282. Rotherham L, Maserumule C, Dheda K, Theron J, Khati M (2012) Selection and application of ssDNA aptamers to detect active TB from sputum samples. *PLoS ONE*. **7**(10): 1-11.

283. Roux KH (2009) Optimization and troubleshooting in PCR. *Cold Spring Harbour Protocols*. **4**(4): doi:10.1101/pdb.ip66.

284. Ruckman J, Green LS, Beeson J, Waugh S, Gillette WL, Henninger DD, Claesson-Welsh L, Janjic N (1998) 2'Fluoropyrimidine RNA-based aptamers to the 165-amino acid form of vascular endothelial growth factor(VEGF165) inhibition of receptor binding and VEGF-induced vascular permeability through interactions requiring the exon 7-encoded domain. *Journal of Biological Chemistry*. **273**: 20556-20567.

285. Ruscito A, DeRosa MC (2016) Small-molecule binding aptamers: selection strategies, characterization, and applications. *Frontiers in Chemistry*. **4**: 14. doi:10.3389/fchem.2016. 00014.

286. Rusconi CP, Scardino E, Layzer J, Pitoc GA, Ortel TL, Monroe D, Sullenger BA (2002) RNA aptamers as reversible antagonists of coagulation factor IXa. *Nature*. **419**: 90–94.

287. Saitou N, Nei M (1987) The neighbor-joining method: a new method for reconstruction of phylogenetic trees. *Molecular Biology and Evolution*. 4: 406-425.

288. Sakamoto T (2017) NMR study of aptamers. *Aptamers*. **1**: 13-18.

289. Sanderson MJ, Smith I, Parker I, Bootman MD. (2014) Fluorescence microscopy. *Cold Spring Harbor protocols*. 2014(10): pdb.top071795. doi:10.1101/pdb.top071795.

290. SantaLucia J (Jr), Hicks D (2004) The thermodynamics of DNA structural motifs. *Annual Review of Biophysics and Biomolecular Structure*. **33**: 415-40.

291. Schuck P, Zhao H (2010) The role of mass transport limitation and surface heterogeneity in the biophysical characterization of macromolecular binding processes by SPR biosensing. *Methods in molecular biology (Clifton, NJ).* **627**: 15-54.

292. Schultz JS (1996) Biological and chemical components for sensors. *In Handbook of Chemical and Biological Sensors*. Taylor RF, Schultz JS (Eds). Institute of Physics Publishing Ltd., Bristol. Pp. 189-199.

293. Schütze T, Wilhelm B, Greiner N, Braun H, Peter F, Mörl M, Volker A. Erdmann, Lehrach H, Konthur Z, Menger M, Arndt PF, Glökler J (2011) Probing the SELEX process with Next-Generation Sequencing. *PLoS ONE.* **6**(12): e29604. https://doi.org/10.1371/journal.pone.0029604

294. Seida AA (2017) Monoclonal antibodies and polyclonal antibodies: A brief comparison. *Advanced Techniques in Clinical Microbiology*. **1**: 2.

295. Seiwert SD, Nahreini TS, Aigner S, Ahn NG, Uhlenbeck OC (2000) RNA aptamers as pathway-specific MAP kinase inhibitors. *Chemistry and Biology*. **7**(11): 833-843.

296. Shao K, Ding W, Wang F, Li H, Ma D, Wang H (2011) Emulsion PCR: A high efficient way of PCR amplification of random DNA libraries in aptamer selection. *PLoS ONE*. 6(9): e24910. doi:10.1371/journal.pone.0024910.

297. Shimizu M, Nagashima H, Sano K, Hashimoto K, Ozeki M, Tsuda K, Hatta H (1992) Molecular stability of chicken and rabbit immunoglobulin G. *Bioscience, Biotechnology, and Biochemistry*. **56**: 270-274.

298. Shtatland T, Gill SC, Javornik BE, Johansson HE, Singer BS, Uhlenbeck OC, Zichi DA, Gold L (2000) Interactions of *Escherichia coli* RNA with bacteriophage MS coat protein: genomic SELEX. *Nucleic Acids Research*. **28**(21): 93 – 103.

299. Simpalipan P, Pattaradolikrat S, Harnyuttanakorn P (2018) Global sequence diversity of the lactate dehydrogenase gene in *Plasmodium falciparum*. *Malaria Journal*. **17**: 16. doi.org/10.1186/s12936-017-2157-5

300. Singh NK, Arya SK, Estrela P, Goswami P (2018) Capacitive malaria aptasensor using Plasmodium falciparum glutamate dehydrogenase as target antigen in undiluted human serum. *Biosensors and Bioelectronics*. **117**: 246-252.

301. Singh P (2016) SPR biosensors: Historical perspectives and current challenges. *Sensors and Actuators B: Chemical*. **229**: 110-130.

302. Skeidsvoll J, Ueland PM (1995) Analysis of double-stranded DNA by capillary electrophoresis with laser-induced fluorescence detection using the monochromatic dye SYBR Green I. *Analytical Biochemistry*. **231**: 359-365.

303. Smith EA, Corn RM (2003) Surface plasmon resonance imaging as a tool to monitor biomolecular interactions in an array based format. *Applied Spectroscopy*. **57**(11): 320A-332A.

304. Smolarsky M, Tal M (1970) Novel method for measuring polyuridylic acid binding to ribosomes. *Biochimica et Biophysica Acta*. **199**: 447-452.

305. Sosic A, Meneghello A, Cretaio E, Gatto B (2011) Human thrombin detection through a sandwich aptamer microarray: interaction analysis in solution and in solid phase. *Sensors (Basel).* **11**(10): 9426-9441.

306. Soukup GA, Ellington AD, Maher JL (1996) Selection of RNAs that bind to duplex DNA at neutral pH. *Journal of Molecular Biology*. **259**(2): 216-22.

307. Spiga FM, Maietta P, Guiducci C (2015) More DNA-Aptamers for Small Drugs: A capture-SELEX coupled with surface plasmon resonance and high-throughput sequencing. *ACS Combinatorial Science*. **17**(5): 326-333.

308. Spill F, Weinstein ZB, Shemirani AI, Ho N, Desai D, Zaman MH (2016) Controling uncertainty in aptamer selection. *Proceedings of the National Academy of Sciences of the United States of America*. **113**(43): 12076-12081.

309. Srivastava IK, Schmidt M, Grall M, Certa U, Garcia AM, Perrin LH (1992) Identification and purification of glucose phosphate isomerase of *Plasmodium falciparum. Molecular and Biochemical Parasitology*. **54**: 153-164.

310. Stellwagen E, Renze A, Stellwagen NC (2007) Capillary electrophoresis is a sensitive monitor of the hairpin-random coil transition in DNA oligomers. *Analytical Biochemistry*. **365**(1):103-110.

311. Stellwagen NC, Stellwagen E (2009) Effect of the matrix on DNA electrophoretic ability. *Journal of Chromatography A*. **1216**(10): 1917-1929.

312. Stenberg E, Persson B, Roos H, Urbaniczky C (1991) Quantitative determination of surface concentration of protein with surface plasmon resonance using radiolabeled proteins. *Journal of Colloid and Interface Science.* **143**: 513-526.

313. Stojanovic MN, de Prada P, Laundry DW (2001) Aptamer-based folding fluorescent sensor for cocaine. *Journal of the American Chemical Society*. **123**: 4928-4931.

314. Stojanovic MN, Kolpashchikov DM (2004) Modular aptameric sensors. *Journal of the American Chemical Society*. **126**(30): 9266-9270

315. Stoltenburg R, Reinemann C, Strehlitz B (2005) FluMag-SELEX as an advantageous method for DNA aptamer selection. *Analytical and Bioanalytical Chemistry*. **383**(1): 83-91.

316. Stoltenburg R, Krafčiková P, Víglaský V, Strehlitz B (2016) G-quadruplex aptamer targeting Protein A and its capability to detect *Staphylococcus aureus* demonstrated by ELONA. *Scientific Reports*. **6**: 33812.

317. Strehlitz B, Nikolaus N, Stoltenburg R (2008) Protein detection with aptamer biosensors. *Sensors*. **8**(7): 4296-4307.

318. Sullenger BA, McNamara J, Gilboa E (2008) Aptamers as agonists. US patent. PCT/US2006/036090. Accessed 26 Jan 2018. Available at: http://www.google.com.pg/patents/EP1933850A2?cl=en.

319. Sun L, Akerman B (2014) Characterization of self-assembled DNA concatemers from synthetic oligonucleotides. *Computational and Structural Biotechnology Journal.* **11**: 66-72.

320. Sun Y, Sriramajayam K, Luo D, Liao DJ (2012) A quick, cost-effective method of purification of DNA fragments from agarose gel. *Journal of Cancer*. **3**: 93-95.

321. Suni II (2008) Impedance methods for electrochemical sensors using nanomaterials. *Trends in Analytical Chemistry*. **27**(7): 604-611.

322. Svitel J, Boukari H, Van Ryk D, Willson RC, Schuck P (2007) Probing the functional heterogeneity of surface binding sites by analysiss of experimental binding traces and the effect of mass transport limitation. *Biophysical Journal*. **92**(5): 1742-1758.

323. Sypabekova M, Bekmurzayeva A, Wang R, Li Y, Nogues C, Kanayeva D (2017) Selection, characterization, and application of DNA aptamers for detection of *Mycobacterium tuberculosis* secreted protein MPT64. *Tuberculosis*. 104: 70-8.

324. Tabarzad M, Kazemi B, Vahidi H, Aboofazeli R, Shahhosseini S, Nafissi-Varcheh N (2014) Challenges to design and develop of DNA aptamers for protein targets. I. Optimisation of asymmetric PCR for generation of a single stranded DNA library. *Iranian Journal of Pharmaceutical Research*. **13**: 133-141.

325. Takahashi M, Wu X, Ho M, Chomchan P, Rossi JJ, Burnett JC, Zhou J (2016) High throughput sequencing analysis of RNA libraries reveals the influences of initial library and PCR methods on SELEX efficiency. *Nature Scientific Reports*. **6**:33697. https://doi.org/10.1038/srep33697.

326. Talman AM, Duval L, Legrand E, Hubert V, Yen S, Bell D, Le Bras, J, Ariey F, Houze S (2007) Evaluation of the intra- and inter-specific genetic variability of *Plasmodium* lactate dehydrogenase. *Malaria Journal*. **6**: 140. doi.org/10.1186/1475-2875-6-140

327. Tan Y, Shi Y, Wu X, Liang H, Gao Y, Li S, Zhang X, Wang F, Gao T (2013) DNA aptamers that target human glioblastoma multiform cells overexpressing epidermal growth factor receptor variant III *in vitro. Acta Pharmacologica Sinica*. **34**: 1491-1498.

328. Tanner JA, Cheung YW, Kotaka M (2013) Nucleic acid aptamers against plasmodium lactate dehydrogenase and histidine-rich protein ii and uses thereof for malaria diagnosis. US Patent 0210023 A1. United States Patent Application Publication. 2013. Available at http://www.google.com/patents/US20130210023. Accessed 21/9/2017.

329. Tasset DM, Kubik MF, Steiner W (1997) Oligonulceotide inhibitors of human thrombin that bind distinct epitopes. *Journal of Molecular Biology*. **272**: 688-698.

330. The TH, Feltkamp TEW (1970) Conjugation of fluorescein isothiocyanate to antibodies. II. A reproducible method. *Immunology*. **18**: 875-881.

331. Thompson JR, Marcelino LA, Polz MF (2002) Heteroduplexes in mixed-template amplifications: formation, consequence and elimination by 'reconditioning PCR'. *Nucleic Acids Research.* **30**(9): 2083–2088

332. Tjitra E, Suprianto S, McBroom J, Currie BJ, Anstey NM (2001) Persistent ICT malaria *P.f/P.v*panmalarial and HRP2 antigen reactivity after treatment of *Plasmodium falciparum* malaria is associated with gametocytemia and results in false-positive diagnoses of *Plasmodium vivax* in convalescence. *Journal of Clinical Microbiology.* **39**: 1025-1031.

333. Tolle F, Wilke J, Wengel J, Mayer G (2014) By-product formation in repetitive PCR amplification of DNA libraries during SELEX. *PLoS ONE*. **9**(12): e114963.

334. Tomar D, Biswas S, Tripathi V, Rao, DN (2006) Development of diagnostic reagents: Raising antibodies against synthetic peptides of PfHRP-2 and LDH using microsphere delivery. *Immunobiology.* **211**: 797–805.

335. Trevino SG, Levy M (2014) High-throughput bead-based identification of structure-switching aptamer beacons. *ChemBioChem*. **15**: 1877-1881.

336. Tse WC, Boger DL (2004) A fluorescent intercalator displacement assay for establishing DNA binding selectivity and affinity. *Accounts of Chemical Research*. **37**(1): 61-69.

337. Tuerk C, Gold L (1990) Systemic Evolution of Ligands by Exponential Enrichment: RNA ligands to bacteriophage T4 DNA polymerase. *Science*. **249**: 505-510.

338. Tuerk C, MacDougal S, Gold L (1992) RNA pseudoknots that inhibit human immunodeficiency virus type 1 reverse transcriptase. *Proceedings of the National Academy of Sciences of the United States of America*. **89**: 6988-6992

339. Turgut-Balik D, Akbulut E, Shoemark DK, Celik V, Moreton KM, Sessions RB, Holbrook JJ, Brady RL (2004) Cloning, sequence and expression of the lactate dehydrogenase gene from the human malaria parasite, *Plasmodium vivax*. *Biotechnology Letters.* **26**: 1051-1055.

340. Tyagi S, Kramer FR (1996) Molecular beacons: probes that fluoresce upon hybidisation. *Nature Biotechnology*. **14**: 303-308.

341. UCSF (2013) Coulombic Surface Coloring. ©2013. University of California, San Francisco (UCSF) Computer Graphics Laboratory. Available at: https://www.cgl.ucsf.edu/chimera/data/ downloads/1.13.1/docs/ContributedSoftware/coulombic/coulombic.html. Accessed: 5 March 2019.

342. Ulrich H, Martins AHB, Pesquero JB (2004) RNA and DNA aptamers in cytomics analysis. *Cytometry*. **59A**(2): 220-231.

343. Varadaraj K, Skinner DM (1994) Denaturants or co-solvents improve the specificity of PCR amplification of a G + C-rich DNA using genetically engineered DNA polymerases. *Gene*. **140**(1): 1-5.

344. Varani L, Spilantini MG, Goebert M, Varani G (2000) Structural basis for recognition of the RNA major groove in the tau exon 10 splicing regulatory element by aminoglycoside antibiotics. *Nucleic Acids Research*. **28**: 710-719.

345. Verma P, Biswas S, Mohan T, Ali S, Rao DN (2013) Detection of histidine rich protein andand lactate dehydrogenase of *Plasmodium falciparum* in malaria patients by sandwich ELISA using in-house reagents. *Indian Journal of Medicinal Research*. **138**: 977-987.

346. Vincent A, Scherrer K (1979). A rapid and sensitive method for detection of proteins in polyacrylamide SDS gels: Staining with ethidium bromide. *Molecular Biology Reports*. **5**: 209. https://doi.org/10.1007/BF00782890

347. Vivas L, Easton A, Kendrick H, Cameron A, Lavandera JL, Barros D, de las Heras FG, Brady RL, Croft SL (2005) Plasmodium falciparum: Stage specific effects of a selective inhibitor of lactate dehydrogenase. *Experimental Parasitology*. **111**: 105-114.

348. Walker NF, Nadjm B, Whitty CJM (2009) Malaria. *Medicine*. **38**: 41-46.

349. Wandtke T, Woźniak J, Kopiński P (2015) Aptamers in diagnostics and treatment of viral infections. *Viruses*. **7**(2): 751-780.

350. Wang C, Zhang M, Yang G, Zhang D, Ding H, Wang H, Fan M, Shen B, Shao N (2003) Single-stranded DNA aptamers that bind differentiated but not parental cells: subtractive systematic evolution of ligand by exponential enrichment. *Journal of Biotechnology*. **102**(1):15-22.

351. Wang J, Meng W, Zheng X, Liu S, Li G (2009) Combination of aptamer with god nanoparticles for electrochemical signal amplification: Application to sensitive detection of platelet-derived growth factor. *Biosensors and Bioelectronics*. **24**(6): 1598-1602.

352. Wang J, Rudzinski JF, Gong Q, Soh HT, Atzberger PJ (2012) Influence of target concentration and background binding on in vitro selection of affinity reagents. *PLoS ONE.* **7**(8): e43940. https://doi.org/10.1371/journal.pone.0043940

353. Wang T, Cong X, Nilsen-Hamilton (2014) *In vitro* selection of aptamers. *In Making and using antibodies: Practical Handbook* (2nd Ed) Howard GC, Kaser MR (Eds) CRC Press, Boca Raton, USA. Pp 184-206.

354. Waring MJ (1965) Complex formation between ethidium bromide and nucleic acids. *Journal of Molecular Biology.* **13**: 269–282.

355. Whelan RJ, Wohland T, Neumann L, Huang B, Kobilka BK, Zare RN (2002) Analysis of biomolecular interactions using a miniaturized surface plasmon resonance sensor. *Analytical Chemistry*. **74**(17): 4570-4576.

356. Whiley DM, LeCornec GM, Baddeley A, Savill J, Syrmis MW, Mackay IM, Sieberth DJ, Burnsh D, Nissend M, Sloots TP (2004) Detection and differentiation of *Plasmodium* species by polymerase chain reaction and colorimetric detection in blood samples of patients with suspected malaria. *Diagnostic Microbiology and Infectious Disease*. **49**: 25-29.

357. White NJ, Olliaro (1996) Stratagies for the prevention of antimalarial drug resistance: rationale for combination chemotherapy for malaria. *Parasitology Today*. **12**: 399-401.

358. Williams R, Peisajovich SG, Miller OJ, Magdassi S, Tawfik DS, Griffiths AD (2006) Amplification of complex gene libraries by emulsion PCR. *Nature Methods*. **3**(7): 545-550.

359. Win MN, Klein JS, Smolke CD (2006) Codeine-binding RNA aptamers and rapid determination of their binding constants using a direct coupling surface plasmon resonance assay. *Nucleic Acids Research*. **34**(19): 5670-5682.

360. Wong I, Lohman TM (1993) A double-filter method for nitrocellulose-filter binding: Application to protein-nucleic acid interactions. *Proceedings of the National Academy of Sciences of the United States of America*. **90**: 5428-5432.

361. World Health Organisation (WHO) (2003) Malaria Rapid Diagnostics: Makin it work. Meeting Report 20-23 January 2003. WHO, Manilla.

362. World Health Organisation (WHO) (2009) Impact of malaria control in *World Malaria Report 2009*. WHO Press, Geneva. pp. 27.

363. World Health Organisation (WHO) (2012a) Changes in malaria incidence and mortality in *World Malaria Report: 2012*. WHO Press, Geneva. pp. 59.

364. World Health Organisation (WHO) (2012b) WHO Malaria Rapid Diagnostic Test performance: results of WHO product testing of malaria RDTs: Round 4 (2012). Geneva: World Health Organisation. http://www.who.int/malaria/publications/rapid_diagnostic/en/. Accessed 11 Nov 2017

365. World Health Organisation (WHO) (2012c) Heat stability in *Malaria Rapid Diagnostic Test performance: Results of WHO product testing of malaria RDTs: 4* (2012). WHO, Italy. pp. 44-50.

366. World Health Organisation (2016) World Malaria Report 2016. Geneva: World Health Organization; 2016. http://www.who.int/malaria/publications/world-malaria-report-2016/report/en/ 148 p. Accessed 21 June 2017.

367. World Health Organisation (2018) World Malaria Report 2018. World Health Organisation. 2018. Geneva: World Health Organization; 2016. https://apps.who.int/iris/bitstream/handle/10665/275867/9789241565653-eng.pdf?ua=1. Accessed 8 February 2019.

368. Wong I, Lohman TM (1993) A double-filter method for nitrocellulose-filter binding: Application to protein-nucleic acid interactions. *Proceedings of the National Academy of Sciences of the United States of America*. **90**: 5428-5432.

369. Wood AE, Bishop GR (2004) Probing the structure of DNA aptamers with a classic heterocycle. *Molecules*. **9**: 67-85.

370. Wu L, Curran J (1999) An allosteric synthetic DNA. *Nucleic Acids Research*. **27**: 1512-1516.

371. Xu B, Zhao C, Wei W, Ren J, Miyoshi D, Sugimoto N, Qu X (2012) Aptamer carbon nanodot sandwich used for fluorescent detection of protein. *Analyst*. **137**: 5483-5486.

372. Xu W, Ellington AD (1996) Anti-peptide aptamers recognize amino acid sequence and bind a protein epitope. *Proceedings of the National Academy of Sciences of the United States of America*. **93**(15): 7475-7480.

373. Xu Y, Yang L, Ye X, He P, Fang Y (2006) An aptamer-based protein biosensor by detecting the amplified impedance signal. *Electroanalysis*. **18**(15): 1449-1456.

374. Xu Y, Cheng G, He P, Fang Y (2009) A review: Eletrochemical aptasensors with various detection strategies. *Electroanalysis*. **21**(11): 1251-1259.

375. Yamamoto R, Baba T, Kumar PK (2000) Molecular beacon aptamer fluoresces in the presence of Tat protein of HIV-1. *Genes Cells*. **5**(5): 389-396.

376. Yang Q, Goldstein IJ, Mei H-Y, Engelke DR (1998) DNA ligands that bind tightly and selectively to cellobiose. *Proceedings of the National Academy of Sciences of the United States of America*. **95**(10): 5462-5467.

377. Yarus M, Berg P (1967) Recognition of tRNA aminoacyl tRNA synthetases. *Journal of Molecular Biology*. **28**:479-490.

378. Ying Y-L, Wang H-Y, Sutherland TC, Long YT (2011) Monitoring of an ATP-binding aptamer and its conformational changes using an α -hemolysin nanopore. *Nanopore Biosensors*. **7**(1): 87-94.

379. Yu H, Zhang W, Yu Q, Huang F-P, Bian H-D, Liang H (2017) Ni(II) complexes with Schiff base ligands: Preparation, characterisation, DNA/protein interaction and cytotoxicity studies. *Molecules*. **22**(10): 1772.

380. Zayats M, Huang Y, Gill R, Ma C, Willner I (2006) Label-free and reagentless aptamer-based sensors for small molecules. *Journal of the American Chemical Society*. **12**: 13666-13667.

381. Zhang DW, Zhang FT, Cui YR, Deng QP, Krause S, Zhou YL, Zhang XX (2012) A label-free aptasensor for the sensitive and specific detection of cocaine using supramolecular aptamer fragments/target complex by electrochemical impedance spectroscopy. *Talanta*. **92:** 65-71.

382. Zhang Y, He Y, Yeung ES (2001) High-throughput polymerase chain reaction analysis of clinical samples by capillary electrophoresis with UV detection. *Electrophoresis*. **22**(11): 2296-2302.

383. Zheng R, Park BW, Kim DS, Cameron BD (2011) Development of a highly specific amine-terminated aptamer functionalized surface plasmon resonance biosensor for blood protein detection. *Biomedical Optics Express*. **2**(9): 2731-2740.

384. Zhou W, Huang PJJ, Ding J, Liu J (2014) Aptamer-based biosensors for medical diagnostics. *Analyst*. **139**: 2627-2640.

385. Zhu Q, Liu G, Kai M (2015) DNA aptamers in the diagnosis and treatment of human diseases. *Molecules*. **20**: 20979–20997.

386. Zink D, Sadoni N, Stelzer E (2003) Visualising chromatin and chromosomes in living cells. *Methods*. **29**: 42-50.

387. Zofou D, Tene M, Ngemenya MN, Tane P, Titanji VPK (2011) *In vitro* antiplasmodial activity and cytotoxity of extracts of selected medicinal plants used by traditional healers of Western Cameroon. *Malaria Research and Treatment*. **2011**: 561342 (6 pages).

388. Zuker M (2003) Mfold web server for nucleic acid folding and hybridization prediction. *Nucleic Acids Research*. **31**: 3406-3415.

389. Zuo X, Song S, Zhang J, Pan D, Wang L, Fan C (2007) A target-responsive electrochemical aptamer switch (TREAS) for reagentless detection of nanomolar ATP. *Journal of the American Chemical Society*. **129**: 1042-1043.

APPENDIX A

The results presented in this Appendix relate to **Chapter 2**.

Transformation efficiencies for ligation reactions for oligonucleotides selected against LDHp and r*Pf*LDH are presented in Table A.1 of this Appendix A.

Table A.1: Transformation efficiencies for ligation reactions for oligonucleotides selected against LDHp and r*Pf*LDH. Bolding indicates transformation efficiencies for oligonucleotides for the oligopeptide target, LDHp, and protein target, r*Pf*LDH, under investigation.

	Blue colonies (*n*)	**White colonies (*n*)**	**Total colonies (*n*)**	**Transformation efficiency (cfu/µg DNA)**
LDHp-selected oligos	20	13	33	**10.17×10^4**
r*Pf*LDH-selected oligos	22	8	30	**8.95×10^4**
Vector control	0	0	0	0
Negative insert control	102	1	103	Undefined
Positive insert control	23	8	31	0.5×10^4

Sixteen (16) white colonies (containing oligonucleotide fragments selected against r*Pf*LDH) and 18 white colonies (containing oligonucleotide fragments selected against LDHp) were re-streaked onto a second set of Luria agar plates, and were hence selected for fragment length screening via PCR amplification. The white colour of these colonies, as opposed to blue, indicates that the *lacZ* gene of the lac operon (coding region) of the β-galactosidase enzyme was disrupted upon insertion of the dsDNA fragments at the T4 DNA ligase nick site (facilitated by the T-overhang in the pGEM vector), preventing synthesis of the enzyme. In the absence of β-galactosidase, X-Gal cannot be cleaved to form 5-bromo-4-chloro-indoxyl. Blue colonies are reflective of the absence of a dsDNA fragment insert as the β-galactosidase enzyme was transcribed using the host cell machinery. With active β-galactosidase present, cleavage of X-Gal to form 5-bromo-4-chloro-indoxyl can occur. This oxidises forming 5,5'-dibromo-4,4'-dichloro-indigo, which is responsible for the blue colour observed in some colonies seen during blue/white screening.

Table A.2 of this Appendix shows the sequences that were obtained from SELEX B, majority of which were primer dimers and concatemers, using this same primer set and library obtained from an overamplified ssDNA pool. The number of basepairs shown in Table 2 was calculated from the forward primer region, i.e. the start of the library sequence, to the end of the reverse primer binding region, i.e. the end of the library sequence.

Table A.2: The sequences that were selected against LDHp and r*Pf*LDH during SELEX B.
Sequences for each colony are in a 5' – 3' direction; reverse primer sequence is in orange, forward primer sequence is in blue and overlapping bases are in red)

Colony Number	Number of basepairs	Sequence (5' – 3')
Sequences resulting from SELEX targeting LDHp		
2	84	GCCTGTTGTGASCCTCCTAACATGCTTATTCTTGTCTCCCTTGCCTGTTGTGAGCCTCCTAACCCCATGCTTATTCTTGTCTCCC
16	119	GCCTGTTGTGAGCCTCCTAACCCCATGCTTATTCTTGTCTCCCATGCTTATTCTTGTCTCCCATGCTTATTCTTGTCTCCCATGCTTATTCTTGTCTCCCATGCTTAT TCTTGTCTCCC
19	85	TGTTGTGAGCCTCCTAACCCCATGCTTATTCTTGTCTCCCGTGCCTGTTGTGAGCCTCCTAACCCCATGCTTATTCTTGTCTCCC
23	43	GCCTGTTGTGASCCTTYCTAACCCCATGCTTATTCTTGTCTCCC
25	106	GCCTGTTGTGAGCCTCCTAACCCCATGCTTATTCTTGTCTCCCATGCTTATTCTTGTCTCCCGTGCCTGTTGTGAGCCTCCTAACCCCATGCTTATTCTTGTCTCCC
32	106	GCCTGTTGTGAGCCTGGGGTTAGGAGGCTCACAACAGGCATGGGAGACAAYAATAAGCACGGGAGACAAGAATAGTCATGGGAGACAAGAATAAGCATG
35	85	TGTTGTGAGCCTCCTAACCCCATGCTTATTCTTGTCTCCCGTGCCTGTTGTGAGCCTCCTAACCCCATGCTTATTCTTGTCTCCC
36	101	GCCTGTTGTGAGCCTCCTAACATGCTTATTCTTGTCTCCCaTGCTTATTCTTGTCTCCCGTGCCTGTTGTGAGCCTCCTAACATGCTTATTCTTGTCTCCC
37	107	GCCTGTTGTSMCTCTTCWAACCCCATGCTTATTCTTGTCTCCCATGCTTATTCTTGTCTCCCGTGCCTGTTGTGAGCCTCCTAACCCCYTGCTTATTCTTGTCTCCC
39	123	GCCTGTTGTGAGCCTCCTAACCATGCTTATTCTTGTCTCCCATGCTTATTCTTGTCTCCCACGCCTGTTGTGAGCCTCCTAACCCCATGCTTATTCTTGTCTCCC
41	130	GCCTGTTGTGAGCCTCCTAACCCCATGCTTATTCTTGTCTCCCATGCCTGTTGTGAGCCTCCTAACCCCATGCTTATTCTTGTCTCCCGTGCCTGTTGTGAGCCTCC TAACATGCTTATTCTTGTCTCCC

Sequences resulting from SELEX targeting r*Pf*LDH		
3	100	GCCTGTTGTGASCCTCCTAACCCCATGCTTATTCTTGTCTCCCATGCTTATTCTTGTCTCCCATGCTTATTCTTGTCTCCCATGCTTATTCTTGTCTCCC
5	91	GCCTGTTGTGAGCCTCCTAACATGCTTATTCTTGTCTCCCGCGCCTGTTGTGAGCCTCCTAACACTTTGCACATGCTTATTCTTGTCTCCC
7	90	GCcTGTTGTGAGCCTCCTAACCCAGAATAGGGACTGCTCGGGATTGCGGATGAGTCTGGGTGGGACATGGCATGCTTATTCTTGTCTCCC
8	107	GCCTGTTGTGAGCCTCCTAACCCCATGCTTATTCTTGTCTCCCATGCTTATTCTTGTCTCCCATGCCTGTTGTGAGCCTCCTAACCCCATGCTTATTCTTGTCTCCC
9	85	GCCTGTTGTGAGCCTCCTAACATGCTTATTCTTGTCTCCCATGCCTGTTGTGAGCCTCCTAACCCCATGCTTATTCTTGTCTCCC
13	78	GCCTGTTGTGAGCCTCCTAACATGCTTATTCTTGTCTCCCGTGCTTATTCTTGTCTCCCATGCTTATTCTTGTCTCCC
17	129	GCCTGTTGTGASCCTYCTAACATGCTTATTCTTGTCTCCCTGCCTGTTGTGAGCCTCCTAACCCCATGCTTATTCTTGTCTCCCGTGCCTGTTGTGAGCCTCCTAACCCCATGCTTATTCTTGTCTCCC
18	82	GCCTGKTGTGASCCTCCTAACATGCTTATTCTTGTCTCCCATGCCTGTTGTGAGCCTCCTAACATGCTTATTCTTGTCTCCC
21	91	GCCTGTTGTGAGCCTCCTAACATGCTTATTCTTGTCTCCCATGCCTGTTGTGAGCCTCCTAACACTTTGCACATGCTTATTCTTGTCTCCC
23	91	GCCTGTTGTGAGCCTCCTAACATGCTTATTCTTGTCTCCCATGCCTGTTGTGAGCCTCCTAACACTTTGCACATGCTTATTCTTGTCTCCC
25	-	TWCGATAGGGCGATTGGGCCCGACGTCGCATGCTCCCGGCCGCCATGGCGGCCGCGGGAATTCGATTGCCTGATGTGARCCTCATGGCACATGCTTATTCTTG GTCCCAACCTGTTGAGAGCCTCCCAACACTTTATTATGCTTATTCTTGTGTCCCCCATATGGGAGAGCTCCCGGCCGCCTGGAKGTCKACCTTGAGGAAGAGCTC CCGACRCCTTGGATGTTGGCTTGAGTATGGTATTAKGTCTTTCCTAAAGCTTGGCGTAATCATGGTCATAGCTGTTTCCTGA
26	78	GCCTGTTGTGAGCCTCCTAACATGCTTATTCTTGTCTCCCATGCTTATTCTTGTCTCCCATGCTTATTCTTGTCTCCC
27	133	GCCTGTTGTGAGCCTYCTAACCCCATGCTTATTCTTGTCTCCCATGCCTGTTGTGAGCCTCCTAACCCCATGCTTATTCTTGTCTCCCATGCCTGTTGTGAGCCTCC TAACCCCATGCTTATTCTTGTCTCCC
28	108	GCCTGTTGTGAGCCTCCTAACATGCTTATTCTTGTCTCCCATGCTTATTCTTGTCTCCCATGCTTATTCTTGTCTCCCATGCCTGTTGTGAGCCTCCTAACATGCTTA TTCTTGTCTCCC
29	128	GCCTGTTGTGAGCCTCCTAACCCCATGCTTATTCTTGTCTCCCATGCCTGTTGTGAGCCTCCTAACCATGCTTATTCTTGTCTCCCATGCCTGTTGTGAGCCTCCTA ACATGCTTATTCTTGTCTCCC
30	107	GCCTGTTGTGAGCCTCCTAACCCCATGCTTATTCTTGTCTCCCATGCTTATTCTTGTCTCCCATGCCTGTTGTGAGCCTCCTAACCCCATGCTTATTCTTGTCTCCC
31	124	GCCTGTTGTGAGCCTCCTAACCATGCTTATTCTTGTCTCCCATGCTTATTCTTGTCTCCCATGCTTATTCTTGTCTCCCATGCCTGTTGTGAGCCTCCTAACCCCATG CTTATTCTTGTCTCCC
32	85	GCCTGTTGTGAGCCTCCTAACCCCATGCTTATTCTTGTCTCCCATGCCTGTTGTGAGCCTCCTAACATGCTTATTCTTGTCTCCC

36	81	GCCTGTTGTGAGCCTcCTAACCCCATGCTTATTCTTGTCTCCCATGCTTATTCTTGTCTCCCATGCTTATTCTTGTCTCCC
37	110	GCCTGTTGTGAGCCTCCTAACATGCTTATTCTTGTCTCCCATGCTTATTCTTGTCTCCCATGCCTGTTGTGAGCCTCCTAACACTTTGCACATGCTTATTCTTGTCTCCC
39	105	GCCTGTTGTGAgCCTcCTAACCATGCTTATTCTTGTCTCCCATGCTTATTCTTGTCTCCCACGCCTGTTGTGAGCCTCCTAACCCCATGCTTATTCTTGTCTCCC

APPENDIX B

Table B.1 in Appendix B represents all sequences with inserts of ~90 bp in length generated against r*Pf*LDH and LDHp following SELEX C. This is presented to support the enrichment of oligonucleotides for the adaptation of binding to the targets and discussion thereof, in **Chapter 3.5.1**.

Table B.1: All sequences of oligonucleotides selected against r*Pf*LDH and LDHp, resulting from colony screening of SELEX pool C

Colony number	Basepair length	Sequence (5' – 3')
		Sequences generated through SELEX using r*Pf*LDH as the target
1	92	GCCTGTTGTGAGCCTCCTAACTCACGGGCAAAAAAAAAACCGTTGTGCACTTGCTGGTTGGCGGCGGTAGGTCATGCTTATTCTTGTCTCCC
2	95	GCCTGTTGTGAGCCTCCTAACTAGCTCGTAGAAAAAAAGAATAGCGTGTGCTGGGACTGCTCGGGATTGCGGACACATGCTTATTCTTGTCTCCC
3	100	GCCTGTTGTGAGCCTCCTAACAAGCTCGTAGAAAAAAAAAAAAAAATAGCGTGTGCTGGGACTGCTCGGGATTGCGGACACATGCTTATTCTTGTCTCCC
4	100	GCCTGTTGTGAGCCTCCTAACCAGCTCGTAGAAAAAAAAAGATATTGCTTCAATTATCTCCTCGCGTTCAATTAACCCAGCATGCTTATTCTTGTCTCCC
5	96	GCCTGTTGTGAGCCTCCTAACTAGCTCGTAGAAAAAAAAAAATAGCGTGTGCTGGGACTGCTCGGGATTGCGGACACATGCTTATTCTTGTCTCCC
6	96	GCCTGTTGTGAGCCTCCTAACTAGCTCGTAGAAAAAAAAAAATAGCGTGTGCTGGGACTGCTCGGGATTGCGGACACATGCTTATTCTTGTCTCCC
9	98	GCCTGTTGTGAGCCTCCTAACCAGCTCGTAGAAAAAAAAGAAGATAGCGTGTGCTGGGACTGCTCGGGATTGCGGACACATGCTTATTCTTGTCTCCC
10	98	GCCTGTTGTGAGCCTCCTAACCAGCTCGTAGAAAAAAAAGAAGATAGCGTGTGCTGGGACTGCTCGGGACTGCGGACACATGCTTATTCTTGTCTCCC
12	97	GCCTGTTGTGAGCCTCCTAACTAGCTCGTAGAAAAAAAAAAAAATAGCGTGTGCTGGGACTGCACGGGATTGCGGACACATGCTTATTCTTGTCTCCC
14	97	GCCTGTTGTGAGCCTCCTAACTAGCTCGTAGAAAAAAAAAAAAATAGCGTGTGCTGGGACTGCTCGGGATTGCGGACACATGCTTATTCTTGTCTCCC
15	94	GCCTGTTGTGAGCCTCCTAACTTTAAAGTTGCTATTTAACCAAAAAAAAAAAAATAAAAAAGTCGAGCCGGCCCCATGCTTATTCTTGTCTCCC

Table B.1 Continued on following page…

Sequences generated through SELEX using LDHp as the target

1	90	GCCTGTTGTGAGCCTCCTAACCAGGAAGCGACCTACTAAAGTGATATTATAGATTCACGGGAGCGTGGTGCATGCTTATTCTTGTCTCCC
2	109	GCCTGTTGTGAGCCTCCTAACTGAGCGCTGGGCGACAATACTTCATGAATGGTAACCGGGAAGGGGGCGACATGCTTATTCTTGTCTCCCATGCTTATTCTTGTCTCCC
3	90	GCCTGTTGTGAGCCTCCTAACTGTTACGCGGGAGAACAATTATGACCAAACCACCGATGTTAAACTCATTCATGCTTATTCTTGTCTCCC
7	90	GCCTGTTGTGAGCCTCCTAACCTAGATTAGACAAACGTGCATTGGGAACATAGCGGTGGCGTCCGAGGTGCATGCTTATTCTTGTCTCCC
11	90	GCCTGTTGTGAGCCTCCTAACCTACTGTTGATATGAGTGATAGGGCGGCGCGCTTATCTAGTGTATTGTGCATGCTTATTCTTGTCTCCC
14	90	GCCTGTTGTGAGCCTCCTAACAGCGTTCACAGCGCAAAAAAGGTAACACGTTTTACTGGACGGGCCGAGCCATGCTTATTCTTGTCTCCC
15	90	GCCTGTTGTGAGCCTCCTAACGAAGATCGCCGCCTCAAATTCCCGCATATAACTAAGCGAAAACCCACCCCATGCTTATTCTTGTCTCCC
18	90	GCCTGTTGTGAGCCTCCTAACAGTCCTCACGTGTCAGGAAATATGTTGAATCATGAGGATAAAACTGTGTCATGCTTATTCTTGTCTCCC

Forward primer regions are marked in magenta colour and reverse primer regions are in blue.

APPENDIX C

The figures and tables shown in Appendix C relate to **Chapter 4**.

Figure C.1 shows photos of the 96-well plates of the ELONA reactions used in the determination of the dissociation constants, and form additional information for **Figure 4.3** and **4.4**.

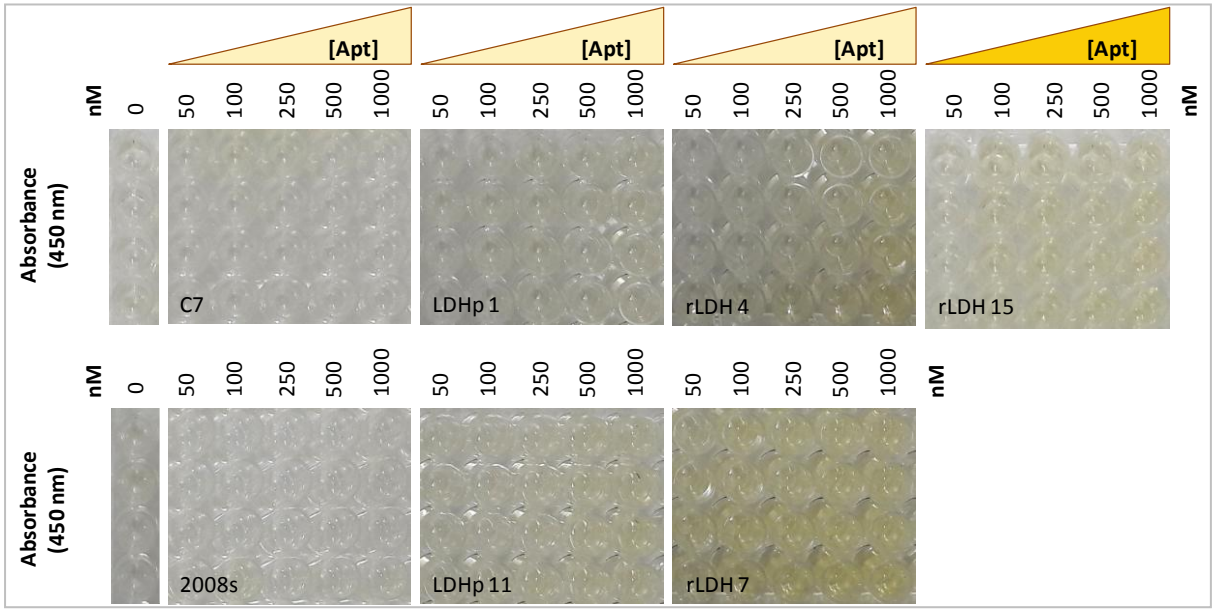

Figure C.1: The corresponding ELONA-assessed colour changes for binding affinity of 0, 50, 100, 250, 500 and 1000 nM biotinylated concatemer control, C7, previously published 2008s (Cheung *et al.*, 2013; Tanner *et al.*, 2013), LDHp 1, LDHp 11, rLDH 4 and rLDH 7 to r*Pf*LDH.

Figure C.2 shows the binding kinetics curves for LDHp 1, rLDH 7, rLDH 15, pL1 and the concatemer, C7, for binding to r*Pf*LDH and r*Pv*LDH, and form additional information to that presented in **Figure 4.9**.

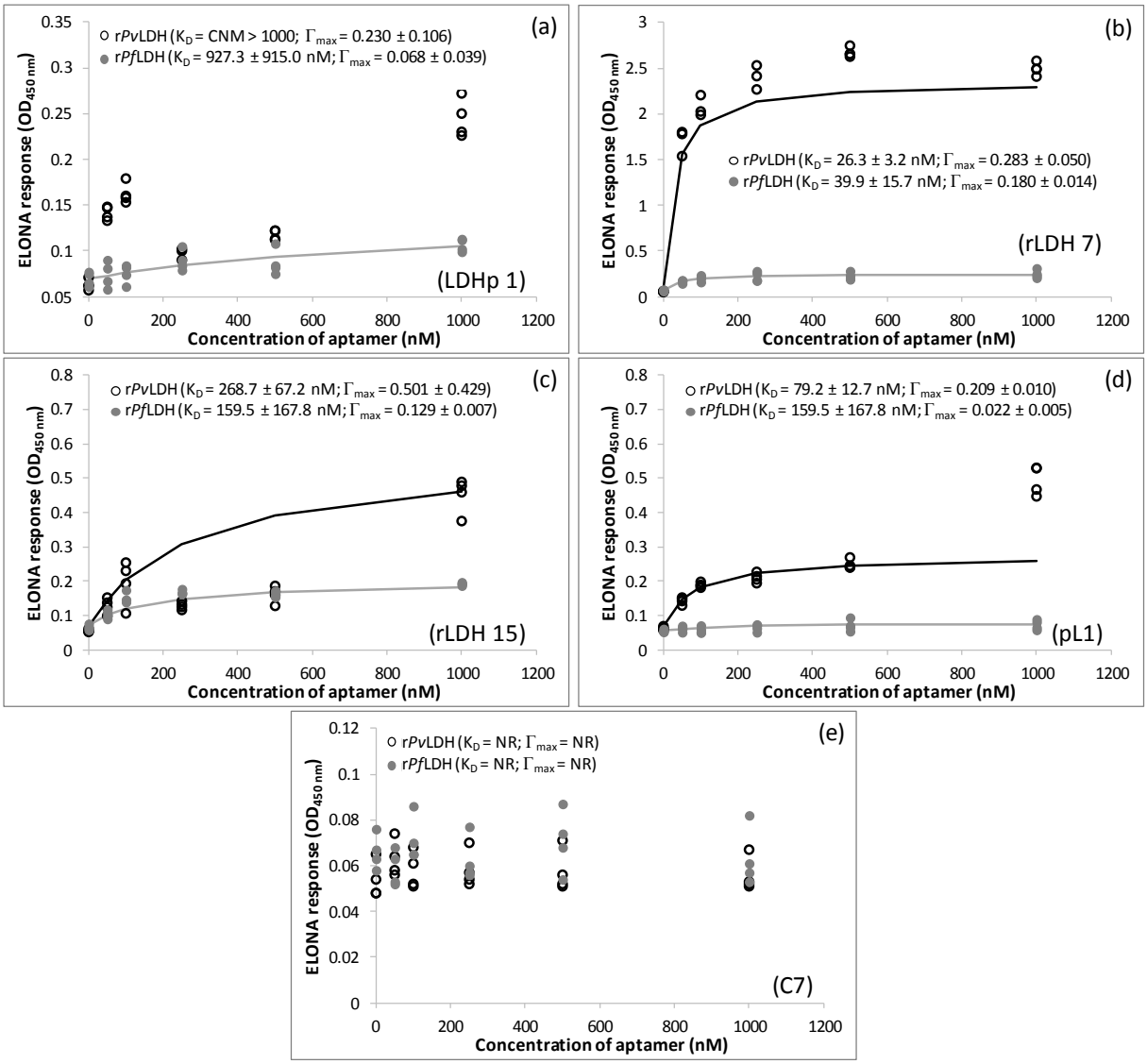

Figure C.2: ELONA-assessed (A_{450nm}) binding kinetics of 0, 50, 100, 200, 500 and 1000 nM biotinylated LDHp 1 (a), rLDH 7 (b), rLDH 15 (c), pL1 (d) and C7 (e) to r*Pf*LDH and rPvLDH (*n* = 4).

Figure C.3 shows the binding kinetics curves for LDHp 1, 3, 11, 14 and 18 binding to LDHp, and form additional information to that presented in **Figure 4.9**.

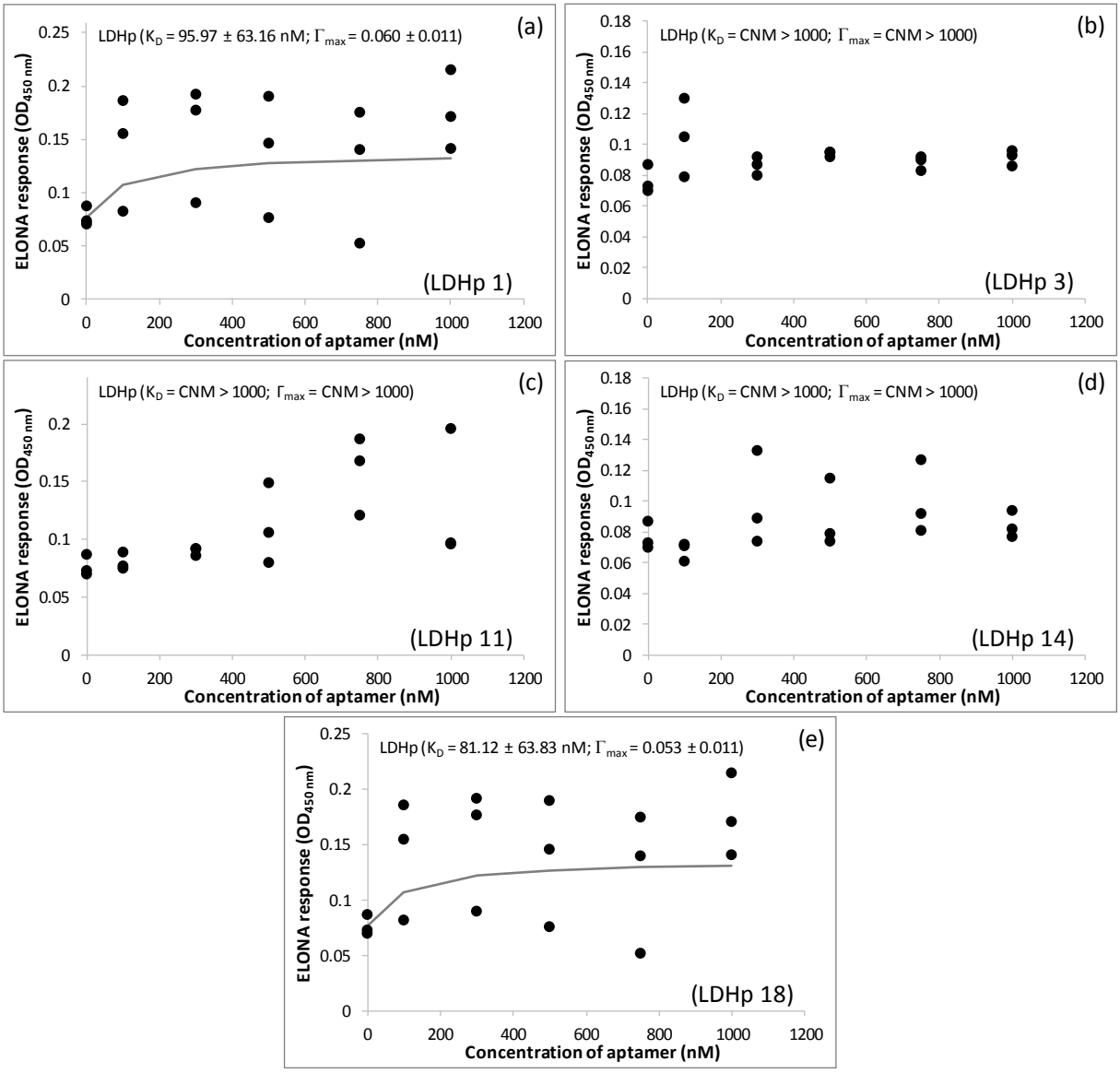

Figure C.3: ELONA-assessed (A_{450nm}) binding kinetics of 0, 100, 300, 500, 750 and 1000 nM biotinylated LDHp 1 (a), LDHp 3 (b), LDHp 11 (c), LDHp 14 (d) and LDHp 18 (e) to the *Pf*LDH-specific peptide, LDHp (*n* = 3).

Figure C.4 shows that GelRed fluorescence increases when the r*Pf*LDH concentration increases, yet increases insignificantly in fluorescence across the LDHp concentration range measured.

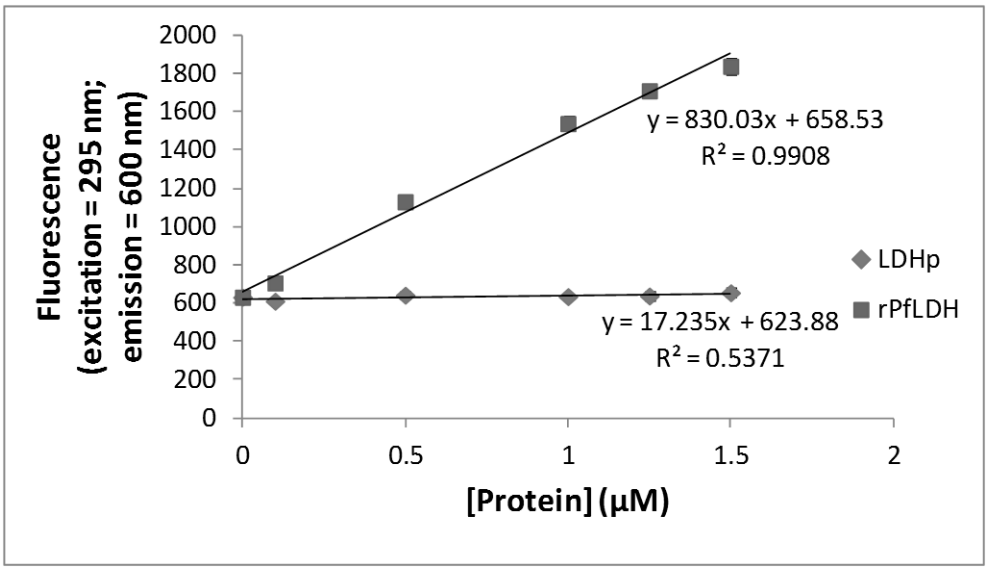

Figure C.4: GelRed intrinsic fluorescent response to increasing concentrations of r*Pf*LDH and LDHp (*n* = 4). Fluorescent excitation: 295 nm; fluorescent emission: 600 nm; protein concentration range: 0 to 1.5 µM; deviation < 5.0 %

Figure C.5 demonstrates GelRed® fluorescence (excitation = 295 nm; emission = 600 nm) whilst intercalated and bound to various concentrations (0, 1, 10, 50, 75 and 100 nM) of aptamer (pL1, LDHp 1, 3, 11, 14 and 18). **Figure C.5** further demonstrates the resulting effect on GelRed-aptamer fluorescence in the presence of the 13-Da *Pf*LDH-specific peptide, LDHp.

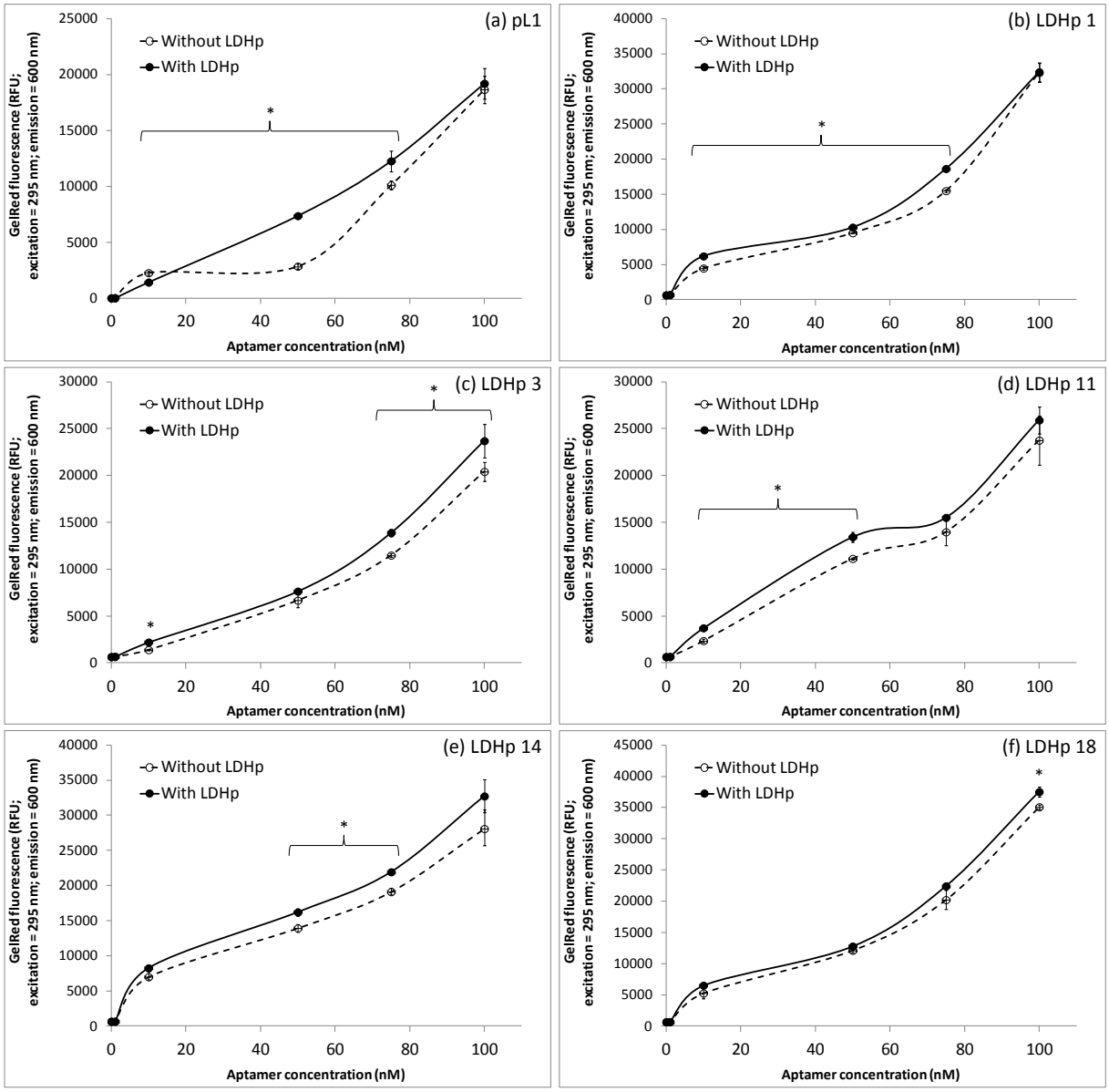

Figure C.5: Fluorescent quenching or enhancement (RFU) of GelRed® dye at various concentrations of aptamer upon LDHp binding (*n* = 3).

Aptamers: pL1, LDHp 1, LDHp 3, LDHp 11, LDHp 14 and LDHp 18.

Tested aptamer concentrations: 1, 10, 50, 75 and 100 nM. Concentration of LDHp was maintained at 0.5 µM.

Statistics: Grouped multiple *t*-test using pairwise comparisons of "Without LDHp" and "With LDHp" at each aptamer concentration;

* Indicates significance: $p \leq 0.05$

APPENDIX D

The material presented in this Appendix relates to **Chapter 5**.

Figure D.1 represents the irreproducibility observed in the Nyquist plots in the absence and presence of LDHp and the MCH-LDHp 11 modified gold stalk electrodes in the assessment of the feasibility of EIS for aptamer-target binding. R_S and C with $p > 0.05$ were determined, while R_{CT} and Z_W had $p < 0.05$ (**Table 5.1**). Note, however, that the concentration of LDHp measured here in was 3.5 µM LDHp, so this figure was included to represent the error observed.

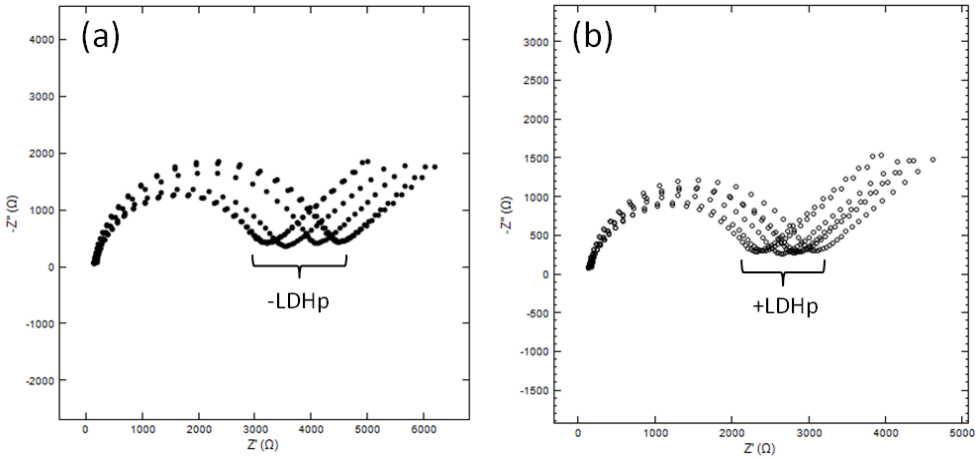

Figure D.1: Replicate Nyquist plots of LDHp 11-MCH gold stalk electrode in the (a) absence (-LDHp) and (b) presence of 3.5 µM LDHp (+LDHp).
Notes: EIS responses were measured with 5 mM $[Fe(CN)_6]^{4-/3-}$ probe in 50 mM potassium phosphate buffer, pH 7.0. Sinusoidal potential: 10 mV (rms); oscillating frequency: 10 kHz to 0.01 Hz.